Rockwell International

Rocketdyne Division
6633 Canoga Avenue
Canoga Park, California 91304

RI/RD85-312

ATOMIZATION AND MIXING STUDY

30 DECEMBER 1985

Contract NAS8-34504

PREPARED BY

A. Ferrenberg
A. Ferrenberg
K. Hunt
J. Duesberg
Advanced Combustion Devices
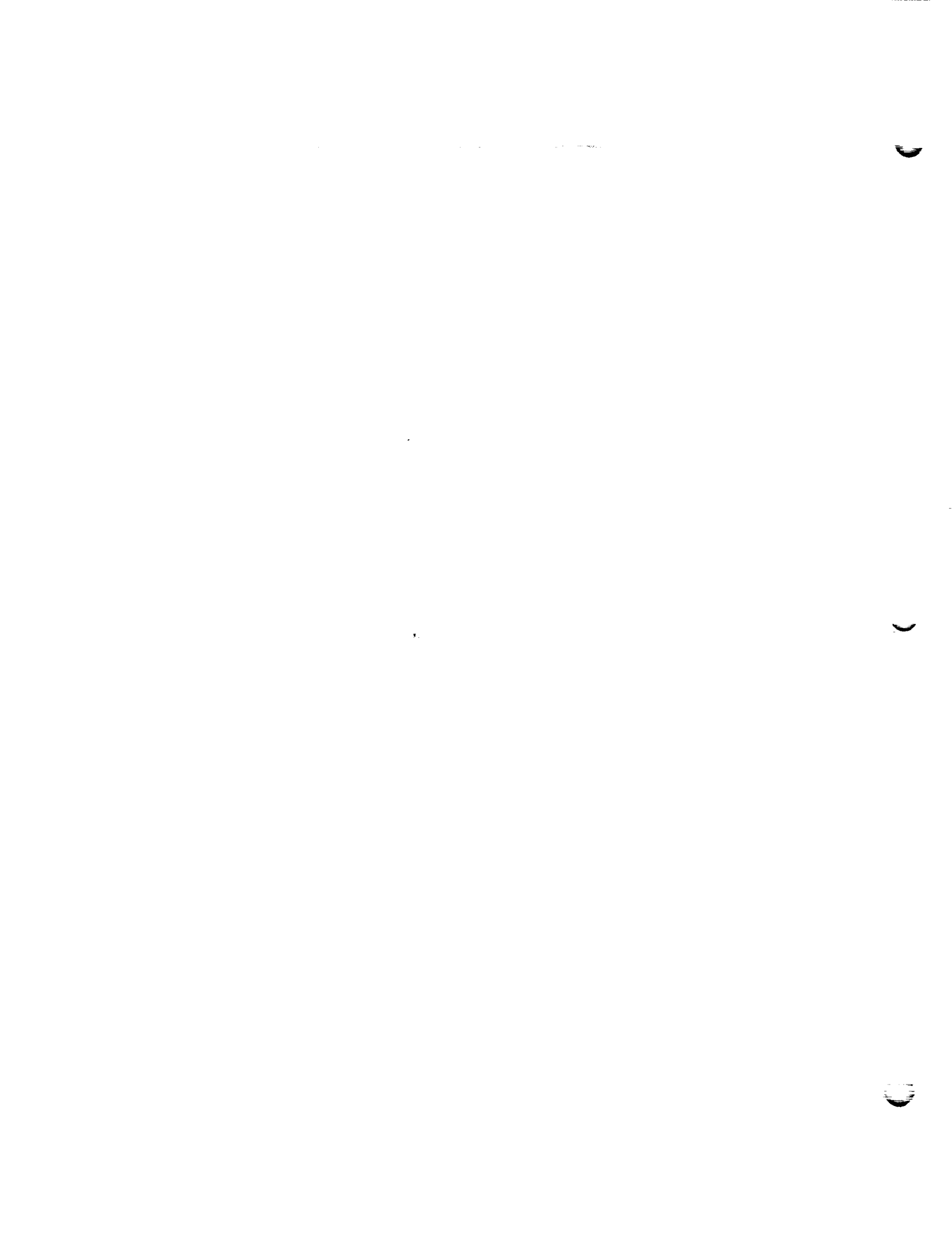
APPROVED BY

F. Kirby
F. Kirby
Program Manager
Advanced Booster Propulsion Program

PREPARED FOR:

NASA/George C. Marshall Space Flight Center
Marshall Space Flight Center, Alabama 35812

FOREWORD

This report describes the work performed during the period of June 1983 through November 1985 under NASA contract NAS8-34504, Atomization and Mixing Study. The Rocketdyne Project Engineer for this work is Dr. Allan Ferrenberg of the Advanced Combustion Devices group under the direction of Mr. James Lobitz. Mr. Frank Kirby is the Rocketdyne Program Manager. Mr. Joseph Duesberg performed the majority of the atomization testing, with some assistance from Mr. Ken Hunt. Mr. Hunt performed all of the mixing testing. Technician support was primarily provided by Mr. Gayle Steele. Other Rocketdyne personnel supporting this work are Mr. Tony Exposito (preliminary droplet sizing interferometry work), Mr. Harry Arbit (basic atomization research literature review), Dr. Robert Jensen (computational analyses in support of gas/liquid mixing methods assessment), and Mssrs. Guido Defever and Robert Saxelby (design support). This program was performed under the technical direction of Mr. Fred Braam of the NASA Marshall Space Flight Center.

CONTENTS

PRECEDING PAGE BLANK NOT FILMED

PAGE iv INTENTIONALLY BLANK

ILLUSTRATIONS

TABLES

I. INTRODUCTION AND SUMMARY

The primary objective of this Atomization and Mixing Study was the obtainment of atomization and mixing performance data for a variety of typical LOX/hydrocarbon injector element designs. Such data are required to establish injector design criteria for such elements, and to provide critical inputs to liquid rocket engine combustor performance and stability analysis, and computational codes and methods. For the most part, these results are sufficiently generic to allow their application to similar injectors employing other propellant combinations.

This program began in February 1982. During the first year of this effort, a literature search and compilation of the liquid rocket injector atomization and mixing data and correlations were performed. Two sets of mixing tests were also performed during the first year: a set of gas/liquid element mixing characterization tests and a smaller set of liquid/liquid triplet element mixing characterization tests. First-year work was reported in an interim technical report (Ref. 1-1). The summary of the liquid rocket injector atomization and mixing correlation and data contained in Ref. 1-1 is presented herein as Appendix A.

During this first year, deficiencies and problems with the atomization test equipment were identified, and action was initiated to resolve them. While these efforts were not a part of this contractual program, they did result in delays and test plan modification in the atomization testing of this program. In addition, the test results of the gas/liquid mixing tests indicated that an assessment of these test methods was required. Finally, the liquid/liquid triplet testing performed indicated a need for a more extensive set of such tests. As a result of these issues, an extension and several modifications of this program were implemented. This work was accomplished during the period of July 1983 through October 1985, and is described in detail in this report.

From October 1983 through December 1984, the gas/liquid mixing assessment methods were analytically and experimentally assessed. During the period of June 1984 through November 1985, several series of liquid/liquid element mixing tests were performed. Finally, in December 1984, after several years of noncontract

testing, problem resolution, and technique development, contract testing to establish the atomization characteristics of selected elements began. This effort culminated in a series of atomization tests during the summer and fall of 1985. All of these efforts and their results are described in detail in this report.

This final report consists of five sections and two appendices:

I   Introduction and Summary

II   Description of Injector Elements

III   Liquid/Liquid Element Mixing Study

IV   Gas/Liquid Element Mixing Testing

V   Atomization Study

Appendix A. Liquid Rocket Atomization and Mixing Technology

Appendix B. Basic Atomization Literature Review

Section II describes the injector elements constructed and tested as a part of this program. The remaining sections are separately summarized in the remainder of this section.

LIQUID/LIQUID ELEMENT MIXING STUDY

The objective of the liquid/liquid mixing study was the acquisition and correlation of cold-flow mixing data for LOX/hydrocarbon injectors. In the primary phase of this study, a series of 71 liquid/liquid mixing tests were performed at Rocketdyne during the period from June 1984 to October 1985. Ten single-element, unlike-triplet injectors were used in a test matrix designed to determine the effect on mixing efficiency of variations in liquid density, impingement distance, element geometry, orifice characteristics, flow rates, and collection

distance, for the overall purpose of evaluating existing triplet injector design correlations and developing improved correlations where necessary.

A secondary phase of the liquid/liquid mixing study was conducted to evaluate the mixing characteristics of a candidate like-doublet injector pattern proposed for use in large LOX/hydrocarbon boosters. A series of tests were performed in October 1985, using four different injector models. In this case, the models featured a multiple-element "unit cell" configuration representative of the overall like-doublet pattern. The test matrix was designed to determine the effect on mixing efficiency of propellant interchange, mass flow throttling, impingement angle, and model scaling.

This program is the largest, and most thorough and comprehensive investigation of the mixing performance of liquid/liquid-triplet elements that has ever been performed. The findings and conclusions of this effort are, in some cases, contradictory to previous findings (based on much less comprehensive test programs) and traditional design practice. Thus, these findings are of great importance and should result in considerable change and improvement in triplet injector designs. In accordance with these findings, the following design criteria and advice to designers of liquid/liquid triplet elements are provided.

1. The use of an optimum value of the Elverum-Morey parameter as a design criterion for liquid/liquid triplets is not justified and should be discontinued. Mixing efficiency increases as the Elverum-Morey parameter increases.

2. The more dense propellant should be injected from the outer orifices.

3. Small, outer to inner, orifice diameter ratios (e.g., 1 or less) are not recommended.

4. The changing of the injection velocity of both liquids by the same percentage, has no effect on the mixing performance, over the range of injection velocities tested.

5. An increase of the outer to inner velocity ratio of the propellants improves mixing performance.

6. The impingement angle has no significant influence on mixing and should be chosen on the basis of other considerations.

7. As a guide to use in the tradeoff of various design considerations, it is recommended that the designer attempt to maximize the parameter.

$$\left(\frac{d_o}{d_i}\right)^{0.29} \left(\frac{\rho_o}{\rho_i}\right)^{0.56} \left(\frac{v_o}{v_i}\right)^{0.25}$$

All of these findings, conclusions, design guidance, and especially the preceding mixing efficiency design parameter, should not be extrapolated or applied beyond the limits of the range of the variables tested in this program without very careful consideration. The range of the variables tested is:

Outer to inner orifice velocity ratio	0.37 to 1.69
Outer to inner orifice diameter ratio	0.92 to 1.58
Outer to inner orifice density ratio	0.76 and 1.32
Impingement angle (between outer streams)	30 to 90 degrees
Orifice diameter	0.117 to 0.236 cm (0.046 to 0.093 in.)
Injection velocities	6.7 to 20.2 m/sec (22 to 66 ft/sec)

The limited testing performed on the like-doublet, multiple-element injector supports the validity of the scaling methods employed. Throttling appeared to have no effect on injector mixing performance. Poorer mixing efficiency was observed for a smaller impingement angle/longer impingement distance variation on the baseline injector.

GAS/LIQUID ELEMENT MIXING STUDY

Single-element, gas/liquid mixing measurements were to be, and have been, performed as a part of this atomization and mixing study. Because of the very poor

collection efficiency measurements obtained on tests already performed, it became necessary to assess and improve the methods by which such measurements are made. Accordingly, a series of studies and experiments were performed, resulting in a number of changes in the apparatus and measurement methods. These changes culminated in a demonstration of the ability to make moderately accurate gas/liquid mixing measurements at low pressure, in lightly loaded (with liquid) flows, and in relatively uniform, one-dimensional flows. Whether these techniques can be successfully applied to the much more heavily loaded and high-pressure flows of interest, is not known. However, it is known that the flow must be relatively straight, (i.e., recirculation must be prevented).

The technique commonly employed for the prevention of recirculation is the use of large quantities of purge gas flow (also referred to as base bleed or curtain flow) circumferentially about the injector. This technique has been applied in all previous gas/liquid mixing measurements. However, while the purge gas greatly reduces or prevents recirculation, it also affects the dispersion of the fuel gas (and perhaps, though certainly to a much lesser extent, the liquid dispersion). Thus, a situation exists where the purge gas is necessary to perform the measurements. At the same time, however, it disturbs or changes the mass flux distributions being measured.

While this problem was recognized in the past, means to assess the magnitude of the effect of the purge gas on the fuel gas distribution did not previously exist. Sufficiently complex, gas dynamic/computer codes capable of estimating the magnitude of this effect now exist. Such an analysis was performed. This analysis indicated a large effect of purge gas on fuel gas distribution. As a result of these studies, the following are concluded:

1. Single-element gas/liquid mixing measurements may be of limited value for comparing the mixing performance of different elements or types of elements, and also may be of very limited value for assessing the relative effects of injector geometry or flow variables. Such measurements serve only as a relative comparison of mixing efficiency.

2. The use of such measurement data as input to the performance analysis codes (e.g., SDER), or to establish design criteria (e.g., optimum values of the Elverum-Morey parameter), is not justified. Further testing of this type is not recommended.

3. Effort should be directed toward the development of a means to assess and measure injector mixing performance.

One very promising means by which this may be accomplished is through the use of multidimensional CFD codes such as the Advanced Rocket Injector Combustor Code being developed under NASA/MSFC Contract NAS8-34928. Such codes can already model cold-flow gas motion with good accuracy and can include the effects of droplets and combustion on gas dispersion. Modeling of the liquid phase (e.g., atomization, stream and droplet breakup, and droplet motion) is currently less developed, but efforts to improve such models are under way.

Another means for the measurement of the mixing performance of injectors is the utilization of advanced combustion diagnostic techniques such as Raman spectroscopy. These diagnostic techniques offer the potential capability to directly and nonintrusively measure combustor gas temperatures and compositions. Thus, they could provide the first direct measurements of hot-fire mixing efficiency.

ATOMIZATION STUDY

The objective of this task was the development of a body of information and empirical correlation by which the atomization characteristics of typical LOX/ hydrocarbon injectors could be assessed or predicted. The survey of the state of the art in this area, presented in Appendix A, discusses the great need for such information and the limited quality and, especially, the applicability of the available data.

To obtain such data and improve upon the droplet-size measurement techniques of the past, the new and very promising technique of droplet sizing interferometry (DSI) was employed. Unfortunately, the application of this powerful new

technique was not as straightforward and simple as originally anticipated. Problems with the DSI, an inability to measure droplet sizes in high-droplet-density sprays, great difficulty in controlling spray recirculation at high pressure, continual difficulties with the monodisperse droplet generator (a DSI calibration tool), various shortcomings of the high-pressure test vessel, and many other problems (as described in Section V) occurred. All of these problems were resolved at no expense to this contract prior to the start of these atomization tests. However, in many cases, the solutions to these problems resulted in a decrease in the scope, quality, or quantity of the atomization testing that could be accomplished during this program. Nevertheless, this effort resulted in the most detailed and complete measurements of the structure of the sprays produced by several of the injector elements of interest. While this effort consisted primarily of tests of coaxial elements, limited testing of gas/liquid-pentad and -triplet elements, and a like-doublet liquid element, was also performed. This program demonstrated the capabilities of the DSI and resulted in the development of procedures and methods for acquiring, compiling, and correlating the vast quantities of data obtainable with the DSI. Specific findings and results from this effort are:

1. Information is provided that indicates the hot-wax technique data, and especially the correlations relating the effects of liquid properties on droplet size, may be of questionable validity or applicability.

2. The Lorenzetto and Lefebvre droplet-size correlating equation is not recommended as a means to estimate droplet sizes for liquid rocket coaxial injectors, especially at mixture ratios greater than 1.

3. The Kim and Marshall droplet-size correlating equation is recommended for the very rough estimation of droplet sizes for liquid rocket coaxial injectors operating at high (main chamber) mixture ratios. This is being recommended only because there appears to be no alternative. Based upon the results of these atomization tests, it is further recommended that the droplet sizes computed from the Kim and Marshall equation be increased by about 30 percent.

4. It is strongly recommended that future efforts to acquire atomization data obtain such data at higher pressures and flow rates.

5. The droplet-size measurement technique employed in this program was the visibility/intensity (V/I) DSI technique. This second-generation DSI technique is inferior to two new DSI techniques now commercially available. However, all of these DSI techniques, as well as all other non-intrusive droplet-size measurement techniques available, have deficiencies that limit their applicability to the study of liquid rocket injector atomization. These deficiencies are the inability to measure droplet sizes in the very dense sprays typical of liquid rocket injectors at nominal flow rates (especially the very fine and dense sprays of gas/liquid injectors), and the inability to distinguish droplets by composition (required to assess unlike liquid injector atomization). Improved capabilities in these areas are needed.

6. The findings of this study demonstrate the need for considerable additional effort in the study of atomization. The validity, and especially the applicability, of all available data and correlations are questionable. The technical challenges and problems are great, but the need for this information to support injector design efforts and the rapidly developing and very promising field of spray combustion modeling is also great.

7. Finally, it is strongly recommended that users of any atomization data and correlations become familiar with the quality, validity, and applicability of them. Furthermore, reports of any analyses based upon such data or correlations should clearly state the limitations and potential errors associated with the utilization of such atomization data.

Additional results and findings are presented in Section V.

APPENDIX A: LIQUID ROCKET ATOMIZATION AND MIXING TECHNOLOGY

This appendix consists of the survey results of the liquid rocket atomization and mixing data, correlations, and measurement techniques previously reported in Ref. 1-1. This appendix is an exact duplicate of that survey as published in July 1983, in Ref. 1-1, and is included herein for the convenience of the reader. It should be noted that certain findings of that survey, regarding mixing assessment techniques and correlations, have been found to be incorrect and have been supplanted by the more recent findings of this program as described in Sections III and IV of this report.

APPENDIX B: BASIC ATOMIZATION LITERATURE REVIEW

Available information on liquid atomization by rocket engine-type injector elements is presented in Ref. 1-1 and Appendix A, in which the literature on atomization by like-doublet, triplet, pentad, and coaxial injector elements was summarized, discussed, and assessed. The general conclusions of that summary were that reported atomization data are largely empirical and ad hoc, only qualitatively understood, and of little general validity or utility. This new review, presented in Appendix B, covers the literature on the more basic or theoretical aspects of liquid atomization. This effort is primarily directed toward studies related to droplet deformation, drag, and breakup, as these processes tend to influence the ultimate size and motion of droplets and are of great importance in efforts to model sprays. Certain more basic and general atomization studies for airblast atomizers are also included. The importance of the atomization process, particularly in combustion applications, has resulted in the publication of hundreds of papers and reviews concerned with various aspects of these subjects. A selection of these studies, representing classical and current procedures, results, and theories, is summarized in this appendix. This summary, together with that in Appendix A, provides a complete description of the state of the art of atomization as it applies to liquid rocket engines. The summary should serve as a useful reference to those familiar with this area and as a basic introduction for those entering this field of study.

II. DESCRIPTION OF INJECTOR ELEMENTS

This section presents the details of the injector elements designed, constructed, and tested as a part of this program. Early in this program, nine typical LOX/hydrocarbon elements were selected for atomization and mixing testing. These were all triplet, pentad, or coaxial elements. The primary characteristics of these baseline elements are presented in Table 2-1. Each of the impinging elements was constructed in the form of a small disc (approximately 2.25 inches in diameter by 0.75 inch thick). A high-pressure mounting assembly was constructed to support and provide liquid and gas manifolding for the interchangeable element discs. The coaxial elements could also be utilized with this mounting assembly. Detail design drawings of the mounting assembly and these nine baseline elements are presented in Ref. 1-1.

The liquid/liquid mixing testing originally planned to be accomplished during this program was very extensively, and successfully, increased. This testing required the construction of additional injectors. The first set of these injectors consisted of eight new liquid/liquid-triplet, single-element discs. These are elements 10 through 17. Detail design drawings of these element discs are presented in Fig. 2-1.

To provide a basis for comparison of the results of these liquid/liquid-triplet tests and earlier Jet Propulsion Laboratory (JPL) tests, a triplet element employing the JPL design practices was constructed. To the greatest extent possible, every important feature of the JPL triplets was incorporated into this element. A JPL triplet orifice design is presented in Fig. 2-2, and the Rocketdyne "copy" of this design is presented in Fig. 2-3 and 2-4. Fig. 2-3 shows the overall assembly, and Fig. 2-4 presents the details of the injector orifice inserts.

The final injectors designed to support the expanded liquid/liquid mixing test program consisted of a set of multiple element, like doublet injectors. This injector pattern was identified under a Rocketdyne IR&D program as a likely candidate for a large LOX/RP-1 booster. This design was based on the concept of a "box" of like doublets of one propellant surrounding each like doublet of the

TABLE 2-1. BASELINE LOX/HYDROCARBON IN;

INJECTOR ELEMENT SELECTI(

	PATTERN	PROPELLANT	P_C (PSIA)	I_C (°R)	MR	ΔP_O (PSI)	ΔP_F (PSI)	ORIFICE DIAMETER (INCHES)		
								OXIDIZER	FUEL	OXII
1	TRIPLET PB (FOF)	LOX/RP-1 (LIQUID/LIQUID)	3500	2100	0.44	700	700	0.0447	0.055	0.;
2	TRIPLET PB (FOF)	LOX/CH_4 (GAS/LIQUID)	2728	2100	0.49	700	346	0.045	0.063	0.;
3	PENTAD PB (FOF)	LOX/CH_4 (GAS/LIQUID)	3500	2100	0.49	700	700	0.0712	0.0587	0.`
4	TRIPLET PB-EDNI (FOF)	LOX/CH_4 (GAS/LIQUID)	3500	2100	0.44	600	850	0.016	0.027	0.(
5	COAXIAL PB	LOX/CH_4 (GAS/LIQUID)	3500	2100	0.49	700	700			
6	TRIPLET PB (FOF)	LOX/C_3H_8 (LIQUID/LIQUID)	5250	1860	0.40	505	905	0.05	0.08	0.;
7	COAXIAL MC	LOX/CH_4 (GAS/LIQUID)	3000	6400	3.5	1000	400			
8	TRIPLET MC (OFO)	LOX/RP-1 (LIQUID/LIQUID)	2000	5900	2.8	350	700	0.065	0.050	0.;
9	COAXIAL MC	LOX/C_3H_8 (GAS/LIQUID)	4000	6400	3.0	1000	800			

)ECTORS

)N

ORIFICE DIAMETER (INCHES)		IMPINGE-MENT ANGLE	V_0 FT/S	V_F FT/S	FREE STREAM LENGTH (INCHES)		REMARKS	OXIDIZER RECESS (I
)IZER	FUEL				OXIDIZER	FUEL		
250	0.239	60°	285	290	0.250	0.289	REF: RI/RD81-129 (NAS8-33243)	
)00	0.276	50°	151	402	0.250	0.275	REF: RI/RD81-129 (NAS8-33243)	
)74	0.248	60°	144	554	0.250	0.289	REF: RI/RD81-129 (NAS8-33243)	
)65	0.062	60°	229	595	0.098	0.112	REF: IR&D	
			75	634	–	–	REF: RI/RD81-129 (NAS8-33243)	0.12{
)5	0.40	60°	207	188	0.25	0.29	ELVERUM-MOREY = 0.66	
			100	500	–	–	REF: RI/RD79-278 (NAS8-33206)	0.1
)5	0.35	60°	171	288	0.29	0.25	ELVERUM-MOREY = 0.66	
			100	600	–	–	SIMILAR TO ELEMENT 7	0.23

2 FOLDOUT FRAME

PRI

COAXIAL ELEMENTS

POST (NCHES)	INNER TUBE ID (INCHES)	INNER TUBE OD (INCHES)	OUTER TUBE ID (INCHES)	INNER TUBE LENGTH (INCHES)	OUTER TUBE UNDISTURBED FLOW LENGTH (INCHES)	INNER TUBE ORIFICE DIAMETER (INCHES)
3	0.088	0.1355	0.1735	2.3	0.525	0.0455
	0.182	0.202	0.247	2.53	0.5	0.086
	0.20	0.23	0.28	2.5	0.5	0.091

3 FOLDOUT FRAME

ELEMENT 10

⌀.188 FLAT
BOTTOM, TO DEPTH
SHOWN, 2PL EQ SP

15°
2PL

⌀.876

⌀.188 FLAT BOTTOM
.550 DEEP
⌀.0500±.0005. THRU
③

②

.800 REF

.563 2PL

④

.250

30°00'±0°15'
2 PL

⌀.0660±.0005 THRU
2PL EQ SP ③

ELEMENT 12

⌀.188 FLAT
BOTTOM, TO DEPTH
SHOWN, 2PL EQ SP
AS SHOWN

15°
2PL

⌀.930

⌀.188 FLAT
BOTTOM, .550
DEEP
⌀.0500±.0005
THRU ③

②

.800 REF

.474 2PL

④

.250

30°00'±0°15'
2PL

⌀.0790±.0005 THRU
2PL EQ SP ③

ELEMENT 11

⌀.188 FLAT
BOTTOM, TO DEPTH
SHOWN, 2PL EQ SP

15°
2PL

⌀.865

⌀.188 FLAT BOTTOM
.550 DEEP
⌀.0500±.0005 THRU
③

②

.800 REF

.582 2PL

④

.250

⌀.0550±.0005 THRU
2PL EQ SP ③

30°00'±0°15'
2 PL

ELEMENT 13

⌀.188 FLAT
BOTTOM, TO
DEPTH SHOWN,
2PL EQ SP, AS
SHOWN

15°
2PL

⌀.840

⌀.188 FLAT BOTTOM
.550 DEEP
⌀.0500±.0005 THRU
③

②

.622 2PL

④

.250

⌀.0460±.0005 THRU
2PL EQ SP ③

30°00'±0°15'
2PL

Figure 2-1. Additional Liquid/Liquid-Triplet Elements

ELEMENT 14

ELEMENT 16

ELEMENT 15

ELEMENT 17
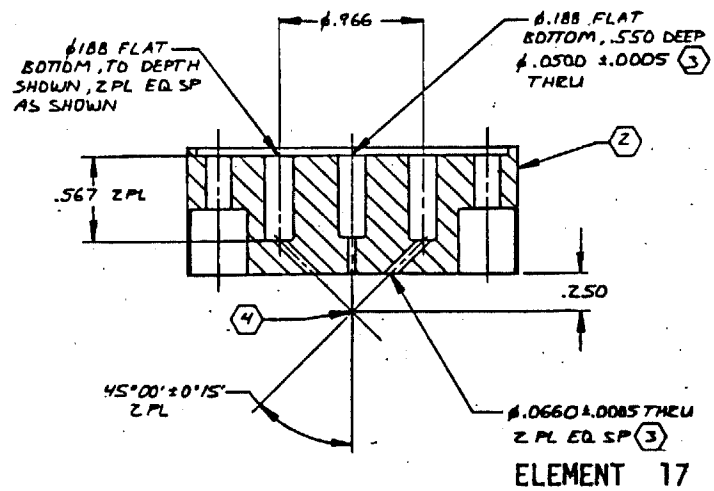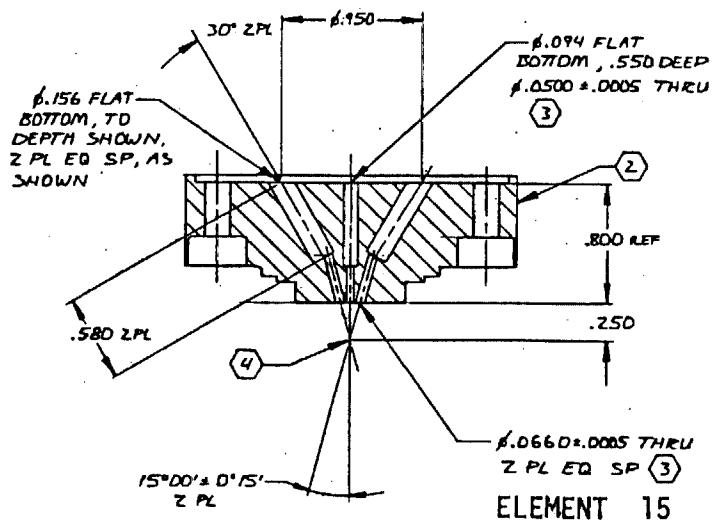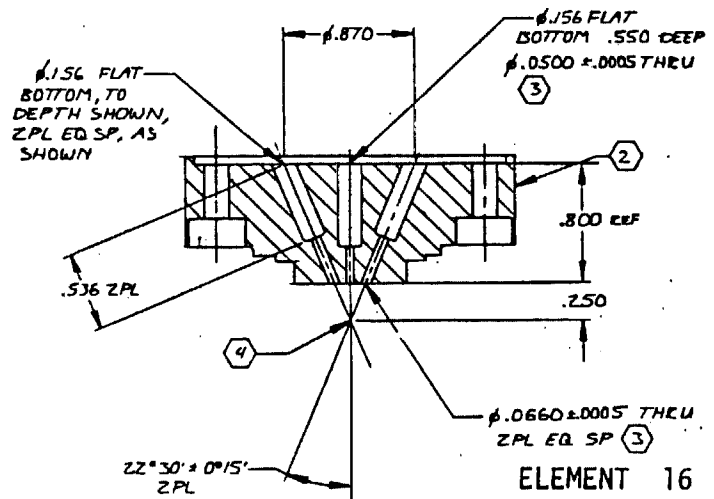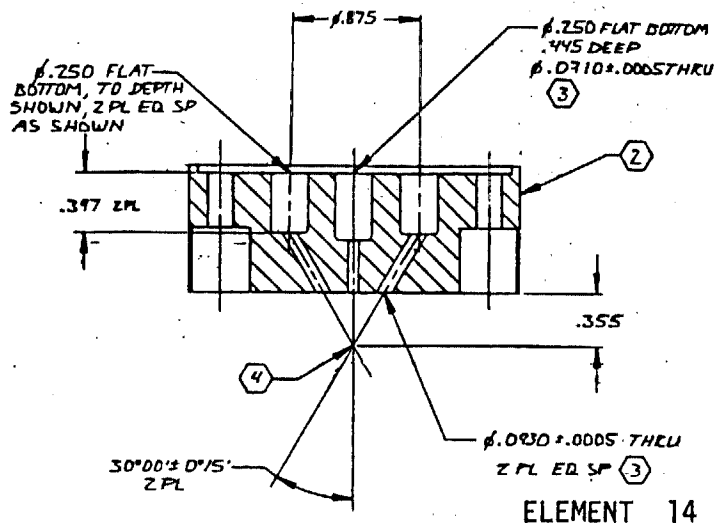
Figure 2-1.   (Concluded)
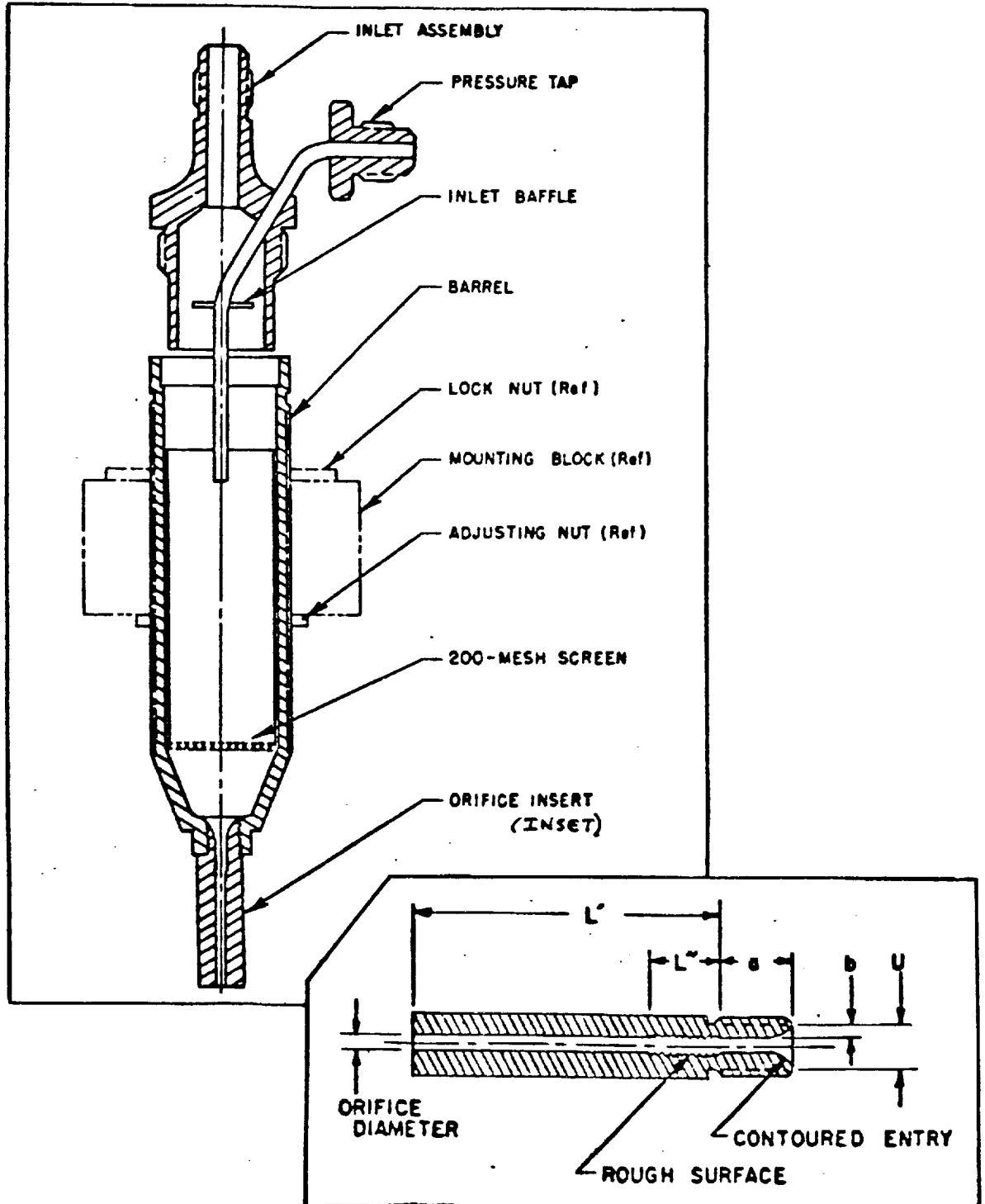
Figure 2-2. Schematic Drawing of Orifice Assembly Employed in JPL Studies
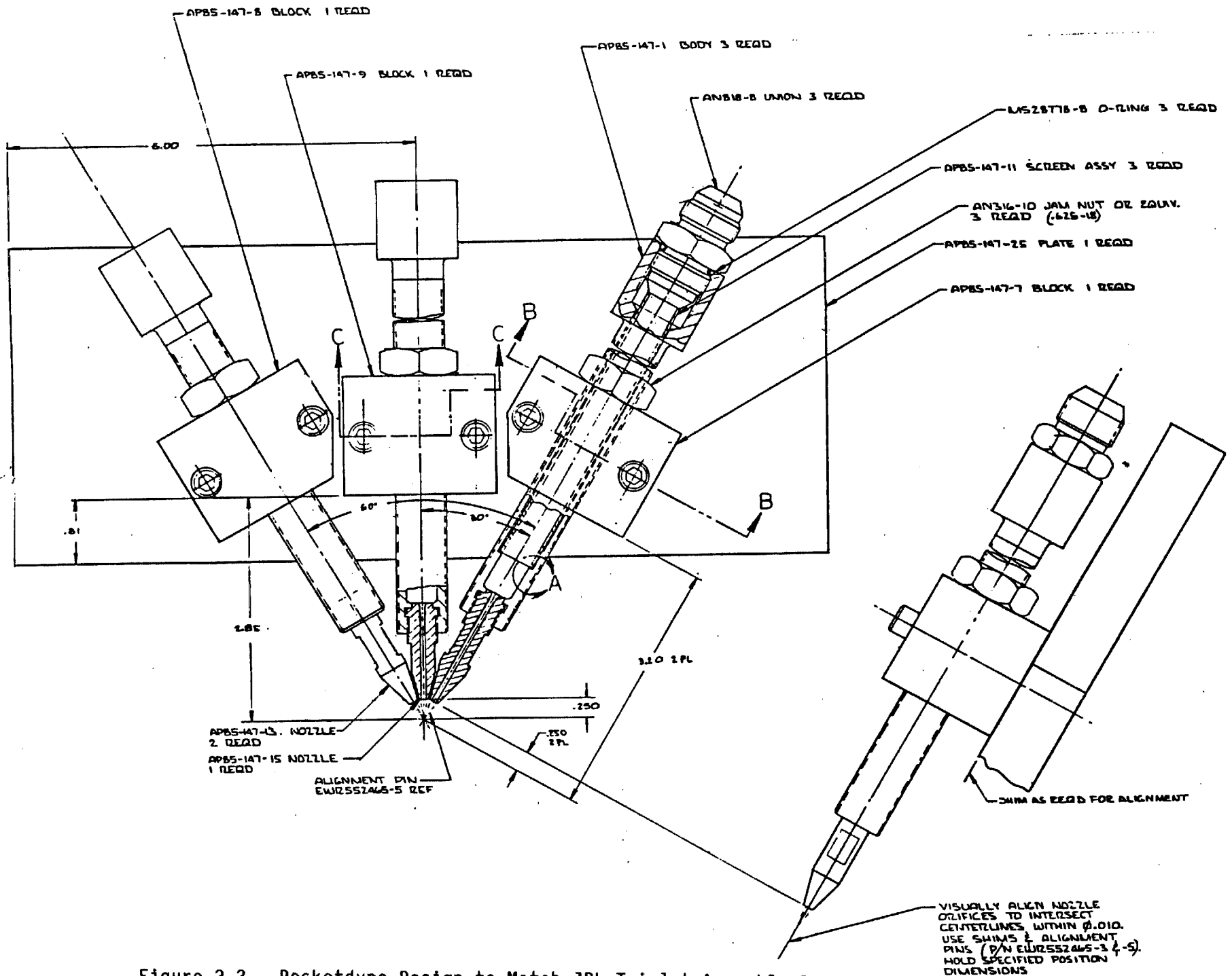
Figure 2-3.   Rocketdyne Design to Match JPL Triplet-Assembly Drawing
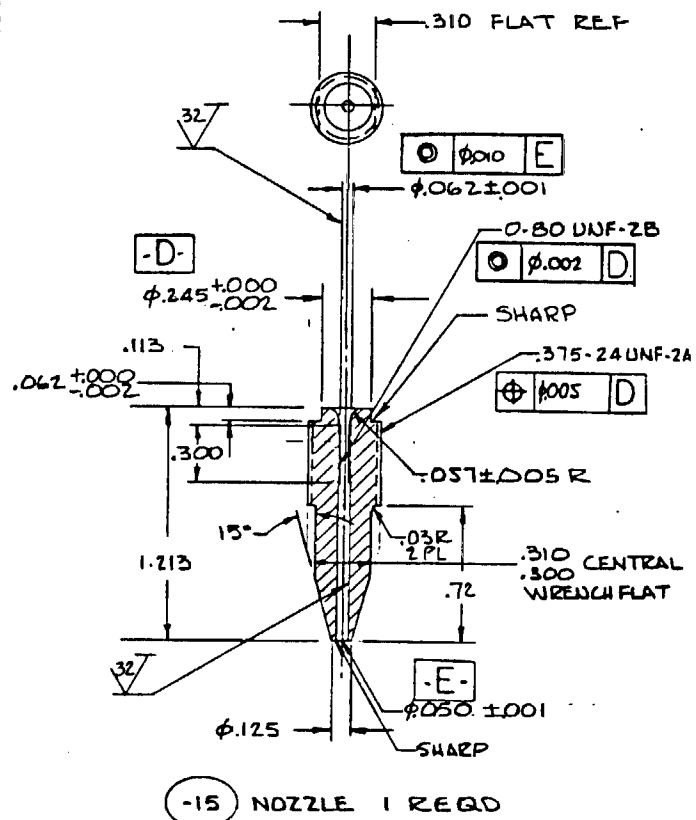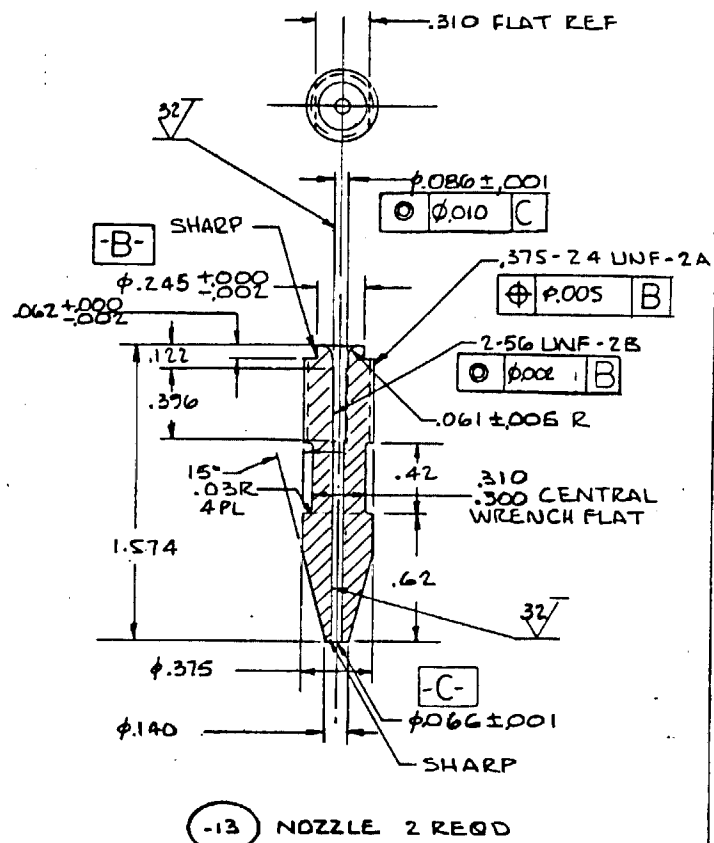
Figure 2-4. Rocketdyne Design to Match JPL Triplet - Orifice Inserts

other propellant. These injectors were constructed from two plexiglass plates bonded together. This novel design concept allowed relatively simple and inexpensive fabrication of these cold-flow injectors. Details of the designs of these injectors are presented in Fig. 2-5 through 2-9. Fig. 2-5 presents the basic plate design employed for all the injectors, while Fig. 2-6 through 2-9 present the major details of each of the injector designs. Rationale for these designs and additional descriptions of these element patterns can be found in Section III.

2.50
FOR -3

10.00
FOR -3

5.00

9E
D

A

A

14A
D

APB5-141 BASE 1 REQD

-3 ELEMENT 1 REQD

.280

63
FOR -3
BEFORE BONDING
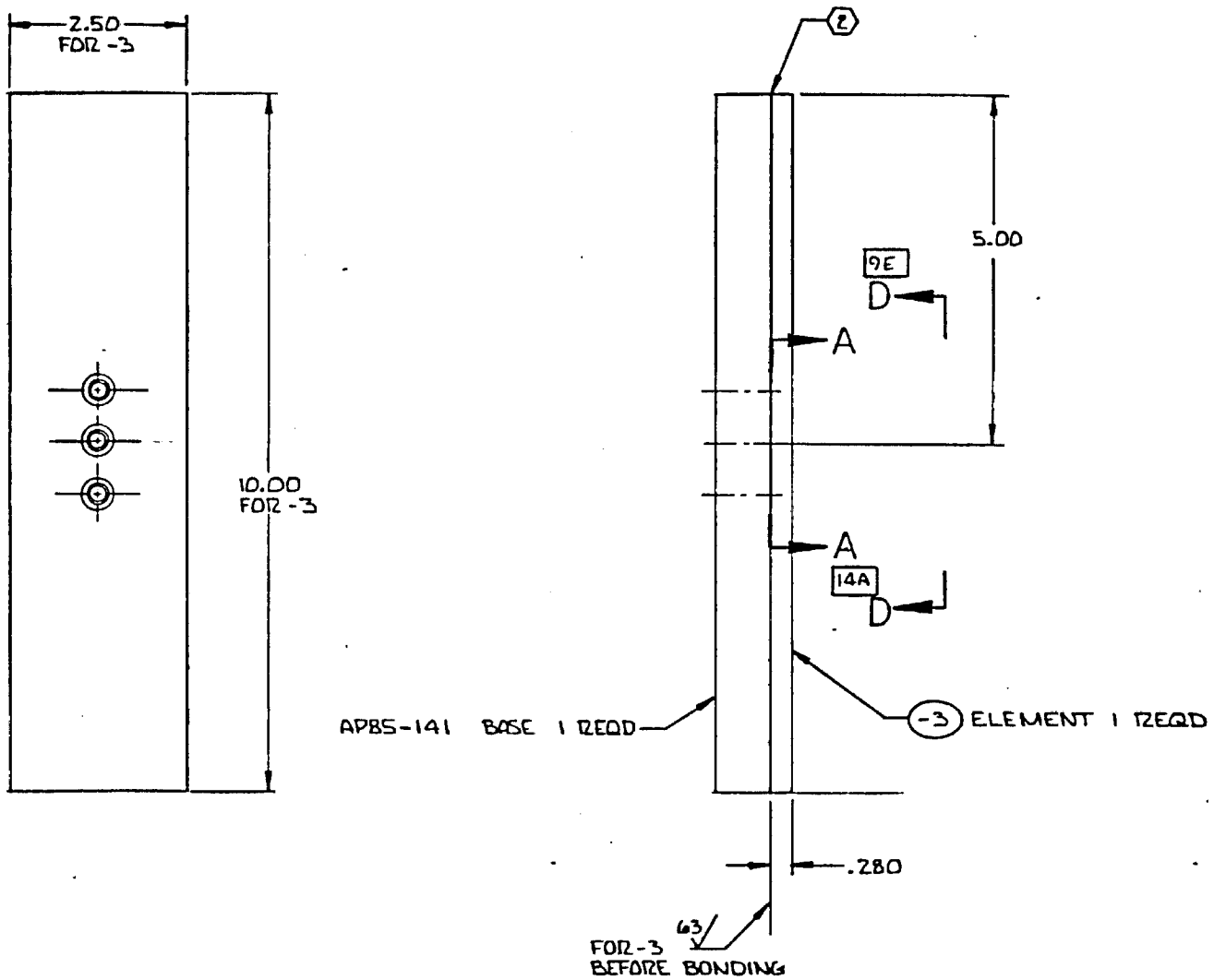
Figure 2-5. Basic Plate Design for Box Pattern Injectors
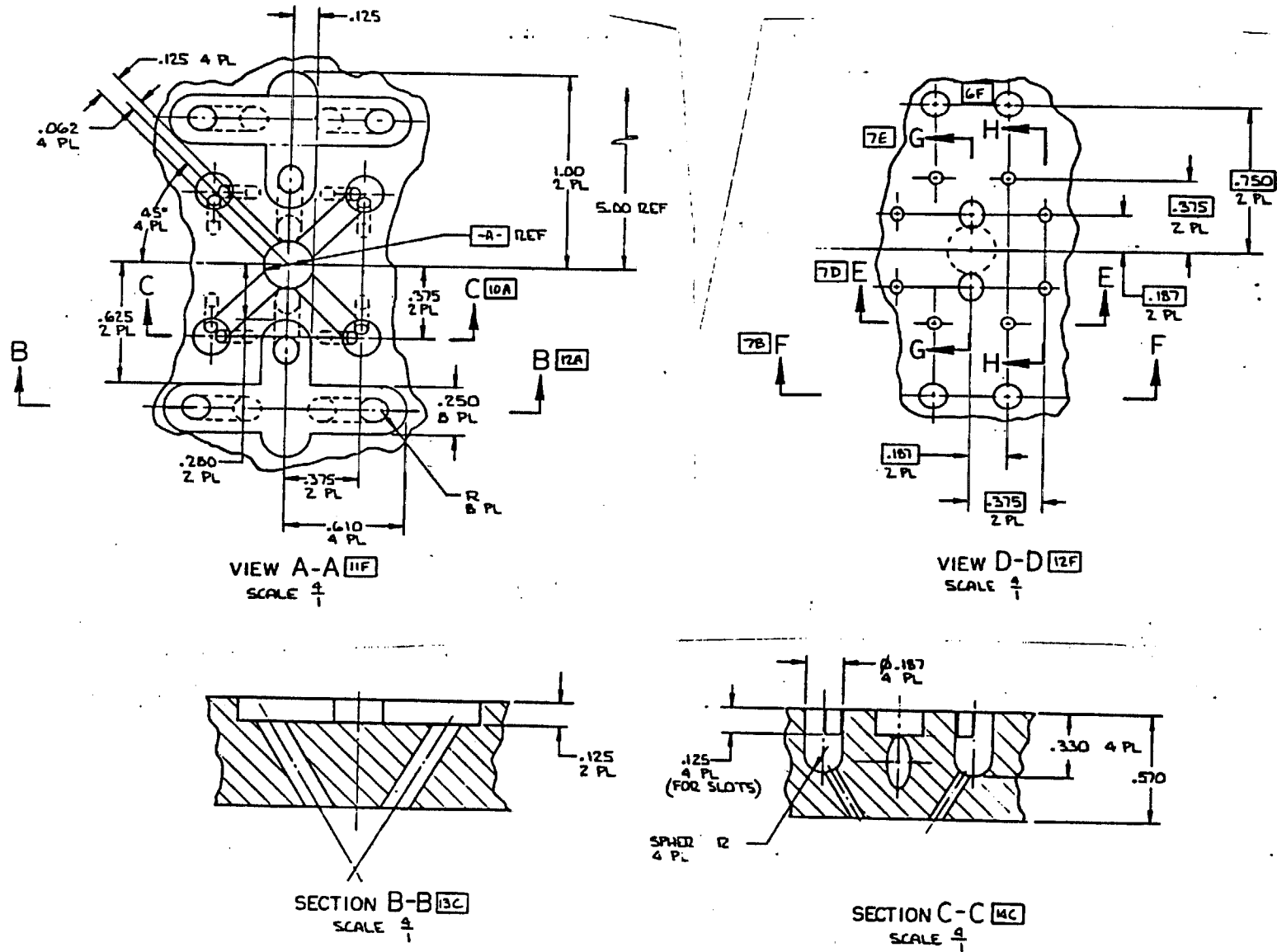
Figure 2-6.   Baseline Element, Fuel Box Around Oxidizer Doublet, 60° Impingement, 2.5 Scale
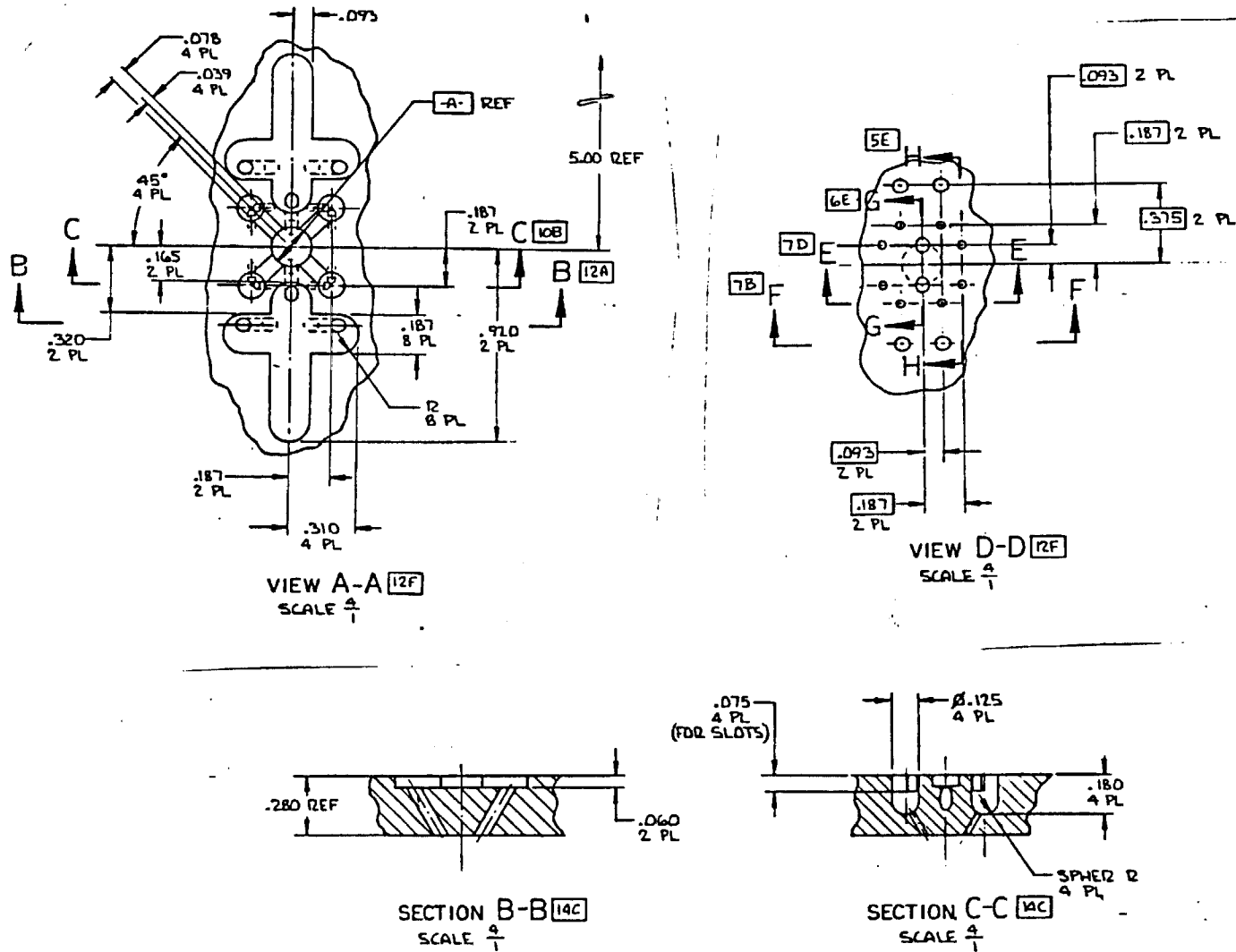
Figure 2-7. Small-Scale Element, Fuel Box Around Oxidizer Doublet, 60° Impingement, 1.25 Scale

VIEW A-A [12F]
SCALE 4/1

VIEW D-D [12E]
SCALE 4/1

SECTION B-B [13C]
SCALE 4/1

SECTION C-C [13C]
SCALE 4/1
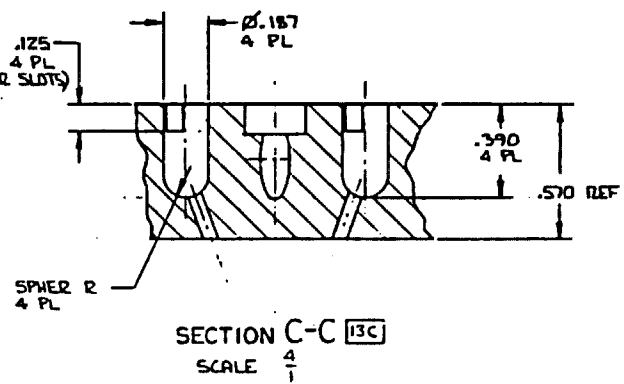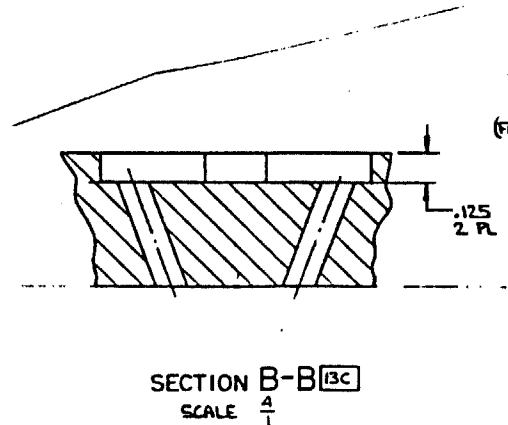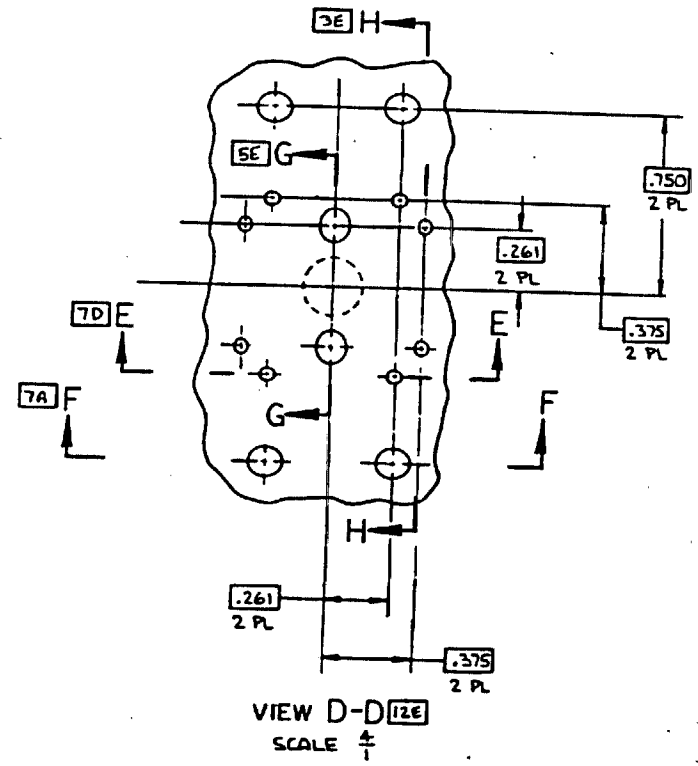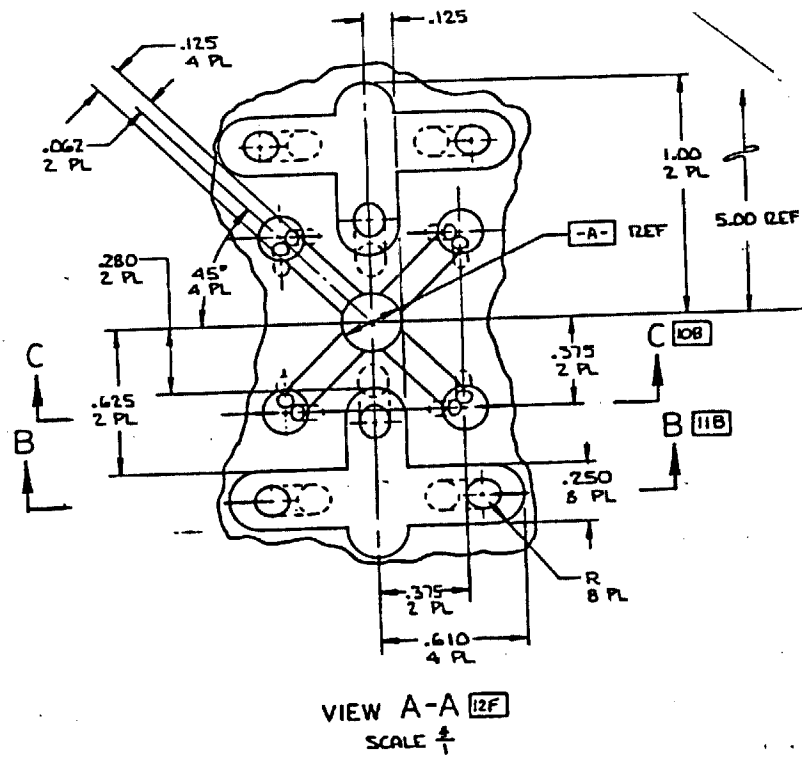
Figure 2-8.   Small-Angle Element, Fuel Box Around Oxidizer Doublet, 40° Impingement, 2.5 Scale

.125
4 PL

.062
4 PL

45°
4 PL

.280
2 PL

.625
2 PL

C

B

.375
2 PL

.610
4 PL

1.00
2 PL

5.00 REF

-A- REF

C 9A

.375
2 PL

B 11A

.250
8 PL

R
8 PL

VIEW A-A 12F
SCALE 4/1

3E H

5E G

7C E

7B F

G

H

.375
2 PL

.750
2 PL

.187 2 PL

.187
2 PL

.375
2 PL

VIEW D-D 12E
SCALE 4/1

E

F

.500 REF

.125
2 PL

SECTION B-B 13C
SCALE 4/1

.125
4 PL
(FOR SLOTS)

Ø.187
4 PL

.320
4 PL

SPHER R
4 PL

SECTION C-C 13C
SCALE 4/1
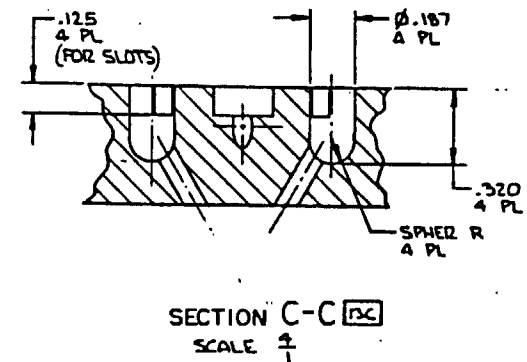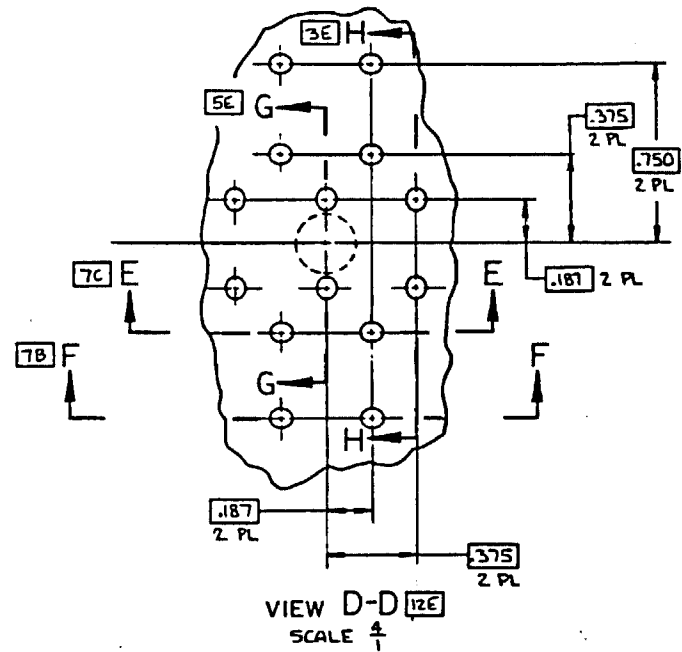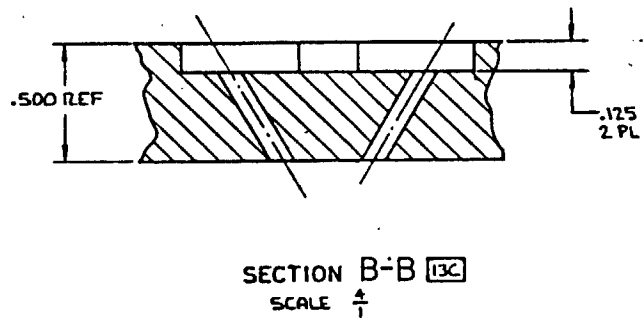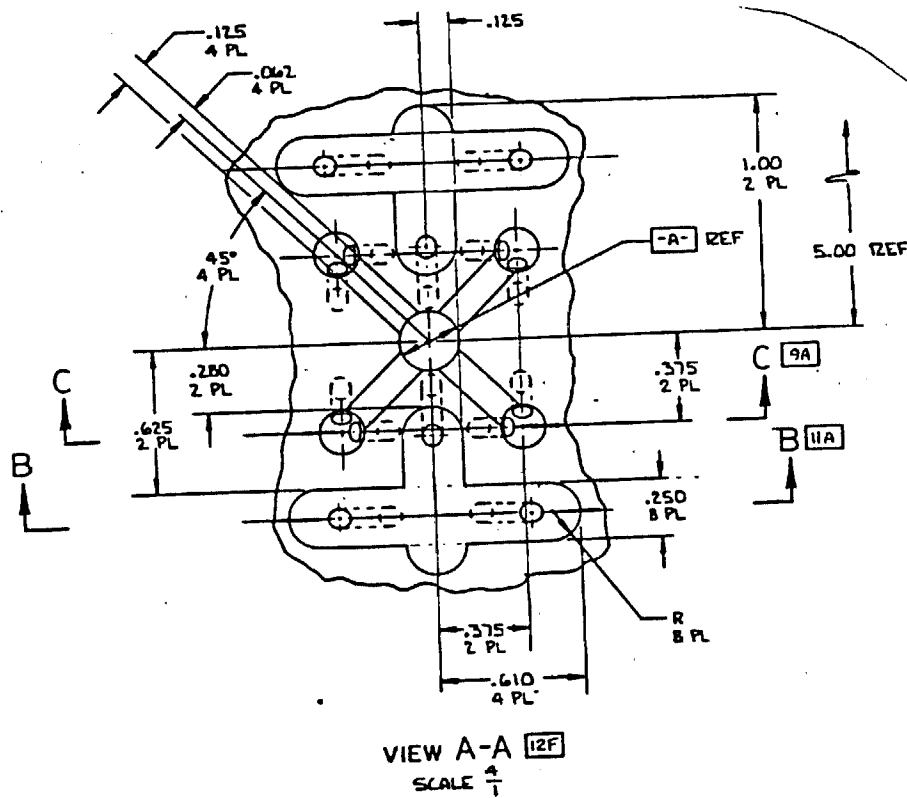
Figure 2-9. Reversed Element, Oxidizer Box Around Fuel Doulet, 60° Impingement, 2.5 Scale

III. LIQUID/LIQUID ELEMENT MIXING STUDY

The objective of the liquid/liquid mixing study was the acquisition and cor-
relation of cold-flow mixing data for LOX/hydrocarbon injectors. In the primary
phase of this study, a series of 71 liquid/liquid mixing tests were performed at
Rocketdyne during the period from June 1984 to October 1985. Ten single-element,
unlike-triplet injectors were used in a test matrix designed to determine the
effect on mixing efficiency of variations in liquid density, impingement geom
etry, orifice characteristics, and collection distance, for the overall purpose
of evaluating existing triplet injector design correlations and developing
improved correlations where necessary.

A secondary phase of the liquid/liquid mixing study was conducted to evaluate the
mixing characteristics of a candidate like-doublet injector pattern proposed for
use in large LOX/hydrocarbon boosters. A series of 11 tests were performed in
October 1985, using four different injector models. In this case, the models
featured a multiple-element "unit cell" configuration representative of the over-
all like-doublet pattern. The test matrix was designed to determine the effect
on mixing efficiency of propellant interchange, mass flow throttling, impingement
angle, and model scaling.

SINGLE-ELEMENT, UNLIKE-TRIPLET STUDY

The efficiency of combustion attained in a rocket engine is highly dependent upon
the uniformity of the mixture ratio produced by the injector. Most engines are
designed to operate at or near overall mixture ratios corresponding to the maxi
mum of the theoretical performance curve. Since any deviation from the large
mixture ratio can result in lower performance, it is evident that not only over
all mixture ratio, but also local mixture ratio must be accurately controlled in
order to achieve the highest possible performance from the engine. The objective
of successful injector design is therefore to deliver the propellants to the com-
bustion zone in a manner such that local variations in mixture ratio across the
injectant spray field are minimized with respect to the overall mixture ratio.

The accepted parameter that defines the mixture ratio uniformity of an injectant spray field was proposed several years ago by Rupe at JPL (Ref. 3-1). Known as the overall mixing efficiency, or Em (E-sub-m) value, this parameter is computed as a mass weighted summation of the mixture ratio variations exhibited by a number of samples collected over a surface in the spray field. The mixing efficiency equation takes the form subsequently shown; each local sample having a mixture ratio different from the overall value is treated as a decrement from perfect mixing, and weighted by the fraction of the overall collected mass it represents.

$$E_m = 100 \left[1 - \left(\sum MF_{sb} \frac{R-R_{sb}}{R} + \sum MF_{sa} \frac{R-R_{sa}}{R-1} \right) \right] \tag{1}$$

In Eq. 1, E_m is the overall mixing efficiency of the element, R represents mixture ratio expressed as oxidizer mass divided by total mass, and MF is the fraction of the total collected mass contained in each individual sample. The subscript sa indicates a sample whose mixture ratio is above the overall value, while sb indicates one whose mixture ratio is below the overall value. Mixing efficiencies range from zero to 100%, with 100% implying that all samples tested have the same mixture ratio, and zero implying that all samples consist of either one component or another.

The problem of optimizing mixing efficiency for various liquid-on-liquid impinging injector element types was investigated by Rupe and his colleagues at JPL, (Ref. 3-1), resulting in injector design correlations that have become widely accepted over the years. These studies were among the first to document the relationship between mixing uniformity and certain hydraulic and relative momentum conditions of the impinging streams. For the case of the coplanar liquid/ liquid triplet, the definitive JPL study was performed by Elverum and Morey (Ref. 3-2), culminating in the correlating parameter bearing their names. All JPL investigators cited the importance of liquid stream stability (i.e., stable, symmetrical velocity profile; similar centerline to mean-stream pressure ratio; and low degree of radial spreading) as a prerequisite for consistent impingement and subsequent mixing characteristics. This emphasis on producing perfectly impinging turbulent streams led to their use of precision-machined test orifices having elliptically contoured entrances, roughened turbulence-inducing sections, and overall lengths of at least 20 diameters.

In the Elverum-Morey study, the propellant simulant combinations employed were water/kerosene and water/carbon tetrachloride. In reporting the results, the authors stated that by interchanging the two liquids in each simulant pair between the inner and outer orifices of a particular element, they were able to investigate the effects of density ratio (ρ_o/ρ_i) variation over a range from 0.54 to 1.85. Based on densities of 0.82, 1.00, and 1.59 g/cm^3 for kerosene, water, and carbon tetrachloride, respectively (Ref. 3-2), the four discrete den- sity ratio possibilities for the reported simulant combinations are more accur- ately seen to be 0.63, 0.82, 1.22, and 1.59. Other variations included in the JPL study were an orifice diameter ratio (D_o/D_i) range of 0.71 to 1.30 (no discrete values reported), and at least two included impingement angles: 60 and 90 degrees. A curve fit of the limited data generated in their study produced a design correlation that has since become known as the Elverum-Morey criteria for triplet injectors:

$$\left(\frac{\dot{m}_o}{\dot{m}_i}\right)^2 \left(\frac{\rho_i}{\rho_o}\right) \left(\frac{A_i}{2\,A_o}\right)^{1.75} = 0.66 \tag{2}$$

where the subscript o implies an outer orifice and subscript i pertains to the inner orifice. The A_o term is the area of one outer orifice. The term on the left is referred to as the Elverum-Morey parameter. Based upon the very limited data of the JPL study, the mixing efficiency appeared to be greatest when this parameter was equal to 0.66. These criteria were reportedly valid only for 60-degree included angles; the optimum value for the 90-degree case was found to be 0.42.

Prior to the Elverum-Morey study, the only accepted injector design correlation was that proposed by Rupe for unlike impinging doublet elements (Ref. 3-3):

$$\frac{\rho_1 V_1^2 d_1}{\rho_2 V_2^2 d_2} = 1.0 \tag{3}$$

The Rupe criteria were hypothesized on the premise that the momenta and diameters of the two streams must be equal to achieve optimum impingement and mixing characteristics, a premise that was substantiated by extensive experimental results. One objective of the Elverum-Morey study was to determine whether or not a correlation of the form proposed by Rupe was applicable to triplet elements. Substitution and rearrangement of Eq. 2 and 3 reveal the similarity between the Rupe [Eq. (4)] and Elverum-Morey [Eq. (5)] forms:

$$\frac{\rho_0 V_0^2}{\rho_1 V_1^2} \left(\frac{A_0}{A_1}\right)^{0.5} = k \tag{4}$$

$$\frac{\rho_0 V_0^2}{\rho_1 V_1^2} \left(\frac{2 A_0}{A_1}\right)^{0.25} = k' \tag{5}$$

On fitting selected data to the Rupe form, Elverum and Morey reported an optimum k value of 0.625 for two triplet elements having diameter ratios (D_0/D_1) of 1.00 and 1.29. They further stated that both correlations [Eq. (4) and (5)] gave the same result for the case of D_0/D_1 equal to 1.26, but diverged for diameter ratios significantly different from 1.26. Algebraic manipulation of Eq. (4) and Eq. (5) reveals that the two forms actually converge at a D_0/D_1 ratio of 1.41. Neither Eq. (4) nor Eq. (5) appears to have a theoretical basis for predicting optimum mixing characteristics for triplet elements, and apparently the empirical correlation shown in Eq. (2) was the best fit for the very limited data of the Elverum-Morey investigation.

Experimental Objectives

The objectives of the liquid/liquid triplet-mixing study were to determine the effect on mixing efficiency of several variations in element geometry and injection conditions, in order to evaluate the validity of the Elverum-Morey criteria, and possibly to develop an improved correlation. In addition to the Elverum-Morey parameter, other comparative stream dynamic parameters, such as momentum ratio and velocity head ratio, were evaluated in their relation to mixing efficiency.

Table 3-1 summarizes the parameter variations assessed in the test program. Water and 1, 1, 1-trichloroethane (TRIC) were used as simulants for RP-1 and LOX, respectively, giving two possible values for stream density ratio: 0.76 and 1.32. Ten triplet elements were employed -- a baseline element sized for an Elverum-Morey parameter value of 0.66 at a nominal oxidizer/fuel mass mixture ratio of 2.8, and nine elements incorporating geometric variations around the baseline. All but two of the elements were fabricated by electrical-discharge-machining (EDM) the orifices. Orifice lengths were generally assigned a value of five diameters, and no entrance contouring was provided. The exceptions in terms of fabrication method were a drilled-orifice element (orifice L/Ds = 5) whose orifice entrances were rounded to a 0.030-inch radius, and a precision machined element (orifice L/Ds = 24) similar to those employed in JPL mixing studies. Both contoured elements were otherwise identical to the baseline EDMed element. Layout drawings of the EDM elements (elements 10 through 17) were presented in Fig. 2-1. The drilled orifice element is the number 8 baseline element presented in Table 2-1, and the details of the element designed to match the JPL elements are presented in Fig. 2-3 and 2-4.

Experimental Procedure

The laboratory apparatus employed in the liquid/liquid testing is shown schematically in Fig. 3-1. The injector elements were installed in a manifolding fixture positioned over a rectangular collection grid comprising 260 (13 rows by 20 columns) 1/8-inch square tubes (Fig. 3-2a), each draining into a corresponding 60-milliliter graduated test tube (Fig. 3-2b). Between the collection grid and the injector element was an air-activated shutter for diverting flow to and from the grid. Propellant simulants were supplied to the injector by gaseous nitrogen pressurization of the two 30-gallon liquid tanks. The procedure for performing an individual run was as follows: target injection flow rates were achieved by regulating the tank pressures with solenoid valves open and the shutter closed; the shutter was opened for a timed liquid collection interval (approximately 20 to 50 seconds); the shutter was closed, followed by the solenoid valves; and finally, the volumes of propellant simulants in each test tube were recorded. Because of the immiscibility and differing densities of the TRIC and water, two separate phases were clearly distinguishable in the test tubes, and volume

TABLE 3-1. OBJECTIVES OF THE LIQUID/LIQUID-TRIPLET MIXING STUDY

PROPELLANT SIMULANTS

    FUEL - WATER (DENSITY = 62.4 LB/FT3)
    OXIDIZER - 1,1,1-TRICHLOROETHANE (DENSITY = 82.6 LB/FT3)

BASELINE ELEMENT

    D_o = 0.066 INCH
    D_1 = 0.050 INCH
    INCLUDED ANGLE = 60 DEGREES
    (SIZED FOR AN ELVERUM-MOREY PARAMETER VALUE OF 0.66 AT
    AN OXIDIZER/FUEL MASS MIXTURE RATIO OF 2.8)

EFFECT OF THE FOLLOWING VARIABLES ON MIXING EFFICIENCY TO BE ASSESSED

PARAMETER	VARIATIONS
MIXTURE RATIO	2.8 +25%
DIAMETER RATIO (D_o/D_1)	1.32 + 20%
IMPINGEMENT ANGLE	60 DEGREES + 30 DEGREES
ORIFICE DIAMETER	NOMINAL, $\sqrt{2}$ X NOMINAL
MASS FLOW RATE THROTTLING	NOMINAL, $\sqrt{2}$ X NOMINAL
FABRICATION METHOD	EDM, SHARP-EDGED; VS DRILLED, CONTOURED ORIFICES
COLLECTION DISTANCE	1, 2, AND 3 INCHES
INJECTANT CONFIGURATION	O-F-O VS F-O-F

VALIDITY OF THE ELVERUM-MOREY CRITERIA TO BE ASSESSED

$$\left(\frac{\dot{m}_o}{\dot{m}_1}\right)^2 \left(\frac{\rho_1}{\rho_o}\right)\left(\frac{A_1}{2 A_o}\right)^{1.75} = 0.66$$

Figure 3-1. Test Apparatus Employed in the Liquid/Liquid Mixing Study
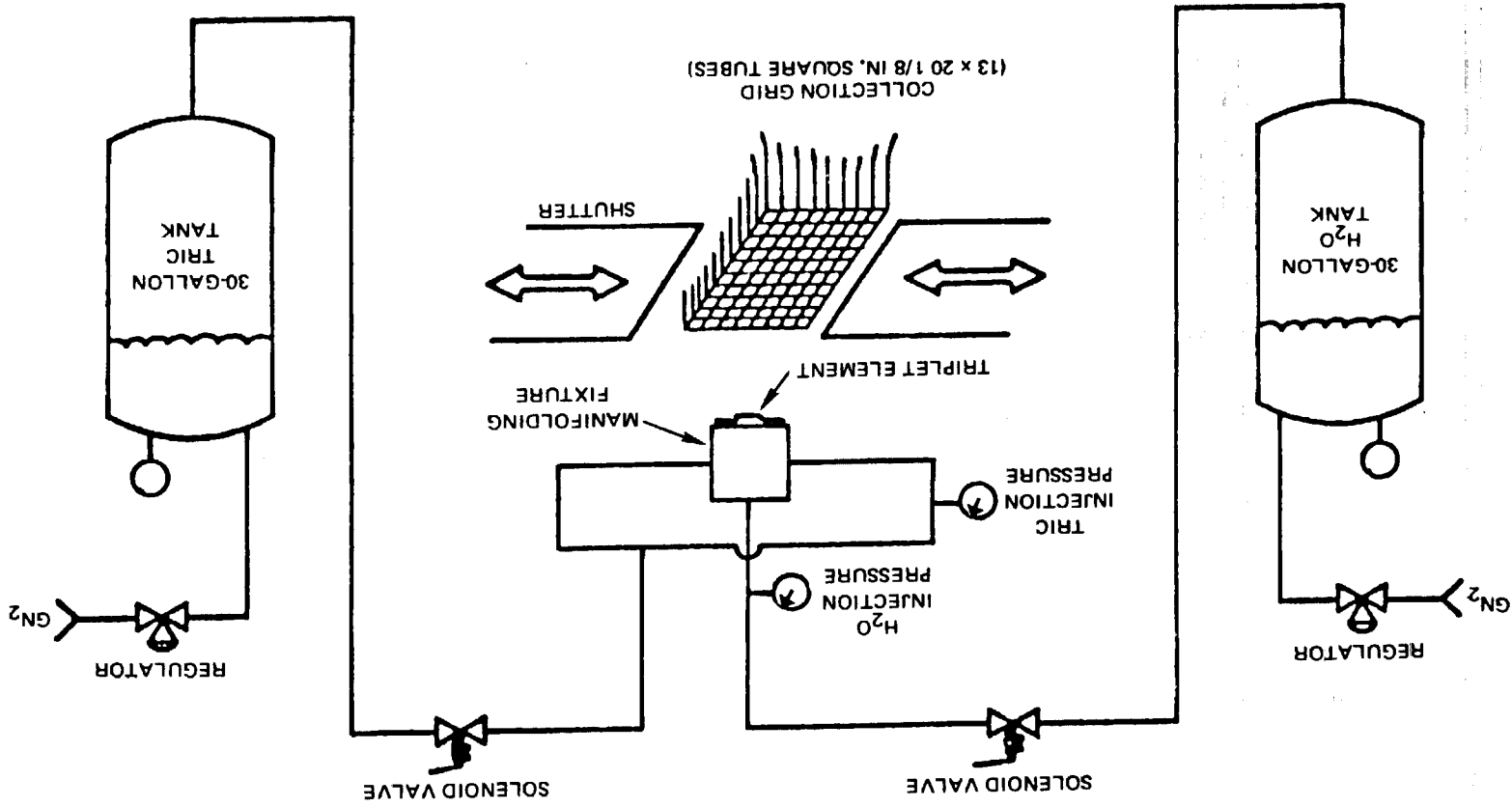
a. Square Tube Assembly

b. Test Sample

Figure 3-2. Liquid/Liquid Mixing Test Apparatus

measurements of each component were recorded to an accuracy of ±0.2 milliliter. Distinction between the two liquids was facilitated by dissolving an inert red dye into the TRIC each time the tank was filled. In many tests, it was necessary to measure and record TRIC and water quantities from nearly all the graduated test tubes. Thus, as many as 520 measurements of propellant distribution were obtained in each test. All these data were input to a computer code that converted them to mixing efficiency data, plots of mass flux distributions, and other data. Details of this code and plots of mass flux distributions from earlier liquid/liquid triplet tests are presented in Ref. 1-1. The primary output for this detailed study of the effects of injector design parameters on mixing efficiency, is the mixing efficiency.

Test Plan and Preliminary Data Analysis

Prior to testing, all the elements were flow calibrated over a narrow pressure drop range corresponding to the range projected for each element in subsequent test runs. Based on the mass-flow-rate versus pressure-drop (discharge coefficient) data obtained, run conditions were formulated for a series of tests designed to meet the parameter variation specifications outlined in Table 3-1. This test plan is presented in Table 3-2. When the plan was formulated, it was assumed that measurement of orifice pressure drops during test runs was sufficient for accurate computation of injectant flow rates, given the discharge coefficient data for each element. Therefore, volumetric flowmeters were not included in the test apparatus. During data analysis following the completion of the testing, however, it became apparent that in some cases a single target pressure drop across an orifice had produced widely disparate mass flow rates over the course of several test runs. The evidence suggested that the inner orifice pressure drop of 30 psid specified for the majority of the test runs often resulted in fluid cavitation, a phenomenon that went undetected during the narrow range flow calibrations.

To clarify the test results, further calibration testing was performed, with both water and TRIC being separately flowed through first the inner and then the outer orifice sides of each element. Calibration data for the element 10 baseline are shown in Fig. 3-3 and 3-4. Figure 3-3 shows data obtained by calibrating the

TABLE 3-2. LIQUID/LIQUID-TRIPLET TEST MATRIX

ELEMENT	TEST NUMBER	COLLECTION DISTANCE (INCHES)	DELTA P OUT (PSI)	DELTA P IN (PSI)	INJECTION PATTERN	TARGET OXIDIZER/FUEL MASS MIXTURE RATIO
TRIPLET 10	1	2	5.7	30.0	O-F-O	2.10
D_o = 0.066 INCH	2	2	10.1	30.0	O-F-O	2.80
D_i = 0.050 INCH	3	2	15.8	30.0	O-F-O	3.50
θ = 60 DEGREES	4	2	22.6	30.0	O-F-O	4.20
(BASELINE	5	2	20.2	60.0	O-F-O	2.80
ELEMENT)	6	2	24.2	60.0	O-F-O	3.50
	7	2	45.3	60.0	O-F-O	4.20
	8	2	20.6	30.0	F-O-F	0.33
	9	2	13.3	30.0	F-O-F	0.41
	10	2	8.6	30.0	F-O-F	0.51
	11	2	4.5	30.0	F-O-F	0.70
	12	1	10.1	30.0	O-F-O	2.80
	13	3	10.1	30.0	O-F-O	2.80
TRIPLET 11	14	2	11.3	30.0	O-F-O	2.10
D_o = 0.055 INCH	15	2	20.0	30.0	O-F-O	2.80
D_i = 0.050 INCH	16	2	30.0	28.8	O-F-O	3.50
θ = 60 DEGREES						
TRIPLET 12	17	2	2.8	30.0	O-F-O	2.10
D_o = 0.079 INCH	18	2	5.1	30.0	O-F-O	2.80
D_i = 0.050 INCH	19	2	7.9	30.0	O-F-O	3.50
θ = 60 DEGREES	20	2	12.8	30.0	O-F-O	4.50
	21	2	21.3	30.0	F-O-F	0.23
	22	2	12.8	30.0	F-O-F	0.30
	23	2	8.5	30.0	F-O-F	0.36
TRIPLET 13	24	2	5.9	30.0	O-F-O	1.00
D_o = 0.046 INCH	25	2	11.7	30.0	O-F-O	1.40
D_i = 0.050 INCH	26	2	30.0	34.8	O-F-O	2.10
θ = 60 DEGREES						
	27	2	29.3	30.0	F-O-F	0.59
	28	2	17.6	30.0	F-O-F	0.77
	29	2	11.7	30.0	F-O-F	0.94

TABLE 3-2. (Concluded)

ELEMENT	TEST NUMBER	COLLECTION DISTANCE (INCHES)	DELTA P OUT (PSI)	DELTA P IN (PSI)	INJECTION PATTERN	TARGET OXIDIZER/FUEL MASS MIXTURE RATIO
TRIPLET 14	30	2	9.0	30.0	O-F-O	2.10
D_0 = 0.093 INCH	31	2	16.0	30.0	O-F-O	2.80
D_1 = 0.071 INCH	32	2	25.0	30.0	O-F-O	3.50
θ = 60 DEGREES						
	33	2	32.6	30.0	F-O-F	0.33
	34	2	21.1	30.0	F-O-F	0.41
	35	2	13.7	30.0	F-O-F	0.51
	36	1	16.0	30.0	O-F-O	2.80
	37	3	16.0	30.0	O-F-O	2.80
TRIPLET 15	38	2	6.5	30.0	O-F-O	2.10
D_0 = 0.066 INCH	39	2	11.5	30.0	O-F-O	2.80
D_1 = 0.050 INCH	40	2	13.0	30.0	O-F-O	3.50
θ = 30 DEGREES						
TRIPLET 16	41	2	6.0	30.0	O-F-O	2.10
D_0 = 0.066 INCH	42	2	10.8	30.0	O-F-O	2.80
D_1 = 0.050 INCH	43	2	16.8	30.0	O-F-O	3.50
θ = 45 DEGREES						
TRIPLET 17	44	2	7.1	30.0	O-F-O	2.10
D_0 = 0.066 INCH	45	2	12.6	30.0	O-F-O	2.80
D_1 = 0.050 INCH	46	2	19.7	30.0	O-F-O	3.50
θ = 90 DEGREES						
TRIPLET 8	47	2	6.9	30.0	O-F-O	2.10
D_0 = 0.065 INCH	48	2	12.2	30.0	O-F-O	2.80
D_1 = 0.050 INCH	49	2	19.0	30.0	O-F-O	3.50
θ = 60 DEGREES						

DRILLED, CONTOURED ORIFICES IN TRIPLET 8 VERSUS EDM, SHARP-EDGED ORIFICES IN ALL OTHERS
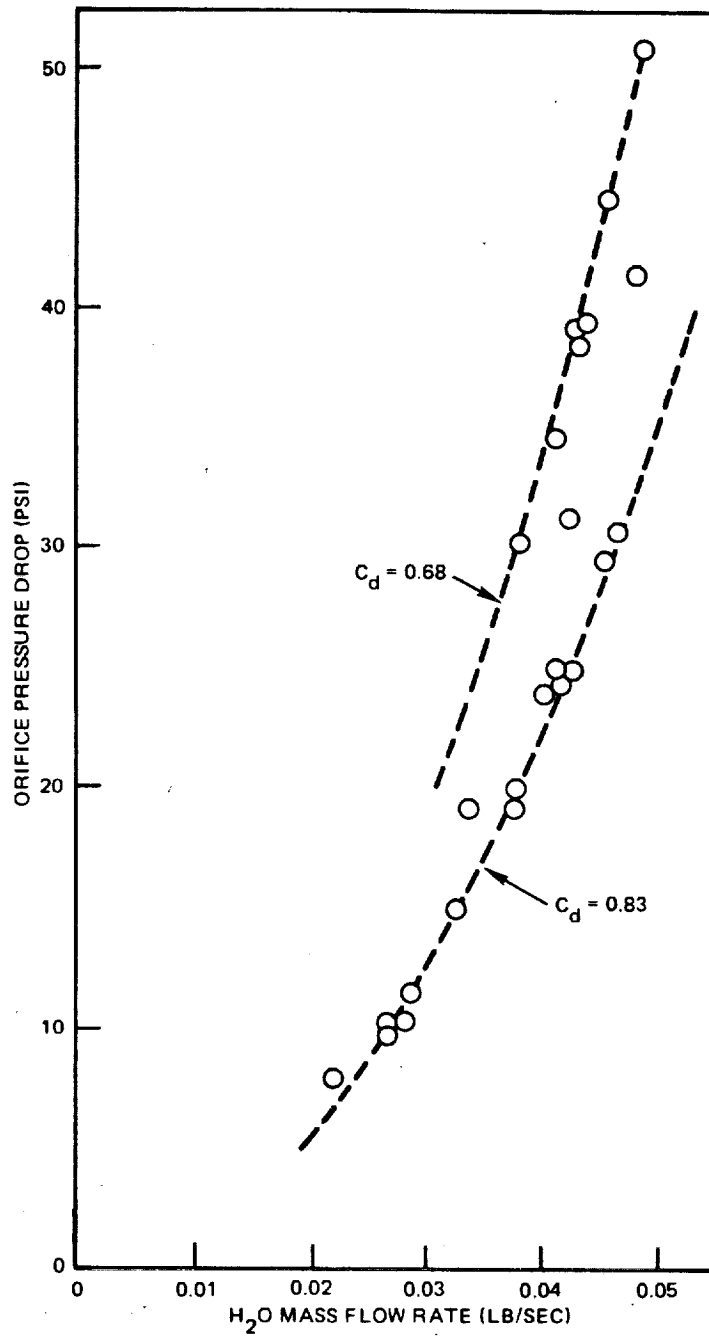
Figure 3-3.   Water Flow Calibration Data for Element 10 Inner Orifice

Figure 3-4. TRIC Flow Calibration Data for Element 10 Outer Orifice Pair
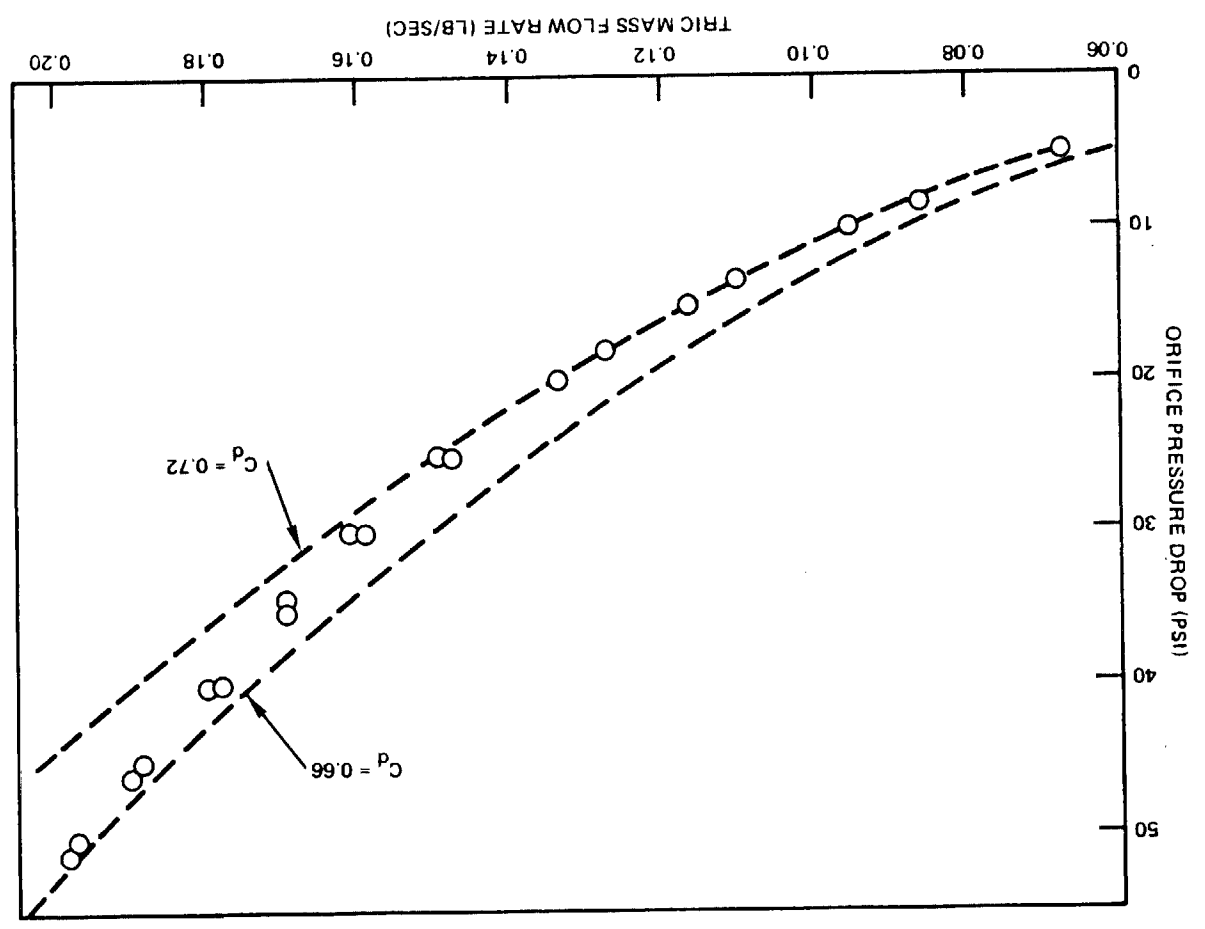
inner orifice with water over a pressure drop range from 10 to 50 psid. Data points at pressure drops less than 25 psid follow the Cd = 0.83 line, while those above 35 psid follow the Cd = 0.68 line. This shift in discharge coefficients between 25 and 35 psid apparently signifies a transition from a noncavitating to a cavitating flow regime. However, as evidenced by the data points near 30 psid, the transition is characterized by a region wherein the exact pressure drop at which the onset of cavitation occurs is uncertain. Unfortunately, the majority of mixing test runs were conducted with inner orifice water pressure drops near 30 psid, resulting in flow-rate uncertainty. The calibration data for TRIC flow through the element 10 outer orifices, presented in Fig. 3-4, do not exhibit the same pronounced Cd shift seen in Fig. 3-3. In this case, a smooth transition occurs from Cd = 0.72 at 5 psid pressure drop to Cd = 0.66 at 50 psid, and whether or not the decrease in Cd is caused by fluid cavitation is uncertain. It is also quite likely that other effects, in addition to or instead of fluid cavitation, are responsible for the variations in discharge coefficient. Increased turbulence, changes in the vena contracta et al, can affect flow rate.

The calibration plots presented for element 10 are typical of those generated by the EDMed (sharp-edged orifice) elements. Element 8, however, with its radially contoured orifice entrances, produced data for both inner and outer orifice sides much like those shown in Fig. 3-4, exhibiting only a gradual decrease in discharge coefficient as pressure drop was increased from 10 to 50 psid (from Cd = 0.80 to Cd = 0.74 for the inner orifice flowing water, and from Cd = 0.82 to Cd = 0.79 for the outer orifices flowing TRIC). Thus, the cavitation phenomenon resulting in flow-rate uncertainty appeared to be characteristic of only the inner orifices of the EDMed elements.

The issues remaining to be resolved, then, were two: an accurate confirmation of mass flow rates in the tests already performed, and a determination of the effect of fluid cavitation on mixing efficiency results. The first issue was resolved by simply calculating the propellant simulant flow rates for all runs directly from the liquid masses collected in the grid and including a small correction for the mass fluxes falling outside the grid as determined by an extrapolation technique. The accuracy of this method was verified by performing tests in which injection flow rates were measured with turbine flowmeters, and compared with the

flow rates determined subsequently by summation of the collected masses. The run conditions for these 12 additional tests (tests 50 through 61) are presented in Table 3-3, and in all cases, the calculated flow rates were within 5% of the metered rates. Thus, the issue of the validity of the flow-rate data was resolved.

TABLE 3-3. ADDITIONAL TESTS CONDUCTED TO ASSESS CAVITATION EFFECTS

ELEMENT	TEST NUMBER	COLLECTION DISTANCE (INCHES)	DELTA P OUT (PSI)	DELTA P IN (PSI)	INJECTION PATTERN	TARGET OXIDIZER/FUEL MASS MIXTURE RATIO
TRIPLET 10	50	2	7.0	23.8	O-F-O	1.94
D_o = 0.066 INCH	51	2	11.5	20.1	O-F-O	2.71
D_i = 0.050 INCH	52	2	18.8	20.1	O-F-O	3.46
θ = 60 DEGREES	53	2	30.0	20.0	O-F-O	4.29
	54	2	50.0	23.0	O-F-O	4.90
(BASELINE	55	2	7.2	32.2	O-F-O	1.99
ELEMENT)	56	2	11.8	30.0	O-F-O	2.63
	57	2	20.0	32.5	O-F-O	3.33
	58	2	31.8	32.2	O-F-O	4.08
	59	2	50.0	32.0	O-F-O	4.87
	60	2	29.7	20.0	O-F-O	4.26
	61	2	31.7	32.1	O-F-O	4.08

The effect of fluid cavitation on mixing efficiency results was also addressed in tests 50 through 61. In runs 50 through 54, inner orifice pressure drops were held under 25 psid to ensure noncavitating flow. Runs 55 through 59 were then conducted such that the injectant flow rates corresponded as closely as possible with the respective conditions of the previous five runs, except that in the latter five runs, the inner orifice pressure drops were increased to ensure cavitating flow. (The fact that identical mass flow rates can be achieved at two different pressure drops is clearly evident in Fig. 3-3, and producing the two conditions experimentally was relatively easy where a turbine flowmeter was used.)

Summary of Test Results

Overall Comparisons. A summary of results for the 61 liquid/liquid mixing tests is presented in Table 3-4, including mixture ratios, propellant simulant collection efficiencies, mixing efficiencies, and the comparative stream dynamic

TABLE 3-4. RESULTS OF COMPLETED LIQUID/LIQUID-TRIPLET TEST MATRIX

TEST NUMBER	ELEMENT NUMBER	OXIDIZER/FUEL MIXTURE RATIO	OXIDIZER (TRIC) COLLECTION EFFICIENCY	FUEL (H_2O) COLLECTION EFFICIENCY	OVERALL MIXING EFFICIENCY (E_m)	OUT/IN MOMENTUM RATIO	OUT/IN VELOCITY HEAD RATIO	RUPE PARAMETER	ELVERUM-MOREY PARAMETER
1	10	2.38	0.90	0.96	0.85	1.22	0.35	0.46	0.48
2	10	2.62	0.91	0.95	0.90	1.49	0.43	0.58	0.58
3	10	2.99	0.89	0.91	0.94	1.94	0.56	0.74	0.76
4	10	4.29	0.87	0.88	0.96	3.99	1.14	1.50	1.56
5	10	2.36	0.89	0.93	0.88	1.21	0.35	0.46	0.47
6	10	2.73	0.87	0.92	0.92	1.61	0.46	0.61	0.63
7	10	3.12	0.87	0.84	0.96	2.11	0.61	0.80	0.83
8	10	0.33	0.81	0.89	0.78	3.40	0.97	1.28	1.33
9	10	0.44	0.89	0.91	0.80	2.00	0.57	0.75	0.78
10	10	0.49	0.92	0.89	0.76	1.60	0.46	0.61	0.63
11	10	0.56	0.97	0.85	0.63	1.23	0.35	0.46	0.48
12	10	2.54	0.99	0.99	0.85	1.40	0.40	0.53	0.55
13	10	2.15	0.87	0.89	0.88	1.00	0.29	0.38	0.39
14	11	1.84	0.94	0.96	0.88	1.06	0.44	0.48	0.54
15	11	2.17	0.92	0.92	0.94	1.47	0.61	0.67	0.76
16	11	3.04	0.91	0.92	0.97	2.89	1.20	1.32	1.49
17	12	2.09	0.90	0.95	0.80	0.66	0.13	0.20	0.20
18	12	2.96	0.89	0.89	0.88	1.33	0.27	0.43	0.40
19	12	3.31	0.91	0.94	0.90	1.66	0.33	0.52	0.50
20	12	4.43	0.91	0.93	0.94	2.97	0.60	0.95	0.89
21	12	0.22	0.96	0.95	0.71	5.41	1.08	1.71	1.62
22	12	0.27	0.98	0.89	0.66	3.51	1.11	1.11	1.05
23	12	0.34	0.99	0.89	0.64	2.32	0.92	0.73	0.69
24	13	0.85	0.99	0.92	0.46	0.33	0.19	0.17	0.22
25	13	1.42	0.93	0.97	0.76	0.89	0.53	0.49	0.60
26	13	2.05	0.91	0.95	0.90	1.87	0.46	0.73	0.69
27	13	0.49	0.96	0.92	0.76	3.24	0.92	1.20	1.25
28	13	0.63	0.98	0.92	0.78	1.96	0.64	0.84	0.87
29	13	0.71	0.99	0.91	0.71	1.56	0.43	0.85	1.05
30	14	2.29	0.92	0.96	0.86	1.16	0.34	0.44	0.46
31	14	2.88	0.91	0.95	0.92	1.82	0.53	0.69	0.72
32	14	3.48	0.99	0.91	0.71	2.67	0.78	1.02	1.06
33	14	2.12	0.95	0.92	0.82	0.97	0.28	0.37	0.38
34	14	3.29	0.95	0.97	0.86	2.35	0.67	0.88	0.92
35	15	3.05	0.99	0.95	0.92	2.02	0.58	0.76	0.79
36	14	2.48	0.99	0.99	0.86	1.35	0.39	0.51	0.54
37	14	2.20	0.82	0.91	0.90	1.07	0.31	0.41	0.42
38	15	2.24	0.99	0.99	0.88	1.06	0.30	0.40	0.38
39	15	2.70	0.99	0.97	0.92	1.53	0.43	0.58	0.59
40	15	3.44	0.99	0.99	0.95	2.49	0.69	0.92	0.96
41	16	2.12	0.96	0.98	0.82	0.97	0.28	0.37	0.38
42	16	3.29	0.95	0.97	0.86	2.35	0.67	0.88	0.92
43	16	3.05	0.95	0.95	0.92	2.02	0.58	0.76	0.79
44	17	1.73	0.89	0.96	0.76	0.65	0.19	0.25	0.25
45	17	2.30	0.90	0.95	0.84	1.14	0.33	0.44	0.45
46	17	2.78	0.86	0.92	0.90	1.68	0.48	0.63	0.66
47	8	1.90	0.89	0.94	0.88	0.80	0.24	0.31	0.32
48	8	2.54	0.89	0.88	0.97	1.45	0.43	0.56	0.58
49	8	3.38	0.88	0.83	0.96	2.55	0.75	0.98	1.02
50	10	1.94	0.88	0.95	0.86	0.81	0.23	0.30	0.32
51	10	2.71	0.87	0.89	0.94	1.59	0.46	0.61	0.62
52	10	3.46	0.85	0.76	0.95	2.59	0.74	0.98	1.02
53	10	4.29	0.85	0.82	0.94	3.98	1.14	1.50	1.56
54	10	4.90	0.74	0.46	0.96	5.21	1.49	1.97	2.04
55	10	1.99	0.88	0.97	0.85	0.86	0.25	0.33	0.34
56	10	2.63	0.84	0.94	0.92	1.50	0.43	0.57	0.59
57	10	3.33	0.85	0.95	0.95	2.40	0.69	0.91	0.94
58	10	4.08	0.84	0.97	0.95	3.61	1.04	1.37	1.42
59	10	4.87	0.75	0.66	0.96	5.21	1.48	1.95	2.02
60	10	4.26	0.82	0.70	0.94	3.94	1.13	1.49	1.55
61	10	4.08	0.83	0.88	0.95	3.61	1.04	1.37	1.42

parameters momentum ratio, velocity head ratio, Rupe parameter [defined in Eq. (4)], and Elverum-Morey parameter. Collection efficiency is defined as the ratio of collected liquid mass to injected liquid mass. Given the methods used to determine injected mass flow rates, collection efficiency was calculated as the ratio of collected mass to the sum of collected mass plus the overshoot estimate. Collection efficiencies exceeded 90% in the majority of test runs. From a qualitative standpoint, the raw volumetric data indicate that collection efficiencies had no appreciable effect on computed mixing efficiencies and performance parameters (i.e., the minor portion of injected mass escaping collection probably comprised approximately the same ratio of the two components as that exhibited by the collected portion of the spray fan). The incidence of gradually decreasing liquid collection efficiency with increasing stream dynamic head is evident, but again, this effect was not expected to appreciably alter computed parameters.

Plots of mixing efficiency versus the comparative stream parameters of velocity head ratio, momentum ratio, Rupe parameter, and Elverum-Morey parameter are presented in Fig. 3-5 through 3-8. Note that the convention adopted in the calculation of these parameters is the ratio of outer to inner streams--the fuel versus oxidizer notation arises only in connection with mass mixture ratio (oxidizer/fuel), and injectant configuration, O-F-O and F-O-F. Because the reversal of injectant configuration from O-F-O to F-O-F consistently resulted in lower mixing efficiencies over the entire range tested for each performance parameter, a distinction between the two configurations has been incorporated into Fig. 3-5 through 3-8. All four plots show a similar trend--mixing efficiency increases as the comparative stream dynamic parameter in question increases, with no optimum value evident. Both of these results run contrary to the findings of Elverum and Morey, who reported no density effect over a wider range of variation, and an optimum value of 0.66 for their correlating parameter, based on their very limited data. While none of the plots exhibits a clear optimization of mixing efficiency over the range tested, any of the four could be employed as a basis for evaluating the effect on mixing efficiency of variations in the individual parameters specified in the test plan. Because the Elverum-Morey parameter is the common design criterion, it was chosen as the basis for comparison of these test results.
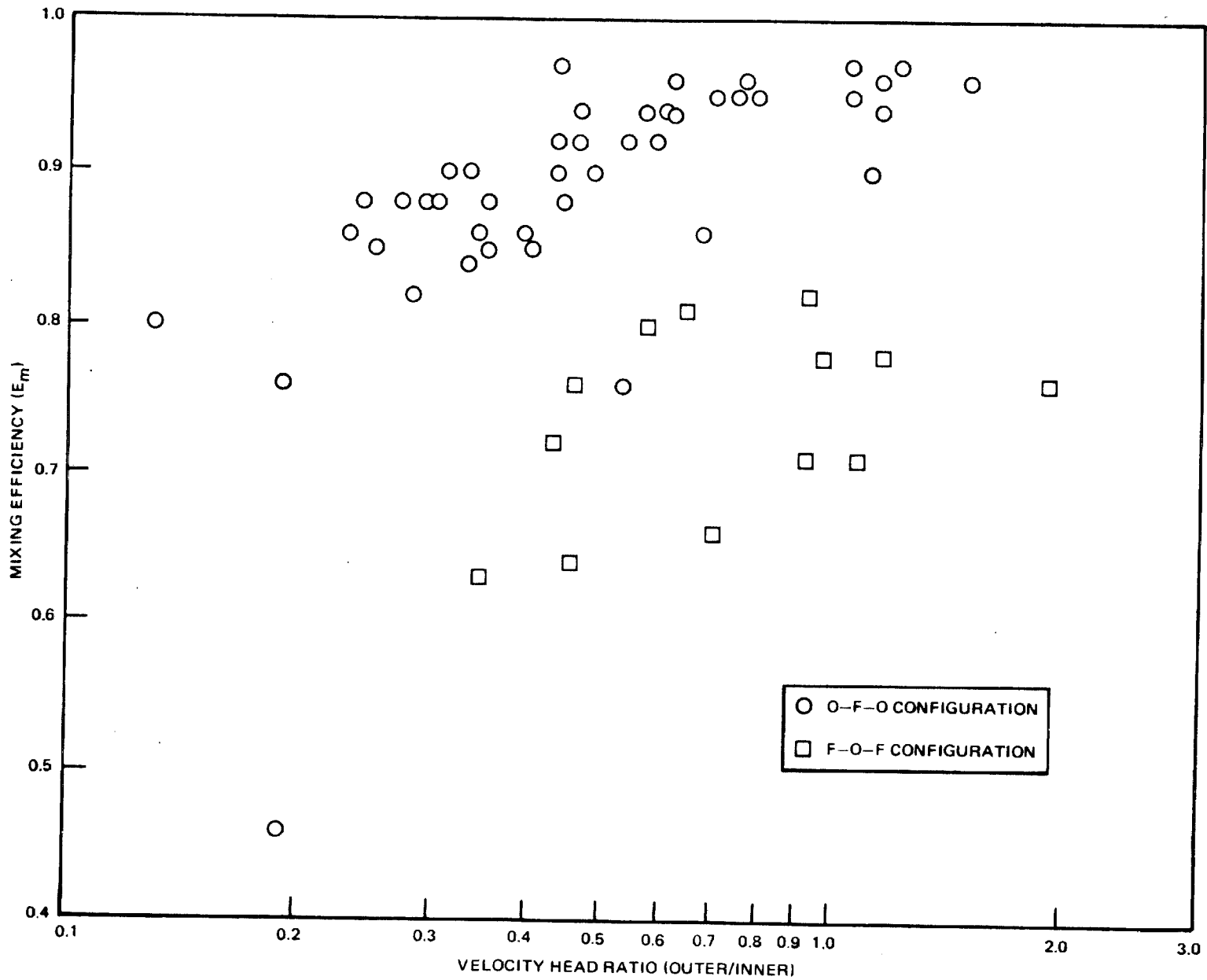
Figure 3-5. Overall Mixing Efficiency vs Velocity Head Ratio for All Test Runs
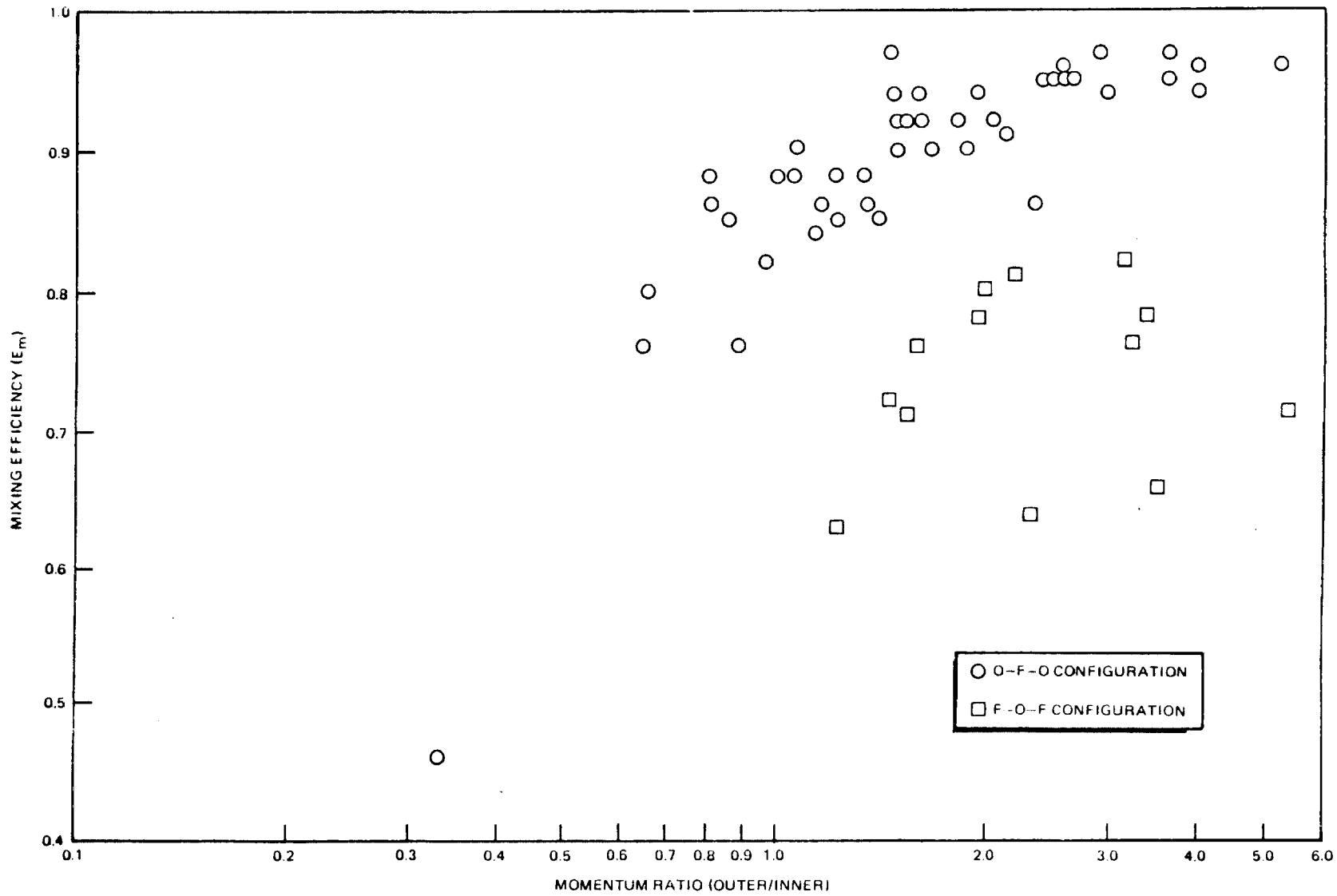
Figure 3-6. Overall Mixing Efficiency vs Momentum Ratio for All Test Runs
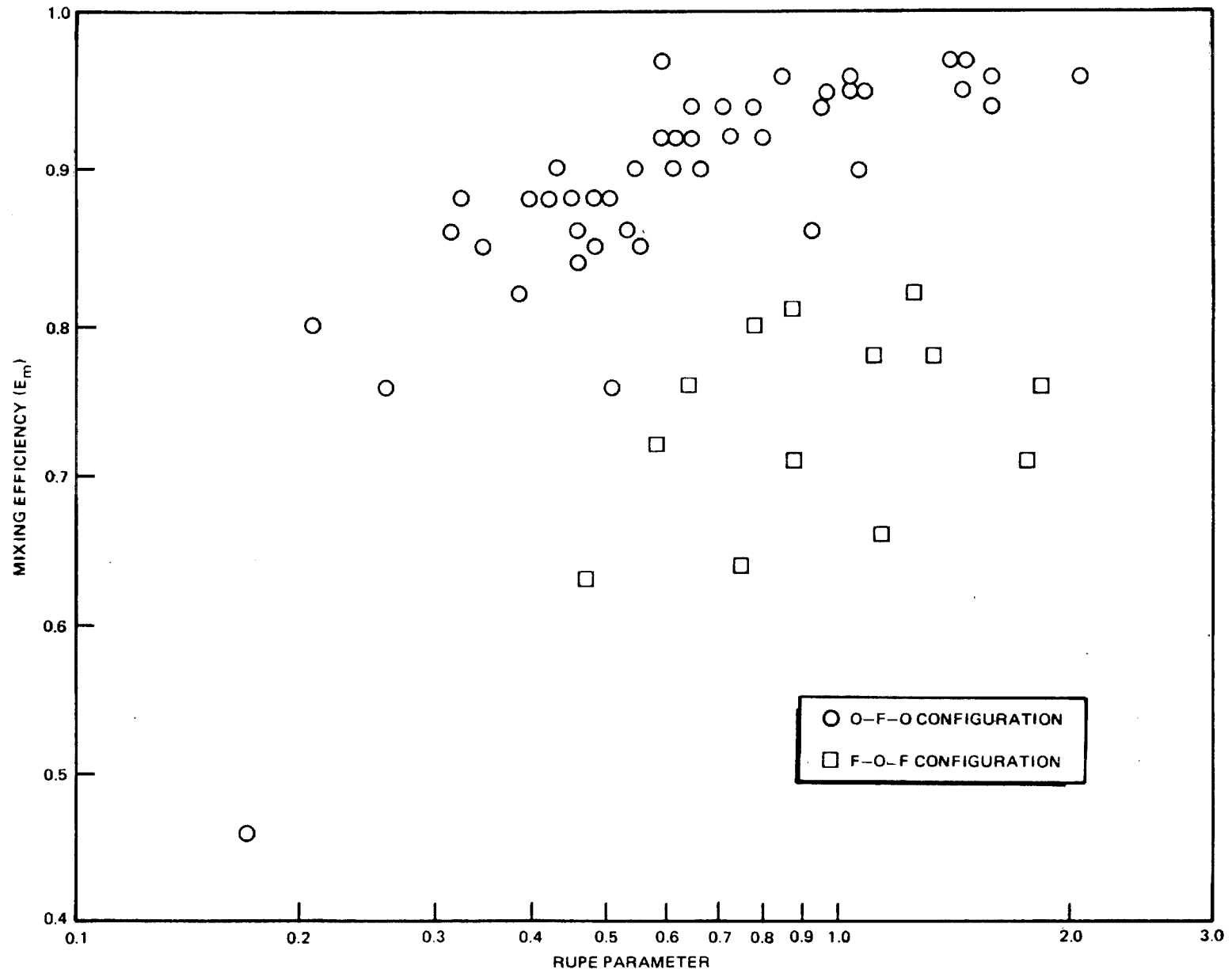
Figure 3-7. Overall Mixing Efficiency vs Rupe Parameter for all Test Runs
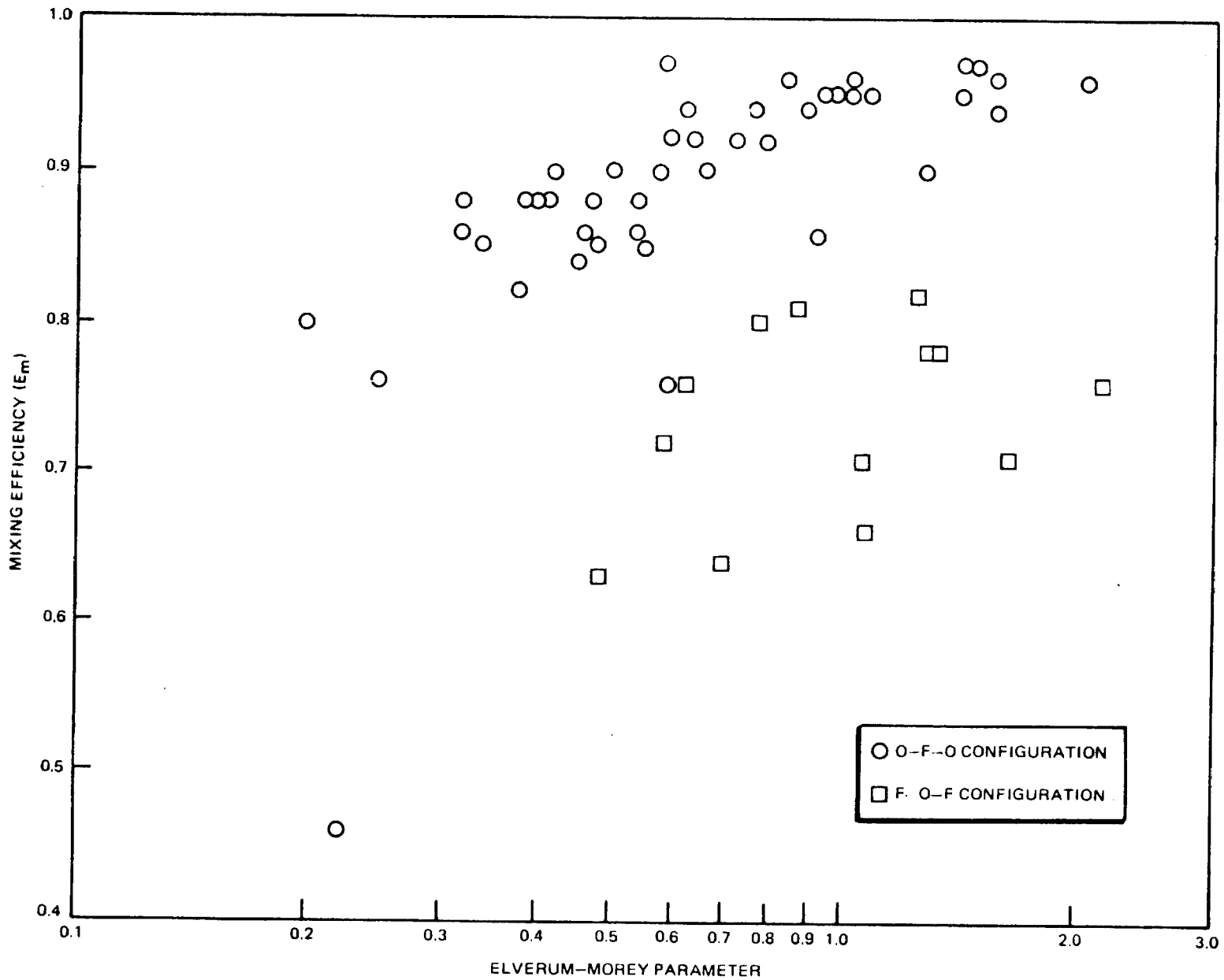
Figure 3-8. Overall Mixing Efficiency vs Elverum-Morey Parameter for all Test Runs

<u>Cavitation Effects</u>. Before further analysis of the data, it was necessary to establish the effect on mixing efficiency of cavitating versus noncavitating flow and collection distance, and to assess the repeatability of specific data points. Foremost among these issues was the question of whether or not fluid cavitation appreciably affected element mixing characteristics. The cavitation issue is important for two reasons. First, because the incidence of cavitation in individual runs was fairly random throughout the test matrix, if mixing characteristics were shown to be appreciably altered by its occurrence, the validity of comparing results between cavitating and noncavitating tests would be suspect (i.e., the internal consistency of the data would be threatened). Second, in actual hot-firing of liquid rocket thrust chambers, propellants are injected into a high-backpressure environment, effectively precluding the incidence of cavitation in the orifices. Therefore, if mixing characteristics were shown to be altered by cavitation, the application of correlations obtained in cavitating test runs to conditions known to be noncavitating would be suspect (i.e., the external applicability of the data would be threatened).

Cavitation in fluids passing through an orifice with a sharp-edged entrance is a complex phenomenon. It is most simply thought to occur when the static pressure in the liquid falls below the vapor pressure of the liquid. Bubbles form that can have large effects on flow characteristics such as discharge coefficients, stream turbulence, and stream coherence, and, in some cases, can lead to detached (from the orifice wall) and hydraulically flipping streams (detached and jumping from one side of the orifice to another side).

The flow and orifice conditions that affect or cause cavitation are not simple. Vena-contracta effects at the entrance, upstream flow conditions, dissolved gases in the liquid, and many other factors influence the initiation, degree, and effects of cavitation. Furthermore, hysteresis effects cause the onset or cessation of cavitation to be dependent upon whether or not the flow rate is increasing or decreasing. As shown in Ref. 3-4, different regimes of cavitation can occur which have differing, and sometimes little, effect on the measured mixing efficiency of like doublets. If the stream is completely attached to the orifice

wall at the orifice exit, upstream cavitation may be expected to have little effect on mixing. Also, according to Ref. 4, if the stream is uniformly detached (and not flipping), unlike, impinging doublet mixing will be little affected. To resolve the issue of the effects of cavitation in the present test program, the simplest approach was to perform tests that differed only by the presence of cavitation, and to observe the effect on mixing efficiency.

Figure 3-9 shows the results of the test runs designed to address the cavitation issue. The cavitating versus noncavitating test pairs at each of the five Elverum-Morey parameter values (i.e., mixture ratio conditions) are seen to closely coincide with respect to mixing efficiency -- the maximum spread in Em is 3% at an Elverum-Morey parameter value of approximately 1.50. Presented in Fig. 3-10 is a plot of another four data pairs, showing the results of repeatability assessment tests. In this case, the maximum spread in mixing efficiency observed between two members of a pair is 2%. In light of this 2% repeatability error, the cavitating/noncavitating data pairs of Fig. 3-9 can be taken as essentially coincident points, thus ensuring the validity of internal comparison and external application of the data generated in the test matrix.

Collection Distance Effects. Figure 3-11 shows the limited number of data points used to determine the effect of varying collection distance on mixing efficiency. Choice of collection distance in mixing studies is essentially arbitrary. The baseline value of 2 inches chosen for this test program is a fairly common standard for studies of this nature, and, in this case, a convenient distance for capturing the triplet spray fans in a large portion of the 1-5/8 by 2-1/2 inches grid with a minimum of overshoot. The four data points plotted in Fig. 3-12 show that mixing efficiency increased from 1 to 2 inches, and again from 2 to 3 inches, by approximately 5% in both cases. Relative spatial distribution of propellant simulants remained essentially the same in both test pairs. While the magnitude of the mixing efficiency increase is greater than the limits of repeatability error, it is still not overly significant, and the trend is in the expected direction (i.e., mixing improves at greater collection distance). It would be hard to rationalize a spray becoming less mixed with axial distance.
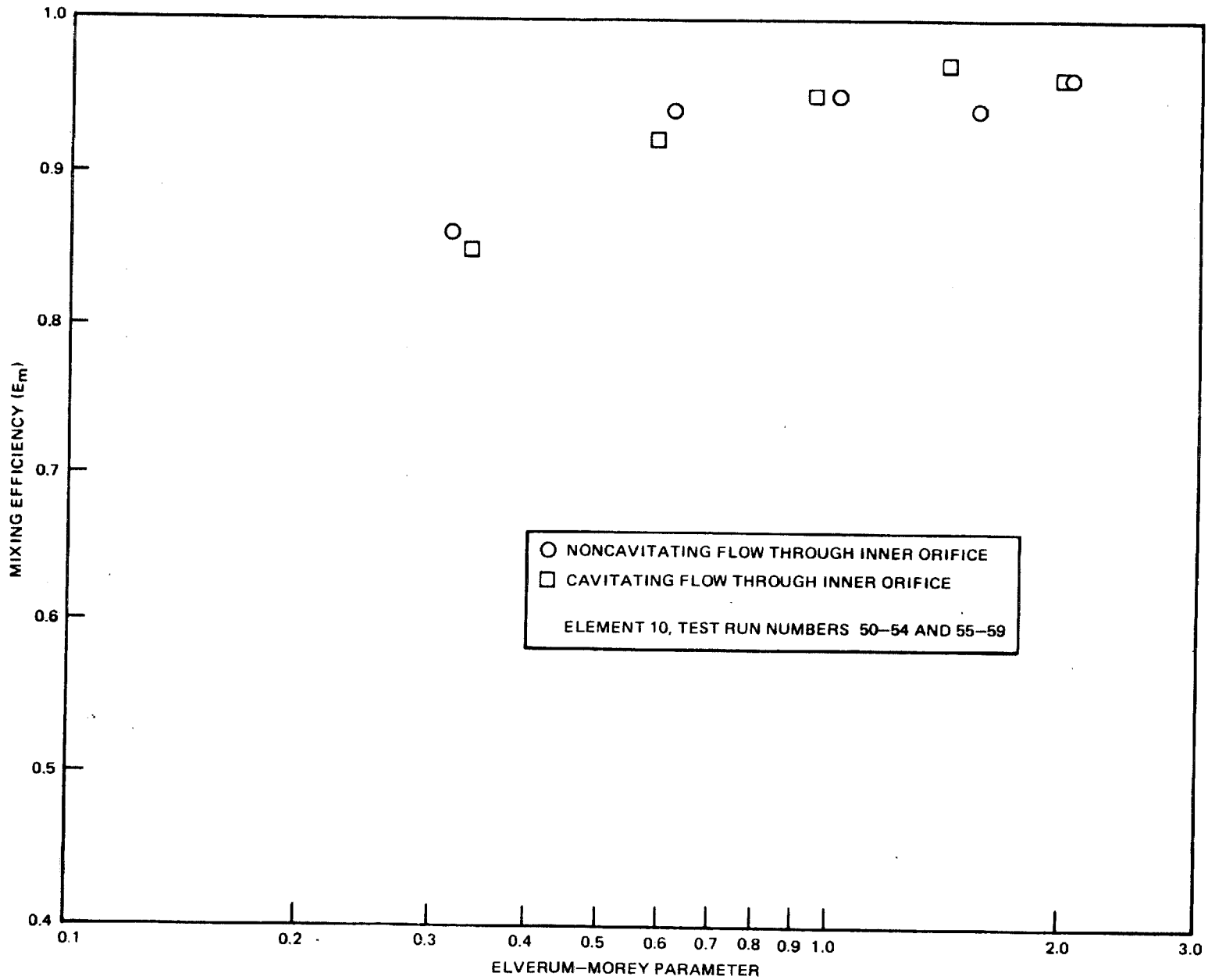
Figure 3-9. Overall Mixing Efficiency vs Elverum-Morey Parameter - Effect of Fluid Cavitation
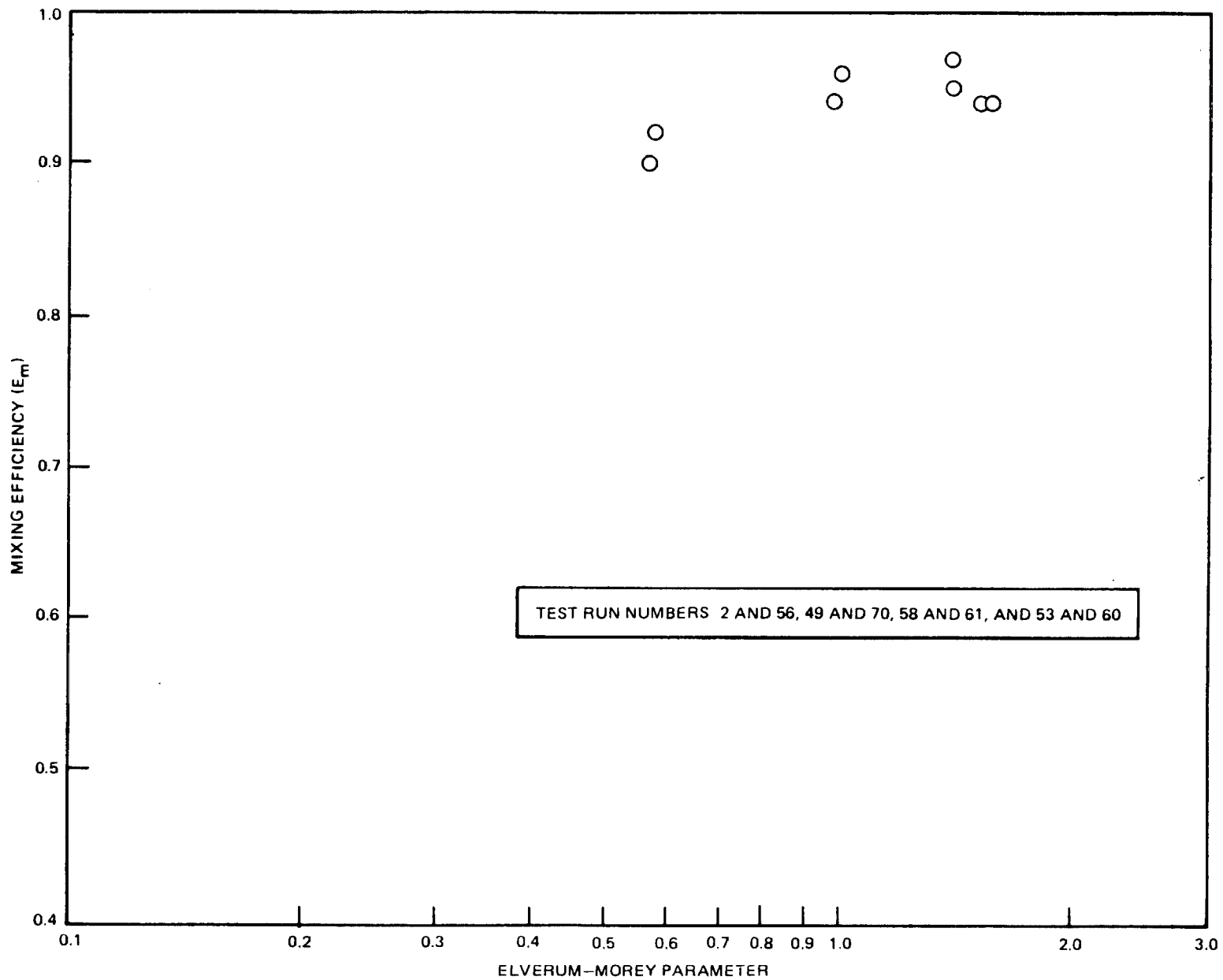
Figure 3-10. Overall Mixing Efficiency vs Elverum-Morey Parameter –
Repeatability Tests
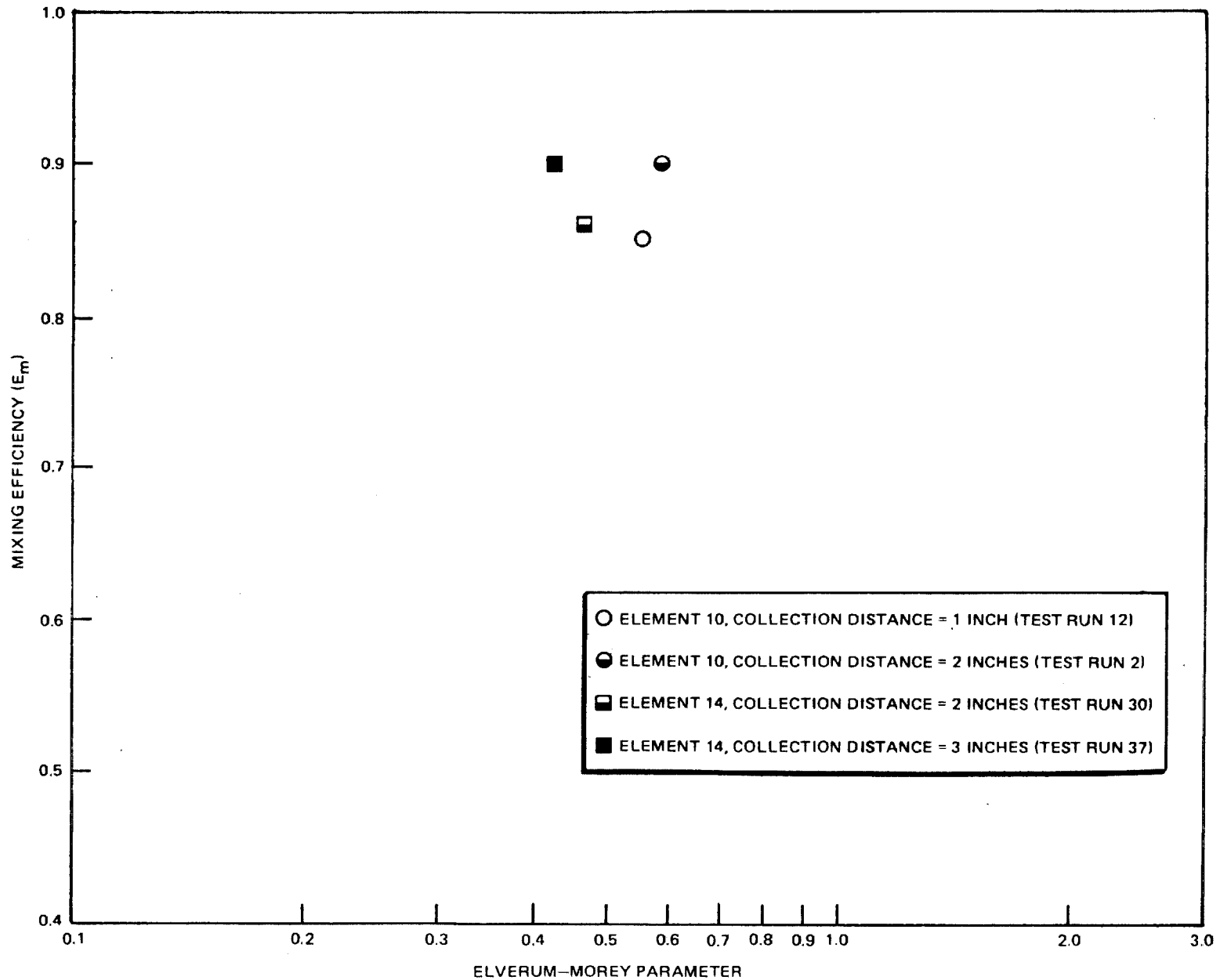
Figure 3-11. Overall Mixing Efficiency vs Elverum-Morey Parameter -
Effect of Collection Distance

MIXING EFFICIENCY (E_m)

COLLECTION DISTANCE (IN.)

○ AEROJET OFO TRIPLET
(MR = 2.63)

△ AEROJET TRANSVERSE LIKE-ON-LIKE DOUBLET
(MR = 2.80)

◇ AEROJET PREATOMIZED OFO TRIPLET
(MR = 2.85)

□ AEROJET EDM'ed LIKE-ON-LIKE DOUBLET
(MR = 2.91)

⬠ ROCKETDYNE OFO TRIPLET 10
(MR = 2.58)

⬣ ROCKETDYNE OFO TRIPLET 14
(MR = 2.25)

(AEROJET MR's FREON/H_2O)

(ROCKETDYNE MR's TRIC/H_2O)
AEROJET DATA FROM REF. 3-5
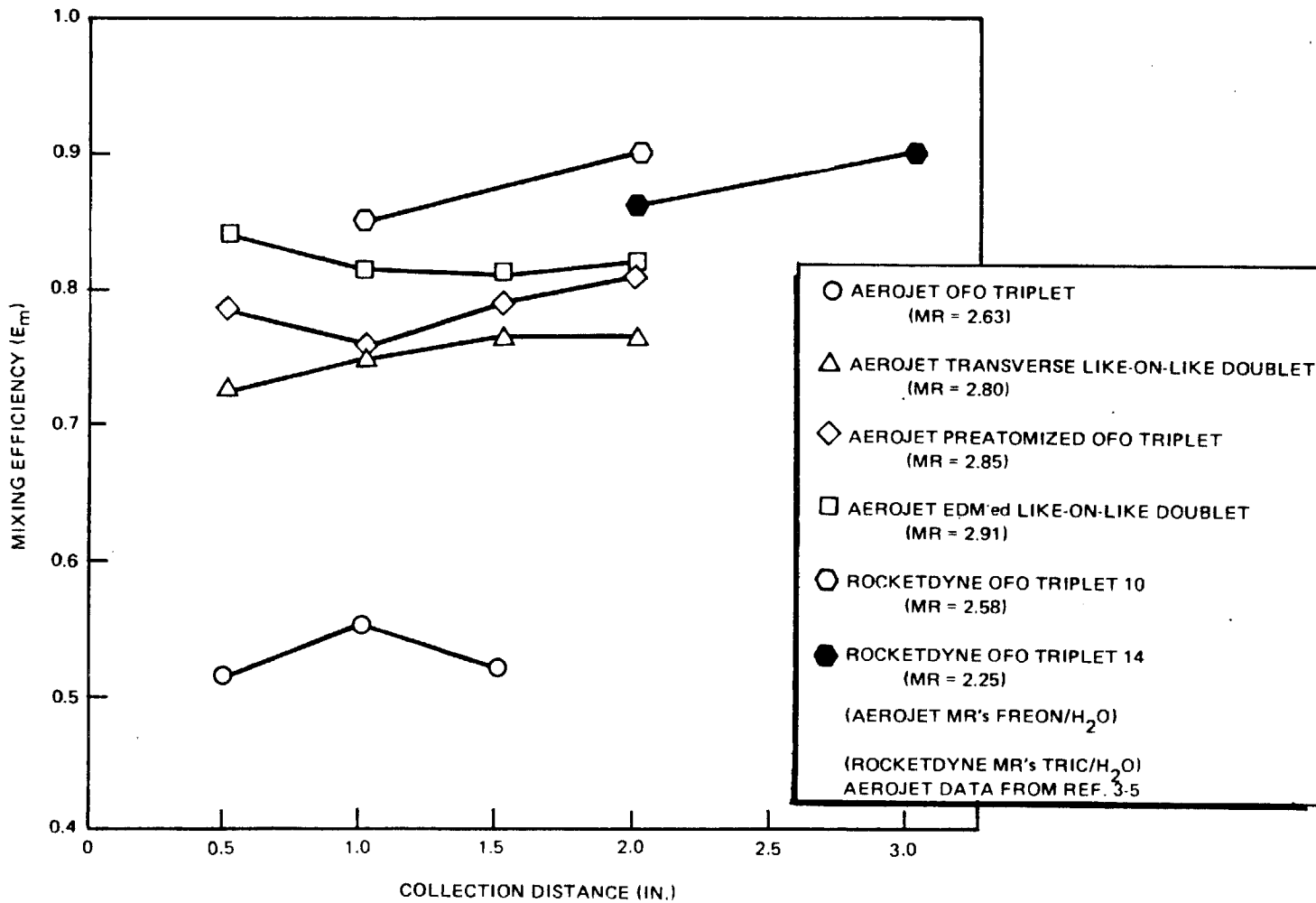
Figure 3-12.   Overall Mixing Efficiency vs Collection Distance for Combined
Rocketdyne and Aerojet Data

Additional collection distance data are provided in the report of an Aerojet study (Ref. 3-5), in which four different injector elements were tested at distances of 1/2, 1, 1-1/2, and 2 inches each. The Aerojet data are presented in Fig. 3-12 alongside the data from this study. No consistent trend is evident in these plots, as mixing efficiency varied anywhere from 2.4% to 6.7% for the elements as collection distance was varied. Furthermore, in some cases the mixing efficiency decreased with collection distance. The test performed as a part of this program and the Aerojet tests indicate that the effect of varying collection distance on mixing efficiency is not substantial, under the conditions of these tests.

Effect of Variations in Individual Parameters. Figures 3-13 through 3-15 show the effect on mixing efficiency of relative stream diameter. Five elements having different outer orifice to inner orifice diameter ratios were tested in the O-F-O configuration to generate the data of Fig. 3-13. These data show no significant effect on mixing efficiency of variations in D_o/D_i, except for the element in which D_o/D_i was less than unity (element 13, D_o/D_i = 0.92). Mixing efficiencies of this element fell significantly lower than those produced by the other elements. Figure 3-14 shows the effect of diameter ratio variation for four elements flowed in the F-O-F configuration, and in this case, the data exhibit no simple trend that can be translated into a generalized diameter ratio effect. The elements with both the highest and lowest diameter ratios experienced poorer mixing. As mentioned previously, configuration reversal from O-F-O to F-O-F consistently resulted in lower mixing efficiency. The data presented in Fig. 3-15 were generated by using elements whose outer orifice to inner orifice diameter ratios were equal, but whose total flow area differed by a factor of 2. In this case, the data indicate that orifice size has no effect on mixing efficiency. This should not be interpreted to imply that larger elements will provide mixing that is as good as smaller elements. Mixing efficiency is a measure of mixing uniformity per unit mass of propellant injected. Larger elements will have larger regions of "off-design" mixture ratio than smaller elements, even though both may have the same mixing efficiency. These larger regions will require longer chamber lengths to be mixed with surrounding gases. Figures 3-13 to 3-15 again illustrate that no definite Elverum-Morey optimum was evident over the range tested.
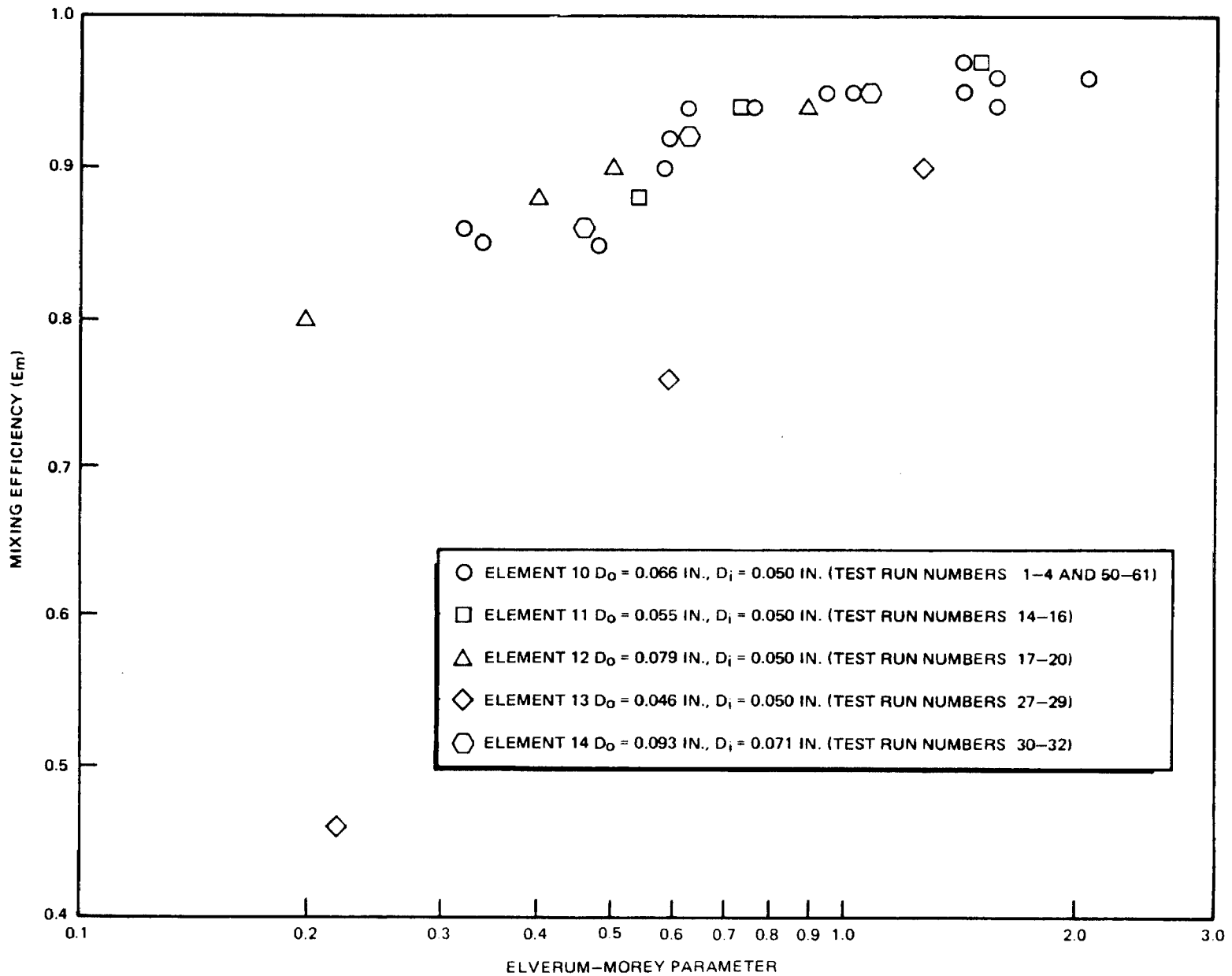
Figure 3-13. Overall Mixing Efficiency vs Elverum-Morey Parameter -
Effect of Diameter Ratio (O-F-O Configuration)
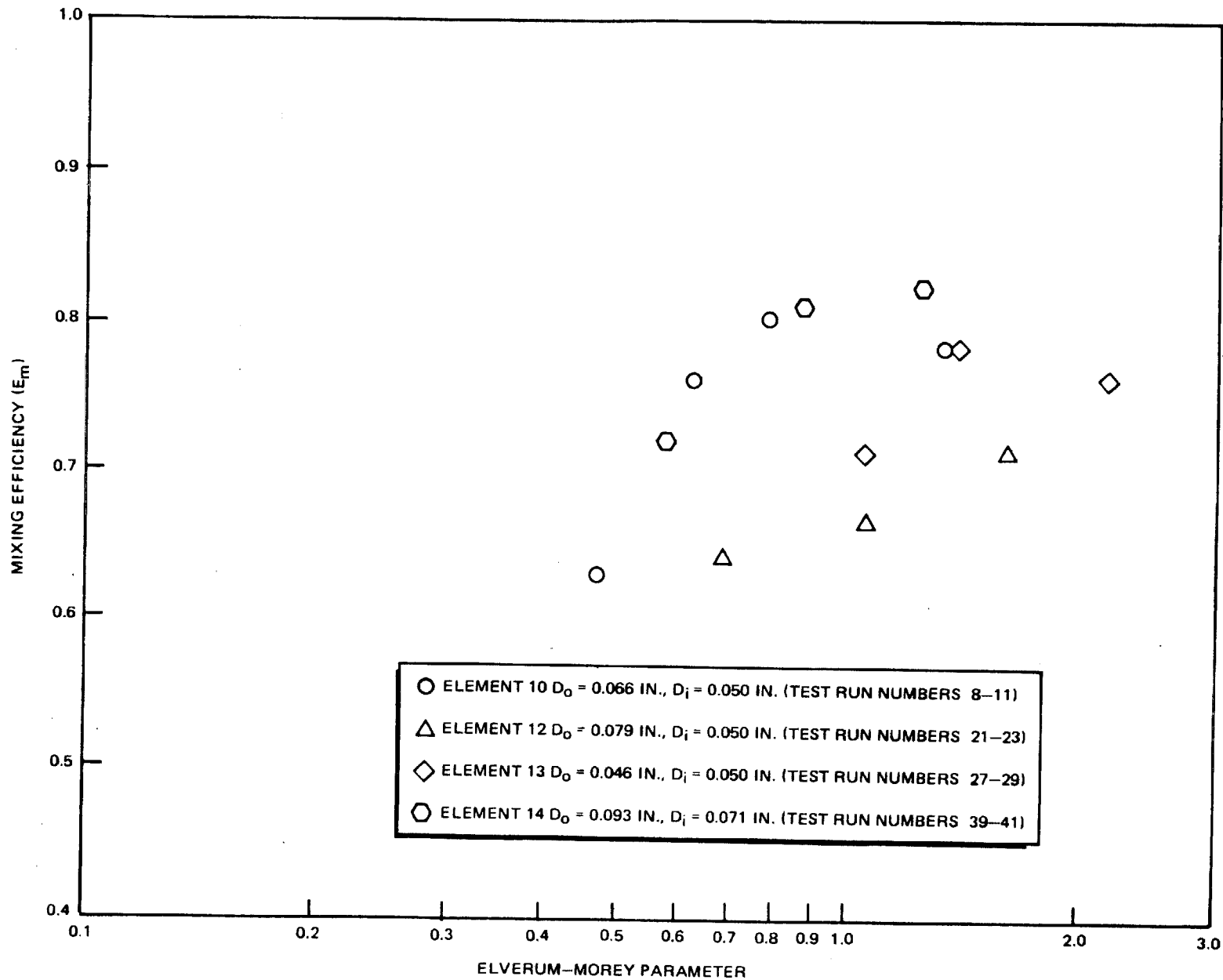
Figure 3-14. Overall Mixing Efficiency vs Elverum-Morey Parameter –
Effect of Diameter Ratio (F-O-F Configuration)
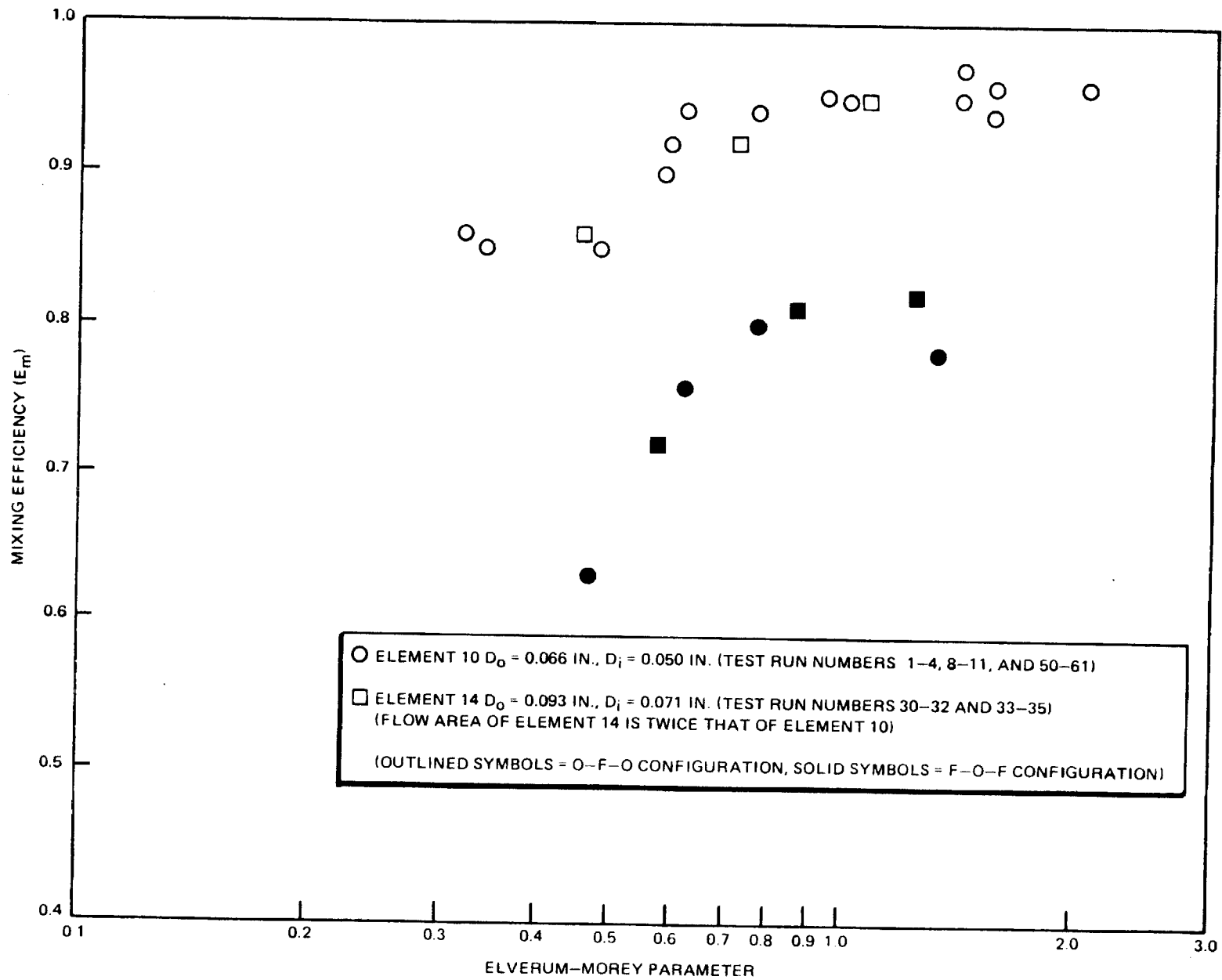
Figure 3-15. Overall Mixing Efficiency vs Elverum-Morey Parameter - Effect of Orifice Scaling

Figure 3-16 shows data generated in tests where impingement angle was varied, with orifice diameters held constant. The four values of total included angle between outer streams were 30, 45, 60, and 90 degrees. Although one of the data points falls anomalously outside the scatter band of the other tests, the results of this test series indicate that impingement angle has no significant effect on mixing efficiency. By contrast, Elverum and Morey reported a pronounced effect: for 60-degree impingement angles, the optimum Elverum-Morey parameter value was computed to be 0.66, while for 90-degree angles, 0.42 was the reported optimum.

The effect on mixing efficiency of increased orifice pressure drop, with mixture ratio held approximately constant, is shown in Fig. 3-17. In four of these test runs, mass flow rates were set at "nominal" values for producing the desired mixture ratios. In the other four runs, elevated pressure drops (approximately twice the nominal values) were achieved to produce approximately the same mixture ratios, with approximately 40% increase in both TRIC and water flow rates. As is evident from the plot, no significant effect on mixing efficiency was observed.

Data presented in Fig. 3-18 illustrate the effect on mixing efficiency of different orifice machining methods. The two elements employed in this test series were dimensionally identical, but in one case the orifices were drilled and provided with rounded (0.030-inch radius) entrances, and in the other, the orifices were EDMed and left with sharp-edged entrances. Although only six data points were generated with element 8, the trend apparent from these points could possibly be construed to exhibit a mixing efficiency maximum near the optimum proposed by Elverum and Morey (approximately 0.65). The element 10 data followed the same general trend observed in the bulk of the test results, with mixing efficiency increasing with increasing Elverum-Morey parameter.

Investigation of Orifice Contouring, Fabrication Method, and Flow Control Feature Effects. The question posed by the results of this fabrication method test series was whether the apparent optimum in the element 8 data was in fact a reproducible trend, or simply caused by data scatter. Furthermore, it was theorized that perhaps the differences between these tests and the limited JPL tests could be the
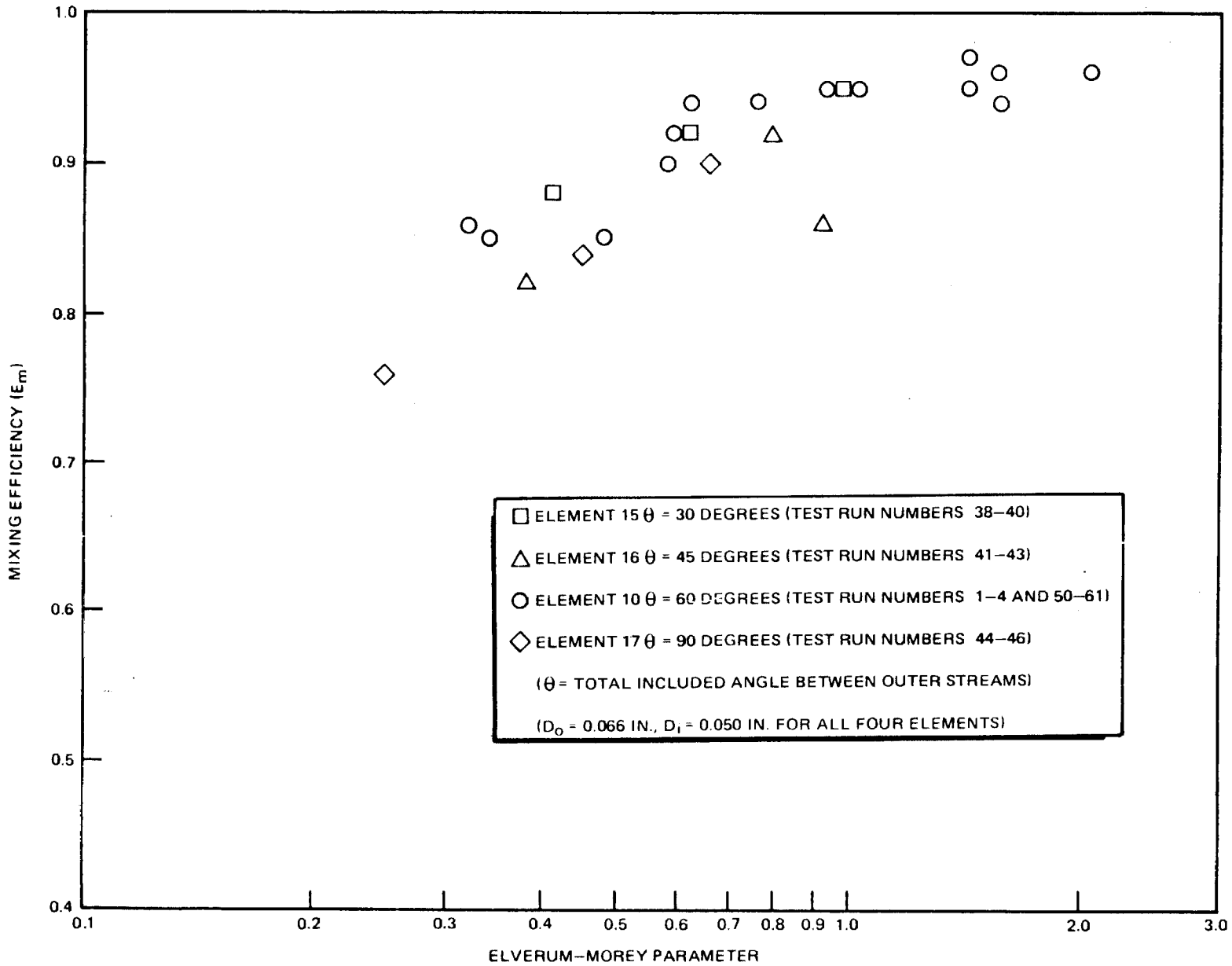
Figure 3-16.   Overall Mixing Efficiency vs Elverum-Morey Parameter -
Effect of Impingement Angle
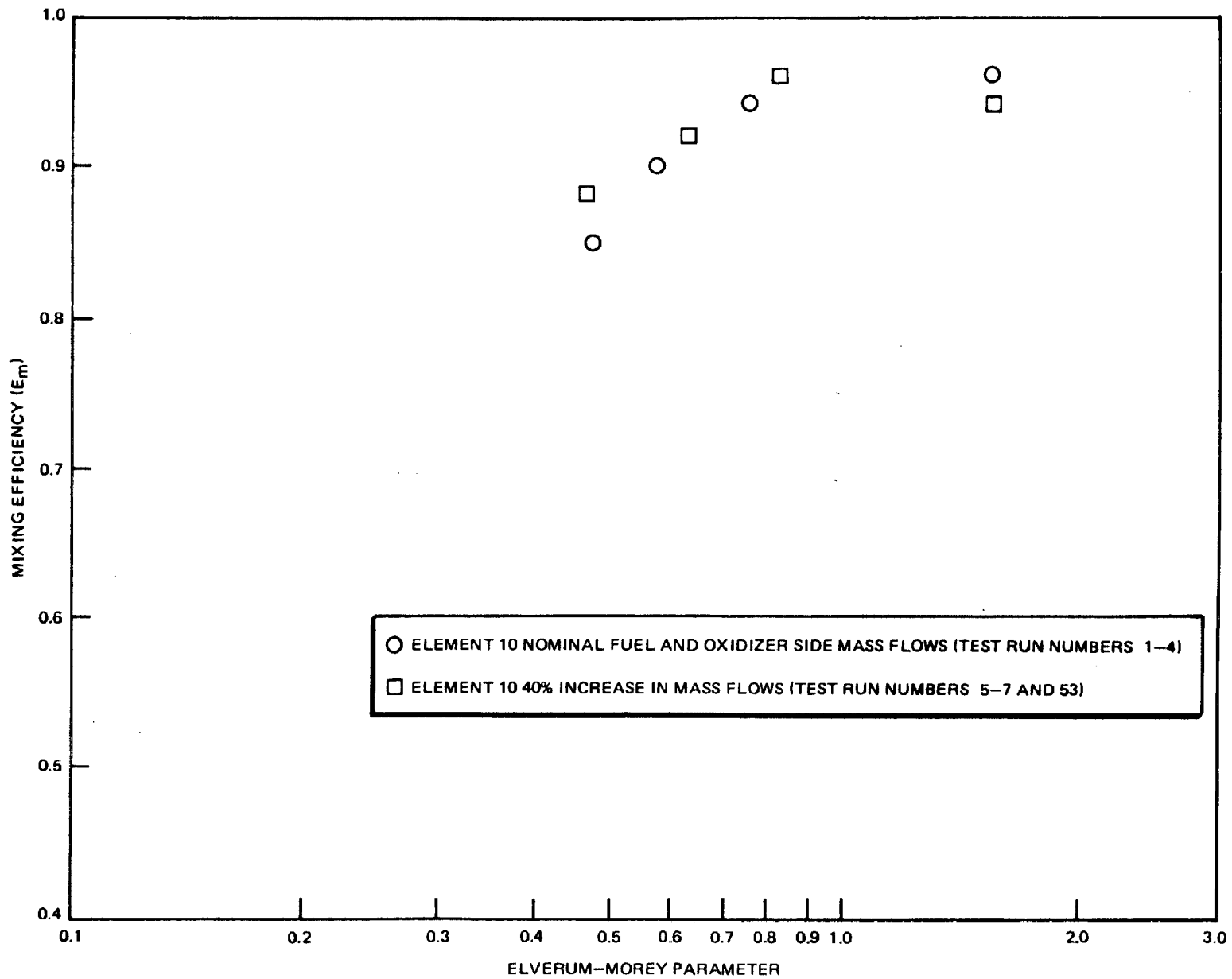
Figure 3-17. Overall Mixing Efficiency vs Elverum-Morey Parameter – Effect of
Injection Velocity at Constant Velocity Ratio (Throttling)

MIXING EFFICIENCY (E_m)

ELVERUM –MOREY PARAMETER

○ ELEMENT 10 SHARP-EDGED, EDM ORIFICES (TEST RUN NUMBERS. 1–4 AND 50–61)

□ ELEMENT 8 CONTOURED, DRILLED ORIFICES (TEST RUN NUMBERS 47–49 AND REF 1-1 TESTS)

(D_O = 0.066 IN., D_I = 0.050 IN. FOR BOTH ELEMENTS)
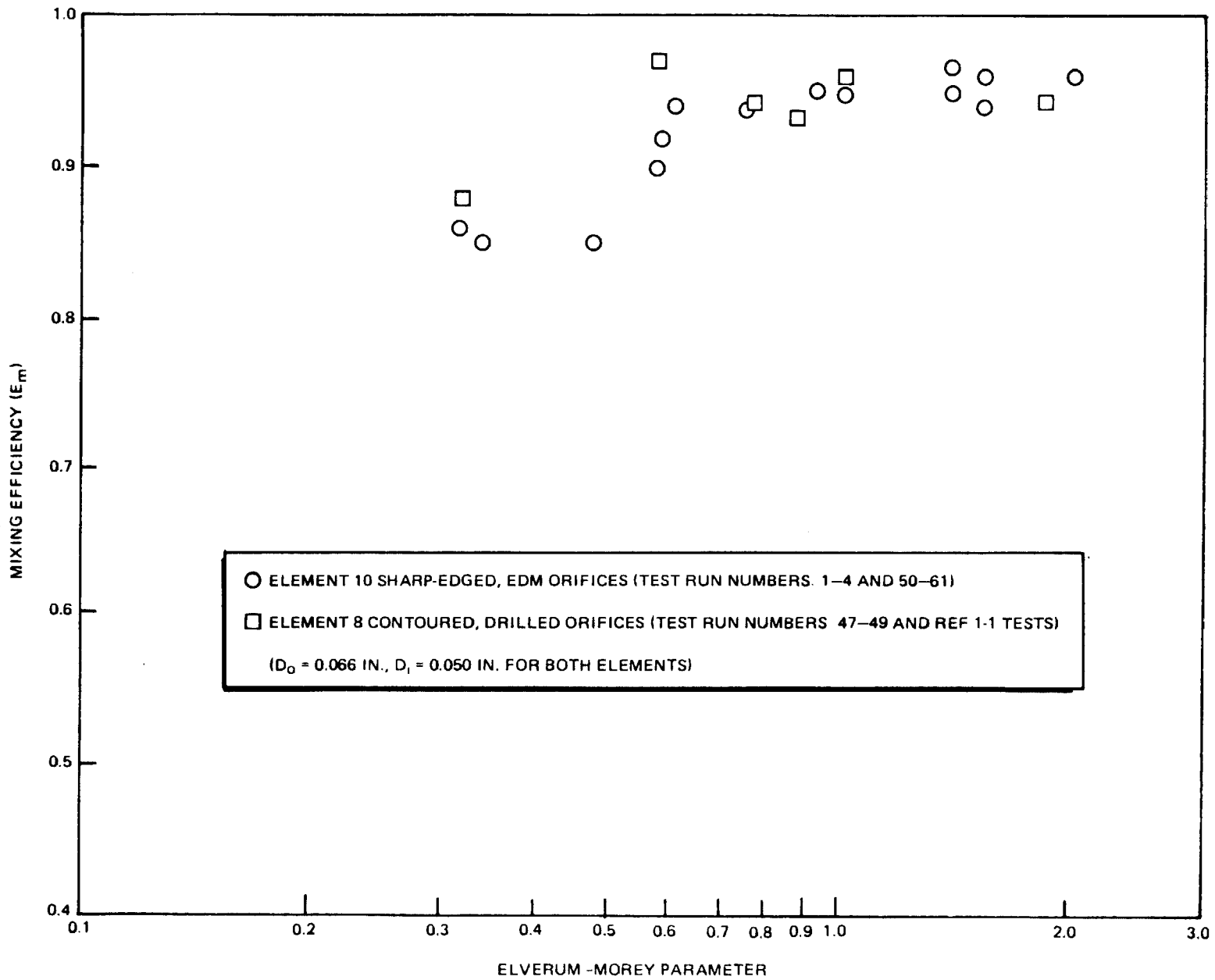
Figure 3-18.   Overall Mixing Efficiency vs Elverum–Morey Parameter – Effect of Fabrication Method

result of the differences in orifice inlet contouring, fabrication method, and/or the JPL specifications for turbulence generation and long length to diameter orifices. Were the conclusions about the Elverum-Morey parameter optimum, indicated by the JPL reports and perhaps by the six tests with element 8, caused by these differences, or were they simply the result of a very small collection of scattered data? This is an important question, as the Elverum-Morey criterium has long been applied as an important triplet design consideration.

To resolve this issue, additional tests were proposed for the element 8, and for an additional element, designated 20, which was fabricated to closely resemble those employed by JPL investigators. Triplet element 20 was formed by positioning three approach tube/orifice insert assemblies on a mounting fixture in a 60-degree impingement configuration with impingement distances identical to those of the one-piece elements 8 and 10. Element 20 orifice diameters matched those of element 10, but lengthy orifice L/Ds, entrance contouring, and inner surface roughening were included, as derived from the JPL standards. A summary of the potentially important differences among the elements 8, 10, and 20 is presented in Table 3-5, and detailed designs of these elements are presented in Section II.

A schematic drawing of an approach tube/orifice insert assembly employed in the JPL mixing studies (Ref. 3-1) is shown in Fig. 2-2. Orifice inserts of this type were precision-machined to include elliptically contoured entrances; a short, roughened section downstream of the entrance for inducing turbulence (achieved by tapping the inside diameter to provide a short length of threading); and overall length-to-diameter ratios exceeding 20.

Table 3-6A shows the additional tests performed with the elements 8 and 20, followed by the results of these tests. Data from the elements 8, 10, and 20 tests are plotted in Fig. 3-19. Pronounced optimums in the elements 8 and 20 data are not evident. The results presented in Table 3-6B and Fig. 3-19 appear to underscore the general trend observed for all elements tested in this study -- mixing efficiency increased steadily as the Elverum-Morey parameter increased from approximately 0.3 to 0.8, then leveled off at a high value with further increase in the Elverum-Morey parameter. This result is in marked contrast to the findings of Elverum and Morey. Included in Fig. 3-19 are five of the actual data points

TABLE 3-5. SUMMARY OF VARIATIONS IN ORIFICE CONTOURING

```
ELEMENT 8:    OUTER ORIFICE DIAMETER 0.065 INCH
              INNER ORIFICE DIAMETER 0.050 INCH
              LENGTH/DIAMETER RATIO 5.0 (ALL ORIFICES)
              ORIFICE ENTRANCE RADIUS 0.030 INCH (ALL ORIFICES

ELEMENT 10:   OUTER ORIFICE DIAMETER 0.066 INCH
              INNER ORIFICE DIAMETER 0.050 INCH
              LENGTH/DIAMETER RATIO 5.0 (ALL ORIFICES)
              ORIFICES ENTRANCES SHARP-EDGED

ELEMENT 20:   OUTER ORIFICE DIAMETER 0.066 INCH
                 ENTRANCE RADIUS 0.061 INCH
                 LENGTH/DIAMETER RATIO 24.0
                 TURBULENCE INDUCEMENT 2-56 THREADED SECTION

              INNER ORIFICE DIAMETER = 0.050 INCH
                 ENTRANCE RADIUS 0.057 INCH
                 LENGTH/DIAMETER RATIO 24.0
                 TURBULENCE INDUCEMENT 0-80 THREADED SECTION
```

TABLE 3-6A. ADDITIONAL TESTS CONDUCTED TO TEST FABRICATION METHOD

ELEMENT	TEST NUMBER	COLLECTION DISTANCE (INCHES)	DELTA P OUT (PSI)	DELTA P IN (PSI)	INJECTION PATTERN	TARGET OXIDIZER/ FUEL MASS MIXTURE RATIO
TRIPLET 20	62	2	9.2	26.9	O-F-O	2.35
D_0 = 0.66 INCH	63	2	12.0	26.5	O-F-O	2.70
D_i = 0.050 INCH	64	2	14.5	26.7	O-F-O	2.96
θ = 60 DEGREES	65	2	18.5	26.5	O-F-O	3.35
	66	2	22.9	26.5	O-F-O	3.73
TRIPLET 8	67	2	9.7	26.7	O-F-O	2.34
D_0 = 0.065 INCH	68	2	12.5	26.7	O-F-O	2.66
D_i = 0.050 INCH	69	2	15.5	26.8	O-F-O	2.96
θ = 60 DEGREES	70	2	19.4	26.5	O-F-O	3.33
	71	2	24.4	26.8	O-F-O	3.71

TABLE 3-6B.   RESULTS OF ADDITIONAL FABRICATION METHOD TESTS

TEST NUMBER	ELEMENT NUMBER	OXIDIZER/FUEL MASS MIXTURE RATIO	OXIDIZER (TRIC) COLLECTION EFFICIENCY	FUEL (H_2O) COLLECTION EFFICIENCY	OVERALL MIXING EFFICIENCY (E_m)	OUT/IN MOMENTUM RATIO	OUT/IN VELOCITY HEAD RATIO	RUPE PARAMETER	ELVERUM-MOREY PARAMETER
62	20	2.35	0.82	0.95	0.88	1.20	0.34	0.45	0.49
63	20	2.70	0.83	0.98	0.92	1.57	0.44	0.58	0.65
64	20	2.96	0.83	0.93	0.95	1.89	0.54	0.71	0.78
65	20	3.35	0.83	0.81	0.95	2.44	0.70	0.92	1.00
66	20	3.73	0.83	0.76	0.95	3.02	0.87	1.15	1.25
67	8	2.34	0.84	0.92	0.91	1.22	0.36	0.47	0.49
68	8	2.66	0.88	1.06	0.95	1.57	0.46	0.60	0.63
69	8	2.96	0.87	0.99	0.96	1.95	0.58	0.75	0.78
70	8	3.33	0.87	0.96	0.94	2.46	0.72	0.94	0.99
71	8	3.71	0.86	0.85	0.95	3.08	0.91	1.18	1.23
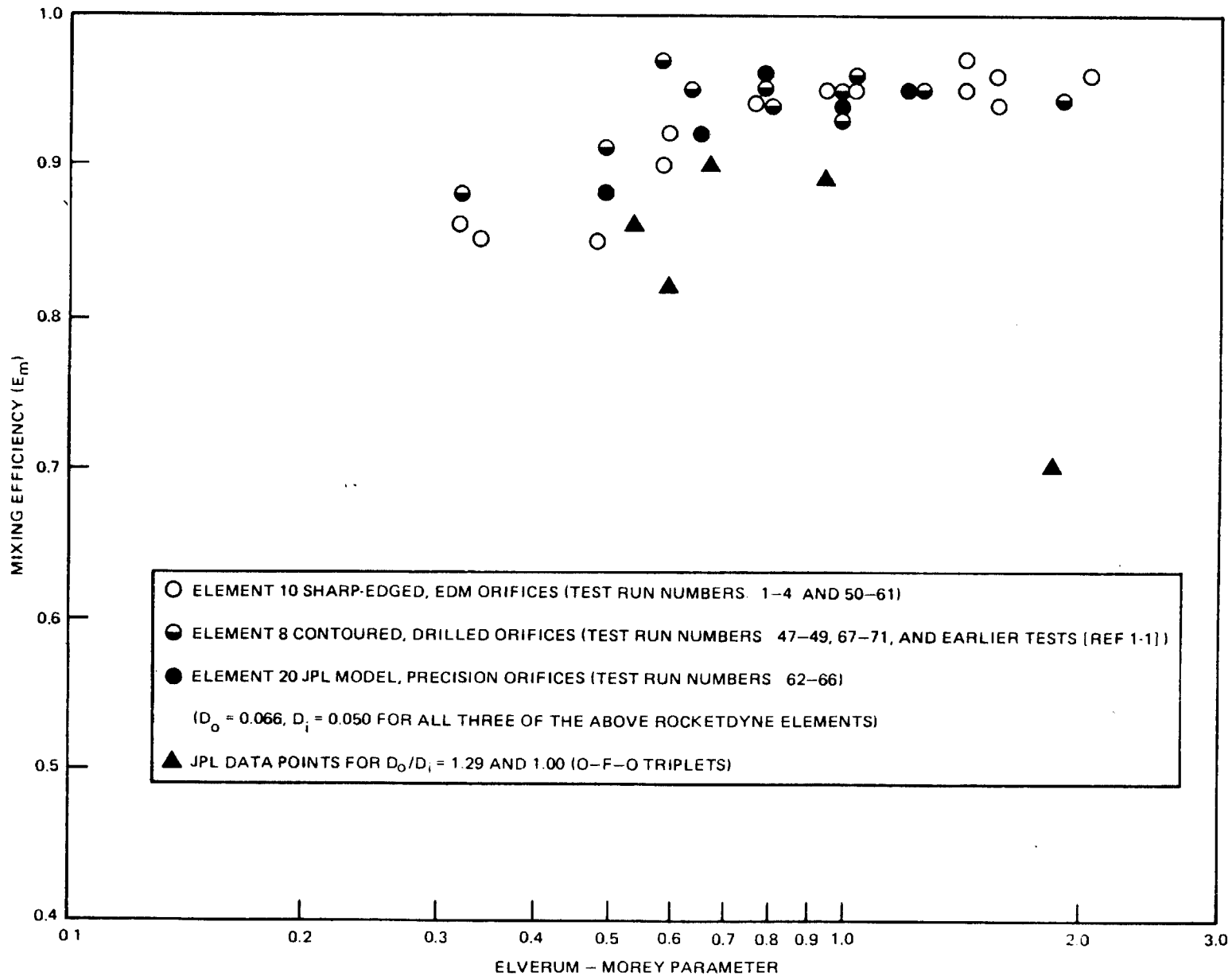
Figure 3-19.   Overall Mixing Efficiency vs Elverum-Morey Parameter -
Rocketdyne vs JPL Data

employed in the Elverum-Morey correlation (Ref. 3-6 and 3-7). Four of these points seem to follow the general trend observed in the present study, while the fifth falls much lower than comparable points produced here. Efforts to uncover all data generated in the JPL triplet studies culminating in the Elverum-Morey correlation proved largely fruitless. The only data available in referenced documents are shown in Table 3-7. Valid comparison of Rocketdyne versus JPL data depends on the assumption that mixing results are independent of the slightly different spray sampling methods employed. While the validity of this assumption has not been directly addressed here, it was reported in a previous JPL study (Ref. 3-4) comparing Rocketdyne and JPL data, that "none of the results appeared to be significantly influenced in any way by differences in apparatus and experimental technique."

Data Correlation

Data from the 71 mixing tests were correlated with the aid of a regression program that computed the relation between the dependent variable (mixing efficiency) and a set of four independent variables (e.g., stream diameter ratio, density ratio, velocity ratio, and impingement angle). These four variables were chosen as the most fundamental physical descriptors of a particular set of injection conditions. Parameters such as momentum ratio or mixture ratio could just as easily have been employed, but they represent combinations of the fundamental quantities. The correlating equation computed was:

$$E_m = 0.81 \left(\frac{d_o}{d_i}\right)^{0.29} \left(\frac{\rho_o}{\rho_i}\right)^{0.56} \left(\frac{V_o}{V_i}\right)^{0.25} (\sin \theta)^{-0.03} \tag{6}$$

The applicability of this correlation is subject to the following limits on the variable ranges:

Outer/inner stream density ratio	0.76 to 1.32
Outer/inner stream diameter ratio	0.92 to 1.58
Included impingement angle	30 to 90 degrees
Outer/inner stream velocity ratio	0.37 to 1.69

TABLE 3-7. SUMMARY OF AVAILABLE DATA FROM JPL TRIPLET STUDIES

TEST NUMBER	REFERENCE NUMBER	D_0 (INCH)	D_1 (INCH)	D_0/D_1	OXIDIZER/FUEL PROPELLANTS SIMULANTS	O-F-O DENSITY RATIO	O/F MASS MIXTURE RATIO	OUT/IN VELOCITY HEAD RATIO	ELVERUM-MOREY PARAMETER	MIXING EFFICIENCY (E_m)
1	3-6	N/A	N/A	1.00	CC14/H20	1.59	1.26	0.50	0.60	0.82
2	3-6	N/A	N/A	1.00	CC14/H20	1.59	1.59	0.79	0.94	0.89
3	3-6	N/A	N/A	1.00	CC14/H20	1.59	2.25	1.59	1.89	0.70
4	3-7	N/A	N/A	1.29	CC14/H20	1.59	2.64	0.40	0.54	0.86
5	3-7	N/A	N/A	1.29	CC14/H20	1.59	2.97	0.50	0.67	0.90
6	3-2	0.082	0.070	1.17	H20/KEROSENE	1.22	1.92	0.40	0.52	N/A
7	3-2	0.082	0.070	1.17	H20/KEROSENE	1.22	2.18	0.52	0.66	N/A
8	3-2	0.082	0.070	1.17	H20/KEROSENE	1.22	2.42	0.63	0.82	N/A

A plot of observed mixing efficiency values for the 71 tests versus the values predicted using Eq. (6) is presented in Fig. 3-20. Fifty-six of the 71 predicted E_m values fell within 6% of the corresponding observed values. It is evident that the majority of points whose predicted Em values deviated from the observed values by more than 6% were those resulting from F-O-F configuration tests. The greatest deviation from this correlation was observed for element 13, which was the only element with a diameter ratio less than 1.

The empirical correlation of Eq. (6) mathematically defines, and agrees with, the findings that were apparent from inspection of the data. For example, the great benefit of having the denser fluid in the outer stream and the relative unimportance of impingement angle are readily apparent in both Eq. (6) and the graphical results previously presented.

Conclusions

The inescapable conclusion to be drawn from the results presented here is that the Elverum-Morey criteria are an invalid correlation for the design of triplet elements composed of sharp-edged entry, low L/D orifices. These types of elements are highly representative of actual rocket engine injector elements. Furthermore, limited data generated with elements composed of contoured entry, high L/D orifices seem to support this conclusion more generally. The invalidity of the criteria is based primarily on the observation here that mixing efficiency does not reach a maximum value at an Elverum-Morey parameter value of 0.66. Certain earlier Rocketdyne testing of F-O-F injectors with $D_o/D_i \leq 1$ (Ref. 1-1) indicates a peak at an Elverim-Morey parameter value near 0.66. Those tests are outside the range of conditions tested in this program. It is possible that the optimum Elverium-Morey parameter is valid under those test conditions.

Another conclusion demonstrated here is the importance of injecting the denser of two liquids through the outer orifice pair of a triplet element, which is seen to produce markedly better mixing efficiency than the reversed configuration (i.e., lighter fluid injected through the outer orifices). This effect may be the result of the greater momentum of the outer streams with denser liquids. Since it is the impingement of the outer streams that causes the breakup and mixing of the

APPLICABLE RANGES OF PARAMETERS

$0.92 < D_o/D_i < 1.58$

$0.76 < \rho_o/\rho_i < 1.32$

$0.37 < V_o/V_i < 1.69$

$30^\circ < \theta < 90^\circ$

ELEMENT	OFO	FOF
8	◉	
10	○	●
11	□	
12	△	▲
13	◇	◆
14	○	●
15	○	
16	◇	
17	○	
20	▭	

$$\text{PREDICTED Em} = (0.81)\left(\frac{D_o}{D_i}\right)^{0.29} \left(\frac{\rho_o}{\rho_i}\right)^{0.56} \left(\frac{V_o}{V_i}\right)^{0.25} (\text{SIN } \theta)^{-0.03}$$
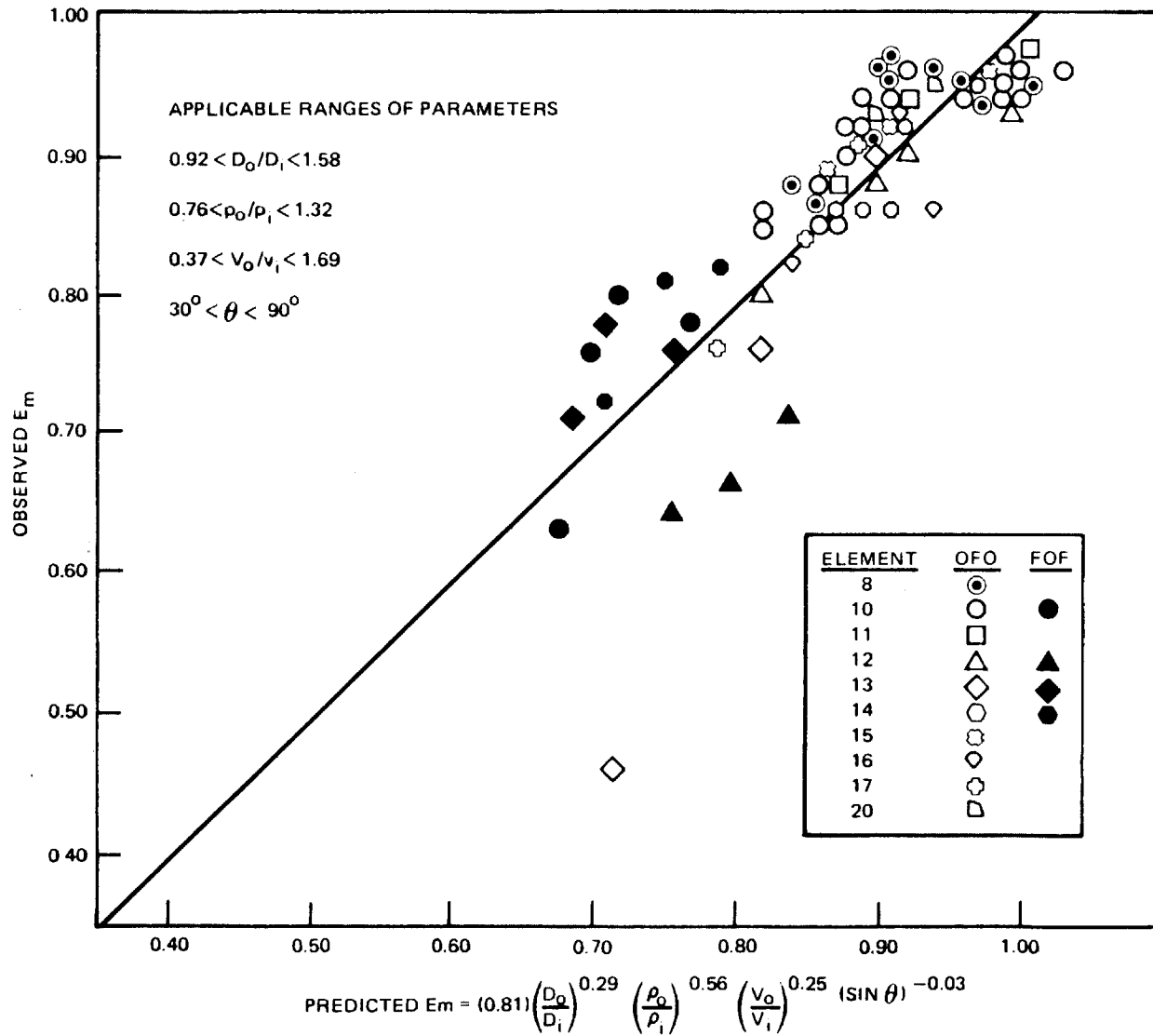
Figure 3-20.   Data Correlation for Liquid/Liquid Triplet Mixing Study

inner stream, increasing the momentum (by increasing the density) of the outer stream would be expected to enhance mixing. Regardless of the reason for this effect, the results of these tests clearly demonstrate a very strong correlation between triplet mixing efficiency and the selection of inner or outer orifices for the more dense propellant. Since the most commonly employed propellant combinations have fuels of lower density than the oxidizer, this finding would dictate the use of oxidizer in the outer streams. In many instances, particularly at preburner mixture ratios, other factors may preclude the use of oxidizer in the outer streams. Liquid/liquid triplets may not be the optimum element choice for such applications. The liquid/liquid triplet testing performed with preburner elements (elements 1 and 6) in an early part of this contractual program (Ref. 1) demonstrated poor mixing efficiency. This may be caused by their F-O-F configuration.

Another factor that appears to have an effect on mixing efficiency is the outer to inner orifice diameter ratio. This is apparent in the empirical correlating equation [Eq. (6)], but is not so readily apparent from the plots of the data (Fig. 3-13 and 3-14). In the O-F-O configuration (Fig. 3-13), there is no discernible difference in mixing efficiency between all the elements tested, except for the element 13, which is the only element with an outer to inner diameter ratio less than 1.0 (actually the only one less than 1.1). Figure 3-14 (F-O-F configuration) seems to indicate that both element 13 (D_0/D_1 = 0.92) and element 12 (D_0/D_1 = 1.58) were relatively poor mixers, while those of intermediate diameter ratios provided better mixing. Thus, the following findings regarding the effect of diameter ratio are indicated.

1.   The empirical correlation indicates that larger values of diameter ratio generally enhance mixing

2.   Figure 3-13 indicates that mixing efficiency is unaffected by diameter ratio except at low values of diameter ratio for O-F-O configurations

3.   Figure 3-14 indicates that both large and small values of diameter ratio inhibit mixing for F-O-F configurations.

While all three of these findings support the conclusion that lower values of diameter ratio reduce mixing performance, they are contradictory regarding the effects of higher diameter ratios. Even this conclusion is somewhat suspect, as it is entirely dependent upon the results obtained with a single element 13. However, this conclusion seems reasonable, since smaller outer streams might be expected to less homogeneously break up and mix with a larger center stream and even minor misimpingements could significantly degrade mixing performance. Additional effort is recommended to confirm this conclusion and to investigate large diameter-ratio elements mixing performance.

The other major parameter affecting the mixing performance of liquid/liquid triplets is the velocity ratio. This is demonstrated in Fig. 3-5, where mixing efficiency versus velocity head ratio $(\rho_o V_o^2 / \rho_1 V_1^2)$ is plotted. For either the O-F-O or F-O-F configuration, the density ratio remains constant. Thus it is apparent that increasing the velocity ratio (V_o/V_1) increases mixing performance for either configuration. The empirical correlation [Eq. (6)] also clearly demonstrates this effect. Limited testing (presented in Fig. 3-17) indicates that it is the velocity ratio rather than the individual velocities which affect mixing. This is an important finding as it provides some basis to support extrapolation of these data to higher injection velocities.

An extensive number of tests with four elements, whose only difference was impingement angle, indicates that impingement angle has no apparent or significant effect on mixing. These results are presented in Fig. 3-16, and the correlating equation demonstrates no significant effect of impingement angle. This, too, is in disagreement with the early JPL findings.

One additional finding of this study is the insignificance of orifice size on mixing efficiency. While the number of tests (presented in Fig. 3-15) is relatively small, there appears to be no effect on mixing efficiency when the orifice area is doubled. This finding appears to contradict common hot-fire test experience on engines that indicates poorer performance for larger elements. However, this poorer performance may be the result of atomization rather than mixing. Also, even though the measured mixing efficiencies of large and small elements may be the same, the regions rich in one or the other propellants are

correspondingly larger for the larger elements. For example, both elements may provide a 10% higher mixture ratio zone in the center of the distribution and a surrounding lower mixture ratio region such that both elements have the same cold-flow mixing efficiency. However, the size of these regions may be expected to scale with the element size. Thus, the larger element would have a correspondingly larger high mixture ratio region, which would not be as readily dispersed and reacted as the smaller high mixture ratio region of the smaller element.

This program is the largest, most thorough, and most comprehensive investigation of the mixing performance of liquid/liquid-triplet elements that has ever been performed. The findings and conclusions of this effort can provide specific guidance to designers of such elements. In accordance with these findings, the following design criteria and advice to designers of liquid/liquid-triplet elements are provided.

1. The use of an optimum value of the Elverum-Morey parameter as design criteria for liquid/liquid triplets is not justified and should be discontinued. Mixing efficiency increases as the Elverum-Morey parameter increases.

2. The more dense propellant should be injected from the outer orifices.

3. Small, outer to inner, orifice diameter ratios (e.g., 1 or less) are not recommended.

4. Changing the injection velocity of both elements by the same percentage, has no effect on the mixing performance, over the range of injection velocities tested.

5. Increasing the outer to inner velocity ratio of the propellants improves mixing performance.

6. Impingement angle has no significant influence on mixing and should be chosen on the basis of other considerations.

7. As a guide to use in trading off various design considerations, it is recommended that the designer attempt to maximize the parameter:

$$\left(\frac{d_o}{d_i}\right)^{0.29} \left(\frac{\rho_o}{\rho_i}\right)^{0.56} \left(\frac{v_o}{v_i}\right)^{0.25} .$$

All these findings, conclusions, design guidance, and especially the preceding mixing efficiency design parameter, should not be extrapolated or applied beyond the limits of the range of the variables tested in this program without very careful consideration. The range of the variables tested are:

Outer to inner orifice velocity ratio	0.37 to 1.69
Outer to inner orifice diameter ratio	0.92 to 1.58
Outer to inner orifice density ratio	0.76 and 1.32
Impingement angle (between outer streams)	30 to 90 degrees
Orifice diameter	0.117 to 0.236 cm (0.046 to 0.093 inch)
Injection velocities	6.7 to 20.2 m/sec (22 to 66 ft/sec)

MULTIPLE-ELEMENT, LIKE-DOUBLET STUDY

Background

Impinging liquid rocket engine injector patterns have traditionally been designed around the concentric ring approach -- a series of concentric, annular propellant manifolding passages that feed corresponding concentric rings of fuel and oxidizer orifices, with impingement occurring between orifices of the same or adjacent rings. This approach has been used primarily because of manufacturing constraints. With the development of more sophisticated fabrication techniques (e.g., electrical discharge machining and electrodepositing processes), a greater degree of flexibility is now possible in injector design. One of the recently developed configurations identified by injector specialists at Rocketdyne is the "repeating box" pattern. In this pattern, the injector face is divided into a grid of square boxes. Impinging elements (usually like-doublets or like-triplets) of one propellant type (fuel or oxidizer) are positioned on the box perimeters, while impinging elements of the other propellant type are positioned in the box centers. The repeating box pattern has been likened to an impinging analog of a coaxial element array, with the spray fans of one propellant type surrounding the fans of the other type.

Subject Injector for LOX/RP-1 Booster

The subject injector for this series of mixing tests has been proposed as a candidate injector for a large LOX/RP-1 booster. The proposed design features a like-doublet version of the repeating box pattern, shown schematically in Table 3-8. Each square box includes four like-doublets on the perimeter (one per side) surrounding one like-doublet in the center. The "box" (perimeter) doublets are each shared by two squares, making the ratio of "box" doublets to "surrounded" doublets four halves to one, or more simply, two to one.

The principal design specifications for the LOX/RP-1 booster injector are also listed in Table 3-8 -- LOX flow rate = 3770 lb/sec, RP-1 flow rate = 1440 lb/sec, injector pressure drop = 400 psid (both sides) -- corresponding to a chamber pressure of 2000 psia. An additional 50% throttling case is also of interest, with a reduced injector pressure drop of 100 psi corresponding to a chamber pressure of 1000 psia. Two injectant configurations are possible -- the "fuel box surrounding oxidizer doublet" configuration or the "oxidizer box surrounding fuel doublet" configuration. Orifice sizes for the two configurations are given in Table 3-8. The latter configuration (oxidizer surrounding fuel) is thought to produce better mixing, while the former (fuel surrounding oxidizer) may be more desirable for boundary layer cooling reasons.

Cold-Flow Testing

The objectives of cold-flow testing were to compare mixing efficiencies between the two injectant configurations, between 40-degree and 60-degree angles of impingement, and between a number of different throttling cases. The experimental apparatus employed was the same as that described in the first section of this report, with water used as the fuel simulant and TRIC as the oxidizer simulant. Turbine flowmeters were used to monitor flow rates. Because of the large size of the proposed hot-fire injector, obviously only a limited portion of the spray pattern could be sampled with the 4.13 by 6.35 cm (1-5/8 by 2-1/2 inches) collection grid. The representative portion selected as the "unit mixing cell" was a single box (four perimeter elements surrounding one central element) plus the two adjacent elements whose spray fans are seen to interact with the fans of the box.

TABLE 3-8. DESIGN SPECIFICATIONS FOR PROPOSED LOX/RP-1 BOOSTER INJECTOR

SCHEMATIC DRAWING OF
REPEATING BOX PATTERN

● ORIFICES OF "BOX" DOUBLETS

• ORIFICES OF "SURROUNDED DOUBLETS

OVERALL INJECTOR DIAMETER = 35.2 INCHES

CHARACTERISTIC LENGTH (X) = 0.30 INCH

NOMINAL PATTERN: "FUEL BOX SURROUNDING OXIDIZER DOUBLET"

NOMINAL PATTERN DESIGN PARAMETERS:

D_o = 0.051 INCH N_o = 22,500
D_f = 0.024 INCH N_f = 45,000

FULL   INJECTOR PRESSURE DROP = 400 PSI (BOTH SIDES)

$\dot{m}_o$ = 3770 LB/SEC $\dot{m}_o$ PER ORIFICE = 0.168 LB/SEC

$\dot{m}_f$ = 1440 LB/SEC $\dot{m}_f$ PER ORIFICE = 0.032 LB/SEC

50% THROTTLE: INJECTOR PRESSURE DROP = 100 PSI (BOTH SIDES)

$\dot{m}_o$ = 1885 LB/SEC $\dot{m}_o$ PER ORIFICE = 0.084 LB/SEC

$\dot{m}_f$ = 720 LB/SEC $\dot{m}_f$ PER ORIFICE = 0.016 LB/SEC

REVERSE PATTERN: "OXIDIZER BOX SURROUNDING FUEL DOUBLET"

REVERSE PATTERN DESIGN PARAMETERS:

D_o = 0.036 INCH N_o = 45,000
D_f = 0.034 INCH N_f = 22,000

FULL   INJECTOR PRESSURE DROP = 400 PSI (BOTH SIDES)

$\dot{m}_o$ = 3770 LB/SEC $\dot{m}_o$ PER ORIFICE = 0.084 LB/SEC

$\dot{m}_f$ = 1440 LB/SEC $\dot{m}_f$ PER ORIFICE = 0.064 LB/SEC

50% THROTTLE: INJECTOR PRESSURE DROP = 100 PSI (BOTH SIDES)

$\dot{m}_o$ = 1885 LB/SEC $\dot{m}_o$ PER ORIFICE = 0.042 LB/SEC

$\dot{m}_f$ = 720 LB/SEC $\dot{m}_f$ PER ORIFICE = 0.032 LB/SEC

A schematic drawing of this representative unit mixing cell is shown in Table 3-9. This mixing cell was selected for cold-flow modeling primarily for low cost and ease of fabrication. However, the small size of a single box (0.30 by 0.30 inch in the hot-fire design) was not particularly compatible with the collection grid dimensions (0.125-inch-square tubes) if adequate mixing resolution was to be ensured. Thus, the cold-flow models designed for these tests were photographically scaled-up versions of the design-scale unit mixing cell. The baseline scaling factor chosen was 2.5, for this reason: an enlargement factor of 2.5 produced a unit mixing cell with sides of 0.75 inch, which could be aligned above the collection grid to coincide exactly with a 6 by 6 array of the 0.125-inch tubes. In this manner, a 36-sample mixing efficiency measurement would be determined for a representative square of the overall repeating box spray pattern.

Four models were fabricated for cold-flow testing, as shown schematically in Fig. 3-21. The baseline model was a 2.5-scale, "fuel box around oxidizer doublet" mixing cell with impingement angles of 60 degrees. Two other 2.5-scale models were fabricated: the first a 40-degree impingement angle version of the baseline, and the second a reversed configuration ("oxidizer box surrounding fuel doublet") model. To produce the 40-degree impingement angle modification of the baseline model, the orifices of each doublet pair were moved slightly farther apart, resulting in an increase in impingement distance from 0.325 inch (60-degree case) to 0.515 inch (40-degree case). The fourth model fabricated was a 1.25-scale version of the baseline model (aligned above a 3 by 3 array of collection tubes during testing). This model was tested primarily to assess the validity of acquiring mixing data from scaled-up models of the subject injector. The majority of mixing tests were conducted on the 2.5-scale models, to effect mixing efficiency comparisons between the two injector configurations, the two impingement angles, and a number of mass flow throttling cases. The 1.25-scale model was then tested under conditions congruous to those employed in a specific baseline model run. A comparison between the 1.25-scale and the 2.5-scale test results would then be an indication of whether photographically scaled-up models can be used to accurately assess mixing characteristics of their small-scale counterparts.

TABLE 3-9. DESIGN SPECIFICATIONS FOR COLD-FLOW MODELS
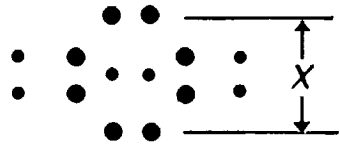
SCHEMATIC DRAWING OF "UNIT CELL"
REPRESENTATIVE OF BOX PATTERN

(1 BOX PLUS 2 ADJACENT DOUBLETS)

CASE 1: SCALING FACTOR = 1.25 (CHARACTERISTIC LENGTH (X) = 0.375 INCH)
NOMINAL PATTERN: "FUEL BOX SURROUNDING OXIDIZER DOUBLET"

D_0 = 0.064 INCH N_0 = 6
D_f = 0.030 INCH N_f = 8

$\dot{m}_0$ PER ORIFICE = 0.26 LB/SEC   TOTAL $\dot{m}_0$ = 1.57 LB/SEC

$\dot{m}_f$ PER ORIFICE = 0.05 LB/SEC   TOTAL $\dot{m}_f$ = 0.40 LB/SEC

CASE 2: SCALING FACTOR = 2.50 (CHARACTERISTIC LENGTH (X) = 0.750 INCH)
NOMINAL PATTERN: "FUEL BOX SURROUNDING OXIDIZER DOUBLET"

D_0 = 0.128 INCH N_0 = 6
D_f = 0.060 INCH N_f = 8

$\dot{m}_0$ PER ORIFICE = 1.05 LB/SEC   TOTAL $\dot{m}_0$ = 6.30 LB/SEC

$\dot{m}_f$ PER ORIFICE = 0.20 LB/SEC   TOTAL $\dot{m}_f$ = 1.60 LB/SEC

CASE 3: SCALING FACTOR = 2.50/CHARACTERISTIC LENGTH (X) = 0.750 INCH)
REVERSE PATTERN: "OXIDIZER BOX SURROUNDING FUEL DOUBLET"
REVERSE PATTERN DESIGN PARAMETERS:

D_0 = 0.090 INCH N_0 = 8
D_f = 0.085 INCH N_f = 6

$\dot{m}_0$ PER ORIFICE = 0.52 LB/SEC   TOTAL $\dot{m}_0$ = 4.16 LB/SEC

$\dot{m}_f$ PER ORIFICE = 0.40 LB/SEC   TOTAL $\dot{m}_f$ = 2.40 LB/SEC
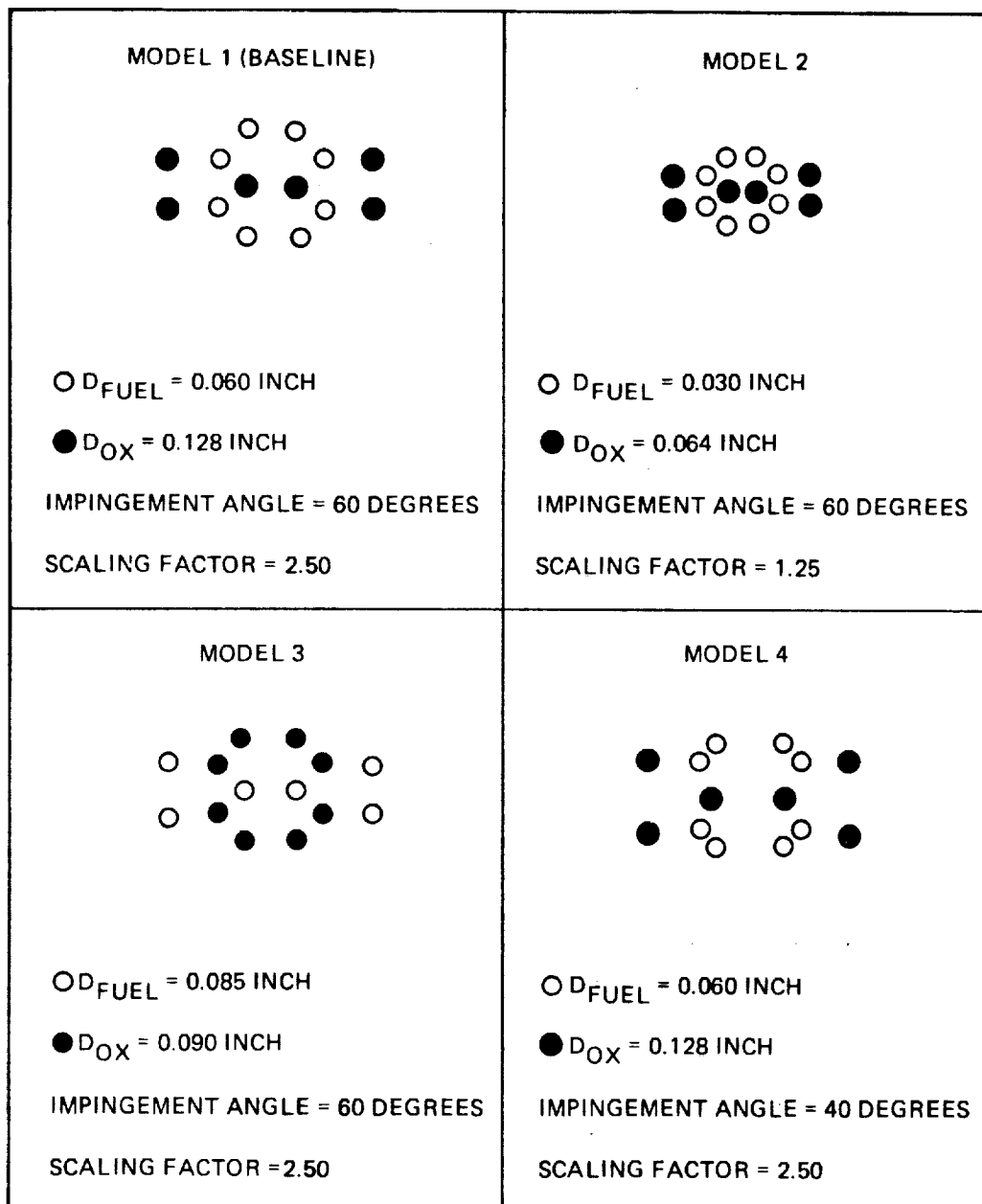
Figure 3-21.   Schematic Drawing of the Four Cold-Flow Models

Mass flow specifications for the test models are presented in Table 3-9, based on design specifications for the hot-fire injector. These conditions were calculated in the following manner: first, it was noted that a 2.5-scale increase in orifice diameter translates to a 6.25-scale (2.5 squared) increase in orifice area, and, therefore, a 6.25-scale increase in mass flow per orifice. (In the 1.25-scale case, the orifice diameter increase translates to a 1.56-scale mass flow increase.) Second, the total hot-fire mass flow rates were reduced to flow rates per individual orifice (lb/sec/oxidizer orifice and lb/sec/fuel orifice), then these values were scaled up by a factor of 6.25 (or 1.56), in the translation to cold-flow orifice sizing. Finally, the translated mass flow per orifice values were multiplied by the number of respective orifices included in the cold-flow models (six or eight, depending on the injectant configuration). Thus, the mass flow conditions specified in Table 3-9 represent constant mass flux enlargements of the corresponding Table 3-8 conditions. However, because of pressure and tankage constraints, these target cold-flow conditions could not be experimentally achieved, and the tests were instead conducted over a reduced mass flow range of approximately 10 to 15% of the Table 3-9 values.

Test Results

A series of 11 test runs was performed with the four injector models, the results of which are presented in Table 3-10. For each run, the test conditions are presented first in terms of TRIC (oxidizer) and water (fuel) injection rates for the model, with a corresponding injected mixture ratio; and additionally in terms of the total mass flow rates of each simulant projected for an entire injector comprising model-size orifices. For example, in test run 1, the projected TRIC mass flow for the overall injector was calculated by dividing the injected (model) TRIC flow rate (0.375 lb/sec) by the number of TRIC orifices (8), and then multiplying the result by the number of oxidizer orifices composing the overall injection pattern -- 45,000.

The baseline collection distance employed in the test runs was 2 inches, with two exceptions: in the one run conducted with the 1.25-scale model, the collection distance was correspondingly reduced by half, to 1 inch, and in one run conducted

TABLE 3-10. RESULTS OF THE TEST SERIES FOR MULTIPLE-ELEMENT LIKE-DOUBLET MODELS

MODEL	RUN NUMBER	COLLECTION DISTANCE (INCH)	INJECTED $\dot{m}_{TRIC}$ FOR MODEL (LB/SEC)	INJECTED $\dot{m}_{H_2O}$ FOR MODEL (LB/SEC)	INJECTED MIXTURE RATIO FOR MODEL	PROJECTED $\dot{m}_{TRIC}$ FOR INJECTOR (LB/SEC)	PROJECTED $\dot{m}_{H_2O}$ FOR INJECTOR (LB/SEC)	PROJECTED MIXTURE RATIO FOR INJECTOR	MIXING EFFICIENCY
2.50 SCALE - OXIDIZER BOX SURROUNDING FUEL DOUBLET	1	2	0.375	0.215	1.74	2112	806	2.62	0.86
	2	2	0.443	0.255	1.74	2486	956	2.60	0.90
MODEL 3	3	2	0.495	0.287	1.72	2787	1076	2.59	0.89
60 DEGREE IMPINGEMENT ANGLE	4*	2	0.559	0.325	1.72	3145	1219	2.58	0.90
2.50 SCALE - FUEL BOX SURROUNDING OXIDIZER DOUBLET	5	2	0.572	0.146	3.92	2143	821	2.61	0.72
	6	2	0.668	0.170	3.93	2505	956	2.62	0.78
MODEL 4	7*	2	0.832	0.216	3.85	3122	1215	2.57	0.82
40 DEGREE IMPINGEMENT ANGLE	8*	1.5	0.851	0.216	3.94	3195	1215	2.63	0.70
2.50 SCALE - FUEL BOX SURROUNDING OXIDIZER DOUBLET MODEL 1	9*	2	0.835	0.217	3.85	3133	1219	2.57	0.90
60 DEGREE IMPINGEMENT ANGLE	10	2	0.741	0.190	3.90	2779	1069	2.60	0.89
1.25 SCALE - FUEL BOX SURROUNDING OXIDIZER DOUBLET MODEL 2 60 DEGREE IMPINGMENT ANGLE	11	1	0.210	0.055	3.82	788	308	2.56	0.92

*DENOTES TESTS CONDUCTED AT BASELINE CONDITIONS FOR 2.5-SCALE MODELS

on the 2.5-scale, 40-degree model, the collection distance was reduced to 1.5 inches with flow conditions held constant, in order to assess the effect of collection distance variation on mixing efficiency. Test runs performed at the chosen baseline injection conditions are marked with an asterisk for comparison purposes. The first four tests were conducted, using the 2.5-scale, oxidizer-around-fuel model, at four mass flow conditions: 67% of baseline, 79% of baseline, 89% of baseline, and baseline. The resulting mixing efficiencies were not significantly affected by the range of throttling -- the increase from 67% baseline to baseline was accompanied by a 4% increase in mixing efficiency, from 86 to 90%. Tests 5 through 7 were conducted, using the 2.5-scale, 40-degree, fuel-around-oxidizer model, at three mass flow conditions: 69% of baseline, 80% of baseline, and baseline. The results of these three tests contrasted with the initial four in two ways: first, the increase in flow rates from 69% baseline to baseline resulted in a 10% increase in mixing efficiency (72 through 82%), and second, the mixing efficiency at the baseline condition (82%) was 8% lower than the corresponding oxidizer-around-fuel baseline value (90%). Test 8 was performed to assess the effect of collection distance variation on mixing efficiency, with flow conditions held near the baseline values. The decrease in collection distance from 2 to 1.5 inches resulted in a mixing efficiency decrease from 82% to 70%. This result indicates that within a short distance downstream of the impingement plane, mixing efficiency measurements are very sensitive to collection distance in multiple-element injector studies. Tests 9 and 10 were conducted, using the baseline model -- 2.5-scale, 60-degree impingement, fuel-around-oxidizer. Two mass-flow conditions were tested: 89% of baseline and baseline, with resulting mixing efficiencies insignificantly affected by the throttling range.

Comparison of runs 1 through 4 with runs 9 and 10 shows virtually the same mixing characteristics for the nominal (fuel-around-oxidizer) and reversed (oxidizer-around-fuel) versions of the 60-degree baseline model. In both cases, mixing efficiencies near 90% resulted, with insignificant mixing variation resulting from mass flow throttling. Comparison of runs 5 through 7 with runs 9 and 10 shows significantly lower mixing efficiencies for the 40-degree model. This effect may be partially explainable in terms of impingement distances -- in the 40-degree model, a 2-inch collection distance translated to 3.9 impingement

lengths, while in the 60-degree model, 2 inches translated to 6.15 impingement lengths. This value (6.15 lengths) corresponds to a collection distance of 3.17 inches for the 40-degree model. Given the increase in mixing efficiency from 70% to 82% for an increase in collection distance from 1.5 inches (2.9 lengths) to 2 inches (3.9 lengths) for the 40-degree model, it is possible that an increase in collection distance from 2 to 3.17 inches would result in mixing efficiencies exceeding 90%. Thus, the poorer mixing performance of the 40-degree impingement angle injector may be caused by the greater impingement distance of that injector.

Finally, test run 11 was conducted on the 1.25-scale model at flow conditions congruous to the baseline values of run 9. A value of 92% resulted from the 9-sample mixing efficiency measurement, as compared to the 36-sample value of 90% for run 9. This result supports the validity of basing general conclusions on the mixing characteristics of a small-scale injector pattern on data obtained from scaled-up models.

In attempting to assess the quality of the mixing provided by these elements, it is important to recognize the following:

1. These results are for 2.5 scale models of the injectors.
2. The collection distance was not scaled. That is, the traditional 2-inch collection distance was employed.
3. Measured mixing efficiency must increase with collection distance, especially with unlike, multiple-element injectors. (Propellants would certainly not become unmixed as they move downstream.) The one test performed to assess collection distance effects on mixing (test 8) indicates a considerable change in mixing efficiency for only a one-half-inch variation in collection distance.

If the collection distance were scaled in proportion to the injector, the measurements would be made at 5 inches. The collection grid employed in these tests was too small to allow testing at this collection distance. Certainly the measured mixing efficiencies at the 5-inch location would be considerably improved over these test results. Thus, these injectors would have considerably better mixing efficiencies than were measured in this program.

Conclusions

The following set of conclusions was inferred from data generated in the present study of the proposed like-doublet repeating box injector pattern:

1. The nominal (fuel-around-oxidizer) configuration and the reversed (oxidizer-around-fuel) configuration are virtually interchangeable with respect to mixing efficiency.

2. The mixing efficiency of the 40-degree impingement angle injector was significantly poorer than the 60-degree impingement angle injectors. Larger impingement angles (and/or shorter impingement distances) appear to promote mixing of the fans of the elements in shorter distances.

3. In the 40-degree impingement angle version of the baseline model, mixing efficiency was significantly increased (72% to 82%) by an increase in mass flow from 67% baseline to baseline conditions. Both the 60-degree nominal baseline model and the 60-degree reversed baseline model produced mixing efficiencies insensitive to throttling over the ranges tested.

4. General conclusions regarding mixing characteristics of the subject injector pattern can be inferred from data obtained with scaled-up models.

5. Mixing efficiencies of these elements would be considerably better if the collection distance were scaled with the injector. The actual mixing efficiencies of these injectors are presumed to be considerably better than reported here.

IV. GAS/LIQUID MIXING TESTING

During the first portion of this program, several of the baseline gas/liquid elements (elements 2, 3, and 4) were subjected to gas/liquid, cold-flow, mixing efficiency measurement tests. Several flow conditions were tested for each element and the results were presented in the interim report (Ref. 1-1). The measurement technique employed in these tests was the standard "impact probe" technique that has been in use for over 15 years. This technique employs a large, total-pressure, pitot tube, which acts as a total pressure measurement device in the standard fashion, and also serves to collect a portion of the liquid spray. The total pressure is used to compute gas velocity and gas mass flux, and the rate of liquid collection is used to compute liquid mass flux. When such measurements are made at various locations throughout the spray field, a map of mass flux and mixture ratio distributions can be constructed, and mixing efficiencies computed. A schematic of the test apparatus is presented in Fig. 4-1. Details of the test and data analysis methods, and the results, are presented in Ref. 1-1.

Another output of the data analysis codes is the collection efficiency. Collection efficiency is simply the ratio of the mass flow rate of each fluid computed from the measured fluxes, to the actual mass flow rate of each fluid. As noted in Ref. 1-1, these collection efficiencies were sufficiently far from the optimum value of 1, to be of some concern. The collection efficiencies from these tests, for both fluids, are presented in Table 4-1. Liquid collection efficiencies were generally low and gas collection efficiencies were high. In some tests, only about one fourth of the injected liquid was being accounted for, and in other tests over twice as much gas was being measured as was being injected. Another concern regarding these gas/liquid mixing test results was their applicability to higher chamber pressure conditions. To investigate the effects of chamber pressure on mixing data, a series of high-pressure tests were planned. These were to be carried out in the high-pressure test vessel that was intended for use in the atomization testing subsequently described. However, before proceeding to higher-pressure testing, it was deemed necessary to resolve the problem(s) responsible for the poor collection efficiencies. It was anticipated that these problems would be even more severe at higher pressure.
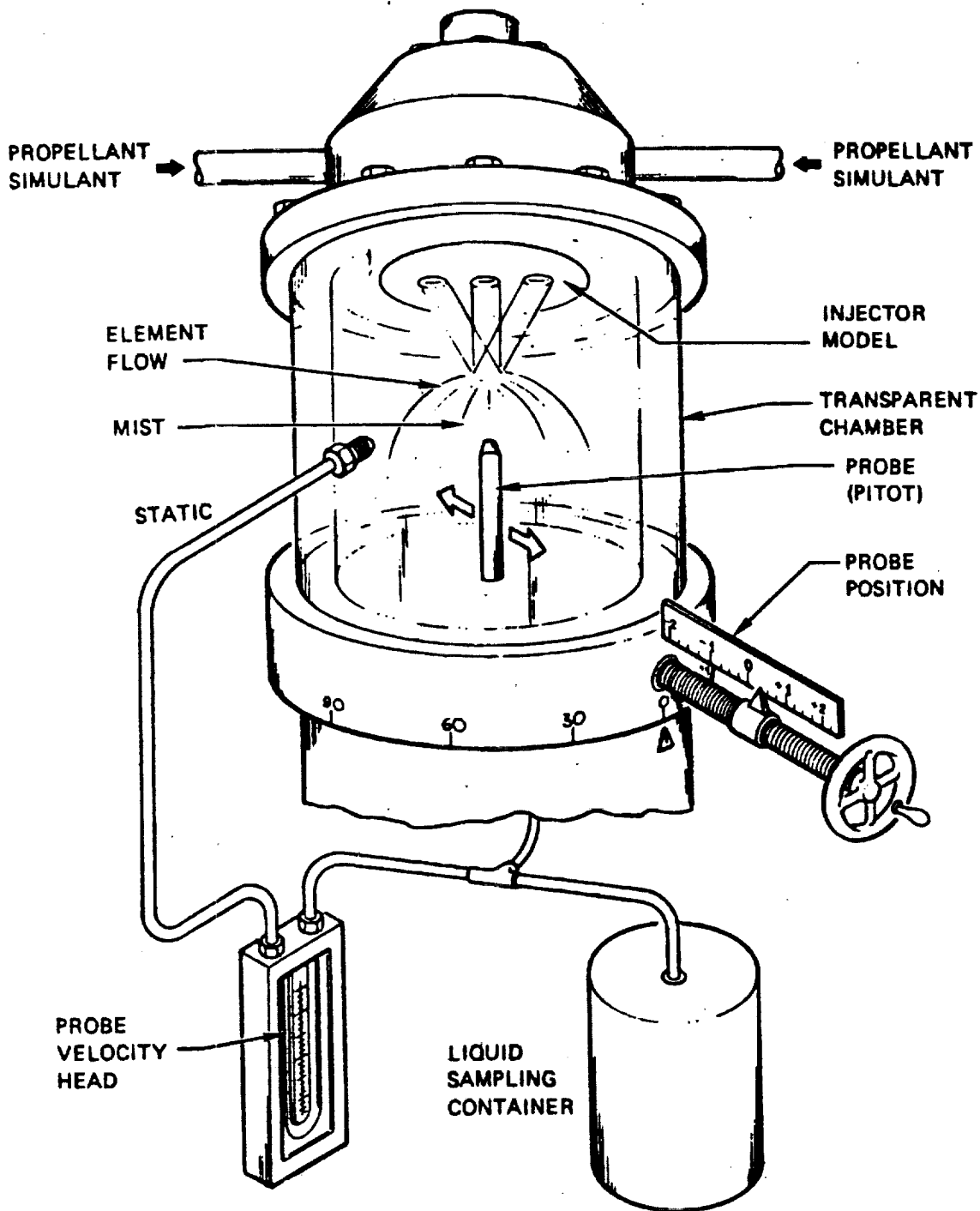
Figure 4-1.   Cold-Flow Gas/Liquid Mixing Measurement System

TABLE 4-1. COLLECTION EFFICIENCY RESULTS

TEST CASE	η_{COL}^{LIQ}	η_{COL}^{GAS}
TRIPLET 2		
NOMINAL HOT-FIRE MOMENTUM RATIO (O/F)	0.48	1.52
+20% NOMINAL MOMENTUM RATIO	0.52	1.59
-20% NOMINAL MOMENTUM RATIO	0.44	1.69
*NOMINAL MOMENTUM RATIO	0.91	1.94
PENTAD 3		
NOMINAL HOT-FIRE MOMENTUM RATIO	.95	1.49
+20% NOMINAL MOMENTUM RATIO	.85	1.19
-20% NOMINAL MOMENTUM RATIO	1.03	2.42
*NOMINAL MOMENTUM RATIO	0.87	0.64
NOMINAL MOMENTUM RATIO	0.93	1.15
TRIPLET 4		
NOMINAL HOT-FIRE MOMENTUM RATIO	0.33	2.07
+20% NOMINAL MOMENTUM RATIO	0.29	1.26
-20% NOMINAL MOMENTUM RATIO	0.23	1.78
*50 PSIG BACKPRESSURES; ALL OTHERS 25 PSIG		

To provide a higher-pressure test capability and eliminate the causes of the poor collection efficiency, a number of potential problems were identified, analyses and experimental studies were performed, and equipment modifications implemented. These are briefly described:

1. High-Pressure Testing Requirement: Gas/liquid mixing testing must be performed at high pressures to allow reasonable simulation of injected gas density. This requirement was especially important for planned testing of coaxial injectors. Thus the high-pressure atomization test vessel was modified to allow its use for gas/liquid mixing tests.

2. Probe and Pressure Line Flooding: Past low-pressure test results indicated that the test probe may have been occasionally filling with water. A new probe was designed and constructed to minimize this

possibility. Water separators were installed to capture any water in the pressure gage lines.

3. Probe Overpressure: Droplets approaching and entering the probe during total pressure measurements transfer momentum to the stagnated gas, thereby increasing the measured pressure. Following study of the work of Dussord and Shapiro (Ref. 4-1), an analytical technique was devised to estimate this effect and incorporated into the data analysis code.

4. Isokinetic Liquid Sampling: If the gas velocity through the probe tip is significantly different from that adjacent to the probe, then the quantity of liquid collected will not be representative of that flowing through that area when the probe is not present. The droplets tend to follow the gas streamlines, especially at high pressures, and go around, rather than into, the probe. To provide isokinetic (constant velocity) liquid collection, the gas flow through the probe was measured and controlled so as to match the measured gas velocity (based upon previous total to static pressure measurements). This was accomplished with a calibrated orifice installed in a line that vented the sample bottle as shown in Fig. 4-2.

5. Liquid Accumulation in Lines Prior to Start of Collection: Since the collection probe must be in place prior to the start of flow through the injector, and since sampling must occur some time after steady flow has been established, liquid may accumulate in the sampling lines. To prevent this, a "dummy" sampling vessel was installed as shown in Fig. 4-2. Prior to the obtaining of a liquid sample, the injector flow was stabilized and the vent valve set to provide a predetermined gas velocity through the probe tip. At the start of the liquid collection time, the flow was diverted from the "dummy" collection vessel to the identical sample collection vessel through the three-way ball valve. Thus steady flow conditions were maintained within the probe and sample line.
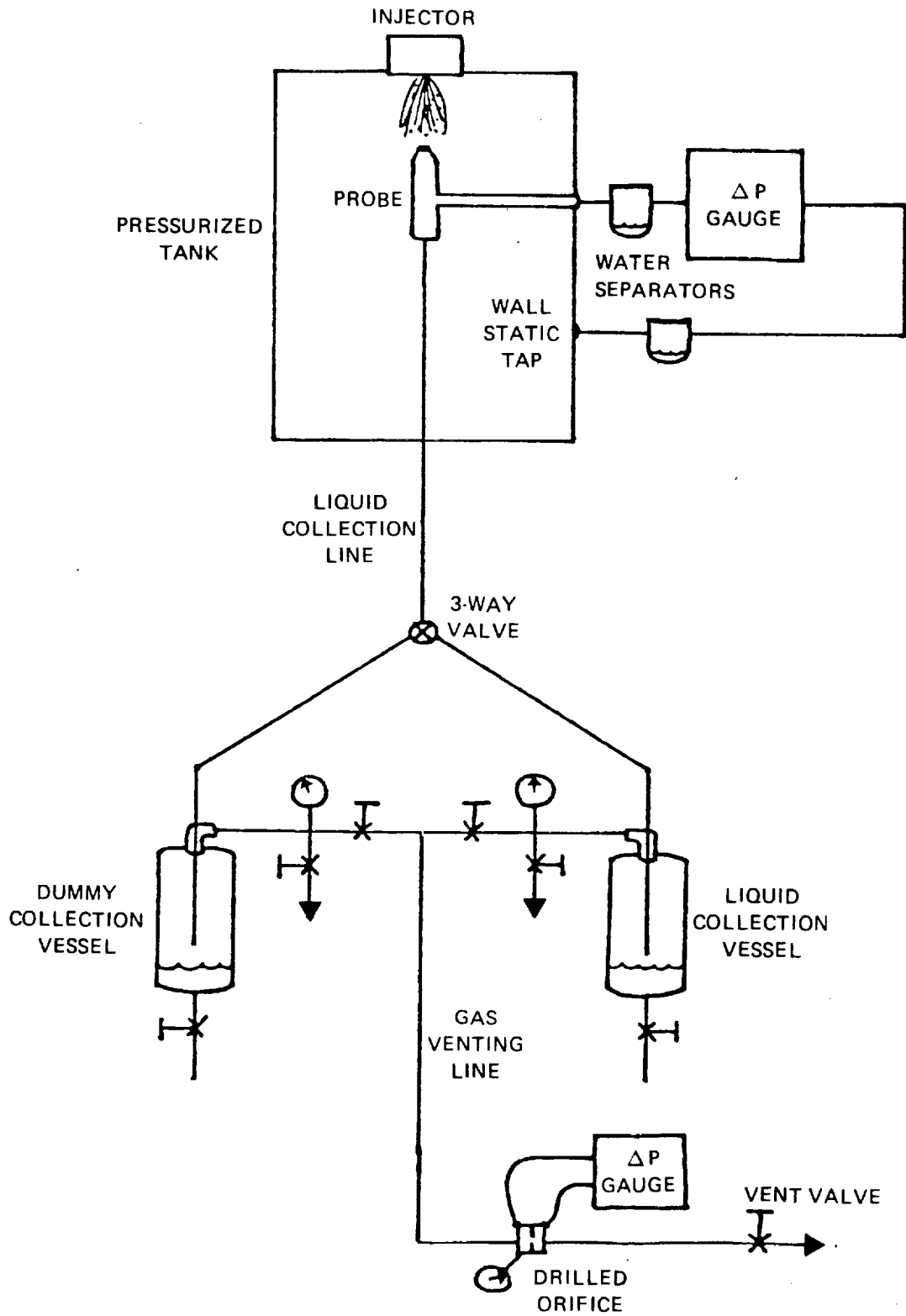
Figure 4-2. New Gas/Liquid Mixing Measurement Test Apparatus

6. Static Pressure Measurement Location: In earlier testing, the static pressure measurement (required for gas mass flux mapping) was made at the test vessel wall. This simplified measurement hardware and was believed to produce only minimal error. Measurements of static pressure across the chamber indicated that only minimal variation of static pressure occurred. However, it was anticipated that this error could be substantial at low velocity or high chamber pressure conditions. Accordingly, the gas/liquid mixing assessment procedure was modified to include a mapping of local static pressure (relative to the wall static tap). Thus the local total pressure (also referenced to wall static) could be related to the local static pressure to obtain more accurate local gas mass fluxes.

7. Data Reduction Programs: To ensure the accuracy of the computer code used to convert the gas/liquid mixing measurement data to mass flux and mixture ratio distributions and plots, and to compute mixing and collection efficiencies, a set of data was analyzed by hand and compared to code output. The sensitivity of the code to the quantity of data (number of measurements made) was also assessed. Results indicate that the code performed accurately, and the results were relatively insensitive to any reasonable quantity of data provided.

8. Recirculation: This appears to be the major problem with gas/liquid mixing measurements. The entrainment and recirculation of gases from outside the spray add considerable mass (several times the fuel gas flow) to the fuel gas. The traditional means by which this problem is circumvented is the addition of a curtain of flowing gas around the injector. This flow is referred to as curtain flow, purge gas, or bleed gas, and it serves to prevent recirculation into the measurement region. The oxygen content of the curtain flow gas is made different from the fuel gas, thus allowing (via oxygen concentration measurements) the curtain gas flow to be "subtracted out" of the measured total gas flow. This approach requires large curtain gas flow rates (in excess of ten times the injector gas flow). For high-pressure testing, the quantity of curtain gas flow would far exceed the existing high-pressure

nitrogen flow capabilities of the atomization and mixing test cell. Furthermore, there was considerable concern that the curtain flow significantly retarded the spreading of the fuel gas, thus affecting the fuel gas mass flux distribution.

Prior to the installation of an expensive high-flow-rate, high-pressure, nitrogen supply system to provide adequate curtain flow, it was deemed advisable to exper- imentally evaluate the changes made in the measurement procedures and apparatus (items 1 through 6). Accordingly, a high-backpressure (800 psig) mixing test was performed with the triplet element (element 2) at high flow rates. Since suffi- cient curtain gas flow was not available, a small narrow-angle, glass cone was placed about the spray in an effort to minimize recirculation. The results of this test were disappointing. Liquid collection efficiency was 223%, gas collec- tion efficiency was 719%, the total pressure was observed to fluctuate and vary over a wide range, and the results were not generally satisfactorily repeatable. The major problem is believed to be recirculation, which the glass shroud did not prevent. The injector flow was visually observed to fluctuate wildly, and des- pite all preventive efforts, water in the pressure lines is suspected to have affected the measurements. Pitot-static pressure measurements in heavily loaded, two-phase flows are very difficult, and there is little experience upon which to draw.

As a result of these findings, the following actions were undertaken:

1. Experiments were performed to demonstrate/determine the ability to make accurate pitot-static pressure measurements in known, well-defined, non- recirculating gas flows with liquid loading.

2. Analyses were performed to assess the effect of curtain flow on the fuel gas distribution.

Pending satisfactory results from these efforts, it was intended that a high- pressure nitrogen system would be "plumbed into" the test facility to provide the necessary curtain flow. These two efforts and their results are presented in the following.

MEASUREMENT CAPABILITY ASSESSMENT TESTS

The objective of these tests was to determine whether the basic measurement technique, with all incorporated refinements, was capable of accurately characterizing mass flux profiles in an ideal two-phase flow field, in the absence of recirculation. The test apparatus used to evaluate the optimum mixing measurement techniques developed under this contract is shown schematically in Fig. 4-3. A 40-horsepower blower was employed to produce a uniform, metered air flow through an 8-inch duct. At the exit section of the duct, a conical spray fan of water droplets was introduced by using a Delavan nozzle. The traversing assembly necessary to position the sampling probe was mounted on the duct outlet.

The sampling matrix comprised 128 data points -- 16 points spaced 0.25 inch apart from duct centerline to a radius of 3.75 inches, along 8 rays spaced by 45-degree increments. Four separate flow-field mappings were performed to obtain the ultimate two-phase, flow-field characterization. Initially, a local flow-field static pressure versus atmospheric pressure mapping was performed, using the static port of a conventional traversing pitot-static tube in gas-only flow. Since the two-phase sampling probe has no local static pressure sensing capability, its total pressure measurements must be referenced to the atmosphere. Thus the local static pressure mapping provides the correction necessary to compute true total pressure versus static pressure measurements at each point in the flow field. Also, when the pitot-static probe was used in gas-only flow, a total versus static pressure mapping was obtained. This was then used to compute the duct velocity profiles. These data indicated the flow was relatively axial (the effects of the upstream tube elbow were apparent, however), and no recirculation was present. These velocity data were subsequently used as the reference for isokinetic probe inlet velocities during liquid collection.

Following pitot-static probe mappings, a gas-only total pressure versus atmospheric pressure mapping was performed with the two-phase sampling probe. With the application of the local static versus atmospheric pressure correction at each point, the total pressure sensing capability of the larger two-phase probe was compared with the pitot-static gas/liquid flow mapping. Gas total pressures were recorded at each matrix point and liquid samples collected over 5-minute
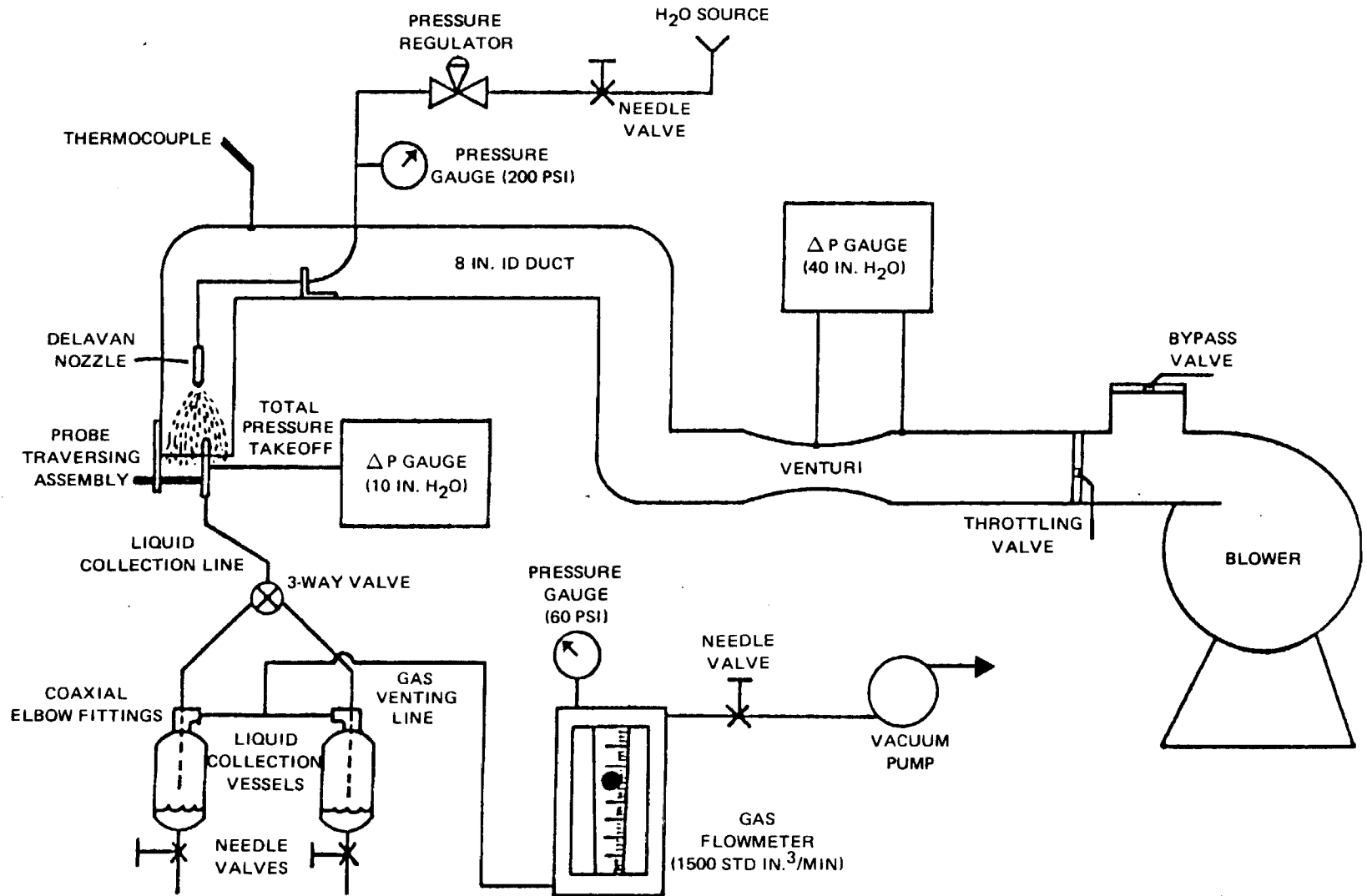
Figure 4-3. Gas/Liquid Mixing Measurement Capability Assessment Test Apparatus

time intervals. Near isokinetic liquid collection was produced at each sampling point by venting the appropriate air flow rate through the gas flowmeter shown in the schematic diagram, under the assumption of steady, incompressible air flow through the probe and liquid collection lines. Results of these tests follow.

Known duct air flow rate	2.568 lb/sec
Known liquid flow rate	0.089 lb/sec
Pitot-static probe, gas only flow	Gas collection efficiency = 1.094
Two-phase probe, gas only flow	Gas collection efficiency = 1.150
Two-phase probe, gas/liquid flow	(No overpressure correction) Gas collection efficiency = 1.160 Liquid collection efficiency = 0.926
	(With overpressure correction) Gas collection efficiency = 1.140 Liquid collection efficiency = 0.926

These measurements indicate that the gas/liquid mixing measurement techniques can produce marginally acceptable results. (Fourteen percent more gas and 7.4% less liquid were measured than were actually present.) However, these were very optimum test conditions (very lightly loaded with liquid - 3.3% water by weight, low pressure, and well-defined, nearly one-dimensional flow). In addition, this spray field was mapped far more extensively than would normally be done.

The next step in the verification of the measurement techniques employed was to be a similar measurement at higher pressure. However, before this effort could begin, results from the analysis of curtain flow effects on the injected gas were completed.

CURTAIN FLOW EFFECTS ANALYSIS

While the preceding results indicated that two-phase mass flux measurement might be possible in the absence of recirculation, the effect of the recirculation preventing bleed gas (curtain flow) on these mass flux measurements had to be ascertained. Recirculation had to be prevented and the bleed gas technique is

the only known means by which this can be accomplished. However, if the bleed gas significantly affected the fuel gas distribution, then the gas mass flux distribution measurements would not be representative of those produced by the injector in the combustor.

To examine this aspect of the problem, an analytical approach was employed. A sophisticated and complex computational fluid dynamics code was used to model the flow of fuel gas in the region between an injector and the normal measurement plane (2 inches below the injector). The code selected for the task was the Advanced Rocket Injector Combustor Code (ARICC) developed by Rocketdyne for NASA under contract NAS8-34929, Turbine Drive Combustor Ignition and Durability Program, and described in Ref. 4-2 and 4-3. ARICC is a time-marching, 2-D (axisymmetric) computational fluid dynamics (CFD) code with provisions for spray mixing and combustion. ARICC was developed from the Los Alamos CONCHAS - SPRAY code (Ref. 4-4). Features of ARICC include:

1. Multispecies mixing and diffusion
2. Lagrangian droplet dynamics
3. Droplet heatup and evaporation
4. Coupled gas - droplet mass, momentum, and energy transfer
5. Equilibrium and kinetic chemistry
6. Subgrid scale turbulence model
7. Choice of wall boundary conditions

The code is modular in format and modules can be added or deactivated, depending on the problem requirements. For this case of gas jet mixing, the chemistry, liquid jet, and droplet modules were not used. Modeling the droplet dynamics would have significantly increased the cost of the analysis.

The problem selected was an F-O-F triplet injector element flowing water and nitrogen into a 900-psia environment. The chamber was 2 inches in diameter by 2 inches long. Injector operating conditions were:

$M/R = 0.49$

$\dot{M}(H_2O) = 0.069 \text{ lbm/s}$ (oxidizer orifice)

$\dot{M}(N_2) = 0.141 \text{ lbm/s}$ (fuel orifices)

The orifice diameters were:

$D_{fuel} = 0.063 \text{ inch}$

$D_{ox} = 0.045 \text{ inch}$

The impingement angle was 50° and the impingement distance was 0.25 inch.

To address the problem in a timely manner using ARICC, several simplifications were made in the representation of the injected flow. The major simplification was to consider only the effect of purge gas on injected gas. (No liquid was assumed to be present.) The water flow was replaced by a stream of water vapor having the same axial mass and momentum flow as the liquid. The water vapor was mixed with the nitrogen flow. Based on conservation of mass and axial momentum, the velocity and diameter of a well-mixed jet of nitrogen and water vapor were calcu- lated. For simplicity, the injected water vapor and nitrogen flow was assumed to be a single specie at the average molecular weight for a flow at a mixture ratio of 0.49. The mass fraction contours of injected fluid could in this manner be easily tracked as a function of time. Three-dimensional details of the flow upstream of the impingement point could not be modeled with a 2-D/axisymmetric flow analysis. In view of this, an axisymmetric injection spud was used to introduce the injected stream to the impingement point. The spud diameter matched the diameter of the actual injector element disc that would be used in the experiment. A spreading angle that is a function of radial distance was imposed on the injected flow at the impingement point. The maximum angle was 45 degrees and corresponds to experimental observations. The mesh at the point of injection was set up with boundaries approximately parallel to the injected fluid streamlines, which served to minimize numerical diffusion. This computational mesh is presented in Figure 4-4.
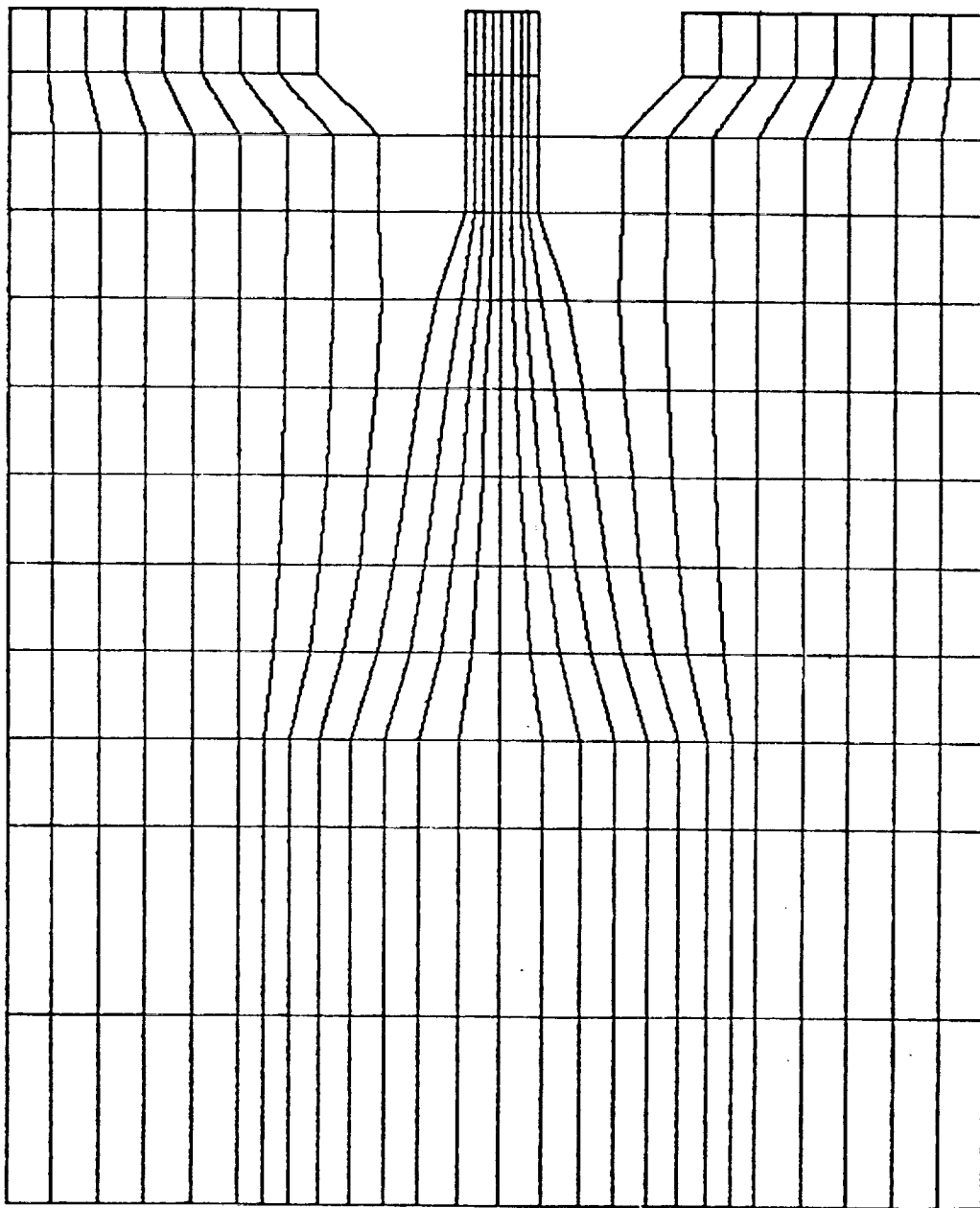
Figure 4-4. Computational Mesh

For the case with purge gas, a nitrogen gas flow of 2 lbm/sec was assumed to flow uniformly over the 2-inch-diameter chamber inlet except for the area taken up by the injection spud. According to Becker et al (Ref. 4-5), the value of the Curtet parameter that is sufficient to preclude recirculation, is 0.78. For the selected triplet conditions and the indicated purge flow, Ct = 0.66. Thus the purge gas flow used in this analysis was somewhat less than what would be employed in a test.

The computations were run until near steady conditions prevailed. Results were then plotted and comparisons of the injected gas distribution in each case were made. Figure 4-5 illustrates the radial velocity profiles at 9.5 stream diameters downstream of the impingement point for both cases. An artificiality in the injected velocity distribution shows up as an annular jet in the velocity profile for the case without curtain flow. An upstream recirculation zone wake is also seen in this profile. The results with purge flow suggest a developing jet profile. Fully developed coaxial jet data scaled up from Abramovich (Ref. 4-6) are shown for comparison with the purge flow case prediction. The close agreement with experimental data provides some degree of confirmation of these computations. Since the computed profile at the collection plane is only 9.5 injected stream diameters beyond the point of impingement, it is not surprising that the velocity profile shows some evidence of a potential core.

Computed injected mass flux profiles are plotted versus radial distance in Fig. 4-6 for the same axial location. Figures 4-7 and 4-8 show injected fluid mass fraction contours for the two cases. Contour lines occur at steps of 0.1 in mass fraction. From these two figures, it can be seen that the jet without curtain flow diffuses much more rapidly in a radial direction than in the case with curtain flow.

Velocity information plotted output from the ARICC code, at the time of these computations, was inadequate for presentation here. However, the velocity information has been used to construct the plots shown in Fig. 4-9. These two unscaled plots present the steady-state flow fields for the cases with curtain flow (left side) and without curtain flow (right side). While the curtain flow does not entirely eliminate the small recirculation zone near the injector, the
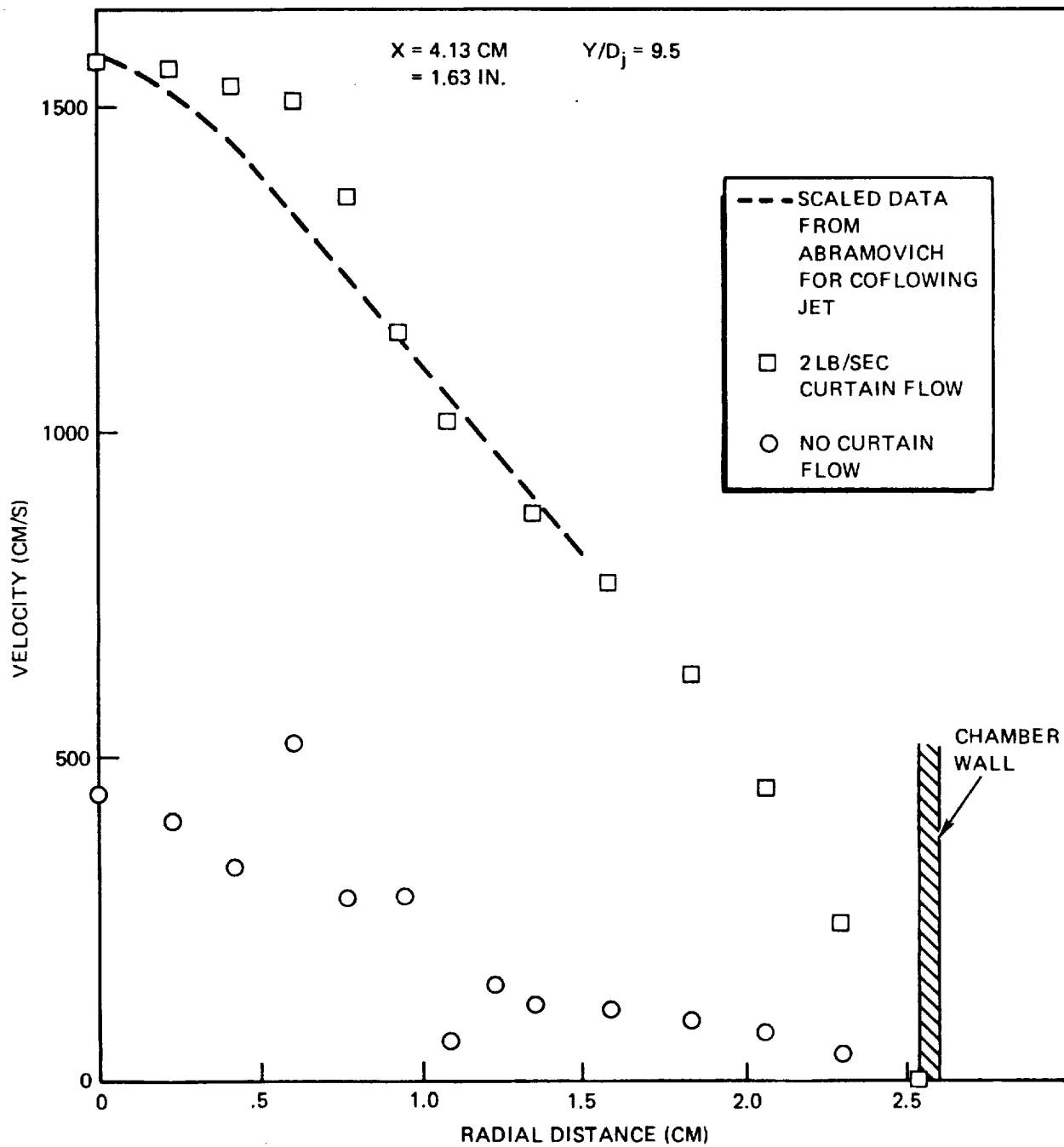
Figure 4-5. Velocity Profiles
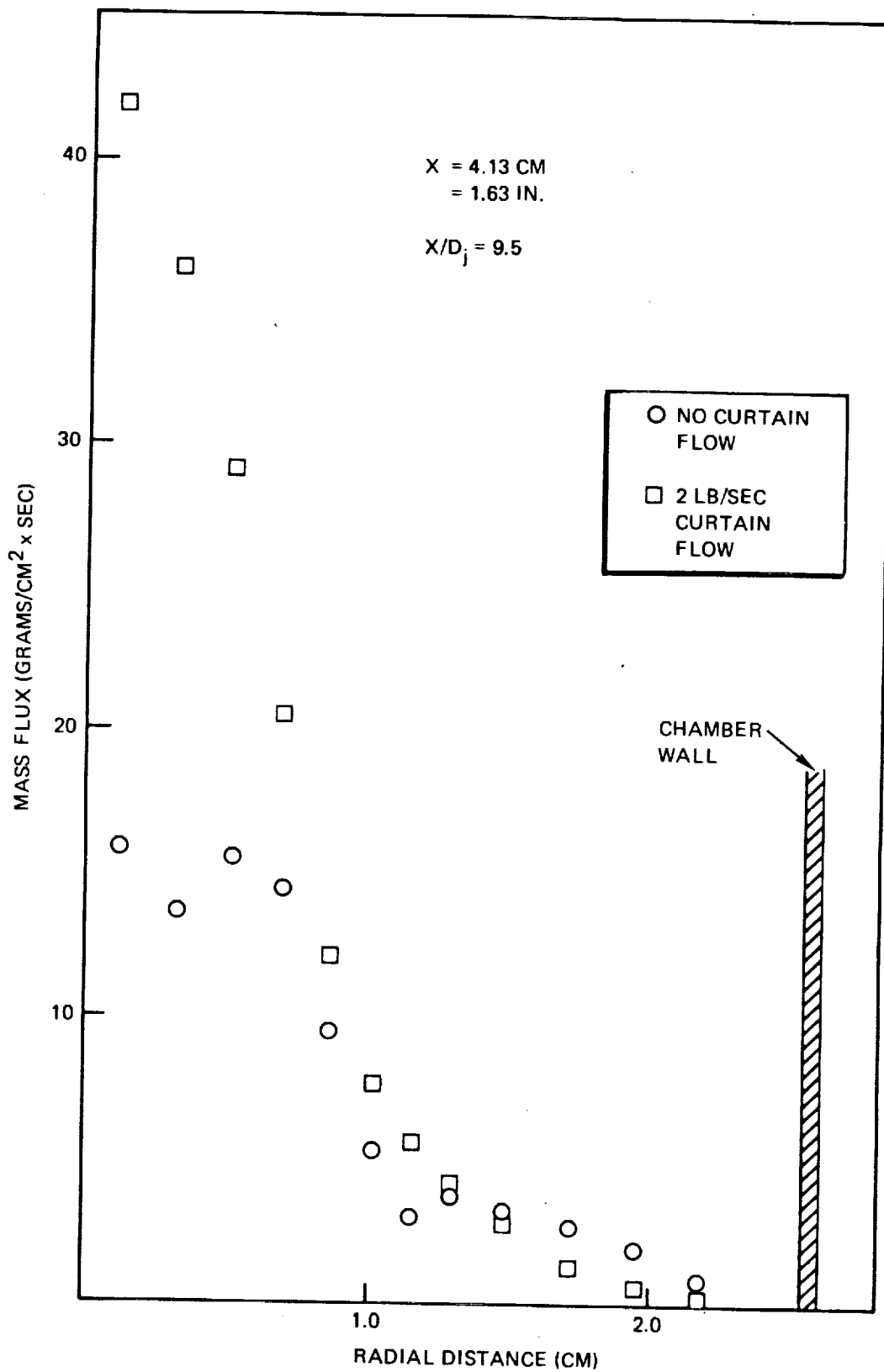
Figure 4-6.   Computed Mass Flux Properties

0.9 MASS FRACTION

0.8

0.7

0.6

0.2
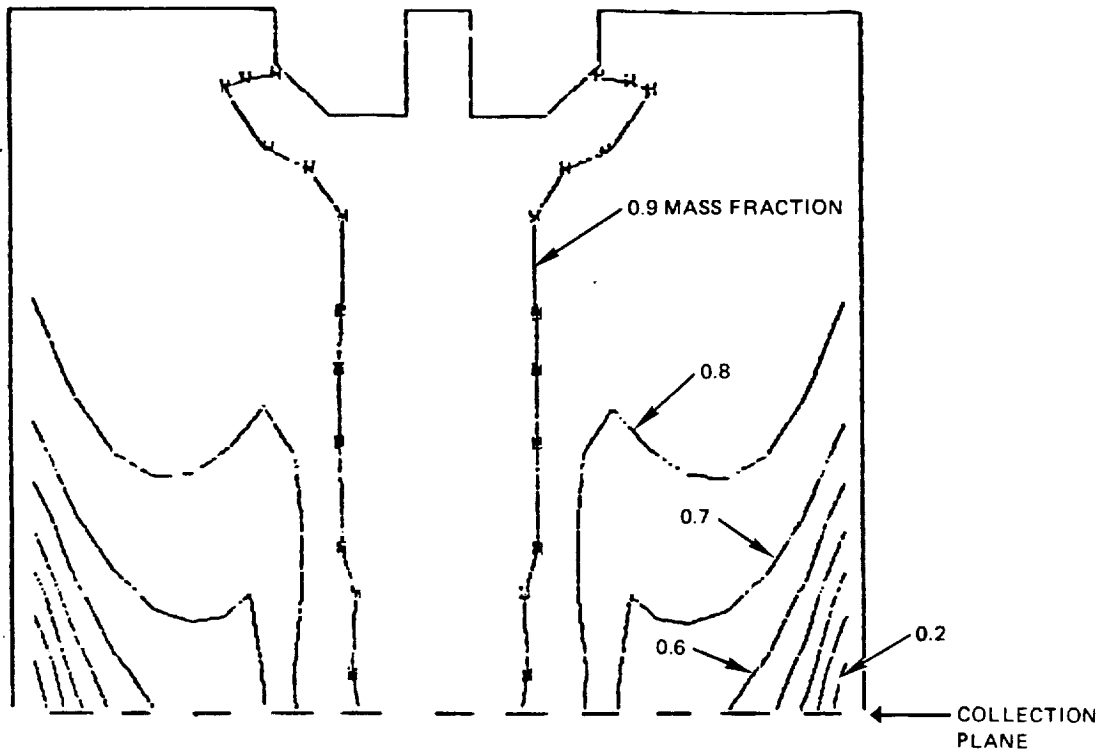
COLLECTION PLANE

Figure 4-7. Injected Species Mass Fraction Contours – With No Curtain Flow

0.9

0.3

0.2

0.1 MASS FRACTION
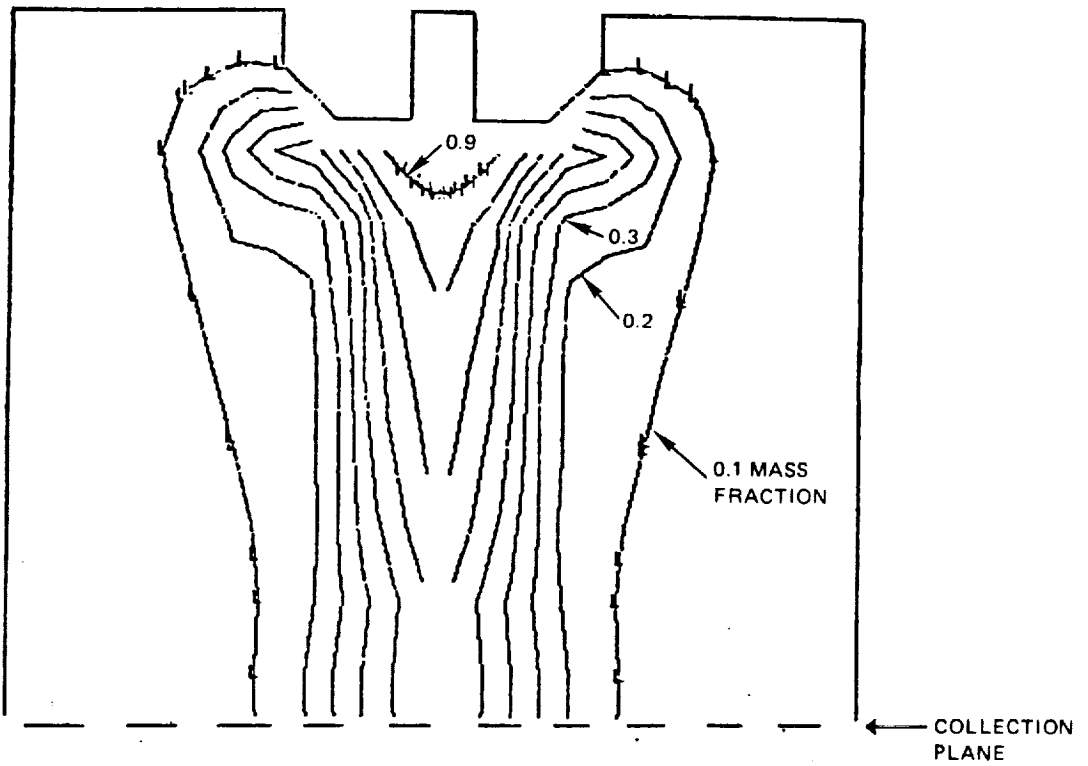
COLLECTION PLANE

Figure 4-8. Injected Species Mass Fraction Contours – With Curtain Flow

COLLECTION
PLANE

WITH CURTAIN FLOW   NO CURTAIN FLOW
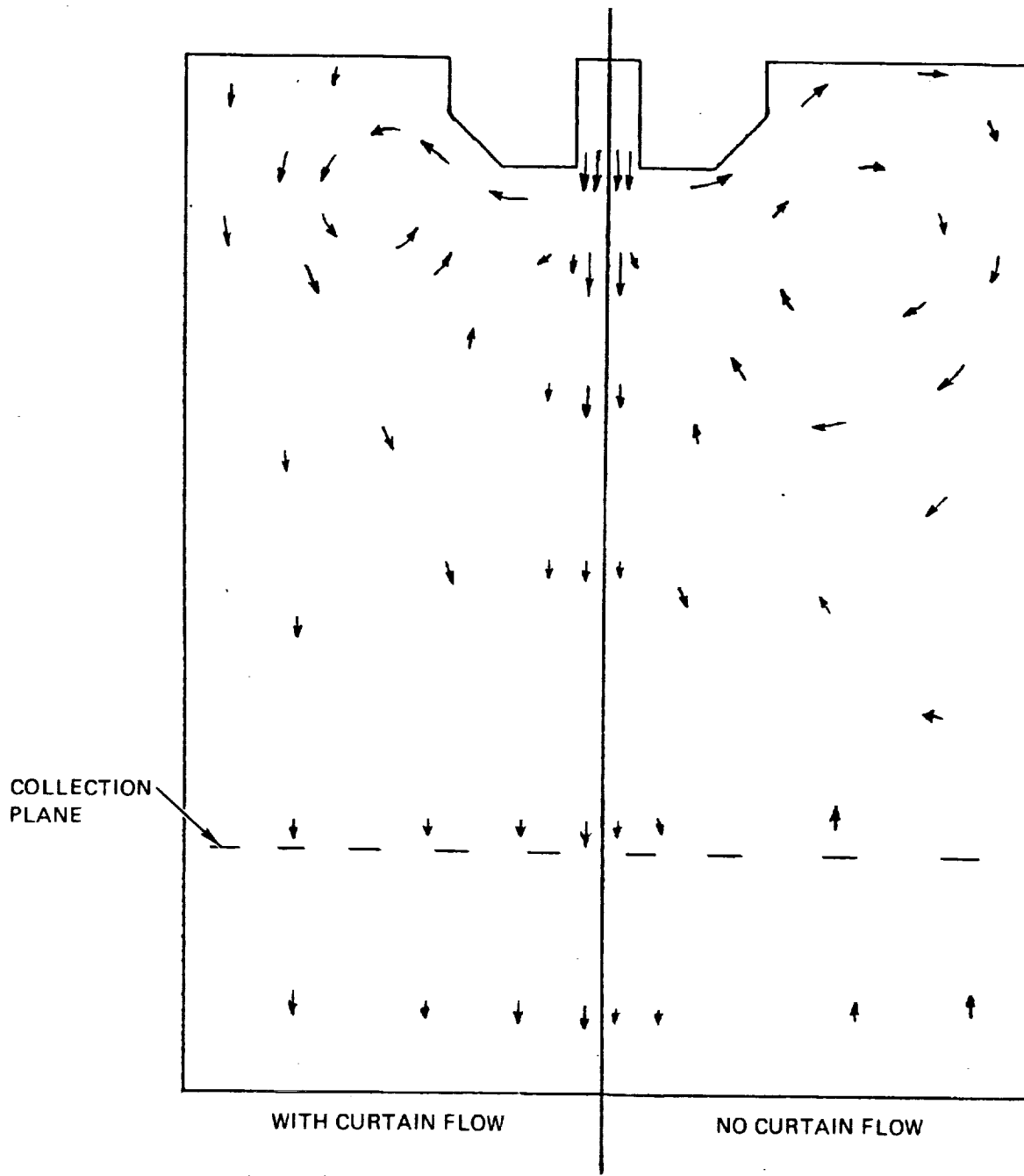
Figure 4-9. Gas Motion - With and Without Curtain Flow

flow at the collection plane is essentially axial. However, without curtain flow, the recirculation zone near the injector is much larger, and a second recirculation zone draws gas from below the collection plane upward and along the periphery of the chamber. Obviously the much greater recirculation of the non-curtain flow case would promote additional mixing. This is the cause of the greater spreading of the injected gas when no curtain flow is provided, as shown in Fig. 4-7.

As a result of these computations, it can be concluded that the purge flow does have a significant impact on the injected mass flux profile at steady state. The purge flow causes a change in the recirculation zone, resulting in a change in the radial flux of injected material. In a flow where a recirculation zone is dominant, the radial flow of mass and momentum is convection dominated. For the case where a purge flow suppresses the recirculation zone, less efficient turbulent diffusion controls the radial spreading of injected gas. Hence, the case with purge flow has a much higher centerline velocity and mass flux of injected gas.

CONCLUSIONS

As a result of these efforts, it is concluded that:

1. The modifications to the gas/liquid mixing measurement procedure and apparatus provide approximate and correct measurements at low liquid-loading levels and low pressure, and in relatively one-dimensional flows with no recirculation. Their ability to obtain correct data at high liquid-loading levels and pressure is not known. Recirculation must be prevented to obtain correct results.

2. The use of large quantities of curtain flow to prevent recirculation results in a very great modification of the fuel gas distribution, thereby invalidating the measured results.

Therefore, with regard to the utility and applicability of gas/liquid mixing measurements, the following are concluded:

1. Single-element gas/liquid mixing measurements may be of limited value for comparing the mixing performance of different elements or types of elements, and also may be of very limited value for assessing the relative effects of injector geometry or flow variables. Such measurements serve only as a relative comparison of mixing efficiency.

2. The use of such measurement data as input to the performance analysis codes (e.g., SDER), or to establish design criteria (e.g., optimum values of Elverum-Morey parameter) is not justified. Further testing of this type is not recommended.

3. Effort should be directed toward the development of a means to assess and measure injector mixing performance.

One very promising means by which this may be accomplished is the use of multidimensional CFD codes such as ARICC. Such codes can already model cold-flow gas motion with good accuracy, and can include the effects of droplets and combustion on gas dispersion. Modeling of the liquid phase (atomization, stream and droplet breakup, and droplet motion) is currently less developed, but efforts to improve such models are under way.

Another means for the measurement of the mixing performance of injectors is the utilization of advanced combustion diagnostic techniques such as Raman spectroscopy. These diagnostic techniques offer the potential capability to directly and nonintrusively measure combustor gas temperatures and compositions. Thus, they could provide the first direct measurements of hot-fire mixing efficiency.

V. ATOMIZATION

INTRODUCTION

Atomization data have long been recognized as one of the most important inputs to any spray combustion model. Both the droplet-size and droplet-size distribution have been shown (Ref. 5-1 and 5-2) to have a large effect on the computed performance of a liquid rocket combustor.

Reference 1-1 contains a detailed assessment and description of available liquid rocket combustor atomization correlations. In summary, the state of the art of atomization modeling is generally inadequate to meet present needs. The physics is only qualitatively understood at best. No quantitative theories exist. The available data and correlations generally are of questionable validity and/or utility. Many of the most critical parameters are unknown (e.g., combustion gas velocity field and multiple element effects) and/or are not simulated in tests (e.g., gas densities, real propellant fluid properties, and combustion gas motion). In addition, the measurement techniques generally used employ questionable assumptions or are incapable of sufficiently detailed or appropriate measurements.

Recognizing the importance of atomization data, and the poor quality of the presently available data, modelers have often used the initial droplet sizes as an adjustable parameter to calibrate their codes. Thus, when the code computations did not predict observed rocket combustor performance, the initial droplet sizes were modified to force agreement. This is the case with the three major performance assessment codes: SDER, CICM, and TPP.

Obviously this degree of uncertainty about one of the most critical inputs to a spray combustion code is not a satisfactory or acceptable situation. And yet, it has been accepted for some time, and little effort has been directed toward improvement. The last extensive program of liquid rocket atomization research was the "hot wax technique" study performed by Rocketdyne and completed in the very early 1970s.

The neglect of such an important area of study may, in part, be the result of a reduction in more basic liquid rocket research funding in order to support engine development efforts. It may also be caused by a lack of knowledge of (1) the importance of atomization data and (2) the inadequate level of quality of available atomization data for combustor analysis codes. And finally, neglect of this important research area is caused, at least in part, by the lack of suitable techniques for measuring droplet sizes accurately and rapidly. (Problems with these techniques are discussed in detail in Ref. 1-1 and 5-3.)

Over the past ten years, the state of the art of droplet-size measurement techniques has improved considerably. Lasers have been employed in a variety of ways to obtain hitherto unavailable information, and small computers have been employed to rapidly convert this information to droplet-size data and to compile and correlate these data. Droplet-size measurement instruments have been developed that utilize such methods as photography, pulsed laser holography, X-ray laser shadowgraphy, Fraunhofer diffraction, pulsed laser TV imaging, pulsed laser photography, high-speed cinematography, and laser interferometry. Many of these instruments and methods are "custom designed" by researchers for their own applications, but several have been developed and are sold commercially. These techniques have been employed in other atomization studies, primarily to evaluate the atomization of diesel, gas turbine, and larger commercial combustor fuel injectors, as well as other spray devices (e.g., agricultural sprayers and flue gas scrubbers).

In 1981, Rocketdyne began an in-house examination of these various drop-size measurement techniques and instruments, with the intent of applying one of these to the study of liquid rocket combustor injectors. These techniques were evaluated with regard to their capabilities in the following areas:

1. Nonintrusive (no flow disturbance)

2. Large sample size. (Several thousand droplets must be measured to obtain accurate distributions)

3. Speed of data acquisition, compilation, and analysis. (Technique must be automated as manual methods are too expensive)

4. 10 to 500 micron droplet-size measurement capability

5. No restrictions on test liquid properties

6. Vacuum to high-pressure test capability. [(Requires that technique be usable in pressure/vacuum vessel (i.e., window and access considerations)]

7. Specific and small measurement location. (Will provide spatial resolution of the spray)

8. Temporal (flux-based) rather than spatial (concentration-based) droplet-size data. (An important and often overlooked consideration. For a detailed description of this consideration, refer to Ref. 5-1 through 5-3, and ASTM standard E799)

9. Droplet velocity measurement capability

10. Applicability to reacting flows

11. Applicability to thick/dense sprays

12. Commercial availability. (Rocketdyne did not wish to become developer of such techniques, if possible)

Most of the techniques considered were relatively new, with little user experience or proven capability. Moreover, no standard spray exists by which to measure the effectiveness, accuracy, et al, of a drop-size measurement technique. Thus it is necessary to rely upon drop generators that produce single drop-size (monodisperse) and very dilute sprays, and upon the "reasonableness" of the measurements of sprays, to assess the validity of an instrument. This inability to verify the droplet-size measurements of new techniques and

instruments is a serious problem that continues to inhibit atomization studies, as it did the Rocketdyne efforts.

By mid-1981, Rocketdyne had selected the technique of droplet sizing interferometry as the most promising technique to employ in the study of liquid rocket atomizers. Arrangements had been made to lease and subsequently purchase a droplet sizing interferometer (DSI), manufactured by Spectron Development Laboratories, and supporting equipment for Rocketdyne IR&D studies of injector atomization characteristics. Also, a windowed pressure vessel was located at Rocketdyne, which appeared satisfactory for high-pressure injector atomization characterization. In October 1981, open-air tests of dilute sprays began. These were part of an IR&D project to develop familiarity with, prove, and implement this droplet sizing technique at Rocketdyne. Based upon the DSI manufacturer's reports and the fact that over a dozen of these systems were then in use in the U.S. and Canada, it was anticipated that this high-pressure droplet sizing capability would be easily and rapidly implemented at Rocketdyne. Accordingly, when this atomization and mixing study contract was announced by NASA-MSFC, Rocketdyne proposed to employ this advanced droplet sizing capability.

By the spring of 1982, the IR&D dilute spray studies had established that the DSI did not perform satisfactorily. While the DSI was easily and repeatably able to accurately determine the droplet size of a narrow stream of monodisperse droplets, the Rocketdyne testing clearly demonstrated that spray test results obtained with different instrument settings were quite inconsistent.

During the next year, Rocketdyne worked with the DSI developers at Spectron Development Laboratories in the development and testing of a second-generation DSI. The Rocketdyne primary function in this joint enterprise was to evaluate the new DSI and assist in the development of operating procedures. In February 1983, it was determined that this second-generation DSI (using the visibility/intensity technique later described) was performing satisfactorily.

Additional effort was then begun to develop and test the high-pressure atomization test capability. The high-pressure, windowed test vessel, DSI and associated equipment, and propellant simulant tankage, plumbing, and control

hardware were installed in a test cell in the Rocketdyne Engineering Development Laboratories. The test vessel (Fig. 5-1) is a 6.2 MPa (900 psig), man-rated, ASTM cylindrical pressure vessel with an inside diameter of 15.2 cm. The windowed section of the vessel is near the top. A single injector element could be mounted in the center of the top of the vessel. Gaseous nitrogen flow (bleed gas) was provided circumferentially about the element to reduce recirculation of the droplets. The injected propellant simulant and the bleed gas were exhausted from the bottom of the tank. The monodisperse droplet generator, which was required for alignment of the DSI, was modified to mount in the center of the top of the tank. A high-pressure feed system, with a very low and precisely controlled flow rate, was designed and constructed for the monodisperse droplet generator. The DSI alignment procedures were modified to account for the high-pressure windows, and the ability of the DSI to correctly measure the sizes of monodisperse droplet streams within the tank was confirmed.

The first attempt to make high-pressure, droplet-size measurements quickly demonstrated the inadequacy of the bleed gas flow. Even at the maximum facility flow rate, the bleed gas was incapable of preventing large quantities of liquid from being recirculated. Liquid was being drawn up along or near the chamber walls and pulled back into the main body of the spray. This recirculating liquid, combined with the main body of spray, was far too dense to allow DSI measurements. The velocity of the injected propellants was creating a low-pressure region near the injector face (in a manner similar to a jet pump). Also, the lower part of the tank was extremely turbulent and agitated. The recirculating gas was entraining some of this agitated liquid and flowing upward, along the cylinder wall, toward this low-pressure region. A variety of baffles and open celled, plastic foam wall liners were built and tested in order to minimize this recirculation. These were only partially successful. A more successful design (presented in Fig. 5-2) consisted of a combination of these baffles and foam, together with a set of tubes aligned axially along the periphery of the cylinder. This arrangement allowed the gases to flow through the tubes from the bottom of the tank to the top. Foam was placed over the tube ends to reduce water ingestion. This technique of controlled and filtered recirculating gases greatly reduced recirculating liquid.
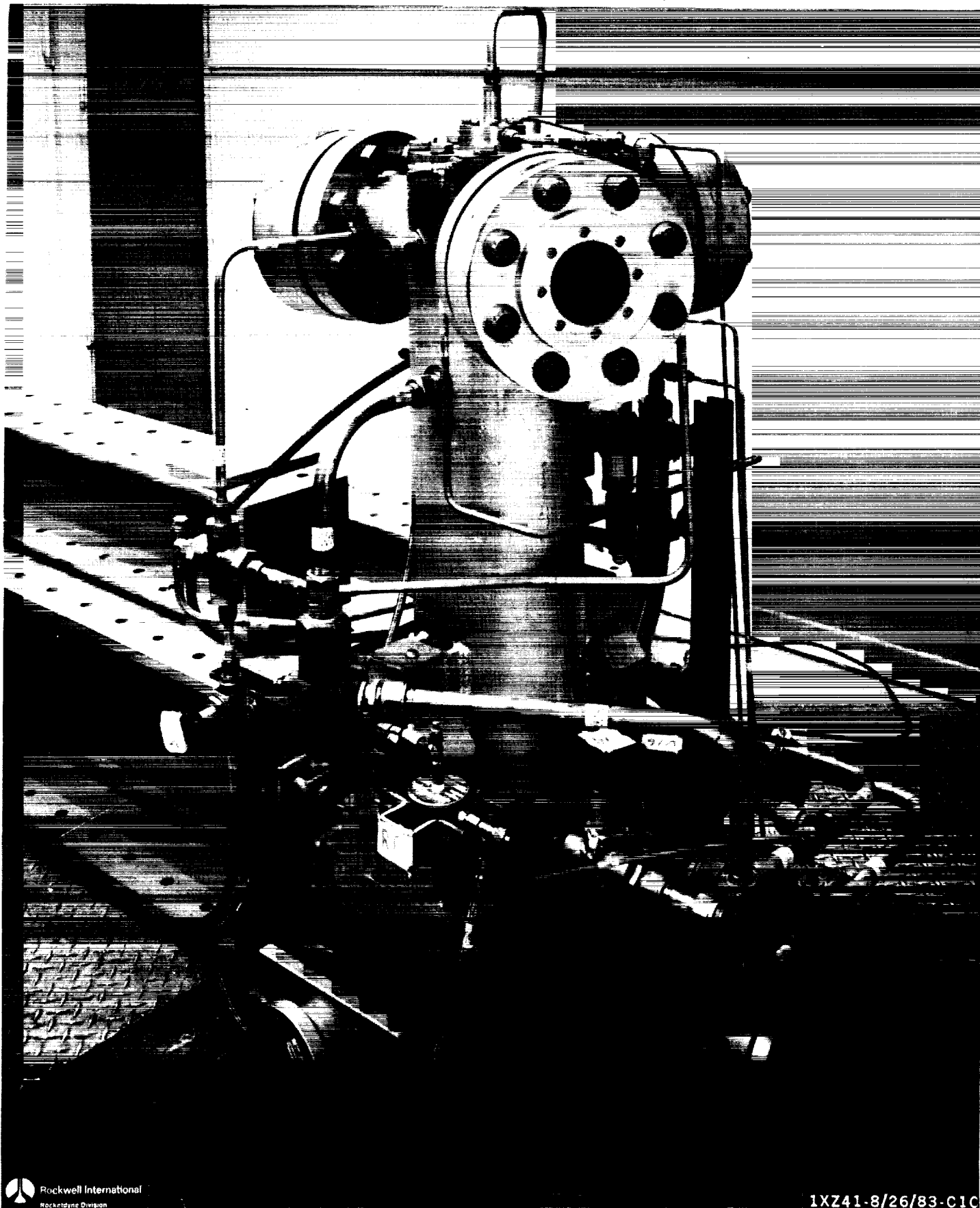
Figure 5-1. High-Pressure Atomization Test Vessel
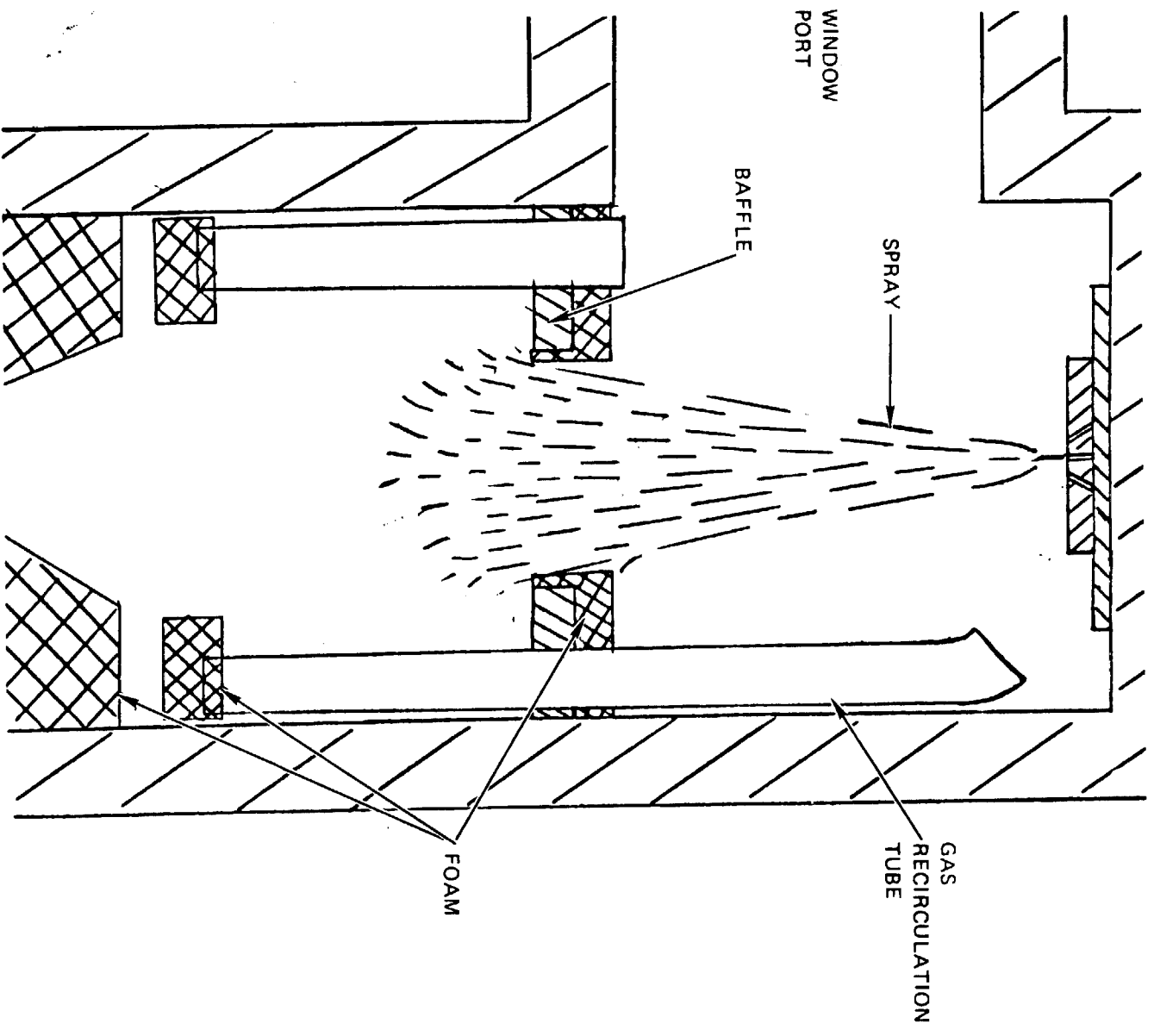
Figure 5-2. Test Vessel Recirculation Control Devices

WINDOW PORT

BAFFLE

SPRAY

FOAM

GAS RECIRCULATION TUBE

The DSI was realigned and calibrated, and attempts were again made to measure droplet sizes in the center of the sprays produced by the gas/liquid injectors at high pressure. Once more, it was found that the sprays were too dense. As will be described in the following section, the DSI establishes a very small measurement region within the spray -- the probe volume. As a droplet passes through this region, its size and velocity are measured. However, only a single droplet can traverse this probe volume at one time if the data are to be valid. The DSI recognizes and discards invalid data. If the droplets are too closely packed (i.e., the spray is too dense), then only rarely will a single droplet traverse the probe volume. The gas/liquid injectors of interest produce such dense sprays of very tiny droplets, that the DSI could not measure droplet sizes except near the edge of the spray. Even the lowest flow rate element (triplet element 4) produced sprays that were too dense. The droplets produced were smaller but just as densely packed. Three approaches were formulated to resolve this problem:

1. Reduce probe volume size: The sizes of the laser beams forming the probe volume were reduced to their minimum diameters. While this reduction improved the situation, it was not sufficient.

2. Develop and use an intrusive probe: A complex cone-shaped probe was designed, built, and tested to accomplish this. This probe is presented in Fig. 5-3. The function of this probe was to intercept a small portion of the spray (the part entering the small end of the cone), separate it from the main body of the spray, and spread the droplets over a larger area. All this must be accomplished without significant droplet breakup or collision with the probe wall. Preliminary testing was disappointing, and it appeared that the development of this technique would be a long-term research project. Therefore, since schedules and budgeting constraints were pressing, this approach was abandoned.

3. Make measurements further downstream of the injector: As sprays move downstream from the injector, they spread and the droplet density decreases. Open-air tests were performed that demonstrated which
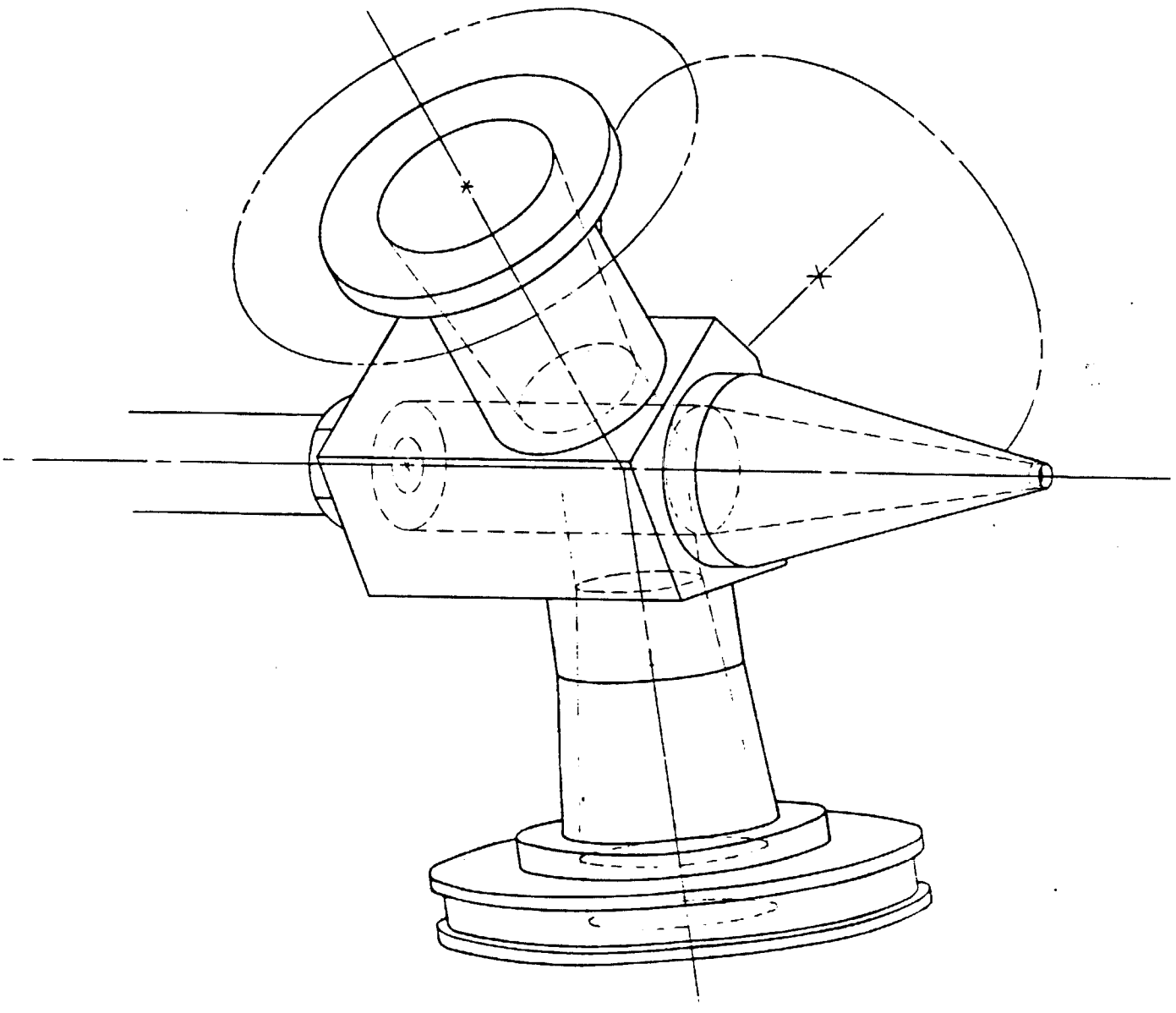
Figure 5-3. Intrusive Probe

measurements could be made far (as much as 1 meter) from a fully flowing injector. Unfortunately the test vessel was designed for spray mappings only a few (up to 10) centimeters below (downstream) of the injector. Also, the test vessel had an inside diameter of only 15.2 cm, which was insufficient to allow adequate spreading of the spray. Thus this approach could not be applied in this test vessel. No other suitable pressure vessel was available.

As a result of this unresolved problem, a decision was made to delete the high-pressure atomization testing and to perform all such tests unconfined (i.e., at atmospheric pressure). An open-air test apparatus was constructed. The test procedures, apparatus, rationale, plan, and results are later described in detail. All this effort to establish this atomization test capability, as described, was performed with Rocketdyne funding, and was not a part of the contractual program.

This decision to test at atmospheric pressure was driven by the previously discussed hardware and instrumentation (DSI) limitations. This approach was employed only as a last resort, as it was recognized that the extrapolation of the test results to the high-pressure conditions of interest would be difficult. Nearly all other atomization research programs have been similarly forced to perform their tests at atmospheric pressure. As reported in Ref. 1-1, essentially no high-pressure atomization data exist for liquid rocket injectors except for some very limited data obtained in support of the SSME development (i.e., coaxial injectors). Thus, a considerable need exists for high-pressure atomization data (one of the original goals of this program). Also, a lack of data to support extrapolation of atmospheric pressure data to high pressure remains (now one of the needs of this program).

DROPLET SIZING INTERFEROMETRY

This subsection describes the droplet sizing interferometry technique employed in this program. While a number of interferometric techniques have been developed to measure droplet sizes, this discussion is limited to the combined visibility/intensity (V/I) DSI technique employed on this program.

As with all DSI techniques, this technique employs a laser, beamsplitter, and appropriate optics to cause the two beams to intersect at a point within the spray where the drop sizes are to be determined (see Fig. 5-4). The intersection of these laser beams produces an interference region—a series of fringes covering the region in space where the beams overlap. This region is referred to as the probe volume. This probe volume may be quite small, perhaps as small as 100 microns in diameter and a few hundred microns in length, and is of an ellipsoidal shape. Collection optics are provided that image this tiny probe volume on a photodetector. Now, as a droplet passes through the probe volume, it scatters light (by refraction and reflection) onto this photodetector. This produces a signal similar to the plot of intensity vs. time shown in Fig. 5-4. This signal is referred to as a Doppler burst or signal, and consists of two components: an ac component superimposed on a gaussian-shaped signal (the "pedestal"). The ac component results from the passage of the droplet over the alternating bright and dark fringes. The pedestal is caused by the gaussian intensity profile of the laser beams. The fringe spacing, which is determined by the optics of the system, and the measured frequency of the ac component can be used to compute the velocity component of the droplet normal to the fringes. The velocity is simply the fringe spacing (the distance the drop travels between fringes) divided by the period of the ac signal frequency (the time required to travel that distance). This technique is commonly referred to as laser doppler velocimetry.

This Doppler signal can also be used to determine the size of the droplet through the concept of visibility. Visibility is a measure of the size of the ac component relative to the pedestal. This relationship and its derivation are described in detail in Ref. 5-4 and 5-5. However, by referring to Fig. 5-5 it may be possible for the reader to obtain a qualitative understanding of how visibility can be related to droplet size. Figure 5-5 presents typical signals that may be obtained for a small droplet (upper plot) and a large droplet (lower plot) passing through the probe volume. The small droplet produces a weaker overall signal than the large droplet, simply because of its smaller size and consequent lesser light-scattering ability. In addition, the small droplet produces a signal in which the ratio of the ac component to the pedestal (i.e., the visibility) is high. Because the droplet diameter is much less than the fringe spacing,

LASER

TRANSMITTER
OPTICS

BEAM
SPLITTER

COLLECTION
OPTICS

INTENSITY

TIME

I_{MAX}

I_{MIN}

PHOTODETECTOR

SIGNAL PROCESSOR
(DETERMINES DOPPLER
FREQUENCY OF
SCATTERED LIGHT)

δ

MEASUREMENT
VOLUME

PARTICLE WITH
VELOCITY U AND
DIAMETER d
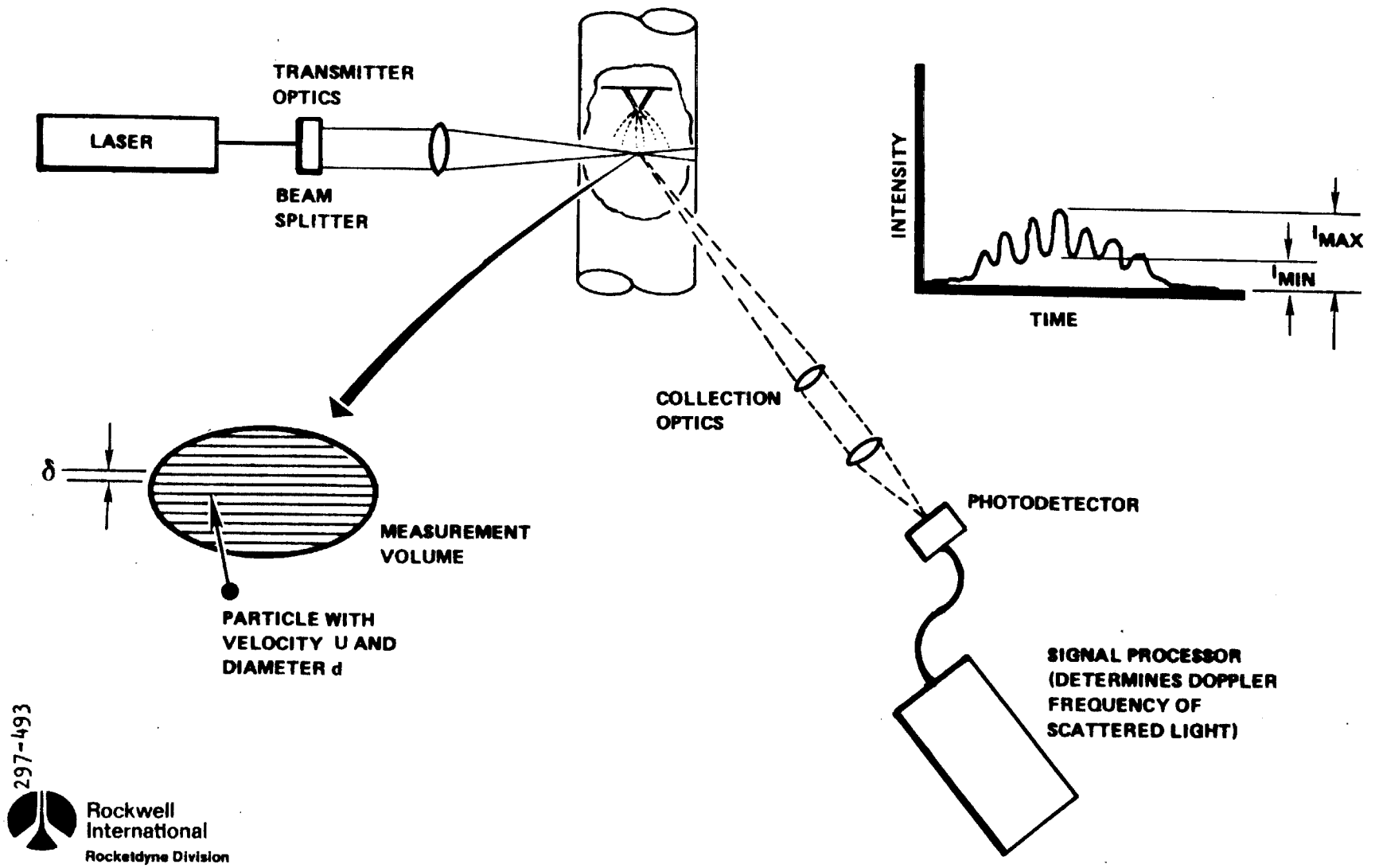
297-493

Rockwell
International
Rocketdyne Division

Figure 5-4.   Droplet Sizing Interferometry

238-934

Rockwell International
Rocketdyne Division
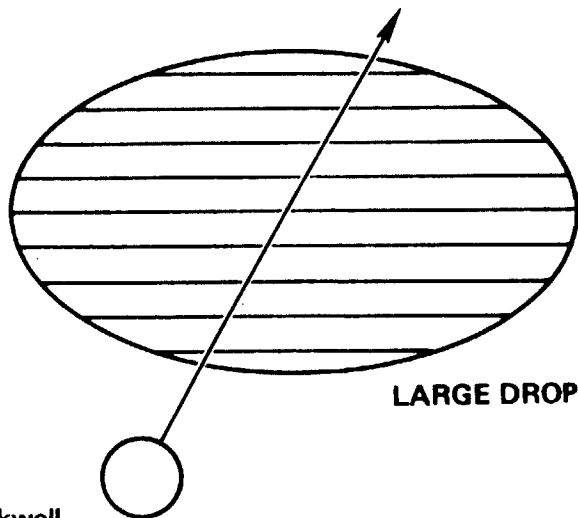
• **SMALL DROP**
HIGH VISIBILITY

DETECTOR OUTPUT

TIME

$$V = \frac{I_{MAX} - I_{MIN}}{I_{MAX} + I_{MIN}}$$
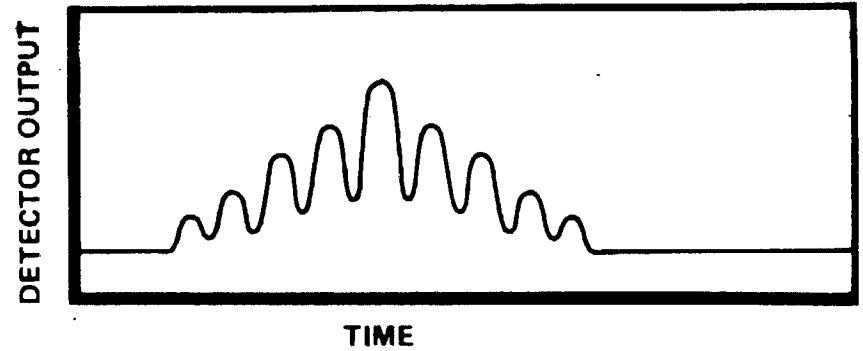
• **LARGE DROP**
LOW VISIBILITY

DETECTOR OUTPUT

TIME

LARGE DROP

Figure 5-5.   Droplet Visibility

smaller droplets have more fluctuation in their Doppler signal. When the droplet is in a bright fringe, the entire droplet is illuminated, and a relatively strong signal is detected. When the droplet passes through a dark fringe, it scatters almost no light, and the signal drops nearly to zero. Conversely, the large droplet overlaps fringes so that it is never totally in darkness or completely, brightly illuminated. Hence, its signal does not fluctuate as much. Thus it can be seen that small droplets produce signals having high ac components relative to the pedestal (i.e., high visibility), and large droplets produce signals having low ac components relative to the pedestal (i.e., low visibility). It is important to recognize that visibility is a relative measurement. Thus, if droplets only pass through the edge of the probe volume, where the fringes are less bright, the strength of both the ac and the pedestal signals is reduced. However, their respective magnitude relative to each other (i.e., the visibility) remains constant.

It is also important to note that this technique requires that only one droplet at a time be present within the probe volume. Also, this technique is based upon the assumption that perfect interference exists between the laser beams. The beams must be of equal intensity and phasing so as to produce fringes of very high contrast (e.g., extremely black, dark fringes and bright, light fringes). If the fringes become smeared (lower fringe contrast), so that the intensity of the bright fringes is reduced and the brightness of the dark fringes is increased, then the ac component of all Doppler signals is decreased. However, the pedestal is relatively unaffected, and therefore, the visibility is also decreased. This condition then makes all the droplets appear larger than they really are.

The original DSI that Rocketdyne planned to utilize was based upon this visibility technique. While the DSI performed very well on a narrow stream of monodisperse droplets, Rocketdyne testing demonstrated its inability to make accurate, or even approximate, measurements in a distributed spray of modest density. The problem was determined to be a result of poor fringe contrast. The major cause of this poor fringe contrast was the passage of droplets through the beams prior to their intersection. This action had the effect of selectively reducing the intensity (or perhaps altering the phasing) of one or the other of the laser

beams. Thus, the fringes were of poor contrast, and the droplet sizes measured were often incorrect.

It was impossible to prevent the droplets from passing through the beams without somehow shielding the beams from the spray (i.e., placing something intrusive into the spray). This solution was not acceptable. Instead, a modification of the visibility technique was employed to circumvent the problem. This modified technique employs the absolute amplitude of the signal (i.e., the intensity of the light scattered by the droplet) as an additional measure of droplet size. The droplet visibility is measured and the droplet size inferred from visibility as previously described. In addition, the peak value of the signal (peak intensity) is measured. This peak intensity is also a measure of droplet size, as larger drops scatter more light. Thus two separate measures of droplet size are obtained, which are compared by the DSI instrumentation and, if they are not within tolerable agreement, that measurement is rejected. Thus, the intensity droplet-size measurement is used to confirm the visibility droplet-size measurement. This combined technique is referred to as the V/I DSI technique. The preceding discussion of the V/I DSI technique is considerably simplified and neglects a number of important issues and features. A more detailed description of this technique is presented in Ref. 5-6.

TEST APPARATUS AND PROCEDURES

Test Configuration

A pictorial view of the test facility is shown as Fig. 5-6. The DSI He/Neon laser is shown in the lower left of this photograph. A single laser beam is split within the laser assembly to form two coherent beams that converge to form the measurement probe volume. In the view shown, the Berglund-Liu droplet generator (upper left) is operating to form a monodisperse droplet stream for calibration of the DSI system. Light scattered by droplets traversing the probe volume is collected by a photodetector cell in the DSI receiver (mid-right). Electrical signals are generated from the reflected/refracted light, and the signals are transmitted to a data processor (not shown) for visibility and intensity evaluation. Valid data from the processor are then stored in the computer for

DSI MEASUREMENT
TEST FACILITY
CONFIGURATION
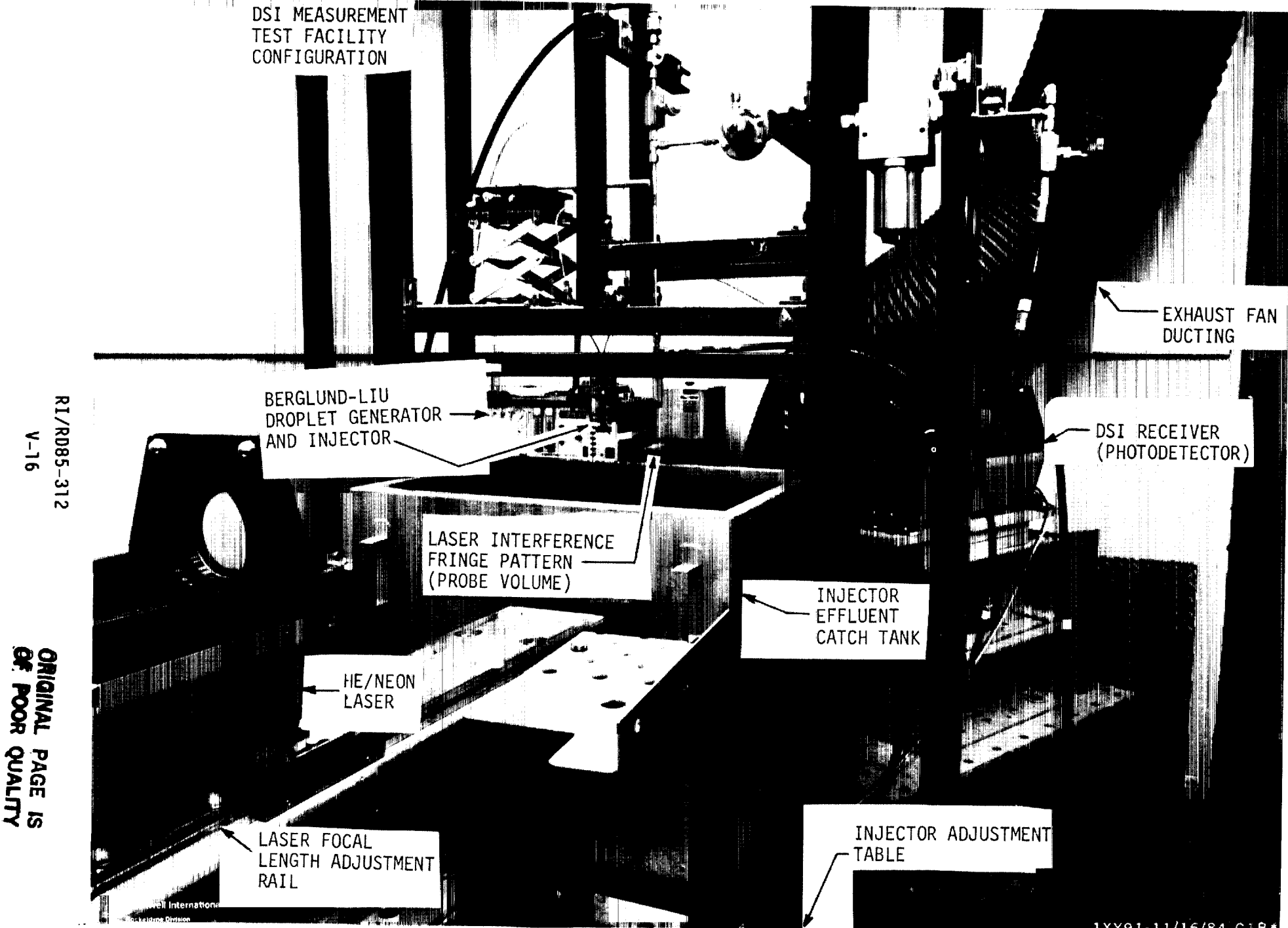
EXHAUST FAN
DUCTING

BERGLUND-LIU
DROPLET GENERATOR
AND INJECTOR

DSI RECEIVER
(PHOTODETECTOR)

LASER INTERFERENCE
FRINGE PATTERN
(PROBE VOLUME)

INJECTOR
EFFLUENT
CATCH TANK

HE/NEON
LASER

LASER FOCAL
LENGTH ADJUSTMENT
RAIL

INJECTOR ADJUSTMENT
TABLE

JXY91-11/16/84-C1B

Figure 5-6. DSI Measurement Test Facility Configuratio

immediate visual presentation. These data may be transferred to a floppy disc for subsequent retrieval and presentation in various forms.

Prior to each test, pretest inspection and alignment are conducted on the DSI system to verify that the system is operating properly. Measurements are conducted to confirm that the laser beam focus, spacing, and beam intensity are satisfactory. The DSI signal processing equipment settings are appropriately set, and the DSI data collection and processing computer software is initialized and appropriate inputs provided. An oscilloscope with a signal storage capability is set up to monitor the Doppler burst signals from the DSI receiver photomultiplier tube.

A Berglund-Liu monodisperse droplet generator is used to calibrate the DSI measurement system prior to each test. The Berglund-Liu droplet generator is designed to generate a stream of precise, constant diameter droplets by dispersing a constant liquid flow rate at a specified injector vibration frequency. The injector vibration is produced by a piezoelectric crystal powered by appropriate signal generation equipment. The DSI optics are adjusted to obtain maximum data rate output and to obtain close agreement (within 5 microns) between the measured DSI droplet size and the known droplet size produced by the Berglund-Liu droplet generator. The Berglund-Liu droplet generating system is very sensitive to contamination within the fluid system, irregularities of the pulsing orifice diaphragm, variations of the fluid upstream pressure, and other unknown factors. Frequently, calibration of the DSI system was prolonged (occasionally for several days) by problems with the Berglund-Liu droplet generator. Many of the problems caused by contamination were eliminated by placing a 0.5-micron filter in the liquid supply system immediately upstream of the injector. Also, immersion of the injector orifice diaphragm in a detergent solution whenever the diaphragm was not in use, reduced calibration delays. At other times, when no detectable cause for problems with the droplet generator was apparent, the replacement of the orifice diaphragm with a new diaphragm improved the performance of the droplet generator.

During the calibration procedure and the subsequent injector testing, a strobe-light was used to visually observe the monodisperse stream or the spray produced by the injector. Scanning of the frequency range of the strobe-light allowed the "periodic frequency" of a specific area of the injector flow field to be determined and "frozen" for visual study over a period of time. This capability aided in the determination of the spray characteristics.

DSI calibration was considered complete when adjustment of the DSI optics resulted in (1) a maximum data rate output at the processor, (2) a proper Doppler signal display on the oscilloscope (i.e., correct number of fringes and symmetrical and nondistorted signal), and (3) the agreement within 5 microns of the predicted Berglund-Liu generated droplet size with the DSI measured droplet size.

After completion of the DSI calibration, the x-y positioning table shown in Fig. 5-5 was adjusted by a thread/screw mechanism to locate the centerline of the injector at the laser probe volume spatial location. No adjustments were made to the DSI system after the calibration.

The desired liquid flow rate for the test was then obtained by adjustment of a small precision value in the injector liquid inlet line immediately upstream of the injector. The injector liquid effluent was collected in a calibrated container for a preset period of time and the valve adjusted to obtain the desired flow rate. The GN_2 flow was determined by measuring the upstream pressure and temperature of a calibrated sonic venturi in the facility gas supply system. To ensure sonic flow conditions, pressure measurements were also observed immediately downstream of the venturi. The GN_2 pressure was also measured immediately upstream of the injector.

All flow and pressure measurements for each injector test series were documented, together with other important test information on test data sheets. A typical test data sheet is presented as Fig. 5-7.

DATE _6-25-85_

SH _1_ OF _2_

TEST TYPE _ATOMIZATION TESTS (SPRAY FIELD MAPPING)_

INJECTOR CONFIG _Co-Ax #7_

DATA DISC # _13_   SERIES _N_

FAN $\times$ ON __ OFF

GN_2 VENT/ORIF _VENT_   DIA _0.032"_ F/M _____

P_{vent} u/s = _180_ psig P_{vent} d/s = _15.5_ psig

P_{inj} u/s = _3.2_ psig   FLOWRATE (LBS/MIN) ~~0.29~~ 0.260

Liquid _Dist. H_2O_

P_{inj} u/s = _____ psig   FLOWRATE (CM^3/MIN) _410 cm³/min_ = ~~2.24~~ 0.90 lb/min

MIXTURE RATIO (O/F) _~~3.75~~ 3.46_

$$D = 317 (.3/18.67)^{0.33} = 80.1 \mu$$

RUN NO	MEAS. LOC (X,Y,Z)	COMMENT
CC	—	Calibration $\begin{cases} \text{Predicted } D = 80.1\mu \\ \text{observed } D \approx 79-81\mu \end{cases}$
1,2,3	0,0,+9.25	1st of 2 Rays Mapped, Table Translation from
4,5,6	+.2,0,+9.25	Origin toward South Wall of Cell Along Y-axis;
7,8,9	+.4,0,+9.25	H_2O Flow Rate Verified @ Each Point
X	+.4,0,+9.25 →	Size/Velocity Correlation Run Corresponding to Run #8
10,11	+.6,0,+9.25	
12,13	+.8,0,+9.25	
14	+1.0,0,+9.25	No Data Criterion @ End of Ray: <1000 Counts/2min.
Y	0,0,+9.25 →	Size/Velocity Correlation Run Corresponding to Run #2

Figure 5-7. Typical Data Sheet

After verification that the target test flow rate and mixture ratio were satis-
factory, an exhaust fan was turned on to prevent recirculation of the injector
effluent. The exhaust fan system consists of a high-volume blower with a large
flexible duct connected to the injector spray catch pan (Fig. 5-6). The exhaust
system is effective in eliminating spray recirculation without affecting test
results. After the start of the blower exhaust system, DSI measurements of the
injector spray were initiated.

ATOMIZATION CHARACTERIZATION TESTING

The intent of these tests was to obtain a detailed mapping of the spray produced
by the nine baseline elements previously described and presented in Table 2-1.
Such mappings consist of droplet-size distribution plots at various points within
the spray. These may then be combined to produce droplet-size distributions
characterizing different portions of the spray and the overall spray. In addi-
tion, various representative droplet sizes characterizing the spray, such as mass
median, Sauter mean, and volume mean, can be computed from these mappings. These
results would then be available for use in the various liquid rocket engine com-
bustor codes.

Droplet Discrimination by Composition

All nine baseline injectors employ both propellants in each individual element.
Three of these are unlike impinging liquid/liquid elements, and the remaining six
are gas/liquid elements. The DSI technique cannot discriminate between droplets
of different composition and can only correctly size droplets of one composition
(one index of refraction) at a time. Thus, if two different types of droplets
are present, the DSI will only correctly measure those of one composition, and
those of the other composition will be incorrectly sized (unless they happen to
have the same index of refraction).

Furthermore, it will not be possible to distinguish one type of droplet from the
other. The two different drop-size distributions would be simply added
together. Almost every droplet-size measurement technique has this deficiency,
but it is only of importance to researchers interested in multiple liquid

atomizers, such as those in liquid rocket engines. With the exception of some small amount of "hot wax" test data (where water and wax were employed), no data exist on the droplet sizes of each type of liquid produced by unlike liquid injectors.

To circumvent this difficulty, tests were planned to investigate the feasibility of making one of the two injected liquids invisible to the DSI. These tests were to be accomplished, using dyes to absorb the incident laser light rather than refract it to the DSI receiver. If only one liquid were so dyed, its droplets would be invisible to the DSI. By an alternative dying of each liquid, the obtaining of separate droplet size data for each liquid was thought to be possible. However, prior to these tests being conducted, this technique was determined unworkable. Rocketdyne IR&D studies indicated that large quantities of mixed-composition droplets would occur. Even immiscible liquids would be expected to form such mixed-composition droplets. These mixed-composition droplets would be only partially visible to the DSI and would be incorrectly sized. As a result, this particular approach was abandoned, and the three liquid/liquid impinging elements were deleted from the testing.

Test Flow-Rate Considerations

Another problem area previously discussed was the chamber and DSI limitations that prevented higher-pressure testing. Thus, the open-air test apparatus described in the preceding section was constructed. This inability to test at higher pressure resulted in additional test difficulties as described below.

Once the pressure at the downstream end of the injectors (the backpressure) was limited to atmospheric pressure, flowing these injectors at any significant percentage of their design flow rates would result in pressure drops across the gas orifices of the injectors of at least several thousand kilo Pascals (several hundred psi). This result would, of course, require that these orifices be choked. If these orifices were operated in such a highly choked condition, the resulting gas flow would experience a rapid expansion upon exiting the injector. Such a flow would be characterized by a gas jet with complex expansion waves, a much larger diameter than the orifice, and a very high velocity. This result was

considered to be unacceptable. As will be subsequently discussed, where the test rationale and conditions are described, the gas stream diameter and velocity are important variables. Thus, all tests were performed with unchoked orifices.

To maintain the injectors unchoked, the gas mass flow rates employed must be very small. Also, since the ratio of gas flow rate (the atomizing force) to liquid flow rate (the quantity on which this force acts) was considered important, it was desirable to maintain mixture ratios comparable to those for which the injectors were designed. Thus, the liquid flow rates were also quite small. This generally resulted in liquid injection velocities of less than 0.5 m/sec. At these low liquid flow rates, the spray behaved in a most peculiar fashion. The two triplet injectors exhibited drastic changes in the spray pattern that were not repeatable. In some cases, streams of larger droplets were observed moving almost horizontally from the impingement point, or at a very large angle from the main body of the spray. This was especially apparent for the smaller triplet (element 4). Measurements of the sizes of these droplets were not obtained as this would have required a major modification of both the optical equipment (to measure these much larger droplets) and the test apparatus (to permit measurements so far from the main body of the spray). Furthermore, these strange spray patterns were not repeatable. At higher liquid flow rates (mixture ratios much higher than reasonable for testing), these effects disappeared and the spray appeared more normal and well behaved. It is believed that these peculiar spray patterns observed with the triplets result from the effects of surface tension (and perhaps small contaminant particles). The triplets, especially the smaller triplet, have much smaller liquid orifices than the other gas/liquid injector elements. At higher liquid injection velocities, surface tension forces would be negligible, but at these low flow rates, surface tension forces may be a significant factor influencing the atomization process. Such effects are, of course, unrepresentative of actual injector performance. Therefore, after several mappings of the main bodies of these sprays and after many attempts to obtain repeatable flows with the two triplet injectors, these two elements were deleted from the testing.

The sprays of the remaining four elements (elements 3, 5, 7, and 9 of Table 2-1, a pentad, and three coaxial elements) were found to be repeatable and relatively

well defined at the desired baseline test conditions. The sprays of the two preburners elements (the pentad and coaxial element 5) exhibited a few large droplets that are probably not typical of realistic sprays. Droplets were observed to form and grow on the face of the pentad and move about until they became large and contacted one of the gas jets. They were then blown off and atomized, producing a brief disturbance of that gas jet. This process occurred at such a low frequency, and had such little apparent effect on the spray, that it was not considered to jeopardize the validity of the droplet-size measurements. The preburner coaxial element produced a spray containing a very few larger droplets (i.e., greater than 100 microns in diameter), which were not included in the measured droplet-size distribution. At higher flow rates, these disappeared.

Thus, the elements tested in this program were the pentad and the three coaxial elements. Certain preliminary checkout tests, the rationale for the test plan, and the final test matrix follow.

Measurement Repeatability

Prior to beginning these tests, it was necessary to perform several checkout tests to ensure the validity and utility of the data. As a part of the test procedure previously described, the DSI was aligned and its droplet sizing capability confirmed via measurements of a monodisperse stream of droplets. This was done prior to each mapping. In addition, a number of measurements and spray mappings were made to confirm the repeatability of the measurements. Even with DSI realignment and recalibration, the repeated mappings never varied significantly (i.e., distribution peaks and representative droplet sizes never varied by more than about 5 microns) from the original mapping.

Measurement Plane

Another concern was the effect of the axial location of the measurement plane. All mapping measurements were made in a plane located 0.235 meter below the injector. This distance was chosen for several reasons. First, as previously discussed, the DSI performs better in dilute sprays. Making measurements at this

distance allows the spray to spread and become more dilute. Secondly, close to the injector, the spray may contain nonspherical liquid particles (ligaments and oscillating, deformed droplets). The DSI technique requires that the droplets be spherical. At greater distances from the injector, all the ligaments should be broken and the droplets stabilized to a spherical shape. To confirm that the spray was stable at the measurement plane, mappings were made at axial locations of 0.222 and 0.235 meter. The results were essentially identical.

Spray Mapping Orientation, Data Compilation, and Data Presentation

Once the DSI is aligned and calibrated, and spray droplet-size measurements begin, vast quantities of data can be obtained in very short times. The DSI measures the sizes and velocities of droplets at a particular probe volume location within the spray and at rates as high as several thousand droplets per second. Droplet-size counting rates in these mappings were generally much lower -- on the order of a few hundred counts per second or less. Droplets are counted for a period of up to 120 seconds, resulting in droplet counts of about 1000 to 10,000. Furthermore, the DSI only counts the droplets passing through the probe volume that lie within a particular velocity range. The velocity range can be modified, but is rarely large enough to encompass the total range of the droplet velocities within the spray. Thus, it is necessary to make two or three droplet-size measurements at each location and to subsequently add the droplets of similar sizes from each of these samples together.

The total number of droplets counted at a particular location within the spray, therefore, could exceed 20,000. Furthermore, to obtain accurate and representative droplet-size data for the entire spray, it is necessary to make measurements at a large number of locations. (The determination of the necessary number of locations is subsequently discussed.) Thus, it can be seen that the quantity of data obtained is immense, and data handling, compilation, and presentation prove a challenging task.

The droplet-size data are stored in a microcomputer that is a part of the DSI system. This computer has the capability to compile and output data from a single run. (All the drop sizes and velocities measured at a single point over

a single velocity range.) Such output consists of the number of droplet counts for each of 53 size groups or bins encompassing the measurement droplet-size range. Droplet velocities are similarly separated into bins. Fig. 5-8 and 5-9 are examples of the DSI standard output. In Fig. 5-8, the left plot is the droplet-size distribution and the right plot, the droplet-velocity distribution. The absicissa values for these plots are printed below the plots, together with a variety of information regarding DSI parameters. Also shown is the total number of counts comprising these distributions (7271 in this case) and the time over which this measurement was made (120.2 seconds). Figure 5-9 presents the plotted data in tabular form. The number of droplets in each size bin is defined in the first two columns and the number of droplets in each velocity bin is presented in the last four columns. Bins with less than five counts are not printed.

Note that the velocity distribution is incomplete. While there are apparently no droplets with higher velocities than were measured here (up to 22.6 m/sec), there are quite obviously many droplets having velocities below the minimum velocity of this measurement (7.25 m/sec). Since it cannot be assumed that slower droplets would have the same size distribution as these droplets, it would be necessary to obtain similar data at this spray location over at least the next lower-velocity range. The droplet counts per second of collection time in each of the nonoverlapping velocity ranges can then be added to obtain the complete distribution for that location. The DSI software can also produce special plots of droplet size vs. velocity.

The standard DSI software does not have the capability to add droplet distribution plots. Furthermore, to obtain representative droplet-size distributions characterizing selected regions of the spray or the entire spray, the distribution at each location must be suitably weighted by the area of the spray represented by that measurement location. The standard DSI software also does not have this capability. Accordingly, an additional data compilation code was constructed to perform these computations. An example of the output of this code is presented in Fig. 5-10, which is a compilation of all the droplet-size data for the coaxial element (element 7) at the flow conditions of test 21. Twenty-one separate droplet-size measurements, taken at various locations within the measurement plane of this spray, and over different velocity ranges, were

COUNTS

DIAMETER (MICRONS)   VELOCITY (METERS/S)
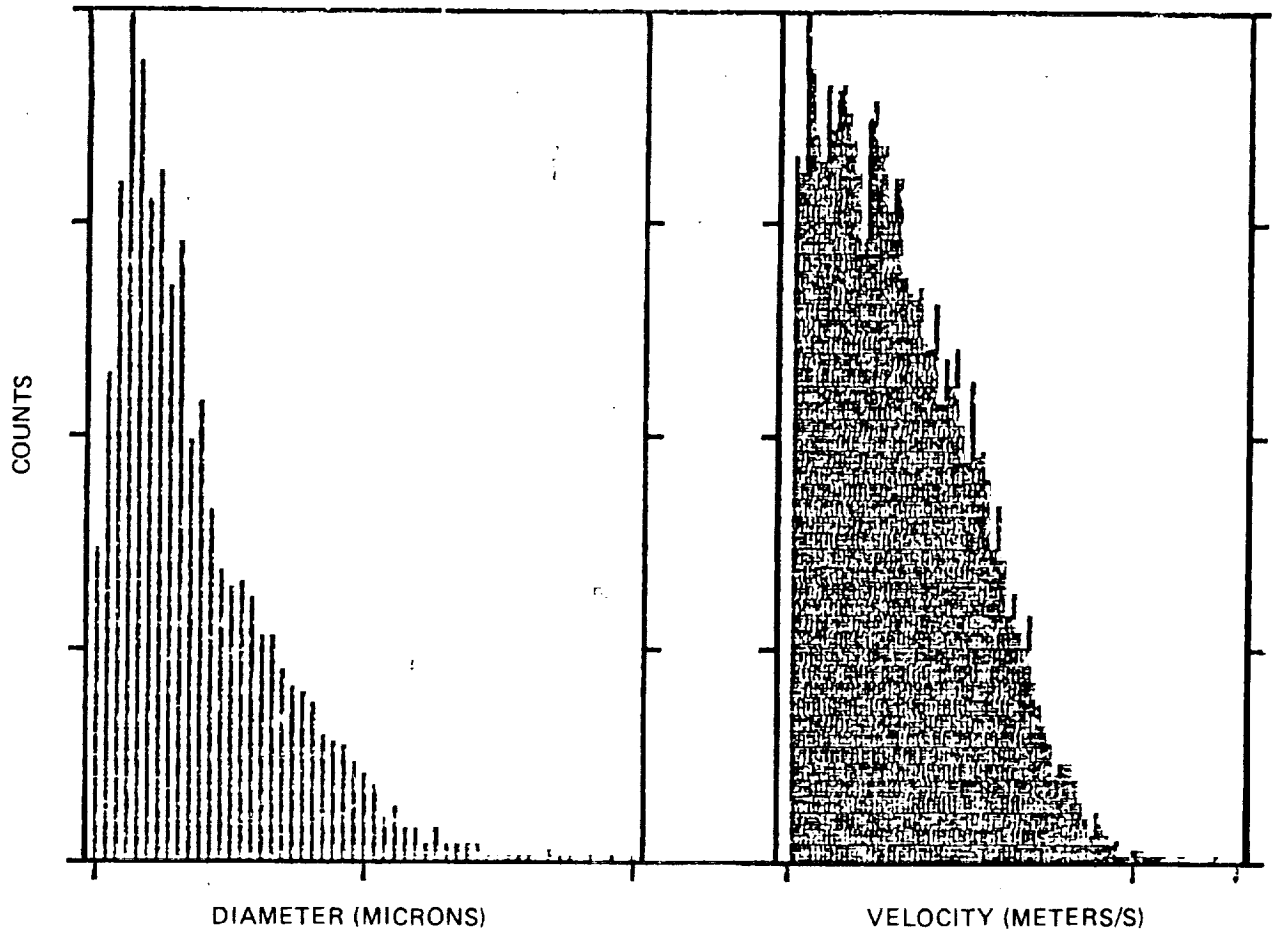
PLOT LABELS
    MIN DIAMETER: 9 MICRONS
    MID DIAMETER: 54 MICRONS
    MAX DIAMETER: 98 MICRONS
    MIN VELOCITY: 7.25 M/S
    MID VELOCITY: 14.88 M/S
    MAX VELOCITY: 22.6 M/S

TIME PERIOD: 120.2 SECONDS   VP-1001 STATUS
VALID VALOCITY SAMPLES: 7271
VALID SIZE SAMPLES: 7271   RANGE: 3
NORMAL ACQUISITION   FRINGE COUNT: 13
LASER WAVE LENGTH: 0.6238 MICRON   % ERROR: 3
COLLECTION FACTOR: 8   COMPARE: 12/6
FRINGE SPACE: 14.5 MICRONS   HIGH VOLTAGE: 329
BEAM SPACE: 40.8 MM   THRESHOLD V (MV): 0.48
XMIT LENS FOCAL LENGTH: 935 MM

Figure 5-8.   DSI Output Plots

R A W   D A T A   L I S T I N G

COMMENTS: INTRUSIVE DSI TESTS

DIA MIC	BIN COUNT	VEL IN M/SEC	BIN COUNT	VEL IN M/SEC	BIN COUNT
84	5	14	6	9.5	127
73	12	14	5	9.4	134
71	11	14	8	9.3	123
69	12	13	10	9.2	149
67	11	13	14	9.2	137
66	21	13	8	9.1	139
64	12	13	12	9	153
62	24	13	16	8.9	151
61	22	12	22	8.8	152
59	40	12	26	8.7	156
57	31	12	27	8.6	183
55	55	12	27	8.5	182
54	63	12	24	8.5	174
52	69	12	32	8.4	192
50	81	11	36	8.3	192
49	88	11	43	8.2	203
47	91	11	49	8.2	199
45	112	11	66	8.1	167
44	121	11	57	8	184
42	126	11	51	7.9	193
40	138	10	72	7.9	200
38	161	10	66	7.8	207
37	161	10	81	7.7	206
35	191	10	95	7.7	196
33	201	10	83	7.6	208
32	199	10	102	7.5	187
30	209	10	109	7.5	194
28	251	10	103	7.4	211
26	330	10	128	7.3	226
25	303	9.9	107	7.3	134
23	446	9.7	117	7.2	188
21	416	9.6	138		
20	497				
18	480				
16	579				
15	614				
13	492				
11	350				
9	225				

Figure 5-9.   DSI Tabular Output
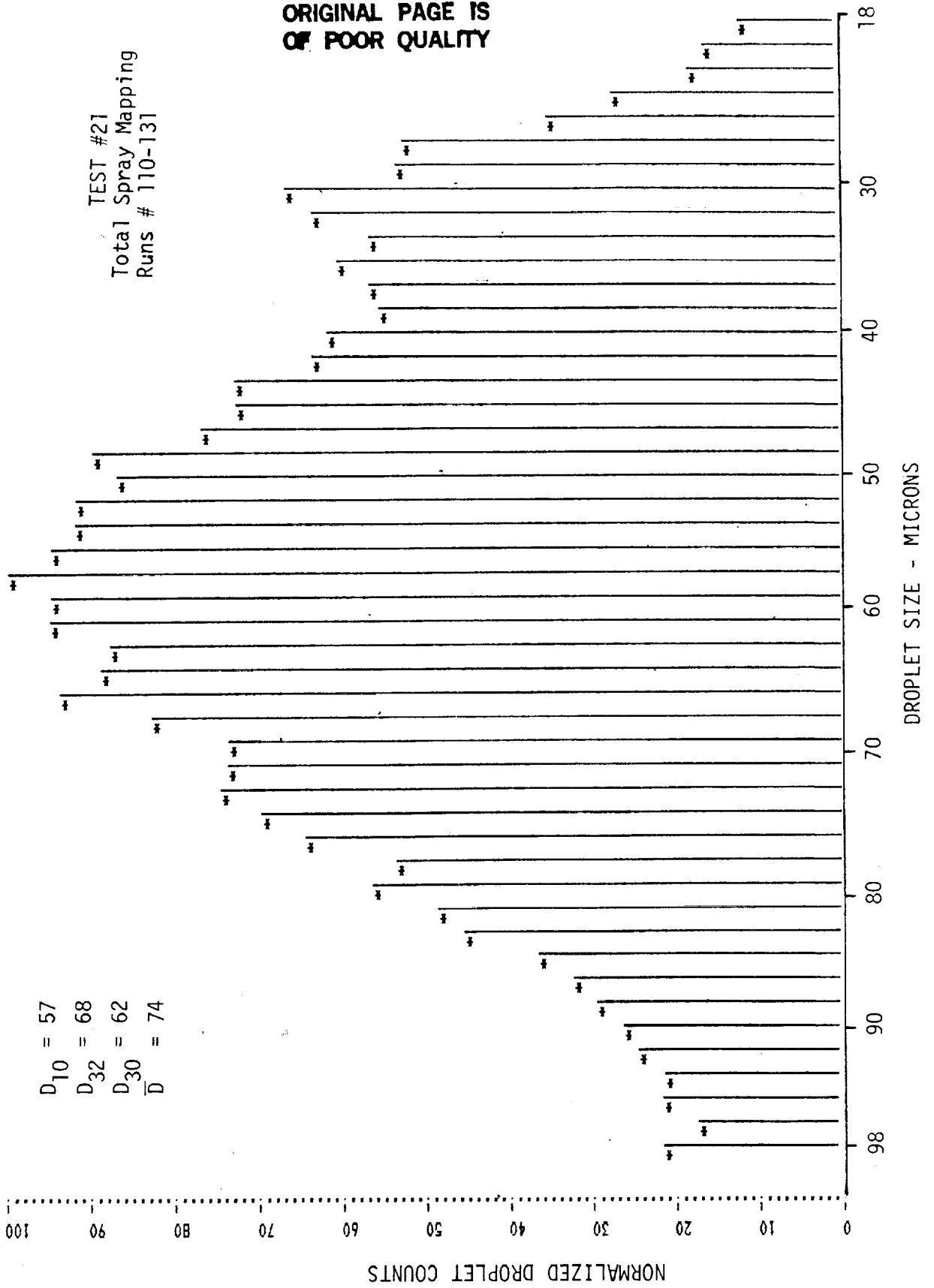
Figure 5-10. Typical Data Compilation Program Output

suitably corrected for sampling time, weighted for the spray area represented by each measurement location, added together, normalized to the largest bin, and plotted. In addition, several representative droplet sizes are computed from these data. These sizes are the mass medium diameter ($\bar{D}$), the volume mean diameters, (D_{30}), the Sauter mean diameter (D_{32}), and the linear mean diameter (D_{10}). It should also be noted that the droplet-size range of Fig. 5-10 is less than that measured by the DSI and presented in Fig. 5-8. The Rocketdyne data compilation program has been constructed to exclude the data in the five bins containing the counts of the smallest droplets. Based upon detailed examination of the methods by which the V/I DSI technique functions, it has been determined by Rocketdyne that these data are of highly questionable validity. Hence, they have been deleted.

Figure 5-10 contains the primary droplet-size information required by spray combustion modeling codes and provides a complete, overall assessment of the atomization characteristics of this spray. If more detailed information is desired, similar plots can be obtained for selected locations within the spray and for particular regions of the spray, as will be subsequently shown.

In many instances during these atomization tests, a substantial portion of the droplets was smaller than could be reliably measured with the DSI. In such cases, only the mass median droplet diameter is presented, as it would be least affected by the presence of the tiny drops. However, it must noted that in such cases, the reported mass median drop size is in error by some unknown amount.

To systematically record and specify the location of the measurements within the spray, a standard three-dimensional Cartesian coordinate system was employed. This system is presented in Fig. 5-11. The center of the injector element is at the x=0, y=0, z=0 point, and any location within the spray can be readily identified by it (x,y,z) location. As previously noted, the element is mounted on a framework resting on an x-y table that can be easily and precisely translated in the x or y directions. Thus, during testing, the coordinate system and spray are traversed in the x and y directions, and the DSI equipment and the probe volume remain stationary.
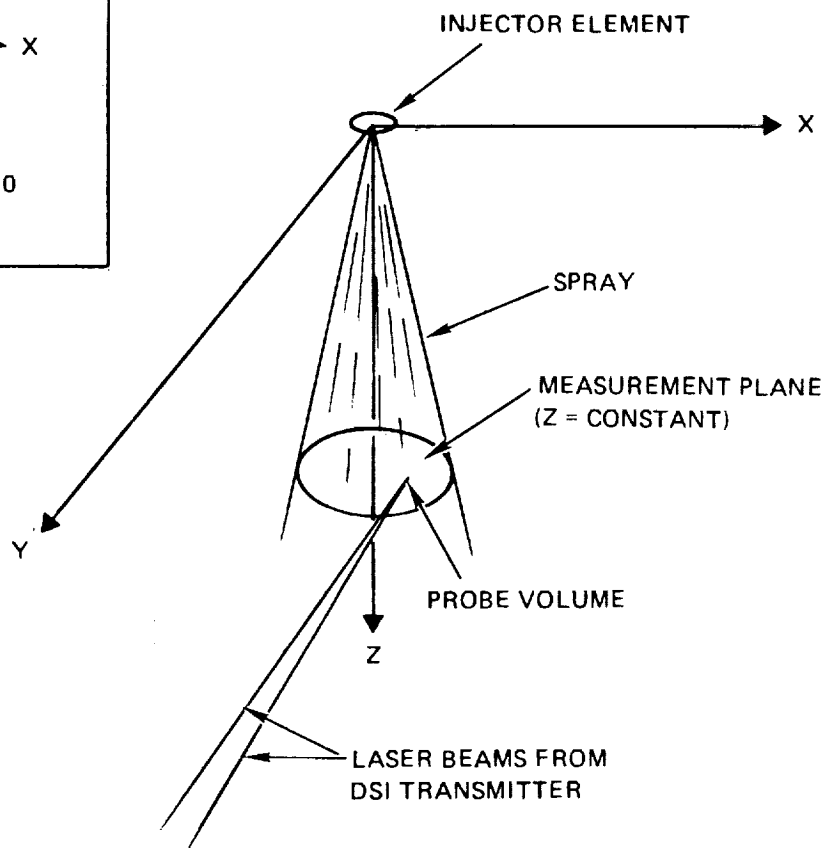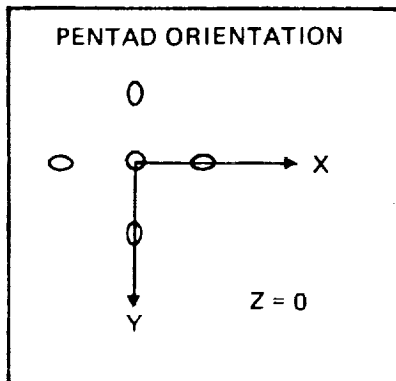
Figure 5-11. Spray Mapping Coordinate System

Element orientation within this coordinate system was as follows. For coaxial elements, the LOX post is centered about the negative z-axis, with the injector face at the z=o location. Thus, the center of the LOX post at its downstream end is (o, o, -R), where R is the LOX post recess of the particular element. The pentad element was oriented so that a particular pair of outer orifices were always aligned along the y axis. Pentad orientation is presented in Fig. 5-11.

Effects of Ambient Air Motion on the Spray

One final issue of concern is the effect of the ambient air motion on the characterization of the spray. As discussed in the section of this report describing the gas/liquid mixing test effort, the spray causes motion and recirculation of the surrounding air. Considerable evidence exists that demonstrates the motion of the surrounding gases can greatly affect the measured droplet size (Ingebo - Ref. 5-7, Zajac - Ref. 5-8 and 5-9, and Falk - Ref. 5-10). To prevent the recirculation of the spray in these tests, a large and deep spray catch pan was installed slightly below the measurement plane. This catch pan was equipped with a 51-cm-diameter duct connected to a blower. This pan provided a constant flow of air downward into the catch pan, thereby containing and preventing the recirculation of the spray. While such a spray removal device was necessary, some concern was expressed that the suction produced by the blower would alter the gas motion sufficiently to change the droplet sizes.

In addition, there was concern that anything disturbing or modifying the manner in which the surrounding gas was ingested into the spray, might affect droplet sizes in the spray. If this effect is strong, it has serious consequences regarding the ability to extrapolate from any cold-flow atomization data to real injectors operating in engines. The presence of the injector face and the adjacent elements, and the expansion of the fuel gas caused by heating and combustion, will most certainly and drastically alter the motion of the surrounding gas. These effects cannot be simulated in cold flow.

To partially investigate this, a series of tests were conducted to determine the effect of the surrounding air motion on the atomization characteristics of the

water spray. If such an effect was observed, and if the effect was significant, then the applicability of this or any atomization data to any combustor would be very difficult and/or of doubtful validity.

For the investigation of this effect, two different configurations were tested. The first set of tests was conducted with the catch pan exhaust fan operating to promote removal of the spray droplets from the measurement region. The exhaust fan inhibits recirculation of the air and water droplets. The data from the tests with the fan operating were compared to tests at the same condition without the fan operating.

The second set of tests was performed with and without a shield (a cone) around the injector spray pattern. The function of the shield (cone) was to minimize or distort the natural influx of the surrounding air into the spray. The objective of these tests was to determine if such a change in air movement would significantly change the spray droplet size and/or velocity characteristics. These tests were also conducted with and without the exhaust fan in operation.

These tests were performed very early in the program (before the installation of flow-measurement devices). The gas and liquid side injector pressure drops were measured, and flow rates estimated from these. However, subsequent to these tests, some leakage was discovered between the gas and liquid sides of the element because of a faulty O-ring. Thus, the actual flow rate computed in this manner could be somewhat in error. Since the intent of these tests was to determine the relative effects of air ingestion variations, the spray produced need only be constant (which it was). These tests employed the large gas/liquid preburner triplet (element 2), flowing at very high liquid flow rates so as to produce a constant and repeatable spray that was free from the unrepresentative spray distortions effects observed at low liquid flow rates.

The cone used in certain of these tests fit tightly about the injector element and was approximately 6 cm in diameter at that end. The cone concentrically enclosed the spray (without touching it) for a distance of 15 cm and was 30 cm in diameter at the open end. The cone ended 7.9 cm above the measurement plane (z = 22.9 cm for these tests).

Measurements were made at a number of points within the spray, and the droplet-size distributions were found to be comparable (i.e., within about 10 microns) at all points measured. The droplet sizes measured were generally very small, and it was apparent that many droplets had diameters less than what could be reliably measured with the DSI (i.e., about 18 microns). It is believed that the upstream leakage between orifices was responsible for this fine atomization. Since large portions of the spray consisted of drops having diameters smaller than could be measured, any computed representative drop sizes would be of little validity. Consequently, these were not computed. Thus, the comparison between conditions must be based upon a direct comparison of the droplet-size and velocity distributions.

Typical droplet-size distributions at the center of this spray are presented in Fig. 5-12 through 5-17. In each figure, the injection pressure drops, and the fan and cone conditions are noted. Figures 5-12 to 5-14 present centerline drop-size distributions for various fan and cone conditions. Figure 5-15 presents the droplet-size distribution near the periphery of the spray, for the fan-off, cone-off condition (comparable to Fig. 5-12); there appears to be little difference in these distributions. Figures 5-16 and 5-17 present data at the same location in a spray with a lower liquid flow rate and a higher gas flow rate. These flow conditions produce an even finer spray than that of Figures 5-12 through 5-15.

Corresponding velocity profiles are presented in Fig. 5-18 through 5-22. Figures 5-18 through 5-20 present the measurements of the velocity distributions of the droplets in the center of the spray at the higher water flow rate. Each of these figures contains two or three velocity-distribution plots corresponding to the size-distribution plots of Fig. 5-12 through 5-14, respectively. Each size-distribution plot was a combined result from two or three runs (note run numbers). Each of the velocity-distribution plots is normalized by the DSI software so that the maximum number of counts always reaches the top of each plot. This must be kept in mind when viewing these plots. For example, in Fig. 5-18, the actual numbers of counts per second at 3.8 m/sec in run 100 is approximately equal to the peak in the distribution of run 101. If these plots had not been normalized then it would be apparent that the high-velocity end of run 101 fits

Injector #2
Fan Off : Cone Off
P_{INJ} : H_2O = 15 PSI N_2 = 2 PSI
LOCATION (0,0, 22.9)
Series II, Runs 100 & 101

DROPLET SIZE - MICRONS
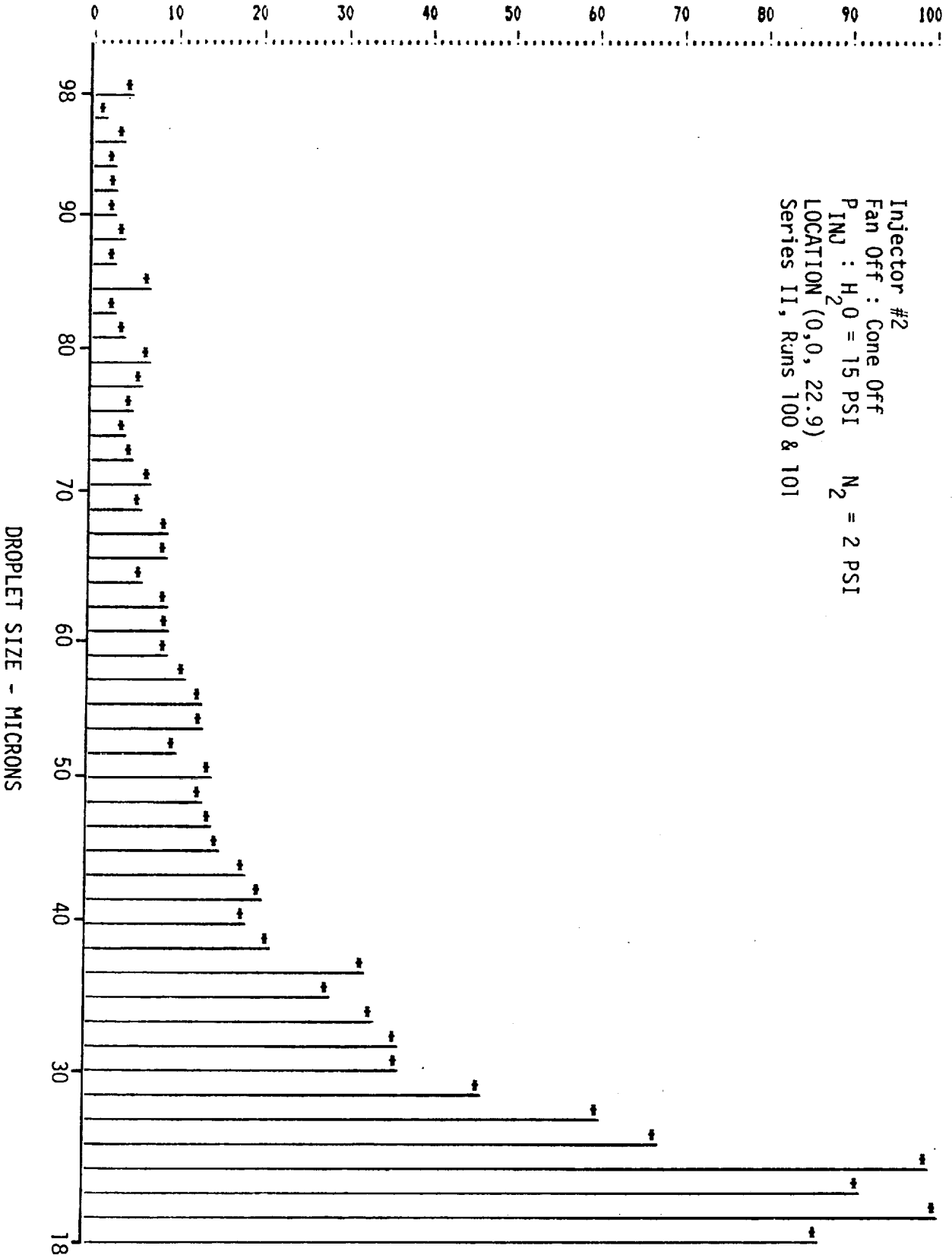
Figure 5-12.   Air Motion Tests, High Liquid Flow Rate Size Plot (1)

INJECTOR #2
FAN ON : CONE OFF
P_{INJ} : H_2O = 15 PSI N_2 = 2 PSI
LOCATION (0, 0, 22.9)
SERIES II RUNS 124 & 125

DROPLET SIZE – MICRONS
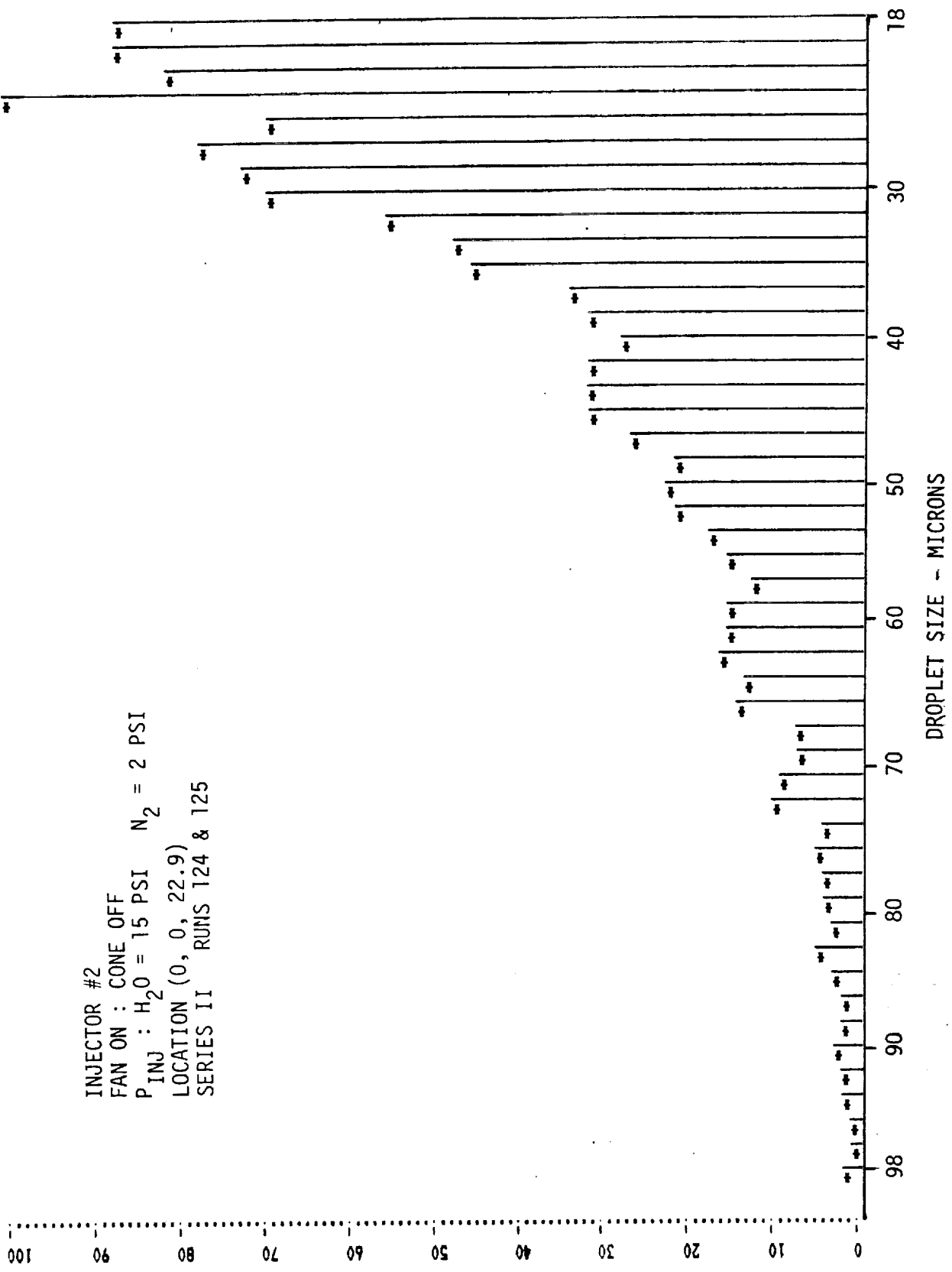
Figure 5-13. Air Motion Tests, High Liquid Flow Rate Size Plot (2)

INJECTOR #2
FAN OFF : CONE ON
P_{INJ} : H_2O = 15 PSI N_2 = 2 PSI
LOCATION (0, 0, 22.9)
SERIES II RUNS 150 & 151

DROPLET SIZE — MICRONS
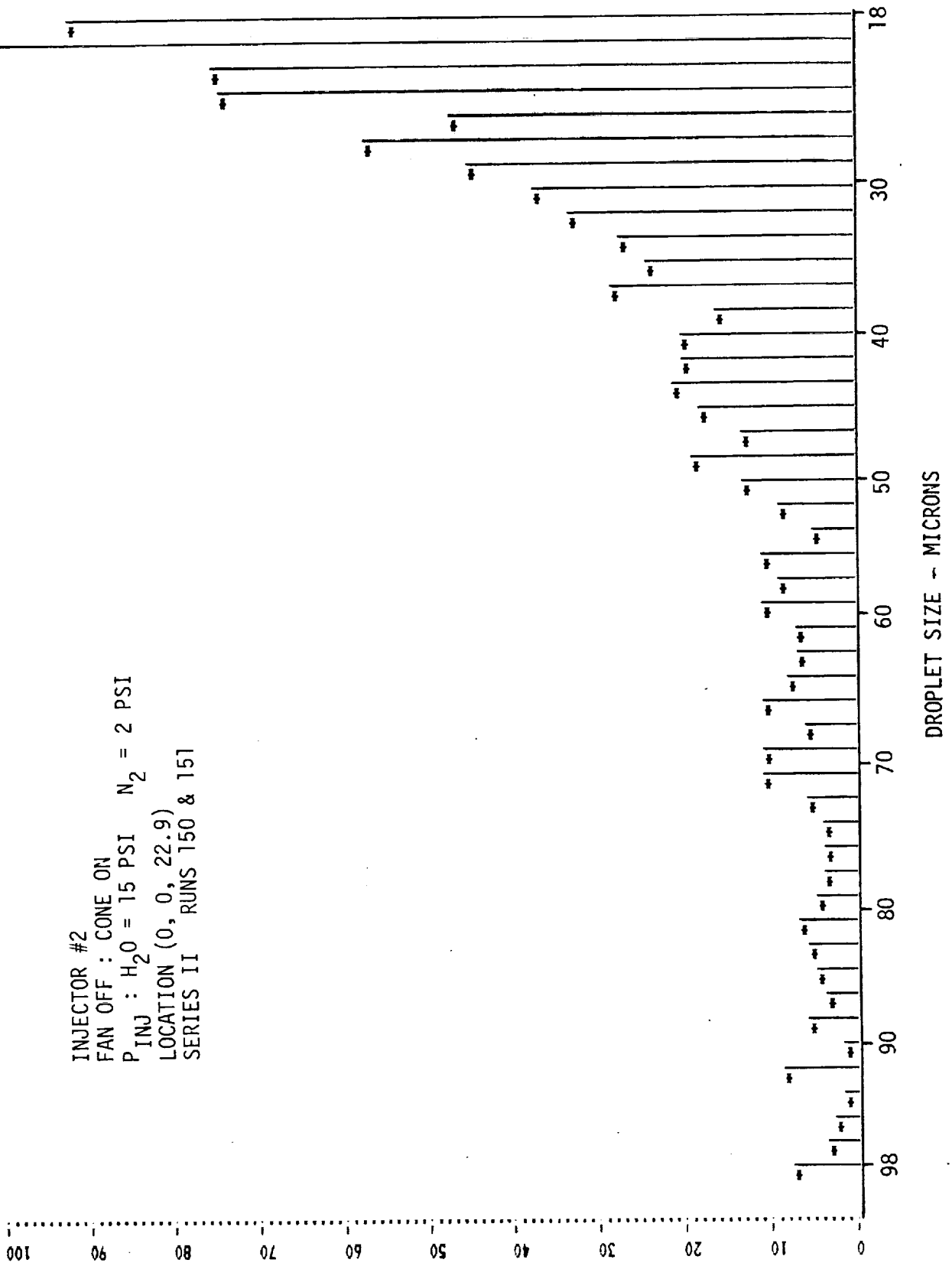
Figure 5-14. Air Motion Tests, High Liquid Flow Rate Size Plot (3)

INJECTOR #2
FAN OFF : CONE OFF
P_{INJ} : H_2O = 15 PSI N_2 = 2 PSI
LOCATION (2.5, 0, 22.9)
SERIES II, RUNS 104 & 105

DROPLET SIZE - MICRONS
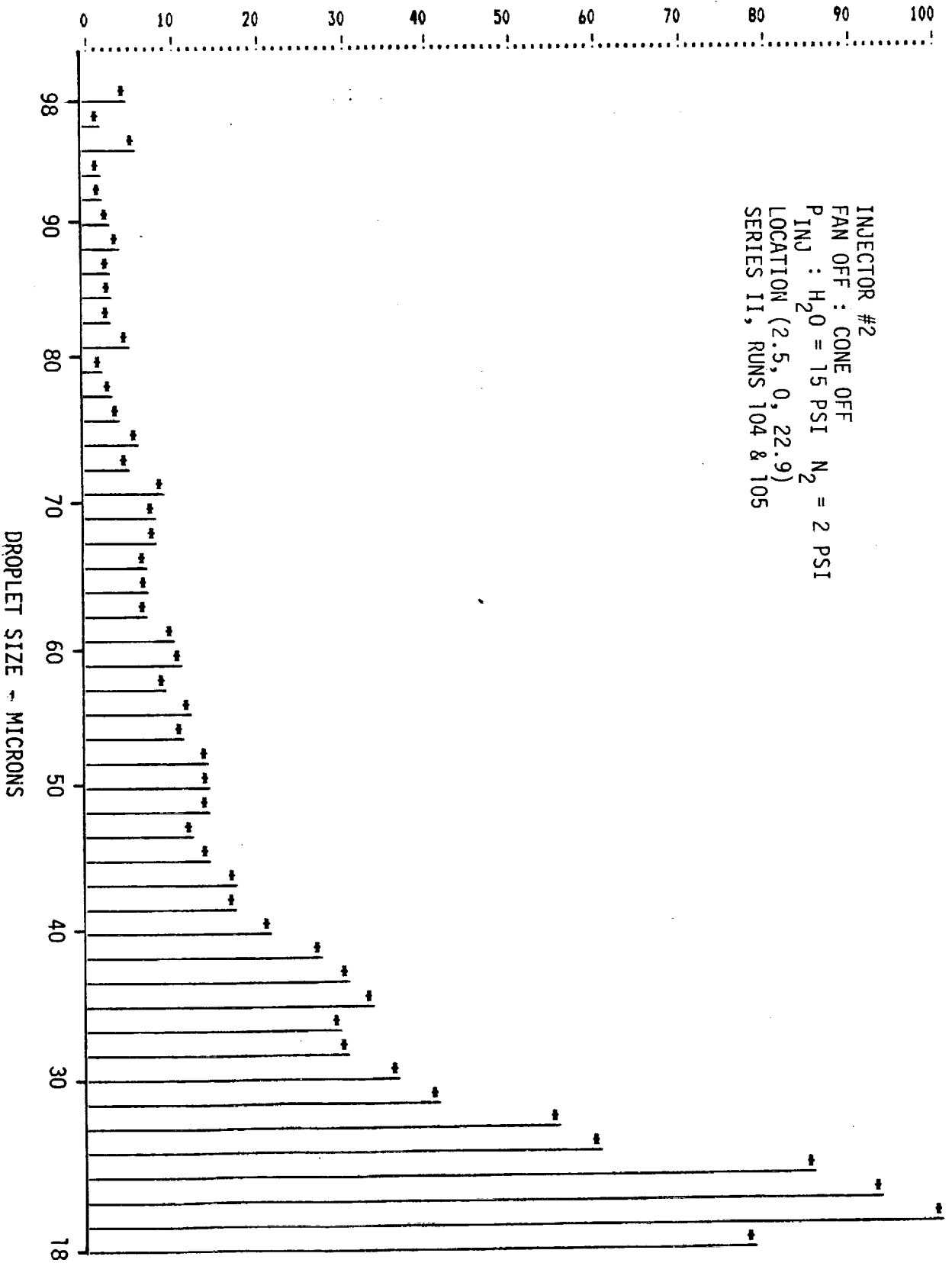
Figure 5-15. Air Motion Tests, High Liquid Flow Rate Size Plot (3)

Figure 5-16. Air Motion Tests, Low Liquid Flow Rate Size Plot (1)

INJECTOR #2
FAN OFF : CONE ON
P_{INJ} : H_2O = 5 PSI N_2 = 8 PSI
LOCATION (2.5, 0, 22.9)
SERIES HH RUNS 23-25

DROPLET SIZE – MICRONS

Figure 5-17. Air Motion Tests, Low Liquid Flow Rate Size Plot (2)

INJECTOR #2
FAN ON : CONE OFF
P_{INJ} : H_2O = 5 PSI N_2 = 8 PSI
LOCATION (2.5, 0, 22.9)
SERIES HH RUNS 3-5

DROPLET SIZE - MICRONS

INJECTOR #2
FAN OFF : CONE OFF
P_{INJ} : H_2O = 15 PSI N_2 = 2 PSI
LOCATION (0, 0, 22.9)
SERIES II   RUNS 100 & 101

RUN 101   RUN 100

1.85   3.82   3.70   7.65   11.60
DROPLET VELOCITY   METERS/SEC
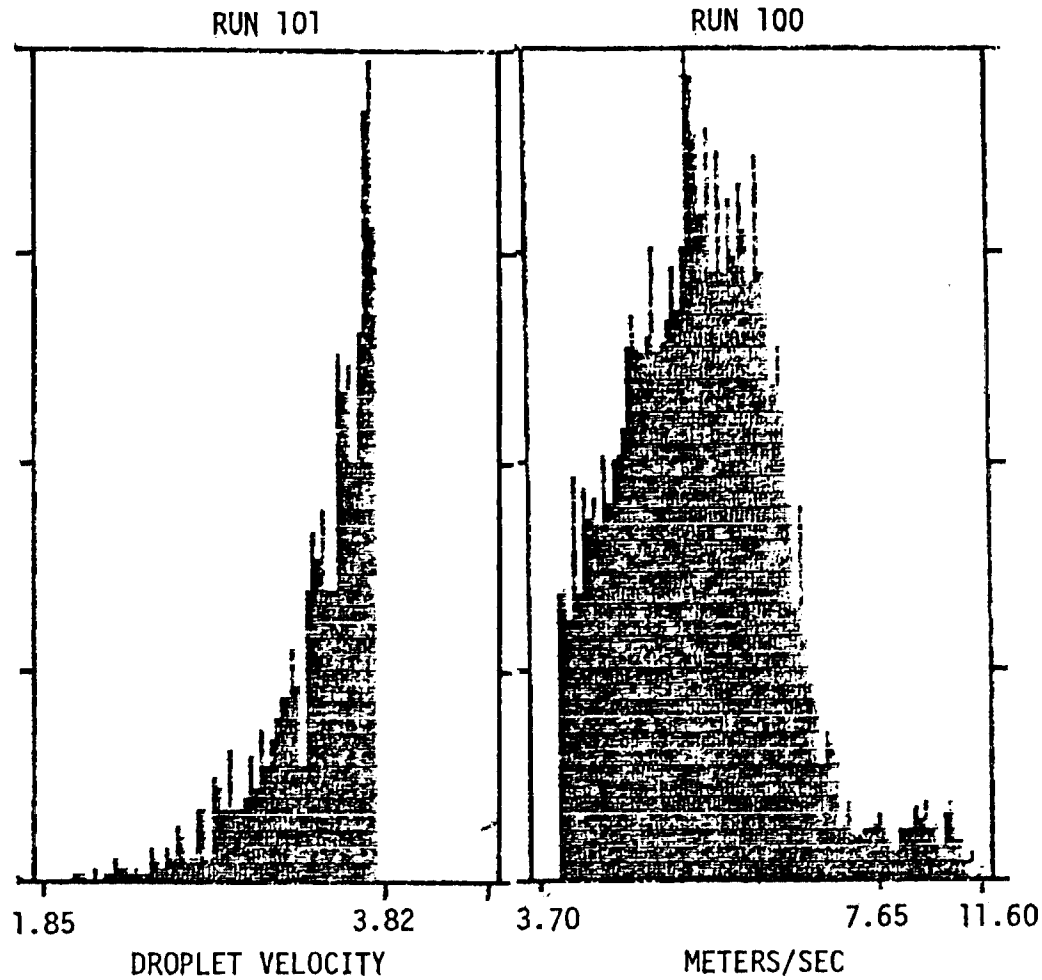
Figure 5-18. Air Motion Tests, High Liquid Flow Rate Velocity Plots (1)

INJECTOR #2
FAN ON : CONE OFF
P_{INJ} : H_2O = 15 PSI N_2 = 2 PSI
LOCATION (0, 0, 22.9)
SERIES II   RUNS 124 & 125

RUN 125   RUN 124

1.85   3.82   3.70   7.65   11.60
DROPLET VELOCITY   METERS/SEC
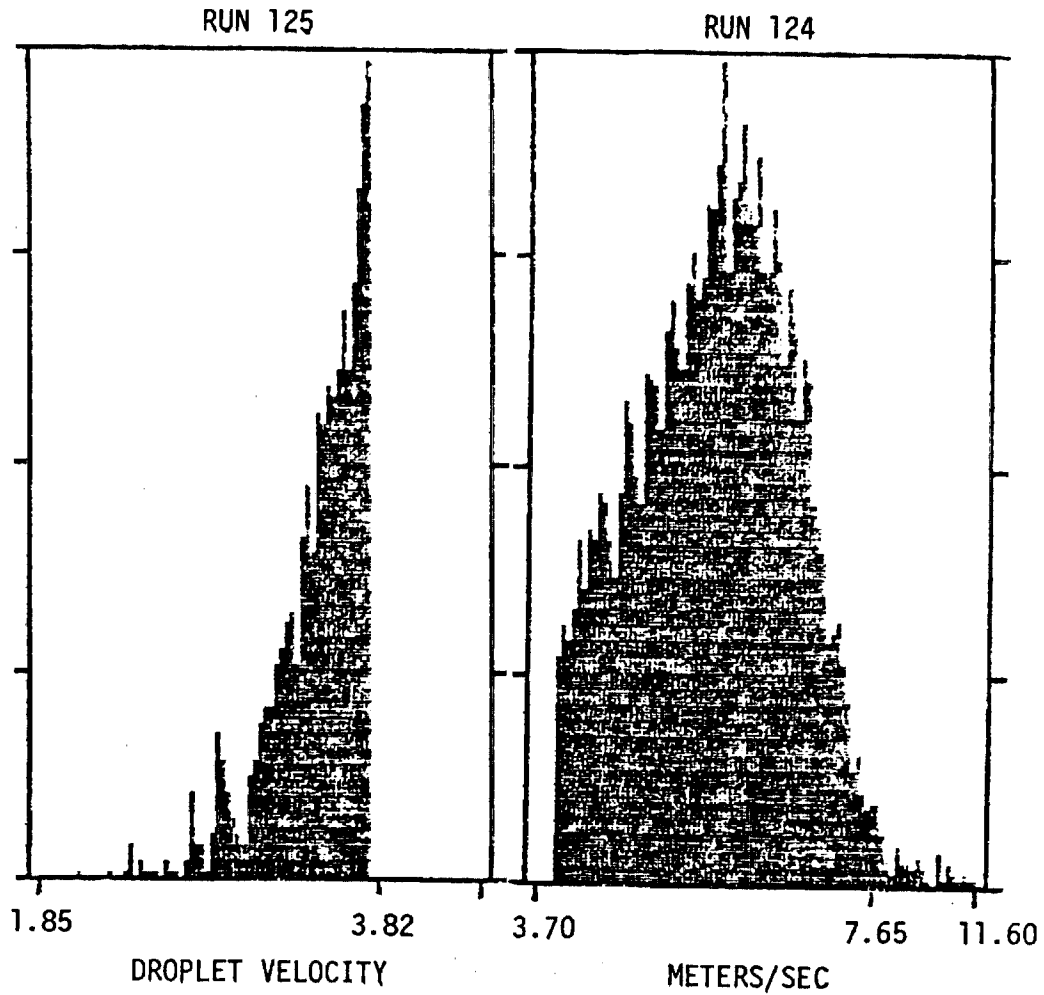
Figure 5-19. Air Motion Tests, High Liquid Flow Rate Velocity Plots (2)

INJECTOR #2
FAN OFF : CONE ON
P_{INJ} : H_2O = 15 PSI N_2 = 2 PSI
LOCATION (0, 0, 22.9)
SERIES II, RUN 150 & 151

RUN 151   RUN 150

1.85   3.82   3.70   7.65   11.60

DROPLET VELOCITY   METERS/SEC
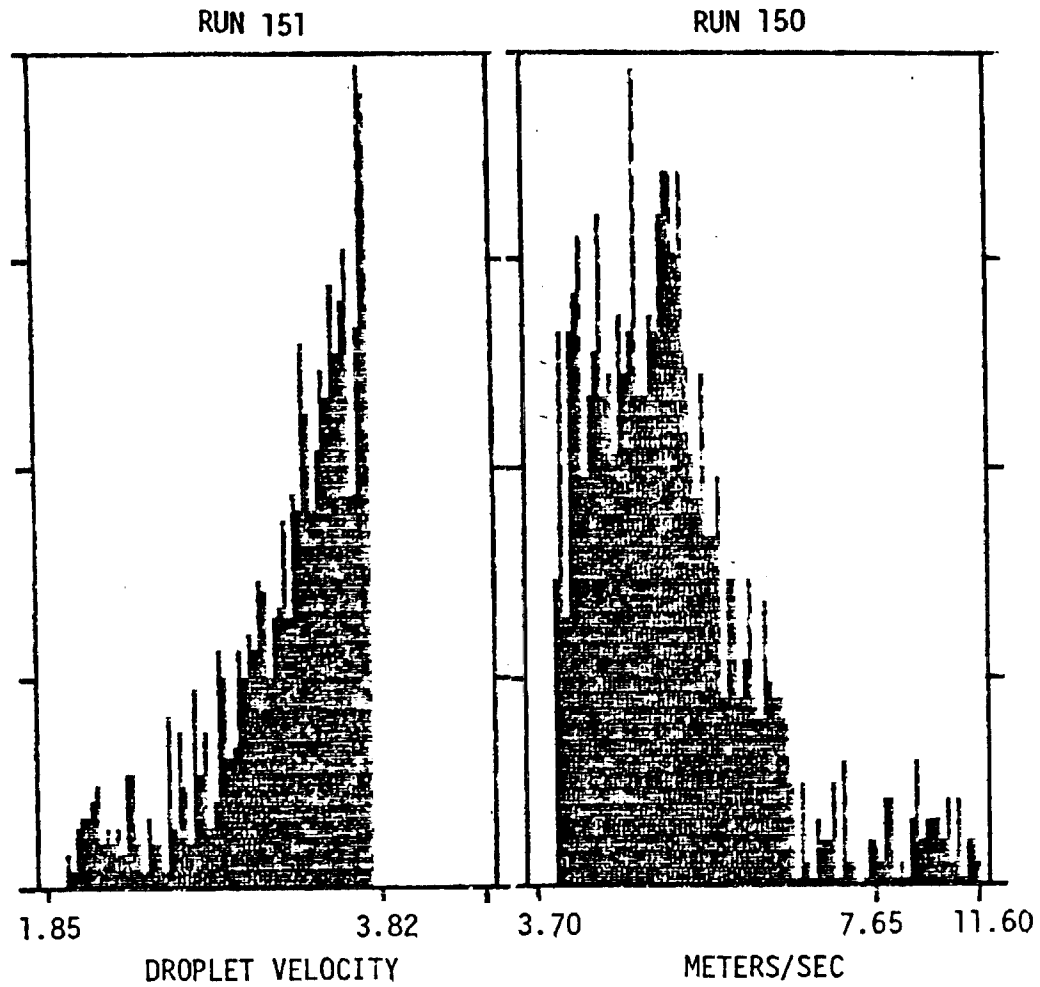
Figure 5-20. Air Motion Tests, High Liquid Flow Rate Velocity Plots (3)

INJECTOR #2
FAN OFF : CONE OFF
P_{INJ} : H_2O = 15 PSI N_2 = 2 PSI
LOCATION (2.5, 0. 22.9)
SERIES II   RUNS 104 & 105

RUN 105   RUN 104

1.85   3.82   3.70   7.65 11.60

DROPLET VELOCITY   METERS/SEC
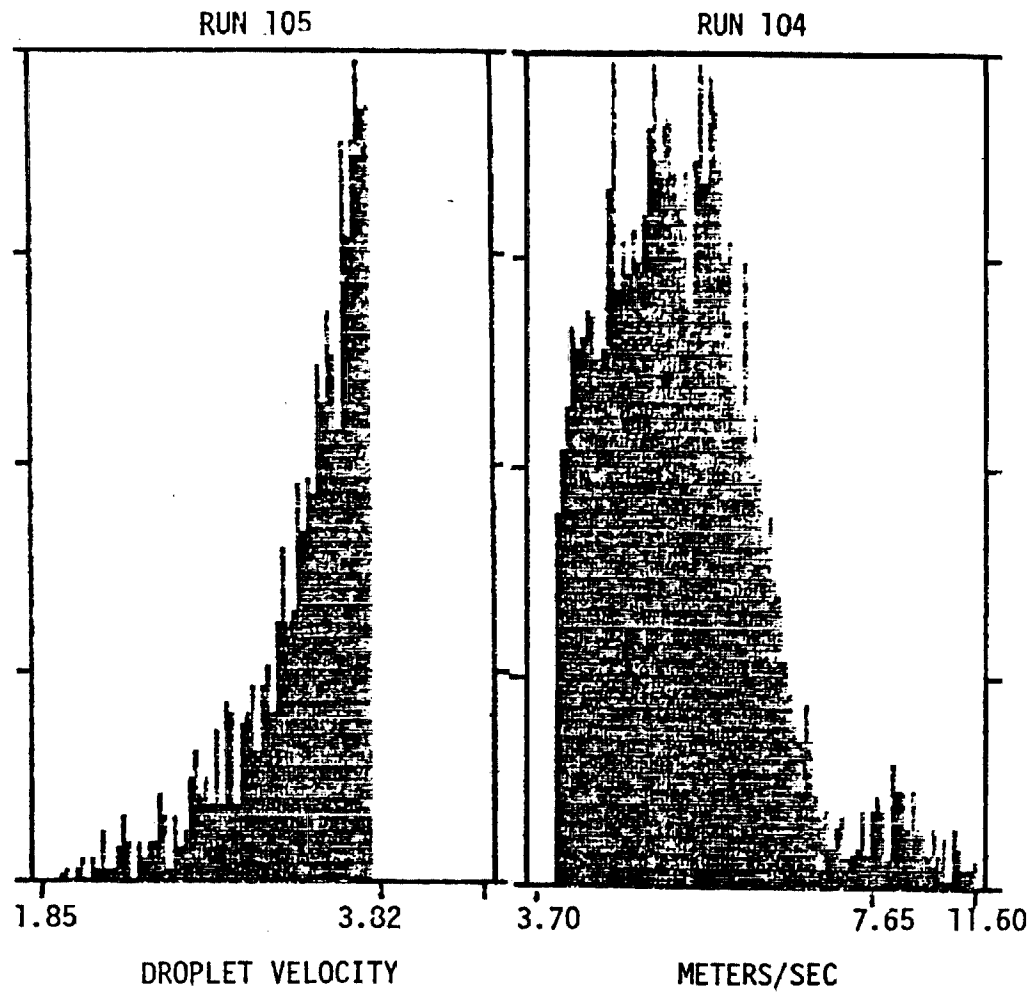
Figure 5-21. Air Motion Tests, High Liquid Flow Rate Velocity Plots (4)

INJECTOR #2
FAN ON : CONE OFF
P_{INJ} : H_2O = 5 PSI N_2 = 2 PSI
LOCATION (2.5, 0, 22.9)
SERIES HH RUNS 3, 4 & 5

RUN 5   RUN 4   RUN 3

1.85   3.82   3.70   7.65   7.25   14.89   22.60
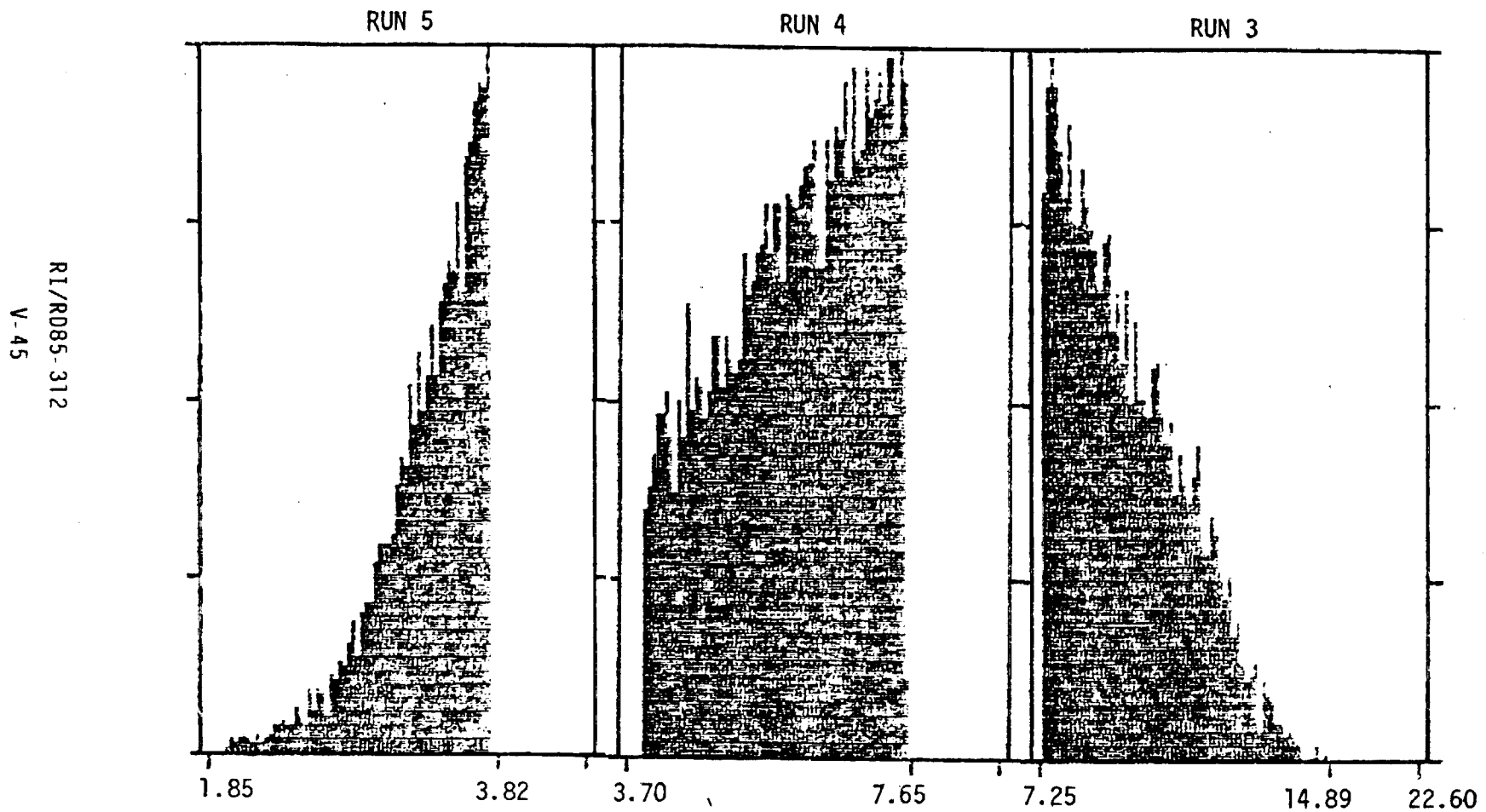
Figure 5-22. Air Motion Tests, Low Liquid Flow Rate Velocity Plots (2)

smoothly with the low-velocity end of run 100. Figure 5-18 demonstrates that nearly all the droplets in the spray at this location (0, 0, 22.9) were traveling at velocities between about 2 and 11 m/sec, and that the peak in the velocity distribution (mode) occurs at approximately 5 m/sec. Comparison of Fig. 5-18 and 5-20 indicates that the cone appears to cause the droplets to move at slightly lower velocities. Comparison of Fig. 5-18 and 5-21 indicates that little difference exists in the droplet velocities at different locations within the spray. Figure 5-22 is the velocity distribution plots corresponding to the size-distribution plot of Fig. 5-17. These mappings were obtained at a lower liquid flow rate and higher gas flow rate. These injection conditions resulted in a large number of droplets moving at higher velocities than in the other (higher liquid and lower gas flow rates) injection condition. The effect of the higher gas injection velocity has resulted in an increase in some of the droplets velocities, as might be expected.

These results are typical of many such measurements performed to assess the effects of the cone and exhaust fan on the spray. The results indicate that the drop-size distribution is not significantly affected by the presence of the cone or the suction of the exhaust fan. The droplet velocities appear to be slightly reduced by the presence of the cone--a result that seems reasonable. The cone would impede the ingestion of air into the upper portion of the spray, creating a lower-pressure region near the injector. This causes air to move upward, along the inner surface of the cone, and toward that lower pressure region. This air flow would oppose and, hence, retard, the spray motion.

The suction of the exhaust fan had no obvious or significant effect on droplet velocities. Thus, it was concluded that the droplet size and velocity results of the planned atomization tests would be unaffected by the suction of the fan (no experimental apparatus effect). Furthermore, at these relatively low flow rates at atmospheric pressure, the effect of a major distortion of the natural inges- tion of air into the spray was minimal. Only the droplet velocities were affected, and that effect was small.

Before leaving this subject, it is instructive to consider how much air has been ingested into the spray. Based upon the injector pressure drops for the high liquid flow rate condition, assuming a discharge coefficient of 0.8 for these

orifices and incompressible gas flow, and using the principle of conservation of axial momentum, the resultant (after impingement) axial velocity of the injected fluids should be approximately 18.5 m/sec. Since the measured velocities ranged from only about 2 to 7 m/sec (see Fig. 5-18 through 5-20), it was obvious that significant quantities of surrounding air were being ingested into the spray and thereby slowing it. A second, simple conservation of momentum computation, assuming an average spray velocity of 5 m/sec, indicates that the quantity of ingested air required is on the order of three times the total mass flow rate of the element. This simple computation provides some indication of the potential importance of the ambient air motion on the spray. While this is still an area of concern, the testing performed in this program to assess the effects of slight modifications to this air motion, indicated that such effects were minimal.

Test Plan and Rationale

The primary intent of these atomization characterization tests was to develop an empirical correlation defining the spray droplet sizes in terms of the flow, geometry, and other governing parameters. Overall spray droplet sizes are commonly characterized by a single representative droplet size, such as the mass median diameter ($\bar{D}$). The choice of the governing parameters varies from the most basic parameters, such as injector velocity, propellant density, stream diameter, and impingement angle, to parameters that combine these factors (e.g., mixture ratio, penetration parameter, and Elverum-Morey parameter) or are directly relatable to engines (e.g., thrust per element). Correlations based upon the most fundamental parameters can be combined to form the less fundamental parameters. Also, the more fundamental parameters offer more general applicability and utility. Therefore, the philosophy of this test program was to employ these more fundamental parameters as the independent test variables. Based upon the extensive study of the atomization literature of Ref. 1-1, the following variables are deemed to be of greatest importance:

Impinging Elements
- Injector velocities, V_L and V_g
- Stream diameters (generally assumed to be equal to orifice diameters), d_L and d_g

- Chamber gas density, ρ_{cg}
- Injector gas density, ρ_g
- Impingement angle, α
- Liquid density, ρ_L
- Liquid viscosity, μ_L
- Liquid surface tension, σ

Coaxial Elements

- Injection velocity, V_L and V_g
- Inner (liquid) stream diameter, d_L
- Outer (gas) stream annulus dimension, Y
- Inner tube recess, R
- Inner tube thickness, t
- Chamber gas density, ρ_{cg}
- Injected gas density, ρ_g
- Liquid density, ρ_L
- Liquid viscosity, μ_L
- Liquid surface tension, σ

While other parameters have been considered (e.g., gas viscosity, and stream turbulence levels and velocity profiles), the listed parameters are those usually previously studied and/or the variables currently considered to be of greatest importance. One nonfundamental parameter also considered important is mixture ratio. Mixture ratio is important to these airblast atomizers as it relates the ratio of the injected liquid (the quantity to be atomized) to the injected gas (which provides the force of atomization).

Since there are no atomization theories sufficiently developed or valid for the types of airblast atomizers employed in liquid rocket engines, the approach generally employed is a straightforward parametric evaluation of the effects of as many of these independent variables as possible. Results are then compiled and an empirical equation developed of the form:

$$\bar{D} \text{ or } D_{32} \text{ et al} = f(V_L, V_g, \rho_g, d_L, d_g, \text{ etc.})$$

Obviously, with so many dependent variables, the size of any test matrix that would comprehensively evaluate each variable would be immense. Accordingly, the approach employed in this program is to use a baseline test condition and to independently evaluate the effects of variations of each of these variables on this baseline condition. Thus, each parameter would be separately varied from the baseline condition, while all other parameters remain constant. While this approach minimizes the size of the test matrix, it necessarily suffers from an inability to identify any synergistic or combined parameter effects. For example, if the gas density effect on atomization varies with liquid viscosity, this would not be observed with such an approach.

The previously described problems that limited the testing to atmospheric back pressure, low flow rates, and only one impinging element (the pentad), precludes large variations of certain of these parameters. Also, for some parameters (e.g., chamber gas density), no variations are possible. Furthermore, in some instances, it is difficult to vary one parameter independently. Despite these difficulties, the approach employed here was, whenever possible, to independently vary one parameter at a time from a baseline condition. When this approach is not feasible, more complex data analysis techniques, such as the regression analysis technique employed in the liquid/liquid mixing study, are required to ascertain the effects of each independent variable.

The general test matrix employed for these tests is presented in Table 5-1. The four basic gas/liquid elements (element 3, a pentad, and elements 5, 7, and 9, coaxial elements, all from Table 2-1) were used. The first series of tests or mappings established the atomization characteristics of these elements under baseline flow conditions. The second series of tests were intended to establish the effects of injector velocity variations at constant mixture ratio.

The next three sets of tests were intended to investigate the effects of liquid viscosity, density, and surface tension, respectively. To vary each of these independently, it was necessary to find liquids having the same properties as water, except for the one property whose effects were to be studied. This proved to be quite difficult. A study of pure liquid properties quickly established

Table 5-1. Atomization Test Matrix

OBJECTIVE	ELEMENTS	MIXTURE RATIO	FLOW RATE	FLUIDS	NUMBER OF MAPPINGS
BASELINE	ALL	BASELINE	BASELINE	H_2O AND N_2	4
FLOW RATE EFFECTS	ALL	BASELINE	2 PER ELEMENT	H_2O AND N_2	8
VISCOSITY EFFECT	7 COAXIAL 3 PENTAD	BASELINE[a]	BASELINE[a]	GLYCEROL/H_2O AND N_2	2
DENSITY EFFECT	7 COAXIAL 3 PENTAD	BASELINE[a]	BASELINE[a]	NaCl/H_2O AND N_2	2
SURF TENSION EFFECT	7 COAXIAL 3 PENTAD	BASELINE[a]	BASELINE[a]	$C_2H_3Cl_3$ AND N_2	2
COMPARE WAX DATA	LIKE DOUBLET	------	[b]	H_2O OR $C_2H_3Cl_3$	8
MIXTURE RATIO EFFECTS	ALL	2 PER ELEMENT	BASELINE GAS VARY LIQUID	H_2O AND N_2	8
GAS DENSITY EFFECT	7 COAXIAL 3 PENTAD	BASELINE[a]	BASELINE[a]	H_2O AND CO_2 H_2O AND He	4

[a]THESE VARIABLES ARE BASED ON VOLUMETRIC RATHER THAN MASS FLOW RATES
[b]HIGH FLOW RATES COMPARABLE TO DICKERSON WAX TECHNIQUE TESTS (REF. 5-11)

that no such pure liquids existed. Attention was then given to mixtures of liquids, and solutions.

An infinite set of such liquids was available; however, there was often little properties test data to support the selection. This search was quickly narrowed by the requirement that the liquids be relatively nonflammable, nontoxic, of low volatility, relatively clear, relatively inexpensive, and compatible with the materials in the feed system and injector assemblies.

In the course of this search for materials, a particular problem was discovered regarding the use of surfactant-type materials to reduce surface tension. Such materials were originally judged to be very attractive for the purpose of this study, as very small amounts appeared quite effective in reducing surface tension. Thus surface tension could be varied without appreciably changing the density or viscosity of the liquid. However, after additional study, it became apparent that this approach was questionable. These materials function by selectively migrating to the surface of the liquid. Thus, their concentration at the surface is much greater than in the bulk of the liquid. Surface tension measurements are based on a determination of the surface tension at the surface of a relatively large quantity of quiescent liquid. Hence, adequate time exists for the surfactant-type materials to migrate to the surface, and the surface area is small relative to the quantity of liquid present. However, the atomization process is characterized by the rapid creation of large amounts of surface area. Thus, it is necessary to question whether these relatively small amounts of sur- factant-type materials will have sufficient time to migrate to the surface, and if sufficient material is present in the liquid to effectively reduce surface tension on the vast surface area of the spray. Because of this concern, only liquids containing relatively large amounts of each of its constituents were considered for use in this study.

Chemical handbooks and other references were employed to identify potential liquid mixtures and solutions. Several promising candidates were identified and materials were procured, mixed, and sent to Truesdail Laboratories of Tustin, California, for properties determination. Some of these materials contained very small quantities of butyl acetate (a surface acting-type of material as

previously discussed), as this was prior to the concerns about such materials. Results of these properties determinations were generally in agreement with whatever literature data existed on these multicomponent liquids. The liquids given in Table 5-2 were chosen for testing. (Their pertinent properties and those of water and LOX are also presented.)

TABLE 5-2. MULTICOMPONENT LIQUIDS AND THEIR PROPERTIES

LIQUID	SURFACE TENSION (dynes/cm)	VISCOSITY (cP)	DENSITY (kg/m^3)
16% GLYCEROL AQUEOUS SOLUTION	69	1.49	1041
17.4% SODIUM CHLORIDE AQUEOUS SOLUTION	77	1.38	1135
1, 1, 1 - TRICHLOROETHANE	22	1.2	1316
WATER	72	0.94	997
LOX (@ NBP)	13.2	0.196	1137

Except for the LOX, all properties are at room temperature. All concentrations are mass percents.

The glycerol solution had properties similar to water (within about 5%), except for a viscosity increase of about 50%. The salt solution was intended to provide a variation in density; however, the viscosity variation from pure water was significant. No suitable surface-tension variation liquid could be identified, so TRIC was employed. This offered a large variation in surface tension with only about 20% and 30% increases in viscosity and density, respectively. No suitable, room-temperature liquids could be found with surface tensions and viscosities comparable to those of LOX. Although they did not provide precisely the desired properties variations, these liquids were the best available for the liquid property effects tests of this atomization study.

Additional tests were planned to investigate mixture ratio variations and changes in the density of the injector gas (via variations in the gas composition). However, slower than anticipated testing (primarily because of difficulties with

the droplet generator used to calibrate the DSI) prevented the accomplishment of the gas density effects tests and most of the mixture ratio effects tests. The planned test conditions for the tests performed are presented in Table 5-3.

One additional, important pair of tests was planned to provide a comparison with the large body of "hot wax", like doublet, atomization test data. As discussed in Ref. 1-1, certain evidence and supporting arguments cast doubt upon the validity of this technique. For the purpose of this comparison, the tests and results of Dickerson (Ref. 5-11) were employed. Dickerson found excellent correlation of his results with the following equation:

$$\bar{D} = 7.84 \times 10^4 \, d_L^{0.57} / V_L^{0.85}$$

where d_L is the orifice diameter employed, in inches, V_L is the wax injection velocity in feet per second, and $\bar{D}$ is in microns. The intent of these tests was to match the test conditions of Dickerson as closely as possible and to compare these results to his wax results. One of the like doublets extensively tested by Dickerson had orifice diameters of 0.066 cm (0.026 inch) and a 60-degree impingement angle. The baseline triplet element fabricated for this program has 0.69 cm (0.027 inch) outer orifices and a 60-degree impingement angle. By flowing only the outer orifices of this element, at flow rates within the range tested by Dickerson, it was possible to closely simulate his tests.

However, one major difference (other than the droplet-size measurement technique) exists between these tests and those of Dickerson- the fluids used. As discussed in Ref. 1-1, the extrapolation of atomization test results from one liquid to another is a major difficulty. Reference 1-1 presents two liquid property correlations commonly applied, and Dickerson recommends one of these (the Wolfe-Anderson correlation), for extrapolation of his results to real propellants. This correlation was employed in this current program to correlate the results of these tests with those of Dickerson. The test conditions for these wax comparison tests are presented in Table 5-4.

TABLE 5-3. ATOMIZATON TEST CONDITIONS - GAS/LIQUID INJECTORS

TEST	INJECTOR ELEMENT	MASS MIXTURE RATIO (OXIDIZER/FUEL)	FLOW RATE GAS (KG/MIN)	FLOW RATE LIQUID CM^3/MIN)	INJECTION VELOCITY (M/SEC) GAS	INJECTION VELOCITY (M/SEC) LIQUID	GAS MACH NUMBER
BASELINE TESTS							
1	PENTAD 3	0.49	0.123	60.0	242	0.40	0.70
2	COAXIAL 5	0.49	0.113	55.0	259	0.21	0.75
3	COAXIAL 7	3.50	0.116	408	152	0.40	0.44
4	COAXIAL 9	3.00	0.171	511	183	0.43	0.53

FLOW RATE EFFECTS TEST (MIXTURE RATIO = CONSTANT)
(Percentage of baseline flow rates in parenthesis after element)

TEST	INJECTOR ELEMENT	MASS MIXTURE RATIO	FLOW RATE GAS	FLOW RATE LIQUID	INJECTION VEL GAS	INJECTION VEL LIQUID	GAS MACH NUMBER
5	PENTAD 3 (120)	0.49	0.147	72.0	291	0.49	0.84
7	COAXIAL 5 (120)	0.49	0.135	66.0	311	0.24	0.90
9	COAXIAL 7 (80)	3.50	0.093	326	122	0.30	0.35
11	COAXIAL 9 (80)	3.00	0.137	409	146	0.34	0.42
6	PENTAD 3 (130)	0.49	0.159	78.0	315	0.52	0.91
8	COAXIAL 5 (130)	0.49	0.147	71.5	337	0.27	0.98
10	COAXIAL 7 (130)	3.50	0.151	530	198	0.52	0.57
12	COAXIAL 9 (130)	3.00	0.222	664	238	0.55	0.69

LIQUID PROPERTIES EFFECTS TESTS (VOLUME FLOW RATE OF LIQUID AND GAS REMAINS THE SAME AS BASELINE. MIXTURE RATIO CHANGES BECAUSE OF LIQUID DENSITY CHANGES.)

TEST	INJECTOR ELEMENT	MASS MIXTURE RATIO	FLOW RATE GAS	FLOW RATE LIQUID	INJECTION VEL GAS	INJECTION VEL LIQUID	GAS MACH NUMBER
	VISCOSITY EFFECTS		(16% GLYCEROL SOLUTION))				
13	PENTAD 3	0.51	0.123	60	795	0.40	0.7
14	COAXIAL 7	3.64	0.116	408	500	0.40	0.44
	DENSITY EFFECTS		(17.4% NaCl SOLUTION)				
15	PENTAD 3	0.56	0.123	60	795	0.40	0.7
16	COAXIAL 7	3.97	0.116	408	500	0.40	0.44
	SURFACE TENSION EFFECTS		(1,1,1 TRICHLOROETHANE)				
17	PENTAD 3	0.64	0.123	60	795	0.40	0.7
18	COAXIAL 7	4.61	0.116	408	500	0.40	0.44

(TESTS 19 AND 20 ARE PRESENTED IN TABLE 5-4)

MIXTURE RATIO EFFECTS TESTS
(Percentage of baseline liquid flow rates in parenthesis after liquid flow rate)

TEST	INJECTOR ELEMENT	MASS MIXTURE RATIO	FLOW RATE GAS	FLOW RATE LIQUID	INJECTION VEL GAS	INJECTION VEL LIQUID	GAS MACH NUMBER
21	COAXIAL 7	2.63	0.116	306 (75%)	152	0.30	0.44
22	COAXIAL 7	5.25	0.116	612 (150%)	152	0.59	0.44

TABLE 5-4. LIKE DOUBLET (WAX DATA COMPARISON) TEST CONDITIONS

TEST	INJECTOR ELEMENT	LIQUID	FLOW RATE (LITERS/MIN)	INJECTION VELOCITY (M/SEC)
19	TRIPLET 4 (OUTER ORIFICES ONLY)	TRICHLOROETHANE	1.46	34
20	TRIPLET 4 (OUTER ORIFICES ONLY)	H_2O	2.75	62

TEST RESULTS AND FINDINGS

The results of these atomization characterization tests are presented in this section. Twenty-two complete spray mappings are presented. Several mappings of the triplet elements were also performed prior to the discovery of the flow irregularities previously discussed. These results have been discarded. The intended flow rates and mixture ratios for all of these tests (as shown in Tables 5-3 and 5-4) were very closely obtained in the testing. Spray mappings were obtained along several rays extending radially outward in the measurement plane from the (0, 0, 23.5) point. Initially measurements were made along two to four such rays in 0.508 cm (0.2 inch) increments. As will be shown, subsequent testing established that very little accuracy was lost if measurements were made along only two rays in 1.016 cm (0.4 inch) increments.

Each test consists of many (sometimes in excess of 100) droplet-size distribution and corresponding velocity distribution data sets. Various combinations of these have been used to construct droplet-size distribution plots for (1) selected points within the spray, (2) along particular rays, (3) inner and outer regions of the spray, and (4) the overall spray. In addition, velocity distribution data and plots of droplet size vs. velocity are available. This vast quantity of data is too extensive to be included in this final report. Accordingly, the results of each test are discussed, observations based upon these data are presented, and specific plots of data are presented either as examples or to support a discussion.

The overall spray droplet-size distribution for test 1 is presented in Fig. 5-23. Note that some portion of the actual droplet-size distribution consisted of droplets having diameters less than could be measured by the DSI. If these droplets had been included, the measured representative droplet diameters, especially the linear mean drop size (D_{10}) would be reduced from those shown in Fig. 5-21. This was a common problem that occurred in many of the spray mappings. The mass median diameter would be least affected by these small droplets. Accordingly, it is the primary representative droplet size employed in these tests.

Figures 5-24 and 5-25 present results obtained from a very extensive mapping of the preburner coaxial element (5) at baseline flow conditions (test 2). One hundred separate droplet-size distribution measurements were made along four different rays (+x axis, -x axis, +y axis, and -y axis.). Measurements were made along these rays to a distance of about 5 cm in 0.508 cm increments.

This series of mappings were then employed to assess the mapping resolution (i.e., number of rays and measurement spacing) required to obtain accurate results. Figure 5-24 is a total spray droplet-size distribution constructed from the data obtained at all measurement locations. Figure 5-25 is a corresponding plot that utilized only the data from every other mapping location. The similarity of these plots demonstrates the adequacy of employing 1.016 cm spacing between measurement points. Data from all pairings of the four rays measured were used to construct an overall spray droplet-size distribution. These results indicated that any two rays would adequately reproduce the more comprehensive, high-resolution results of Fig. 5-24. Similar comparisons of measurement resolution in some of the subsequent tests further supported the findings of this test regarding measurement location requirements.

The droplet distributions measured at each location in this test were surprisingly uniform throughout the spray. However, slightly larger drops appeared to exist in the central part of the spray. Velocity profiles at two points within the spray are presented in Fig. 5-26 and 5-27. These clearly demonstrate that the droplets are generally traveling faster near the center of the spray. Also, the number of droplets counted (samples) in the center of the spray is much
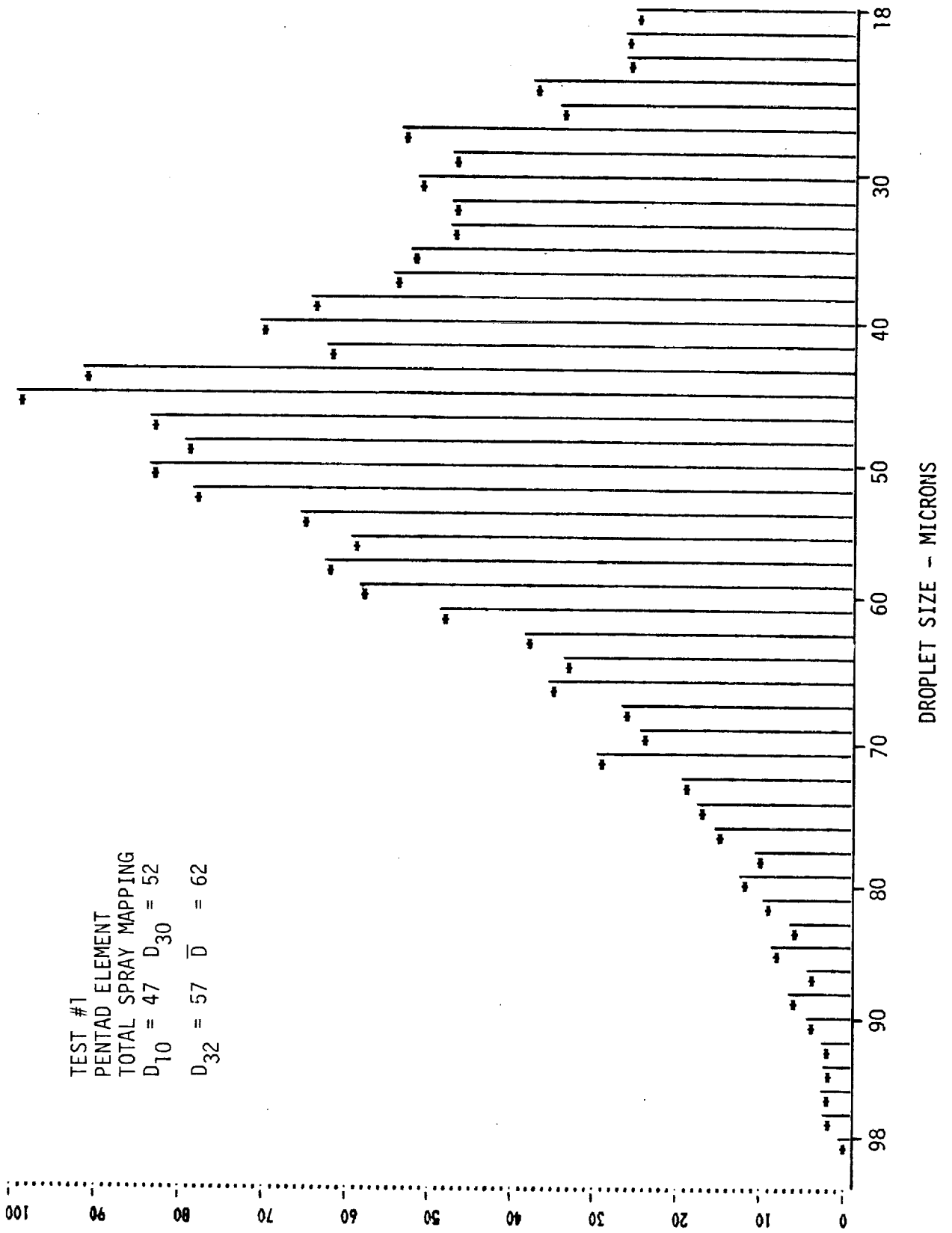
Figure 5-23. Spray Droplet-Size Distribution, Test 1

TEST #1
PENTAD ELEMENT
TOTAL SPRAY MAPPING
$D_{10} = 47$ $D_{30} = 52$
$D_{32} = 57$ $\overline{D} = 62$

DROPLET SIZE - MICRONS

RI/RD85-312

V-57

TEST #2
COAXIAL ELEMENT #5
TOTAL SPRAY MAPPING (HIGH RESOLUTION)
$\overline{D} = 45$

DROPLET SIZE - MICRONS
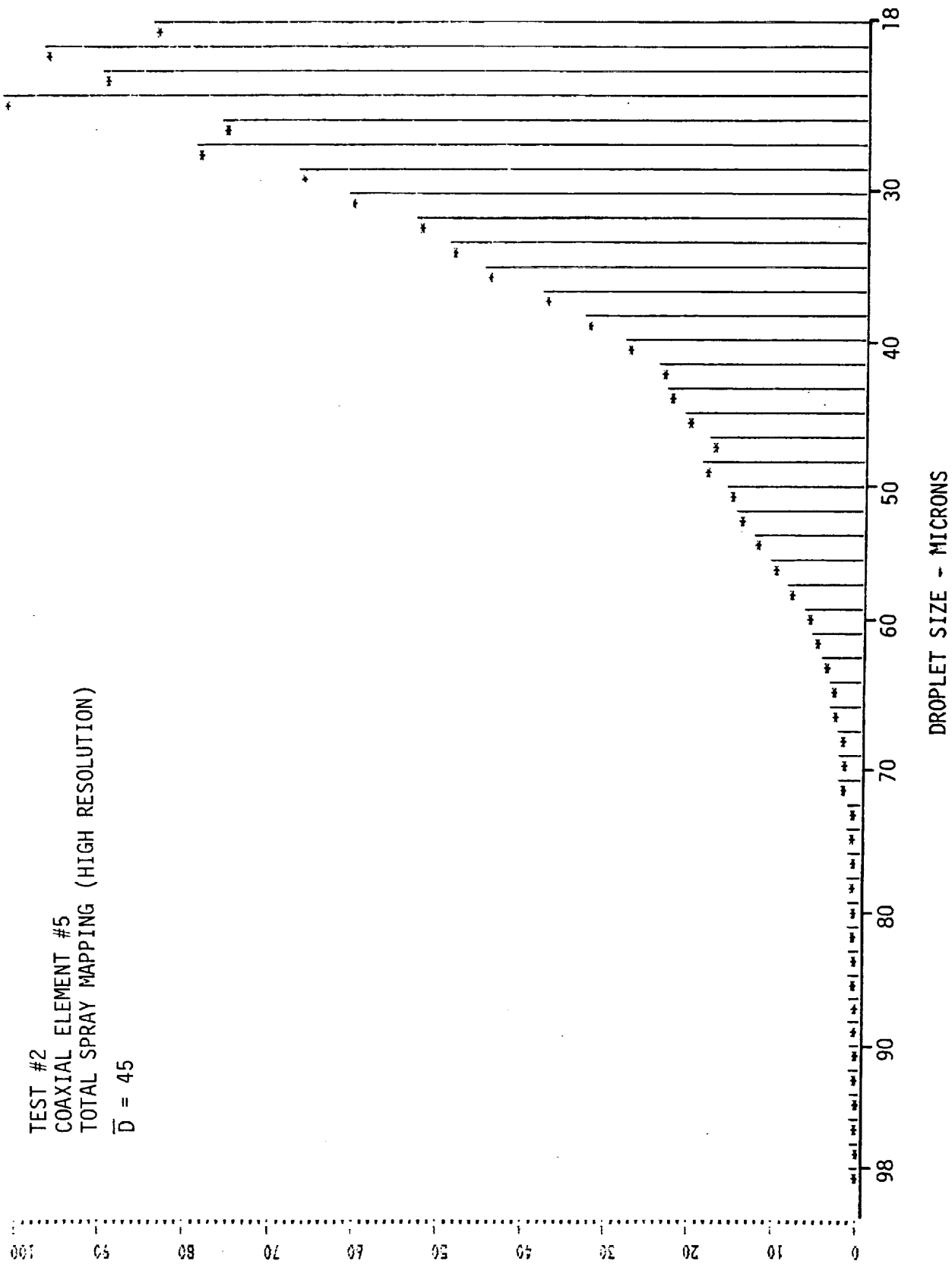
Figure 5-24. Spray Droplet-Size Distribution, Test 2 (0.508 cm point spacing)
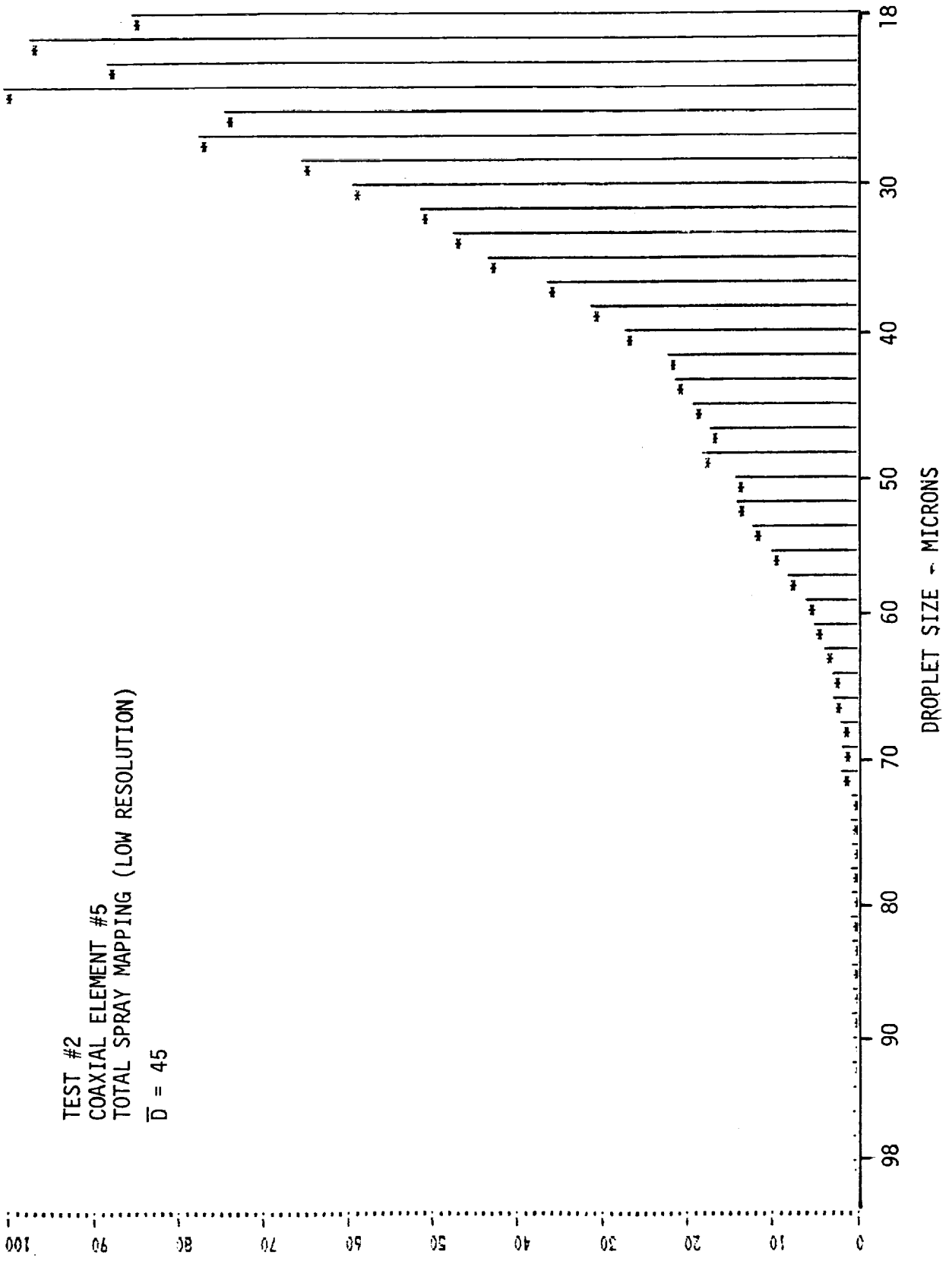
Figure 5-25. Spray Droplet-Size Distribution, Test 2 (1.016 cm point spacing)
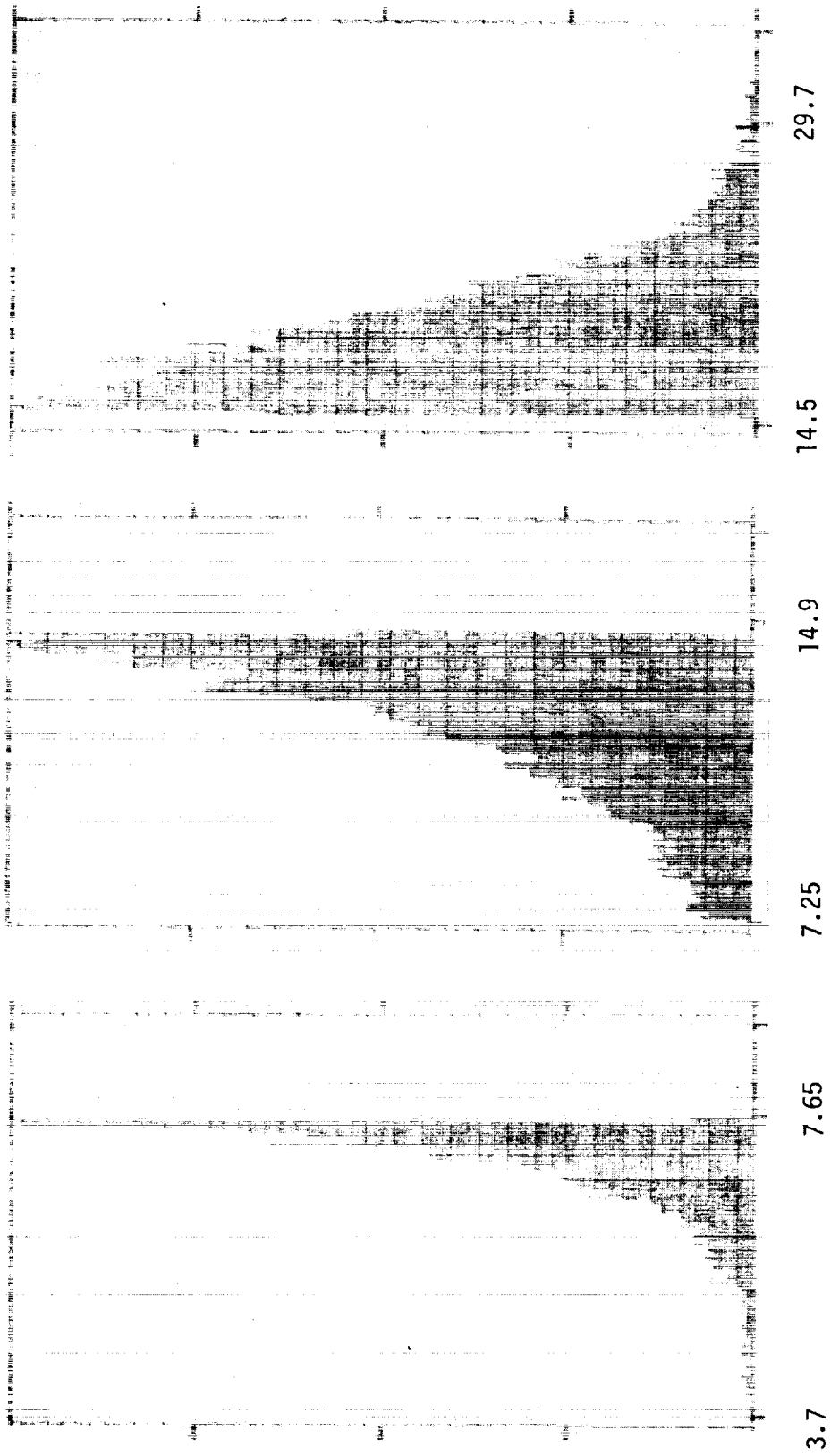
TEST #2
COAXIAL ELEMENT #5
TOTAL SPRAY MAPPING (LOW RESOLUTION)
$\overline{D} = 45$

VELOCITY (METERS/SEC)

RELATIVE COUNTS

8440 SAMPLES.

10,000 SAMPLES

1636 SAMPLES

Figure 5-26. Droplet Velocity Distributions, Test 2, Location (0, 0, 23.5)
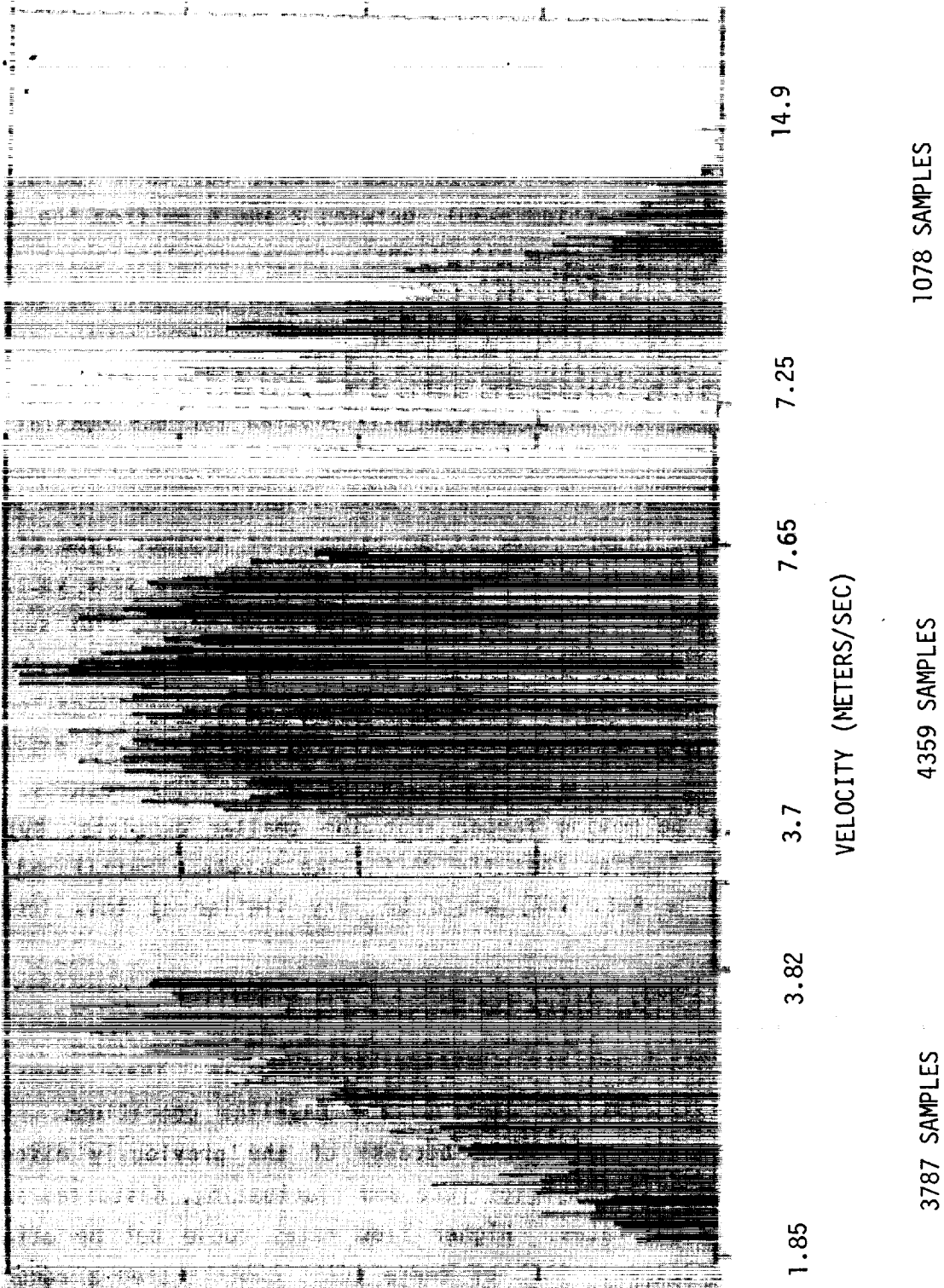
Figure 5-27. Droplet Velocity Distributions, Test 2, Location (0,-4.6, 23.5)

greater than near the edge. All data obtained are based upon a maximum 2-minute measurement time.

The overall spray droplet-size distribution for test 3 (coaxial element 7 at baseline flow conditions) is shown in Fig. 5-28. Also presented are droplet-size distribution plots for the inner core region (Fig. 5-29), out to a radius of 2 cm, and the outer annular region (Fig. 5-30), between 2 and 4 cm from the center of the spray. These results indicate that slightly larger droplets exist in the outer region. However, the difference is quite small, and the spray is surprisingly uniform.

Figure 5-31 presents the overall droplet-size distribution for the coaxial element (element 9) at baseline flow conditions (test 4). As in the previous test, the droplets in the outer region of the spray were slightly larger than in the central core of the spray. Figure 5-32 is an example of another type of data commonly obtained in all these tests. This is a plot of droplet size vs. velocity obtained at the (0, 0, 23.5) location within the spray. This plot suggests only a weak functional relationship between droplet velocity and diameter, a finding substantiated by plots of similar data collected at other locations in the measurement plane. Measurements of this type were obtained at different measurement locations in many of these tests, with very similar results. The larger droplets appear to be moving faster than the smaller droplets, but the difference is small. This implies that the difference between spatial and temporal droplet-size data (see Ref. 1-1) would be very similar at this location within the spray.

Tests 5 and 6 were intended to establish the effect of the injection velocities of the fluids on the atomization characteristics of the spray. These tests were performed at flow rates of 120% and 130% of the baseline conditions. Lower liquid flow rates were judged undesirable because of the previously discussed issues of droplets forming on the injector face and fluctuating, distorted sprays observed at lower liquid flow rates. Higher flow rates could not be attained without choking the gas orifices. Both of these tests demonstrated a reduction in droplet size from the baseline case (test 1). Figures 5-33 and 5-34 present spray droplet-size distributions, based upon measurements along the positive

TEST #3
COAXIAL ELEMENT #7
TOTAL SPRAY MAPPING

$\overline{D}$ = 66

DROPLET SIZE – MICRONS
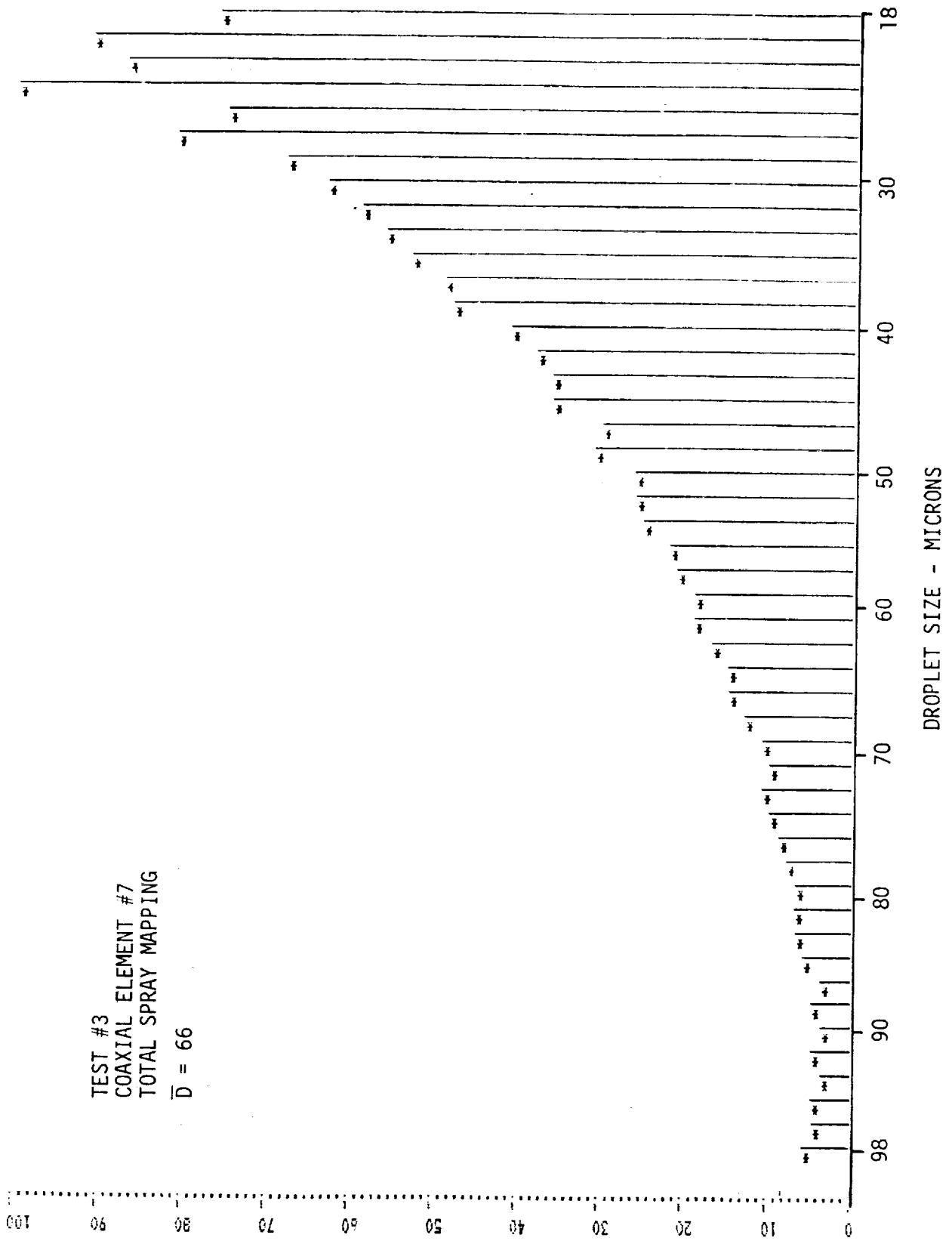
Figure 5.28. Spray Droplet-Size Distribution, Test 3

TEST #3
COAXIAL ELEMENT #7
INNER CORE (r = 0 to 2 cm)

$\overline{D}$ = 62

DROPLET SIZE - MICRONS
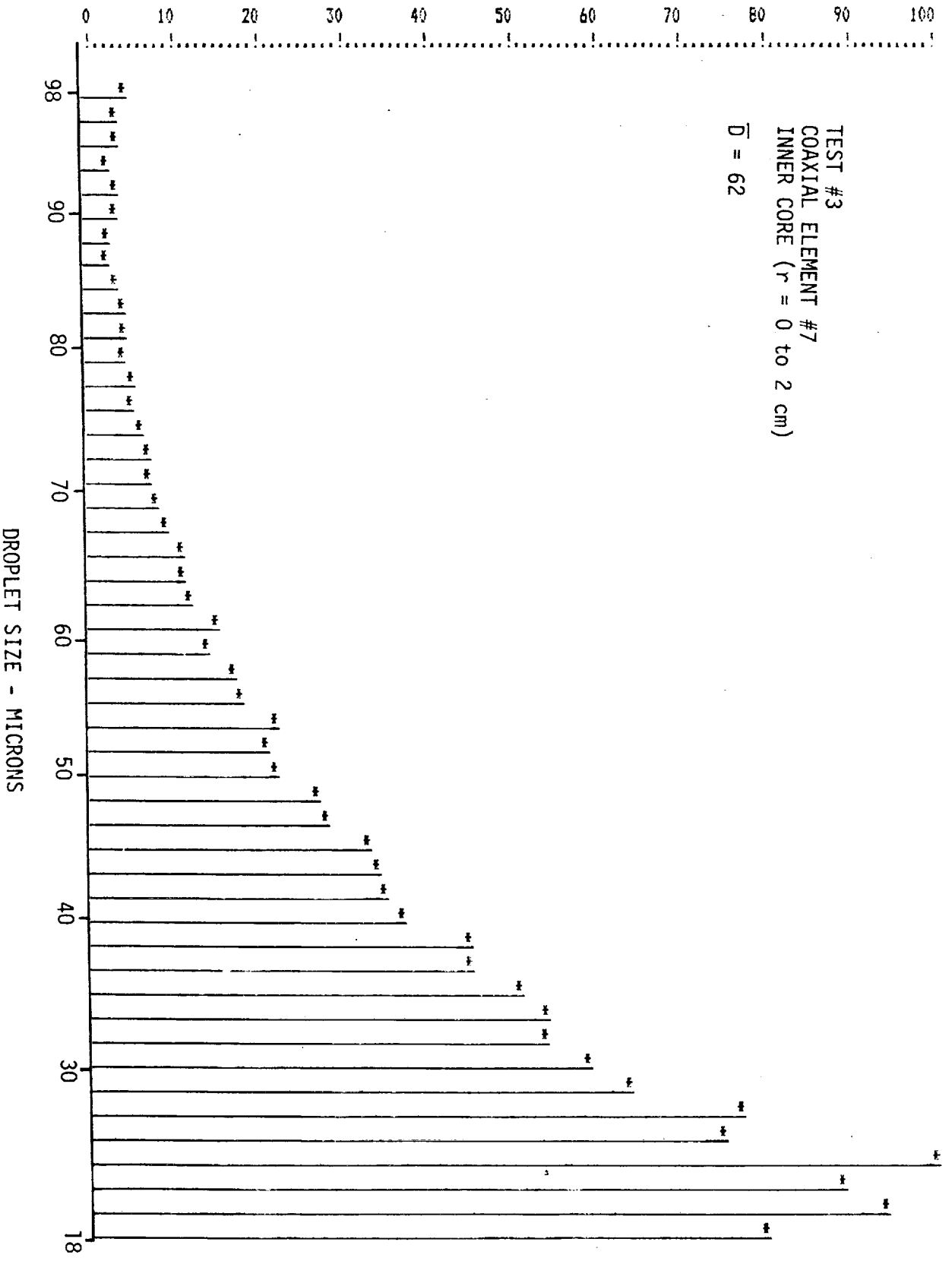
Figure 5-29. Inner Core Droplet-Size Distribution, Test 3

TEST #3
COAXIAL ELEMENT #7
OUTER ANNULUS (r = 2 to 4 cm)

$\overline{D}$ = 69

DROPLET SIZE — MICRONS
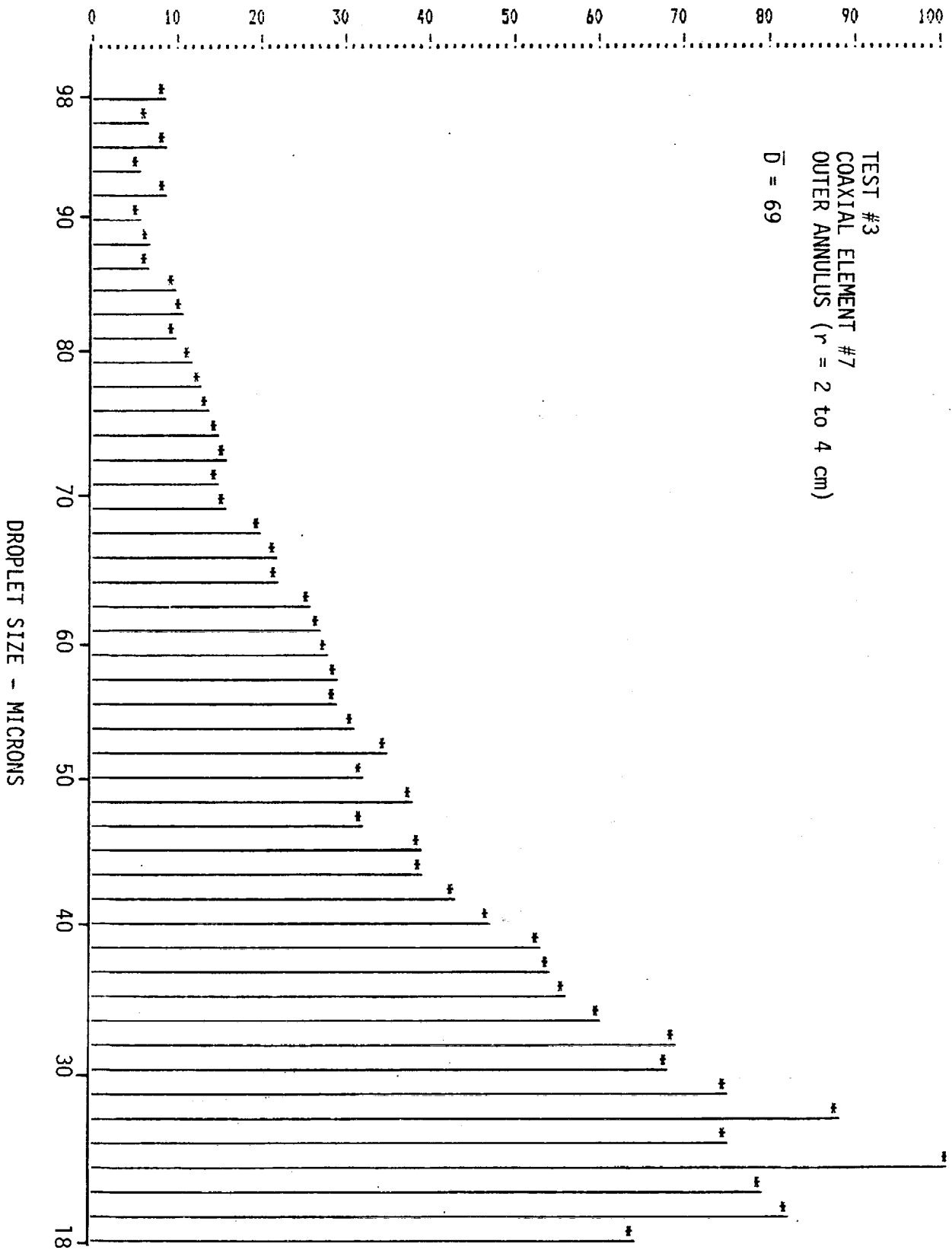
Figure 5-30. Outer Annulus Drop-Size Distribution, Test 3

TEST 4
COAXIAL ELEMENT #9
TOTAL SPRAY MAPPING

$\overline{D} = 67$

DROPLET SIZE – MICRONS
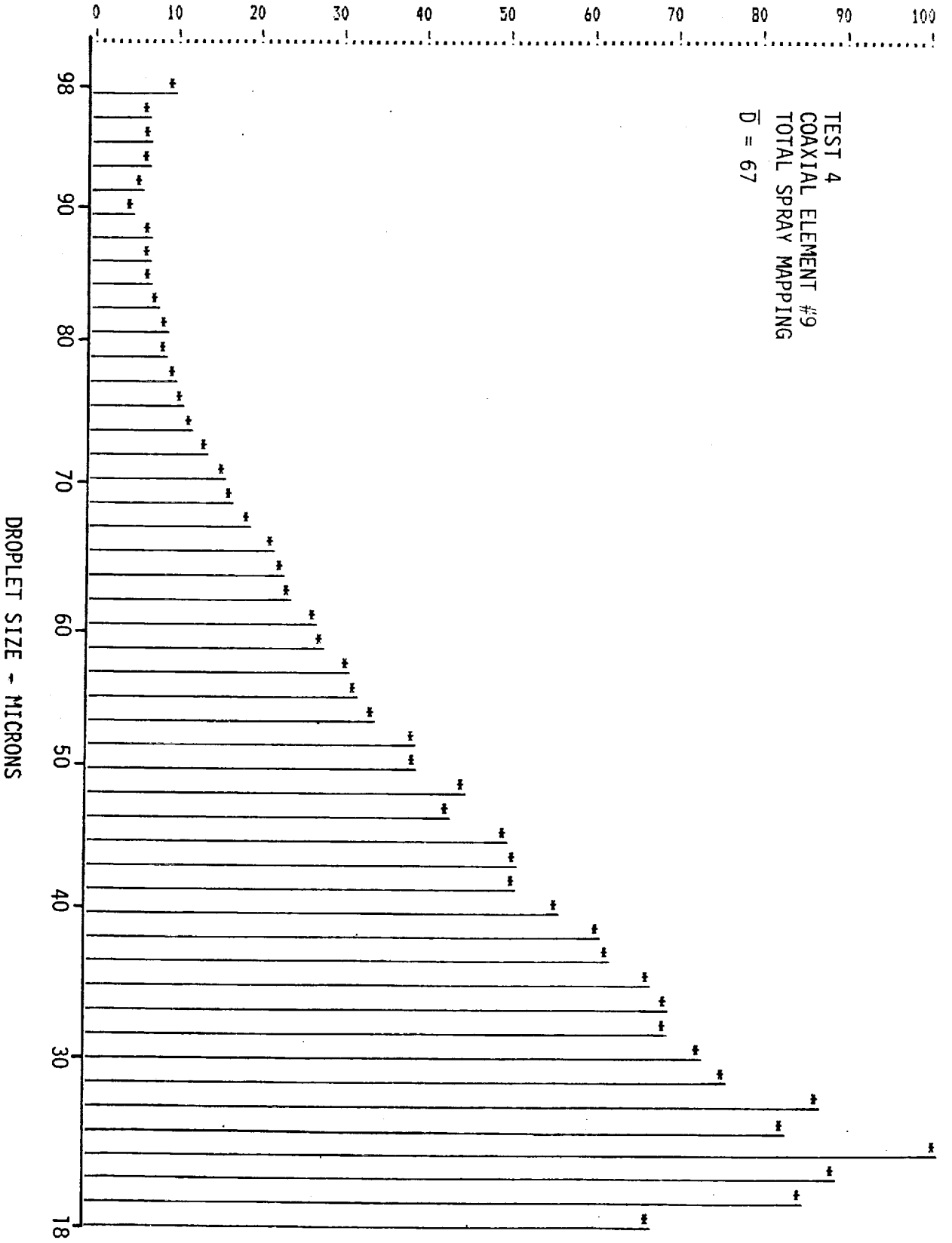
Figure 5-31. Spray Droplet-Size Distribution, Test 4

VELOCITY (METERS/SEC)

DROP SIZE (MICRONS)
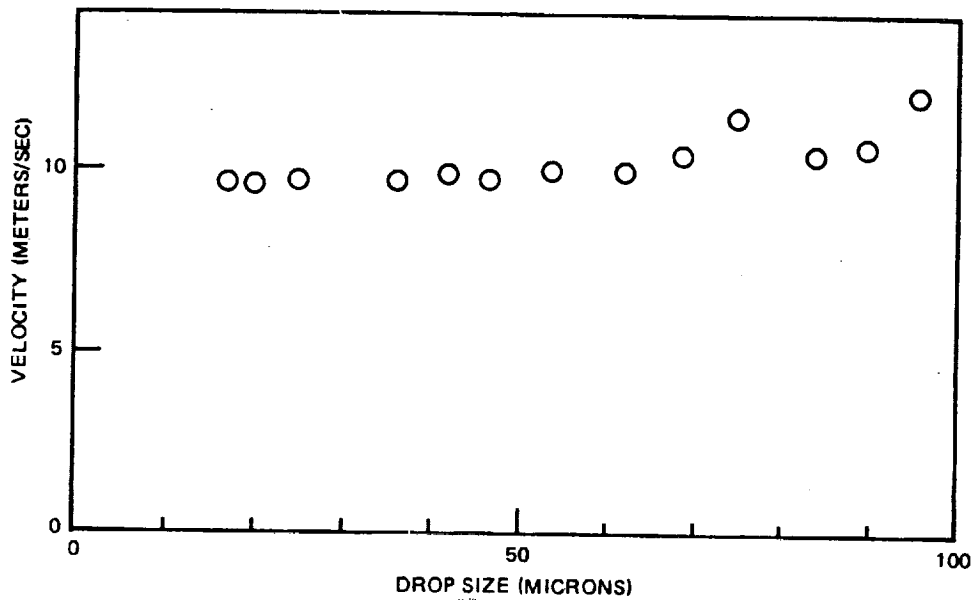
TIME PERIOD. 20.45 SECONDS   VP-1001 STATUS
VALID VELOCITY SAMPLES: 3072
VALID SIZE SAMPLES: 3072   RANGE: 3
NORMAL PAIR ACQUISITION   FRINGE COUNT. 18
LASER WAVE LENGTH:0.5328 MICRON   % ERROR: 3
COLLECTION FACTOR: 8   COMPARE: 12/5
FRINGE SPACE: 14.5 MICRONS   HIGH VOLTAGE 316
BEAM SPACE: 40.8 MM   THRESHOLD V (MV).0.47
XMIT LENS FOCAL LENGTH: 935 MM

Figure 5-32. Droplet Size vs Velocity at (0, 0, 23.5), Test 4

TEST #6
PENTAD ELEMENT
RAY (o, o, 23.5) to (4.06, 0, 23.5)

$D_{10} = 36$ $D_{30} = 40$

$D_{32} = 44$ $\overline{D} = 49$

DROPLET SIZE - MICRONS

Figure 5-33. Positive X-Axis Spray Droplet-Size Distribution, Test 6
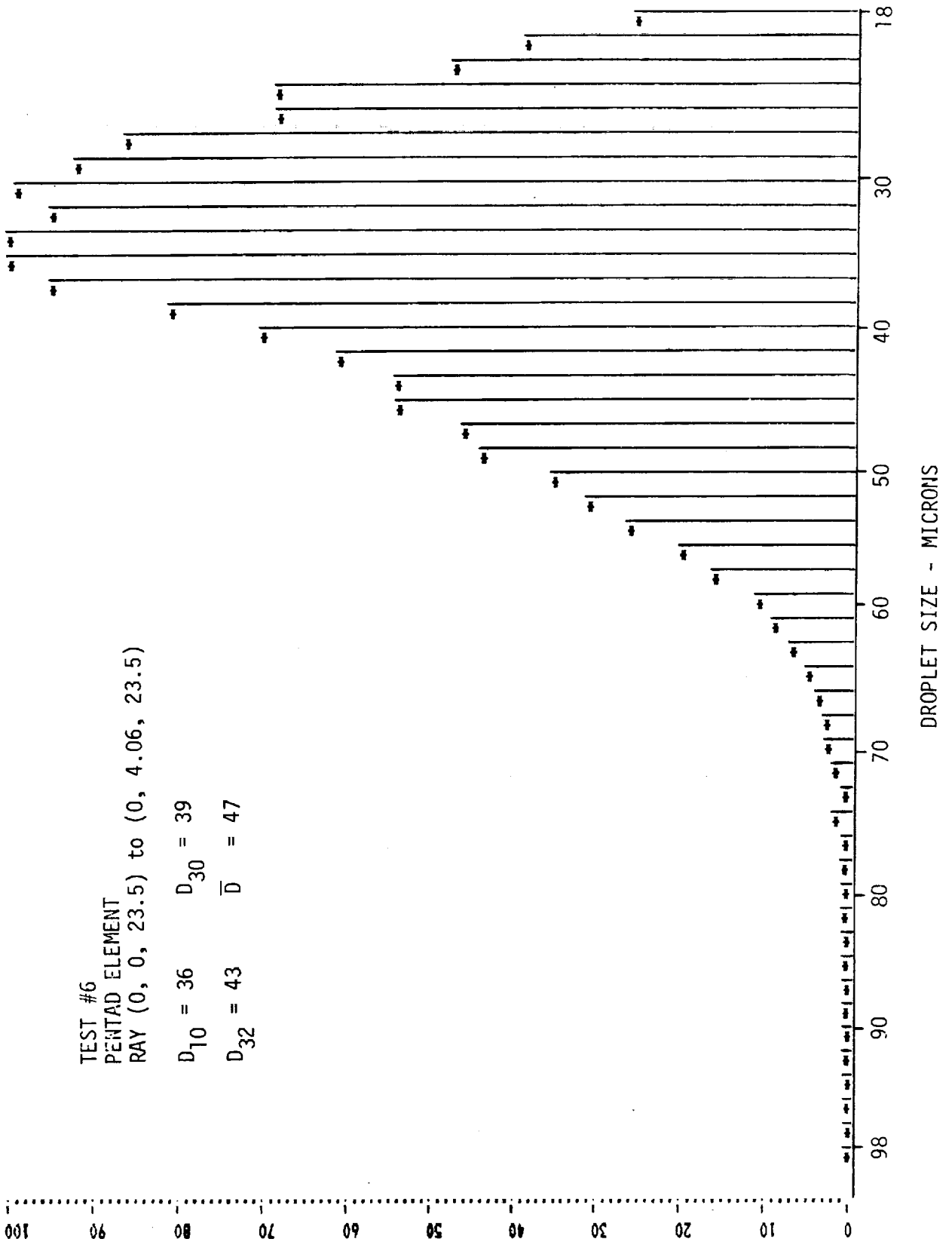
Figure 5-34. Positive Y-Axis Spray Droplet-Size Distribution, Test 6

TEST #6
PENTAD ELEMENT
RAY (0, 0, 23.5) to (0, 4.06, 23.5)

$D_{10} = 36$ $D_{30} = 39$

$D_{32} = 43$ $\overline{D} = 47$

DROPLET SIZE - MICRONS

x-axis and the positive y-axis, respectively, for the 130% flow-rate case (test 6). These figures again demonstrate the commonly observed uniformity of these sprays. Unfortunately, no droplet-size measurements were obtained along any diagonal rays. However, observations of the pentad spray (using a strobe light source) indicated no apparent fans or lobes from this pentad. The spray appeared similar to that of a coaxial element.

Tests 7 and 8 were performed to assess injector velocity effects (at constant mixture ratio) on the atomization characteristics of the spray produced by the preburner coaxial element (element 5). Tests were performed at 120% and 130% of the baseline flow rate. Both test conditions produced significantly larger droplets than the baseline case. Also, both tests demonstrated a distinct difference between results obtained along the two rays mapped. In both tests, the droplet-size distributions measured along the +y axis had a mass median diameter that was 10 microns lower than that of the +x axis. These results, for the 120% flow rate case, are presented in Fig. 5-35 and 5-36. No such difference in drop sizes along any of the four rays measured in the baseline flow-rate case were observed.

In tests 9 and 10, the higher mixture ratio coaxial element (element 7) was tested at 80% and 130% of its baseline flow rate. The higher liquid baseline flow rates for this element allow some reduction in liquid flow rate without producing unrealistic sprays. The overall spray droplet-size distributions for this element, at 80% and 130% of baseline flow levels, are presented in Fig. 5-37 and 5-38. These results, together with the baseline test (test 3) appear to indicate a slight increase in droplet size with flow rate. However, measurements performed at the (0, 0, 23.5) location at 80%, 100%, 130%, and 150% of baseline showed no obvious trend. In all cases, droplet velocities increased with flow rate.

Tests 11 and 12 consisted of spray mappings of the coaxial element (element 9) at 80% and 130% of the baseline flow rate. The results of these tests, together with the baseline test, are inconclusive. Change in the droplet-size distributions among tests 4, 11, and 12 are small and indicate no trends.
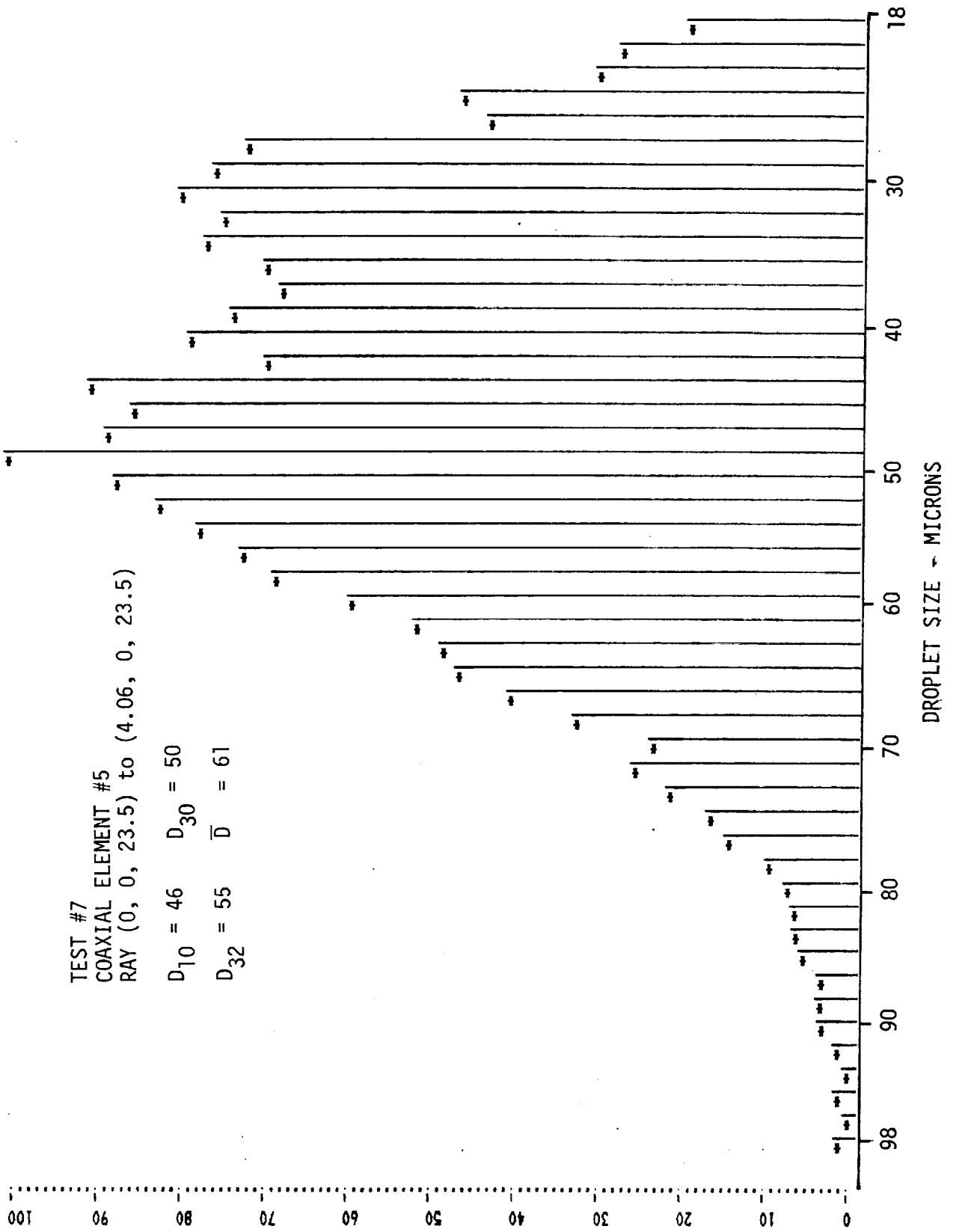
Figure 5-35. Positive X-Axis Spray Droplet-Size Distribution, Test 7

TEST #7
COAXIAL ELEMENT #5
RAY (0, 0, 23.5) to (4.06, 0, 23.5)

$D_{10} = 46$ $D_{30} = 50$
$D_{32} = 55$ $\overline{D} = 61$

DROPLET SIZE - MICRONS

TEST #7
COAXIAL ELEMENT #5
RAY (0, 0, 23.5) to (0, 4.06, 23.5)

D_{10} = 43 D_{30} = 45
D_{32} = 49 $\overline{D}$ = 52

DROPLET SIZE – MICRONS
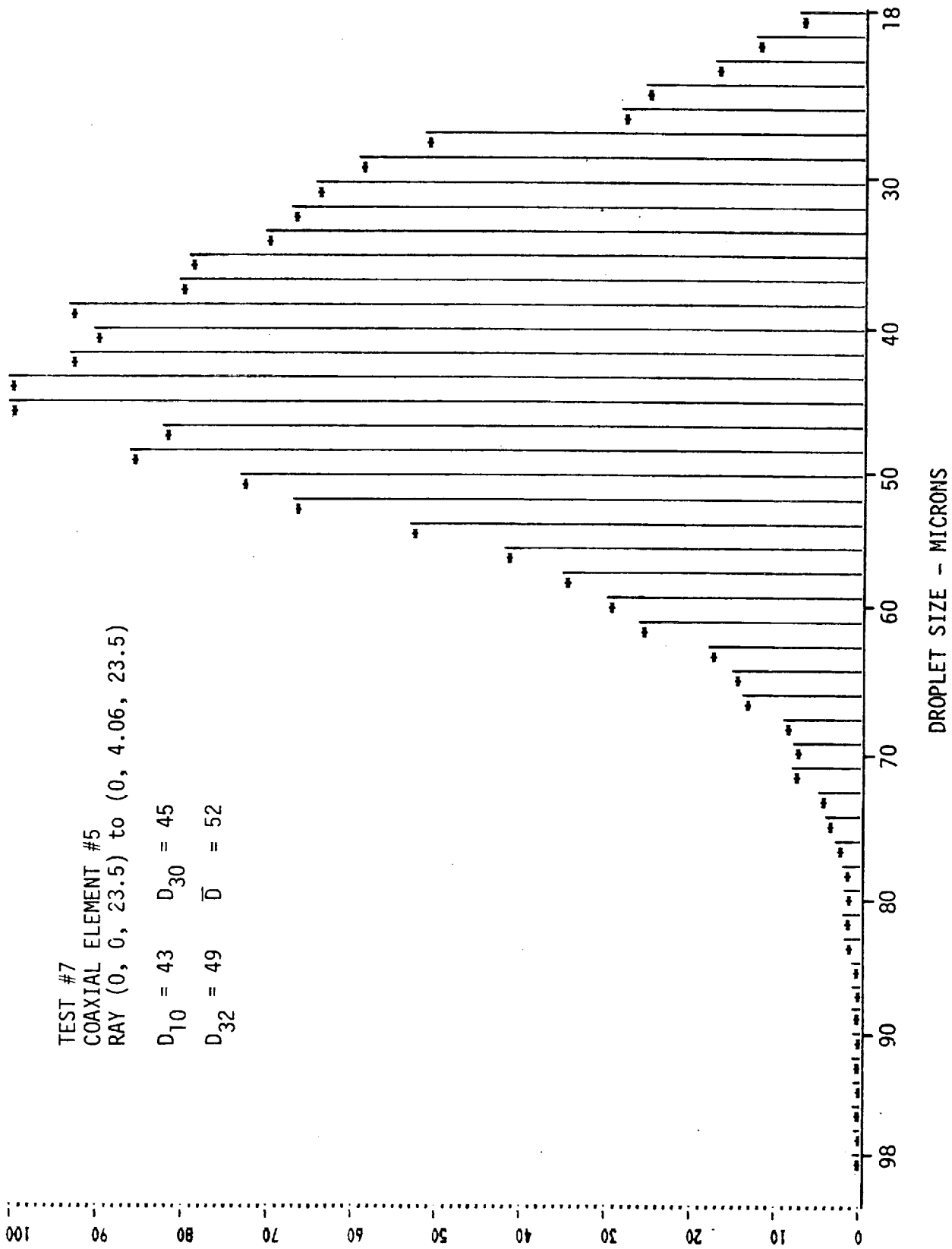
Figure 5-36. Positive Y-Axis Spray Droplet-Size Distribution, Test 7
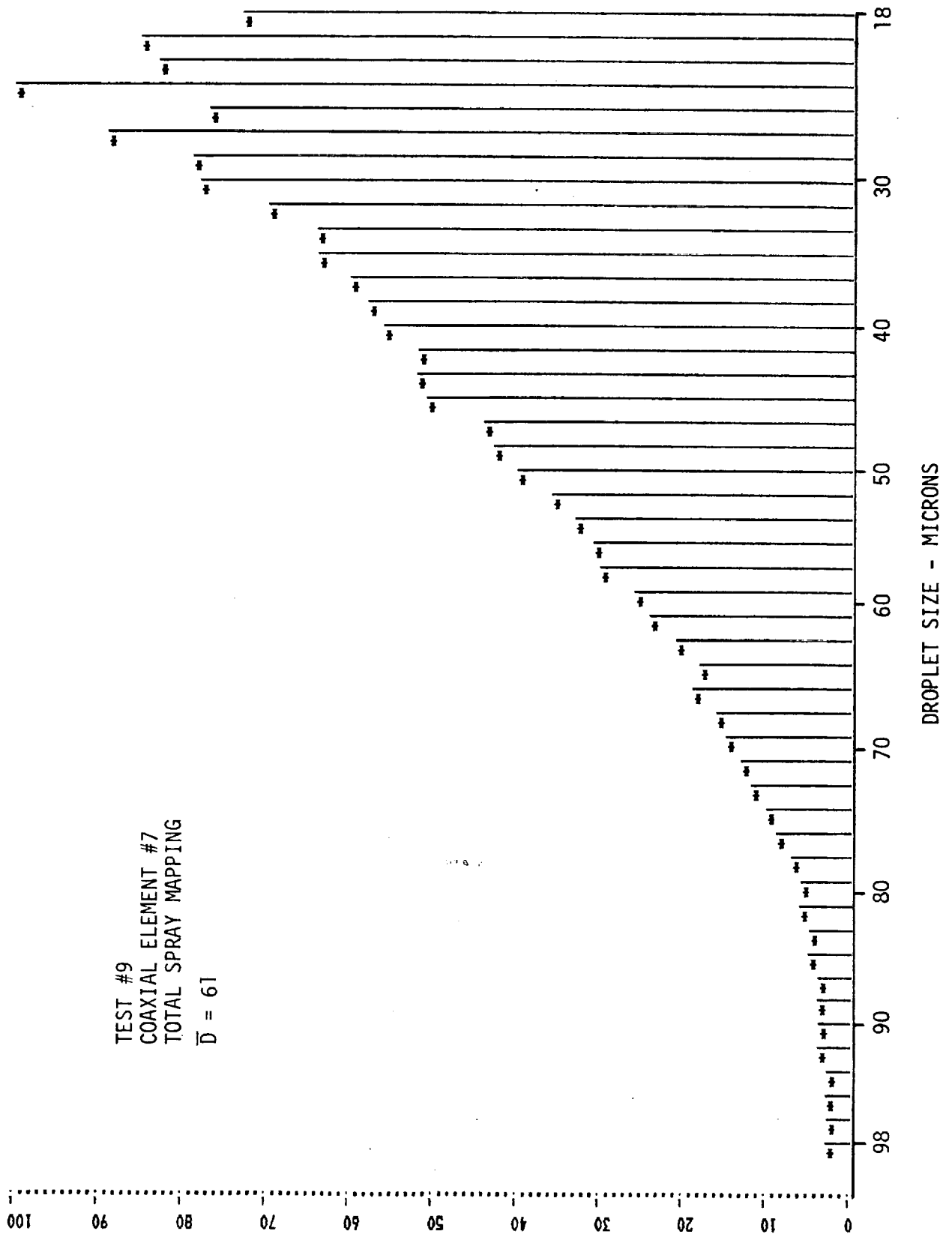
Figure 5-37. Spray Droplet-Size Distribution, Test 9

TEST #9
COAXIAL ELEMENT #7
TOTAL SPRAY MAPPING
$\overline{D} = 61$
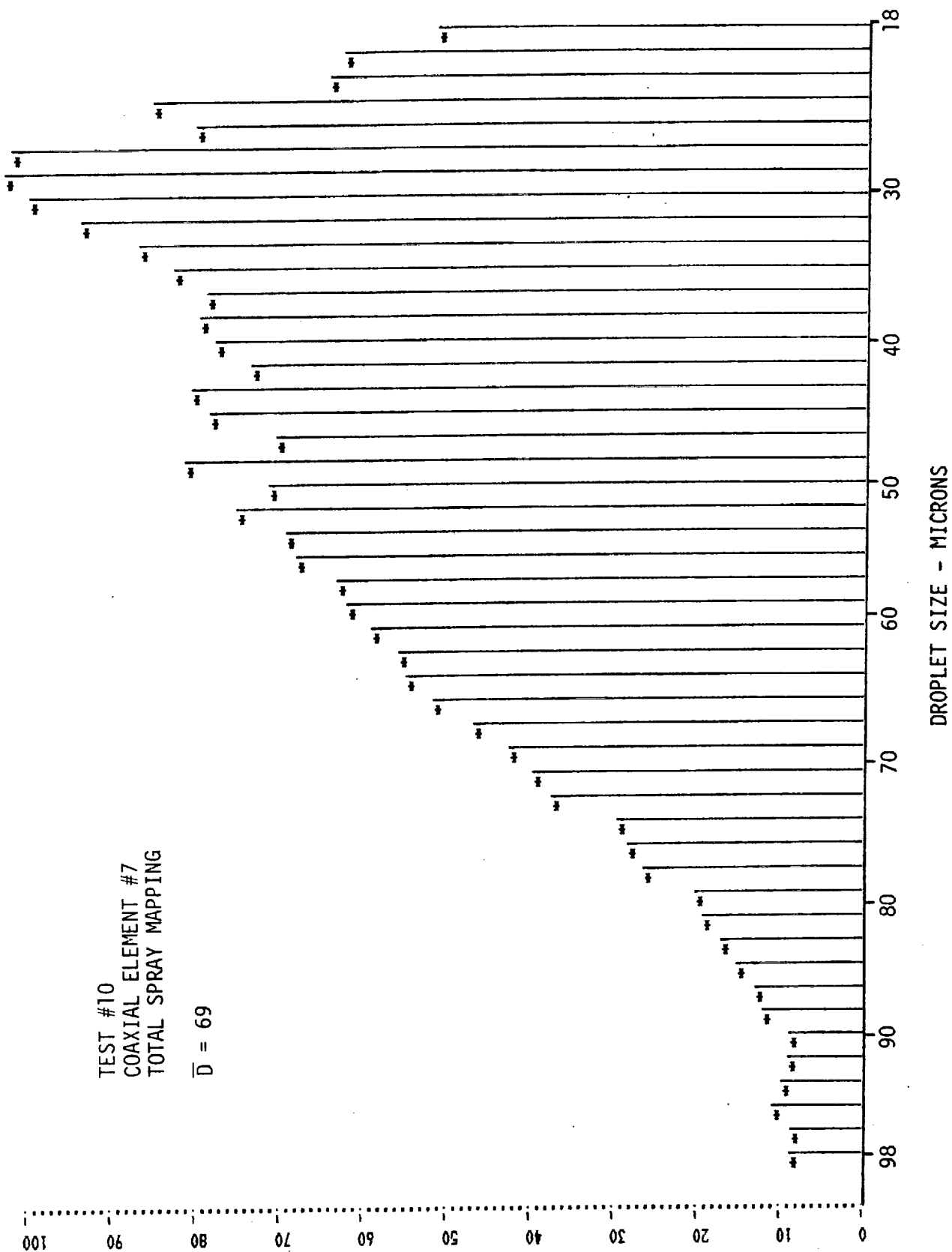
DROPLET SIZE – MICRONS

Figure 5-38. Spray Droplet-Size Distribution, Test 10

TEST #10
COAXIAL ELEMENT #7
TOTAL SPRAY MAPPING

$\overline{D} = 69$

DROPLET SIZE - MICRONS

The properties effects test employed the pentad element and the smaller main chamber coaxial element (element 7), flowing different liquids. Baseline volumetric flow conditions were employed. The nitrogen flow rate was maintained at the baseline value and the liquid volumetric flow rate was set equal to the baseline volumetric flow rate. Density variations in the liquids employed resulted in corresponding variations in the mass mixture ratio from the baseline case.

To investigate the effects of viscosity, a mixture of distilled water and glycerol was prepared. This mixture consisted of 16% glycerol by mass. The overall spray droplet-size distributions for the pentad (test 13) and the coaxial element (test 14) are presented in Fig. 5-39 and 5-40, respectively. Comparing these results with the corresponding baseline tests (Fig. 5-23 and 5-28, respectively) demonstrates the following: the effect of viscosity on the pentad element is large -- the more viscous fluid produced a much finer spray. The effect of viscosity on the coaxial element spray is smaller and opposite -- the more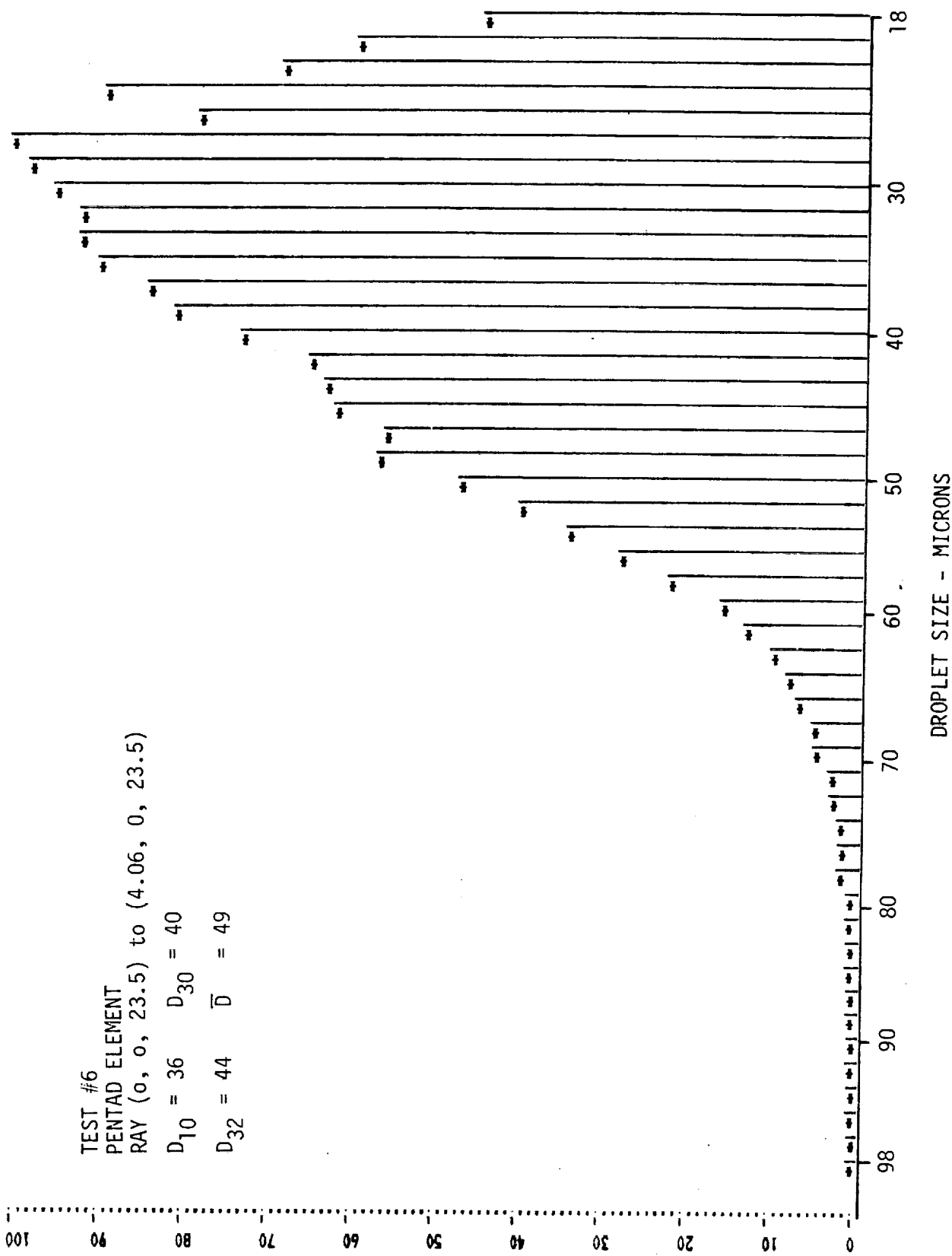 viscous fluid produced slightly larger droplets. It is generally believed, and confirmed by others investigating fluid properties effects on atomization, that the effect of higher viscosity is to increase droplet diameters. Viscosity is thought to retard the shearing of the fluid and thereby allow larger fluid particles to escape from the primary atomization region. The pentad element, operating at this low flow rate, was already subject to flow abnormalities, as previously discussed. It may be that the increased fluid viscosity further aggravated this problem and produced this surprising, and possibly unrealistic, result.

Tests 15 and 16 utilized the same pentad and coaxial elements as the previous pair of tests. The liquid employed was a salt (pure sodium chloride with no additives) dissolved in distilled water (17.4% NaCl by mass). This resulted in a liquid of greater density, but also of significantly greater viscosity, than pure water. The pentad test (test 15) resulted in droplet sizes comparable to those of the viscosity effects tests (test 13). Droplets near the center of the spray were found to be considerably smaller than those near the periphery of the spray, as shown in Fig. 5-41 and 5-42. This effect is also apparent, though to a lesser

TEST #13
PENTAD ELEMENT
TOTAL SPRAY MAPPING

$\overline{D} = 52$

DROPLET SIZE — MICRONS
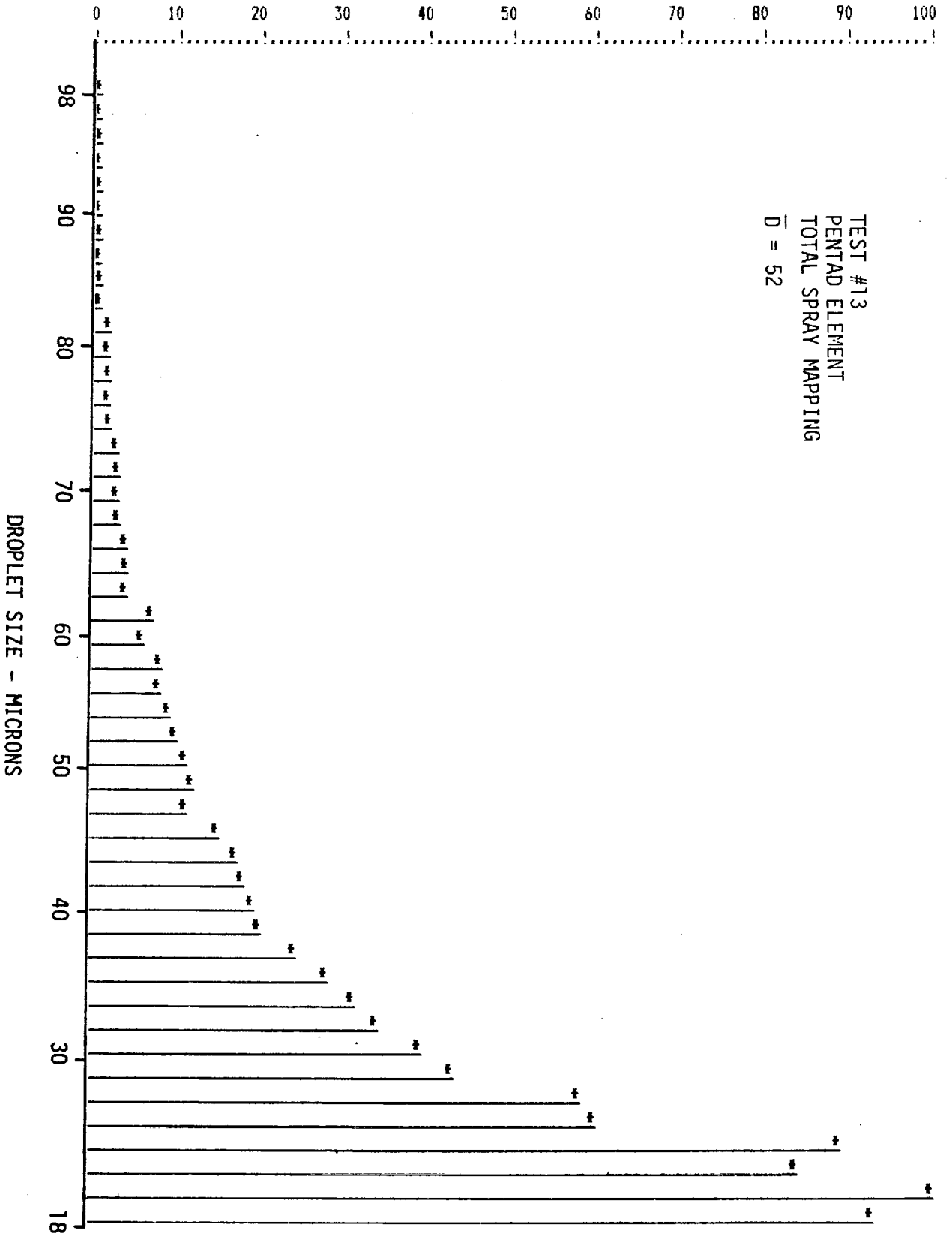
Figure 5-39. Spray Droplet-Size Distribution, Test 13

TEST #14
COAXIAL ELEMENT #7
TOTAL SPRAY MAPPING

$\overline{D} = 74$

DROPLET SIZE ÷ MICRONS
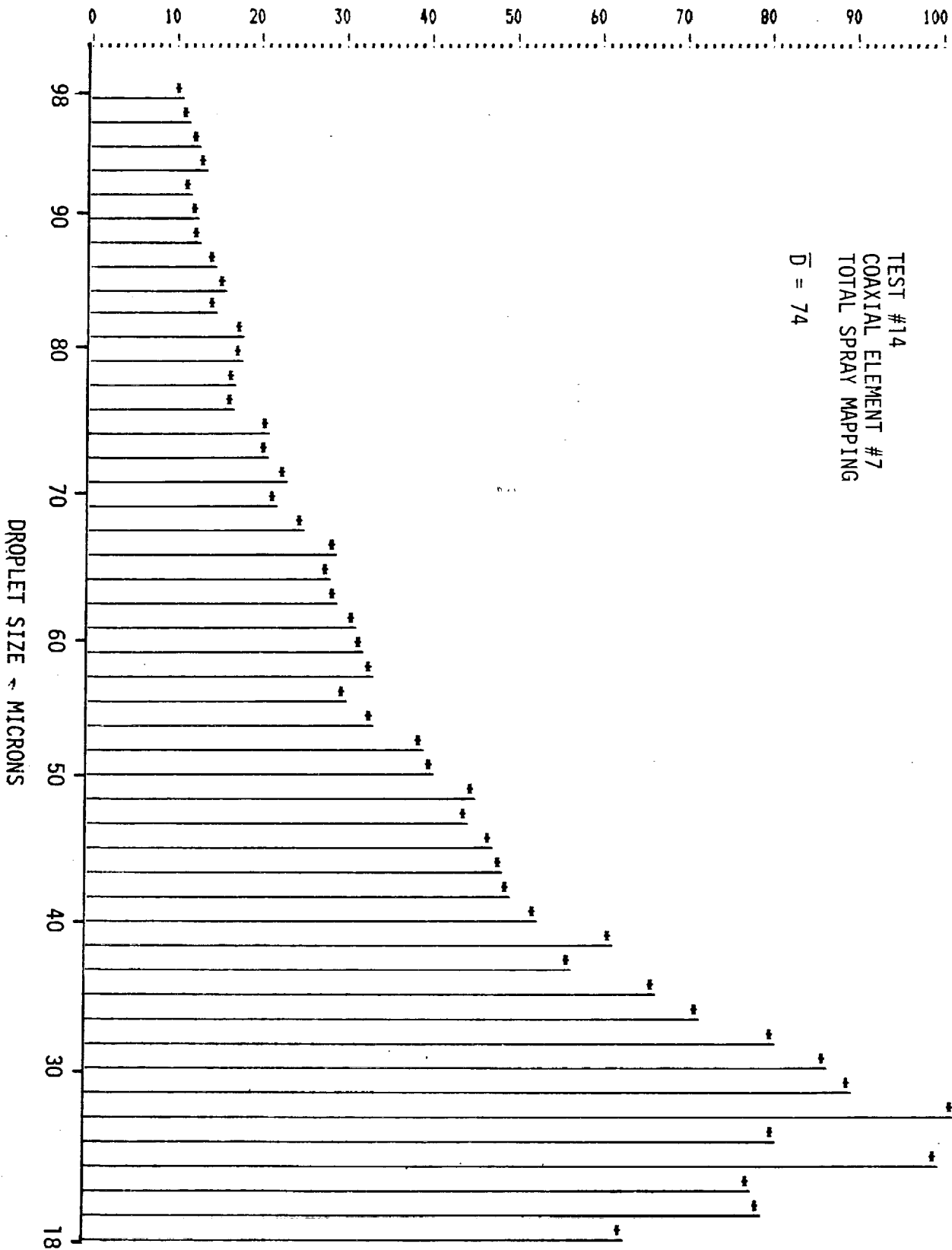
Figure 5-40. Spray Droplet-Size Distribution, Test 14

TEST #15
PENTAD ELEMENT
INNER CORE (r < 3.3 cm)

$\overline{D} = 49$

DROPLET SIZE — MICRONS
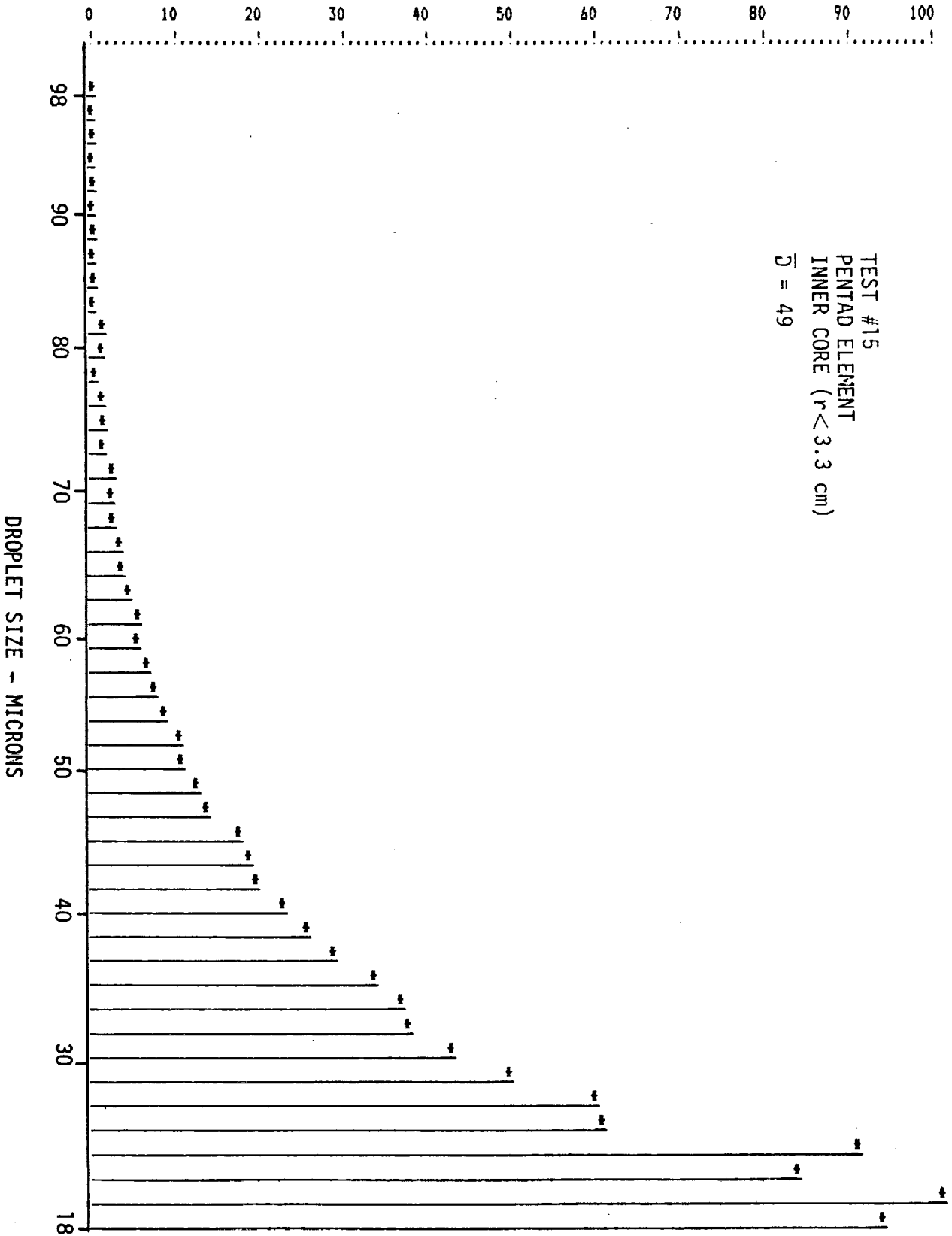
Figure 5-41. Inner Core Droplet-Size Distribution, Test 15

TEST #15
PENTAD ELEMENT
OUTER ANNULUS (r > 3.3 cm)

$\overline{D} = 61$

DROPLET SIZE - MICRONS
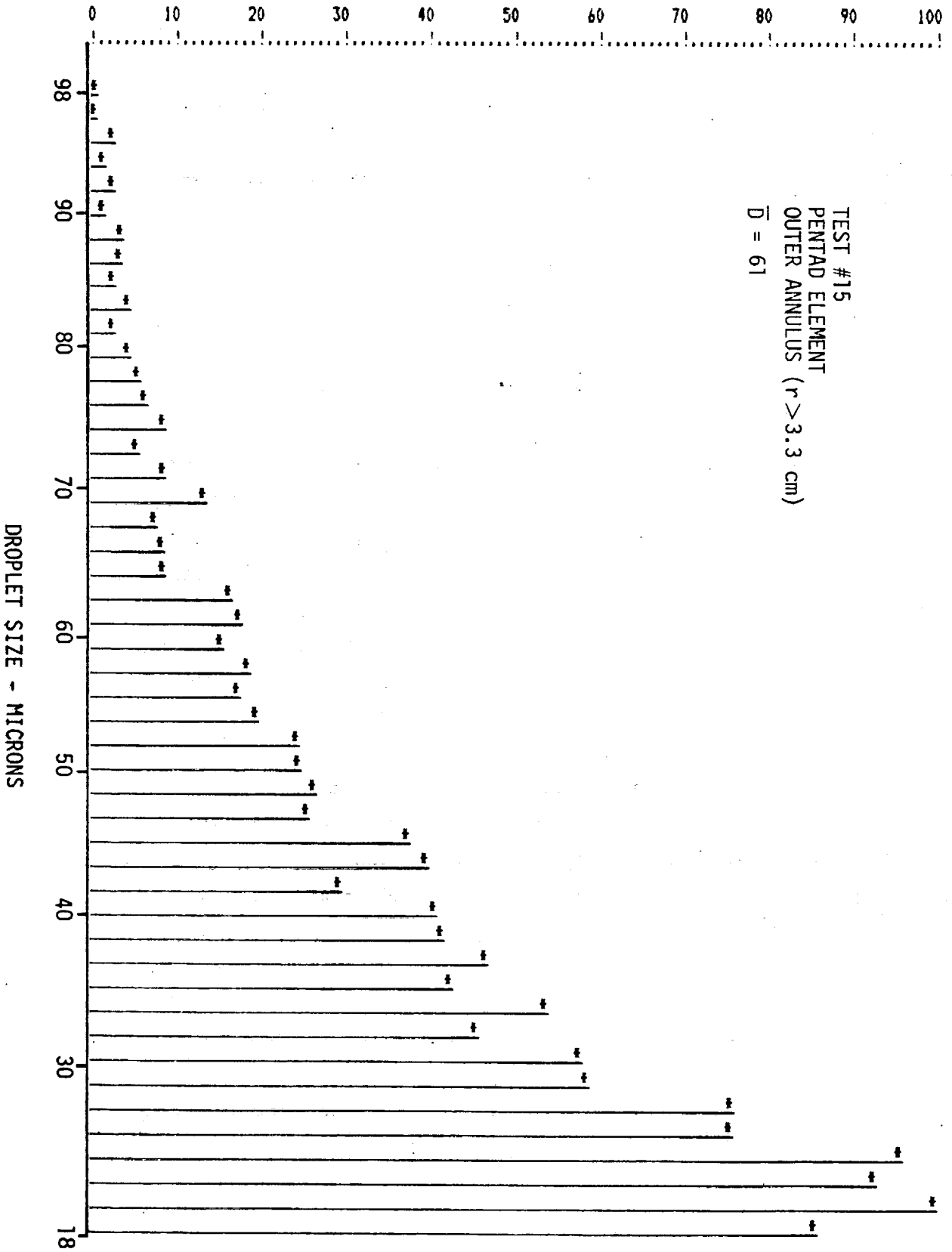
Figure 5-42. Outer Annulus Droplet-Size Distribution, Test 15

degree, in the viscosity effects test (test 13) and the baseline conditions test (test 1) with this pentad element.

The coaxial element density effects test (test 16) produced a spray with an over-all droplet-size distribution very similar to the baseline test (test 3) shown in Fig. 5-28. Also, as with the baseline test, the droplets near the periphery of the spray were larger than those near the center.

The final pair of tests in these properties effects tests employed pure 1, 1, 1, --trichloroethane liquid. This liquid provided significant deviation of density and viscosity from pure water, but the major difference was the change in surface tension. The overall spray droplet-size distribution for the pentad element is presented in Fig. 5-43. Note the change in the droplet size (abscissa) scale. This is caused by the substantial index of refraction difference between water and trichloroethane, which modifies the DSI droplet measurement range. The index of refraction changes for the other liquids used was insignificant. This test again demonstrated larger droplets in the outer region of the spray.

The total spray droplet-size distribution for the coaxial element flowing tri-chloroethane and nitrogen at baseline volumetric flow rates is presented in Fig. 5-44. Comparison of this case with the baseline (Fig. 5-28) shows how strongly the computed mass median diameter is affected by a few larger droplets. Test 18 produced a droplet distribution with a peak (mode) at about 26 to 30 microns, as compared to the test 3 peak at 20 to 24 microns. Yet, test 18 has a smaller mass median droplet size. Even though the majority of the measured drop-lets in test 18 are larger than those of test 3, the mass median diameter in test 18 is smaller than that of test 3. This is the result of the presence of a rela-tively small number of very large droplets in test 3. The value of $\bar{D}$ is highly sensitive to these larger droplets. This reduction in larger droplets may be caused by the lower surface tension, which is the cohesive force holding the droplet together. Again, most of the very largest droplets were found to be in the outer periphery of the spray.

The hot-wax test comparison results (tests 19 and 20) are discussed shortly. Tests 21 and 22 were performed with coaxial element 7. The nitrogen flow rate

TEST #17
PENTAD ELEMENT
TOTAL SPRAY MAPPING

$\bar{D} = 56$

DROPLET SIZE ~ MICRONS
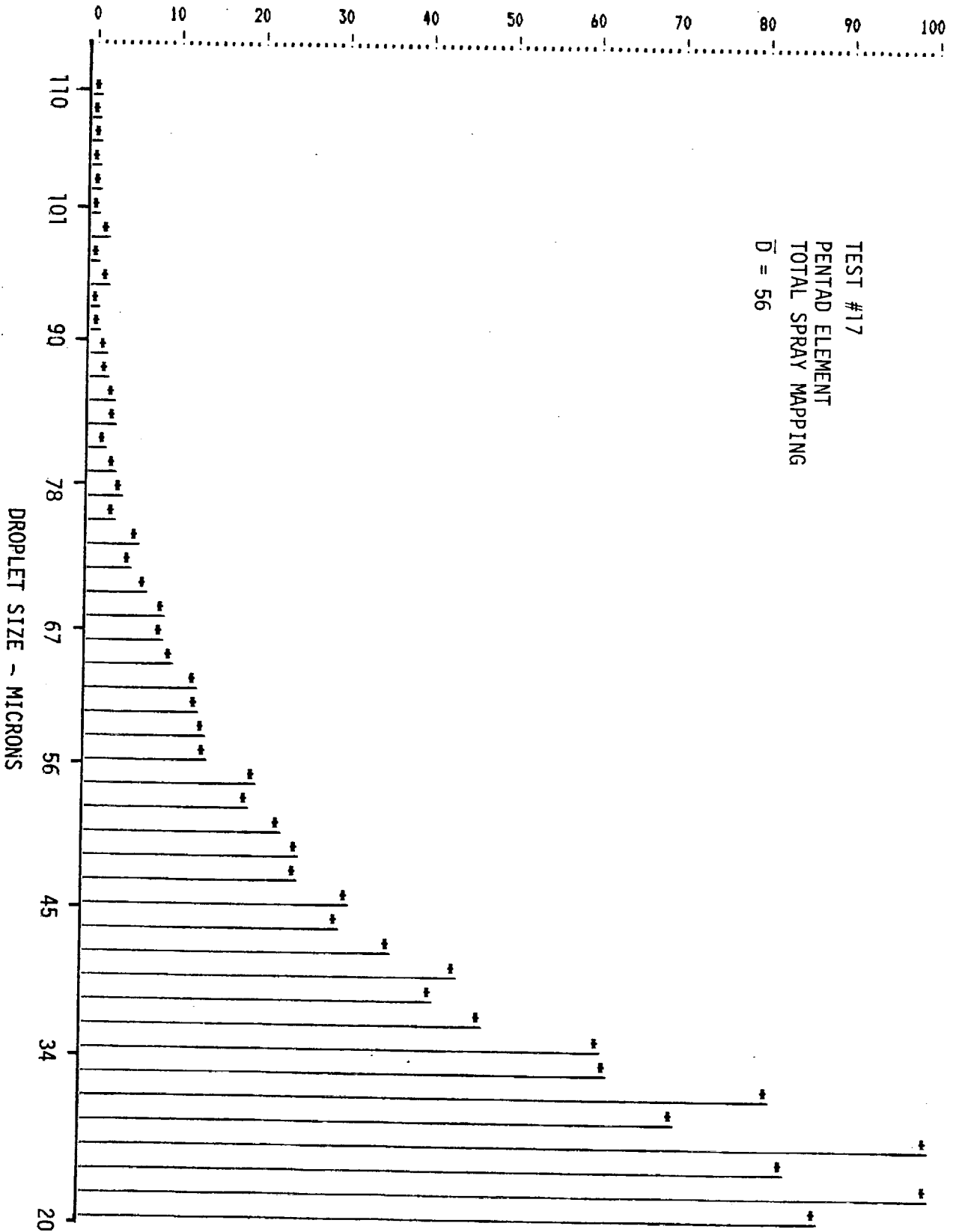
Figure 5-43. Spray Droplet-Size Distribution, Test 17

TEST #18
COAXIAL ELEMENT #7
TOTAL SPRAY MAPPING

$\overline{D}$ = 62

DROPLET SIZE - MICRONS
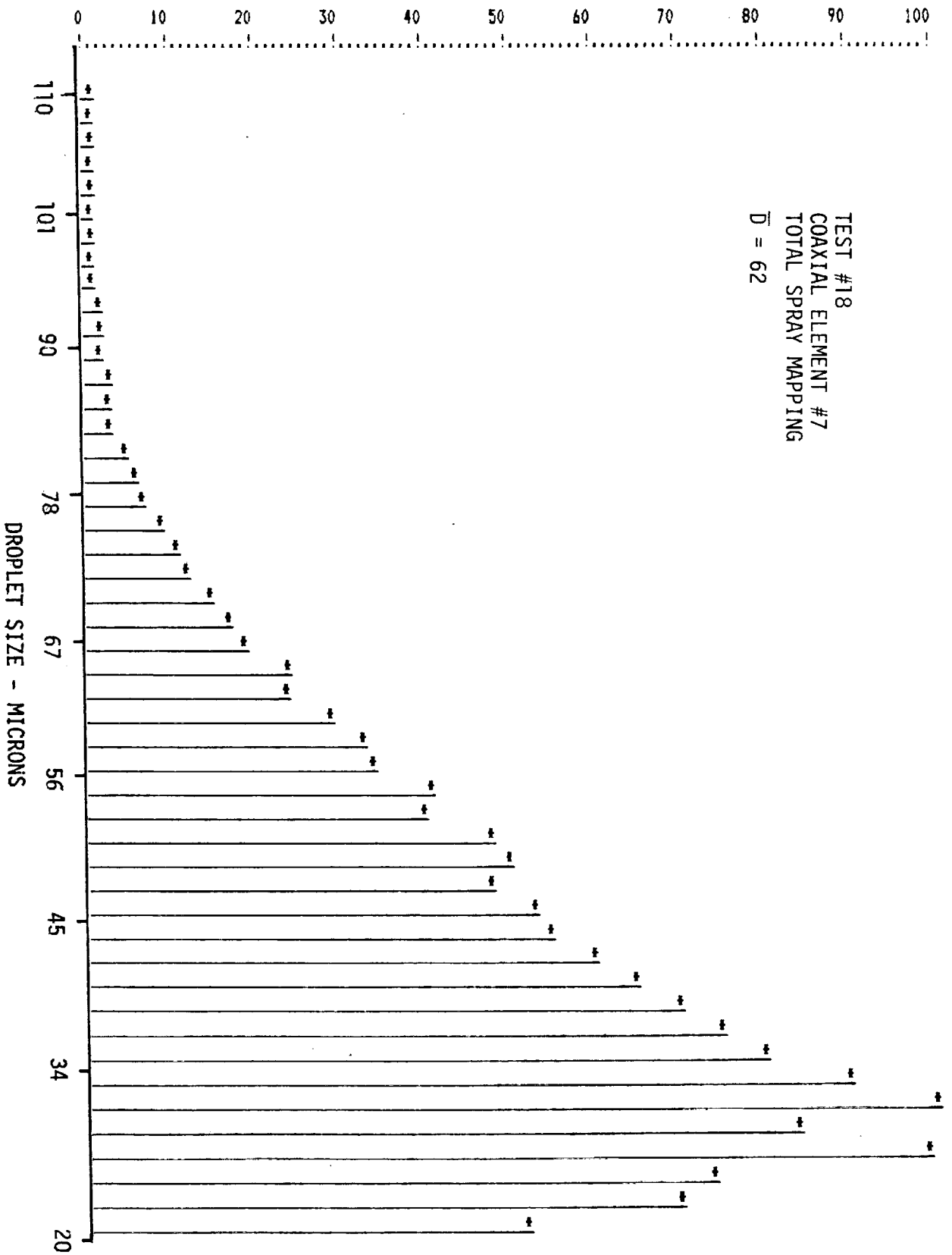
Figure 5-44. Spray Droplet-Size Distribution, Test 18

was maintained at the baseline value and the water flow rate was set at 75% (test 21) and 150% (test 22) of the baseline value. The overall spray droplet-size distribution in these tests is presented in Fig. 5-45 and 5-46. The low liquid flow-rate test (test 21) exhibited much larger droplets than the baseline case. Some of these droplets were larger than the largest size that could be measured with the DSI configuration (fringe spacing) utilized. Undoubtedly, the actual $\bar{D}$ of this spray would be considerably larger than that measured, if these additional large droplets were included. The higher liquid flow-rate test produced a droplet-size distribution similar to that observed in the baseline test.

Two additional tests (test 19 and 20) were performed to provide a comparison with the hot-wax test results of Dickerson (Ref. 5-11). As previously described, these tests used the outer orifices of the small triplet (element 4) flowing water (test 20) and trichloroethane (test 19). This like-doublet was quite similar to one of Dickerson's elements. The overall spray droplet-size distributions for these tests are presented as Fig. 5-47 and 5-48. Flow rates in these tests were very much higher (1.49 and 2.75 liter/min) than all other tests. This was possible because there was no concern about choking a gas orifice. The DSI performance was nominal during these much higher flow-rate (more dense spray) tests.

These tests provided liquid injection velocities within the range tested by Dickerson, almost exactly matched his like-doublet geometry, and injected into the open air in a manner very similar to that of the hot-wax tests. In test 20, droplet sizes at several different flow rates were examined. Lower injection rates resulted in larger droplets, which is in qualitative agreement with Dickerson's findings and those of all other like-doublet atomization investigators (see Ref. 1-1). Both of these tests produced very homogeneous sprays with little variation in droplet size from the inner to the outer region. Also, a distinct "fan pattern" was apparent in the data, with the spray being considerably wider in one dimension than the other. (In test 19, the dimensions at the main body of the spray at the measurement plane were 5.0 by 8.1 cm.)
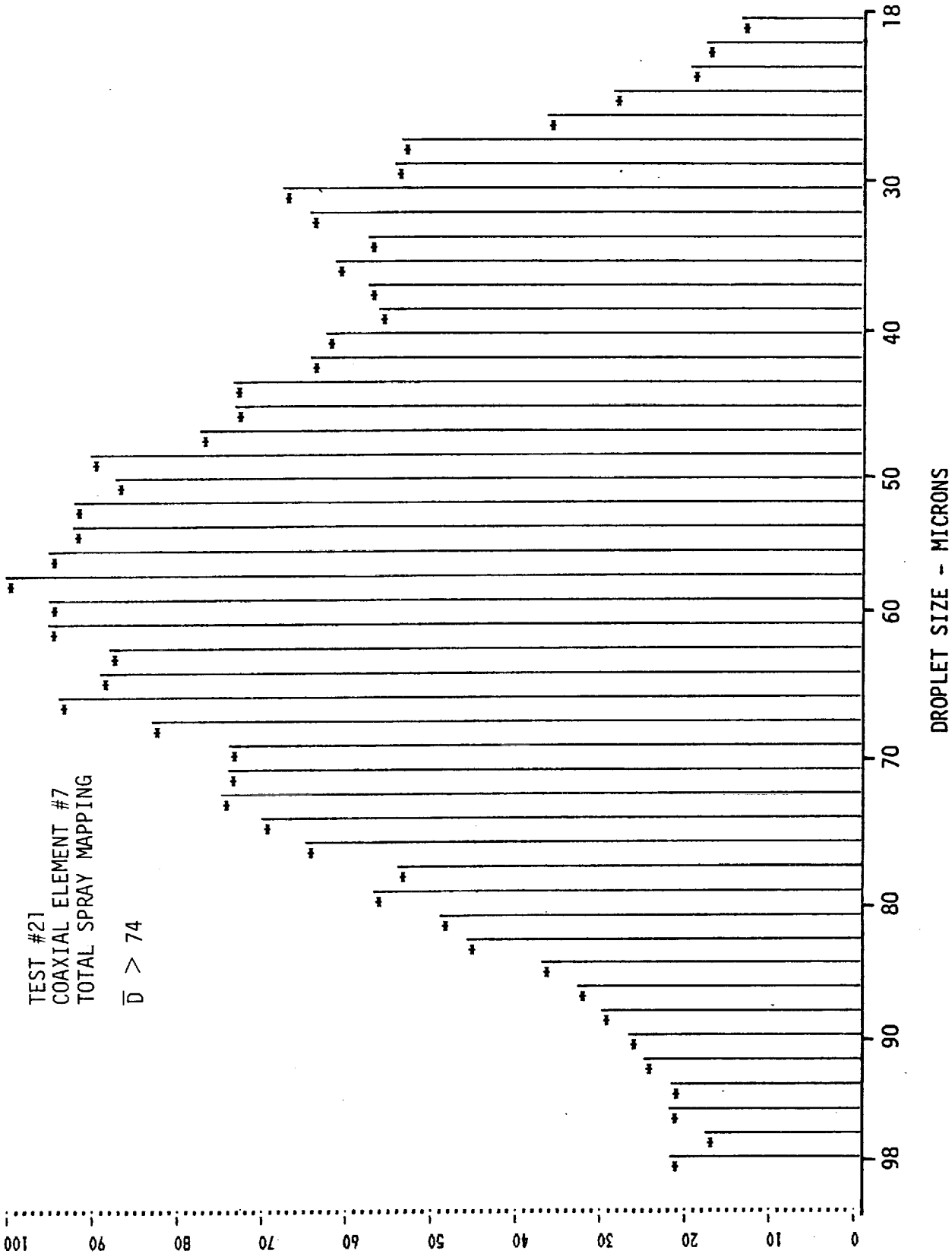
Figure 5-45. Spray Droplet-Size Distribution, Test 21

TEST #21
COAXIAL ELEMENT #7
TOTAL SPRAY MAPPING

$\overline{D} > 74$

DROPLET SIZE – MICRONS

RI/RD85-312

V-84
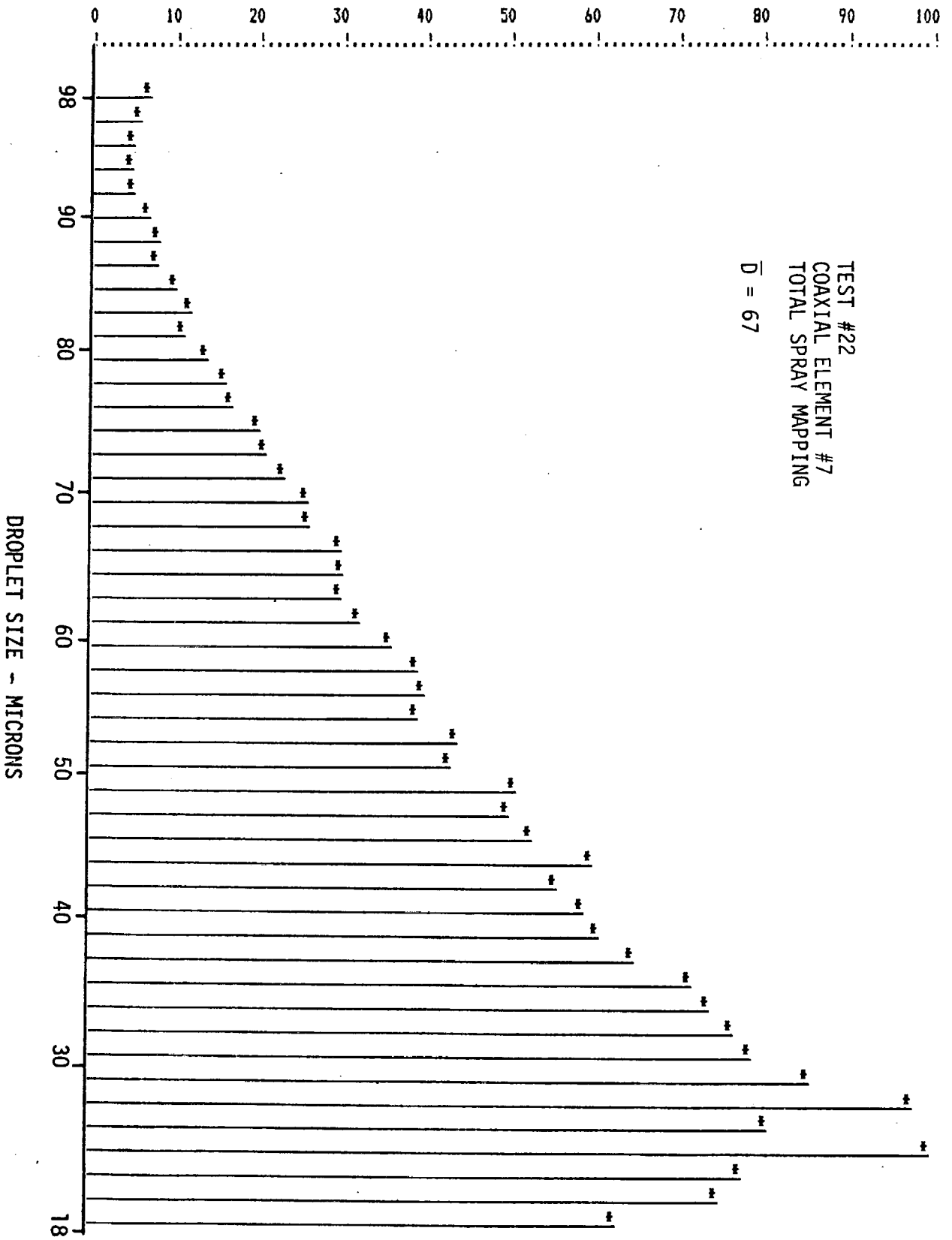
Figure 5-46. Spray Droplet-Size Distribution, Test 22

TEST #22
COAXIAL ELEMENT #7
TOTAL SPRAY MAPPING

$\overline{D} = 67$

DROPLET SIZE — MICRONS
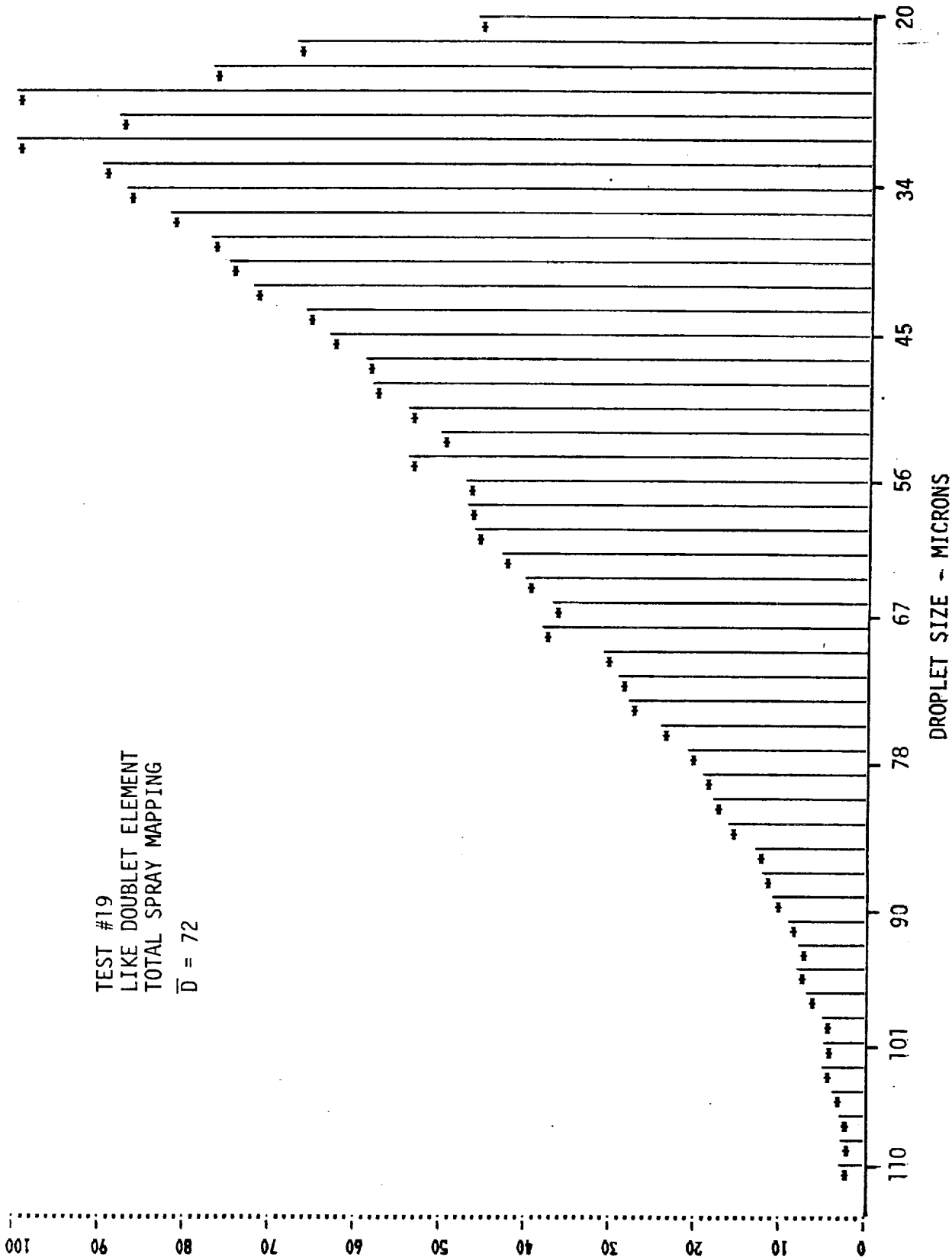
Figure 5-47. Spray Droplet-Size Distribution, Test 19

TEST #19
LIKE DOUBLET ELEMENT
TOTAL SPRAY MAPPING
$\overline{D} = 72$

C-3
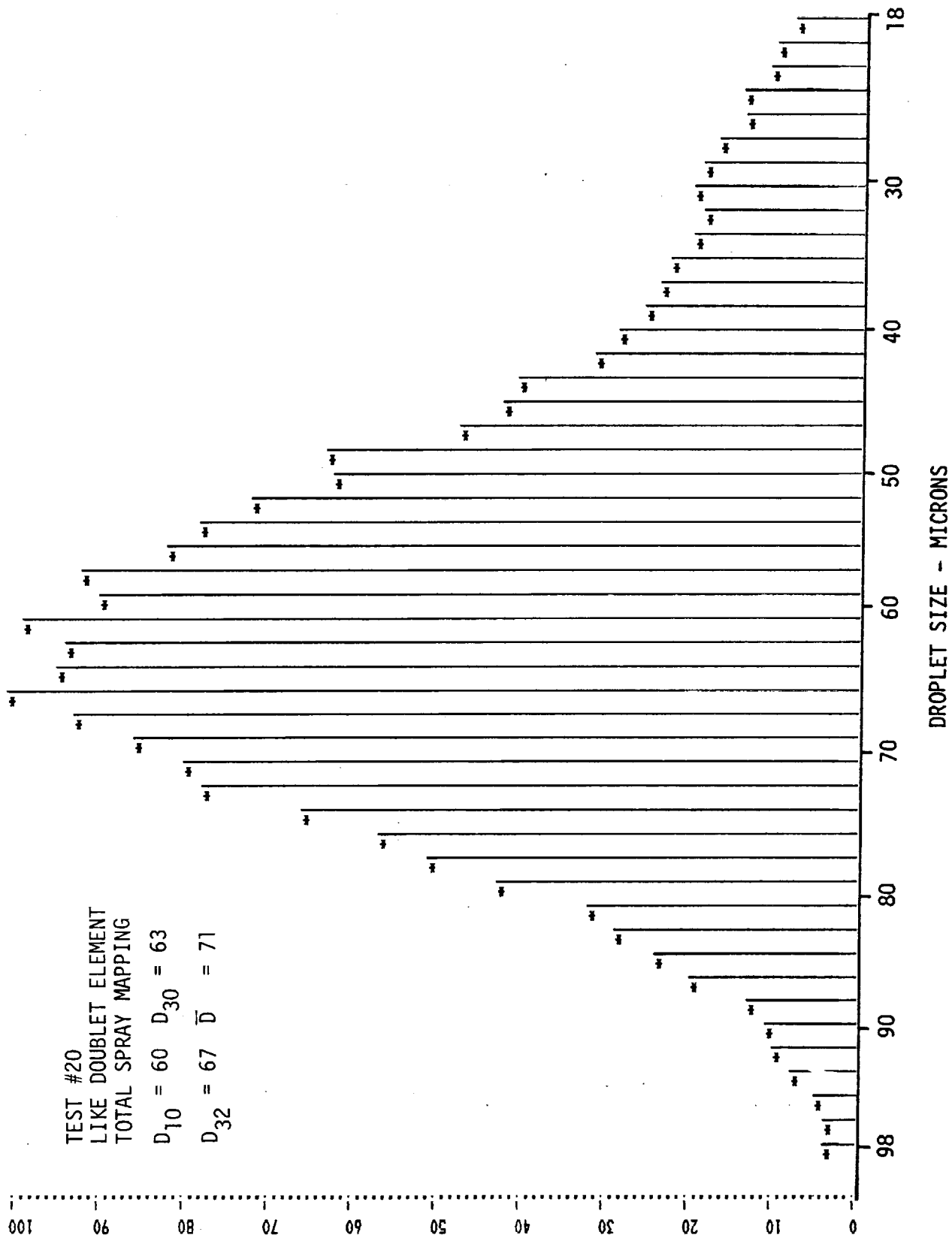
Figure 5-48. Spray Droplet-Size Distribution, Test 20

TEST #20
LIKE DOUBLET ELEMENT
TOTAL SPRAY MAPPING

$D_{10} = 60$ $D_{30} = 63$
$D_{32} = 67$ $\overline{D} = 71$

A summary of the actual test conditions and the measured, total spray, mass median droplet diameters is presented in Table 5-5. As previously mentioned, in some tests a significant portion of the droplet-size distribution was below the size measurement range employed in these tests (and in test 21). In the tests in which this effect appears to be greatest, the mass median droplet diameters are marked with an appropriate greater than (>) or less than (<) symbol. The test variables noted in Table 5-5, together with appropriate geometric variables for each injector, are the basic and most fundamental variables upon which droplet-size correlating equations are based.

ANALYSIS OF RESULTS

Analysis and discussion of the hot-wax test comparisons will be presented first. The Dickerson correlation for like doublets is

$$D = 7.84 \times 10^4 \; d_L^{\;0.57} / V_L^{\;0.85} .$$

The correlation for the effect of liquid properties recommended by Dickerson is the Wolfe-Anderson correlation:

$$\frac{\bar{D} \text{ (fluid A)}}{\bar{D} \text{ (fluid B)}} = \left(\frac{\sigma_A}{\sigma_B}\right)^{1/2} \left(\frac{\mu_A}{\mu_B}\right)^{1/3} \left(\frac{\rho_B}{\rho_A}\right)^{1/6} .$$

Properties for wax, water, and trichloroethane are

LIQUID	ρ (dynes/cm)	ρ_L (kg/m^3)	μ_L (cP)
WAX (shell 270 at 95°C)	25	764	3
WATER	72	997	0.89
TRICHLOROETHANE	22	1316	1.2

TABLE 5-5. ATOMIZATION TEST RESULTS

TEST	ELEMENT	GAS VELOCITY (M/SEC)	LIQUID VELOCITY (M/SEC)	LIQUID DENSITY (kg/m^3)	SURFACE TENSION (dynes/cm)	VISCOSITY cP	D
BASELINE TESTS							
1	PENTAD	242	0.39	997	72	0.94	62
2	COAXIAL 5	259	0.21				<45
3	COAXIAL 7	152	0.40				<66
4	COAXIAL 9	175	0.43				67
FLOW-RATE TESTS							
5	PENTAD	291	0.49				50
6	PENTAD	315	0.52				49
7	COAXIAL 5	311	0.24				56
8	COAXIAL 5	337	0.27				59
9	COAXIAL 7	122	0.30				69
10	COAXIAL 7	198	0.52				61
11	COAXIAL 9	146	0.34				74
12	COAXIAL 9	238	0.55				69
VISCOSITY TESTS							
13	PENTAD	233	0.39	1041	69	1.49	<54
14	COAXIAL 7	152	0.39	1041	69	1.49	74
DENSITY TESTS							
15	PENTAD	242	0.39	1135	77	1.38	<50
16	COAXIAL 7	152	0.39	1135	77	1.38	<67
SURFACE TENSION TESTS							
17	PENTAD	240	0.39	1316	22	1.2	<56
18	COAXIAL 7	149	0.38	1316	22	1.2	62
WAX DATA COMPARISON TESTS							
19	LIKE DOUBLET	---	33.6	1316	22	1.2	72
20	LIKE DOUBLET	---	62.0	997	72	0.94	71
MIXTURE RATIO TESTS							
21	COAXIAL 7	152	0.30	997	72	0.94	>74
22	COAXIAL 7	156	0.60	997	72	0.94	67

Through the use of these properties, the correlations for wax to water and wax to trichloroethane are

$$D_{WATER} = 1.08 \; D_{WAX}$$
$$D_{TRIC} = 0.63 \; D_{WAX}.$$

Following the employment of Dickerson's droplet-size correlating equation and the preceding properties correlation for test 19 and 20 conditions, the predicted mass median droplet size would be 117 and 118 microns, respectively. As shown in Fig. 5-47 and 5-48, the measured mass median values were 72 and 71 microns, respectively. Thus, considerable disagreement lies between these test results and those of the earlier hot-wax technique test results.

This disagreement can be attributed to one or more of four factors:

1. A basic flaw in the hot-wax technique as employed by Dickerson
2. An incorrect liquid properties correlating equation
3. A basic flaw in the DSI measurement technique as employed in this program
4. Some unrecognized difference in the element geometry or flow conditions between these sets of tests

Item 4 seems highly unlikely. As previously discussed, all the geometric and flow variables considered of importance were very nearly the same in both sets of tests. The three other potential causes of this difference are discussed in the following paragraphs.

As discussed in Ref. 1-1, a number of reasons and certain experimental evidence indicate that some flaw may exist in the hot-wax technique. In using the wax technique, it is necessary to be concerned with such potential error issues as (1) the wax droplet density change upon freezing and its relationship to droplet size, (2) the proper collection and sampling of the wax particles -- particularly the fines, (3) abrasion of wax particles during the sieving process, (4) drop-size resolution provided by the sieving process, (5) spherical uniformity of the particles, and (6) agglomeration of freezing particles during and after the atomization process. Many of these issues have been addressed by investigators

employing this technique; however, in most cases, some questions remain.

One very basic question regarding this technique is the effect of the droplet cooling and freezing on the atomization process. When the 367 K liquid wax is sprayed into the cooler air (as was done in Dickerson's tests), the wax immediately begins to cool, and the properties of the wax undergo significant change during this process. Furthermore, the outer portions of the droplets are cooled and frozen first, thereby limiting additional atomization. These effects would tend to limit the atomization, thus producing larger droplets. If significant cooling of the surfaces of the wax droplets occurs prior to the completion of atomization, then the validity of the wax data is highly suspect.

As discussed in Ref. 1-1, the liquid properties correlating equations in common use are of questionable applicability. Another properties correlating relationship that could be applied with as much justification as Wolfe-Anderson's relationship, is that of Ingebo (Ref. 5-12):

$$\frac{\bar{D}\ (\text{fluid A})}{\bar{D}\ (\text{fluid B})} = \left(\frac{\sigma_A\ \mu_A}{\rho_A}\right)^{1/4}\left(\frac{\rho_B\ \mu_B}{\rho_B}\right)^{1/4}$$

This correlation yields wax to TRIC and wax to water droplet-size correction factors of 0.48 and 0.90, respectively. The use of these properties correction factors with Dickerson's droplet-size equation results in predicted mass median droplet sizes of 89 microns (test 19) and 98 microns (test 20). These sizes are closer to the measured values of 72 and 71 microns, respectively. Valid and proven properties correlating equations are an important requirement for comparing data obtained with different fluids. This is especially important, since nearly all cold-flow atomization data must be extrapolated to real propellants (e.g., LOX). Unfortunately, such correlating equations are not available.

The final potential cause of the differences between the hot-wax test results and those of this program involve the validity of the DSI measurements. At the start of each test, the DSI measuring capability is confirmed via measurement of a stream of monodisperse droplets of known size. However, this does not guarantee

the validity of the measurements of the more distributed and dense sprays of interest. The lack of a recognized, established, standard spray for confirmation of the performance of droplet-size measurement instruments, is a serious problem that is being addressed by an ASTM subcommittee. At present, the only available confirmation of the DSI consists of the monodisperse droplet stream measurements and the repeatability, consistency, and "reasonableness" of the data.

It is impossible to determine which of the preceding factors is responsible for the observed disagreement between the wax data and the corresponding tests of this program. Certainly, part of the problem is the lack of valid liquid properties correlations. These results demonstrate the great need for such correlations, and cast some doubt on the validity of the hot-wax technique test results. Attention is now directed toward the results of the other atomization tests.

Examination of Table 5-5 shows very little variation in mass median droplet size with any of the parameters tested. The DSI measurements are considered valid within approximately 10 microns, and, in most cases, the spread in the data lies within these limits. This result is somewhat surprising as considerable variations were employed for some of the important parameters (e.g., gas injection velocity). The very low liquid flow rates necessary for these tests are a source of concern. These low liquid flow rates were responsible for the large and unrealistic deviations from expected spray appearance for the triplet elements, and for lesser spray anomalies observed with the other two preburner elements (the pentad and coaxial 5). The test using the two main chamber coaxial elements is considered to be the most valid. However, no discernable trends in any of the data are apparent. With so little spread in the data, many more tests would be required to assess the effects of changes to the governing parameters. Attempts were made to correlate the data in a variety of ways but they met with no success. The regression analysis technique that was so successfully applied to assess the liquid/liquid triplet mixing test results, was used in this endeavor with no success. There were too little data, too little spread in the data, and too many variables for such an analysis.

However, a number of observations can be made from these data that are of some importance to future research in this area. Also, the DSI provides previously unavailable information regarding the internal structure of the spray. These findings regarding general spray characteristics are:

1. These sprays were surprisingly homogeneous. Droplet mass median diameter variations between the inner and outer regions of the spray were generally less than 10 microns.

2. In general, at any location within the spray, the average velocity of the larger droplets was only slightly greater than the average velocity of the smaller droplets.

3. The droplets in the center of the spray have a larger average velocity than those near the periphery.

4. A slight but general tendency for the larger droplets to be nearer to the outer edge of the sprays produced in these tests was shown. The preburner coaxial element (element 5) may be an exception.

5. The effects of flow-rate and liquid properties variations on the measured droplet sizes were mixed or very small (within the estimated measurement accuracy of the DSI). For example, higher flow rates appeared to decrease droplet sizes for the pentad, increase droplet sizes for the coaxial element (element 5), and have no consistent or discernible effects on the other two coaxial elements.

These results provide the first detailed mapping of liquid rocket injector elements. Data on droplet sizes as a function of location within the spray, droplet size vs. velocity information, and detailed velocity mappings through the spray are available. This information can be of value to efforts for the development of spray combustion models. To model spray combustion, the spray must be modeled. Detailed information of the spray structure, droplet sizes, and droplet velocities provides the necessary data for comparison with the output of the spray modeling codes. Such "anchoring" and improvement of the various

submodels of these codes is necessary in the development of, and to ensure the validity of, the overall spray combustion codes for liquid rocket engines.

In much the same way that the results of tests 19 and 20 were used to compare with previous hot-wax test results, these coaxial test results can be used to evaluate droplet-size correlations obtained by other investigators. A liquid rocket coaxial injector would be more generally referred to as a plain-jet (pneumatic or airblast) atomizer. However, a wide variety of plain-jet airblast atomizers exists and, many of this type are quite different, in form, function, and operating principle, from those employed in liquid rockets. When comparing results, it is necessary to ensure that the injectors are similar.

An excellent summary of airblast atomizer research and findings has been prepared by Lefebvre (Ref. 5-13). In this survey paper, two droplet-size correlating equations are identified, which offer some potential applicability to liquid rocket coaxial injectors. These equations are that developed by Lorenzetto and Lefebvre (Ref. 5-14) and that developed by Kim and Marshall (Ref. 5-15). These equations were developed through empirical correlation of the results of a large number of spray droplet-size measurements. The atomizers employed in these studies are presented in Fig. 5-49. Also shown in Fig. 5-49 are the range of the variations of the parameters tested by both of these investigators and the range employed for the main chamber coaxial elements (elements 7 and 9) tested here. SSME main injector conditions are also presented as a reference point. D is the liquid jet diameter and A is the area of the gas jet. All tests were performed at atmospheric backpressure. The correlating equations developed by Lorenzetto and Lefebvre and Kim and Marshall are

$$\bar{D} = 5.36 \times 10^{-3} \frac{\sigma^{0.41} \mu_L^{0.32}}{\left(\rho_g V_R^2\right)^{0.57} A_g^{0.36} \rho_L^{0.16}}$$

$$+ 3.44 \times 10^{-3} \left(\frac{\mu_L}{\rho_L \sigma}\right)^{0.17} \frac{W_L}{W_g} V_R^{-0.57}$$

(Kim and Marshall)

TABLE 5-6. INJECTION CONDITIONS INVESTIGATED AND SSME MAIN COMBUSTION CHAMBER CONDITIONS

LIQUID

AIR
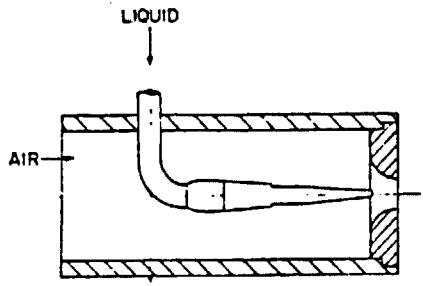
AIR — LIQUID

Lorenzetto and Lefebvre Atomizer (Ref. 5-14)   Kim and Marshall Atomizer (Ref. 5-15)
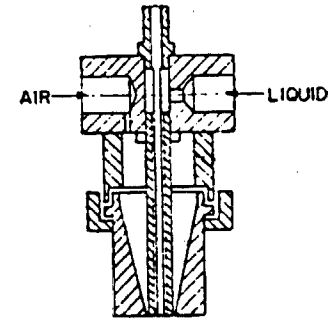
INJECTION CONDITIONS

| INVESTIGATOR | LIQUID PROPERTIES | | | BACKPRESSURE | INJECTION VELOCITY | | MIXTURE RATIO | D | A |
	SURFACE TENSION (N/m) x 10^3	DENSITY (kg/m^3)	VISCOSITY (kg/m/sec) x 10^3	(atm)	GAS (m/sec)	LIQUID (m/sec)	(Liquid/Gas)	(m) x 10^3	(m^2) x 10^6
Lorenzetto and Lefebvre	26-76	794-2180	1-76	1	60-180	<3	0.063-1	0.4-1.6	27-507
Kim and Marshall	29.6-31.2[a]	782-834	8.7-49.2[a]	1	75-393	Negligible	0.025-16	1.4-5.6	5.7-6
This Program (coaxial 7 and 9)	22-77	997-1316	0.94-1.49	1	122-238	0.3-0.6	2.6-5.3	4.6-5.1	10-13
SSME MC	13[b]	1137[b]	0.2[b]	210	322	32	3.3	4.78	56.7

[a] These values appear to be reported incorrectly in Ref. 5-13. Values from Ref. 5-15 are shown here.

[b] LOX properties at normal boiling point.

$$D_{32} = 0.95 \left[\frac{(\sigma\ W_L)^{0.33}}{V_R\ \rho_L^{0.37}\ \rho_g^{0.30}} \right] \left[1 + \frac{W_L}{W_g} \right]^{1.7}$$

(Lorenzetto and Lefebvre)

$$+\ 0.13\ \mu_L \left[\frac{d_L}{\sigma\ \rho_L} \right]^{0.5} \left[1 + \frac{W_L}{W_g} \right]^{1.7}$$

Note that both these equations contain gas density terms, even though all the tests were performed at atmospheric backpressure. These terms were included to preserve the dimensionality of the equations and, perhaps, with some understanding of the effect of gas density on atomization from other investigations (generally with different types of atomizers). The reader should also consider the injectors employed in the development of the correlations. Both these injectors provide some degree of radial inward motion of the injector gas, which is not realistic in comparison with liquid rocket coaxial injectors. The Kim and Marshall atomizer has a smaller gas flow annulus than a typical coaxial element, and no recess of the center tube. The Lorenzetto and Lefebvre atomizer has an extremely large gas flow annulus and center tube recess, and a very small liquid tube diameter, as compared to typical coaxial elements. Finally, the method by which the droplets were measured (and the measurement location) must be considered. Lorenzetto and Lefebvre used a light scattering technique (presumably based on Fraunhofer diffraction), and Kim and Marshall employed the hot-wax technique. Problems and issues related to these measurement techniques are discussed in Ref. 1-1 and 5-1.

Now, a combustion modeler or combustor designer requires droplet-size information to assess combustor performance, stability, et al. The proper choice of droplet size has been shown (e.g., Ref. 5-2) to be of great importance in such computations. Despite a large array of questions regarding the applicability of such correlations, the analyst generally can use no better correlations than those just presented. One recent example of this is a study by Carroll et al (Ref. 5-16), which used the Lorenzetto and Lefebvre correlation to assess SSME performance. As is apparent from Fig. 5-49, this assessment requires a drastic extrapolation of the Lefebvre equation beyond the test conditions under which it

was developed (particularly the backpressure and liquid velocity). Even modest extrapolation of such correlating relationships is extremely dangerous, as the relationships are strictly empirical (i.e., there is no physical basis for their form). Those who apply and use results and models employing these correlating relationships must be aware of the very great lack of accuracy incorporated into such results and models.

While the data obtained in this program can do little to extend these correlations to higher pressures, etc., these results can be used to assess the correlating equations at conditions somewhat closer to actual coaxial injector designs. The coaxial element (elements 7 and 9) baseline flow conditions are in general agreement with the test conditions of Lorenzetto and Lefebvre and Kim and Marshall with the following major exceptions:

1. Kim and Marshall tests employed substantially lower surface tension and higher viscosity liquids.

2. Lorenzetto and Lefebvre utilized much lower mixture ratios, far lower than typical main chamber combustion conditions.

3. Lorenzetto and Lefebvre used much smaller liquid injector tip diameters.

4. Kim and Marshall employed smaller gas annulus widths.

5. Lorenzetto and Lefebvre used very much larger gas annulus widths.

6. While both injectors differ from the coaxial injectors of this program, the Lorenzetto and Lefebvre design appears most different.

To assess the effects of these differences and compare correlations, the baseline test conditions and geometrics for the coaxial injectors (elements 7 and 9) were input to both of the correlating equations, with the following results ($\bar{D}$ values in microns)

	Coaxial 7	Coaxial 9
Lorenzetto and Lefebvre equation $\bar{D}$*	575	443
Kim and Marshall equation	49	37
Measured $\bar{D}$	66	67

*Assumes $\bar{D}/D_{32}$ = 1.2 as recommended by Lefebvre (Ref. 5-13)

Even this relatively modest extrapolation of these correlations demonstrates the great errors introduced -- especially with the Lorenzetto and Lefebvre equation. While the DSI-measured droplet sizes could conceivably be in error by 20 to 30 microns (no reason exists to suspect this, however), it is inconceivable that they could be in error by 400 to 500 microns. If these correlations do not provide reasonable estimates for these modest extrapolations, then their accuracy must be of even greater concern when they are extrapolated to the much more different conditions of operating liquid engines.

Inspection of the correlating equations indicates one major factor influencing droplet size in the Lorenzetto and Lefebvre equation that has a much smaller effect in the Kim and Marshall equation. This is the effect of mixture ratio. In the Lorenzetto and Lefebvre equation, this factor increases droplet size by a factor of 10. Since Lorenzetto and Lefebvre tested at much lower mixture ratios, the applicability of the equation at the higher mixture ratios of interest is especially doubtful. Additional attempts were made to correlate the coaxial element test results of this program with the Kim and Marshall correlation, with the following results:

Test	Measured $\bar{D}$	Kim-Marshal Equation $\bar{D}$
2	<45	11
7	56	9
8	59	9
9	69	57
10	61	41
11	74	42
12	69	30
14	74	69
16	<67	50
18	62	69
21	>74	40
22	67	67

With the exception of the preburner element tests (tests 2, 7, and 8), the Kim and Marshall equation produces results not excessively different from these tests. However, it continues to predict generally lower values of mass median droplet size than were measured. The measured droplet sizes are, on the average, 36% larger than the Kim and Marshall computed sizes.

ATOMIZATION TESTING CONCLUSIONS AND RECOMMENDATIONS

The original intent of this study was to develop droplet-size correlating equations and information that could be employed, with reasonable confidence, to assess injector designs, and to provide important data to the combustor analysis computer codes. The previously discussed problems encountered in the course of this program resulted in the test conditions being limited to low flow rates and atmospheric backpressure. It was anticipated that such tests would provide sufficient variations in the results to allow their extrapolation to conditions of greater interest. However, this was not found to be the case. Accordingly, except for the very general confirmation of the Kim and Marshall correlation, it was not possible to extract specific droplet-size correlating equations from these results.

The following are the major conclusions, recommendations, and findings of these atomization characterization tests. Supporting rationale for these has been discussed in the preceding section.

1. These tests have provided the first detailed velocity and size distribution mappings for several gas/liquid injectors. In addition to the insight now available regarding the structure of these sprays, these data can be used to anchor and validate the spray models being developed as a part of the efforts to construct liquid rocket engine combustion codes.

2. These results provide information that indicates that the hot-wax technique data, and especially the correlations relating the effects of liquid properties on droplet size, may be of questionable validity or applicability.

3. These tests demonstrate the capability of droplet sizing interferometry to provide extensive and detailed spray information that was previously unavailable. Unfortunately, this effort also demonstrates the great difficulty encountered in attempting to employ the DSI, and especially the monodisperse droplet generator, under conditions of greatest interest (e.g., high pressure and dense sprays).

4. The Lorenzetto and Lefebvre droplet-size correlating equation is not recommended as a means for estimating droplet sizes for liquid rocket coaxial injectors, especially at mixture ratios greater than 1.

5. The Kim and Marshall droplet-size correlating equation is recommended for the very rough estimation of droplet sizes for liquid rocket coaxial injectors operating at high (main chamber) mixture ratios. This equation is recommended only because no alternative appears to exist. Based upon the results of these atomization tests, it is further recommended that the droplet sizes computed from the Kim and Marshall equation be increased by about 30%.

6. It is strongly recommended that future efforts to acquire atomization data obtain such data at higher pressures and flow rates. It is universally agreed that the effects of gas density and flow rate are important but there is scarcely any data to assess these effects. Such high-pressure and high-flow-rate testing would be expected to provide data that could be used to develop droplet-size correlating equations of high accuracy and applicability.

7. The DSI can satisfactorily obtain data at the flow rates and pressure tested in this program. Very much higher pressures and flow rates may result in sprays too dense to allow such measurements by the DSI.

8. Higher-pressure test facilities must be designed so as to greatly reduce the natural recirculation of the spray, and must do so in a manner that least affects the spray.

9. These tests have demonstrated that the sprays produced at these conditions are relatively homogeneous in terms of droplet size. Also, since droplet velocity is relatively independent of size, there is little difference between concentration and flux based results (spatial versus temporal data). If this condition continues to be true at other test conditions, it may be possible to reduce the spatial resolution of the DSI measurements or to use a different (and simpler) measurement technique, such as the Fraunhofer diffraction method. However, DSI measurements will remain a requirement to ensure that these conditions continue to exist.

10. The droplet-size measurement technique employed in this program was the V/I DSI technique. This second-generation DSI technique is inferior to two new DSI techniques now available. However, all of these DSI techniques, as well as all other nonintrusive droplet-size measurement techniques available, have deficiencies that limit their applicability to the study of liquid rocket injector atomization. These are the inability to measure droplet sizes in the very dense sprays typical of liquid rocket injectors (especially the very fine and dense sprays of gas/

liquid injectors), and the inability to distinguish droplets by composition (required to assess unlike liquid injector atomization). Improved capabilities in these areas are needed.

11. The findings of this study demonstrate the need for considerable additional effort in the study of atomization. The validity, and especially the applicability, of all available data and correlations are questionable. The technical challenges and problems are great, but the need for this information to support injector design efforts and the rapidly developing and very promising field of spray combustion modeling is also great.

12. Finally, it is strongly recommended that users of any atomization data and correlations become familiar with their quality, validity, and applicability. Furthermore, reports of any analyses based upon such data or correlations should clearly state the limitations and potential errors associated with the use of such atomization data.

VI. REFERENCES

1-1 Ferrenberg A., and V. Jaqua, "Atomization and Mixing Study Interim Report," NASA CR 170943, Rocketdyne Report No. RI/RD83-170, July 1980

3-1 Rupe, J. H., "The Liquid Phase Mixing of a Pair of Impinging Streams," Progress Report No. 20-195, Jet Propulsion Laboratory, California Institute of Technology, Pasadena, California, August 6, 1953

3-2 Elverum, G. W., and T. F. Morey, "Criteria for Optimum Mixture Ratio Distribution Using Several Types of Impinging Stream Injector Elements," Memorandum No. 30-5, Jet Propulsion Laboratory, California Institute of Technology, Pasadena, California, February 25, 1959

3-3 Rupe, J. H., "A Correlation Between the Dynamic Properties of a Pair Impinging Streams and the Uniformity of Mixture Ratio Distribution in the Resulting Spray," Jet Propulsion Laboratory, California Institute of Technology, Pasadena, California, March 28, 1956

3-4 Hoehn, F.W., J.H. Rupe, and J.G. Sotter, "Liquid Phase Mixing of Bipropellant Doublets," Technical Report 32-1546, Jet Propulsion Laboratory, California Institute of Technology, Pasadena, California, February 15, 1972

3-5 Fang, J., "Final Report: LOX/Hydrocarbon Fuel Carbon Formation and Mixing Data Analysis," Contract NAS 3-22823, Aerojet Liquid Rocket Company, Sacramento, California, July 20, 1983

3-6 Combined Bimonthly Summary No. 40, Jet Propulsion Laboratory, California Institute of Technology, Pasadena, California, p. 28, December 20, 1953 to February 20, 1954

3-7 Combined Bimonthly Summary No. 59, Jet Propulsion Laboratory, California Institute of Technology, Pasadena, California, pp. 48-50, April 1, 1957 to June 1, 1957,

4-1 Dussourd, J., and A. Shapiro, "A Deceleration Probe for Measuring Stagnation Pressure and Velocity of a Particle Laden Gas Stream", Jet Propulsion, January 1958

4-2 Liang, P., and M. Chang, "Development of a Three-Phase Combustion Code for Modeling Liquid Rocket Engines," 21st JANNAF Combustion Meeting, October, 1984

4-3 Jensen, R. and P. Liang, "Modeling of Dense Sprays from LOX/H$_2$ Coaxial Injectors Under Supercritical Conditions," 22nd JANNAF Combustion Meeting, October 1985.

4-4 Cloutman, L. D., et al, CONCHA - SPRAY, A Computer Code for Reactive Flows With Fuel Sprays, LA-9294-MS, May 1982.

4-5 Becker, H. A., et al, Concentration Intermittancy in Jets, 10th Symposium on Combustion, pp 1253-1263, 1965.

4-6 Abramovich, G.N., The Theory of Turbulent Jets, MIT Press, Cambridge, 1963.

5-1 Ferrenberg, A., and M. Varma, "Atomization Data Requirements for Rocket Combustor Modeling," 21st JANNAF Combustion Meeting, Laurel, Maryland, October 1984.

5-2 Ferrenberg, A., and M. Varma, "Atomization Data for Spray Combustion Modeling," AIAA/SAE/ASME Joint Propulsion Conference, Monterey, California, July 1985

5-3 Ferrenberg, A., "Liquid Rocket Injector Atomization Research," Liquid Particle Size Measurement Techniques, ASTM STP 848, J. Tishkoff, R. Ingebo, and J. Kennedy, Editors, 1984.

5-4 Bachalo, W.D., "Method for Measuring the Size and Velocity of Spheres by Dual-Beam Light-Scatter Interferometry," Applied Optics, Vol. 19, February 1980.

5-5 Bachalo, W.D., C.F. Hess, and C.A. Hartwell, "An Instrument for Spray Droplet Size and Velocity Measurements," ASME 79-WA/GT-13, 1979.

5-6 Hess, C.F., "A Technique Combining the Visibility of a Doppler Signal with the Peak Intensity of the Pedestal to Measure the Size and Velocity of Droplets in a Spray," AIAA-84-0203, January 1984.

5-7 Ingebo, R., and H. Foster, "Drop Size Distributions for Crosscurrent Breakup of Liquid Jets in Airstreams," NACA TN 4087, October 1957

5-8 Zajac, L., "Droplet Breakup in Accelerating Gas Flow, (Primary Atomization)," Part 1, Rocketdyne Report R-9337-1, NASA-CR-134478, October 1973

5-9 Zajac, L., "Droplet Breakup in Accelerating Gas Flow, (Secondary Atomization)," Part 2, Rocketdyne Report R-9337-2, NASA-CR-134479, October 1973

5-10 Falk, A., "Coaxial Spray Atomization in Accelerating Gas Stream, Final Report," Rocketdyne Report R-9753, NASA-CR-134825, June 1975

5-11 Dickerson, R., "Like and Unlike Impinging Injection Element Droplet Sizes," _J. Spacecraft_, Vol. 6, No. 11, November 1969

5-12 Ingebo, R., "Drop Size Distributions for Impinging-Jet Breakup in Airstreams Simulating the Velocity Conditions in Rocket Combustors," NACA TN 4222, 1950

5-13 Lefebvre, A., "Airblast Atomization," _Prog. Energy Combust. Sci._, Vol. 6, 1980

5-14 Lorenzetto, G., and A. Lefebvre, "Measurements of Droplet Size on a Plain-Jet Airblast Atomizer," _AIAA Journal_, Vol. 15, 1977

5-15 Kim, K., and W. Marshall, "Drop Size Distributions From Pneumatic Atomizers," _AIChE Journal_, Vol. 17, No. 3, May 1971.

5-16 Carroll, R., D. Connell, and C. Limerick, "Performance Comparison of the Current SSME and a New Main Injector - Main Combustion Chamber Using the JANNAF Methodology," 22nd JANNAF Combustion Meeting, Pasadena, California, October 1985.

APPENDIX A

This appendix is a reprinting of pages 5 through 106 and 139 through 141 of the "Atomization and Mixing Study - Interim Report" (Ref. 1-1), published as NASA-CR-170943, July 1983. The appendix is included in this report in order to provide the reader with a complete and single report describing the state of the art of atomization and mixing technology.

It should be noted that the work described in the main body of this report has demonstrated that certain findings and statements of Appendix A are incorrect or not generally applicable. In particular, the findings regarding gas/liquid mixing and liquid/liquid triplet mixing design criteria are superseded by the findings reported in Sections III and IV of this report.

ATOMIZATION

This section describes the state of the art in the area of liquid rocket injector atomization. The need for this information, the parameters of importance, the manners in which the data are correlated and reported, the droplet size measurement techniques employed, and the specific correlations and data pertaining to rocket engine injectors (triplets, pentads, coaxial, and some doublet data), are described, discussed, and assessed. In the study of the atomization literature, emphasis was placed on experimental programs and empirical results directly related to liquid rocket injectors. The more theoretical or basic research efforts are to be studied in a subsequent phase of this program. A bibliography of the atomization reports reviewed to prepare this assessment is included in the list of references at the end of this section.

In liquid rocket engines, the combustion process generally is considered to be evaporation limited, i.e., the evaporation of the propellants is the slowest step in the combustion process and, therefore, very important to model correctly. Droplet evaporation rate is a strong function of droplet size and velocity relative to the gas phase. Some computer codes calculate drop velocity and motion. This is important in properly assessing evaporation, stability, spacecraft contamination by ejected propellant droplets, performance, and wall effects (e.g., wall film buildup, heat transfer). Droplet acceleration is due to an imbalance between droplet inertial forces (a function of drop diameter cubed) and drag forces (generally a function of drop diameter squared). Thus, the droplet size is an important parameter in the assessment of droplet evaporation rate and motion.

It is possible to write the equations governing the motion and evaporation of a droplet. The forms of these equations and most of the parameters are known fairly well over many operating regimes of interest. The equations are ordinary differential equations that can be solved readily. However, as with all differential equations, any such solution requires knowledge of the initial or boundary conditions. And this is the problem--these initial conditions are not known well enough. These conditions are the droplet size and velocity distributions at the

locations where the droplets are formed. Given these initial conditions, the governing equations can be solved, and this is precisely what the combustor codes do. However, errors in the initial conditions produce corresponding errors in the predictions.

This problem has long been recognized and a number of experimental programs have been performed to establish these initial conditions. Due to the complexity of the physical processes occurring during atomization, these initial droplet conditions generally are characterized by empirical correlations. Some of these correlations and experiments are described later. Both mixing and atomization experiments often are performed with propellant simulants. This introduces a set of corrections that must be employed to extrapolate to the actual propellants of interest. Another set of corrections generally must be applied to extrapolate the test data to the operating conditions (pressures, temperatures, etc.) of interest. Thus, the establishment of these critical initial conditions depends entirely upon a relatively small quantity of empirical data, relating the effects of a few of the many parameters affecting these complex physical processes, and several sets of corrections to this data.

The utilization of such atomization data and correlations in the combustor analysis codes is a major source of difficulty and error. This has been demonstrated repeatedly in code development programs at Rocketdyne. The three major performance codes in use at Rocketdyne (TPP, CICM, and SDER) all attempt to use such correlations. In all three cases, it has been found to be necessary to modify the experimental correlations to force the codes into agreement with large-scale, rocket engine performance tests. Such "calibration" of computer models with the actual hardware they attempt to model is a standard procedure when dealing with complex unknown phenomena, although it is obviously a technique of last resort. Codes that are calibrated in such a manner can be relied upon to produce good results as long as they are applied to designs and conditions not significantly different from those that they were calibrated against. However, the accuracy of the codes becomes increasingly questionable as they are applied to situations and problems significantly different from the calibration points.

The poor performance of these drop size correlations indicates that something is wrong with the measurement techniques, the correlations developed from the measurements, and/or the manner in which they are applied. The assessment of the state of the art, as described in the remainder of this section, provides reason to suspect all of these.

PARAMETERS AFFECTING ATOMIZATION

The physical processes occurring during atomization cannot be reduced currently to sets of equations derived from basic physical principles. The most common case of the break up of a single jet of liquid has been theoretically studied for over 100 years, and these theoretical studies have been unable to predict, to an adequate degree, the characteristics of the droplets produced. Impinging streams and other fan-forming injectors also have been investigated theoretically. These studies and experimental efforts, combined with the strictly empirical investigations of others, provide an indication of the parameters of importance in the atomization process. However, there is considerable disagreement regarding the relative importance of specific variables.

The properties of a liquid propellant that are considered of importance are the surface tension, viscosity, and density. For a propellant injected as a gas, the only thermodynamic property generally considered of importance is the gas density. The geometric variables of importance for impinging-type injectors are the orifice diameter, orifice length, orifice entrance conditions, number of orifices (triplet or pentad), free jet distance (i.e., distance from the orifice to the impingement point), and impingement angle. Flow variables to be considered are the velocities of the liquid streams and the existence of turbulence in these streams.

For coaxial injectors, the geometric variables of potential importance are the propellant flow areas, the inner tube (LOX post) wall thickness, and the recess of the LOX post. The flow variables of greatest concern are the liquid velocity and the relative gas to liquid velocity.

Another parameter that has been shown to be of very great importance is the velocity of the combustion gases relative to the injected fluids. This parameter affects the aerodynamic breakup of the large droplets and ligaments after they have separated from the spray fan. This is often referred to as secondary atomization and many basic research efforts have been performed to evaluate this. Separation of atomization into primary and secondary atomization processes is certainly an oversimplification, but it has been employed. The importance of the combustion gas velocity is unfortunate, since the actual velocity field in the combustor cannot be determined adequately. The combustion gas velocity field depends entirely upon the droplet evaporation rate and distribution, which in turn is highly dependent on initial droplet size, which in its turn is greatly affected by the combustion gas velocity field. Thus, all of these phenomena are interrelated highly and must be considered together. Even in cold flow tests, the local gas velocity field in unknown. There is no such thing as "spraying into still air," as the spray itself transfers momentum to the gas and sets it in motion.

Another important parameter that is difficult to quantify is the liquid velocity. Generally, this is assumed to be the average velocity at the orifice exit assuming the orifice is flowing full. But this is not the velocity of the liquid in the fan, or of the ligaments, which is probably the velocity of greater concern.

The effects of combustion on atomization are unknown. Matching the density and velocity field of the combustion gases in a cold flow atomization test may not be sufficient. Burning droplets may break up differently (secondary atomization) than nonburning droplets due to the effect of the burning gas envelope about them.

Our knolwedge of many of the parameters affecting rocket engine atomization comes primarily from the study of doublets. Details of many of these studies are included later in this report where the relative importance of the parameters affecting atomization are discussed in greater detail.

ATOMIZATION CORRELATING EQUATIONS

The objective of atomization studies is to develop quantitative relationships defining the effects of the various governing parameters on the characteristics of the spray. The characteristics generally most desired are a representative droplet size (a mean or average value) characterizing the spray, and a droplet distribution defining how the number of droplets in the spray varies with droplet size. Other parameters of interest are the distribution of droplets in space, and the velocities of the droplets.

The data generally most desired is the number of drops of each size in a given spray. Often the data is obtained in the form of numbers of droplets counted, n, in each of many uniform size ranges (e.g., 5 to 10μ, 15 to 20μ, etc.) as shown in Fig. 1a. However, this discrete form of data presentation has the undesirable characteristic that as the width, ΔD, of the size ranges is varied the count will change. In order to quantify the data in the form of a continuous mathematical expression, the data is often converted to the form of Fig. 1b. Here, the number of droplets per unit size range (e.g., per micron) is plotted. This continuous function is called a distribution function f, and is determined by evaluating $\frac{n(D)}{\Delta D}$ as ΔD approaches zero. n(D) is the number of drop-lets having diameters between $D - \frac{\Delta D}{2}$ and $D + \frac{\Delta D}{2}$. This distribution function is the mathematical expression that best defines the size distribution of the droplets. All the other forms and techniques for expressing droplet size distributions can be derived mathematically from this distribution function, f, where

$$f = \lim_{\Delta D \to 0} \frac{n}{\Delta D}$$

Another useful function is the fraction of droplets in the spray at diameter D, which is

$$f/n_t = \lim_{\Delta D \to 0} \frac{n/n_t}{\Delta D} \quad \text{where } n_t = \text{total droplet count}$$

a. Number of drops per size group

$$f = \lim_{\Delta D \to 0} \frac{n}{\Delta D} \quad \text{or} \quad n = \int_{D-0.5\Delta D}^{D+0.5\Delta D} f dD \qquad v = \frac{1}{6}\pi D^3 n$$

$$v = \frac{1}{6}\pi D^3 \int_{D-0.5\Delta D}^{D+0.5\Delta D} f dD$$

b. Number of distribution function

$$N(D) = \sum_{0}^{D} n = \int_{0}^{D} f dD$$

c. Volume of drops per size group

$$V(D) = \sum_{0}^{D} v = \frac{1}{6}\pi \int_{0}^{D} D^3 f dD$$

$$\frac{dV}{dD} = \frac{1}{6}\pi D^3 \frac{dN}{dD}$$

d. Cumulative number distribution

e. Cumulative volume distribution

$$R = V/V_{tot}$$

1.0

f. Normalized cumulative volume distribution
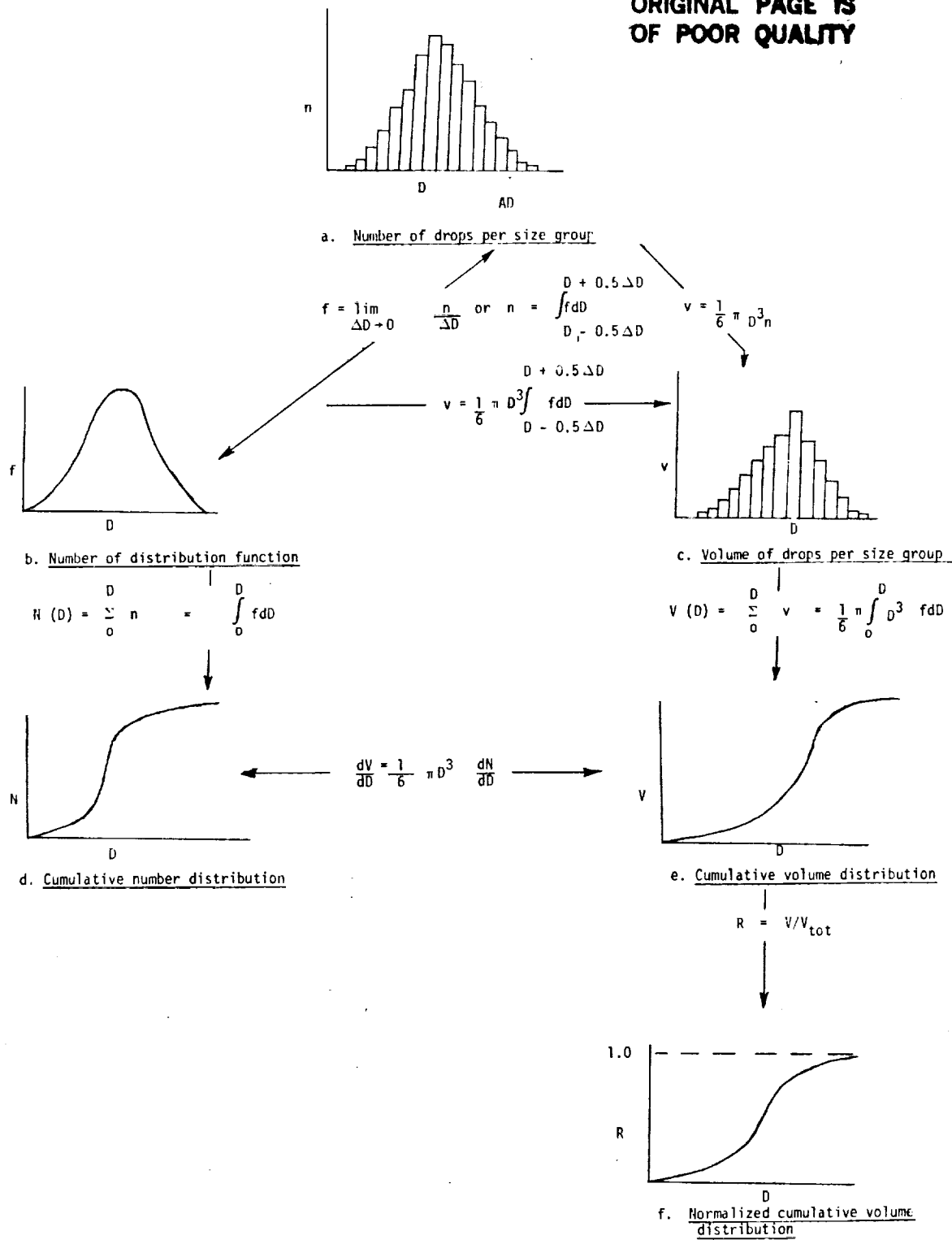
Figure 1. Droplet-Size Distributions and Relationships

In some applications, the volume of liquid in the spray as a function of drop diameter is of interest. Multiplying the number of drops in each diameter range by the volume of a drop of that diameter converts the number distribution to a volume distribution (Fig. 1c). It is also possible to construct a volume distribution function (not shown in Fig. 1) analagous to the size distribution function. Another useful representation is a cumulative distribution. The cumulative number, N, of droplets at any diameter D is the sum of the number of all droplets having diameters less than D (Fig. 1d).

$$N(D) = \sum_0^D n = \int_0^D f \, dD \qquad \text{or} \qquad \left(\frac{dN}{dD}\right)_D = f(D)$$

Similarly, the cumulative volume distribution, V, of the droplets at any diameter D is the sum of the volumes of all drops in the spray having diameters less than D (Fig. 1e).

$$V(D) = \sum_0^D v = \int_0^D \left(\lim_{\Delta D \to 0} \frac{V}{\Delta D}\right) dD \qquad \text{or} \qquad \left(\frac{dV}{dD}\right)_D = \frac{1}{6} \pi D^3 f$$

The normalized cumulative volume distribution, R, (Fig. 1f) is the volume distribution divided by the total volume of all the droplets measured, i.e.,

$$R = \frac{V}{V_{tot}}$$

The cumulative volume distribution (often normalized) is the most commonly utilized manner for graphically presenting the data.

The mathematical expressions defining the drop size distribution that are encountered most commonly are

$$\frac{dV}{dD} = AD^5 \exp(-BD^n) \qquad\qquad \text{Nukiyama – Tanasawa}$$

$$\frac{dV}{dD} = BnD^{n-1} \exp(-BD^n) \qquad\qquad \text{Rosin – Rammler}$$

$$\frac{dV}{dY} = \delta \pi^{-1/2} \exp(-\delta^2 Y^2) \qquad\qquad \text{Log probability}$$

where $Y = \ln(D/\bar{D})$

and A, B, , and   are the adjustable constants. Many other distribution
functions have been utilized and a more complete list and description of these is
contained in Ref. 11. Since:

$$\frac{dV}{dD} = \frac{1}{6}\pi D^3 \quad \frac{dN}{dD} = \frac{1}{6}\pi D^3 f$$

these distributions actually define the desired distribution function, f. Given
the distribution function, f, the cumulative volume (or number) distribution can
be obtained by integrating the distribution function, f, over various size ranges.

More often, the data is plotted in terms of the cumulative volume, or normalized
cumulative volume, versus drop diameter. For some droplet measurement tech-
niques, particularly the frozen wax technique, it is this cumulative volume (or
mass) distribution which is measured directly. Evaluation of the slope of this
distribution then can be performed to define the droplet number distribution or
distribution function. Cumulative distributions tend to "smooth" the data, mask
inaccuracies due to too few droplet measurements, and reduce the apparent differ-
ences between different distributions. Usually, only the cumulative volume dis-
tribution is reported, so this problem is overlooked often. One very comprehen-
sively reported investigation (Ref. 66), which presented all of the data and
plots of V and $\frac{dV}{dD}$ versus D, demonstrates this problem. Figure 2 is a cumu-
lative volume plot of the data from one set of droplet size measurements as pre-
sented in that report. The data appear to be in good agreement with the integral
of the particular distribution function chosen. However, the plot of the actual
volume distribution, $\frac{dV}{dD}$, and the data (Fig. 3) demonstrate that this appar-
ent agreement between the distribution function and the data is misleading.
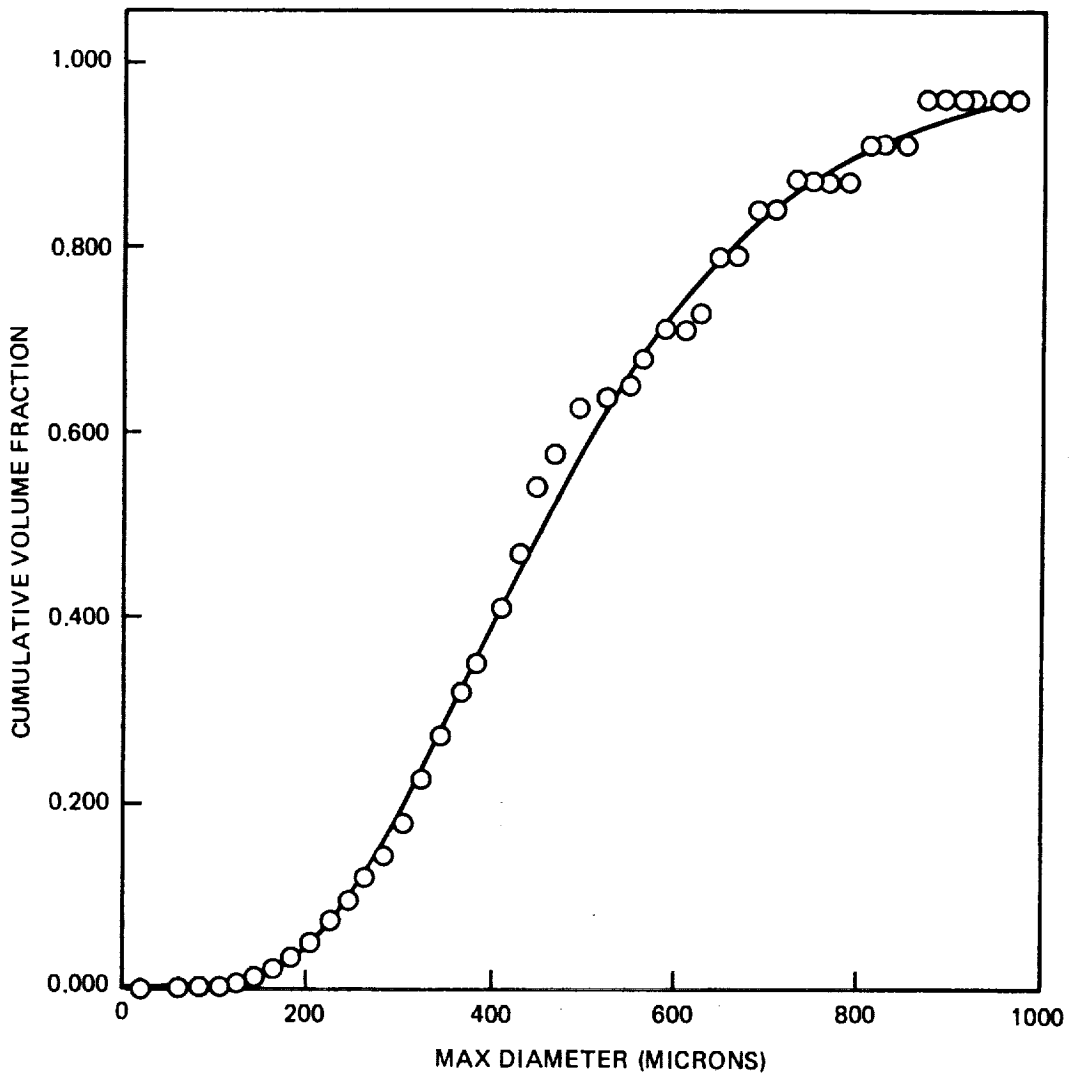
Figure 2. Droplet Cumulative Volume Distribution and Equation (Ref. 66)
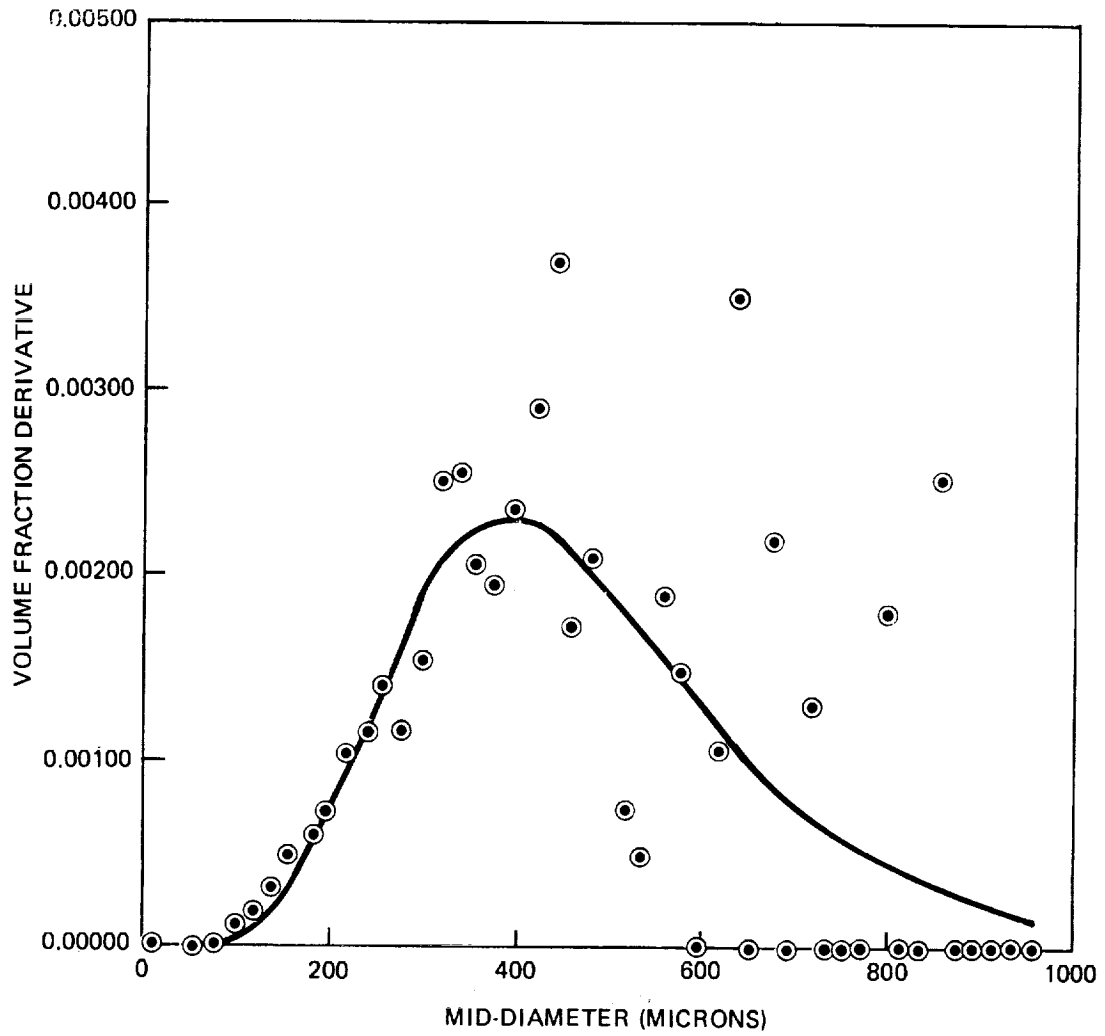
Figure 3. Derivatives of Droplet Cumulative Volume Distribution Data and Equation (Ref. 66)

Often the drop distribution is characterized by a single value--a representative drop diameter. Some such common representative diameters are the mean or average drop diameter, volume mean diameter, Sauter mean diameter, or mass median diameter. The mean or average diameters are defined according to the following general relationship:

$$D_{pq} = \left[\frac{\sum n_i D_i^p}{\sum n_i D_i^q} \right]^{\frac{1}{p-q}}$$

where i denotes size range considered.

n_i = number of droplets in size range i

D_i = middle diameter of size range i

Thus, D_{10} is the linear average diameter of all the droplets measured, D_{30} is the diameter of the droplet having the average volume of all the droplets measured, and D_{32} is the diameter of the droplet whose volume to surface area ratio is the average of all the droplets in the spray (referred to as the Sauter mean diameter). The mass median droplet diameter is the droplet whose size is such that one half of the mass (or volume) of the spray is contained in droplets having a larger diameter. On a plot of R versus D (Fig. 1f), the mass median diameter is the diameter occurring at a value of R = 0.5. All of these representative diameters can be calculated from the distribution function, f.

Most of the correlations developed to define the effect of various geometric and operational variables on droplet size define this effect in terms of the influence these parameters have on one of these representative diameters. These usually take a form:

$$\text{Representative diameter} = A \, X_1^{\,m} \, X_2^{\,p} \, X_3^{\,q} \, \ldots \ldots$$

where the X terms are the variables, or collections of variables, of interest, and A, m, p, q, ... are the adjustable constants by which the relationship is made to fit the data. In some instances, sums of terms, each similar in form to the right-hand side of the above equations, are employed. It must be recognized that such relationships as this do not completely characterize the spray, and that two sprays with the same mass median or Sauter mean diameter are not the same. It is often the smallest drop size and/or the largest drop size that are of greatest importance (e.g., in assessing stability and performance respectively). The mean or median droplet size does not provide this information. Thus, it is important to also characterize the droplet size distribution--i.e., to establish the correlating equation defining the distribution function, f.

DROPLET MEASUREMENT TECHNIQUES

A variety of techniques have been employed to measure droplet sizes. All of these techniques are subject to inaccuracies and questions associated with the basic assumptions employed, their manner of use, and/or the quantities of data usually obtained. Details of these techniques can be found in the literature, including some of the references contained in the bibliography. The discussion here is limited to the three primary techniques previously employed to obtain atomization data for rocket engine injectors. The findings obtained regarding rocket engine injection atomization utilizing these techniques is discussed subsequently.

Imaging Techniques

These include photography and holography and have been the most extensively employed methods for droplet sizing. They generally require a fairly dilute spray and offer the advantage of actually "seeing" the droplets as they exist at the point and time where knowledge of their size is desired. Although multiple exposure techniques can be employed to obtain droplet velocity data, none of the experimental programs discussed herein did so. As will be discussed shortly, velocity information is essential to the determination of accurate droplet size distributions when imaging techniques are employed. Imaging techniques have been employed to measure droplet sizes in reacting flows. This is an important and valuable feature that apparently has only been employed for the case of a rocket engine combustor in the investigations reported in Ref. 26, 72, 73, and 76.

A major problem with the use of imaging techniques has been the need for human analysis of the images. Although computerized techniques have been developed recently for analysis of photographic images, all of the rocket injector atomization work described herein employed at least some degree of human involvement in the analysis of the droplet images. It is necessary for someone to determine which droplets are to be counted (i.e., which droplets are in focus), and in most cases, to manually measure the droplet sizes. This causes errors in two ways-- human judgment and insufficient droplet counts to define the spray.

Another problem associated with imaging techniques is the time (i.e., cost) required to manually identify, count, and measure the droplets. This often prevents the counting of a sufficient number of droplets to assure an accurate distribution. A large number of droplets must be counted. The number of small drops may be over 1000 times as great as the number of large ones, and yet these large drops are often the most important to include. In Ref. 5, it is calculated that it is necessary to count 5500 droplets to be 95% confident that the Sauter mean diameter is correct to within 5%. Rarely are so many droplets counted per sample with imaging techniques.

Perhaps the most important problem associated with imaging techniques is that these techniques only measure the concentration of droplets in a given volume of space (i.e., spatial distribution) rather than the true droplet distribution, the temporal distribution. This problem is recognized in the older literature (Ref. 11), but appears to have been neglected by many others. The nature of this problem is discussed in detail in the following.

In a steady-state flow of droplets, the number of droplets, and the number of droplets of each size entering a particular region in space per unit time must be constant. It is possible to write a droplet number conservation equation (analagous to a mass conservation equation) as follows:

$$N_i = \rho_i A V_i$$

where N_i = number of droplets of size group i entering a region or control volume (drops/sec)

ρ_i = local concentration of droplets of size i (drops/cm^3)

A = cross sectional area of region perpendicular to the direction of flow (cm^2)

V_i = velocity of the droplets of size group i (assuming all drops in size group i are travelling at the same velocity) (cm/sec)

Now, the temporal distribution of droplets produced by an injector can be obtained by counting the droplets per second of each size group i crossing A, that is, by measuring the values of the N_i terms. As long as the droplets are moving in one direction (i.e., the spray is not spreading), measurements of the N_i values at any location in the spray will not change. However, the imaging techniques measure the droplet concentrations, i.e., the ρ_i terms. As long as the droplet velocities remain constant as the spray moves downstream, these ρ_i terms also will remain constant. However, if the droplet velocities change in such a way that the smaller drops are no longer moving at the same speed as the larger drops, then the ρ_i terms also change. The N_i values must remain constant for this is a steady flow situation. Thus, an imaging technique measures the ρ_i terms, and the ratios of the ρ_i terms is not the ratios of the actual number of droplets of each size group in the spray. The only time that the imaging techniques produce true drop size distributions is when all the droplets move at the same velocity. This condition rarely, if ever, occurs in nature or in experiments.

One particularly noteworthy effort that appears to demonstrate this effect is the work of George (Ref. 72, 73, 76). In these experiments, measurements were made at several axial locations downstream of the injector utilizing an imaging technique (holography). In all these tests, the gas velocity exceeded the liquid injection velocity. In such a case, the small droplets would be accelerated more rapidly than the larger droplets. This would cause the spatial concentrations of smaller drops to decrease faster than for the larger drops as we move downstream from the injector face. Thus, we should expect to see more larger drops than smaller drops in the holograms as we move downstream. This effect was observed (Ref. 73) and was quite significant. The value of D_{30} was found to increase by 50 microns or more over a 2-inch change in axial distance. Also, a simple computer simulation of droplet dynamics in a constant velocity gas flow (Ref. 84) demonstrates significant differences (40% or more variation in representative droplet sizes) between temporal and spatial measurements.

RI/RD085-312

A-15

This problem of spatial versus temporal distributions places some doubt on the utility of the results obtained with imaging techniques. Not only are the distributions measured not the true distributions, but the distributions will vary at different locations due to differences in velocities of the various size droplets. This may account for much of the disagreement between various investigators. The only situation in which the temporal and spatial distributions are the same is when the velocities of the droplets are not a function of droplet size. Spraying into "still" air will never produce this condition; and spraying into flowing air only will approximate this condition beyond some unknown distance downstream from the injector (where the droplets and gas velocities are equal).It is the temporal distribution that is needed for the combustor models.

Liquid Droplet Capture Technique

This technique involves the capture of a sample of the spray on a solid surface (e.g., a glass slide) or in another liquid. The droplets captured are measured under a microscope or photographed for later analysis. Most of the work utilizing this type of technique was performed before 1960 and the technique seems to have been supplanted, to a large extent, by photographic and other methods. In many cases the captured droplets are no longer spherical (e.g., droplets captured on a surface) and corrections to account for this must be applied.

This type of measuring technique requires the use of highly nonvolatile liquids and, when the droplets are captured in another liquid (e.g., a heavy oil or glycerine), further requires that the droplet liquid be immiscible in the capturing liquid. This limits the choice of liquids that can be utilized. Also, the droplets must be captured gently so as to prevent droplet shattering.

In many applications of this technique, it is obviously the temporal distribution of droplets that is obtained. For some sampling methods, however, there is some question as to whether it is the spatial or temporal distributions that are measured. Such questionable methods include the slide "waving" technique, where a glass slide is passed rapidly through a spray.

Like the imaging technique, the liquid droplet capture technique requires considerable manpower to count and size the droplets. Thus, the size of the sample counted may be a serious source of error. Also, this technique requires the spray to be diluted sufficiently to prevent a significant amount of coalescense of the droplets in the sample. In order to accommodate this requirement, one technique often employed is a spray splitter. The spray impinges on a plate containing a hole or slit through which only a portion of the spray may pass. Only this small portion is allowed to fall on the collection surface. This same procedure also is used occassionally with imaging techniques to dilute the spray. One aspect of this spray splitting procedure that occassionally is overlooked is the effect and probability of droplets colliding with the edge of the splitter plate. Such collisions can shatter droplets thereby causing the sampled spray to have a droplet distribution different from that of the main spray. This problem is analyzed in some detail by Dickerson (Ref. 47).

Droplet Freezing Technique

This technique has been applied extensively in the study of rocket engine injectors. Much of this work that is related directly to rocket engine injectors was performed at Rocketdyne during the period 1967 through 1975, and utilized wax as the injected liquid. Fluids other than wax have been used and droplet capture and freezing in liquid nitrogen also has been performed. All of the work described herein utilizing this technique was done with wax.

The frozen wax technique offers several advantages over other methods. The liquid wax is injected into the atmosphere or a large pressure vessel where the droplets rapidly cool and solidify, and then are collected and sampled. The sample then is subjected to a sieving operation where the wax droplets are separated into size groups. Each size group then is weighed and a plot of droplet mass (volume) versus size is constucted. Thus, the cumulative volume, volume distribution, and mass median diameter are measured directly, without the great time and manpower associated with the sizing and counting of individual droplets. Also, the true or temporal distribution of droplets is measured, since all the droplets produced by the spray over a long period of time (several seconds) are collected. And finally, the number of frozen wax droplets included in the sample is on the order of millions. This technique does not suffer from a lack of a sufficient sample size to be statistically accurate.

One serious disadvantageous feature of the hot-wax technique is the limited choice of materials that can be applied conveniently. Since the properties of the actual propellants are different from the simulants, it is necessary to establish the effects of these properties (surface tension, density, and viscosity) on the atomization process. Thus, the capability to perform tests with different fluids having widely varying properties is important. Another feature of the wax technique that merits consideration is the density increase upon freezing. Because of this, some earlier investigators have corrected the wax droplet sizes by multiplying the measured droplets' volumes by the ratio of the solid to liquid densities. However, the physics of the freezing phenomena indicates that the droplets should freeze on the outside first. If this is correct, then the frozen drops should be hollow and no density change drop size correction is required. Dickerson (Ref. 47) has discovered that the droplets indeed are hollow, and that the volume of the central void is approximately equal to the size change due to freezing--at least for the larger drops.

One of the most serious criticisms of most of the hot-wax investigations involves the problem of defining the temperature (and hence the properties) of the liquid wax during atomization. In most investigations, the hot liquid wax is injected into a relatively cold gas (e.g., the atmosphere). For these cases, it is necessary to question whether the wax has cooled significantly prior to the completion of atomization. Zajac (Ref. 58) presents data showing that the surface tension and viscosity of the particular wax utilized (shell 270) increase by 12% and 83%, respectively, between 93 C (the nominal injection temperature) and 66 C (slightly above the wax fusion temperature). Certainly, the surfaces of the wax ligaments and droplets must be cooler than the bulk wax injection temperature. Thus, the wax properties at the injection temperature may not be the same as those existing during atomization. Longwell (Ref. 1) presents results suggesting the wax technique erroneously may give large droplets due to viscosity increases as the liquid cools during atomization. However, Hasson and Mizrahi (Ref. 23) present extensive data demonstrating that the wax technique produces significantly and erroneously small droplets (they corrected for an assumed shrinkage of the droplets upon freezing, but this correction is not great enough to account for the observed difference). Several investigators (Ref. 29, 70, 71, 78) performed hot-wax experiments in which the wax was injected into hot gas and subsequently

cooled after atomization was complete. In these investigations the potential problem of wax cooling during atomization should have been eliminated or minimized.

DROPLET SIZE MEASUREMENT RESULTS AND CORRELATIONS FOR ROCKET ENGINE INJECTORS

This section presents all the pertinent atomization results that were found relating to triplet, pentad, and coaxial injectors. Since very little data pertaining to these injector types has been found, and since most of our knowledge of atomization comes from the study of like doublets, a discussion of like doublets also is included.

The expressions relating representative droplet diameter to injector geometry, operating conditions, and environment vary with each investigator. The most common representative diameters utilized are the Sauter mean (D_{32}), volume or mass mean (D_{30}), and mass median ($\overline{D}$). Conversion between these diameters requires that the droplet size distribution be known, and a generalized conversion requires that the distribution function be known and integrable. Generally, such information is not available, so a direct comparison between these representative diameter equations cannot be accomplished (one exception to this is described later). However, inspection of the exponents of some of the more important variables (e.g., liquid velocity, V_L, and orifice diameter, d_j), indicates considerable disagreement between these equations. This may be due to the previously discussed questions and problems regarding the measurement techniques, testing over different ranges and conditions, the use of different fluids, unmeasured and/or uncontrolled variables (the most important being the local gas velocity, V_g), and/or other unknown causes. In a few cases, these drop size equations contain variables that are not varied significantly during the testing. In many cases (all cases for the triplet, coaxial, and pentad injectors), all of the potentially significant variables have not been tested. The equations developed from such data are incomplete. All of the droplet size equations described herein are strictly empirical or are based only in part on very limited theoretical considerations.

Like Doublet Correlations

The most extensively studied rocket engine type injector is the like doublet. Much can be learned through a review of these doublet studies about atomization processes and measurements in general that is relevant and important to the study of triplets, pentads, and even coaxial injectors. Table 1 is a list of selected impinging doublet injector atomization studies showing the droplet size correlations derived and the conditions of the experiments.

One of the earliest studies of impinging element injectors was the work of Tanasawa, et. al. (Ref. 9). This study employed totally opposed impinging streams to develop the equation presented in Table 1, and also indicated that liquid viscosity is of little importance. Although it is not clear, it appears that other properties were varied with viscosity. Subsequent studies indicated that viscosity effects cannot be neglected.

Prof. Dombrowski of Imperial College performed a number of investigations (Ref. 32, 33, 34, 35, 40, 45) of atomization of impinging streams utilizing photography. Many of these experiments were performed in a pressurizable vessel with a weak gas flow to prevent droplet recirculation. Some of these results (Ref. 33) show the surprising result that increasing chamber gas density first causes a decrease in droplet size, but at higher chamber pressures (>1 mPa) the effect of gas density is to increase droplet size. In order to cover both these regions, two droplet size equations were fit to the data as shown in Table 1. Reference 33 also presents data showing the effect of chamber gas density on ligament and droplet velocity. Dombrowski (Ref. 40) also demonstrates the differences in the spray fans and the droplets formed by laminar and turbulent streams. Turbulent stream droplet size correlations did not fit laminar stream data. Measurements of the liquid velocities in fans were performed and show that these liquid velocities can exceed the average stream velocity if the streams are flowing laminar. An explanation of this phenomena is presented. This difference between laminar and turbulent streams' drop sizes is an important finding that was not considered by some later investigators. Dombrowski's work utilized photography that measures the spatial distribution or concentration of droplets.

TABLE 1. SELECTED LI

REFERENCE	MEASUREMENT TECHNIQUE	CORRELATION
TANASAWA, ET. AL. (1957)	DROPLET CAPTURE (VARIOUS FLUIDS)	$D_{32} = 1.73 \dfrac{d_j^{.75}}{V_L^{0.5}} \left(\dfrac{\sigma}{\rho_L}\right)^{.25}$
DOMBROWSKI AND HOOPER (1962)	PHOTOGRAPHY (WATER, ETHANOL, AND WATER/ GLYCERINE SOLUTION	$D_{32} = .0077 \left(\dfrac{\sigma}{\Delta P}\right)^{.16} \left(\dfrac{\rho_L}{\rho_g}\right)^{.1}$ $.0012 < \rho_g < .009 \text{ g/cm}^3$ $D_{32} = .0468 \dfrac{\sigma^{.12}}{\Delta P^{.2}} \left(\dfrac{\rho_g}{\rho_L}\right)^{.25}$ $.016 < \rho_g < .025 \text{ g/cm}^3$ $\Delta P \text{ IN psi}$
DROMBROWSKI AND HOOPER (1964)	PHOTOGRAPHY (WATER)	$D_{32} = \dfrac{4}{V_L^{.79} (\sin\frac{\alpha}{2})^{1.16}}$
INGEBO (1958)	PHOTOGRAPHY (n-HEPTANE) 8 INCH FROM INJECTOR	$D_{30} = \dfrac{1}{.3(V_L/d_j)^{1/2} + .0125\lvert V_L - V_g \rvert}$
DICKERSON, ET. AL. (1968)	HOT WAX SPRAYED INTO AIR	$\bar{D} = 8.41 \times 10^5 \dfrac{d_j^{.57}}{V_L^{.85}}$
ZAJAC (1971)	HOT WAX SPRAYED INTO AIR	$\bar{D} = 3.7 \times 10^5 \dfrac{d_j^{.57}}{V_L^{.75}} \left(\dfrac{P_c}{P_j}\right)^{-.52}$ LAMINA JETS $\alpha = 60$ $\bar{D} = 2.85 \times 10^6 \dfrac{d_j^{.57}}{V_L} \left(\dfrac{P_c}{P_j}\right)^{-.1}$ TURBUL JETS $\alpha = 60$ $\bar{D}_\alpha = (1.44 - .0073\alpha) \bar{D}$

CONDITIONS		
$\alpha = 180°$ $V_g = 0$ $d_j = .04 - .1$ cm	$V_L = 1.0 - 5.0$ m/s $\sigma = .029 - .075$ Nt/m $\mu_L = .005 - 3.5$ POISE	RESULTS INDEPENDENT OF VISCOSITY
$\alpha = 110°$ $d_j = .053$ cm $\Delta P = 25 - 100$ psi	$\rho_L = 800-1000$ kg/cm^3 $\sigma = .024 - .073$ Nt/m $\mu_L = 1 - 5$ cP $V_g \sim 0$	NOTED THAT RAPID DROP DECELERA-TION CAUSED DROP CONCENTRATION TO INCREASE
$V_L = 7.3 - 19.5$ m/s $\alpha = 50 - 140°$		TURBULENT FLOW ONLY LAMINAR DATA DID NOT FIT
$d_j = .074 - .226$ cm $V_L = 9.15 - 30.5$ m/s $V_g = 19.8 - 91.4$ m/s	$\alpha = 90°$ $\mu_L = .386$ cP $\rho_L = 680$ kg/m^3 $\sigma = .020$ Nt/m	$\Delta V \neq V_L$ $D_{30} \propto \left(\dfrac{\mu_L \sigma}{\rho_L}\right)^{.25}$ (INGEBO 1957)
$d_j = .066 - .206$ cm $V_L = 15.5 - 45.3$ m/s $\alpha = 60°$ $V_g = 0$	WAX PROPERTIES (?) $\mu_L = 3.0$ cP $\rho_L = 764$ kg/m^3 $\sigma = .017$ Nt/m	ADJACENT FANS (WATER) HAD NO EFFECT ON $\bar{D}$, BUT DID AFFECT DISTRIBUTION
$d_j = .152 - .206$ cm $V_L = 9.14 - 67.0$ m/s $\alpha = 45-90°$ $V_g = 0$ $\dfrac{P_c}{P_j}$ = RATIO OF CENTERLINE TO AVERAGE DYNAMIC PRESSURE (A MEASURE OF VELOCITY PROFILE)	WAX PROPERTIES	ORIFICE ENTRANCE CONDITIONS, MISIMPINGEMENT, JET DISINTE-GRATION, TURBULENT VS LAMINAR, VELOCITY PROFILE, L/d (ORIFICE), L/D (FREE STREAM), ET. AL., INVESTIGATED.

TABLE 1. (Concl...

REFERENCE	MEASUREMENT TECHNIQUE	CORRELATION	
GEORGE (1973)	HOLOGRAPHY N_2H_4 DROPS BURNING IN N_2O_4 H_2O DROPS IN N_2 1" TO 4" FROM INJECTOR	$D_{30} = A_o + A_1 V_L + A_2 \ln \rho_L + A_3 \dfrac{\rho_g V_g^2 d_j}{12\sigma}$ COLD FLOW $D_{30} = \dfrac{d_j}{B_1 + B_2 d_j + B_3 W_L}$ HOT FLOW	$d_j = .15 - .244$ $V_L = 18.6 - 38.7$ $\alpha = 60°$ $V_g = 75.6 - 114$
ZAJAC (1973)	HOT WAX INJECTED INTO WARM, FLOWING N_2 IN A VARIABLE AREA DUCT	$\overline{D} = \tau \overline{D}_C \left\{ 1 - 1.77 \times 10^{-3} \overline{D}_C \left(\dfrac{V_{gm} - V_L}{V_L} \right) \text{EXP} \left[-.24 \dfrac{V_{gm} - V_L}{V_L} \right] \right. \mid \dfrac{V_{gm} - V_L}{}$ $\text{FOR } -1 \leq \dfrac{V_{gm} - V_L}{V_L} \leq 1.25$ $\overline{D} = \tau \left\{ \overline{D}_C (1 - 1.52 \times 10^{-3} \overline{D}_C) - 12 \ln \left(\dfrac{V_{gm} - V_L}{V_L} \right) \right\}$ $\text{FOR } \dfrac{V_{gm} - V_L}{V_L} > 1.25$ $\text{WHERE } \overline{D}_C = 2.01 \times 10^5 d_j^{.375} / V_L^{.75} = 10.9 \, \overline{D}_o^{.66} / V_L^{.09}$ $\tau = \left[1 + 5.8 \times 10^{-6} \dfrac{\overline{D}_C V_L}{L} \left(\dfrac{V_L}{V_{gm}} \right)^{.5} \right]^{.41}$ $L \geq 5 \text{ cm}$	
ALL D VALUES IN MICRONS, ALL OTHER VALUES IN THE EQUATION SHOULD BE INPUT IN CGS UNITS			

CONDITIONS		
cm	ρ_g = 24. - 36. kg/m^3 (HOT)	HOT AND COLD FLOW DID NOT CORRELATE
m/s	ρ_g = 1.1 kg/m^3 (COLD)	
	ρ_L = 1001 - 1017 kg/m^3 (HOT)	DROP SIZE DISTRIBUTION WAS SPATIALLY UNIFORM
m/s	ρ_L = 10^3 kg/m^3 (COLD)	D_{30} INCREASES WITH AXIAL DISTANCE

$\dfrac{V_L}{}$] }

V_L = 23.2 - 76.2 m/s

α = 60°

WAX PROPERTIES

$\rho_g \sim 1$ kg/m^3

$\overline{D}_c$ = DROP SIZE WHEN $V_{gm} = V_L$ (140 < $\overline{D}_c$ < 360)

$\overline{D}_o$ = DROP SIZE WHEN $V_{gm} = 0$

V_{gm} = MAX GAS VELOCITY (V_{gm} < 305 m/s)

L = LENGTH OVER WHICH GAS IS ACCELERATED

2 **FOLDOUT FRAME**

As previously discussed, this is not the true or temporal distribution, and the spatial concentration can vary with location and with changes in the droplet decelerating forces (in this case, changes in gas density). In Ref. 33, it is noted that rapid drop decelerations at high gas densities caused droplet concentrations to increase. Apparently, the possibility that the amount of increase in droplet concentration might vary with the size of the droplet was never considered.

During the late 1950s and early 1960s, a number of investigations of atomization were performed at NASA-Lewis (Ref. 12, 13, 15, 21, 25, 26, 39, 49). These include studies of the effects of various parameters on impinging stream fans, single stream crosscurrent injection, and photographic measurements of droplet sizes produced by impinging streams. One of the most often quoted references of these is the work of Ingebo (Ref. 15). He performed experiments utilizing like doublets injecting heptane into a low-velocity gas stream. The heptane was injected in the direction of the gas flow (concurrently) and the droplets were photographed and counted throughout the spray at a distance of 8 inches from the injector. The heptane streams were flowing in the turbulent regime. One of the most unique and important features of this work was the use of the flowing gas stream to simulate the combustion gas motion in a rocket combustor. Unfortunately, one of the greatest problems then (and now) is that we are unable to adequately define the actual combustion gas velocity field in a rocket combustor. And Ingebo's work demonstrates the great importance of this effect. The droplet size correlating equation developed from this data (Table 1) contains a term $(V_L - V_g)$, which accounts for this gas velocity effect on droplet size. Ingebo also utilized the data to evaluate the constants in a Nukiyama - Tanasawa general droplet size distribution equation to obtain:

$$\frac{dR}{dD} = \left(\frac{3.915}{D_{30}}\right)^6 \frac{D^5}{120} \exp\left(-3.915 \, D/D_{30}\right)$$

Furthermore, in an earlier investigation (Ref. 13), Ingebo established a relationship for the effect of injected liquid properties on droplet size as:

$$D_{30} \quad \left(\frac{\mu_L \sigma}{\rho_L}\right)^{.25}$$

However, this relationship was determined in experiments involving crosscurrent injection of single streams into flowing gases. Its applicability to cocurrent injection may be questionable, yet, it is often utilized.

In a subsequent study (Ref. 26), Ingebo utilized a moving camera to photograph burning ethanol droplets and measured their velocities. At a distance of 0.1 m from the injector, the drops were observed to be traveling at a higher velocity than their injection velocity. Most importantly, the small droplets were observed to have been accelerated much more than the larger droplets. 35 micron droplets had undergone a velocity increase 9 times as great as 344 micron droplets. Again, this would indicate that the spatial concentration of each size of droplets would be rapidly and differently varying with distance from the injector. The effect this would have on the measured spatial droplet size distribution apparently was not considered.

In 1964, several studies (Ref. 36 through 38) were reported by investigators at Aerojet General. Brown (Ref. 38) captured droplets on glass slides that were produced by the injection of a stream of liquid into flowing cold and hot (up to nearly 1300 K) gas. One of the important features of this work was the recognition that the spray affects the gas velocity. An attempt was made to quantify this effect in a droplet size relationship with a term containing the mass flowrate ratio of liquid to gas. In another of these investigations, Wolfe and Anderson (Ref. 37) performed experiments and developed a relationship for the breakup of large droplets (i.e., secondary atomization) based upon the earlier work of Weiss and Worsham (Ref. 29). This relationship includes a liquid properties effect of the form,

$$D_{30} \propto \sigma^{1/2} \, \mu_L^{1/3} \, \rho_L^{-1/6}$$

In the early 1970s, photography and the new technique of holography were utilized at AFRPL to measure droplet sizes (Ref. 54, 66, 72, 73, 76). Kuykendal (Ref. 54) investigated the effects of liquid velocity, orifice diameter, impingement angle, stream alignment, orifice length, and surface finish for like doublets flowing water. Droplet size equations were developed to define these effects, but the average drop sizes were based upon a relatively small drop count (occasionally less than 100), and these equations appear to disagree greatly with most other similar studies. George (Ref. 72, 73, 76) utilized holography to measure droplet sizes in both hot flow (hydrazine drops burning in nitrogen tetroxide) and cold flow (water in N_2). The form of the droplet size correlations developed in that effort are presented in Table 1.

During the late 1960s and early 1970s, a very elaborate hot-wax capability was developed at Rocketdyne and many atomization investigations were performed (Ref. 47, 48, 50, 51, 52, 55, 56, 58, 60, 61, 63, 64, 65, 67-71, 74, 78). Two of the most comprehensive of these investigations are those of Dickerson, et. al. (Ref. 47) and Zajac (Ref. 58). Their correlations for like doublets are presented in Table 1. Both of these efforts were performed by spraying wax into "still" air. Dickerson's droplet size correlations, as reported in Ref. 47, are not in agreement with his subsequent paper (Ref. 52). Discussions with Dickerson revealed that the earlier liquid velocity data was incorrect, and the correlations of his latter paper include the correction. Dickerson evaluated the atomization characteristics of a variety of impinging injectors, with great emphasis on doublets. Experiments were performed with impinging fans from unlike pairs of like doublets utilizing water as the other fluid. These tests indicate that impinging fans tend to broaden the droplet size distribution but have little effect on D. Droplet size distributions for several of the injectors tested are presented in Fig. 4. Note that both axes have been normalized in such a way that all distributions must pass through the point (1.0, 0.5). Also, as previously discussed, it is the slope of these cumulative volume distributions that truly defines the spray. Thus, the apparently small differences in the plots of Fig. 4.are, in fact, large differences of great importance.
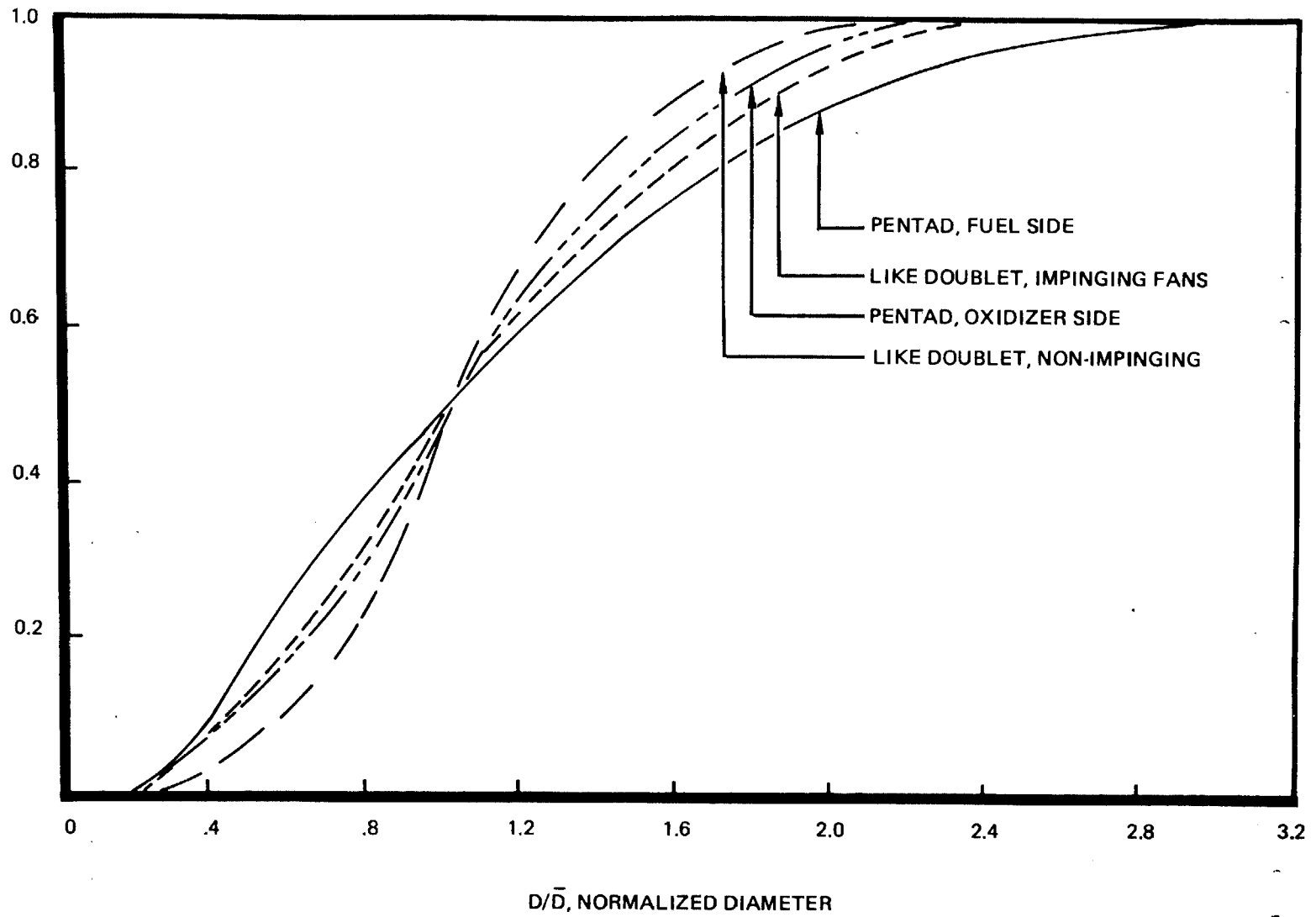
Figure 4. Normalized Droplet Size Distributions
for Selected Injectors (Ref. 52)

The single most comprehensive study of atomization of rocket engine-type injectors is the work of Zajac (Ref. 58). Zajac examined the effects of liquid velocity, orifice diameter, velocity and diameter ratios, orifice length, free jet length (distance from orifice to impingement point), angle of impingement, orifice entrance conditions (geometric and flow conditions), misimpingement, and propellant miscibility for like and unlike doublets are well as triplets and pentads. In addition, he measured transient pressure distributions within the free streams (a measure of velocity profile and turbulence). Zajac found that streams flowing turbulent acted considerably different than laminar streams with regard to atomization (Dickerson had neglected this, but earlier investigators, e.g., Dombrowski (Ref. 40), already had indicated this). Thus, it was necessary to establish two droplet representative diameter equations, one for turbulent and one for laminar. Velocity profile also was found to be important, but only in laminar flow. Free stream breakup prior to impingement was shown to be important and can occur at a free stream length of from 5 to 10 orifice diameters in turbulent streams. The much higher gas densities in a real combustor could cause breakup in shorter lengths.

The state of the art circa 1971 was that the wax technique yielded sufficient quantity and apparent quality of data to define droplet sizes and size distributions of hot wax droplets sprayed from like doubltes into still air. Several problems remained, as follows:

1. How valid is the hot-wax technique? Does wax significantly change properties before atomization is complete?

2. How can hot-wax results be correlated to that of real propellant?

3. What is the effect of the actual rocket combustor environment (hot, high-density combustion gases moving at high velocity) on the atomization process?

In an attempt to solve some of these problems, tests were performed with combinations of waxes to examine viscosity effects (Ref. 69) and a large pressure tank was utilized to simulate high-density gases (Ref. 64, 69, 74, et. al.). In addition, several attempts (Ref. 65, 68, 74, et. al.) were made to validate these

droplet size correlations by utilizing them in computer models of rocket engines and comparing the results of these models with the actual hot-fire tests the models were attempting to simulate. In one program (Ref. 65), a test engine operating on wax and liquid oxygen was utilized. Although all of these efforts reported some degree of success, these three basic questions still remain essentially unanswered.

One of the most unknown aspects of this problem was (and is) the effect of the combustion gas velocity on droplet size. The actual velocity field existing in and around the spray in cold-flow experiments is never measured. The actual velocity field existing in and around the spray in an operating engine also is unknown. And finally, the effect of a known flowfield on the formation and breakup of a spray fan or stream (primary atomization) is essentially unknown. There is, however, a considerable body of work performed to evaluate the effects of gas flowfields on the deformation and breakup of individual droplets (secondary atomization). Such efforts demonstrate the great complexity of this latter process.

In an effort to establish the effect of gas velocity on the size of droplets produced by impinging liquid streams, experiments have been performed in low-pressure wind tunnels. In such experiments, the gas velocity is defined as the velocity that existed prior to the introduction of the spray. The effect of the spray on the gas velocity, although often recognized, is not taken into account--very crudely included by Brown (Ref. 38), and is not measured. Similarly, the liquid velocity in the gas is assumed to be the average liquid velocity at the injector orifice exit, and not the actual liquid velocity in the spray fan. Thus, in attempting to correlate this very important effect of relative gas velocity (gas velocity relative to liquid velocity), the velocities used are incorrect and are, at best, only representative of the true velocities. Despite this, these experiments do provide an indication of the importance of the relative gas velocity. Probably the most extensive of these efforts for impinging like doublets are the work of Ingebo (Ref. 15) and George (Ref. 76), as previously discussed, and the latter investigations of Zajac (Ref. 70 and 71).

Zajac utilized a doublet injecting hot wax cocurrently into a ducted hot (60 C) nitrogen stream. He separated the atomization process into two parts (i.e., primary and secondary) and studied these separately. In the primary atomization study, the effect of constant velocity and accelerating gas streams on the sizes of droplets initially formed was investigated. In the secondary atomization study, known droplet size distribution sprays were subjected to accelerations to observe droplet breaking. The rate and degree of acceleration was controlled by varying the length and area of the duct downstream of the injection location.

Zajac found that many of the parameters investigated in his previous work were of little importance compared to the effect of relative gas velocity. Much of his data was plotted in the form of Fig. 5, showing droplet size versus a nondimensionalized relative gas velocity. Note that all of the investigations in which the liquid was injected into "still" air would be plotted at the -1 value of the nondimensionalized velocity. Shown in Fig. 5 are volume mean diameter data from Ingebo showing the effect of gas velocity on droplets produced by two different injectors, mass median diameter data from Zajac, and the calculated droplet size based upon tests with $V_g = 0$. The data from Zajac presented here was obtained with a constant gas velocity (i.e., duct area remained constant). Figure 5 demonstrates the great efect of gas velocity on droplet size.

Based upon his experiments with accelerated and constant velocity flows, Zajac constructed the droplet size correlation equations shown in Table 1. These equations compute the mass median droplet size based upon the gas and liquid velocities, the droplet size, D_c occurring when the maximum gas velocity equals the injected liquid velocity (i.e., $V_g-V_L/V_L = 0$), and a parameter , which includes the distance over which the gas is accelerated (at V_g = constant, L = infinity). The parameter D_c is computed from the liquid velocity and orifice diameter. A study of the derivation of these equations indicates they are applicable to turbulent flow only.

The correlation of Zajac is, to some extent, supported by the earlier work of Ingebo, and the very important effect of relative gas velocity is demonstrated. Unfortunately, the application of such results to real combustors is difficult since the combustion gas velocity cannot be defined adequately.
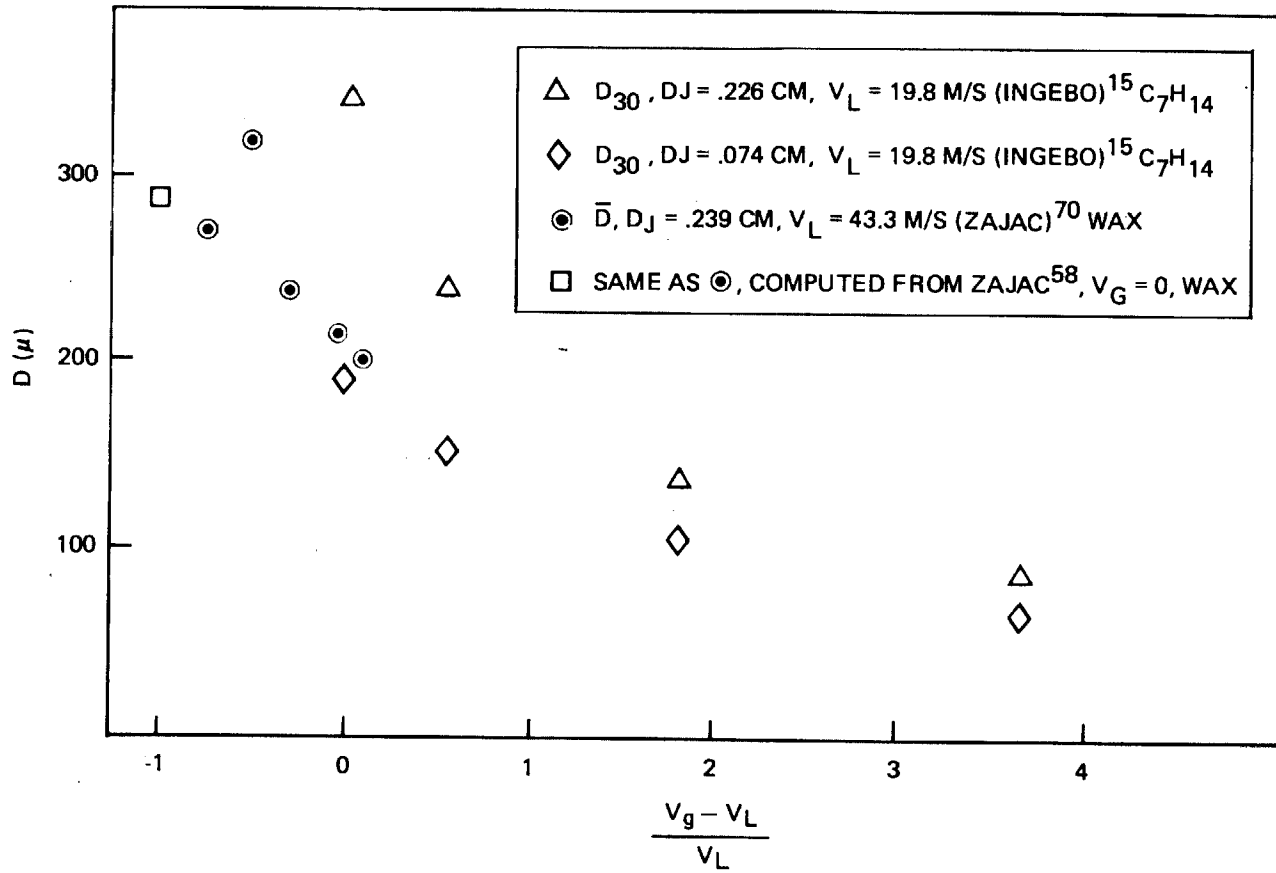
Figure 5. Effect of Gas Velocity on Droplet Size

Since about 1975, there has been very little atomization work directly relateable to rocket engine like doublet injectors. This is certainly not because the problem has been considered solved. Despite all the earlier efforts to define the initial droplet sizes produced by like doublets in combustors, our knowledge in this area is very crude and/or qualitative. All of the droplet size data to date is of questionable accuracy and/or validity due to real or possible droplet size measurement technique problems as previously discussed. The droplet size correlations and distributions developed from this data are generally, strictly empirical. They are mere curve fits of the test data and, as such, may be neglecting important untested variables and are certainly not of the proper form. These correlations are based upon data that demonstrated poor or usually unknown repeatability, considerable spread, and often a relatively low quantity of droplet counts. To some extent, these features of the data are masked by the extensive use of semilogarithmic plots of the data and cumulative droplet size distribution plots.

Perhaps the greatest problems involve the application or utility of the atomization data. Extrapolation of the cold-flow data using wax or other liquids to the actual propellants and to the conditions existing in a rocket combustor requires many questionable assumptions and estimates. One of the most important and, unfortunately, most questionable of these extrapolations involves the combustion gas velocity, as previously discussed. Also, since the correlations developed are empirical, extrapolation to any conditions outside the ranges tested is dangerous. And finally, the attempts to utilize the correlations in rocket combustor codes have not been successful. All of the major rocket combustor codes in use at Rocketdyne (i.e., TPP, SDER, CICM) have arbitrary multipliers of the initial droplet sizes, either as a part of the code or as an input, in order to force agreement between the codes and hot-fire engine test data.

Properties Correlations for Like Doublets

In addition to all the like doublet "lessons learned" discussed above that are applicable in general to rocket engine-type injectors, these studies provide the only known corrections or correlations by which we may relate real propellant atomization to that of the simulants used in atomization experiments. Although

many of the droplet size correlating equations contain liquid properties effects, probably the two properties correlations quoted most generally are

$$D_{30} \; (\frac{\mu \; \sigma}{\rho_L})^{.25} \qquad \text{Ingebo (Ref. 13)}$$

and

$$D_{30} \; \mu_L^{.333} \; \sigma^{.5} \; \rho_L^{-.167} \qquad \text{Wolfe and Anderson (Ref. 37)}$$

Ingebo's correlation comes from a droplet size correlation equation defining the droplet sizes produced by the breakup of a single stream injected transversely into an airstream. Wolfe's and Anderson's correlation is based on the breakup of already formed droplets in gas streams (i.e., secondary atomization). The applicability of either of these relationships to like doublets can be questioned. In addition, no attempts to establish the effect of liquid properties on droplet size distributions were found in the literature. Also, properties correlations for unlike doublets, triplets, pentads, or coaxial injectors, or any gas/liquid injector apparently do not exist.

Another aspect of the liquid properties correlations problem that often is overlooked is the actual values of the properties of the real propellants and the simulants at their injection conditions. Since liquids are generally, relatively incompressible, since viscosity usually is not considered to be a function of pressure, and since density, viscosity and surface tension data for many propellants and test fluids is readily available only at room temperature and one atmosphere or at the liquid's normal boiling point (for cryogenics), these room temperature and one atmosphere or NBP properties data often are utilized. This can cause considerable error. Liquid oxygen is a propellant of considerable interest which serves as a good example. For LOX at 134 K (the SSME preburner LOX injection temperature) the density increases by 11% and the viscosity increases by 52% between 17 and 340 atm (data from NBS Table TN 384). LOX properties are, of course, a fairly strong function of temperature, and choosing the wrong temperature (e.g., using NBP data) also can cause great errors.

Surface tension is a particularly difficult property for which to find nonroom temperature and one atmosphere or non-NBP data. Surface tension is a strong function of temperature and techniques are available to compute the effect of temperature. For LOX, the surface tension changes from 13.2 dynes/cm at its NBP of 90 K to 6.4 dynes/cm at its SSME injection temperature of 134 K. As part of an attempt to determine the effect of pressure on surface tension, papers were found that indicated a very strong effect (e.g., O.K. Rice, "The Effect of Pressure on Surface Tension,: Journal of Chem. Physics, Volume 15, #5, May 1947). However, based upon discussions with Prof. A. Adamson and Dr. R. Massoudi of the University of Southern California's Chemistry Department, this effect apparently is not due to pressure, but rather to the absorption of gases into the liquid. The effect of pressure alone on surface tension should be on the order of a 1% increase per 100 atm pressure. This absorption of gases also probably would have a great effect on other properties. Since the time available for absorption, i.e., the time between injection and atomization is so short, very little absorption would be expected. If this is the case, the effect of pressure on surface tension should be of little concern.

Triplet Correlations

Very little data was found regarding the atomization characteristics for triplets. This data is synopsized in Table 2. All these investigations were performed at Rocketdyne utilizing the hot-wax technique. In all these tests, the wax was injected into "still" air at ambient pressure.

As a small part of Zajac's earlier investigation (Ref. 58), a particular liquid/liquid triplet having all three holes the same size was subjected to atomization testing. In order to separately evaluate the droplet size produced by the inner and outer streams, wax and hot water were employed. The wax was injected through the inner orifice and the water through the outer orifice, and the liquids then were reversed on a subsequent test. The only variables investigated were the liquids' velocities, and these were varied in such a way as to maintain a constant mixture ratio. Most of these tests were performed under laminar flow conditions. At high velocity (turbulent flow), the data begins to markedly deviate from the correlating equation presented in Table 2.

TABLE 2. DROPLET SIZE CORR[

REFERENCE	MEASUREMENT TECHNIQUE	CORRELATION	
ZAJAC (1971)	WAX AND WATER	D_c & $\bar{D}_o \propto 3.03 \times 10^4 \, V_L^{-.575}$ V_L (cm/s) IS VELOCITY OF LIQUID IN ORIFICE OF INTEREST (CENTER OR OUTER)	$\alpha = 30°$ $V_L = 9.1$ $d_c = d_o$ $\rho_g = 1.1$
McHALE AND NURICK (1974)	WAX AND WATER	PLOTS NEW DATA AND ZAJAC's VS W_e ($^L/d$) $W_e = \dfrac{\rho_L V_L^2 d}{\sigma}$ L = ORIFICE LENGTH	d_c OR $d_o = .05$ $\dfrac{d_o}{d_c} = .52$ L = ORI $\rho_g = 1.1$
MEHEGAN, ET. AL. (1970)	WAX AND HOT GAS (N$_2$) CENTER ORIFICE GAS	2 DATA POINTS	$d_c = 1.4$ $d_o = .52$ $\rho_g = 1.1$

SUBSCRIPT:

  C - CENTER
  O - OUTER

FOLDOUT FRAME

CONDITIONS		
WAX AND WATER PROPERTIES		POSSIBLE DEVIATION AT HIGH VELOCITY
4 - 45.7 m/s	MR $\sim$ CONSTANT	WATER TURBULENT
= .17 cm		WAX TURBULENT ABOVE $\sim$23 m/s
kg/m^3	$\dfrac{(\rho V^2 d)_c}{(\rho V^2 d)_o} = .34 - .38$	
1 - .17 cm	$\dfrac{\rho_c V_c^2 d_c}{\rho_o V_o^2 2 d_o} = 1$	LAMINAR ONLY
2 - 1.0		$\overline{D}$ FOR TRIPLET GREATER THAN $\overline{D}$ FOR UNLIKE DOUBLET AT SAME V_L
FICE LENGTH = 7-50d		
kg/m^3 (P_c = ATMOSPHERIC)		
8 cm	$\rho_c V_c^2 = 7.58 \times 10^4$ Pa (11 psi)	
cm		
kg/m^3	$\dfrac{X_p}{d_c} = 5.39$ AND 9.74 (DEFINED SAME AS FOR PENTADS)	

ζ FOLDOUT FRAME

McHale and Nurick (Ref. 74) performed the most extensive study of triplets to date, utilizing the wax and hot-water technique previously used by Zajac. Although they did not fit the data with an equation, they did plot the data versus Weber number times the orifice length to diameter ratio (Fig. 6). All of their work was done with laminar flow and the low-velocity triplet data of Zajac's is included in Fig. 6. The fact that the droplet size was a strong function of the orifice length to diameter ratio is in agreement with the work of Zajac on doublets. Since the flow is laminar, the velocity profile significantly can affect atomization, and the length to diameter ratio determines how close to fully developed the velocity profile has become. This effect is included in Zajac's correlation for doublets in the P_c/P_j term (Table 1).

The data of Fig. 6 confirms Zajac's earlier work regarding the lack of difference in drop size when by the central and outer streams are of the same size. Note that the ordinate is normalized by the orifice diameter. Also, Fig. 6 is a logarithmic plot. As previously mentioned, such plots tend to minimize significant differences and scatter in the data. At low Weber numbers, which Zajac did not investigate, the normalized mass median drop size for the center and outer streams was no longer the same.

Figure 6 contains all the known droplet size data for liquid/liquid triplets (except for a few higher velocity tests of Zajac). All of the data in Fig. 6 is from laminar flowing orifices, while most future triplet designs would be flowing turbulent. All of the data was obtained with wax and hot water, so there is no way to evaluate liquid properties effects and, hence, to extrapolate this data to actual propellants. And finally, none of this data includes the very important effects of combustor gas velocity.

The only data available regarding gas/liquid impinging elements was obtained by Mehegan, et. al. (Ref. 55). Two tests were performed with triplets utilizing two wax streams impinging on a central hot, gaseous nitrogen stream. These test conditions also are presented in Table 2.
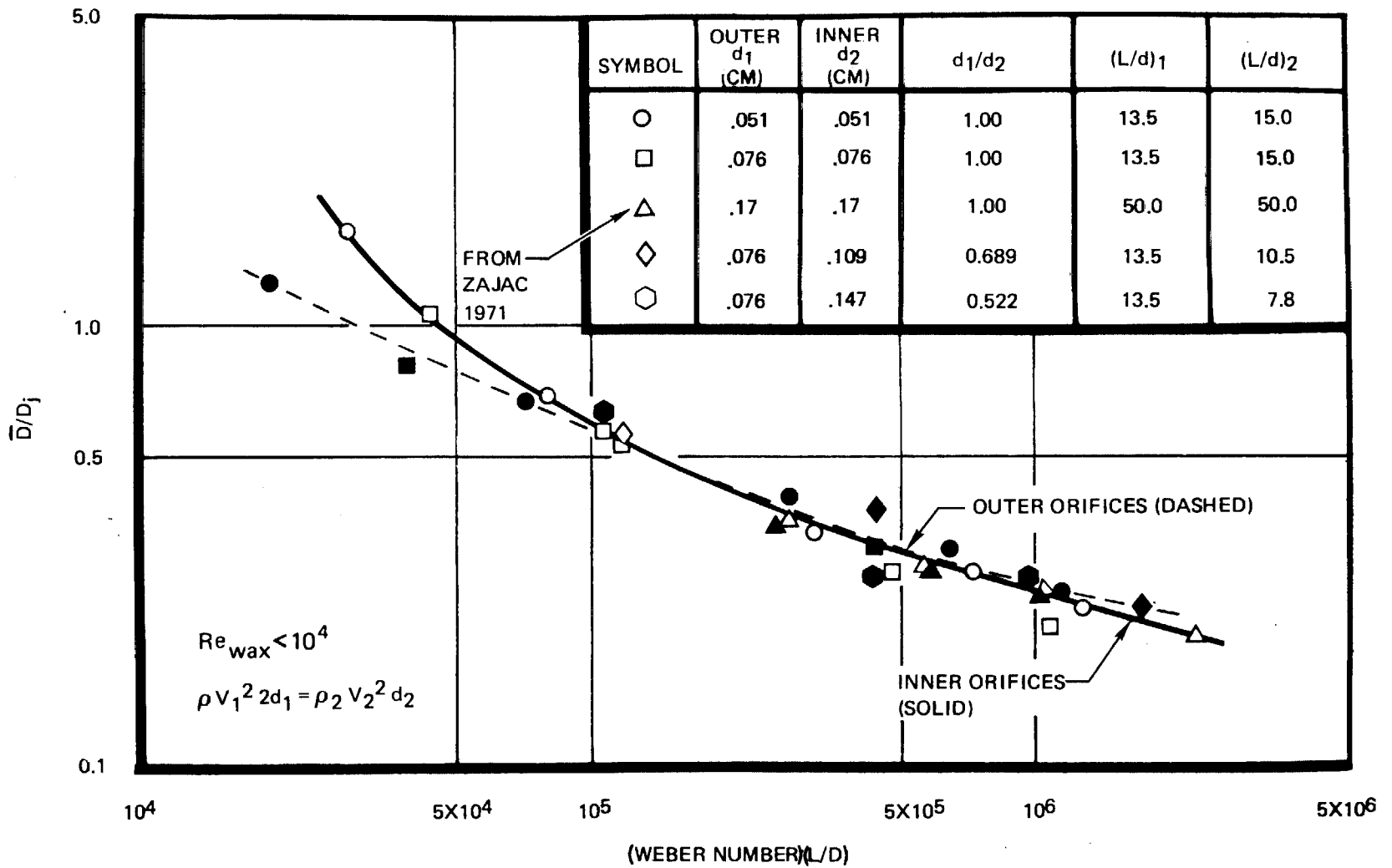
Figure 6. Correlation of Relative Droplet Diameter with Weber Number and Orifice L/d for Triplets (Ref. 74)

Pentad Correlations

The state of the art for pentad atomization knowledge is essentially the same as for triplets. What little data is available was obtained from Rocketdyne wax tests. All of these tests were performed by injection of the propellant simulants into "still" air. The data is synopsized in Table 3.

As a part of Dickerson's (Ref. 47) investigation of injector atomization characteristics, a number of tests were performed on a set of pentad injectors. Droplet size correlating equations were developed relating the mass median drop size to the orifice diameters and injection velocities. Separate equations were obtained for the inner and outer orifices. Wax and hot water were used as the test liquids in a manner similar to the previously discussed triplet tests. In addition, droplet size distribution data were obtained. Normalized volume distribution plots from this work were presented earlier (Fig. 4), and show the different distributions obtained for the center and outer orifices. In addition, the droplet size distribution equations for this data are presented in Ref. 52. As previously discussed, the droplet size correlating and distribution equations presented in Ref. 47 are incorrect, and the equations in this latter paper (Ref. 52) are correct. Dickerson also notes that the quality of the wax spheres was poorer than usual for these pentad tests.

Zajac (Ref. 58) performed a few similar tests and found that the very few higher velocity tests were in crude agreement with the correlations of Dickerson. Most of Zajac's tests were at lower velocities and were in great disagreement with Dickerson's correlating equation (Dickerson did not perform tests at these lower velocities). The deviation at the low velocities is speculated to be due to velocity profile and/or laminar flow effects. Zajac speculates that the flow regime of the outer streams is more important than that of the inner stream.

As a part of the investigation of Mehegan, et. al. (Ref. 55) of gas/liquid injectors, atomization characteristics were determined for a set of pentads. These experiments employed wax and hot gas, with the central orifice always flowing the gas. These tests were performed at atmospheric pressure with variations in gas and liquid velocity and orifice sizes. No correlating equations were developed.

REFERENCE	MEASUREMENT TECHNIQUE	CORRELATION	
DICKERSON (1969)	WAX AND WATER	$$\bar{D}_c = 8.26 \times 10^5 \frac{d_c{}^{.1} d_o{}^{.12}}{V_c{}^{.086} V_o{}^{.89}}$$ $$\bar{D}_o = 5.66 \times 10^6 \frac{d_o{}^{.68}}{V_o{}^{.56} V_c{}^{.57} d_c{}^{.35}}$$	$\alpha = 30$ $\rho_g = 1.$ d_o AND $d_c = .0$ WAX AND H_2O PR
ZAJAC (1971)	WAX AND WATER	AGREES WITH DICKERSON EXCEPT AT LOW V_L (SEPARATE EQUATIONS SHOULD BE DERIVED FOR LAMINAR)	$\rho_g = 1.$ d_o AND $d_c = .1$ $V_L = 9.$
MEHEGAN, ET. AL. (1970)	WAX AND N_2 (OR H_e) CENTRAL ORIFICE GAS GAS HEATED >140 F	$\bar{D} \propto (\rho_g V_g{}^2)^{-\frac{1}{4}}$ $\quad$ $\bar{D} \propto d_o/d_c$ $\bar{D} \propto \frac{X_p}{d_c}$ FOR $\frac{X_p}{d_c} > .8$, OTHERWISE INDEPENDENT MR NOT IMPORTANT LARGER DROPLETS FOR PENTADS THAN TRIPLETS	$\alpha = 45$ $d_c = .6$ $d_o = .1$ V_c (GAS) = 18 WAX PROPERTIES

SUBSCRIPT:

c = CENTER STREAM   ALL d VALUES IN cm
o = OUTER STREAM   ALL v VALUES IN cm/s
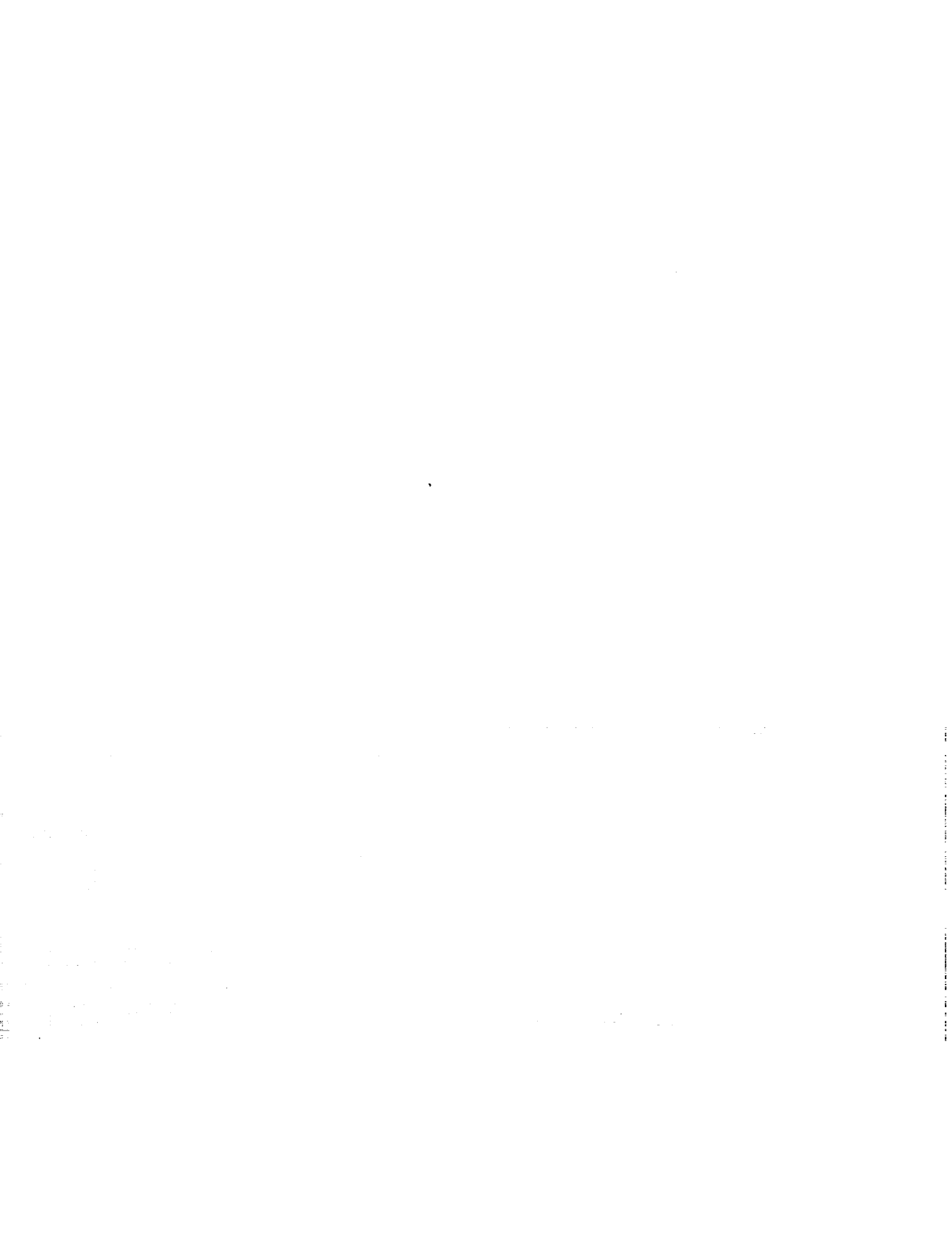
CONDITIONS

° (ANGLE BETWEEN CENTER & OUTER STREAMS)	V_L = 16.8 - 77.7 m/s
1 kg/m^3	DIFFERENT DISTRIBUTIONS FOR INNER AND OUTER STREAMS
635 - .218 cm	
OPERTIES	POORER QUALITY WAX SPHERES

1 kg/m^3 α = 30°	VELOCITY PROFILE EFFECTS MAY BE IMPORTANT
6 - .218 cm	
14 - 18.3 m/s	RELATIVELY FEW TESTS

°	
6 - 2.1 cm	ρ_g = 1.1 kg/m^3
7 - .52 cm	$\dfrac{d_o}{d_c}$ = .161 - .317
3-914 m/s	$\dfrac{x_p}{d_c}$ = .293-1.14 = $2.5\left[\dfrac{\dot{m}_L V_L}{\dot{m}_g V_c}\cos^2(90-\alpha)\right]^{\frac{1}{2}}$
	(PENETRATION PARAMETER)

ζ FOLDOUT FRAME

However, the proportionality relationships shown in Table 3 were observed. Higher gas dynamic forces ($\rho_g v_g^2$) tended to reduce drop size, and the degree of penetration of the outer liquid streams into the central gas stream also affected atomization. This degree of penetration is quantified in a mixing assessment parameter, the pentration parameter, which is defined as shown in Table 3. The droplet size was observed to increase with the penetration factor at higher values.

The capability to assess the atomization characteristics of pentads is only slightly better than that of triplets. At present, there is no way to extrapolate to the actual propellants. Also, there is no data by which to assess the effects of combustion gas motion.

Coaxial Correlations

The standard coaxial injector (gas flowing through the annulus about a central liquid stream) has been studied more extensively than gas/liquid triplets and pentads. Again, all of this work was performed at Rocketdyne utilizing the hot-wax technique. These efforts are synopsized in Table 4.

As a part of the investigation of gas/liquid injectors by Mehegan, et. al. (Ref. 55), a number of tests of the effects of inner tube recess, gas and liquid velocities, and mixture ratio on mass median droplet size were performed. These tests were performed with a large coaxial element. The results of these tests are presented graphically in Fig. 7. Since it is generally believed that the liquid stream breakup is dependent strongly on aerodynamic forces, the velocity difference between the gas and liquid is often of great concern. The effect of inner tube recess also is shown to be of great importance in Fig. 7. A smaller element also was tested, which indicated little effect of recess, but this data was considered questionable. Also, the sizes of the droplets produced by this large injector were quite large.

TABLE 4. DROPLET SIZE CORRELATI(

REFERENCE	MEASUREMENT TECHNIQUE	CORRELATION	
MEHEGAN, ET. AL. (1970)	WAX AND HOT N_2 SPRAYED INTO ATMOSPHERE	$\bar{D} \propto \dfrac{1}{R}$ $\bar{D} \propto \dfrac{1}{V_g V_L}$ $\bar{D} \propto \dfrac{\dot{W}_L}{\dot{W}_g}$ $R = $ RECESS IN UNITS OF d_L	$d_L = $ CENTER TU[$Y = $ ANNULUS G/ $\dfrac{\dot{W}_L}{\dot{W}_g} = 5.7 - 13.\{$ $V_L = 1.6 - 12.$
BURICK (1972)	WAX AND HOT N_2 SPRAYED INTO PRESSURIZED TANK	INCREASE V_g (BY DECREASING Y AT CONSTANT $\dot{W}_g$) DECREASES $\bar{D}$ GREATLY FOR SMALLER Y INCREASE V_L (BY DECREASING d_L AT CONSTANT $\dot{W}_L$) DECREASES $\bar{D}$	$d_L = .177, .27$ $Y = .013, .04[$ $\dfrac{\dot{W}_L}{\dot{W}_g} = 3 - 7.5$ $V_L = 12.2 - 42$
McHALE AND NURICK (1974)	WAX AND HOT N_2 SPRAYED INTO PRESSURIZED TANK	D/Y DECREASES AS $\rho_g V_g^2$ INCREASES BUT THE EFFECT IS LESS AT HIGHER V_L	$\rho_g = .9 - 4.3$ $V_L = 1.2 - 16.[$ $V_g = 91.4 - 30!$ $\dfrac{\dot{W}_L}{\dot{W}_g} = 6$
FALK (1975)	WAX AND HOT N_2 SPRAYED INTO FLOWING GAS	$\bar{D} \propto V_L$ (CONSTANT d_L) SMALL EFFECT $\bar{D} \propto 1/V_g$ (ESPECIALLY WHEN $V_{CG} = 0$) $\bar{D} \propto \dot{W}_L/\dot{W}_g$ (ESPECIALLY WHEN $V_{CG} = 0$) $\bar{D} \propto 1/L$ (NEGLIGIBLE EFFECT EXCEPT AT LARGE D_0 $D_0 = $ DROP SIZE WHEN $V_{CG} = 0$	$d_L = .14 - .41$ $Y = .25 - 1.4[$ $V_g = $ ANNULUS G/ $= 61-305$ m/$ $V_L = 23 - 76$ m/ $V_{cg} = $ SIMULATED VELOCITY $L = $ LENGTH OV[ACCELERAT[

	CONDITIONS	
BE ID = .704 cm $\quad$ V_g = 112 - 339 m/s AP = .259 cm $\quad\quad$ R = 0 - 2d_L B 5 m/s		GENERALLY THESE LARGE COAXIAL ELEMENTS PRODUCED LARGE DROPS A SMALLER ELEMENT WAS TESTED AND SHOWED DIFFERENT EFFECT OF R. THIS DATA WAS CONSIDERED QUESTIONABLE
4, .345 cm $\quad\quad$ R = 0 - 4 d_L 5, .104 cm $\quad\quad$ ρ_g = 3.1 - 22.7 kg/m^3 7 m/s		POST RECESS HAD NO EFFECT DIFFERENT RESULTS FOR DIFFERENT SIZE ELEMENTS PLOTS OF DISTRIBUTION DATA
kg/m^3 $\quad\quad\quad$ R = 0 - 1d_L 8 m/s $\quad\quad\quad$ d_L = .41 cm 5 m/s $\quad\quad\quad$ Y = .13 cm		SLIGHT $\overline{D}$ DECREASE AS R INCREASES
cm $\quad\quad\quad$ $\dfrac{\dot{W}_L}{\dot{W}_g}$ = .1, .5, 2.0 5 cm AS VELOCITY 5 /s COMBUSTION GAS MAX = 61-244 m/s ER WHICH GAS WAS ED = 5-20 cm		SAME DROP SIZE DISTRIBUTION AS ZAJAC LIKE DOUBLETS

⌐ **FOLDOUT FRAME**
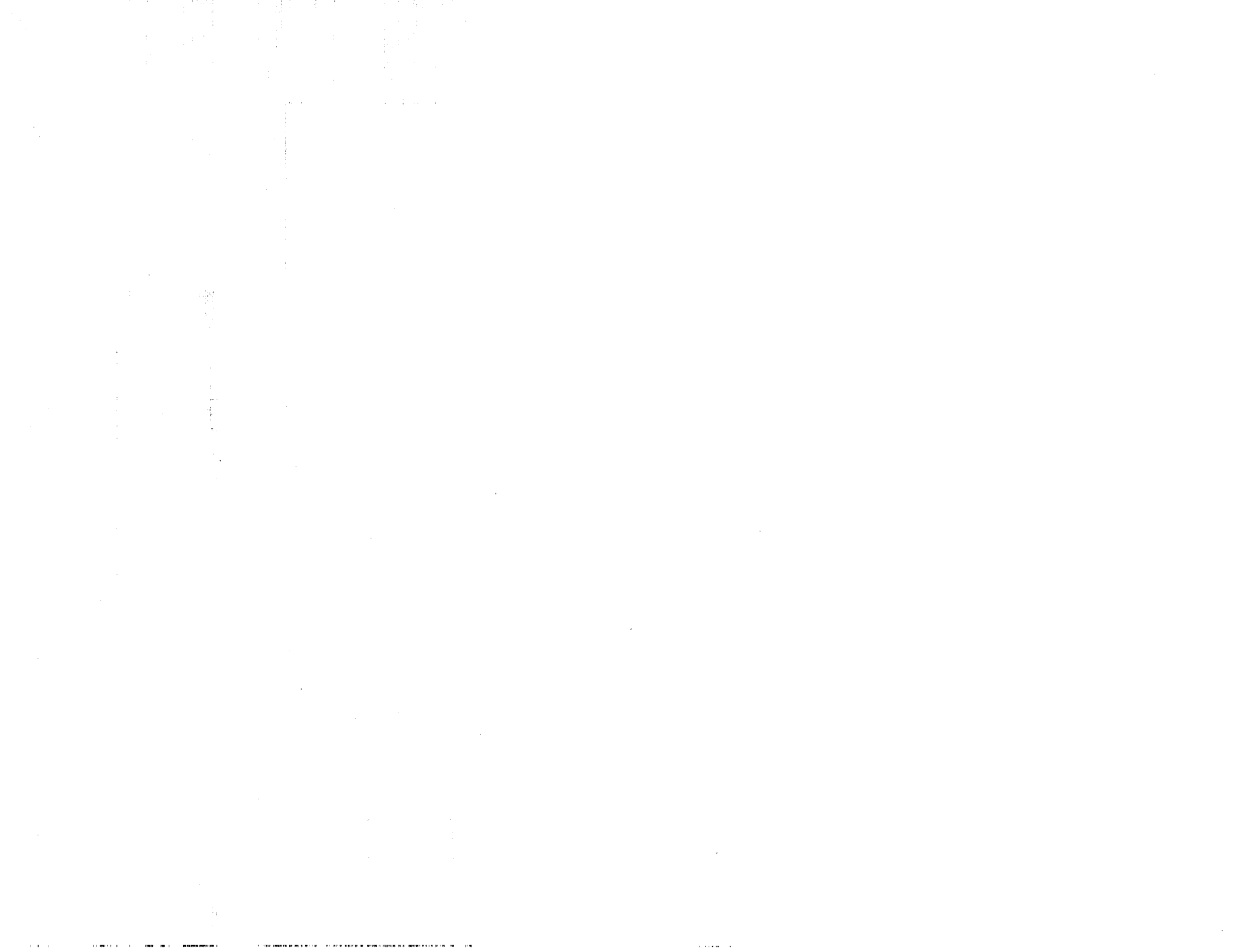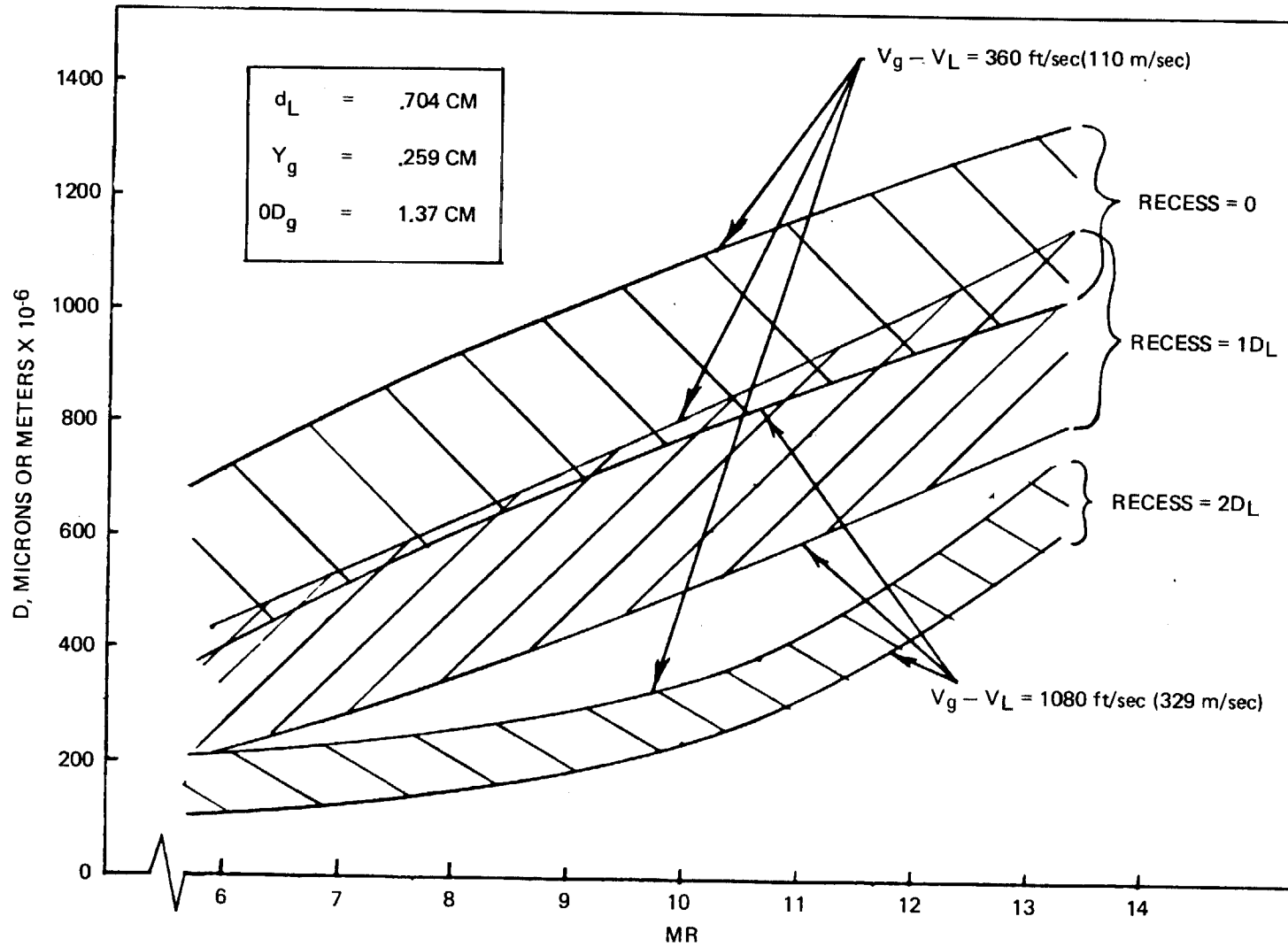
Figure 7. Mixture Ratio Influence on Dropsize
for Coaxial Injectors (Ref. 55)

Investigations by Burick (Ref. 64 and 67) and McHale and Nurick (Ref. 74) util-
ized hot wax and nitrogen injected into a pressurized chamber to examine coaxial
element atomization. The combined work of these two studies, along with the pre-
viously discussed work of Mehegan, indicate that recess only reduces D at low
pressures and/or for large elements. Burick correlated his data as shown in
Fig. 8. Again, the normalization and logarithmic plotting of the data masks the
"spread" of the data. Although McHale and Nurick were investigating primarily
the atomization characteristics of noncircular orifices, they did perform limited
tests on circular orifices. Their data indicates that increased annulus gas
dynamic pressure (ρ_g v_g^2) reduces droplet size, especially at low liquid
velocity. References 67 and 74 present droplet size distribution plots.
Although McHale and Nurick state that recess is a major factor influencing drop-
let size, this conclusion is based upon tests of all of their injectors, which
are primarily noncircular. The limited testing performed with circular coaxial
elements indicates a 10 to 20% reduction in drop size as recess is increased to
$R = d_L$. Even the noncircular elements do not show an effect of recess anywhere
near as significant as that found by Mehegan, et. al.

Falk (Ref. 78) investigated the atomization characteristics of coaxial elements
injecting wax and hot nitrogen cocurrently (i.e., axially) into a duct flowing
hot nitrogen. This work utilized the same test apparatus and techniques as the
analagous work of Zajac (Ref. 70 and 71) on like doublets. One potentially very
important finding of this work was that the droplet size distribution of these
coaxial injectors could be described by the distribution function defined by
Zajac for like doublets. Also, the mass median droplet sizes observed in both of
these investigations were essentially the same at high relative gas velocity.
This would seem to indicate that the manner in which the liquid is broken up
(i.e., the type of injector) has no effect on the ultimate droplet size in the
presence of a sufficiently accelerating combustion gas. If this is truly the
case, it is a most important discovery that will direct the course of future
studies of rocket engine injectors.
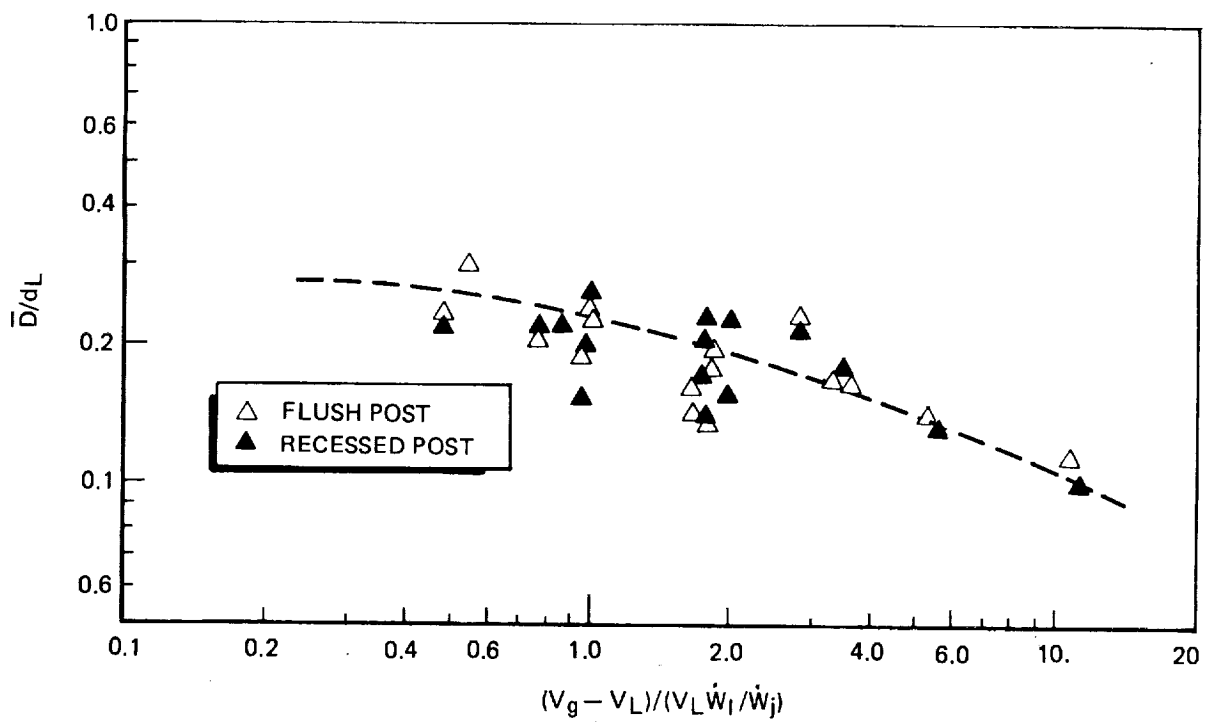
Figure 8. Correlation of Cold-Flow Atomization for Coaxial Injectors (Ref. 67)

Some of Falk's results, showing the effect of simulated combustion velocity on droplet size, are presented in Fig. 9. This data indicates that injectors, which form larger droplets when no combustion gas motion is simulated (i.e., when $V_{cg} = 0$), show more effect of this gas motion than injectors producing smaller droplets. Recognizing this important influence of the relative combustion gas velocity on the droplet size, Falk correlated the data in a manner shown in Fig. 10. This correlation is based only upon the relative, simulated, combustion gas velocity and D_o, the mass median droplet size produced by an injector in the absence of this gas flow.

ATOMIZATION SURVEY - FINDINGS, CONCLUSIONS, AND RECOMMENDATIONS

The state of the art regarding our knowledge of atomization processes is generally quite poor. The physics is poorly and, at best, only qualitatively understood. Only very rudimentary quantitative theories exist. The available data and correlations are generally of questionable validity and/or utility. Many of the most critical parameters are unknown (e.g., combustion gas velocity field, multiple element effects) and/or are not simulated in tests (e.g., gas densities, real propellant fluid properties, combustion gas motion). This sad state of affairs appears to be attributable to two primary causes: the great complexity of atomization processes, and the inaccuracies, errors, and limitations associated with droplet size measurement techniques. Nevertheless, the available data does provide information regarding the importance and relative effects of a number of variables on droplet size.

Probably the most critical of these parameters affecting droplet size is the combustion gas velocity field. This is unfortunate since the actual velocity field in a rocket combustor, and in atomization experiments, is unknown. Combustion gas velocity also is the one parameter that greatly increases the complexity of the atomization assessment problem. This is due to the fact that atomization is highly dependent on the combustion gas velocity field, and in turn, the combustion gas velocity field is established by the rate of combustion, which is determined by the rate of propellant evaporation, which is highly dependent on how well the propellants are atomized (i.e., initial droplet sizes) and mixed. Thus, all of these problems are coupled and the solution of any one requires at least an approximate solution of each of them.

Gas/Liquid Coaxial Element

V_g = 305 m/sec (1000 ft/sec)
V_L = 22.9 m/sec (75 ft/sec)
$\dot{W}_L / \dot{W}_g$ = 2.0
L = 10.16 cm (4.0 inch)
▲ d_L = .411 cm (0.162 inch)
△ d_L = .239 cm (0.094 inch)
■ d_L = .140 cm (0.055 inch)

V_{gac} = 0

$\bar{D}$, Microns

$(V_{cg} - V_L)/V_L$
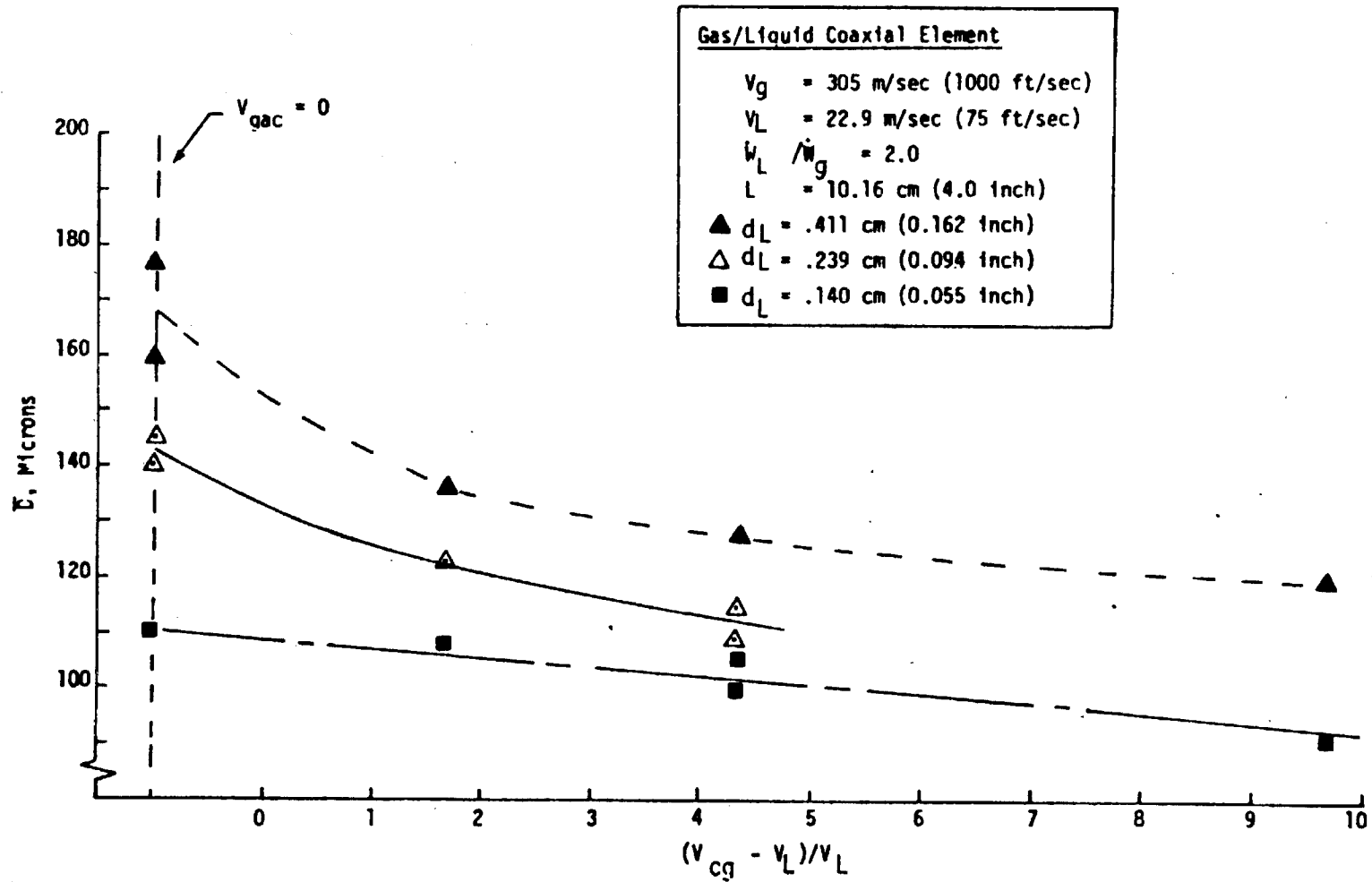
Figure 9.   Influence of Combustion Gas Simulant Velocity on
Mass Median Dropsize - Coaxial Injectors (Ref. 78)
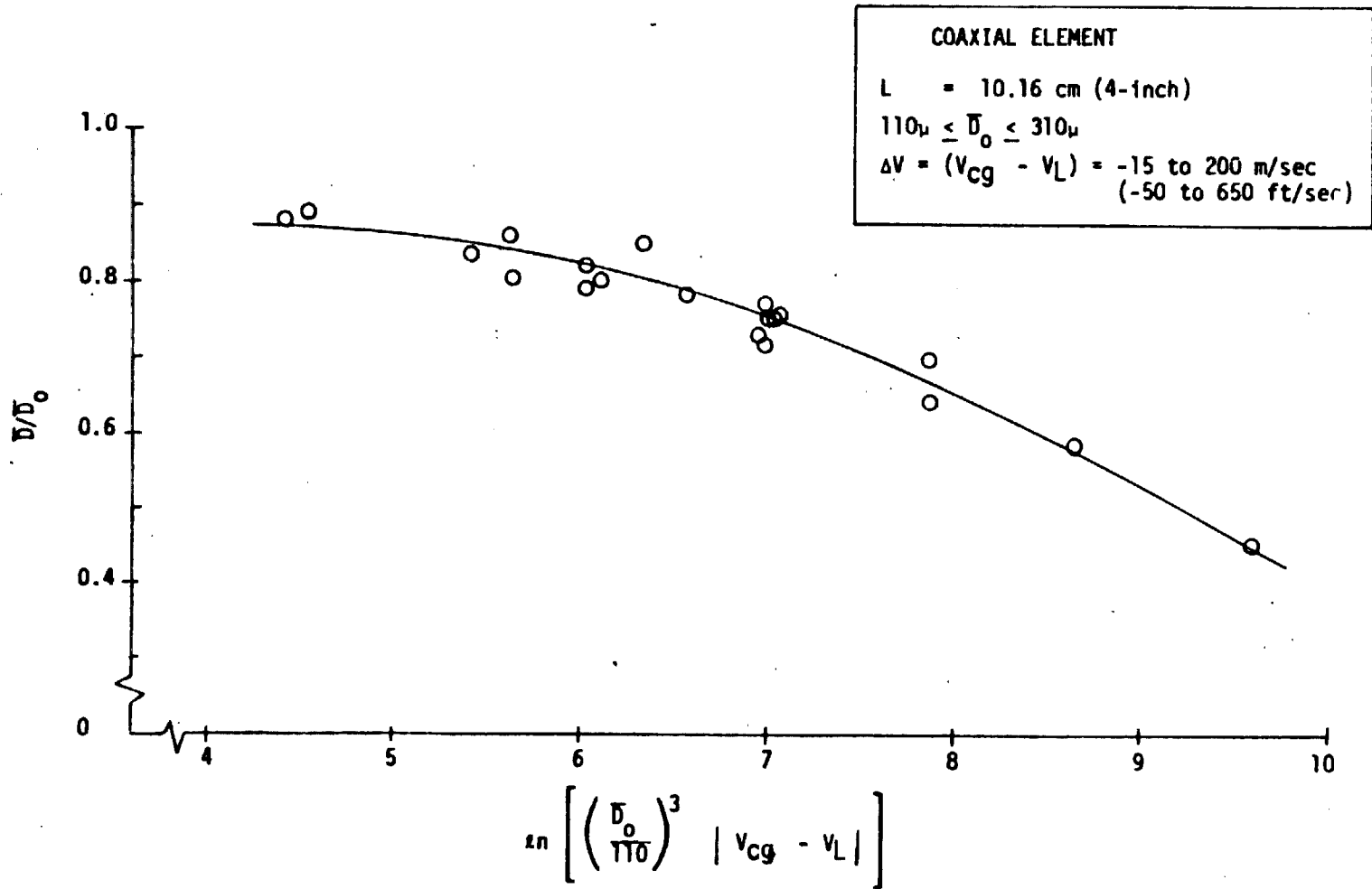
Figure 10. Correlation of Droplet Breakup (Atomization) Data
— Coaxial Injectors (Ref. 78)

All of the droplet size measurement techniques applied to atomization studies have serious limitations and potential and/or known sources of error. Imaging techniques measure the spatial concentrations of the various size droplets. Such spatial concentrations can be utilized only rarely to define the actual droplet size distribution or representative droplet size characterizing all of the droplets produced by a given spray (temporal distribution). Spatial and temporal distributions are often quite different. Thus, the photographic techniques and the droplet freezing (i.e., hot wax) technique do not measure the same thing.

In order to utilize cold-flow atomization data, it is necessary to be able to account for the effects of the different liquids' properties on the droplet sizes. The only data available for this purpose applies to like doublets, is of questionable validity and applicability, and differs from one investigation to another. No methods have been proposed to accomplish this properties effects correlation for any gas/liquid injector or for any liquid/liquid injector except like doublets. No attempts have been amde to assess injected fluids properties effects on droplet size distributions.

Very little information could be found regarding the atomization characteristics of triplet, pentad, and coaxial injectors. Such data, as is available, is presented along with a representative sampling of the data for like doublets.

The following actions are recommended for the purpose of (1) improving our knowledge of atomization processes, (2) developing the droplet size data required by the combustor analysis codes, and (3) utilizing the data in such codes. These actions are divided into near and long-term approaches.

Near term: For the most immediate future, it is recommended that droplet size data for combustor analysis be determined in the following manner. First, the existing data can be utilized (it should be verified first, however) and/or tests can be performed to better define D_o, the droplet size produced in the absence of any simulated combustion gas motion. This can be considered primary atomization. Then the data and correlations of Falk (Ref. 78) and Zajac (Ref. 70 and 71) can be employed to estimate the effect of gas velocity on droplet size. In order to do this it is, of course, necessary to estimate the combustion gas

velocity where the injector is to be employed. This can be accomplished through the use of combustor performance computer codes that generally compute the axial velocity of the gas. Thus, at least the major (hopefully) gas phase velocity component will be estimated. Since the computed axial gas phase velocity will depend on initial droplet sizes, a few iterations of this process may be necessary. That is, the codes can be used to predict V_g, which then can be used to estimate D, which will be input to the codes to predict a new V_g, etc.

Another problem in the use of cold flow droplet size data is that it is necessary to convert from the test fluids to the real propellants. With great reservation, and only because no better information is available, the properties effects correlations of Ingebo (Ref. 13) or Wolfe and Anderson (Ref. 37) are recommended for this purpose, when liquid, like impinging elements, are being considered.

The method described above provides a rudimentary technique for estimating a representative droplet size. Drop size distributions in general, and representative droplet size information for gas/liquid injectors, cannot be estimated via this technique due to the lack of data regarding combustion gas velocity effects and fluid properties' effects on atomization. Even when applied to the case of like doublets, which have been most extensively studied, this technique may be little better than a consistent guessing method.

In order to better utilize this technique and improve its accuracy the following are recommended:

1. Experiments to investigate gas velocity effects on droplet sizes

2. Additional tests to better define D_o for the injectors of greatest interest, especially gas/liquid injectors. Most of the geometric and operational variables have not been tested

3. Experiments to establish fluid properties effects for all types of injectors, like and unlike liquid and gas/liquid injectors, and separate effects for primary and secondary atomization

Such studies and experiments will provide the basis for improvements to atomization assessment methods and will establish the nature, feasibility, and desireability of pursuing the long-term approach.

Long term: As previously discussed, due to the importance of the combustion gas motion on atomization, the problem becomes coupled with those of droplet evaporation, combustion, and three-dimensional fluid mechanics with momentum and mass sources and sinks. Unless some simplifying assumptions are identified earlier, the only available solution would consist of a coupling and solution of all the equations governing these processes. This would probably involve a long-term effort consisting of a number of programs to model (probably with a computer code) various parts of the problem, experimentally verify these models, and combine them in one comprehensive model. Such an approach offers the greatest potential for a comprehensive, accurate, proven solution to the problem of spray definition for rocket engine injectors. If a satisfactory measurement technique exists, experiments with operating, small-scale rocket combustors should be performed to validate the atomization model. In its ultimate form, such a model would include multiple element effects and would predict mixing efficiencies.

NOMENCLATURE

Some atomization nomenclature is defined in text.

A   area (cm^2)

d   injector orifice diameter (cm)

D   droplet diameter (microns)

D   mass median diameter

D_o droplet mass median diameter observed when $V_g = 0$

D_c droplet mass median diameter observed when $V_g = V_L$

f   droplet distribution function, (drops/micron)

$$f = \lim_{\Delta D \to 0} \frac{n}{\Delta D}$$

L   length over which gas is accelerated in atomization studies in accelerating gas flows (cm)

n   number of droplets counted in a given size range

n_t total number of droplets counted

N   cumulative number distribution,

$$N(D) = \sum_0^D n$$

N_1 flowrate of droplets of size group 1

ΔP injector orifice pressure drop (Pascals)

R   normalized cumulative volume distribution, $R = V/V_{tot}$

W   mass rate of flow (kg/s)

V   velocity (m/s)

V_{gm} maximum gas velocity

V   cumulative volume distribution,

$$V(D) = \sum_0^D v$$

v   volume of all drops in a given size range (cm^3)

V_{tot} total volume of all droplets counted

V_1 velocity of drops of size group 1

V_{cg} simulated combustion gas maximum velocity (gas/liquid injectors only)

Y annulus gap for coaxial injectors (cm)

Z axial spatial coordinate

α impingement angle

μ viscosity (cP)

ρ density

ρ_i concentration of drops of size group i (drops/cm^3)

σ surface tension (dynes/cm)

Subscripts

g   gas (either local chamber gas or injected gas)

i   size group of droplets

j   jet or orifice

L   large drops

L   liquid

s   small drops

REFERENCES

1. Longwell, J.P.: "Fuel Oil Atomization," D. Sc. Thesis, MIT, 1943.

2. Hinze, J.: "Critical Speeds and Sizes of Liquid Globules," Appl. Sci. Res., 1948, Vol A1.

3. Lane, W.: "Shattering of Drops in Streams of Air," Industrial & Engineering Chemistry, Chemical Defense Experimental Establishment, England, June 1951, Vol. 43, No. 6.

4. Mugele, R., and H. Evans: "Droplet Size Distributions in Sprays," Industrial & Engineering Chemistry, Chemical Defense Experimental Establishment, England, June 1951, Vol. 43, No. 6.

5. Bowen, I., and G. Davies: "Particle Size Distribution and Estimation of Sauter Mean Diameter," Shell Petroleum Co. (London), October 1951, Report No. I.C.T. 28.

6. Heidmann, M., and J. Humphrey: "Fluctuations in a Spray Formed by Two Impinging Jets," ARS Journal, May-June 1952, Vol. 22, No. 3.

7. Moore, B., and A. Hussman: "Fuel Injection Studies with Impinging Jet Nozzles", Penn State University, October 1955, ONR Contract 656(07), AD 119844.

8. Fraser, R., and P. Eisenklam: "Liquid Atomization and the Drop Size of Sprays," Trans. Instn. Chem. Engrs., 1956, Vol. 34.

9. Tanasawa, Y., S. Sasaki, and N. Nagai: "The Atomization of Liquids by Means of Flat Impingement," Technology Reports of the Tohoku University, 1957, Vol. 22, No. 73.

10. Graves, C., and D. Bahr: "Atomization and Evaporation of Liquid Fuels," Basic Considerations in the Combustion of Hydrocarbon Fuels with Air, NACA Report 1300, Chapter 1, 1957.

11. Putnam, A., et. al.: Injection and Combustion of Liquid Fuels, Battelle Memorial Institute, March 1957, WADC-TR-56-344, AD 118142.

12. Heidmann, M.F., R.J. Priem, and J.C. Humphrey: "A Study of Sprays Formed by Two Impinging Jets," March 1957, NACA TN 3835.

13. Ingebo, R., and H. Foster: "Drop Size Distributions for Crosscurrent Break-up of Liquid Jets in Airstreams," October 1957, NACA TN 4087.

14. Fuhs, A.: "Spray Formation and Breakup and Spray Combustion," February 1958, AFOSR-TN-58-414, AD 158217.

15. Ingebo, R.: "Drop Size Distributions for Impinging Jet Breakup in Air-streams Simulating the Velocity Conditions in Rocket Combustors," March 1958, NACA TN 4222.

16. Weiss, M.A., and C.H. Worsham: "Atomization in High-Velocity Airstream," ARS Journal, April 1959.

17. Rossman, T.: "A High-Speed and High-Resolution Photographic Technique for the Observation of Propellants Injected into a Firing Chamber," May 1959, AFOSR-TN-59-8 (2 parts).

18. Benson, G., M.E. Walil, P. Myers, and O. Uyehara: "Fluorescent Technique for Determining the Cross Sectional Drop Size Distributions of Liquid Sprays," ARS Journal, May 1960, Vol. 30, No. 5.

19. Rossman, T.: "Observation of Propellants Injected into a Firing Rocket Chamber," July 1960, AFOSR-TR-60-98.

20. Dykema, O.: "A Study of Injector Geometry by Spray Analysis," Rocketdyne Report 60-19, August 1960.

21. Heidmann, M.: "Photography & Analysis of Time Variation in Drop Size Dis-tribution of a Liquid Spray," Fifth International Congress on High-Speed Photography, Paper N-7, Washington, D.C., October 1960.

22. Taylor, G.: "The Dynamics of Thin Sheets of Fluid," Proceedings of the Royal Society of London, November 1970, Vol. 259 A.

23. Hasson, D, and J. Mizrahi: "The Drop Size of Fan Spray Nozzles: Measure-ments by the Solidifying Wax Method Compared With Those Obtained by Other Sizing Techniques," Trans. Instn. Chem. Engs., Chemical Engineering Depart-ment, Technion, Haifa, Israel, 1961, Vol. 39.

24. Ungureanu, C.: "Some Results Concerning the Distribution of Drops of Fuel Atomized Through Low-Pressure Injectors," Rumanian periodical Energetica, 1961, Vol. 4, No. 3, (FTD-TT-63-29/1+2+3+4).

25. Heidmann, M.F., and H. Foster: "Effect of Impingement Angle on Drop Size Distributions and the Spray Pattern of Two Impinging Water Jets," July 1961, NASA TN D-872.

26. Ingebo, R.: "Size Distribution and Velocity of Ethanol Drops in a Rocket Combustor Burning Ethanol and Liquid Oxygen," ARS Journal, April 1961 (also see NASA-TN-D-290, June 1960).

27. Popov, M.: "Model Experiments on the Atomization of Liquids," NASA-TT-F-65, July 1961.

28. Fraser, R.: "Liquid Atomization," Journal of Royal Aeronautical Society, Imperial College, London, November 1961, Vol. 65.

29. Weiss, M., and C. Worsham: "Nozzle Sprays in Air Streams," Chemical Engineering Science, Esso Research & Engineering Co., New Jersey, December 1961, Vol. 16, No. 1 and 2.

30. Lewis, J.: "Studies of Atomization and Injection Processes in the Liquid Propellant Rocket Engine," Rocket Propulsion Establishment TM No. 241, Westcott, Great Britain, December 1961.

31. Lambris, S., L. Combs, and R. Levine: "Stable Combustion Processes in Liquid Propellant Rocket Engines," 5th Colloquium of the Combustion and Propulsion Panel, 1962, NATO, AD 283525.

32. Dombrowski, N., and P. Hooper: "The Effect of Ambient Density on Drop Formation in Sprays," Chemical Engineering Science, Imperial College, London, 1962, Vol. 17.

33. Dombrowski, N., and P. Hooper: "The Performance of Characteristics of an Impinging Jet Atomizer in Atmospheres of High-Ambient Density," Fuel, 1962, Vol. 41.

34. Fraser, R., P. Eisenklam, N. Dombrowski, and D. Hasson: "Drop Formation from Rapidly Moving Liquid Sheets," A. I. Ch. E. Journal, Imperial College, London, November 1962, Vol. 8, No. 5.

35. Dombrowski, N., and P. Johns: "The Aerodynamic Instability and Disintegration of Viscous Liquid Sheets," Chemical Engineering Science, Imperial College, London, 1963, Vol. 18.

36. Brown, R., and K. Leonard: "Methods of Describing Droplet Size Distributions from Atomized Solutions," Aerojet Report 0395-04(15) SP, AD 434106, March 1964.

37. Wolfe, H., and W. Anderson: "Kinetics, Mechanism, and Resultant Droplet Sizes of the Aerodynamic Breakup of Liquid Drops," Aerojet General Report 0394-09(18)SP, AD 437340, April 1964.

38. Brown, R.E.: "The Atomization of a Solution of 2, 4 - Dihydrobenzophenone in Bis (2 Ethylhexyl) Hydrogen Phosphate," Aerojet General Report 0395-04(20)SP, AD601462, May 1964.

39. Clark, R.: "Breakup of a Liquid Jet in a Transverse Flow of a Gas," August 1964, NASA TN D-2424.

40. Dombrowski, N., and P. Hooper: "A Study of the Sprays Formed by Impinging Jets in Laminar and Turbulent Flow," Journal of Fluid Mechanics, 1964, Vol. 18, Part 3.

41. Lewis, J.: "Some Basic Studies of Liquid Propellant Injection Processes," Journal of the Royal Aeronautical Society, Rocket Propulsion Establishment, England, November 1964, Vol. 68.

42. Lapple, C., J. Henry, and D. Blake: "Atomization - A Survey and Critique of the Literature," Stanford Research Inst., Report No. 6, April 1967, AD 821314.

43. Luna, R., and W. Klikoff: "On Aerodynamic Breakup of Liquid Drops," Sandia Laboratories Research Report SC-RR-66-2716, June 1967.

44. Hiroyasu, H.: "Mathematical Expressions for Drop Size Distribution in Sprays," NASA-CR-72272, November 1967.

45. Dombrowski, N., and G. Munday: "Spray Drying," Biochemical and Biological Engineering Science, Academic Press, 1968, Chapter 16.

46. Adelberg, M.: "Mean Drop Size Resulting From the Injection of a Liquid Jet into a High-Speed Gas," AIAA Journal, June 1968, Vol. 6, No. 6.

47. Dickerson, R., K. Tate, and N. Barsic: "Correlation of Spray Injector Parameters with Rocket Engine Performance," Rocketdyne Report R-7499, AFRPL-TR-68-147, June 1968.

48. Sloat, T.: "Dropsize Measurements with Large-Thrust Coaxial and Triplet Elements," Rocketdyne Internal Letter IC69-344-24, June 1969.

49. Ingebo, R.: "Maximum Drop Diameters for the Atomization of Liquid Jets Injected Concurrently Into Accelerating or Decelerating Gas Streams," NASA-TN-D-4640, July 1968.

50. Knight and Nurick: "Interim Report, Correlation of Spray Dropsize Distribution and Injector Variables," Rocketdyne Report R-7995, September 1969.

51. Sloat, T., and D. Campbell: "Atomization Characteristics of Gas/Liquid Injectors," 6th Liquid Propellant Combustion Instability Conference, Chicago, September 1969.

52. Dickerson, R.: "Like and Unlike Impinging Injection Element Droplet Sizes," J. Spacecraft, November 1969, Vol. 6, No. 11.

53. Walkden, A., and R. Kell: "Characteristics of High-Flux Sprays From Colliding Water Jets," Trans. Instn. Chem. Engrs., General Electric Co., Wimbly, Middlesex, England, 1969, Vol. 49.

54. Kuykendal, W.: "The Effect of Injector Design Variables on Average Drop Size for Impinging Jets," AFRPL-TR-70-53, May 1970.

55. Mehegan, P., D. Campbell, and C. Scheuerman: "Investigation of Gas Augmented Injectors," Rocketdyne Report R-8361, NASA-CR-72703, September 1970.

56. Nurick, W., and R. McHale: "Noncircular Orifice Holes and Advanced Fabrication Techniques for Liquid Rocket Injectors," Rocketdyne Report R-8224, NASA-CR-108570, September 1970.

57. Huang, J.: "The Breakup of Axisymmetric Liquid Sheets," J. Fluid Mech, 1970, Vol. 43, Part 2.

58. Zajac, L.: "Correlation of Spray Dropsize Distribution and Injector Variables," Rocketdyne Report R-8455, Contract NAS7-726, February 1971.

59. Kim, K., and W. Marshall: "Drop Size Distributions From Pneumatic Atomizers," A. I. Ch. E. Journal, University of Wisconsin, May 1971, Vol. 17, No. 3.

60. Nurick, W.: "Analysis of Sprays From Rocket Engine Injectors," _Journal of Spacecraft and Rockets_, Rocketdyne, July 1971, Vol. 8, No. 7.

61. Zajac, L., and W. Nurick: "Correlation of Spray Dropsize and Injector Variables," 8th JANNAF Instability Conference, October 1971.

62. Simpkins, P., and E. Bales: "Water Drop Response to Sudden Accelerations," _Journal of Fluid Mech._, Bell Labs & Stevens Inst. Tech., 1972, Vol. 55, Part 4.

63. Combs, L.: "Catalog of Injector Spray Correlations," Rocketdyne, NASA Contract NAS7-746, 1972.

64. Burick, R.: "Atomization and Mixing Characteristics of Gas/Liquid Coaxial Injector Elements," _Journal of Spacecraft_, May 1972, Vol. 9, No. 5.

65. Nurick, W.: "Study of Spray Disintegration in Accelerating Flow Fluids," Rocketdyne Report R-9017, NASA-CR-114479, June 1972.

66. George, D., and F. Spaid: "Holography As Applied to Jet Breakup & An Analytical Method for Reducing Holographic Droplet Data," AFRPL-TR-72-72, September 1972.

67. Burick, R.: "Space Storable Propellant Performance Program Coaxial Injector Characterization," Rocketdyne Report R-8973-2, NASA-CR-120936, October 1972.

68. Falk, A.: "Space Storable Propellant Performance Gas/Liquid Like Doublet Injector Characterization," Rocketdyne Report R-8973-1, NASA-CR-120935, October 1972.

69. Nurick, W.: "Physical Property Effects on Spray Atomization," Rocketdyne IR&D Report ITR-73-014-C, September 1973.

70. Zajac, L.: "Droplet Breakup in Accelerating Gas Flow, (Primary Atomization)," Part 1, Rocketdyne Report R-9337-1, NASA-CR-134478, October 1973.

71. Zajac, L.: "Droplet Breakup in Accelerating Gas Flows (Secondary Atomization)," Part 2, Rocketdyne Report R-9337-2, NASA-CR-134479, October 1973.

72. George, D.: "Rocket Injector Hot-Firing and Cold-Flow Spray Fields," AIAA/SAE 9th Propulsion Conference, Las Vegas, November 1973.

73. George, D.: "Rocket Injector Hot-Firing and Cold-Flow Spray Fields," 10th JANNAF Combustion Meet, December 1973, CPIA No. 243, Vol. 3.

74. McHale, R., and W. Nurick: "Noncircular Orifice Holes and Advanced Fabrication Techniques for Liquid Rocket Injectors (Phases I, II, III, & IV)," Rocketdyne NASA CR-R-9271, May 1974.

75. Buschulte, W.: "Liquid Propellant Atomization by Injector Elements and Its Effects on Combustion Chamber Efficiency," Israel Journal of Technology, 1974, Vol. 12.

76. George, D.: "Droplet Size Distribution Functions For Rocket Combustor Spray Fields," 11th JANNAF Combustion Meet, December 1974, CPIA No. 261.

77. Anon: "Analysis of Rocket Engine Injection/Combustion Processes," Rocketdyne Report R-9668P-1, March 1975.

78. Falk, A.: "Coaxial Spray Atomization in Accelerating Gas Stream, Final Report," Rocketdyne Report R-9753, NASA-CR-134825, June 1975.

79. Rizkalla, A., and A. Lefebvre: "The Influence of Air and Liquid Properties on Airblast Atomization," Journal of Fluids Engineering, Cranfield Inst. Tech., Trans ASME, September 1975.

80. Rao, K., and A. Lefebvre: "Fuel Atomization in a Flowing Airstream," AIAA Journal, October 1975, Vol. 13, No. 10.

81. Farmer, W.: "BRL Particle Sizing Interferometer," University of Tennessee Space Institute, Tullahoma, Tenn., circa 1980.

82. Lefebvre, A.: "Airblast Atomization," Prog. Energy Combustion Science, Purdue University, 1980.

83. Elkotb, M.: "Fuel Atomization for Spray Modeling," Progress in Energy & Combustion Science, Cairo University, 1982, Vol. 8, No. 1.

84. Ferrenberg, A.: "Liquid Rocket Injector Atomization Research," Proceedings of ASTM Symposium on Liquid Particle Size Measurement Techniques, Kansas City, June 1983.

Cold flow mixing tests frequently have proven to be a significant aid in predicting potential performance, or diagnosing problems with rocket engine injector components. Cold flow tests are not sufficiently reliable so as to serve as a replacement for hot-fire testing, but should be considered as complementary to hot-fire tests, aiding in minimizing the number of hot-fire tests required to obtain an optimum configuration. In almost every case, an injector or element that performs poorly in cold flow testing will not perform well in hot-fire testing. However, the counter side of this statement cannot be applied universally. An element can be excellent in cold flow mixing, but the combustion reaction may override the hydromechnical mixing provided by the injection streams. This effect is most notable with storable hypergolic propellants, where a phenomena of reactive demixing "blowapart" is frequently a significant factor in combustion performance. There have been other reports of combustion systems suffering from reactive demixing, but none have been as well documented as the hypergolic reaction systems.

Aerodynamic forces in the combustion zone also are factors that cannot be simulated in cold flow mixing tests. Gas forces in recirculation can be strong factors influencing mixing and atomization. There are, however, useful correlations between cold flow mixing and combustion results, and the relative cost factor between cold flow and hot-fire tests generally is a rational reason for utilizing cold flow tests as an injector design and development tool.

The key objective, to establish correlations between cold flow mixing data and hot-fire results, requires a large empirical data base as well as a consistent assessment of the data and an applied scientific evaluation of the resultant correlating parameters. Therefore, an assessment criteria was established, which allowed compilation of existing cold flow experimental data acquired within the industry on element types suitable for LOX/hydrocarbon injector advancement.

The triplet, pentad, and coaxial element injection devices were selected for study based on available hotfire and cold flow experience with LOX/hydrocarbon

propellants. The cold flow correlating parameters used for these devices were identified and an extensive literature survey conducted to obtain related cold flow data. Data from the literature search was compiled into a displayable format. The information then was plotted by the appropriate correlating parameter(s) against mixing efficiency, a standard measure of cold flow performance.

In addition to the literature survey, five impinging triplet elements, one pentad element, and three coaxial elements were fabricated for cold flow testing. The sizing of these elements encompassed designs for both preburner (gas generator) and main injector mixture ratios at high chamber pressure. The propellant combinations were LOX/methane (gas/liquid), LOX/RP-1 (liquid/liquid), and LOX/propane (liquid/liquid and gas/liquid). The low-pressure cold flow mixing test program was conducted with these elements at several flow conditions. Measures of mixing efficiency were established and plotted as a function of mixing parameters. Maps depicting mixture ratio-normalized mass distribution were constructed from the cold flow tests to provide a good visual indication of relative mass and mixture ratio concentrations for the different element types.

INJECTOR MIXING CORRELATING PARAMETERS

Mixing correlation parameters are mathematical expressions based upon injector element geometry and flow conditions. Their utility as injector design criteria depends upon (1) their ability to be related to mixing efficiency and (2) the existence of optimum values of these correlation parameters at which mixing will be maximized.

Numerous correlating parameters have been proposed for different injector configurations, propellant conditions, and hot fire related operating conditions. The scientific basis for the parameters generally has been derived from momentum and stream diameter relationships of the injection element. A survey of available literature showed that of these relationships, most correlating parameters were derived for liquid/liquid impinging-type injectors. Many of the experimenters have established formulas to plot data from numerous test conditions on a single curve, or at least, within a family of curves.

The correlating parameters used in the literature survey data reduction and in the subsequent low-pressure mixing tests are presented in Table 5. A description of these important parameters is discussed below. Illustrations of the three element types studied under this program (coaxial concentric tube, triplet, and pentad) are presented in Fig. 11 through 12, with the appropriate terminology and physical parameters identified.

Rupe Factor/Rupe Number

The best example of an injector correlating parameter for mixing criteria is the Rupe Factor, or Rupe Number, developed for use on unlike impinging doublets elements. This basic expression (Eq. 2) primarily was developed in the '50s by its namesake, Jack Rupe of Jet Propulsion Lab (JPL). He ran a great number of cold flow mixing tests and conducted related hot fire experiments. Applying stream momentum and diameter ratios, he developed an expression, since referred to as the "Rupe Factor," which indicated the best mixing when it equalled unity. This parameter also can be expressed as the diameter ratio over the momentum ratio. Since this expression is a ratio, the mathematical range of this factor from zero to one is the same as from one to infinity, which is difficult to interpret. For this reason, the expression has been revised to the "Rupe Number" (Eq. 3), which has a total range from zero to one and an optimum value of 0.5.

This expression has been utilized widely for sizing of unlike doublets and has demonstrated good correlation over a wide range of conditions. This does not mean that a Rupe number of 0.58 reflects a certain quantitative level of mixing efficiency, but that in sizing an element for a given design, mixing, for most cases, optimizes very near the 0.5 value.

Momentum Ratio

Other element types have been analyzed in a similar manner as the Rupe Number, and modified momentum/diameter relationship expressions have been derived for triplet and pentad impinging element patterns. These parameters are based on more limited cold flow data and virtually no hot fire data, and should be used more cautiously in universal application than the doublet expressions.

TABLE 5. INJECTOR ELEMENT CORRELATING PARAMETERS

PARAMETER	COMMON APPLICATION	EXPRESSION	OPTIMUM VALUE	LEGEND
• MOMENTUM RATIO	IMPINGING ELEMENTS	$\dfrac{\rho_{FU}\,A_{FU}}{\rho_{ox}\,A_{ox}}\left(\dfrac{\dot{m}_{ox}}{\dot{m}_{fu}}\right)^2$ (1)	NONE	**VARIABLES** $\dot{m}$ = MASS FLOW RATE, Kg/SEC V = VELOCITY, M/SEC A = ELEMENT DISCH FLOW AREA, M^2 D = ELEMENT HOLE DIA, M ρ = PROPELLANT DENSITY, Kg/M^3 MR = MASS MIXTURE RATIO, OXID/FUEL θ = VERTICAL ANGLE BETWEEN INNER AND OUTER STREAMS, DEGREES **SUBSCRIPTS** ox = OXIDIZER FU = FUEL g = GAS L = LIQUID in = INSIDE OR CENTRAL ORIFICE out = OUTER ORIFICES
• RUPE FACTOR	UNLIKE IMPINGING DOUBLET ELEMENTS, LIQUID/LIQUID	$\dfrac{\dot{m}_{FU}\,V_{FU}\,D_{ox}}{\dot{m}_{ox}\,V_{ox}\,D_{FU}}$ (2)	1	
• RUPE NUMBER		$\dfrac{1}{1 + \text{RUPE FACTOR}}$ (3)	0.5	
• ELVERUM – MOREY CRITERIA	IMPINGING TRIPLET ELEMENTS, LIQUID/LIQUID	$\left(\dfrac{\dot{m}_{out}}{\dot{m}_{in}}\right)^2\left(\dfrac{\rho_{in}}{\rho_{out}}\right)\left(\dfrac{A_{in}}{A_{out}}\right)^{1.75}$ (4)	0.66	
	IMPINGING PENTAD ELEMENTS, LIQUID/LIQUID	$\left(\dfrac{\dot{m}_{out}}{\dot{m}_{in}}\right)^2\left(\dfrac{\rho_{in}}{\rho_{out}}\right)\left(\dfrac{A_{in}}{A_{out}}\right)^{1.25}$ (5)	2.75	
• PENETRATION FACTOR	IMPINGING ELEMENTS, GAS/LIQUID, CENTRAL GAS STREAM	$1.25\sin(\theta)\left(\dfrac{\dot{m}_{out}}{\dot{m}_{in}}\right)\left(\dfrac{\rho_{in}}{\rho_{out}}\right)^5\left(\dfrac{D_{in}}{D_{out}}\right)$ (6)	0.5	
• VELOCITY HEAD RATIO	GAS/LIQUID, LIQUID/LIQUID IMPINGING AND COAXIAL ELEMENTS	$\dfrac{\rho_{FU}}{\rho_{ox}}\left(\dfrac{A_{FU}\,\dot{m}_{ox}}{A_{ox}\,\dot{m}_{FU}}\right)^2$ (7)	1	
• COAX PARAMETER	COAXIAL CONCENTRIC TUBE ELEMENTS, GAS/LIQUID	$\dfrac{\left(\rho_g\,V_g\right)^2}{MR\,V_L}$ (8)	?	

LIQUID

GAS

POST RECESS DEPTH (CUP DEPTH)

INNER TUBE I.D. (LOX POST)

INNER TUBE O.D.

OUTER TUBE I.D. (FUEL SLEEVE)

Figure 11. Coaxial Concentric Element

ORIFICE
LENGTH

2θ

θ = IMPINGEMENT ANGLE

FREE STREAM
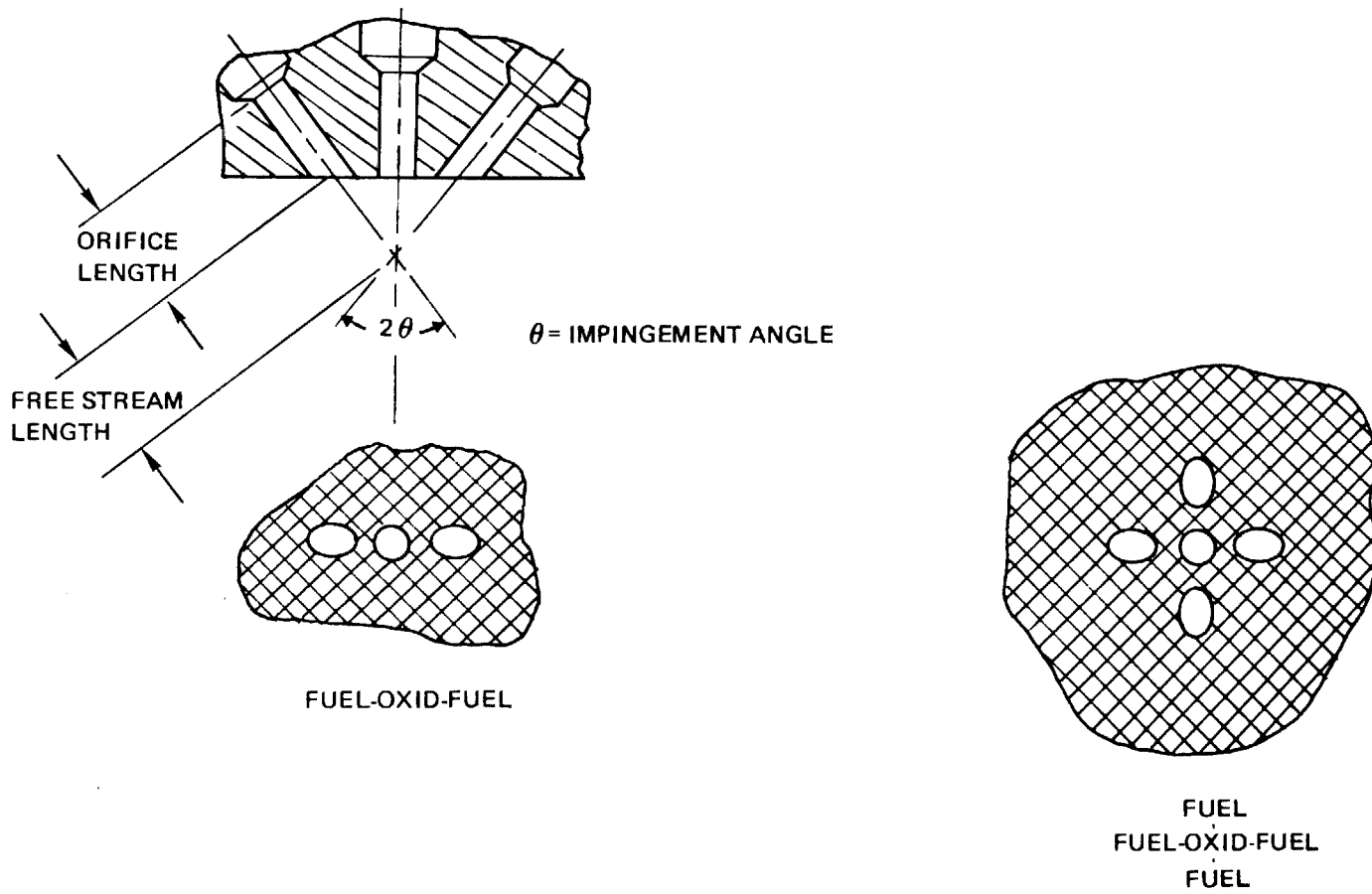LENGTH

FUEL-OXID-FUEL

FUEL
FUEL-OXID-FUEL
FUEL

Figure 12.   Impinging Triplet and Pentad Elements

As previously mentioned, the primary root for almost all impinging element mixing parameters is the momentum ratio. As a general rule, the momentum ratio always is expressed as the oxidizer total momentum over the fuel total momentum regardless of the number or placement of oxidizer streams relative to fuel streams within the element. Relating this ratio to the values available to the designer, we have the form of momentum ratio as shown in Table 5, (Eq. 1). There is no design optimum for this parameter and, again, this is a ratio with theoretical values from zero to infinity, where values over one indicate that the oxidizer has higher momentum than the fuel.

Elverum-Morey Factor

The equivalent of the Rupe Factor for triplet and pentad elements was developed by Rupe's colleages, Elverum and Morey, and is based also on momentum/diameter (area) relationships as shown in Table 5, (Eq. 4). For the triplet element, with two outer angled streams and a central axial stream, the relationships are set as inner and outer streams rather than oxidizer and fuel streams, since both fuel-oxidizer-fuel and oxidizer-fuel-oxidizer triplets are in general use.

For liquid/liquid triplets, within the range of study by Elverum and Morey, the optimum value for this expression was 0.66. Triplet injectors have been used most commonly for hypergolic storable propellants, and use of the Elverum-Morey Factor has been successful under these conditions. For the nominal mixture ratio of liquid oxygen and liquid hydrocarbons*, very little data has been available. A modified Elverum-Morey expression, Table 5 (Eq. 5), was designed for pentads and has a purported optimum value of 2.75.

---

*The typical mixture ratio for storable propellant combinations, such as NTO/MMH or UDMH/IRFNA, is between 1.5 and 2.5 ox/fu for main injector operation. The mixture ratio for liquid/liquid LOX/hydrocarbon propellants, i.e., RP-1/LOX, is optimum near 2.8 ox/fu for main injector maximum Isp, and near 0.4 ox/fu for fuel-rich preburner (turbine drive combustor) applications.

Penetration Factor

This parameter has been developed for gas/liquid triplet injectors where two liquid streams impinge on a central gas stream. It relates the predicted penetration of the liquid streams to the central gas flow. Optimum mixing is predicted if the liquids barely penetrate to the center, with liquid droplets being sheared off and entrained by the gas flow on the way. The penetration factor is presented in Table 5, (Eq. 6).

A value of 0.5 is the theoretical optimum. Lower numbers infer that the liquid is being deflected away by the gas or is not fully penetrating the gas stream. Over penetration, on the other hand, produces a liquid fan within the gas flow, which also reduces the uniformity of gas/liquid mixing. This factor was created from a combination of analysis and cold flow experiments, and hot fire data appears to support the basic premise. Pentads and other impinging patterns with liquid streams impinging on a central gas core also would be expected to correlate with some form of the penetration parameter. However, data is limited for these applications.

The use of this factor for the reverse case of gas streams impinging on a central liquid, or any other extremes in the density relationships, is questionable. Triplets with the gaseous reactant in the outer streams have been used in numerous cases, but there is little data on any correlating parameters. Some limited information suggests that high levels of gas to liquid momentum ratio are beneficial to the mixing process in impinging element injectors.

Velocity Head Ratio

Another parameter that does not have a stated optimum value is the velocity head ratio shown in Table 5, (Eq. 7). This roughly relates to the very practical

consideration of "Delta P" ratio, or pressure drop ratio. The usual starting point in an injector design is based on the desired level of pressure drop at the design flowrates. Isolation between feed system and chamber pressure disturbances generally dictates a desire for a high level of injection orifice pressure drop, and system pressure limitations would like a low pressure drop. A compromise solution usually results in an injector delta P of about 15 to 20% of chamber pressure, and an initial starting point would be for both oxidizer and fuel systems to be roughly the same value. Therefore, an injector design that has velocity head ratios significantly distant from 1 would require some compensation in design approach (i.e., supplementary orifices, etc.).

As mentioned previously, there is no theoretical optimum for the velocity head ratio, but the values close to 1 are desirable for system integration. Many times, sizing the injection orifices to optimize one of the other parameters will result in an unacceptable level of velocity head ratio. For this reason, the velocity head ratio should be computed at the same time as the other parameters, and evaluated and adjusted concurrently.

Coaxial Parameter

The gas/liquid coaxial concentric tube injector element has had wide, successful usage for hydrogen/oxygen combustion. Cold flow and hot fire experience with this element still has not provided a good correlating parameter. In this element, typical design practice has been to provide a low-velocity central liquid stream (liquid oxygen) sheathed by a high-velocity gas flow (gaseous hydrogen or fuel-rich preburner gases) as shown in Fig. 11. Mixing and atomization are provided primarily by the shear forces between gas and liquid and by the momentum of the expanding gases.

Recessing the liquid stream upstream of the exit plane of the outer (gas) stream is popularly held to increase both atomization and mixing. Cold flow testing has not established a strong correlation with this practice, although hot fire results generally reflect a performance increase that usually is accompanied by an increase in face heating.

Increasing the gas velocity (relative to the liquid velocity) generally improves mixing. This design approach should not be employed blindly, since some references suggest that mixing can be impacted adversely by velocity ratios that are too high. This would tend to suggest that some correlating parameter for optimization may be possible. Very high gas velocity apparently can reverse the gas liquid relationship, "blowing out" the center of the spray and dispersing excess liquid to the outside of the spray cone.

A review of existing data, as a part of this effort, indicates trends that may be useful for providing a general optimizing expression for the coax element. Falk and Nurick of Rocketdyne (NASA CR-72703 R-8361) have suggested the coaxial parameter presented in Table 5, (Eq. 8). However, no optimum value of this parameter has been established. One of the objectives of the remainder of this program is the establishment of a coaxial element mixing parameter.

MIXING TEST METHODS

Liquid/Liquid Mixing Test Methods

The liquid/liquid testing for mixing efficiency is relatively easy and low cost, if facilities are available. The procedure for liquid/liquid mixing utilizes a grid-like sample device, which ducts the individual position captured liquid into an appropriate sample container (Fig. 13). This technique utilizes two immiscible liquids as propellant simulants, typically water and a high-density, low-vapor pressure solvent such as 1,1,1-trichloroethane. The fluids collected in the sample tubes separate by the variation of density and their quantities in each tube are measured (Fig. 14). Typically, the sample grid represents hundreds of data points, and a computer data reduction process is required to provide meaningful quantitative data.

Different fluid combinations have been employed for liquid/liquid mixing in an effort to better match injected reactant conditions, while addressing concerns for toxicity, flammability, and general questions of safety, convenience, and cost. Other solvents used for these purposes have included many of the lower

a.   Square Tube Assembly

b.   Test Sample
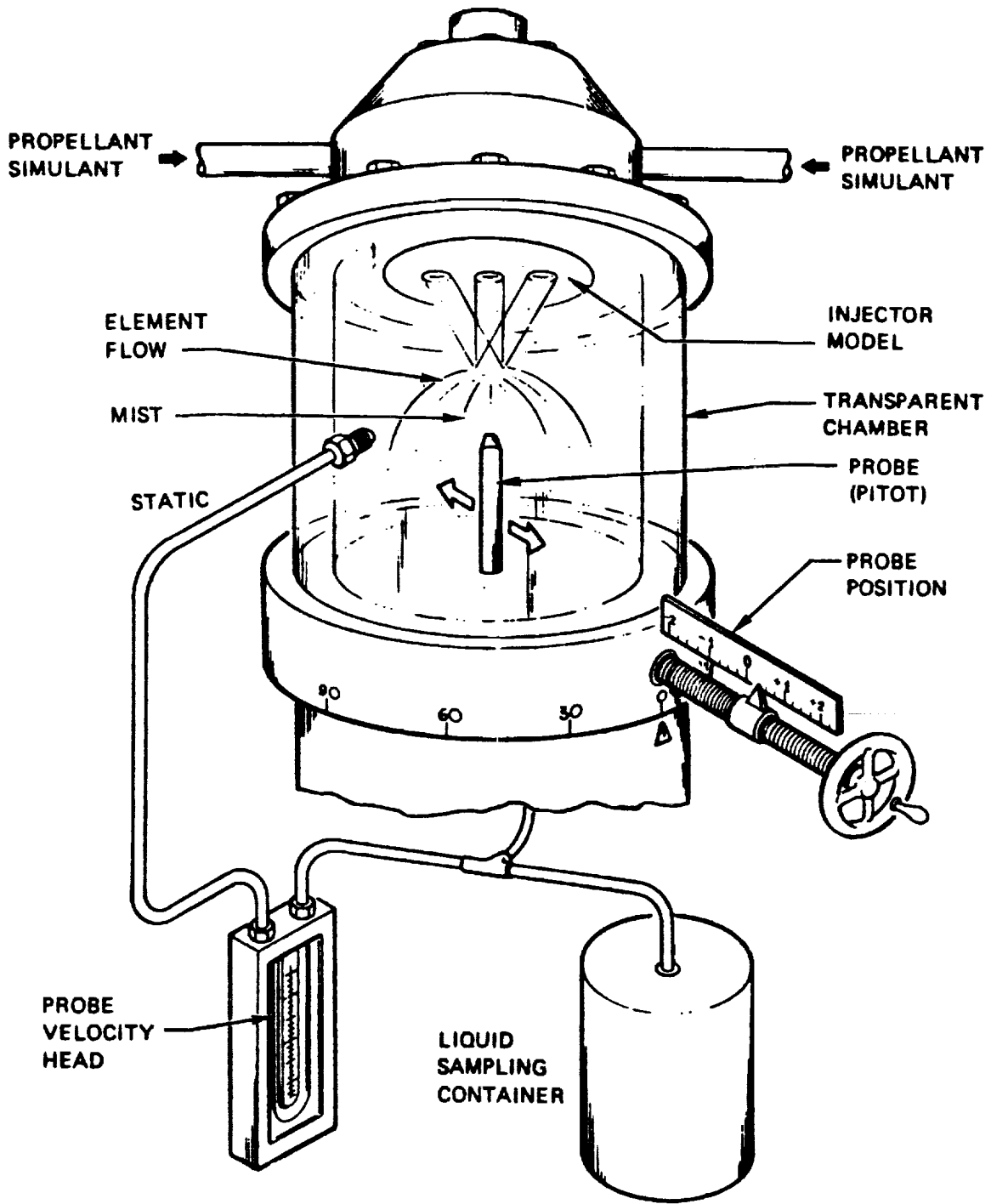
Figure 13.   Liquid/Liquid Mixing

Figure 14. Cold Flow Gas/Liquid Mixing Measurement System

vapor pressure "freon" compounds, perchlorethylene (a dry-cleaning solvent), as well as fuel-type hydrocarbon liquids. At least one past program at Rocketdyne utilized a water/brine system, with the mixture ratio of the sample determined by an electric salinity meter. Data acquisition using this method was significantly slower than the immiscible fluid method, and accuracy was poor in the low mass flow outer zones.

Gas-Liquid Mixing Test Methods

Gas-Liquid mixing tests are significantly more time consuming than the liquid-liquid mixing, which probably is the reason that gas-liquid data is more limited. A gas-liquid mixing measurement system has been utilized extensively at Rocketdyne for hydrogen/liquid oxygen concentric elements (with the gas annulus surrounding the liquid core). The schematic of the process is shown in Fig. 15. The sample element is installed at the "head end" of a transparent, pressurized chamber, with a traversable probe mounted at the desired sampling plane. Water typically is used for the liquid oxygen simulant and a nonreactive gas simulates the hydrogen fuel (or hydrogen-rich hot gas in a staged combustion cycle). Typically, the gas used is nitrogen, sometimes diluted with helium to provide a desired density. Gas density is controlled by tank back pressure, and the mixture of gases supplied. A "base bleed" gas usually is supplied through the face around the injection element to minimize recirculation from the injected flow, and to simulate partially the axial gas flow present in a combustion chamber. A tracer gas (frequently oxygen) is included in this base bleed flow to allow this local gas flow to be measured and extracted mathematically from the measured element gas flow in each sample.

The sample is extracted from the gas-liquid element flowfield by the use of a sharp edge probe that can be positioned in the desired sample area. The liquid spray in the sample zone is collected physically by the opening in this probe, and accumulated in a sample container over a measured time period. The gas flow flux in the sample zone is determined from the relationship between total and static pressure (corrected for the liquid in the two-phase flow). The gas measurement may require a second correction for the entrained "base bleed" flow, and the data for this correction is obtained from an "on-line" gas analysis technique.

As might be deducted from the preceding description, each sample requires a sufficient time to stabilize the required readings and collect the liquid. When compared to the hundreds of sample points simultaneously obtained in the liquid-liquid testing, the increase in test time for gas-liquid testing is readily apparent. Testing with concentric elements permits a reasonable assumption of circular symmetry, allowing a reduced number of required sample measurements. However, the more complex "fan" shapes of gas-liquid triplets and pentads require careful study of the sample locations, and require more sample points than for a co-ax test. Previous work with triplets and pentads in a gas/fluidized solid system, Ref. 30, and triplets in a gas-gas system have indicated the shape of expected mass distribution, and show that numerous sample points are required to characterize these element types.

COLD FLOW MIXING DATA REDUCTION

The data reduction procedures for the liquid-liquid and the gas-liquid cold flow mixing tests are very similar. As in the testing itself, the data reduction for the liquid-liquid testing is a bit more straight forward. The total sample grid usually encompasses all the injected flow, and the grid openings usually have no open spaces between them. Therefore, the collected totals should equal the injected totals, thus providing a good cross-check on the data. This is the first factor computed in gas/liquid mixing tests, and is referred to as the "collection efficiency."

Collection Efficiency

To calculate the collection efficiency of the test system, fluid input values are compared with fluid collected values. The input values of mass flowrate is frequently calculated theoretically by the Injector Pressure Drop Equation (9), based on previous cold flow resistance calibration of the test model:

$$W_{input} = \frac{\pi}{4} ND^2 C_d (2\rho\Delta P)^{1/2}$$

(9)

where

W = mass flowrate

N = total number of oxidizer or fuel holes

D = diameter of orifice

C_d = dimensionless discharge coefficient as determined from the calibration flow test

ρ = density of simulant

ΔP = injector pressure drop

If direct flow measurement capability exists in the cold flow mixing facility, the values from these measurements are used.

The collected values of mass flowrates are calculated from the test data; summing all of the individual sample measurements:

$$\dot{W} \text{ collected} = \frac{\rho Q}{t} \tag{10}$$

where:

ρ = density

Q = local corrected sample volume

t = collection time in seconds

Collection efficiency of the system is calculated then by:

$$\eta_{col} = \frac{W \text{ collected}}{W \text{ input}} \tag{11}$$

where a value of "1" represents perfect collection efficiency. Large deviations in the collection efficiency would indicate problems in the system or the data for the testing. Unfortunately, collection efficiency rarely is included in reports of mixing tests and in some cases may not even be calculated. Liquid/ liquid mixing testing is relatively simple and collection efficiency generally

$C-4$

is not needed or obtained. However, the much greater complexity of gas/liquid testing requires the "check" on test methods and procedures that collection efficiency provides.

Mixing Efficiency

The most meaningful expression for assessing mixing efficiency is the E_m (E-sub m) value proposed several years ago by Jack Rupe at JPL. This is an expression for the mass mixture ratio distribution of the samples based purely on the relationship of the samples to the overall mixture ratio with no regard to such factors as theoretical stoichiometry, etc.

This value is computed as a mass weighted summation of the mixing errors in all the samples. In practice, it is computed as a summation of decrements based on how far the mixture ratio of each sample deviates from the overall mixture ratio, and weighted by the mass fraction of each of these samples. The range of this expression is from zero to 100%, with 100% indicating all samples are the same mixture ratio, and zero indicating the samples are all one component or the other.

The nominal form for computation of E_m is expressed by:

$$E_m = \left[100 \ \ 1 - \sum MF_{sb} \ \frac{R-R_{sb}}{R} + \sum MF_{sa} \ \frac{R-R_{sa}}{R-1} \right] \qquad (12)$$

where

E_m = mixing efficiency from 0 to 100%

R = overall mixture ratio as expressed by weight flow oxidizer/weight flow total

R_{sb} = mixture ratio of sample below overall mixture ratio

MF_{sb} = mass fraction of sample below overall mixture ratio

MF_{sa} = mass fraction of sample above overall mixture ratio

R_{sa} = mixture ratio of sample above overall mixture ratio

Each local sample that is not at the overall mixture ratio thus provides a mixing efficiency decrement proportional to how far it is from the nominal mixture ratio, and what mass fraction of the total flow it represents. For example, if a sample representing 50% of the total mass has a mixture ratio fraction of 0.35 when the overall is 0.70, the total mixing loss from this sample is

$$100 \left(0.5 \frac{0.70 - 0.35}{0.70}\right) = 25\% \text{ loss in mixing efficiency}$$

This factor is much more sensitive to mixing deficiencies than combustion efficiency-related factors, which are "rounded off" by theoretical curves and the relationship between test mixture ratio and stoichiometric mixture ratio.

Mixing Limited C-Star

A frequently used parameter to describe mixing test results is mixing limited C-star or $_c^*$ mix (ETA C-star mix). This can be applied only to tests for a specific reactant combination, and actually only for an assumed chamber pressure. It is a prediction of the expected hot fire C-star efficiency (assuming total vaporization). The product of vaporization efficiency and mixing limited C-star efficiency is the predicted combustion efficiency.

At Rocketdyne, the mixing limited C-star is computed by a single stream tube performance model technique. The computer program is provided with a theoretical C-star function and the theoretical C-star value (M/sec) is calculated for each sample mixture ratio. Each sample collected mass is multiplied by the sample C-star, and these products are summed for the entire sample. This answer is divided by the total mass collected to provide the mixing limited C-star.

$$\text{Mixing Limited C-star} = \frac{C_1^* \times \text{Mass}_1 + C_2^* \times \text{Mass}_2 \dots + C_N^* \times \text{Mass}_N}{\text{Total Sample Mass}} \quad (13)$$

The mixing limited C-star efficiency then is determined by comparing this value to the theoretical C-star for the overall mixture ratio:

$$\eta_{c*} = \frac{\text{mixing limited } C*}{\text{theoretical } C*} \qquad (14)$$

A C-star efficiency of one indicates that at uniform mixture ratio, $E_m = 1$, mixing limited C-star is equal to theoretical C-star. This parameter is used to make a rough estimate of performance potential for given operating conditions of certain mixture ratio and mixing efficiency.

REVIEW OF EXISTING DATA

An extensive literature search was conducted on past experience in determining and evaluating mixing efficiency for triplet, pentad, and coaxial elements. Numerous document references were accessed and reviewed, and a bibliography of the pertinent reports reviewed is presented herein. The intent of this search primarily was to find reports containing quantitative cold flow mixing test data for these injectors.

The literature search yielded fewer reports than had been anticipated, although several valuable references were encountered. The abundance of data involved liquid/liquid impinging doublets followed by liquid/liquid triplets and pentads. Gas/liquid reports were almost entirely limited to coaxial elements and presented little data regarding gas/liquid triplets or pentads.

The data from each report was re-reduced in order to provide a uniform basis for comparison. In each instance, the objective was to obtain as close to raw data as possible from the information in the report. Using a computer program designed for this task, a table of injection parameters relating to measured performance was constructed. Information from each report thus was computed in the same consistent fashion for best comparison of results.

As expected, many important test conditions typically were omitted from the reports, such as the distance from the injector face to the sample plane, the

relative size of the sample grid, and the number of sample points in the test plane. For gas/liquid coaxial element data there had been controversy on the use of averaged data for sample grid points, and the reports typically did not elaborate on data reduction methods. With these limitations and constraints in mind, the data was analyzed and reviewed for some generalized conclusions.

The data was extracted from all the reports that had usable mixing data and has been prepared in summary chart form (Table 6). The data has been organized by element types and propellant condition (i.e., gas-liquid triplet, liquid-liquid pentad, etc.). All of the normally used injector sizing and operating parameters are displayed (if they were available or calculable from the report information). Where a report provided information on more than one element type or propellant condition combination, it has been listed in appropriate multiple locations in the charts, with cross-reference to the other elements. These charts are intended as a summary reference source, rather than a quick graphic comparison, and a review of data comparing similar configurations can be accomplished with minimum confusion. Most of the data also is presented elsewhere in this report in graphic form, with mixing efficiency plotted against the common injection parameters.

Triplet - Liquid/Liquid

Two documents for liquid/liquid triplets, were found each containing significant single element data on several configurations (Ref. 5 and 7). The data was relatively consistent and indicated a reasonable correlation with the Elverum Morey Factor (Fig. 15 and 16). These plots depict the Elverum Morey Factor on a logarithmic scale since this factor is computed as a ratio. In both references, it can be stated generally that maximum mixing efficiency occurs near the 0.66 value for the factor. Elements with near the same orifice diameters appear to provide the highest maximum mixing efficiency, and multiple elements reflect interelement mixing with higher average values and reduced sensitivity to the parameters. A "reverse" triplet (two oxidizer streams on a central fuel) (Ref. 5) appears to have a significantly different characteristic as a result of having the high density liquid on the outside. Further evaluation of these
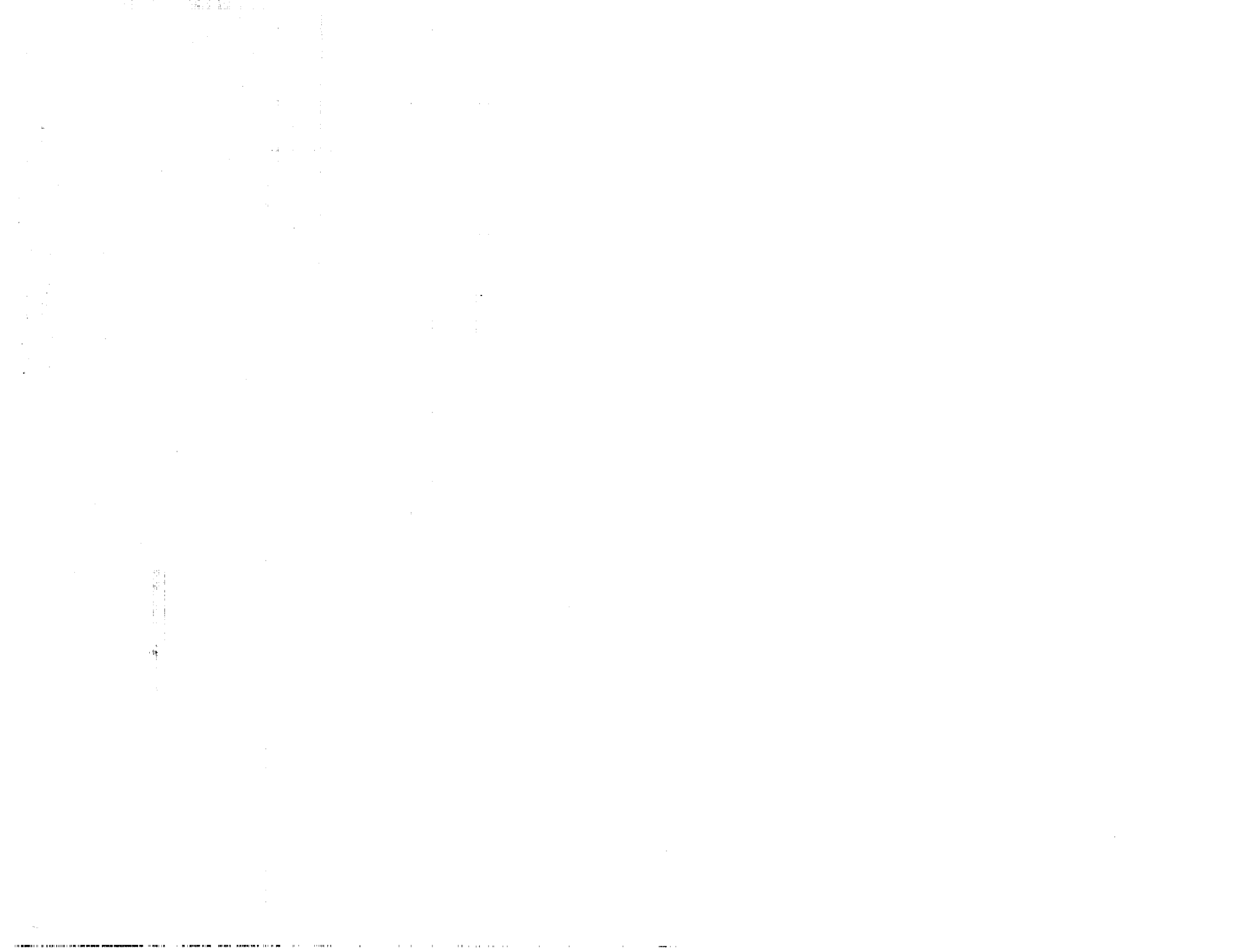
TABLE 6.   SUMMARY OF PREVIOUS COI

TRIPLET

DATE	REPORT I.D. TITLE	PROPELLANTS SIMULATED	SIMULANTS	ELEMENT CONFIGURATION	OPERATING RANGE					
					INJECTION PATTERN	ELEMENT SIZE RANGE (DIA IN)	SIMULATED MR	MOMENTUM RATIO	VELOCITY RATIO	VE HEA
2 8/80	ITUR-80-8 COLD FLOW INVESTIGATION OF UNLIKE TRIPLETS FOR LOX/RP1 (CHEUNG JAQUA)	LOX/RP-1	TRICHLOROETHYLENE & WATER	UNLIKE TRIPLETS LIQ/LIQ	SINGLE F-O-F O-F-O θ=30° MULTI-ELEMENT (LIQ/LIQ) RADIAL CANTED 30° CANT ANGLE θ=30° θ=30°	F — O — F 0.043 - 0.076 - 0.043 0.030 - 0.062 - 0.030 0.030 - 0.030 - 0.030 O — F — O 0.030 - 0.030 - 0.030 MULTI F — O — F 0.030 - 0.062 - 0.030	F-O-F 1.71 2.67 1.28 - 2.71 2.57 - 3.57 O-F-O 2.76 3.45 MULTI F-O-F 2.06 3.63	F-O-F 1.22 3.21 1.57 2.34 1.36 2.64 O-F-O 2.37 3.66 MULTI F-O-F 1.34 4.77	F-O-F 0.77 - 1.70 0.50 - 0.65 0.53 - 0.74 O-F-O 0.85 - 1.05 MULTI F-O-F 0.85 - 1.16	
AUG 90	NASA 7408 R 7460, R 7542, R 7808 LUNAR MODULE ASCENT ENGINE PROGRAM (BUERGIN)	N₂O₄ & N₂H₄/UDMH (50-50)	TRICHLOROETHYLENE & WATER	TRIPLETS, MIXED DOUBLET UNLIKE DOUBLET LIQ/LIQ	TRIPLET F-O-F 192 MULTI-ELEMENTS	INJECTOR O — F UNIT 1 0.0044 - 0.0039 (192 ELEMENTS) UNIT 2 0.0497 - 0.0397 96 ELEMENTS 0.0463 - 0.0399 96 ELEMENTS	1.40 1.52 0.99 1.99	0.73 0.76 0.45 1.73		
MAY 74	NAS CR-68770 NON CIRCULAR ORIFICE HOLES AND ADVANCE FABRICATION TECHNIQUES FOR LIQUID ROCKET INJECTORS COMPREHENSIVE PROGRAM SUMMARY REPORT (McHALE, NURICK)	SINGLE ELEMENT LIQUID/LIQUID STUDIES 4 TO 50-60	WATER/ TRICHLOROETHYLENE	UNLIKE TRIPLETS LIQ/LIQ	F-O-F FUEL OX FUEL TYPICAL TRIPLET ELEMENT	ELEMENT #F #O 0.030 - 0.030 0.030 - 0.043 0.030 - 0.0575 0.030 - 0.030	0.35 1.83 0.87 3.47 1.35 - 2.73 0.54 - 1.22	0.22 - 5.80 0.18 - 4.85 0.35 1.48 0.45 2.48	0.74 - 1.87 0.45 - 2.27 0.85 - 1.38 0.74 - 1.88	0.3 0.3 0.7 0.5
SEPT 73	R-9315 EXPERIMENTAL INVESTIGATION OF COMBUSTOR EFFECTS ON ROCKET THRUST CHAMBER PERFORMANCE (NURICK, HINES)	LOX & GH₂	WATER & HELIUM	TRIPLET LIQ/GAS	TRIPLET O-F-O REVERSE θ=30° 96 MULTI-ELEMENTS	O — F 0.048 - 0.161	2.3 7.8	0.08 0.50	0.03 - 0.064	0.4
APR 81	LS 14 COLD FLOW (MEHEGAN)	NF₃ + H₂ OX? (CH₄ + H₂ (F)	AIR N₂ + H₂	TRIPLET, SINGLE & MULTI-ELEMENT GAS/GAS	O-F-O REVERSE θ=30°	O — F — O MULTI 0.040 - 0.030 - 0.040 SINGLE 0.030 - 0.067 - 0.030	7.16 3.2	3.84 - 0.39		10.
FEB 73 JUN 71	R-8871 OR NASA CR 120808 AND A/AA 71-673 HYDROGEN/OXYGEN APS ENGINES VOL 1 HIGH PRESS THRUSTER (FASTER)	GO₂-GH₂	GO₂/GN₂	TRISLOT GAS/GAS	0.202 GH₂ 0.030" GO₂ 0.103 GH₂ 0.030" T3-A INJECTOR INNER ROW 18 ELEMENTS	30° TRISLOT 45° TRISLOT 60° TRISLOT BASELINE ENLARGED Oₓ AREA ENLARGED FL AREA	6.28 4.4 8.9 4.4 8.9 6.28 4.4 8.9 4.4 8.9		2.1 4.0	
1 17/77	ITR 76-011 C COAL COMBUSTION FOR MHD COLD FLOW MIXING STUDIES (JAQUE/YU)	COAL/AIR	COAL/GN₂	UNLIKE TRIPLET SOLID/GAS	TRIPLET O-F-O REVERSE O — F — O 0.202 0.12 - 0.202 0.302 0.19 - 0.202	UNLIKE TRIPLET	TRIPLET 2.4 5.5	TRIPLET 30 39.0		

INJECTION PARAMETERS (CALCULATED FROM INPUT)				PERFORMANCE PARAMETERS			
LOCITY RATIO	ELVERUM-MOREY (TRIPLET/PENTAD)	PENETRATION FACTOR	OTHER	MIXING EFFICIENCY, E_m	ηc^*_{MIX}	OTHER	COMMENTS
	F-O-F	F-O-F		F-O-F	F-O-F		COLD FLOW STUDY FOR LOX/RP TYPE OPERATION WITH UNLIKE IMPINGING TRIPLETS. QUASI 3-D PLOTS OF MASS DISTRIBUTION SHOW TRIPLET UNBALANCE EFFECTS
2.05	0.43 - 1.05	0.49 - 0.77		0.82 0.93	0.81 0.96		
1.05	0.77 1.63	0.58 - 0.84		0.76 0.93	0.85 0.87		
0.77	0.86 1.04	0.84 - 0.76		0.76 0.91	0.79 0.83		
- 0	O-F-O	O-F-O		O-F-O	O-F-O		
1.98	1.27 - 1.95	1.29 - 6.70		0.87 0.94	0.87 0.95		
MULTI F-O-F	MULTI F-O-F	MULTI F-O-F		MULTI	MULTI		
1.91	0.43 1.36	0.43 - 0.76		0.87 0.98	0.83 - 0.97		
							COLD FLOW MIXING TESTS TO OBTAIN CALIBRATION AND CHARACTERIZATION DATA PRIOR TO HOT FIRE
				0.77 0.93	0.93 0.96		TRIPLET MIXED DOUBLET AND UNLIKE DOUBLET TESTED FOR LEM ASCENT ENGINE. UNLIKE DOUBLET CHOSEN AS FINAL DESIGN
				0.93 0.98	0.94 0.99		PRIMARY TEST VARIABLE WAS MIXTURE RATIO (1 TO 3). 18 COLD-FLOW MIXING TESTS CONDUCTED. 129 HOT FIRE TESTS. NO COLD FLOW ATOMIZATION TESTS
0.13	0.13 3.2	0.41 - 2.89	SINGLE INJECTOR ELEMENT WAS STUDIED. MIXING PROCESSES AND ATOMIZATION WERE INVESTIGATED INDEPENDENTLY FROM COLD FLOW. FROZEN WAX WAS USED	0.45 0.93		EQUATION FOR OPTIMUM MIXING OF CIRCULAR TRIPLET ELEMENTS WAS PRESENTED. LIST OF VARIABLES AFFECTING ATOMIZATION IS ALSO AVAILABLE.	INFLUENCE ON ELEMENT SHAPE UPON PERFORMANCE OF INJECTORS. DIFFERENT LIKE DOUBLET INJECTORS WERE DESIGNED. COLD FLOW AND HOT FIRE TESTED. NON CIRCULAR ORIFICES WERE INVESTIGATED. THE REPORT ALSO CONTAINS DESIGN CRITERIA FOR UNLIKE TRIPLET AND RECTANGULAR CONCENTRIC TUBE ELEMENTS
7.54	0.13 3.3	0.33 - 1.91		0.38 0.90			
2.82	0.3 - 1.3	0.38 0.78		0.78 0.93			
4.11	0.28 - 1.8	0.81 - 1.48		0.71 0.93			
2.92	0.30 1.88	0.25 0.82		0.80 0.80	0.82 0.95		FULL SCALE HOT-FIRE TESTS. SINGLE ELEMENT MIXING AND ATOMIZATION TESTS
0.28	1.10 0.12			0.986 0.974			COLD FLOW MASS AND MIXTURE RATIO DISTRIBUTION TEST PROGRAM TO EXPERIMENTALLY EVALUATE THE LS-14 INJECTOR ELEMENT CONTRIBUTION TO THE COMBUSTOR THERMAL GRADIENT AND SUBSEQUENT NOZZLE DEGRADATION PROBLEM
			PERFORMANCE IS COMPROMISED FOR SMALLER IMPINGEMENT ANGLE. ELVERUM-MOREY CRITERIA WAS USED TO SIZE THE ELEMENTS $$\left(\frac{W_f}{W_o}\right)^2 \left(\frac{\rho_o}{\rho_f}\right)\left(\frac{A_o}{2Af}\right)^{1.75} = .98$$	0.77	0.96		COMPREHENSIVE STUDY FOR HIGH PRESSURE INJECTOR CONCEPT. 4 INJECTORS WERE COLD FLOW TESTED. CONCENTRIC, TRIPLET, DIFFUSE FACE AND TRISLOT. 2 WERE SELECTED FOR HOT-FIRE TESTS. CONCENTRIC AND TRISLOT ηc^* FROM HOT FIRE IS WITHIN 2% OF COLD FLOW. COLD FLOW SAMPLING AT 7" FROM FACE
				0.82 0.88	0.97 0.98		
				0.83 0.92	0.98 0.98		
				0.87	0.98		
				0.82 0.89	0.97 0.98		FUEL SLOT OVERLAP CONFIGURATION AND SMALLER IMPINGEMENT ANGLE WERE INVESTIGATED. GOOD CORRELATION BETWEEN COLD FLOW AND HOT FIRE WAS OBTAINED. HOT-FIRE DATA SUMMARY IS AVAILABLE
				0.72 0.93	0.93 0.95		
	TRIPLETS 0.1 10.3			TRIPLETS 0.44 0.93			STUDY FOR PULVERIZED COAL/AIR TYPE OPERATION WITH UNLIKE TRIPLETS AND PENTAD. ELEMENTS TESTED FOR MASS AND MR DISTRIBUTION

2 FOLDOUT FRAME

TABLE

DATE	REPORT I.D TITLE	PROPELLANTS SIMULATED	SIMULANTS	ELEMENT CONFIGURATION	OPERATING RANGE				
					INJECTION PATTERN	ELEMENT SIZE RANGE (DIA in)	SIMULATED MR	MOM RA
8/88	AFRPL TR-88-152 VOL I STUDY OF DROPLET EFFECTS ON STEADY STATE COMBUSTION (ROCKETDYNE)	50/50 N_2O_4; N_2H_4; ClF$_3$; UDMH IRFNA	WATER/ TRICHLOROETHYLENE	PENTAD SINGLE & MULTI-ELEMENT LIQ/LIQ	REVERSE θ - 30°	SINGLE D - F 0.104 - 0.185; 0.070 - 0.138 MULTI D - F 0.041 - 0.073	1.72 - 2.47; 1.87 - 2.47	1.20; 1.20
JUN 88	AFRPL TR-88-147 CORRELATION OF SPRAY INJECTOR PARAMETERS WITH ROCKET ENGINE PERFORMANCE (DICKERSON, TATE, BARSIC)	N_2O_4; N_2H_4-UDMH 50-50	WATER/ TRICHLOROETHYLENE	PENTAD LIQ/LIQ	OXIDIZER FUEL θ - 30° REVERSE	OX - FU 0.103 - 0.185; 0.070 - 0.138; 0.221 - 0.400	0.83 - 1.71; 0.82 - 2.11; 0.33 - 2.53	0.46; 0.40; 0.81
NOV 88	NASA CR-72487 R 7677 SPACE STORABLE PROPELLANT PERFORMANCE STUDY (FALK, CLAPP, NAGAI)	FLOX 82% O$_2$ & LPG 55% METHANE/ 45% ETHANE	TRICHLOROETHYLENE & WATER	PENTAD LIKE DOUBLET LIQ/LIQ	PENTAD REVERSE θ - 30° MULTI-ELEMENT	O - F 0.026 - 0.038; 0.025 - 0.032; 0.037 - 0.0373; 0.040 - 0.0486	2.72 - 5.82; 2.38 - 5.18	1.27; 1.19
10/11/71	NASA CR-72877 R 8415 SPACE STORABLE THRUSTER HIVES (McFARLAND, JAQUA)	FLOX/C$_3$H$_8$	WATER & PERCHLOROETHYLENE	UNLIKE PENTADS LIQ/LIQ	REVERSE θ - 30° NORMAL θ - 30°	O - F 0.026 - 0.042; O - F 0.073 - 0.071	3.43 - 7.16; 7.86 - 7.82	2.36; 13.04
8/30/67	NASA CR-72263 R-7199 TWO STATE BIPROPELLANT INJECTION SYSTEM STUDIES (MEHEGAN)	LOX/GH$_2$/ HOT GAS	WATER/GN$_2$ H$_2$	PENTAD LIQ/GAS		PENTAD D - 0.213 in²; F - 1.88 in²; G - 3.89 in²	0.73 - 0.87 - 8.1	PENT HOT 13; FUEL 8.3
9/70	NASA CR-72703 R-8361 INVESTIGATION OF GAS-AUGMENTED INJECTORS (MEHEGAN, CAMPBELL AND SHUETRMAN)	LOX GH$_2$; FLO$_2$ CH$_4$; LF$_2$ GH$_2$	WATER GH$_2$/H$_2$	PENTAD LIQ/GAS	REVERSE PENT/D θ - 40° NORMAL PENTAD θ - 40°	PENTAD REVERSE O - F 0.246 - 0.81; 0.435; 0.125; 0.309 - 0.81; 0.584 - 0.377; 0.185 - 0.82 NORMAL O - F 0.334 - 0.81	REVERSE 0.3 - 13.0; NORMAL 4.6 - 7.4	0.16; 0.827
1/17/77	ITR 78-011-C COAL COMBUSTION FOR MHD COLD FLOW MIXING STUDIES (JAQUA/YU)	COAL/AIR	COAL/GN$_2$	UNLIKE PENTAD SOLID/GAS	PENTAD REVERSE	PENTAD D - 0.213; F - 0.133	PENTAD 4.0 - 5.5	PENT 9.0

FOLDOUT FRAME

6. (Continued)

PENTAD

INJECTION PARAMETERS (CALCULATED FROM INPUT)						PERFORMANCE PARAMETERS				
MOMENTUM RATIO	VELOCITY RATIO	VELOCITY HEAD RATIO	ELVERUM/MOREY FACTOR (TRIPLET, PENTAD)	PENETRATION FACTOR	OTHER	MIXING EFFICIENCY, E_m	η_{c^*} MIX		OTHER	COMMENTS
										STUDIED THE EFFECTS OF INJECTOR-INDUCED MASS MR AND DROPLET DISTRIBUTION CHARACTERISTICS ON STEADY STATE COMBUSTION PERFORMANCE. STUDY SHOWED CORRELATION BETWEEN INJECTOR DESIGN AND COMBUSTION EFFICIENCY
										EVALUATION OF DROPSIZE MEASUREMENT TECHNIQUE (1) HIGH SPEED PHOTOGRAPHY (2) FROZEN WAX (3) HOLOGRAPHY. FROZEN WAX WAS PROVEN TO BE THE MOST SUPERIOR TECHNIQUE. INJECTORS WERE DESIGNED, COLD FLOW AND HOT FIRE TESTED TO CORRELATE. HOT FIRE η_{c^*} WITH COLD FLOW THE RESULTS WERE WITHIN 1%
										FULL-SCALE COLD-FLOW MIXING AND HOT FIRE PERFORMANCE TESTS CONDUCTED. EXCELLENT DATA QUALITY
										ANALYTICAL AND EXPERIMENTAL STUDY OF 25 LB$_f$ THRUSTER. CORRELATION OF STEADY-STATE AND PULSE MODES. 2-D PLOTS OF MASS FLOW AND MIXTURE RATIO DISTRIBUTION
						N/A				COMPREHENSIVE STUDY FOR LARGE THRUST PER ELEMENT INJECTORS. TWENTY INJECTOR DESIGNS WERE REVIEWED INITIALLY AND FOUR WERE CHOSEN FOR COLD FLOW AND TWO FOR HOT FIRE. LIQUID MASS DISTRIBUTION MAPS PRESENTED FOR SELECTED INJECTORS
										ANALYTICAL COLD FLOW, HOT FIRE PERFORMANCE CORRELATION TECHNIQUES DEVELOPED FOR INJECTOR DESIGNS FOR GAS/LIQUID INJECTORS. COLD FLOW TESTS DETERMINED DROPLET SIZES AND DISTRIBUTION AND THE MASS AND MIXTURE RATIO DISTRIBUTION FOR LARGE THRUST PER ELEMENT DESIGNS
						PENTAD				STUDY FOR PULVERIZED COAL/AIR TYPE OPERATION WITH UNLIKE TRIPLETS AND PENTAD. ELEMENTS TESTED FOR MASS AND MR DISTRIBUTION

2 FOLDOUT FRAME

DATE	REPORT I.D. TITLE	PROPELLANTS SIMULATED	SIMULANTS	ELEMENT CONFIGURATION	OPERATING RANGE				
					INJECTION PATTERN	ELEMENT SIZE RANGE (DIA IN)	SIMULATED MR	MOMENTUM RATIO	VELOCITY RATIO
FEB 70	NASA CR 135388 R/PC78.114 PREBURNER OF STAGE COMBUSTION ROCKET ENGINE (YOST)	LOX/GH₂	NOT MENTIONED	COAXIAL LIQ/GAS	16 ELEMENTS EQUALLY SPACED		8.57		11.0 - 15.0
MAY 74	NASA CR-92770 NON CIRCULAR ORIFICE HOLES AND ADVANCE FABRICATION TECHNIQUES FOR LIQUID ROCKET INJECTORS COMPREHENSIVE PROGRAM SUMMARY REPORT (BeHALE, BURICK)	SINGLE ELEMENT LIQUID/LIQUID STUDIES NTO/50-50	WATER/ TRICHLOROETHYLENE	CONCENTRIC TUBE INJECTOR LIQ/GAS	CIRCULAR / RECTANGULAR		CIRCULAR 0.38 - 5.61 RECTANGULAR 6.0		CIRCULAR 8.35 - 71.5 RECTANGULAR 38.0 - 63.0
JUNE 73	(a) PT 73 - 38 (b) PT 73 - 37 SPACE SHUTTLE MAIN ENGINE a. COLD-FLOW MIXING CHARACTERIZATION OF THE SSME PREBURN ELEMENTS b. COLD-FLOW MIXING CHARACTERIZATION OF THE SSME MAIN AND BAFFLE ELEMENTS (FALK)	(a) LOX/GH₂ (b) LOX/Gas/ HOT GAS	(a) H₂O/GH₂/N₂ (b) H₂O/GH₂/N₂	(a) COAXIAL (b) LIQ LIQ/GAS GAS	(a) FACEPLATE 60 PER ROW – 6N + 6 N = ROW NO PPB – 204 ELEMENTS IN 6 ROWS GPB – 139 ELEMENTS IN 6 ROWS (b) MAIN INJECTOR 600 ELEMENTS IN 13 ROWS	(a) PPB FUEL – .0125 GRID – .0002 GPB FUEL – .01277 GRID – .00407 (b) MAIN ELEMENT FUEL – .0270 GRID – .204 BAFFLE ELEMENT FUEL – .0270 GRID – .204	(a) PPB 0.5 - 1.14 GPB 0.4 - 1.32 (b) MAIN ELEMENT 0.4 - 0.8 BAFFLE ELEMENT 4.0 - 5.0		(a) PPB 6.7 - 24.3 GPB 4.0 - 24.0 (b) MAIN ELEMENT 14.0 - 33.3 BAFFLE ELEMENT 13.0 - 41.0
MAY 72	JOURNAL OF SPACECRAFT AND ROCKETS (VOL. 9, NO. 5) ATOMIZATION AND MIXING CHARACTERISTICS OF GAS/LIQUID COAXIAL INJECT. ELEMENTS (BURICK) OCT 70 NASA CR-120825 R-8573-2 SPACE STORABLE PROPELLANT PERFORMANCE PROGRAM COAXIAL INJECTOR CHARACTERIZATION (BURICK) MAY 70 NASA CR-120825 INJECTOR DESIGN GUIDELINES FOR GAS/LIQUID PROPELLANT SYSTEMS (FALK, BURICK)	FLOX GN₂	WATER GH₂/GO₂	COAXIAL SINGLE ELEMENT LIQUID CYL/GAS ANNULUS LIQ/GAS	R = OXIDIZER POST RECESS		3 - 7.5		100 < V₀ < 600 6 < V₁ < 100
SEP 70	NASA CR-72703 R-8061 INVESTIGATION OF GAS AUGMENTED INJECTORS GRE/HEGAR, CAMPBELL, SCHUELER (REAR)	LOX GH₂ FLOX CH₄ LF₂ GH₂	WATER GH₂/N₂	COAXIAL LIQ/GAS	GAS LIQ	COAXIAL A_LIQ A_GAS 0.080 - 0.887 0.262 - 0.860 0.100 - 0.210	4.0 - 10.3		V₀/V_L 3.30 - 91.4
AUG 67	NASA CR-72003 R-7188 TWO STATE BIPROPELLANT INJECTION SYSTEM STUDIES (BREHEGAN)	LOX/GH₂ HOT GAS	WATER GH₂/N₂	TRIAXIAL HOT GAS INSIDE LOX/FUEL ANNULI COAXIAL IMPINGING RECESSED CUP LIQ/GAS	FUEL LOX HOT GAS CJA CJA – G – CJA CJA	TRIAXIAL O - 2.80 in² F - 1.35 in² G - 3.80 in² COAXIAL O - 0.51 in² F - 1.34 in² G - 3.39 in²	G F O .650 0.50-0.52-7:1 0.75-1.57-6.7	TRIAXIAL HOT GAS 40.5 FUEL 18.5 COAXIAL IMPACT HOT GAS 71.0 FUEL 11.9	
FEB 73 JUN 71	R-8577-1 OR NASA CR125005 AND AIAA 71-673 HYDROGEN/OXYGEN APS ENGINES VOL 1 HIGH PRESS THRUSTER (PASTER)	GO₂/GH₂	GO₂/GN₂	COAXIAL GAS/GAS	BASE LINE ELEMENT	ID OD ID POST POST SLEEVE BASE 40 TAPER .141 .104 .299 BLUNT .141 .104 .299 TAPER .141 .104 .299 - 125 RECESS BLUNT .141 .104 .299 - 125 RECESS TAPER .141 .104 .299 TAPER .299 .251 .299	4.4 - 8.0 4.2 - 8.4 4.3 - 8.4 4.4 - 8.3 4.4 - 8.0		

(continued)

AL

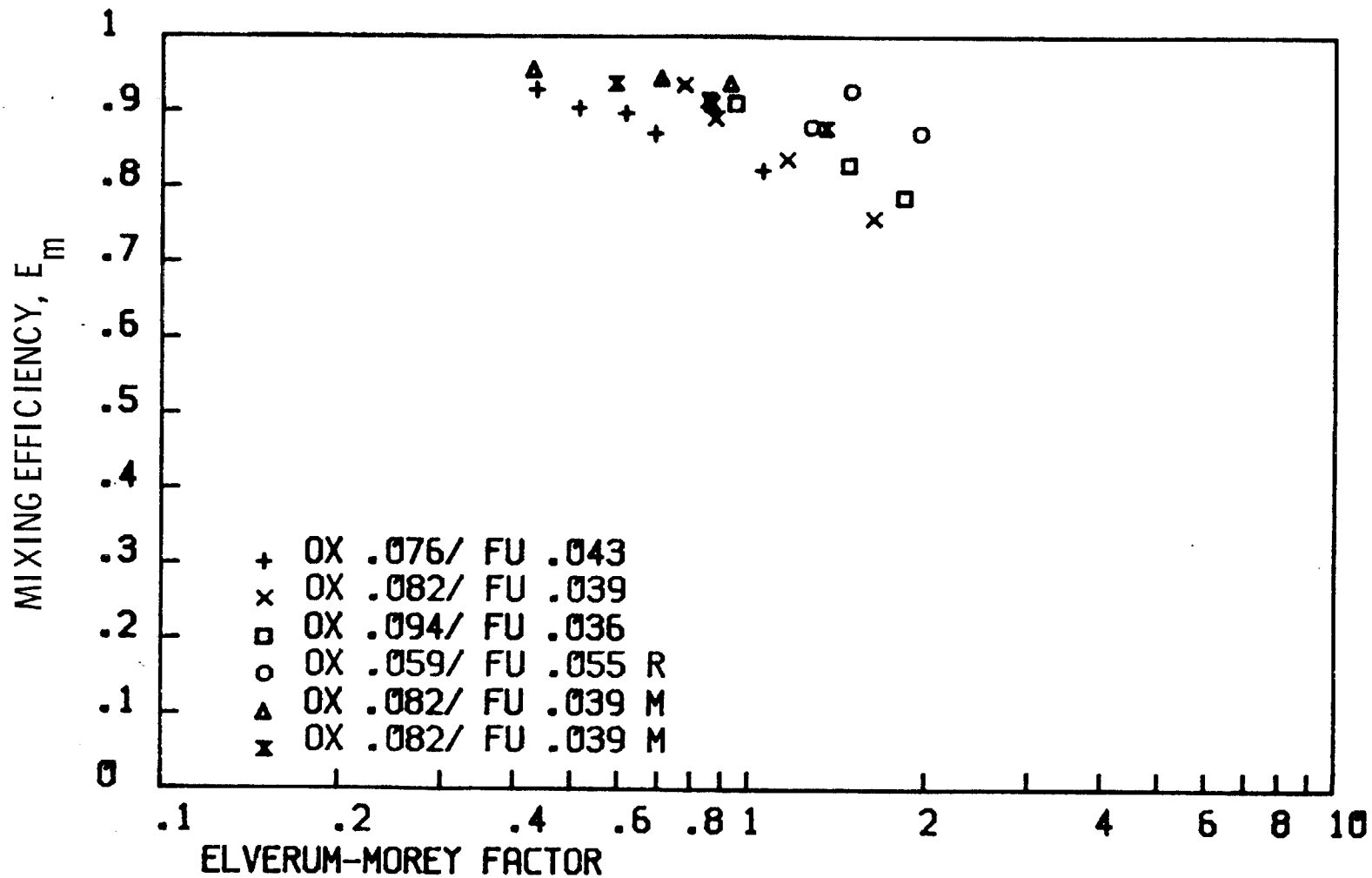| INJECTION PARAMETERS (CALCULATED FROM INPUT)				PERFORMANCE PARAMETERS			
VELOCITY HEAD RATIO	SILVERMAN/MOREY FACTOR (TRIPLET, PENTAD)	PENETRATION FACTOR	OTHER	MIXING EFFICIENCY, E_m	$\eta_c{}^*$ MAX	OTHER	COMMENTS
			THE COAXIAL INJECTOR COMBUSTION MODEL (C.I.C.M.) WAS USED TO PREDICT THE PERFORMANCE			PREBURNER INJECTORS AND MAIN INJECTOR WERE BUILT AND HOT-FIRE TESTED FOR MAIN INJECTOR $\eta_c{}^*$ RANGE FROM 98.3% FOR MR = 0.9 TO 99% FOR MR = 1.25	COMPLETE STUDY OF A REGENERATIVE COOLED LOX/HYDROGEN STAGED COMBUSTION. TABLES OF ELEMENT DESIGN PARAMETERS ARE AVAILABLE IN CONJUNCTION WITH BOTH PREBURNER AND MAIN INJECTOR ELEMENTS AND THE ADVANCED SPACE ENGINE (ASE).
			$2.6 D_L < R < 12 D_L$ and $2043 < \frac{\mu S}{\rho_L} < 2940$			TABLES OF PHYSICAL VARIABLES AND DIMENSIONLESS GROUP REQUIRED FOR THE DESCRIPTION OF GAS/LIQUID CONCENTRIC ELEMENT MIXING AND ATOMIZATION FROM DIMENSIONAL ANALYSIS	COLD FLOW MIXING AND COLD FLOW ATOMIZATION WERE STUDIED. RECTANGULAR CONCENTRIC TUBE INJECTOR WAS HOT-FIRE TESTED TO EVALUATE THE EFFECT OF THE ELEMENT GEOMETRY UPON INJECTOR PERFORMANCE. ANALYTICAL COMBUSTION MODEL WAS DEVELOPED TO CORRELATE E_m AND D WITH $\eta_c{}^*$ ERR AND $\eta_c{}^*$ VAP.
				(a) PPB 0.900 - 0.984; SPB 0.80 - 0.956; (b) MAIN ELEMENT 0.771 - 0.986; BAFFLE ELEMENT 0.900 - 0.992	(a) PPB 0.9846 - 0.9980; SPB 0.900 - 1.000; (b) MAIN ELEMENT 0.993 - 0.997; BAFFLE ELEMENT 0.972 - 0.992		SPACE SHUTTLE ELEMENTS HAVE BEEN COLD FLOW EVALUATED (MIXING) OVER PLANNED OPERATING RANGE. SINGLE-ELEMENT TESTS COULD POSSIBLY BE COMPARED WITH LATER HOT-FIRE RESULTS. SUPER-CRITICAL PROPELLANTS. EXCELLENT QUALITY COLD-FLOW DATA AVAILABLE.
			PHYSICAL PARAMETERS V_g, V_L, AND P_g INFLUENCE ON MIXING AND ATOMIZATION FOR GAS/LIQUID INJECTORS.	R = 0 0.50 - 0.95; R = 10 0.80 - 0.95		CORRELATION MADE BETWEEN MIXING DATA (E_m) AND THE PARAMETER $P_G V_G{}^2$/ $\rho_L \cdot V_L{}^2$	REPORT ON ATOMIZATION AND MIXING EFFECTS ON COAXIAL ELEMENTS WITH VARYING POST RECESS AND LIQUID AND GAS FLOW AREAS. PROGRAM WAS CONDUCTED TO CHARACTERIZE GAS/LIQUID COAXIAL INJECTOR IN ORDER TO OBTAIN HIGH $\eta_c{}^*$ WITHOUT SACRIFICING HARDWARE DURABILITY. VARIOUS SINGLE ELEMENT GEOMETRIC CONFIGURATIONS WERE COLD FLOW AND HOT-FIRE TESTED. ALSO FULL SCALE INJECTOR WAS BUILT AND TESTED. $\eta_c{}^*$ HOT-FIRE WAS WITHIN 3% OF $\eta_c{}^*$ COLD FLOW.
			Δ(Vg-VL) 300 - 940; POST RECESS/D_L 0.0 - 3.0	0.904 - 0.950			ANALYTICAL COLD FLOW, HOT-FIRE PERFORMANCE CORRELATION TECHNIQUES DEVELOPED FOR INJECTOR DESIGNS FOR GAS/LIQUID INJECTORS. COLD FLOW TESTS DETERMINED DROPLET SIZES AND DISTRIBUTION AND THE MASS AND MIXTURE RATIO DISTRIBUTION FOR LARGE THRUST PER ELEMENT DESIGNS.
	0.95						COMPREHENSIVE STUDY FOR LARGE THRUST PER ELEMENT INJECTORS. TWENTY INJECTOR DESIGNS WERE REVIEWED INITIALLY AND FOUR WERE CHOSEN FOR COLD FLOW AND TWO FOR HOT-FIRE. LIQUID MASS DISTRIBUTION MAPS PRESENTED FOR SELECTED INJECTORS.
			LARGER η_c ANNULUS INCREASES $\eta_c{}^*$ BY 3%	0.70 - 0.91; 0.75 - 0.92; 0.70 - 0.90; 0.90 - 0.95; 0.94 - 0.98	0.90 - 0.95; 0.92 - 0.97; 0.94 - 0.98; 0.90 - 0.95; 0.95 - 0.99	FIGURE 14. CORRELATION OF COLD-FLOW PERFORMANCE PREDICTION OF HOT-FIRE RESULTS	COMPREHENSIVE STUDY FOR HIGH PRESSURE INJECTOR CONCEPT. 4 INJECTORS WERE COLD FLOW TESTED: CONCENTRIC, TRIPLET, TRIPLET FACE AND TRIPLET. 2 WERE SELECTED FOR HOT-FIRE TESTS: CONCENTRIC AND TRIPLETS. FROM HOT-FIRE & WITHIN 2% OF COLD FLOW. COLD FLOW SAMPLING AT 3" FROM FACE. FUEL SLOT OVERLAP CONFIGURATION AND SMALLER IMPINGEMENT ANGLE WERE INVESTIGATED. GOOD CORRELATION BETWEEN COLD FLOW AND HOT-FIRE WAS OBTAINED. HOT-FIRE DATA SUMMARY IS AVAILABLE.

Figure 15. Mixing Efficiency of Liquid/Liquid Triplets (ITUR-80-9)
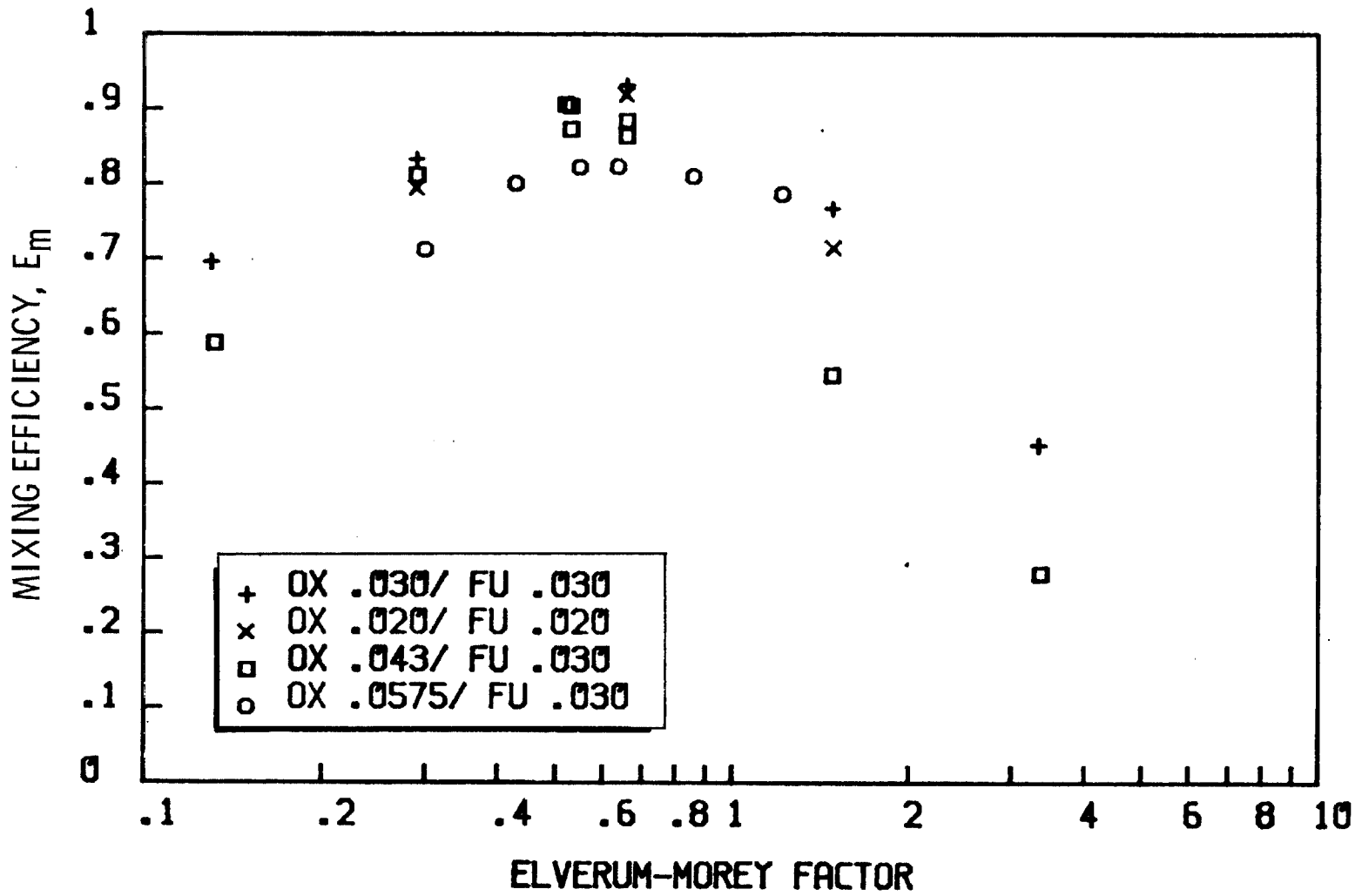Depicting Elverum-Morey Factor Influence

Figure 16.   Mixing Efficiency of Liquid/Liquid Triplets (NASA CR-R-9270)
Depicting Elverum-Morey Factor Influence

characteristics would appear to be warranted since liquid/liquid hydrocarbon mixtures favor a reverse triplet configuration at main chamber mixture ratios.

Triplet - Gas/Liquid

One report was found on LOX/hydrogen work (Ref. 34) which provided data on a liquid/gas/liquid configured element. Suprisingly, the penetration factor, designed for liquid/gas/liquid elements, did not produce the desired correlation of maximum mixing efficiency (E_m) at the 0.5 theoretical optimum value (Fig. 17). Visual aids from the report depict the gas/liquid normalized mass flux profiles for each of three cold flow tests. Figure 18 depicts representative samples of those three tests. The sample mixture ratio is equivalent to the overall inlet mixture ratio where the dashed lines (gas) intersect the solid lines (liquid). It can be inferred from the distribution plots that the balance of gas and liquid was optimum at the under-penetrated condition (penetration factor 0.4), which contributed to the maximum-measured mixing efficiency. At penetration factors greater than 0.4, the gas blowout produced by the impinging liquid jets was visible. This contributed to the poorer mixing efficiency noted.

The Elverum-Morey criteria for this element, shown in Fig. 19, did reflect a correlation between the 0.66 optimum value and the peak mixing efficiency. In this test, the oxidizer-to-fuel density ratio was over 600, markedly removed from the design application range of 1.7. These parameters bear additional testing since there are good designs for liquid/gas/liquid elements in LOX/ hydrocarbon gas generators and preburners.

Pentad - Liquid/Liquid

Documents obtained with mixing data for liquid/liquid pentad elements consisted primarily of reverse configuration* element studies (Ref. 3, 4, and 10). In these

---

* A reverse pentad generally is considered to have the denser liquid (oxidizer) in the outboard streams and the less dense liquid (fuel) as the centrally located stream.
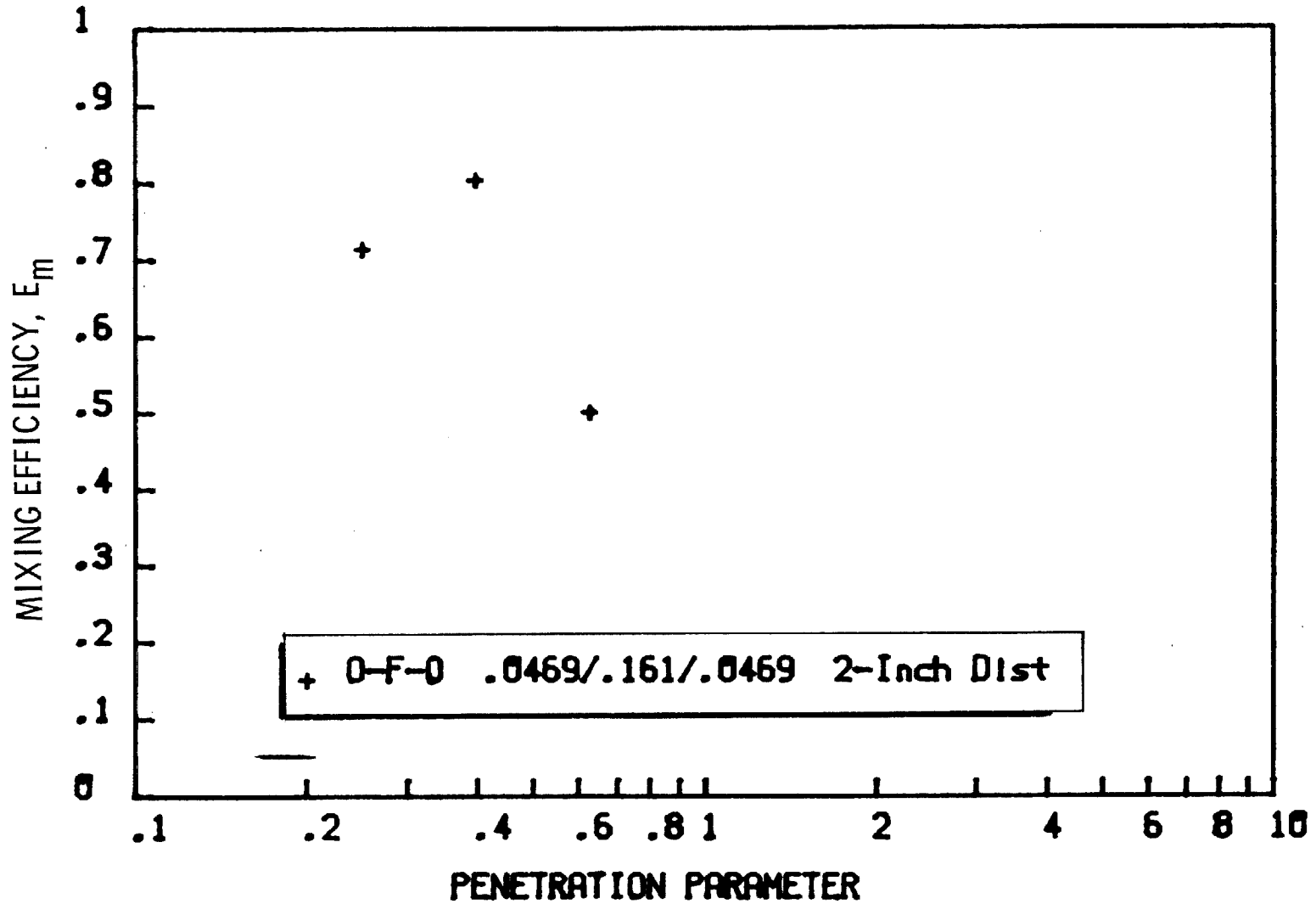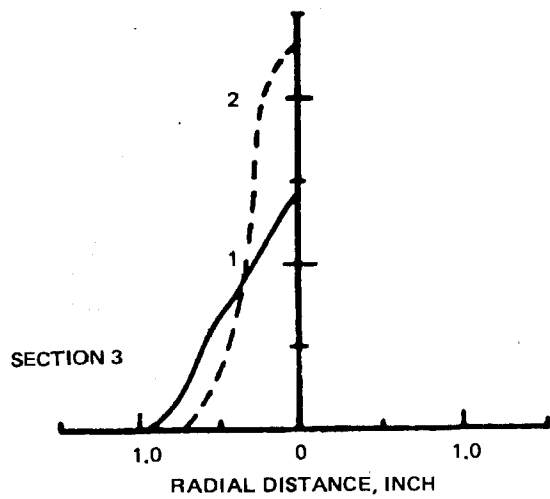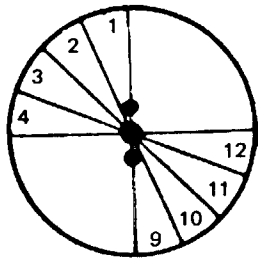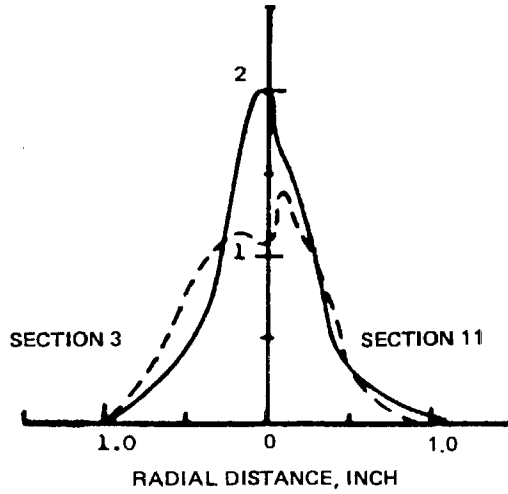
Figure 17.   Mixing Efficiency of a Gas/Liquid Triplet (R-9315)
Depicting Penetration Factor Influence

DEFINITION OF
FLOW SECTIONS

SECTION 3

RADIAL DISTANCE, INCH

1.0   0   1.0

PENETRATION
FACTOR = 0.25

SECTION 3   SECTION 11

RADIAL DISTANCE, INCH

1.0   0   1.0

PENETRATION
FACTOR = 0.395

SECTION 3   SECTION 11

RADIAL DISTANCE, INCH

1.0   0   1.0
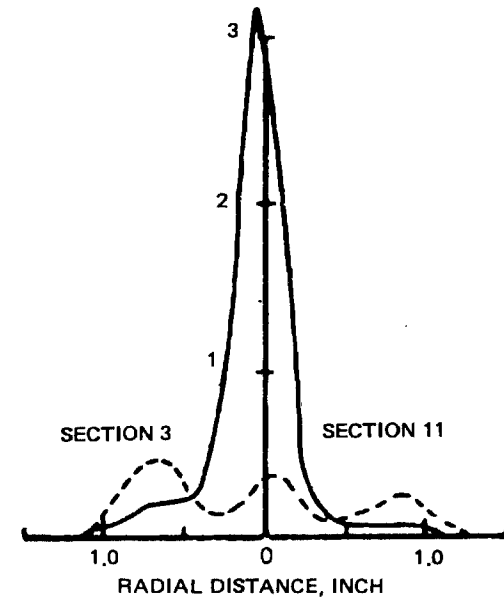
PENETRATION
FACTOR = 0.62

Figure 18.   Normalized Cold Flow Mass Flux Profiles for LOX/GH$_2$,
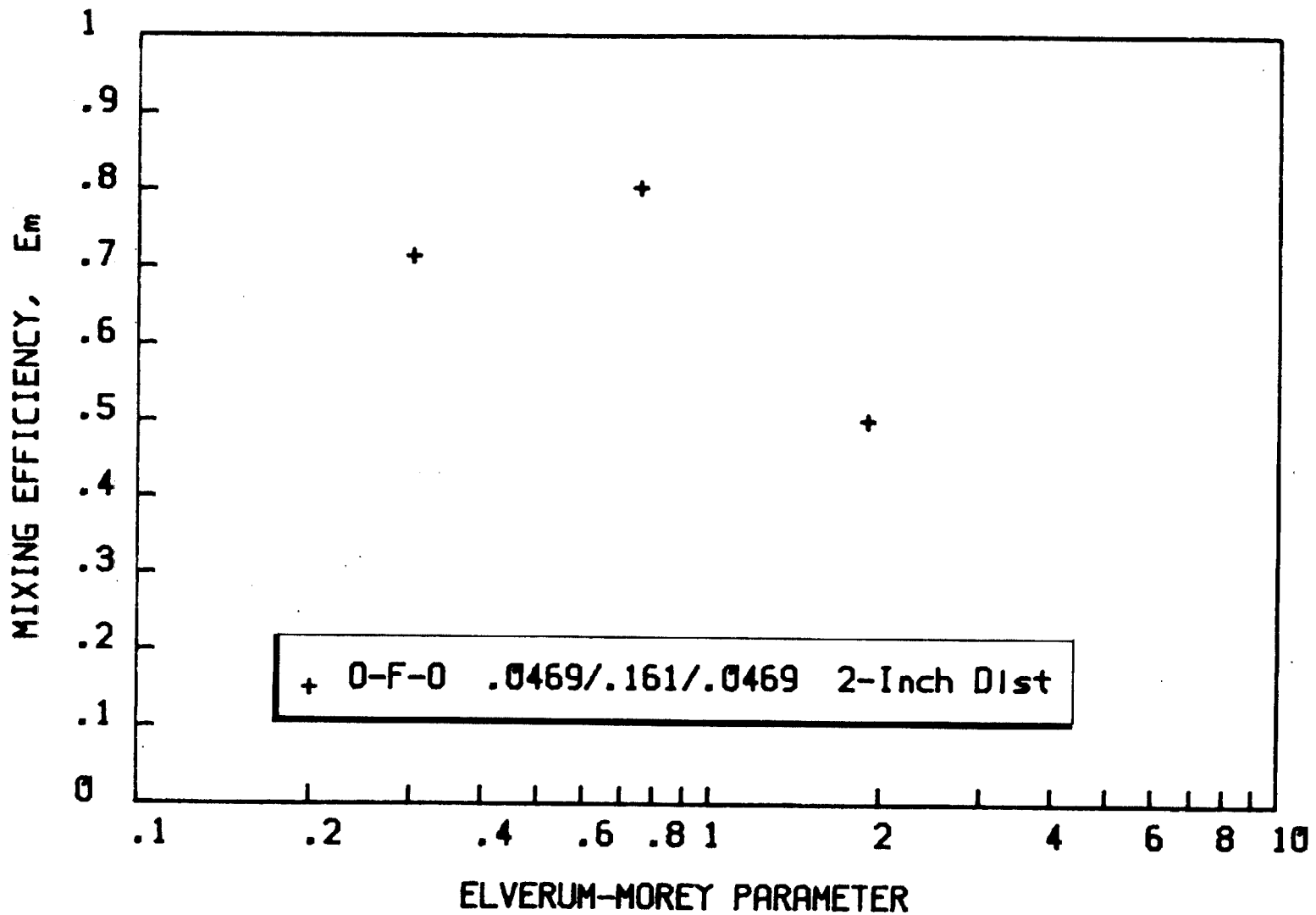Liquid/Gas/Liquid Triplet, 2-inch Collection Tubes (Ref. 34)

Figure 19. Mixing Efficiency of a Liquid/Gas/Liquid Triplet (R-9315)
Depicting Elverum-Morey Factor Influence

studies, the overall level of mixing efficiency was generally good. Single element characteristics did not adhere to the Elverum-Morey theoretical optimum very well for the large element tests shown in Fig. 20 (Ref. 3), although the multi-element tests did show peak mixing efficiency near the 2.75 optimum value for the same experimentors. This is either a result of secondary mixing enhancement from the multiple element configuration or is indicative of absolute size limitations in parameter application. Other data presented in Fig. 21 and 22 indicate some small degree of correlation with the 2.75 optimum parameter value.

Pentad – Gas/Liquid

The volumetric unbalance realized with gas/liquid propellant combinations frequently dictates the use of pentad (four on one) elements. With the gaseous reactant on the four outside elements, this bears some resemblance to an impinging concentric element.

With the gaseous component of the reaction system in the center stream, the case resembles an extension of the liquid-gas-liquid triplet where a form of the penetration factor becomes the most likely mixing parameter.

One document was located with gas/liquid pentad data (Ref. 31), which includes test data for both configurations, liquid-gas-liquid and gas-liquid-gas. This data was replotted against three different parameters, momentum ratio, Elverum-Morey ratio, and penetration factor.

Both pentad configurations showed improved mixing characteristics with increased oxidizer (liquid) momentum (Fig. 23), regardless of the orientation of the oxidizer stream(s). This is not understood fully since prior experience on other programs, such as the gas/fluidized-solid program (Ref. 30), indicated contrary relationships, i.e., an increase in performance with a reduction in momentum of the central-fluidized stream with maximum performance occurring at a relatively high gas to liquid momentum ratio.

Figure 20. Mixing Efficiency for Liquid/Liquid Pentads (AFRPL-TR-66-147) Depicting Elverum–Morey Factor Influence

Figure 21. Mixing Efficiency for Liquid/Liquid Pentads
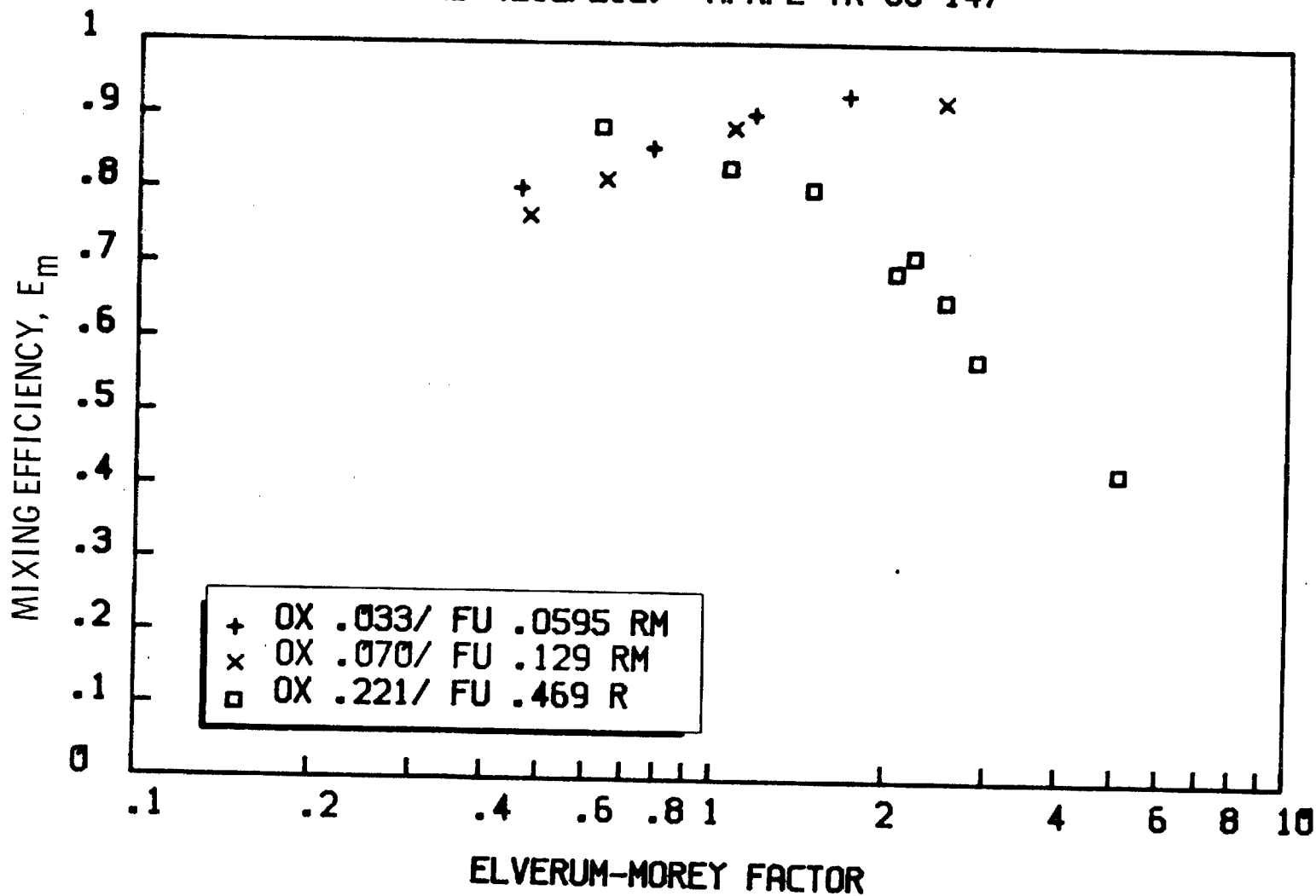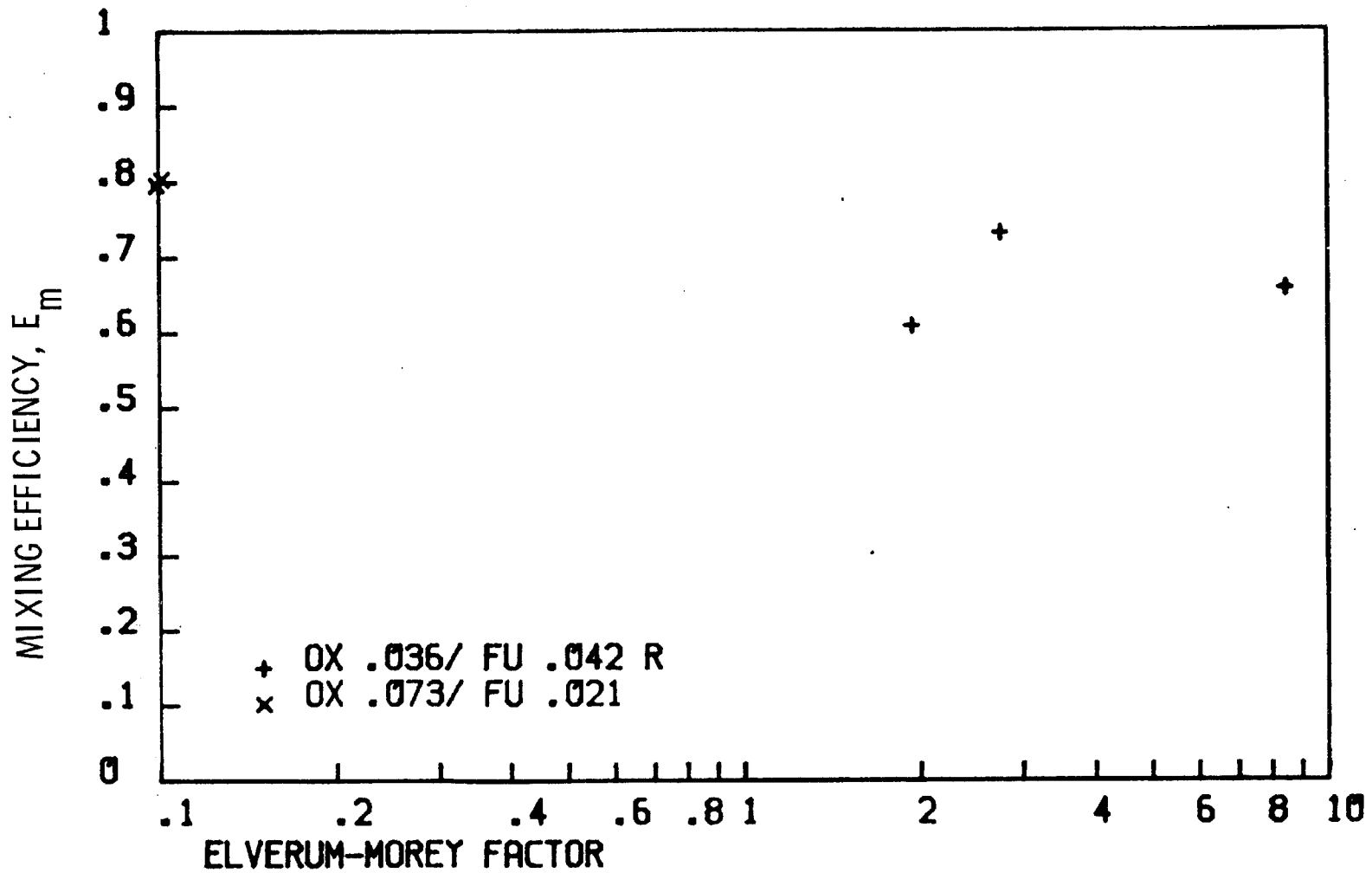(NASA CR-72827 R-8415) Depicting Elverum-
Morey Factor Influence
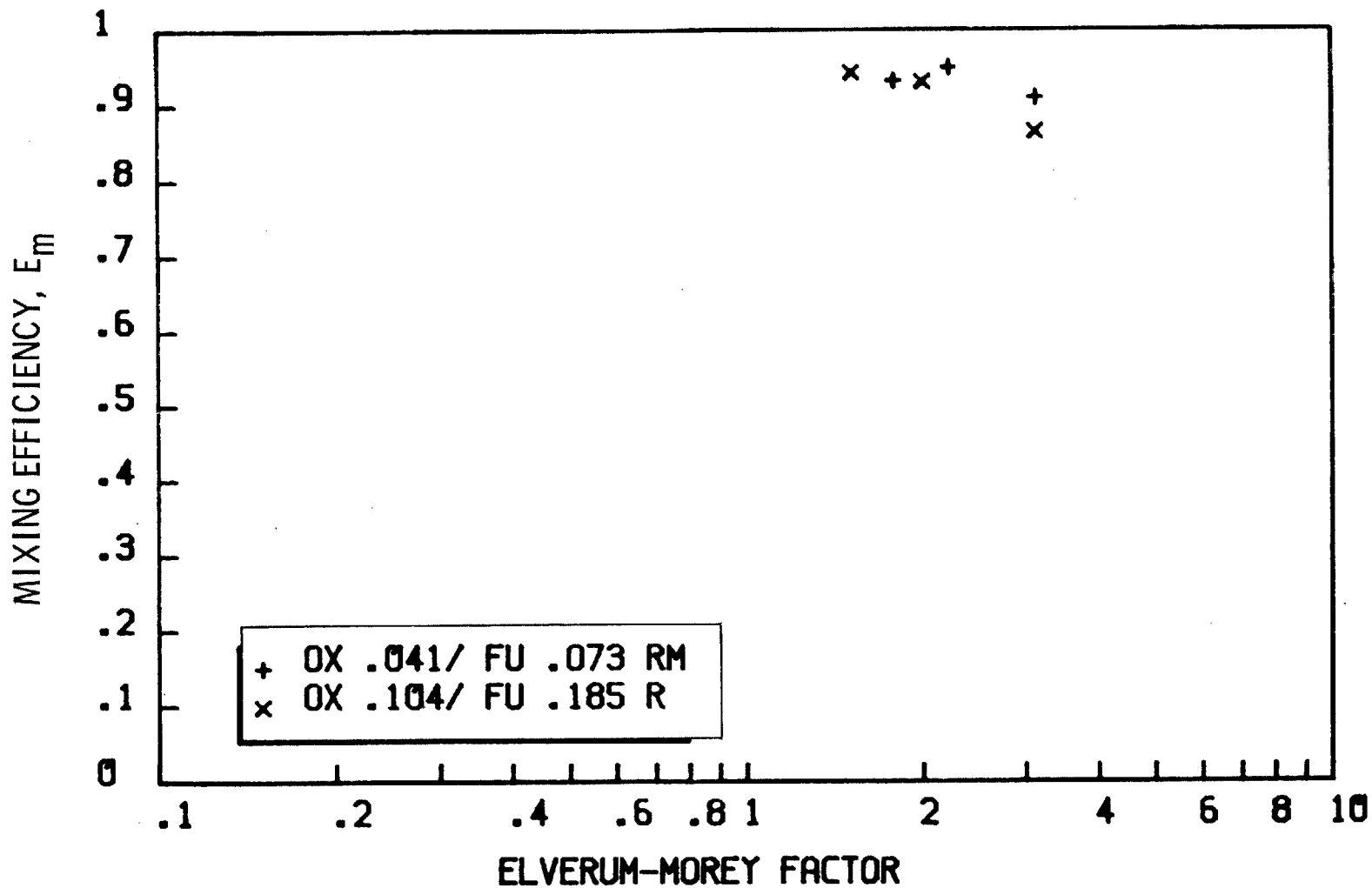
Figure 22. Mixing Efficiency for Liquid/Liquid Pentads
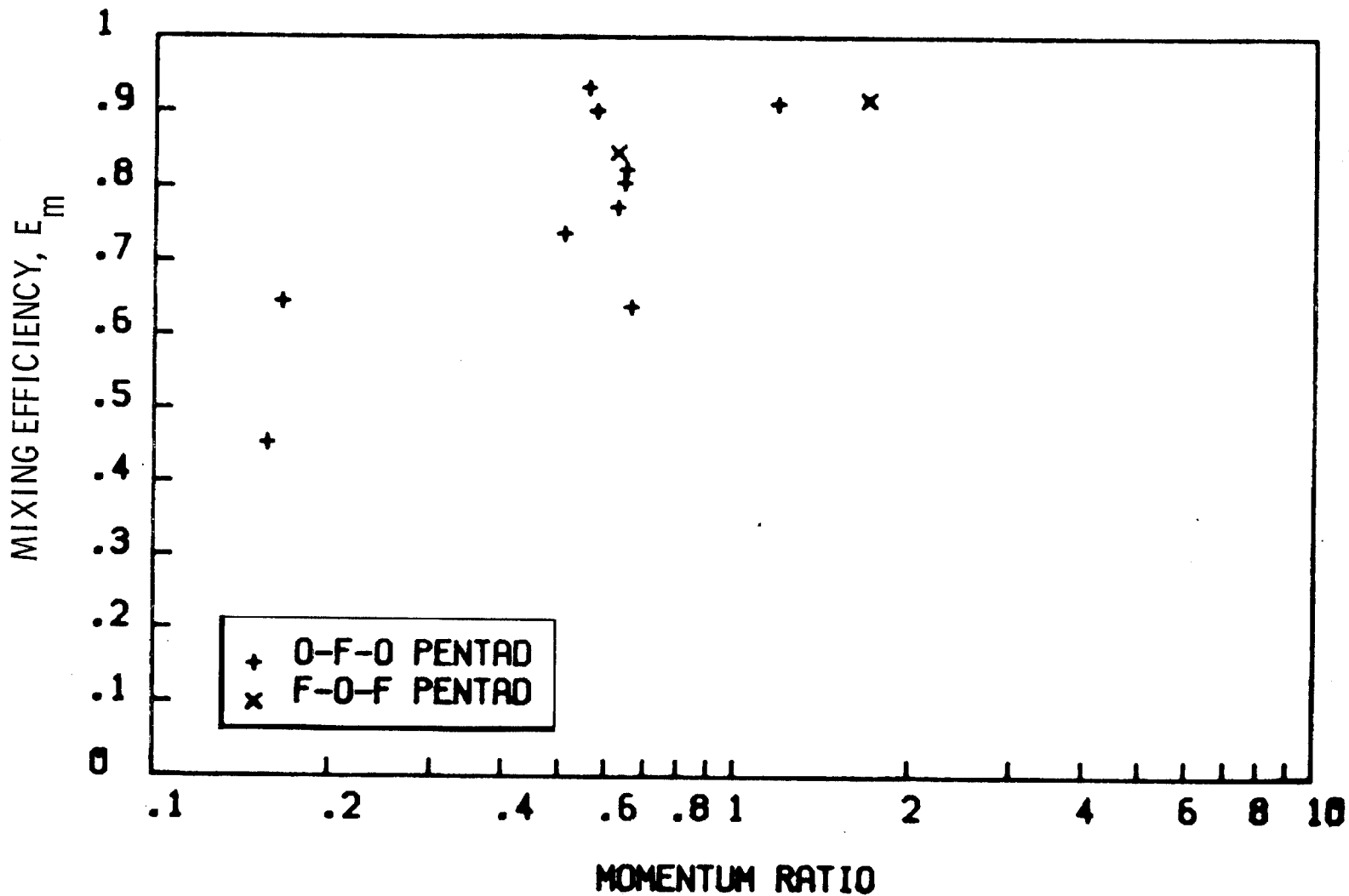(AFRPL-TR-66-152) Depicting Elverum-Morey
Factor Influence

Figure 23. Mixing Efficiency for Gas/Liquid Pentads
(NASA CR-72703 R-8361) Depicting Momentum
Ratio Influence

Extrapolating the liquid-gas-liquid test data along the Elverum-Morey curve, Fig. 24 suggests a trend toward the 2.75 optimum value for pentads, whereas the gas-liquid-gas data do not obey the parameter functions. Extrapolating the penetration factor data for the gas-liquid-gas element may indicate a trend toward the 0.5 optimum value (Fig. 25). The liquid-gas-liquid element apparently does not adhere to the penetration factor function.

Concentric Coaxial Element

Several report references were obtained in the literature search containing cold flow mixing data for coaxial elements. Some of these were from the Space Shuttle Main Engine (SSME) Program. The mixing data from these sources were plotted against the conventional parameters applicable to coaxial injectors, namely LOX post recess and velocity ratio.

In most concentric element configuration, relatively large improvements in mixing are anticipated as the central tube (oxidizer post) recess is increased to one liquid stream diameter. Data presented in Fig. 26 (Ref. 7) depict less effect than had been expected. The curve indicates poor overall mixing efficiency (E_m = 50 to 65%) with very little improvement obtained as recess is increased. However, Falk and Burick report in their studies (Ref. 19) that cup recess does improve mixing. This conflict needs to be resolved by additional testing, especially in the areas of hydrocarbon fuels.

The influence of gas-to-liquid velocity ratio on the level of mixing efficiency is presented in Fig. 27 and 28, depicting the characteristics of SSME LOX/hydrogen preburner and main injector elements in cold flow test. In these figures, mixing efficiency is consistantly high. Propellant density matching was achieved for these tests, which also resulted in nominal matching of hot fire (design range) velocity and momentum ratios simultaneously.

Additional tests conducted by Rocketdyne (Ref. 31 and 7) are presented in Fig. 29 and 30, respectively, depicting the effects of velocity ratio on mixing efficiency. The latter figure shows the influence of gas-to-liquid density ratio

PENTAD (GAS/LIQ)   NASA CR-72703   R-8361
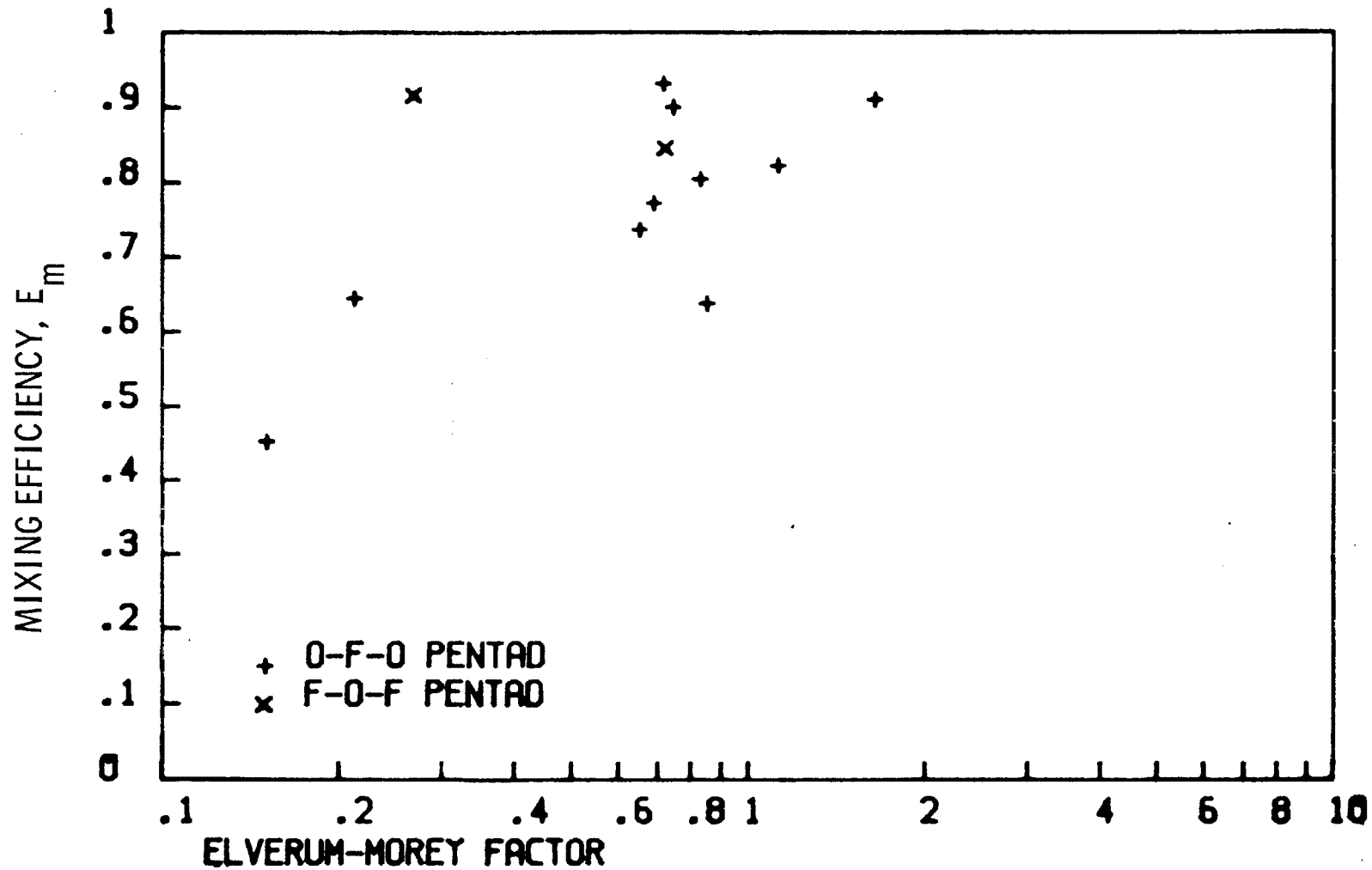
Figure 24. Mixing Efficiency for Gas/Liquid Pentads
(NASA CR-72703 R-8361) Depicting Elverum-
Morey Factor Influence
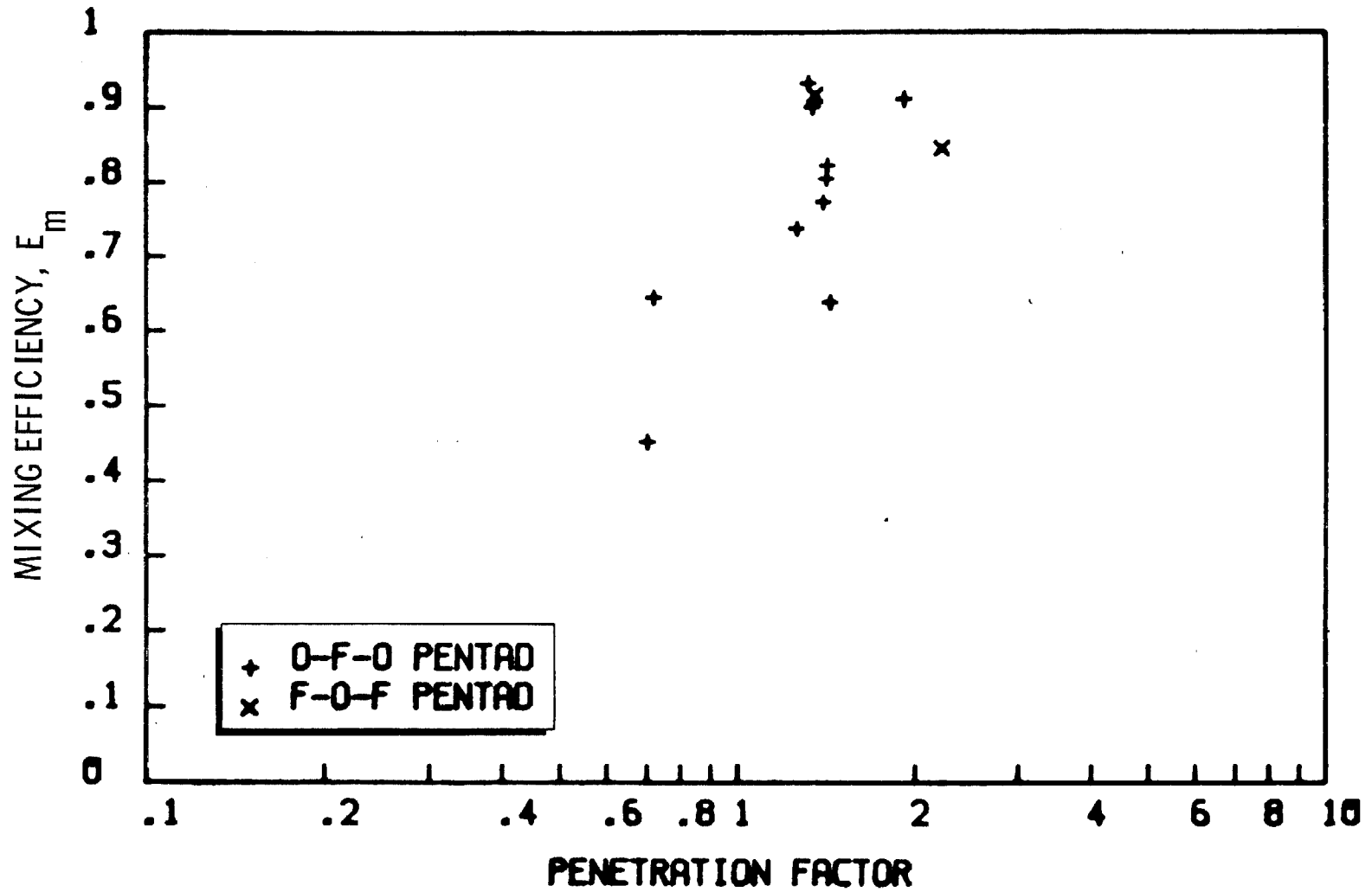
Figure 25.   Mixing Efficiency for Gas/Liquid Pentads
(NASA CR-72703 R-8361) Depicting Penetration
Factor Influence

Figure 26.   Mixing Efficiency for Coaxial Element (NASA CR-R-9270)
Depicting LOX Post Recess Influence
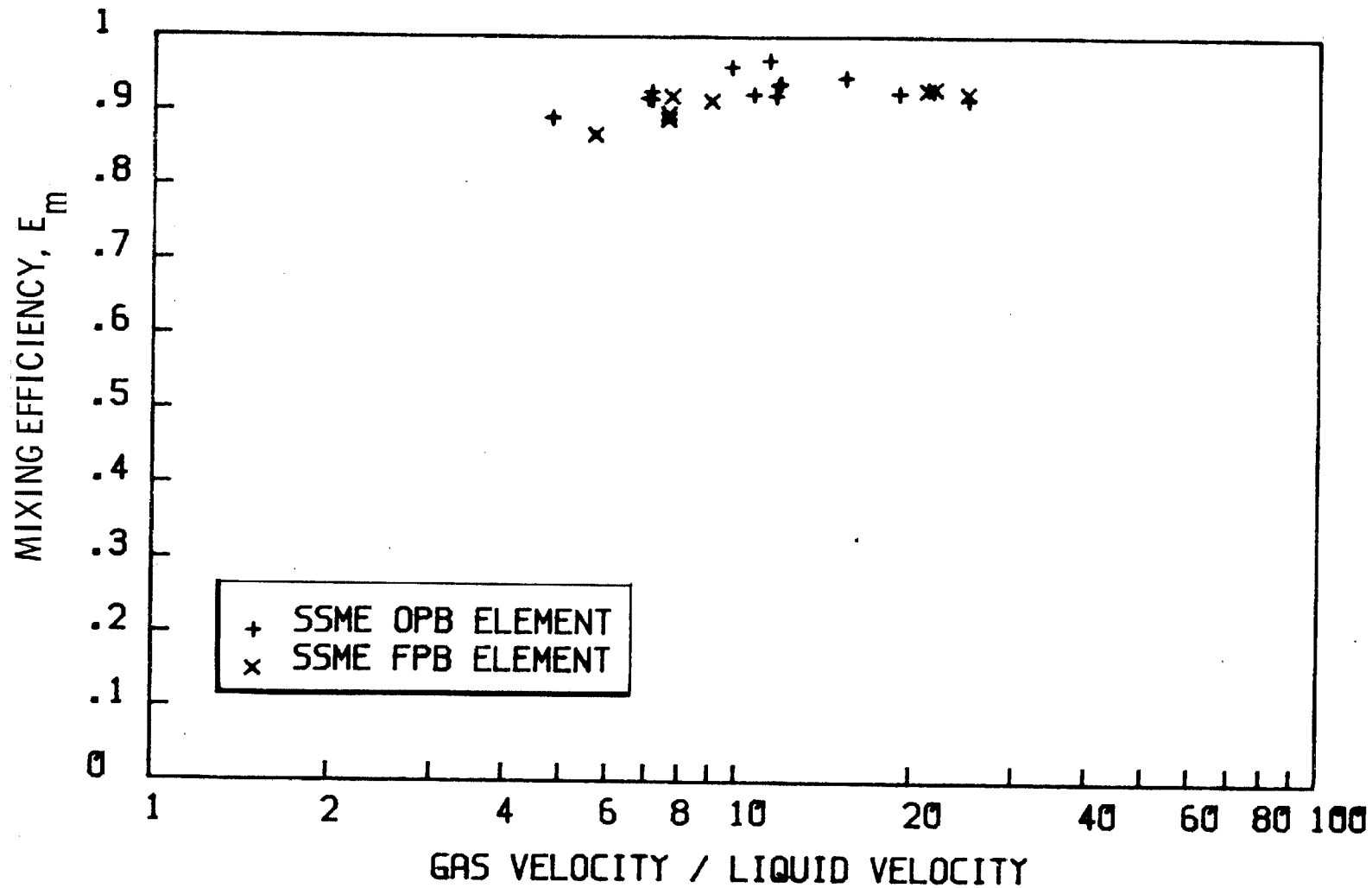
Figure 27. Mixing Efficiency for Coaxial Elements (IL PT 73-30)
Depicting Velocity Ratio Influence

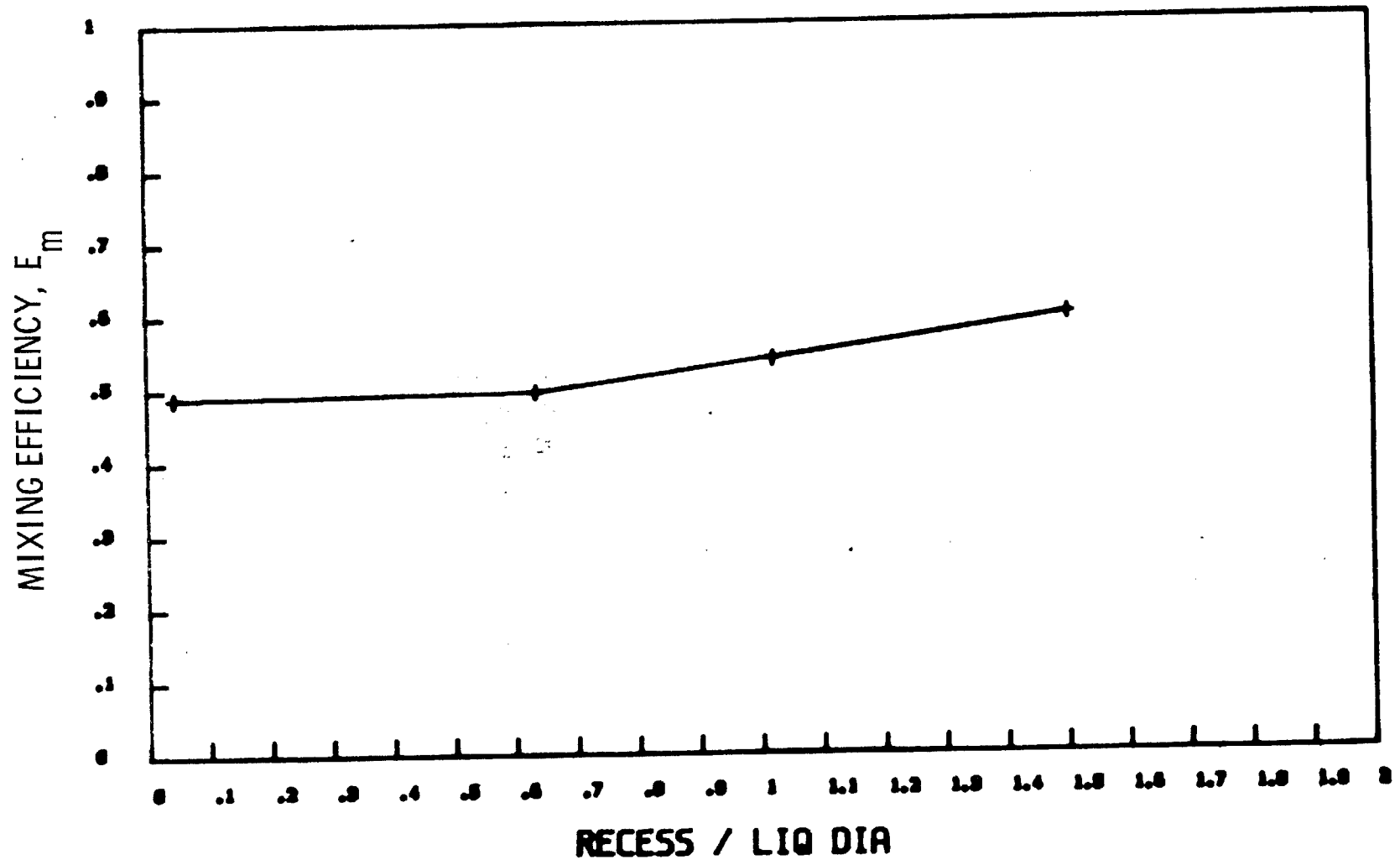Figure 28. Mixing Efficiency for Coaxial Elements (IL PT 73-37) Depicting Velocity Ratio Influence
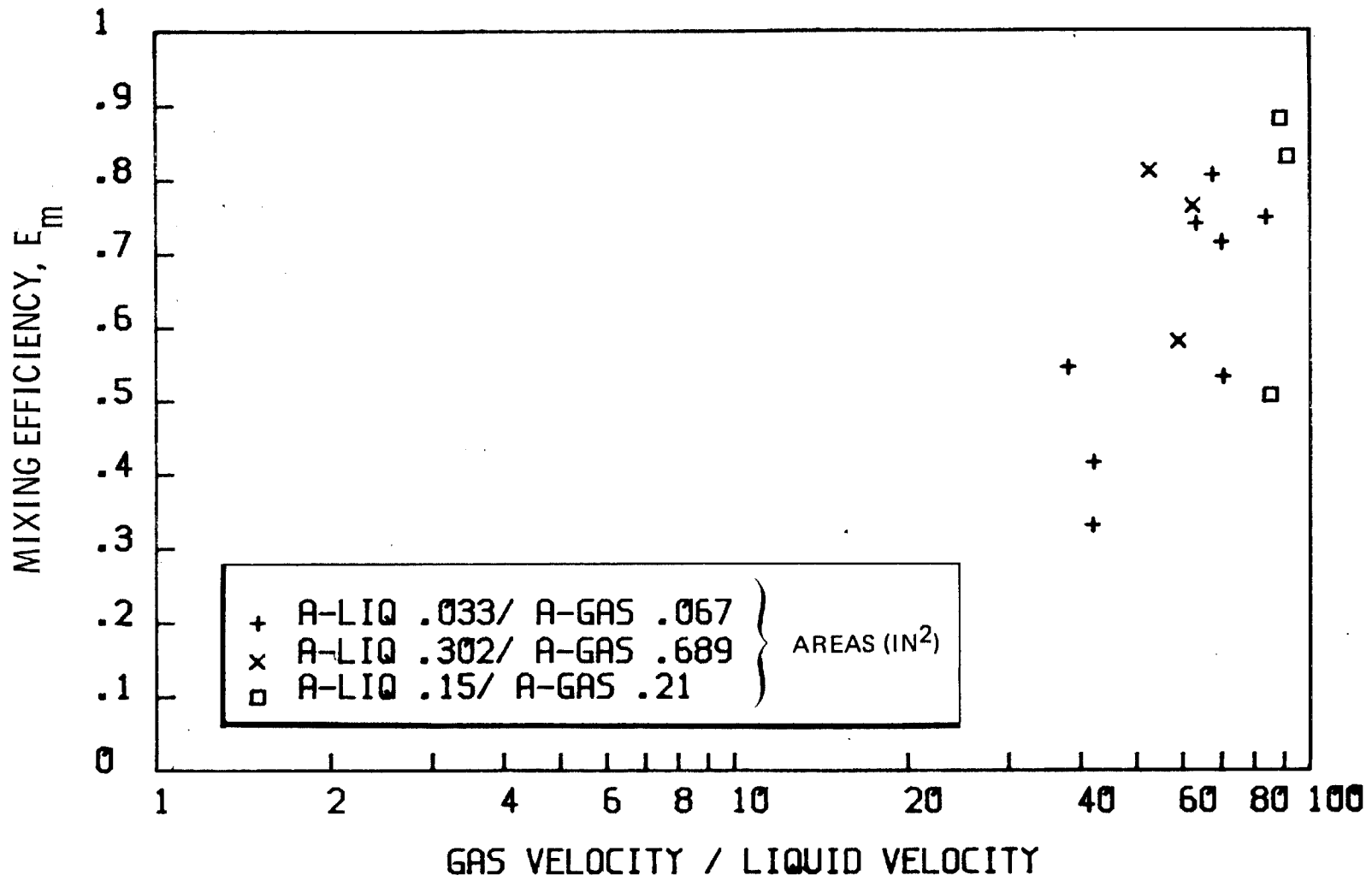
Figure 29. Mixing Efficiency for Coaxial Elements
(NASA CR-72703 R-8361) Depicting
Velocity Ratio Influence

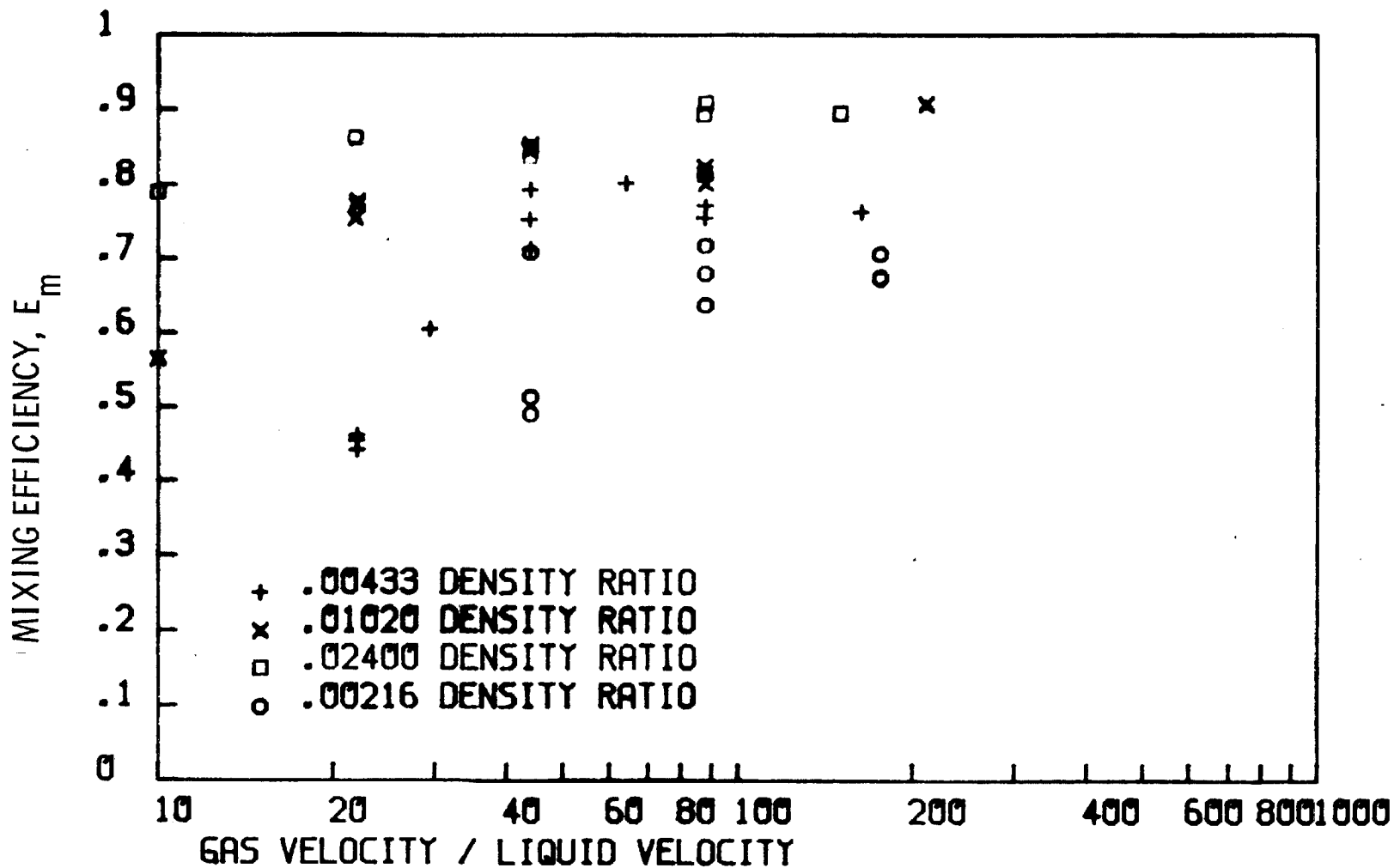# COAXIAL (GAS/LIQ)   NASA CR-R-9270

Figure 30.   Mixing Efficiency for Coaxial Elements
(NASA CR-R-9270) Depicting Velocity
Ratio for Varying Density Ratios

as well, and clearly indicates that higher gas-to-fuel density ratios produce higher mixing efficiencies for a given velocity ratio. This relationship strongly suggests that a velocity-density product, such as momentum ratio, will not peak at an optimum value, but will approach ideal mixing as the gas momentum continuously increases. For this reason, an alternate parameter (Table 5. Eq. 8) has been considered in an effort to characterize the data with a single expression. The coax parameter (Ref. 19) was applied to the SSME preburner and main injector data as shown in Fig. 31 and 32). Because of the high overall mixing efficiency of that data, no predominant trends were evident.

LITERATURE SURVEY CONCLUSIONS AND RECOMMENDATIONS

As a result of the literature review and data examination, most of the initial impressions regarding the state of the cold flow data have been confirmed. Large discrepancies exist in test results noted between the various experimenters, and there does not appear to be any proven correlating parameters for coaxial element mixing efficiency. In general, the available data is insufficient to confidently confirm or establish the optimum value of the correlating parameters for impinging elements.

Although the gas/liquid triplet element has significant potential for future liquid-oxygen/gaseous-hydrocarbon propulsion systems, very little quantitative data exists to either support design calculations or provide correlating expressions for combustion modeling. Most hydrocarbons considered for advanced booster applications will be delivered to the injectors as warm or hot gas with densities relatively high as compared to hydrogen or combustion gases used in current concentric element injectors. This higher density favors impinging elements rather than the concentric element. The gas annulus gap required for the denser fuels in a coaxial element injector may approach small absolute values that ultimately result in poor concentricity and element contamination problems. Greater emphasis should be placed on obtaining mixing data on gas/liquid impinging (especially triplet) elements.
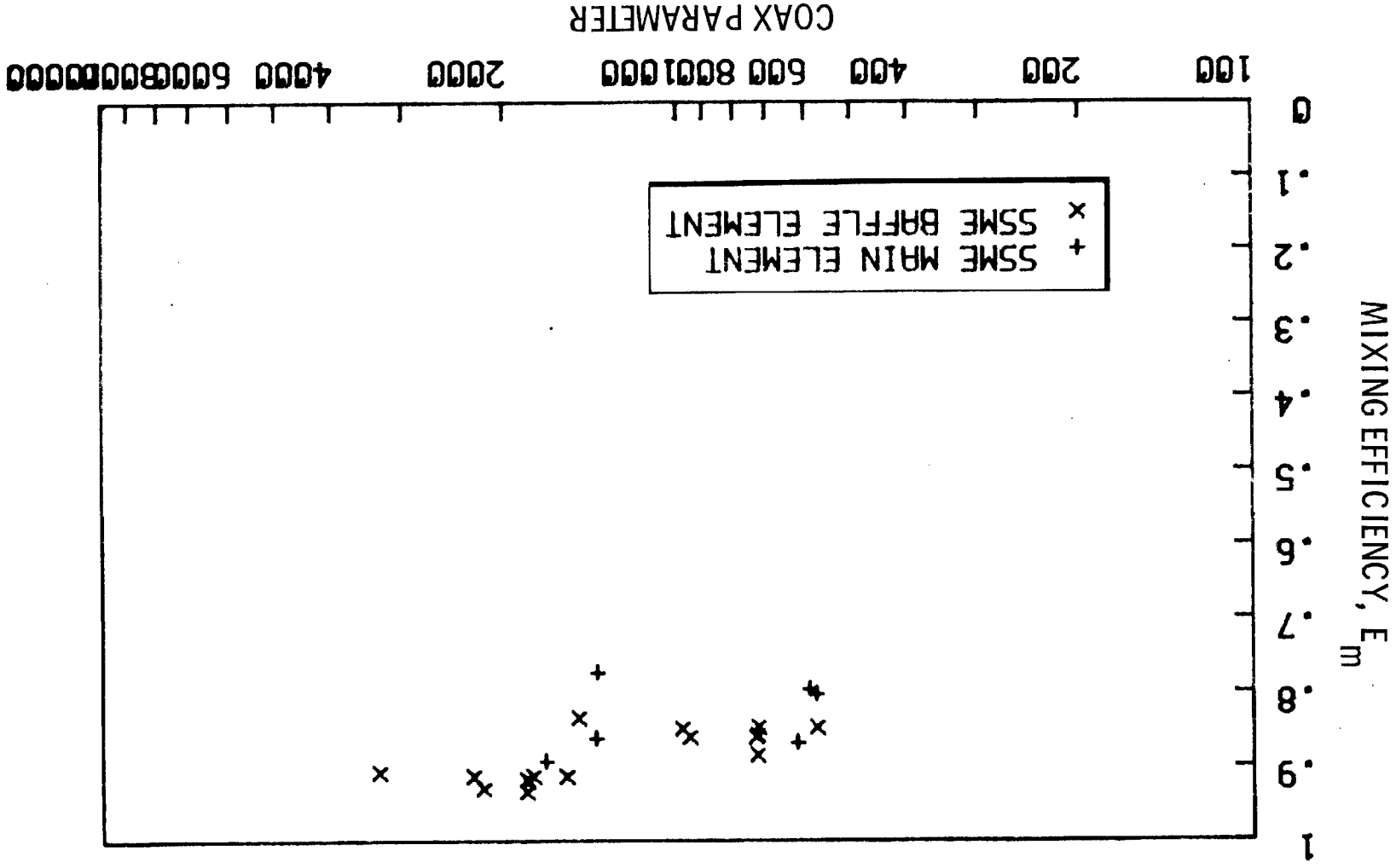
Figure 31. Mixing Efficiency for Coaxial Elements (IL PT 73-37) Depicting Falk and Burick Parameter Influence

RI/RD85-312
A-101
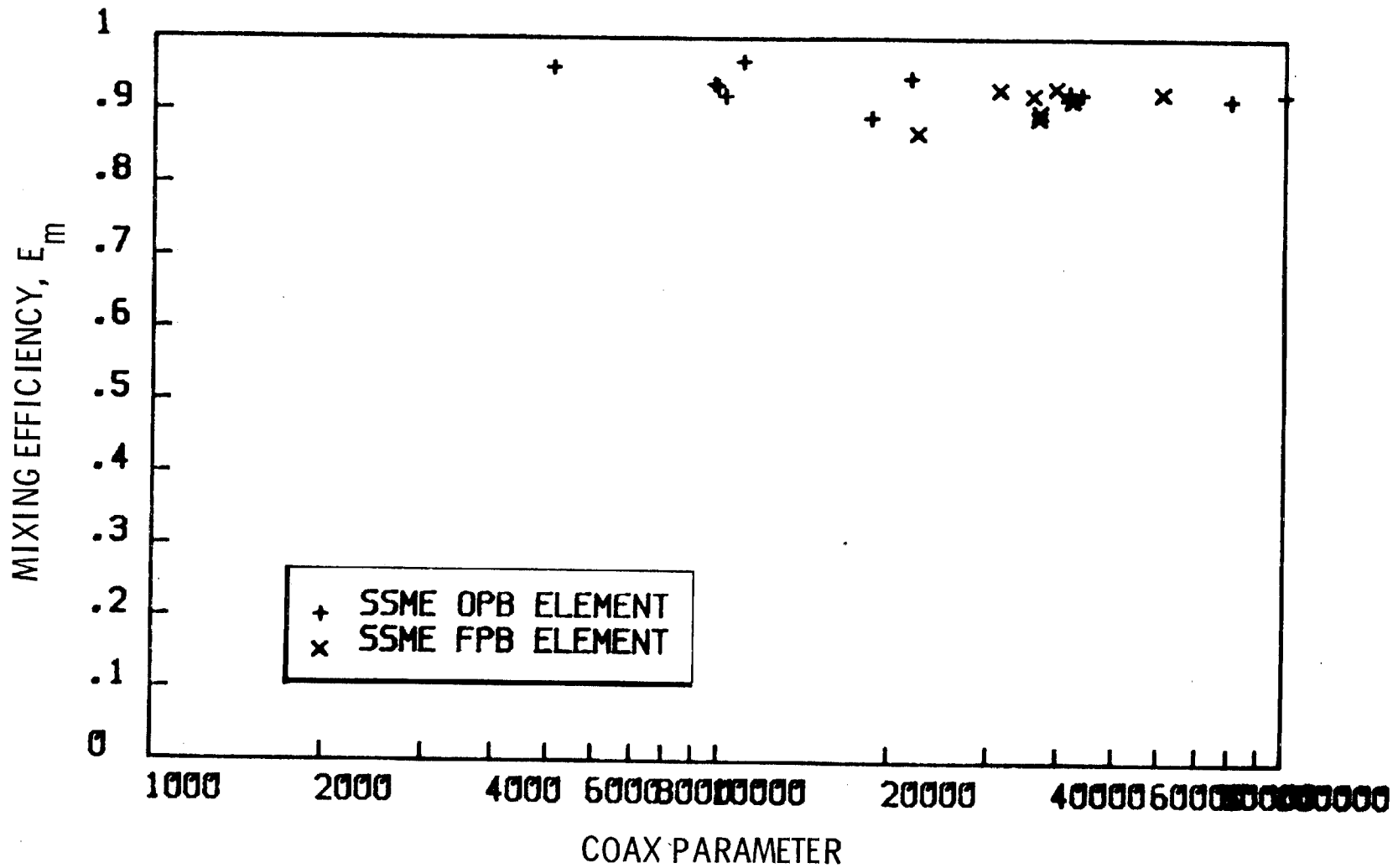
Figure 32. Mixing Efficiency for Coaxial Elements (IL PT 73-30)
Depicting Falk and Burick Parameter Influence

REFERENCES

1. Murthy, S.N.B.: "Turbulent Mixing In Nonreactive and Reactive Flows," Plenum Purdue University, W. Lafayette, IN, 1974

2. Evans, David D., Howard B. Stanford, Robert W. Riebling: "The Effect of Injector-Element Scale on the Mixing and Combustion of Nitrogen Tetroxide - Hydrazine Propellants," (Technical Report 32-1178), Jet Propulsion Laboratory, California Institute of Technology, Pasadena, CA, 1 November 1967

3. Dickerson, R., K. Tate, N. Barsk: "Correlation of Spray Injector Parameters with Rocket Engine Performance," Rocketdyne, Canoga Park, CA, June 1968

4. Study of Droplet Effects on Steady-State Combustion (AFRPL-TR-66-152-VOL 1), Volume 1: Measured Spray Parameter Analysis and Performance Correlation, Rocketdyne, Canoga Park, CA, August 1966

5. Cheung, T.T., V. W. Jaqua: Cold Flow Investigation of Unlike Triplet Elements for Liquid Oxygen/Liquid Hydrocarbon Injectors (ITUR 80-9), 8 February 1980

6. Joshi, P., A. Jakubowski, J. Schetz: Effect of Injector Geometry on Penetration, Spread, and Structure of a Liquid Jet Injected Normal to a Supersonic Air Stream, Virginia Polytechnic Institute, September 1973

7. McHale, R. M.: Noncircular Orifice Holes and Advanced Fabrication Techniques for Liquid Rocket Injectors (NASA CR-R-9270), Rocketdyne, Canoga Park, CA, May 1974

8. Riebling, Robert W.: "Effect of Orifice Length-to-Diameter Ratio on Mixing in the Spray From a Pair of Unlike Impinging Jets," Journal of Spacecraft and Rockets Volume 7, No. 7, JPL, Pasadena, CA, July 1970

9. Riebling, Robert W.: "Criteria for Optimum Propellant Mixing in Impinging - Jet Injection Elements," Journal of Spacecraft and Rockets, Volume 4, No. 6, JPL, Pasadena, CA, June 1967

10. McFarland, B. L., V. Jaqua: Space Storable Thruster Investigation (NASA CR-7287, R-8415), Rocketdyne, Canoga Park, CA, 10 November 1971

11. Nagai, C. K., R. N. Gurnitz, S. D. Clapp: Cold Flow Optimization of Gaseous Oxygen/Gaseous Hydrogen Injectors for the Space Shuttle APS Thruster AIAA/SAE 7th Propulsion Joint Specialist Conference, Rocketdyne, Canoga Park, CA, June 1971

12. Hinde, P. T.: Basic Aspects of Gas - Mixing and Kinetics in Rocket Engine Combustion Chambers, Rocket Propulsion Establishment, Ministry of Technology, London, February 1979

13. Falk, A.Y.: Cold Flow Mixing Characteristics of the SSME Main and Baffle Elements, Rocketdyne Report No. PT73-37, Canoga Park, CA, 14 February 1974

14. Paster, R. D.: Hydrogen - Oxygen APS Engines, Volume II: Low Pressure Thruster (NASA CR-120806, R-8837-2), Rocketdyne, Canoga Park, CA, February 1973

15. Nurick, W. H., R. M. McHale: Noncircular Orifice Holes and Advanced Fabrication Techniques for Liquid Rocket Injectors (NASA CR-108570, R-8224), Rocketdyne, Canoga Park, CA, 15 September 1970

16. Yost, M.: Preburner of Staged Combustion Rocket Engine, Rocketdyne, Canoga Park, CA, February 1978

17. Gill, G. S.: A Qualitative Technique for Concentric Tube Element Optimization, Utilizing the Factor (Dynamic Head Ratio - 1), Societe Europeenne de Propulsion, Vernon, France, January 1978

18. Dykema, Owen W.: Liquid Mixing of an Impinging Jet Using Immiscible Liquids (R.R. 60-28), Rocketdyne, Canoga Park, CA, 30 November 1960

19. Falk, A. Y., R. J. Burick: Injector Design Guidelines for Gas/Liquid Propellant Systems (NASA CR-120968, R-8973-3), Rocketdyne, Canoga Park, CA, May 1973

20. Buschulte, W.: Propellant Mixing By Injectors and its Efficiency Effect, 26th German Federal Republic, International Astronautical Congress of the International Astronautical Federation, 12 November 1975

21. Falk, A. Y.: Coaxial Spray Atomization in Accelerating Gas Stream (NASA CR-134825, R-9753), Rocketdyne, Canoga Park, CA, June 1975

22. Hoehn, F. W., J. H. Rupe, J. G. Sotter: Liquid-Phase Mixing of Bipropellant Doublets (Technical Report 32-1546), 15 February 1972

23. Trotter, C.: Swirling Hydrogen Jet Mixing With a Coaxial Airstream, Department of Chemical Engineering and Fuel Technology, Sheffield, England, August 1970

24. Nurick, W. H.: "Analysis of Sprays from Rocket Engine Injectors," Journal of Spacecraft and Rockets, Volume 8, No. 7, Rocketdyne, Canoga Park, CA, July 1971

25. Burick, R. J.: "Atomization and Mixing Characteristics of Gas/Liquid Coaxial Injector Elements," Journal of Spacecraft and Rockets, Volume 9, No. 5, Rocketdyne, Canoga Park, CA, May 1972

26. Fricke, Hans D., Charles J. Schorr: "Measurement of Gaseous Mixing Down-stream of Coaxial And Adjacent Orifices," Journal of Spacecraft and Rockets, Volume 9, No. 8, Bell Aerospace Company, Buffalo, NY, August 1972

27. Falk, A. Y.: Space Storable Propellant Performance Gas/Liquid Like-Doublet Injector Characterization (NASA CR-120935, R-8973-1), Rocketdyne, Canoga Park, CA, October 1972

28. Analysis of Rocket Engine Injection/Combustion Processes Technical Proposal R-9668P-1, Advanced Programs, Rocketdyne, Canoga Park, CA, 5 March 1975

29. Mehegan, P. F.: Two-Stage Bipropellant Injection System Studies (NASA CR-72303, R-7199), Rocketdyne, Canoga Park, CA, 30 August 1967

30. Jaqua, V., T. Yu: Coal Combustion For MHD Cold Flow Mixing Studies (ITR-76-011-C), Rocketdyne, Canoga Park, CA, 17 January 1977

31. Mehegan, Campbell, Scheverman: Investigation of Gas-Augmented Injectors (NASA CR-72703 R-8361), Rocketdyne, Canoga Park, CA, September 1970

32. Huebner, A. W.: High-Pressure LOX/Hydrocarbon Preburners and Gas Generators, (Final Report) Contract NAS8-332431, Rocketdyne, Canoga Park, CA, April 1981

33. Wheeler, D., and F. Kirby: High-Pressure LOX/Methane Injector Program (RI/RD79-278) Contract NAS8-33206

34. Nurick, W. H.: "Experimental Investigation of Combustor Effects on Rocket Thruster Chamber Performance," (RI/RD 9315), September 1973

APPENDIX B

BASIC ATOMIZATION LITERATURE REVIEW

INTRODUCTION

Available information on liquid atomization by rocket engine-type injection elements was summarized in Appendix A, in which the literature on atomization by like-doublet, triplet, pentad, and coaxial injection elements was summarized, discussed, and assessed. The general conclusions of that summnary were that reported atomization data are largely empirical and ad hoc, only qualitatively understood, and of little general validity or utility.

Part II of the review, reported herein, covers the literature on the more basic or theoretical aspects of liquid atomization. This effort is primarily directed toward studies related to droplet deformation, drag, and breakup, as these processes tend to influence the ultimate size and motion of droplets and are of great importance in efforts to model sprays. Some of the more basic and general atomization studies for airblast atomizers are also included. The discussions of droplet distribution functions, definitions of average droplet diameters in sprays, droplet-size measurement techniques, and problems of spatial versus temporal droplet distributions which are presented in Appendix A of this atomization literature review (Ref. B-22, also see Ref. B-89) are, of course, equally applicable to this airblast atomizer research.

The importance of the atomization process, particularly in combustion applications, has resulted in the publication of hundreds of papers and reviews concerned with various aspects of this subject. A selection of these studies, representing classical and current procedures, results, and theories related to liquid atomization, are briefly summarized in this report. This summary, together with that in Ref. B-22, provide a complete description of the state of the art of atomization as it applies to liquid rocket engines. It should serve as a useful reference to those familiar with this area and as a basic introduction for those entering this field of study.

DISCUSSION

Conversion of a volume of liquid to a spray of droplets can be accomplished by a variety of methods, most of which function by the imposition of a high relative velocity between the liquid and its surrounding gas. In "pressure" atomizers, a high-velocity jet of liquid is discharged through an orifice into a low-velocity gas; in "airblast" atomizers, a low-velocity liquid is exposed to a high-velocity gas stream. Various mechanical means (e.g., impingement of two or more liquid jets on each other, impingement of a jet on a solid surface, or added swirl to the liquid and/or gas) are frequently employed to augment or enhance the rate or extent of atomization.

This review will be concerned primarily with the breakup of the large drops initially formed in the atomization process. The discussion will be presented in terms of four interrelated aspects of the process:

1. Criteria and requisite time for breakup of liquid drops
2. Drop deformation and drag coefficient as functions of time
3. Sizes of droplets formed in breakup of large drops
4. Effects of system parameters on the atomization process

Criteria and Requisite Time for Breakup of Liquid Drops

If a large liquid drop is exposed to a gas whose relative velocity is sufficiently high to overcome the restoring force of its surface tension, the drop will disintegrate into a cloud of daughter droplets (secondary breakup). Two basically different modes of drop breakup have been observed, the "bag" type and the "shear" (or "stripping") type; these are described in the section of this report entitled "Droplet Deformation and Drag Coefficient".

Early Drop Breakup Studies

General reviews of the early work (to about 1965) on liquid particle breakup in gas streams have been published by Forsnes (Ref. B-24), Lapple et al (Ref. B-57), and Luna (Ref. B-61).

A theoretical analysis of drop breakup was presented by Hinze (Ref. B-37). He described the deformation of a liquid sphere caused by the normal pressure distribution resulting from a flow of gas over its surface. Closed-form solutions of the linearized hydrodynamic equations were obtained for very high and very low liquid viscosity. Hinze also postulated the existence of a critical Weber number as a criterion for drop breakup (Ref. B-36):

$$We = \rho_G \, d_L \, \overline{\Delta V}^2 / \sigma_L \tag{B-1}$$

Where ρ_G is the gas density, d_L is the original drop diameter, $\overline{\Delta V}$ is the relative gas/liquid velocity, and σ_L is the surface tension. An analytical derivation of a criterion for the critical breakup condition of drops of low and high viscosity exposed to a gradually increasing gas flow and for high-viscosity drops suddenly exposed to a constant-velocity gas flow gave:

$$(\delta/r)_{max} = 0.095 \, (We)_{max} \tag{B-2}$$

where δ is the radial deformation of the drop and r is the original drop radius. For low-viscosity drops suddenly exposed to a constant-velocity gas flow,

$$(\delta/r)_{max} = 0.17 \, (We)_{max} \tag{B-3}$$

The analysis also yielded equations for the breakup time of drops suddenly exposed to a constant flow:

$$t_b \approx 1.15 \frac{r}{\overline{\Delta V}} \left[\frac{\rho_L}{\rho_G} \left(\frac{\delta}{r} \right)_{max} \right]^{0.5} \quad \text{(low viscosity)} \tag{B-4}$$

$$t_b \approx 10 \frac{\mu_L}{\rho_G \, \overline{\Delta V}^2} \left(\frac{\delta}{r} \right)_{max} \quad \text{(high viscosity)} \tag{B-5}$$

where ρ_L and μ_L are the liquid density and viscosity, respectively.

The limited experimental data then available for the case of gradually increasing gas velocity (Ref. B-66) indicated the following approximate values:

$$(\delta/r)_{crit} \simeq 1 \quad (We)_{crit} \simeq 10 \quad \text{(low viscosity)}$$

$$(\delta/r)_{crit} \simeq 2 \quad (We)_{crit} \simeq 20 \quad \text{(high viscosity)}$$

The difference between the two cases was ascribed to the extra time delay in drop deformation resulting from high viscosity, which gives the drop time to accelerate and thus lowers the relative velocity below the critical value.

Note that for low viscosity liquids, Eq. B-4 reduces to

$$t_b \simeq (d_L/2 \ \overline{\Delta V}) \ (\rho_L/\rho_G)^{0.5} \tag{B-6}$$

This is the form used by subsequent investigators, although some experimental values were up to ten times longer than predicted (Ref. B-13 and B-71).

Taylor (Ref. B-90) presented a crude boundary layer analysis of the shear breakup mode. Boundary layer stripping results from tangential friction, which was not considered by Hinze (Ref. B-36), who assumed zero tangential stress. Taylor solved for the boundary layers of both gas and liquid, assuming two-dimensional uniform flow, and obtained the velocity profiles of both fluids. The rate of loss of liquid from a drop by tangential drag is given by:

$$\frac{dV}{dt} = -K \ \pi \ d^2 \left[\frac{\overline{\Delta V} \ \nu_L}{2b} \right] \tag{B-7}$$

where V is the drop volume (or mass), K is a constant on the order of unity, d is the drop diameter, ν_L is the liquid kinematic viscosity, and b is the boundary layer thickness.

From experimental data, Taylor established a value of 2.7 for the critical Weber number in steady, long-duration gas flow, where the Weber number was defined as

$$We = \rho_g \, r \, \overline{\Delta V}^2 / 2 \, \sigma_L \tag{B-8}$$

He also pointed out that the relative velocity required for drop breakup in transient gas flow is different from that in steady flow, and that

$$\frac{(We)_{crit - transient \, flow}}{(We)_{crit - steady \, flow}} = \frac{1}{\sqrt{2}} \tag{B-9}$$

as long as the drop oscillation period ($0.258 \, r^{1.5}$ for water) does not exceed approximately two times the gas flow duration.

Lane (Ref. B-56) studied the breakup of water drops in transient and steady streams of air. In steady flow, bag mode breakup was observed, with the following correlation of the experimental data for the critical condition:

$$\overline{\Delta V}^2_{crit} \, d = K \approx 612 \tag{B-10}$$

A theoretical analysis of the steady-flow case, treating the critical condition as the point at which the drag force equals the surface tension, gave an expression for the drag coefficient:

$$C_D = (16 \, \sigma_L)/(D \, \rho_G \, \overline{\Delta V}^2) \tag{B-11}$$

With an assumed drag coefficient of 0.4, the value of K in Eq. B-10 was about 1200, twice the experimental value. The difference was ascribed to deformation of the drop into a nonspherical shape before breakup. Lane observed that about 70% of the original mass of a drop undergoing bag mode breakup was in the heavy rim; after the bag burst into a mist, the rim broke into larger droplets.

Lane observed shear mode breakup in transient flow tests and concluded that this was a combination of boundary layer stripping and the cresting of capillary waves formed on the drop surface. He found that Taylor's estimate of the ratio of critical velocities in transient and steady flow was fairly accurate. Lane also concluded that the daughter droplet mass mean diameter (MMD) decreased with increasing gas velocity, but only up to a limiting velocity, beyond which no further decrease occurred. The lower limit of the MMD was about 15 microns. Another observation was that since the disintegrating drop accelerates and decreases the relative velocity, the latter stages of breakup should produce larger droplets.

Following Lane's work, Hinze (Ref. B-38) modified his original Weber number criterion for drop breakup by including the effect of viscosity:

$$(We)_{crit} = C [1 + \alpha N_{vi}] \tag{B-12}$$

where C is We_{crit} for negligible-viscosity liquids, α is a function of viscosity and

$$N_{vi} = \mu_L/(\rho_G \sigma_L d)^{0.5} \tag{B-13}$$

The critical Weber number was not only dependent on liquid viscosity but also on the time-variation of the relative gas/liquid velocity. It was smaller for a suddenly applied gas velocity and larger for higher viscosity liquids. Experimental data with low-viscosity liquids gave a critical Weber number of approximately 13 for the transient case and about 22 for steady gas flow.

Gordon (Ref. B-30) supplemented the investigations of Hinze by considering the cases of intermediate drop viscosity and surface tension. For bag-type drop breakup, he derived a theoretically based critical diameter:

$$d_{crit} = \frac{160}{\rho_G \overline{\Delta V}^2} \tag{B-14}$$

For drops larger than the critical size and with negligible velocity, the breakup time for drops with low viscosity and surface tension is given by

$$t_b = \frac{2\ d_{crit}}{\overline{\Delta V}} \left(\frac{\rho_L}{\rho_G}\right)^{0.5}$$ (B-15)

For drops with higher viscosity and low surface tension

$$t_b = \frac{32\ \mu_L}{\rho_G\ \overline{\Delta V}^2}$$ (B-16)

the indicated independence of breakup time and drop diameter is probably unreal, but comparison with then-available data showed that the estimated breakup times were off by less than a factor of 2.

Morrell (Ref. B-67) postulated that the breakup mode is controlled by the action time (flow duration) of the gas flow on the drop. If the action time is greater than the natural period of the drop, the drop disintegrates by the bag mode. When the action time is less than the oscillation period, the shear mode occurs. From the results of experiments on the breakup of a liquid jet by a transverse shock wave, Morrell later concluded (Ref. B-68) that the flow duration merely affects the extent of drop breakup.

Shock Tube Studies of Drop Breakup

Shock tubes provide a convenient method for studying the atomization of single drops in a stream of high velocity gas. The drop, suspended from a thin wire or released from a support and allowed to hang free, is exposed to a shock wave, whose intensity controls the gas properties in its wake. High-speed motion pictures of the subsequent atomization permit close examination of the details of the process.

Such studies were carried out by a number of investigators. Their results indicate that the influence of the incident shock, the internal motion of the liquid, and the increased vaporization caused by the temperature increase across the shock are negligible and that the only effect of the shock is to induce a high relative liquid/gas velocity in its wake. With these conditions, dimensional analysis shows that the drop breakup time is a function of the Weber, Reynolds, and Mach numbers and the gas/liquid density and viscosity ratios. The actual functional relationships must be determined experimentally and are independent of the particular cause of the relative gas/liquid velocity.

Hanson et al (Ref. B-33) studied the aerodynamic shattering of drops in a shock tube, over a wide range of liquid viscosity. In contrast with the finding of Lane (Ref. B-56), they observed bag mode breakup with transient gas flow, providing evidence that the breakup mode is not a function of the type of flow, steady or transient. Hanson et al also found that the bag mode occurred near the critical breakup velocity, and the stripping mode occurred at higher velocities. A transitional mode was also reported (the "bag-stamen" mode), in which the bag develops a re-entrant portion resembling the stamen of a flower. The "stamen" increases in length and stands alone as the rim and the remaining portion of the bag blow downstream and disintegrate. The authors suggest that Lane's expression for the critical breakup condition (Eq. B-10) has the correct form

$$\overline{\Delta V}^m_{crit} \, d = K \tag{B-17}$$

but that the values of the constants m and K must be experimentally determined for particular liquids and flow conditions. The effect of viscosity on the critical breakup velocity was found to be negligible for viscosities less than approximately 10 centistokes; above 10 centistokes, increasing viscosity (at constant drop diameter) raises the critical velocity.

For water, the critical Weber number ranged from 3.6 (D = 600µ, $\overline{\Delta V}_c$ = 84 ft/sec) to 6.6 (D = 120µ, $\overline{\Delta V}_c$ = 239 ft/sec); for methanol, the range was 6.0 (D = 625µ, $\overline{\Delta V}_c$ = 60 ft/sec) to 8.4 (D = 118µ, $\overline{\Delta V}_c$ = 157 ft/sec).

Viscous liquids required higher critical Weber numbers for drop breakup. At Weber numbers slightly greater than critical, the drops disintegrated in the bag mode, in which surface tension is important. For Weber numbers substantially greater than critical, shear-type breakup, in which surface tension is not important, was observed. The experimental data also indicated that the critical Weber number was not constant for liquids of about the same viscosity. Instead, it varied inversely with drop diameter.

With the product of Weber and Reynolds numbers as correlating factor, the critical velocity was expressed by

$$(We\ Re)_{crit} = \frac{\rho_G\ d^2}{2\ \sigma\ \nu_G}\ \overline{\Delta V}^3_{crit} \tag{B-18}$$

whence, if ρ_G, σ, and ν_G are constant

$$\overline{\Delta V}_{crit} \propto \sigma^{1/3} \tag{B-19}$$

which fit the test data.

Engel (Ref. B-21) studied the shear mode breakup of water drops in a shock tube and gave detailed descriptions of her observations. However, the only variables used were drop size and shock strength; liquid properties were not changed.

Rabin and Lawhead (Ref. B-78) observed both bag and shear-type breakup of burning and nonburning drops of fuel in shock tubes. The breakup mechanism and the critical velocity were dependent on the duration and velocity of the flow plateau following the shock front. Their photographs showed that shear-type breakup always occurred at gas velocities considerably higher than critical and that the drops were shattered by the flow behind the shock wave, not by the shock front itself.

A later report by these authors (Ref. B-79) summarized their experimental study of the breakup of fuel drops by weak shock waves. Duration of the gas flow behind the shock wave was varied by changing the length of the pressure section in the shock tube. Effects of gas flow velocity and duration, chamber pressure, and liquid surface tension on the shattering of burning and nonburning drops were investigated.

The solenoidal retraction of the wire upon which the drop was suspended usually resulted in the formation of a "primary" drop (500 to 1600 micron diameter) and a "satellite" drop (50 to 300 micron diameter). Usually, the larger drops exhibited shear breakup, while the smaller drops exhibited bag breakup, at the same gas velocity and flow duration. It was again verified that the drop was not shattered by passage of the shock front; it was the flow that followed which caused the breakup. Although no theoretical explanation of the choice of breakup mode was presented, it was confirmed that gas velocities much higher than critical always resulted in shear breakup. The critical velocities in these experiments were comparatively low (60 to 100 ft/sec at one atmosphere; 10 to 15 ft/sec at 34 atmospheres). Flow durations were 1.0 to 2.5 msec.

At atmospheric pressure, both types of drop breakup were observed; at elevated pressures, only the shear mode occurred. No significant differences in breakup characteristics were seen between burning and nonburning drops, aside from a slightly lower critical velocity for burning than for nonburning because of lower surface tension in the former.

The test data could not be correlated in terms of the drop Weber number alone. Instead, it was postulated that shear breakup (which is more pertinent than the bag mode in rocket engine combustor applications) occurs when the tangential component of the aerodynamic forces on the drop is greater than the surface tension forces and

$$(We) \ (Re)^{-0.5} = C \qquad \qquad (B-20)$$

The value of C for nonburning drops was found to be 0.5. For burning drops, the C value was not constant, probably because of the unknown surface tension.

Shock tube photographic studies of 1800-micron RP-1 drops in shear breakup were made by Rojec (Ref. B-85). After exposure of a drop to high velocity gas, no changes were observed for 20 to 100 microseconds. At that time, small ripples, or capillary waves, appeared on the drop surface, with wavelength inversely proportional to the gas velocity, and the downstream side of the drop was deformed into a truncated cone. The surface waves increased in amplitude with time until ligaments and droplets began to be shed. This shedding of daughter droplets began from about 40 microseconds after exposure to the gas flow (at a velocity of 1250 ft/sec)to about 115 microseconds after exposure (at 320 ft/sec).

The time required for complete breakup of the parent drops could not be determined directly because they broke off from their supports and were carried out of the field of view. However, by extrapolation of the available data, the time for complete breakup could be estimated: at V_G = 200 ft/sec, t_b = 800 microseconds; at V_G = 500 ft/sec, t_b = 500 microseconds.

This photographic evidence supports the assumption that shear mode atomization by a high-velocity gas stream proceeds by the growth, cresting, and disintegration of capillary surface waves. These capillary waves are characterized by very small wavelengths, on the order of 100 microns, which result in small-radius surface curvatures. Since the pressure exerted by surface tension forces is inversely proportional to the radius of curvature, the liquid-gas interfacial surface tension is important in the analysis of capillary wave dynamics.

An analysis for the case of plane liquid surfaces (Ref. B-64 and -65) derived an expression for the mean diameter of the generated droplets. It was postulated that when a capillary wave reaches its critical amplitude, it erodes to form a ligament, from which droplets of a diameter proportional to the wave length (λ) are formed:

$$d = F\lambda \tag{B-21}$$

where the dimensionless parameter F was assumed to be independent of λ and was found to be nearly independent of the fluid characteristics.

A similar analysis for drop atomization would be excessively complicated because of surface curvature, divergent propagation of capillary waves from the forward stagnation point, and the magnitude of the deformation that occurs when liquid drops are subjected to high velocity gas flows. However, an experimental study was conducted of the rate of mass loss from liquid drops subjected to a high relative gas velocity (Ref. B-15 and -16). A shock tube was employed, in conjunction with high-speed motion pictures from streak and framing cameras. The liquid was RP-1 (1400-micron drops) and the driver gas was nitrogen. Analysis of the streak data gave the mass loss history of the drops and the diameters of the product droplets. The correlating expression was

$$\dot{m} = 3.53 \times 10^{-5} \left(\frac{S_d \, \mu_L}{d} \right) \left(\frac{d \, \overline{\Delta V} \, \sqrt{\rho_G \rho_L}}{\mu_L} \right)^{2.8} \left(\frac{\rho_G \, \overline{\Delta V}^2 \, d}{\sigma} \right)^{-0.42} \tag{B-22}$$

where m is the mass loss rate of the drop and S_d is the surface area of a sphere with equivalent mass. Equation B-22 applies only to a quasi-steady-state process.

The atomization rate of a drop is zero from the instant of drop exposure to the gas flow until the capillary waves reach sufficient amplitude to crest. It is therefore important to define the "drop breakup time" as the time elapsed before the drop begins to disintegrate, the time required for the disintegration itself, or the sum of these. Most published reports are ambiguous in this regard, which increases the difficulty of comparing different results.

Buzukov (Ref. B-5) investigated drop breakup in a shock tube. A dimensional analysis using the Navier-Stokes equation without viscous effects gave the breakup time of a drop as

$$t_b = K \frac{d}{\overline{\Delta V}} \left(\frac{\rho_L}{\rho_G} \right)^{0.5} \tag{B-23}$$

which is identical in form to Eq. B-6 and B-15, derived by Hinze (Ref. B-36) and Gordon (Ref. B-30). Buzukov also observed bag mode breakup near the critical velocity and shear mode at higher velocities. He concluded that the Weber number was the controlling parameter and that the breakup of capillary wave crests was the basic mechanism of the shear mode.

Several other shock tube investigations (Ref. B-21, -50, -79, -80, -85, and -97) have indicated the same relation for drop breakup time in the shear mode as Eq. B-23:

$$t_b \sim \frac{d}{\overline{\Delta V}} \left(\frac{\rho_L}{\rho_G}\right)^{0.5} \quad \text{or} \quad t_b \sim d \left(\frac{\rho_L}{q}\right)^{0.5} \tag{B-24}$$

where q is the dynamic pressure. Defining β as the gas/liquid density ratio and τ_b as a dimensionless droplet breakup time, $[\overline{\Delta V} \, t_b/d]$, then

$$T_b \equiv \tau_b \sqrt{\beta} = \text{constant} \tag{B-25}$$

This equation shows that the Weber number, Reynolds number, and gas/liquid viscosity ratio are of little importance in shear-mode breakup time. Similar results have been obtained for liquid jets (Ref. B-7 and B-69). Reported values of T_b are 3.5 (Ref. B-72), 4.5 (Ref. B-50), and ranging from 4 at low subsonic gas velocity to 5.5 at sonic velocity (Ref. B-80).

Fishburn (Ref. B-23) reported the results of a boundary layer analysis of drop undergoing constant acceleration and deformation in high-velocity gas stream in which $We \gg Re^{0.5}$. He concluded that drops deform and fragment at the same dimensionless time regardless of initial size.

Several approximate theoretical analyses (Ref. B-5, -7, -67, -80, and -97) using varied approaches have led to expressions similar to Eq. B-24. However, an analysis (Ref. B-14) that treated shear breakup as stemming from the generation and shedding of capillary waves did not lead to Eq. B-24 or the expected limiting behavior, but did appear to give some agreement with expermental data.

In a departure from other drop breakup theories, Wolfe and Anderson (Ref. B-97) postulated that the breakup is a rate process. They theorized that the customary analysis, which equates the maximum force tending to break up a drop to the surface tension force, is valid only for small rates of stress loading and not for shock processes nor for situations in which the stress tending to break up the drop undergoes a change in less time than that required for the breakup. Their approach applied kinetic theory to the breakup process, in addition to the hydrodynamic/mechanical aspects.

Aerodynamic pressure drag and aerodynamic friction drag were considered to be the factors responsible for bag and shear drop breakup, respectively. A qualitative theoretical derivation, using rate process theory to relate drop deformation to these aerodynamic forces, gave the following expressions relating drop breakup time to the gas and liquid flow parameters:

$$t_b = \frac{d}{(A^2 + B \, P)^{0.5} - A} \tag{B-26}$$

where

$$A = 16\mu_L / d \, \rho_L$$

$$B = 2/\rho_L$$

$$P = C_D \left(\frac{\rho_L \, \overline{\Delta V}^2}{2}\right) - \frac{k \, \sigma}{d}$$

k = constant (Reflects drop curvature and breakup mode).

For liquids with negligible viscosity and surface tension (and $C_D = 1$), Eq. B-26 becomes

$$t_b = \left(\frac{d}{\overline{\Delta V}}\right) \left(\frac{\rho_L}{\rho_G}\right)^{0.5} \tag{B-27}$$

Again, this is the same relationship, Eq. B-23, as that suggested by many other investigators.

Breakup time in Eq. B-26 and B-27 is the time from inception of the aerodynamic flow around the drop to complete disintegration of the drop. If the frictional drag on a drop is twice the pressure drag, as generally assumed, then the pressure factor in Eq. B-26 becomes

$$P_b = \left(\frac{C_D}{3}\right)\left(\frac{\rho_G \overline{\Delta V}^2}{2}\right) - \frac{K_b \sigma}{d} \tag{B-28}$$

$$P_s = \left(\frac{2 C_D}{3}\right)\left(\frac{\rho_G \overline{\Delta V}^2}{2}\right) - \frac{K_s \sigma}{d} \tag{B-29}$$

for the bag and shear modes, respectively. Constants K_b and K_s reflect the effect of surface tension in each type of breakup. Experimental data indicated that $K_b = 4$ and $K_f = 2$, and that the droplet sizes produced by the bag and shear modes of drop breakup were essentially the same.

From capillary wave theory, Wolfe and Anderson developed the following expression for the mass mean diameter of the droplets resulting from shear mode breakup of a drop:

$$MMD = \left[\frac{136 \, \mu_L \, \sigma^{3/2} \, d^{1/3}}{\rho_G^2 \, \rho_L^{1/2} \, \overline{\Delta V}^4}\right]^{1/3} \tag{B-30}$$

This equation is stated to be valid for cases in which the dynamic pressure forces are much greater than the viscous or surface tension forces. Agreement of their shock tube data with both the breakup time and mean diameter equations was fairly good.

Ranger and Nicholls (Ref. B-80) studied shear-mode droplet break at high Weber numbers in a shock tube. Drop diameters were in the range 750 to 4400 microns. At lower gas velocities, the drop deformed into an ellipsoidal configuration, followed rapidly by stripping of the surface to a micromist.

At high gas velocities, these processes occurred essentially simultaneously. The micromist was observed to follow the gas streamlines, indicating that it was composed of very small droplets.

Ranger and Nicholls derived the same breakup time equation as other investigators (Eq. B-23). Reported values of the constant K in this expression are:

$$K = 0.57 \qquad \text{Hinze (Ref. B-36)}$$
$$K = 2.0 \qquad \text{Gordon (Ref. B-30)}$$
$$K = 0.20 \qquad \text{Ranger \& Nicholls (Ref. B-80)}$$
$$K = 1 \qquad \text{Wolfe \& Anderson (Ref. B-97)}$$
$$K = 1 \qquad \text{Clark (Ref. B-7)}$$
$$K = 1 \qquad \text{Buzukov (Ref. B-5)}$$

The value of the drop drag coefficient was estimated as $C_D \sim 3$, the breakup distance was on the order of 25 drop diameters, and the size of the daughter droplets was estimated to be approximately 10 microns.

A review published in 1967 (Ref. B-61) summarized the state of the art at that time:

1. The best criterion for drop breakup is a critical Weber number, which is a function of liquid viscosity and the variation of gas flow with time (i.e., steady vs. transient).
2. For low-viscosity liquids (Ohnesorge number, $(\mu/\rho\, \sigma\, d)^{0.5} < 1$), the critical Weber number is between 1 and 10. For $Oh > 1$, We_{crit} may go as high as 30.
3. Drop breakup requires sufficient time of exposure to the gas stream, so We_{crit} is a necessary but not sufficient requirement.

4. Near the critical velocity, a bag mode drop breakup occurs. At higher gas velocities, a shear or stripping mode occurs, consisting of boundary layer stripping and cresting and breakup of unstable surface waves. The diameter of the droplets formed is on the order of magnitude of the most unstable wavelength, approximated by:

$$\lambda = \frac{3 \pi \sigma}{\rho_G \overline{\Delta V}^2} \tag{B-31}$$

(For water/air with a relative velocity of 500 ft/sec, this wavelength is 23 microns).

Miscellaneous Studies

Harper et al (Ref. B-34) analyzed an accelerating liquid sphere as a boundary value problem to determine the conditions under which small surface waves would become unstable and grow. The study concluded that a liquid sphere would be subject to surface instability if the product of the bond number and drop acceleration exceeded a critical value:

$$\frac{(\rho_L - \rho_G) \, d^2}{\sigma} \left(\frac{d \, \overline{\Delta V}}{dt} \right) > \gamma \tag{B-32}$$

where (d $\overline{\Delta V}$/dt) is the acceleration of the drop relative to the gas.

Kreczkowski (Ref. B-55), in a recent investigation of drop breakup in a wind tunnel, observed the bag, transition, and stripping modes. He considered the breakup to be controlled by three dimensionless groups: Weber number, Laplace number, and the liquid/gas viscosity ratio, where the Laplace number is:

$$La = \frac{\rho_L \, \sigma \, d}{\mu_L^2} \tag{B-33}$$

The critical Weber number increased with liquid viscosity and the effect of viscosity on breakup time was minimal. Variation in viscosity by a factor of 1000 resulted in a breakup time increase of only a factor of 2.

Volynskiy and Lipatov (Ref. B-91) derived a critical Weber number of 5.4 (Eq. B-1) for the disintegration of a drop of low-viscosity fluid by ellipsoidal deformation at low Reynolds numbers. At high Reynolds numbers, a critical Weber number of 15 tO 22 is suggested by the data of Korsunov and Tishin (Ref. B-54).

The capillary wave analysis by Mayer (Ref. B-64) discussed above, which assumes that waves formed on the liquid surface amplify, crest, and shed ligaments that rapidly disintegrate to droplets, was extended by Adelberg (Ref. B-1 and -2). He postulated a region of high aerodynamic forces, in which the product of the Weber and Reynolds numbers is greater than 10^6, where another type of breakup, called acceleration wave breakup, occurs. This breakup mode occurs when the surface waves are accelerated by the high-velocity gas stream and requires freestream dynamic pressure above about 300 lb/ft^2. The acceleration wave mechanism of jet breakup is probably negligible for subsonic flows (Ref. B-2). Experimental studies of acceleration wave jet breakup are discussed in a subsequent section of this report ("Effect of System Parameters on the Atomization Process").

Williams (Ref. B-96) reviewed earlier studies of fuel jet breakup in subsonic and supersonic gas flows, and described the three mechanisms of jet and drop atomization: shear stripping, capillary wave, and acceleration wave.

Borisov et al (Ref. B-3) presented criteria for drop breakup by several mechanisms. Defining the Weber number as one-half the customary value,

$$We = \frac{\rho_G \overline{\Delta V}^2 d}{2 \sigma} \qquad (B-34)$$

they gave We > 3 as the requirement for drop breakup.

The observed breakup modes included the bag and shear types, as well as intermediate modes, and conformed to the following criteria:

Mode	Criteria

Simple division
Parachute type (bag) $4 \leq We \leq 20$
Chaotic (intermediate) $0.1 \leq We\ Re^{-0.5} \leq 0.8$

In these modes, sizes of the secondary drops were
of the same order of magnitude as the original drop.

Stripping (shear)

Yields mist of fine droplets $10 \leq We \leq 10^4$

$0.5 \leq We\ Re^{-0.5} \leq 10$

Explosive $10^3 \leq We \leq 10^5$

$10 \leq We\ Re^{-0.5} \leq 10^2$

In this high-gas-velocity regime, droplet breakup is related to a Rayleigh-Lamb-Taylor instability and the Bond number ($Bo = \rho_L d^2/\sigma$).

Breakup times were given as follows:

t_1 = time for drop deformation to the critical stage, when shear breakup begins

$$t_1 = \left(\frac{d}{\Delta V}\right) \left(\frac{\rho_L}{\rho_G}\right)^{0.5} \tag{B-35}$$

t_2 = characteristic drop acceleration time = time for ΔV to decrease to one-half its original value

$$t_2 = \frac{4}{3}\left(\frac{\rho_L\, d}{\rho_G\, C_D\, \overline{\Delta V}}\right) \tag{B-36}$$

t_3 = characteristic boundary layer establishment time

$$t_3 = 0.36\left(\frac{d}{\overline{\Delta V}}\right)\left(\frac{\rho_L}{\rho_G}\right)^{0.5} \tag{B-37}$$

t_4 = drop destruction time in the explosive breakup mode

$$t_4 = 10\ \text{We}^{-0.25}\ t_1 \tag{B-38}$$

Craig (Ref. B-10) recently reported the results of an experimental investigation of the aerodynamic breakup of liquid drops (e.g., water, ethanol, and mercury). Holographic and laser velocimetry were used for droplet-size measurements. With original water and ethanol drop sizes in the range of 100 to 600 microns, the observed critical Weber numbers (on the order of 100) were up to an order of magnitude higher than those previously considered to be necessary for breakup. Only the bag mode of drop breakup was observed. However, other recent studies gave values of the critical Weber number (based on original drop diameter) in general agreement with the results of the earlier investigators: 6 to 10 (Ref. B-12), 12 (Ref. B-19), 10 (Ref. B-28), and 4 (Ref. B-35).

Fox and Dabora (Ref. B-25) studied the breakup of drops in a spray. The criterion for stripping mode breakup was found to be We > 20. The breakup times for this mode were lower for drops in the wake of other drops than for free drops. This was attributed to the effect of an increase in the effective gas density, caused by the presence in the gas of droplets sheared from preceding drops.

Gel'fand and Borisov (Ref. B-28) emphasized the necessity of considering the effects of drop breakup in models of spray combustion. They presented calculations of drop Weber and Reynolds numbers and breakup times as functions of chamber length, for several experimental conditions and showed that there was quite sufficient chamber dwell time for drop breakup to occur. The predominant mode of droplet breakup is stripping.

An important consideration in studies of liquid drops and sprays is the effect of drop aggregations on the behavior of individual drops. This factor was examined by O'Rourke (Ref. B-75) in a theoretical investigation of the dynamics an evaporation of drops in sprays. He defines three spray regimes:

"Very thin sprays": Total mass and volume of liquid are negligible in comparison with those of the gas. Therefore, the gas is an infinite sink as far as the drops are concerned, and collisions between drops need not be considered in analyses.

"Thin sprays": The drops have negligible volume but significant mass in comparison with the gas. Because of their small volume, interaction between drops is not important, but because the mass of liquid in a given volume of the spray field is of the same order as the mass of the gas, evaporation from the drops affects the gas phase properties.

"Thick sprays": The drops occupy a significant volume fraction of the spray field, which nevertheless consists of discrete drops in a continuous gas phase. In this regime, drop interactions, such as collisions and modifications of drop drag and vaporization rates resulting from close spacing, are important. Drop collisions may be so significant that the size distributions produced by the atomization process may be completely altered by subsequent coalescence and shattering.

Petela (Ref. B-76) also recognized that there are different types of sprays (or different regions within a single spray) in which drops of given diameter and velocity may not behave in the same manner. He proposed modeling of the atomization process by computation of minimum stable drop sizes for each of three breakup mechanisms: turbulent breakup at the orifice exit, aerodynamic breakup, and breakup by microexplosions.

The changing character of drop sizes and drop-size distributions within a spray undergoing evaporation, combustion, or acceleration was originally pointed out by Shapiro and Erickson (Ref. B-86).

Drop Deformation and Drag Coefficient as Functions of Time

Drop Deformation and Breakup Mechanisms

A spectrum of drop breakup modes exists, ranging from the "bag" type at one extreme to the "shear" type at the other. In bag-type breakup, the aerodynamic force of the relative liquid/gas velocity deforms the drop into an ellipsoidal shape, with its major axis perpendicular to the flow direction. This deformation has been called "disk-shaped", "saucer-shaped", and "toroidal-shaped" by various authors. As the deformation continues, the center of the drop opens like a bag in the direction of the flow and appears as a thin film of liquid anchored to a heavier rim around the drop perimeter and "stretched" in the flow direction until the bag is several times larger than the original drop or the circumferential ring of liquid. When a critical condition is reached, the bag breaks into a shower of small droplets and the rim disintegrates into several large droplets. Photographs of bag mode breakup are shown in Ref. B-33, -55, -56, -62, -79, and -97.

In the shear breakup mode, capillary waves formed on the surface of the liquid are stripped off as ligaments that rapidly break into droplets much smaller than the parent drop. When the relative liquid/gas velocity is sufficiently high, the stripping action appears as a shower of droplets being torn from the surface of the drop. Typical photographs of shear mode breakup are shown in Ref. B-21, -55, -56, -79, -80, -85, and -97.

In addition to the two extreme breakup modes, combined bag and shear breakup (called the "bag-stamen" and "bag-shear" modes), have been observed photographically (Ref. B-33, -55, and -97.).

The bag-type drop breakup process occurs at a lower Weber number than the shear type and requires that the disrupting aerodynamic force be imposed for substantially larger times. The shear-type breakup mode occurs when the flow field imposes shear forces on the drop surface faster than the drop inertia will permit it to distort as a single mass, resulting in stripping of a spray of daughter droplets.

The shock tube tests of Rabin et al (Ref. B-79) showed a decrease in the critical velocity of a given drop size as the flow duration was increased. Hence, a critical drop diameter was postulated for a stated flow duration.

The time required for a drop to deform sufficiently from its original spherical shape to one which induces breakup ("deformation time") was found to be inversely proportional to the drop diameter. The deformation time was assumed to be inversely proportional to the gas flow velocity and may be the same as the pre-breakup time previously mentioned.

An analytical model of drop deformation was presented by Chiu (Ref. B-6), based on small perturbations and drop vibrations.

Collins and Charwat (Ref. B-9) constructed a fairly complex model that calculates drop stripping, drag coefficient, deformation, and velocity as functions of time. Model predictions showed good agreement with the experimental data then available.

Drop Drag Coefficients

A number of empirical correlations for the estimation of drop drag coefficients have been proposed, most of which are related to the Reynolds number, defined by

$$ Re = \frac{d \, \rho_G \, \overline{\Delta V}}{\mu_G} \qquad (B-39) $$

Time variation of the drag coefficient would therefore follow the corresponding variation of Reynolds number.

1. Gilbert et al (Ref. B-29) reported the following empirical expression for the drag coefficient of a single spherical particle.

$$C_D = 0.48 + 0.28 \, Re^{-0.85} \qquad (B-40)$$

This value was also used by Ishikawa and Murakaino (Ref. B-49) in a study of sprays generated by diesel engine type orifice atomizers.

2. Ingebo (Ref. B-41) obtained the following equation for accelerating groups of solid spheres and drops in the Reynolds number range 0.5 to 78:

$$C_D = 27/Re^{0.84} \qquad (B-41)$$

The reliability of this correlation has been questioned by Clift and Gauvin (Ref. B-8):

3. Rabin et al (Ref. B-78 and -79) measured drag coefficients experimentally in their shock-tube study of single-drop breakup. For drops smaller than about 100 microns, the drag coefficients agreed roughly with those of Ingebo (Ref. B-41). For larger drops, however, there were considerable differences, probably because smaller drops deform only slightly from spherical shape at gas velocities below critical, while larger drops deform into disk shape even at subcritical velocities. Their findings indicate an expression of the form:

$$C_D = 0.386 \, Re^{0.177} \qquad (B-42)$$

for droplet Reynolds numbers between 10^2 and 10^4.

4. Hughes and Gilliland (Ref. B-39) proposed a modification of the standard Stokes solid sphere drag coefficient (C_d = 24/Re) to fit experimental data in the Reynolds number range 0.5 to 200:

$$C = \left(\frac{24}{Re}\right) \left(1 + \sqrt{1.11 \times 10^{-2} \; Re}\right)^2 \left(\sqrt{1+\delta} + \sqrt{\delta}\right) \quad (B\text{-}43)$$

where $\delta = 3.75 \times 10^5$ (Re We)

$$We = \rho_G \; \overline{\Delta V}^2 \; d/\sigma$$

5. Crowe et al (Ref. B-11) studied the effects of burning and acceleration on the drag coefficients of particles suspended and accelerating in gas streams at Reynolds numbers 250 to 1600. Boundary layer analyses indicated that burning and acceleration tend to reduce the drag coefficient. Shock tube experiments were carried out on burning and nonburning solid particles to measure the drag coefficients as functions of gas density and relative velocity The values measured for burning particles were imprecise, probably because of nonuniform burning rates. The following correlation of the experimental data for nonburning particles was reported for "low" gas velocities:

$$\log_{10} C_D = 2.586 - 1.705 \; \log_{10} Re + 0.25 \; (\log_{10} Re)^2 \quad (B\text{-}44)$$

$$(200 < Re < 1600)$$

6. Yuen and Chen (Ref. B-98) suggest that the equation for the drag coefficient for solid spheres can be applied to liquid drops in a gas stream if the Reynolds number is based on the following combination of liquid and gas viscosities:

$$\mu = \mu_L + 0.33 \; (\mu_G - \mu_L) \quad (B\text{-}45)$$

They note that the drag coefficient of a drop in a spray cloud is lower than that of an isolated drop of the same diameter because the aggregate of drops causes motion of the gas and changes the relative velocity.

7. For drops undergoing shear mode breakup--and therefore at comparatively high Reynolds numbers--the following values of the drag coefficient (based on initial drop size and flow conditions) have been suggested: 3.0 (Ref. B-80), 2.5 (Ref. B-50), and 2 (Ref. B-79).

   Groeneweg (Ref. B-32) constructed a model of drop motion that included drag and evaporation as part of a study of the statistical description of a spray in terms of drop velocity, size, and position.

The critical shortcoming in experimental measurements of drop drag coefficients is the difficulty of determining the effects of such factors as deformation, acceleration, vaporization, and turbulence. Considerable variation between data reported by various investigators is therefore not unexpected.

Sizes of Droplets Formed in Breakup of Large Drops

The following expression was derived (Ref. B-97) for the "mean" droplet size resulting from the breakup of a drop by aerodynamic forces that are much larger than either the viscous or surface tension forces (i.e., at high Weber numbers):

$$D_{mean} = \left[\frac{136 \, \mu_L \, \sigma^{3/2} \, d^{1/2}}{\rho_G^2 \, \rho_L^{1/2} \, \overline{\Delta V}^4} \right]^{1/3} \tag{B-46}$$

The photographic studies of the shock-induced breakup of an 1800-micron drop by the shear-mode mechanism, which were previously discussed (Ref. B-85) showed that the daughter droplets are very much smaller than the parent drop, on the order of 50 microns. No breakup of the daughter droplets was observed in these experiments.

Effects of System Parameters on the Atomization Process

Typical available information on the effects of system parameters--particularly liquid properties--on the degree of atomization is summarized in this section. Appendix A is specifically limited to liquid rocket atomizers while the injectors described here are designed for other applications. They may, however, have some applicability and utility in assessing the atomization characteristics of liquid rocket injectors.

Airblast Atomization

When the velocity of the gas stream is substantially higher than that of the liquid, the process is referred to as "airblast" atomization. Two general types of airblast atomizers have been studied. One uses the "prefilming" concept, in which the liquid is spread out into a thin continuous sheet and is then subjected to the atomizing action of high velocity air*. To be fully effective, this system requires both sides of the liquid sheet to be exposed to the gas, which complicates design, since it entails two separate gas flows through the atomizer. In the second, or "plain-jet" concept, the liquid is injected into the high-velocity gas stream in the form of discrete jets. The objective in both cases is the same: to use the available energy of the flowing gas to achieve the maximum degree of atomization. A recent review of airblast atomization by Lefebvre (Ref. B-58) was the source of many of the references and much of the discussion in this section.

Drop-Size Correlations

The drop-size correlations developed for airblast atomization, like those for liquid rocket-type injector atomization, are highly empirical. Their applicability is limited as a result of problems in drop-size measurement techniques, incomplete or no variation of fluid properties, and improper development of data

---

* Most of the airblast atomization studies have used air; any gas might be used as well.

correlations. In addition, various investigators use different average drop sizes and, without data on size distributions, conversion to a common basis for comparison is difficult**.

Nevertheless, sufficient information is available to permit some generalized conclusions as to the effects of fluid properties and flow parameters on the degree of atomization produced by airblast atomizers.

For convenience of reference, the most significant of the various correlations proposed for the mean drop sizes produced by all types of airblast atomizers are summarized in Ref. B-58. It is strongly recommended that these correlations be very carefully considered before applying them to any type of liquid rocket, gas/liquid injectors. These are all empirical relationships with little or no theoretical basis. Their application will generally require the extrapolation of these correlations far beyond the range of test conditions used in their development. Also, a great variety of airblast atomizers is available, and plain-jet airblast atomizers come in many different shapes and forms. It is very important that these factors be carefully considered prior to application of these correlations. As shown in Section V, Atomization Study, even the relatively minor extrapolation of one of these correlations (Lorenzetto and Lefebvre--Ref. B-82) to the conditions of the tests performed in this program, can result in very major errors. The nomenclature used in this section is listed in Table B-1.

Effects of System Variables on Mean Drop Size

Liquid Properties. The liquid properties of importance in airblast atomization are viscosity, density, and surface tension. The adverse effect on spray quality of an increase in viscosity at varying levels of gas velocity and constant liquid

---

** Note, however, that the ratio of mass mean diameter to Sauter mean diameter has been reported to be 1.20 ± 0.006 (Ref. B-33)

TABLE B-1. NOMENCLATURE FOR AIRBLAST ATOMIZATION

A, B	EXPERIMENTAL CONSTANTS
D	DROP SIZE, m
D_o	LIQUID ORIFICE DIAMETER; INITIAL JET DIAMETER, m
D_L	DIAMETER OF ATOMIZER CUP (AT LIP), m
D_p	DIAMETER OF PREFILMER LIP, m
L	LENGTH, m
L_c	CHARACTERISTIC ATOMIZER DIMENSION, m
P	PRESSURE, Pa
Q	VOLUMETRIC FLOW RATE, liters/sec
Re	REYNOLDS NUMBER, $UL\rho/\mu$
U	VELOCITY, m/sec
W	MASS FLOW RATE, kg/sec
We	WEBER NUMBER, $U^2 L\rho/\sigma$
ρ	DENSITY, kg/m^3
σ	SURFACE TENSION, kg/sec^2 OR N/m
μ	DYNAMIC VISCOSITY, kg/m/sec OR $N\text{-}sec/m^2$
υ	KINEMATIC VISCOSITY, m^2/sec
MMD	MASS MEAN DIAMETER, m
SMD	SAUTER MEAN DIAMETER, m
SUBSCRIPTS	
G	GAS
L	LIQUID
R	GAS RELATIVE TO LIQUID

flow rate is shown for a prefilming and a plain jet atomizer in Fig. B-1 (Ref. B-83) and Fig. B-2 (Ref. B-60), respectively. Viscosity forces tend to suppress the formation of capillary waves on the liquid surface, which precedes atomization, and also resist deformation of subsequently formed ligaments into drops.
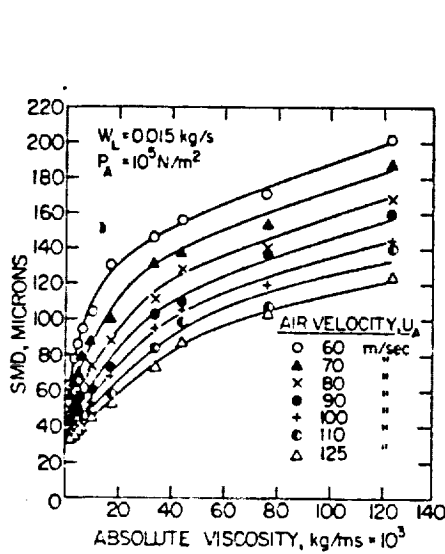

Figure B-1. Variation of Mean Drop Size With Liquid Viscosity for a Prefilming Atomizer (Ref. B-83)
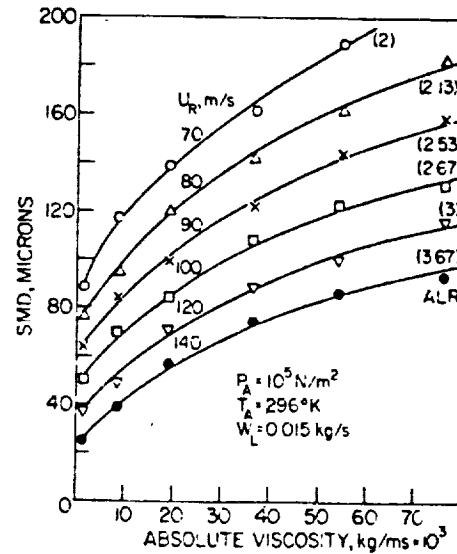
Figure B-2. Variation of Mean Drop Size With Liquid Viscosity for a Plain-Jet Atomizer (Ref. B-60)

Surface tension forces tend to impede atomization by resisting disturbances or distortions of the liquid surface, thereby opposing the creation of surface waves and delaying the onset of ligament formation. The effect of surface tension on drop size is illustrated in Fig. 3 (Ref. B-83) and Fig. 4 (Ref. B-60) for a prefilming and a plain jet atomizer, respectively.

Liquid density affects droplet size in a complex manner, the net result of which is that the influence of density is minor. For prefilming atomizers, drop size increases slightly with density, while the opposite occurs with plain-jet nozzles, as shown in Fig. 5 (Ref. B-82) and Fig. 6 (Ref. B-60), respectively.
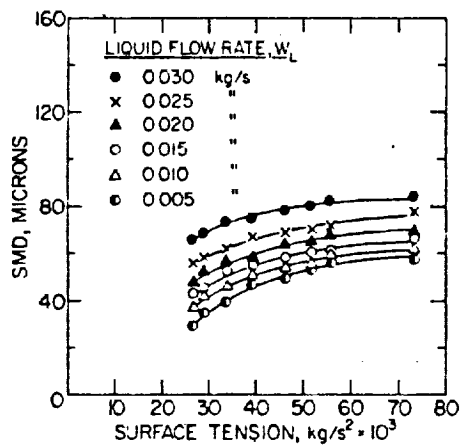
Figure B-3. Variation of Mean Drop
Size With Surface Tension
for a Prefilming Atomizer
(Ref. B-83)
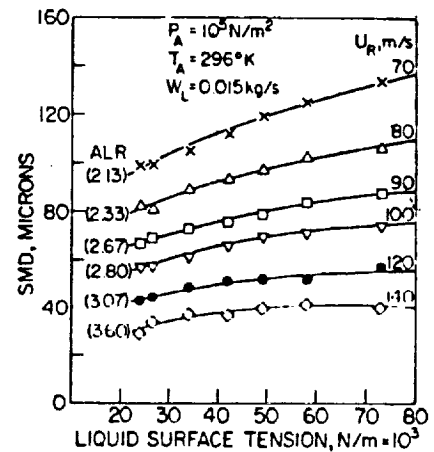
Figure B-4. Variation of Mean Drop
Size With Surface Tension
for a Plain-Jet Atomizer
(Ref. B-60)
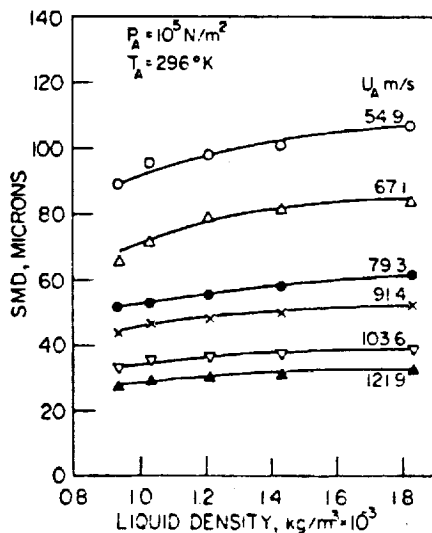
Figure B-5. Variation of Mean Drop
Size With Liquid Density
for a Prefilming Atomizer
(Ref. B-82)
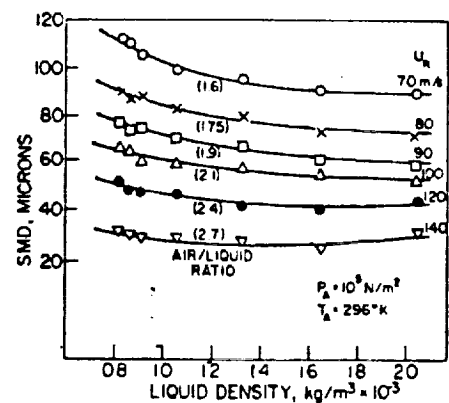
Figure B-6. Variation of Mean Drop
Size With Liquid Density
for a Plain-Jet Atomizer
(Ref. B-60)

Gas Properties. Gas velocity is the most important factor controlling mean
drop size in airblast atomizers, as shown in Fig. B-1, -2, -4, -5, and -6. For
typical low-viscosity liquids, the Sauter mean diameter (SMD) is approximately
inversely proportional to air velocity. A second important factor is the air/
liquid mass flow-rate ratio, as shown for prefilming atomizers in Fig. 7 (Ref.
B-84) and Fig. 8 (Ref. B-20). Atomization quality starts to decline when the
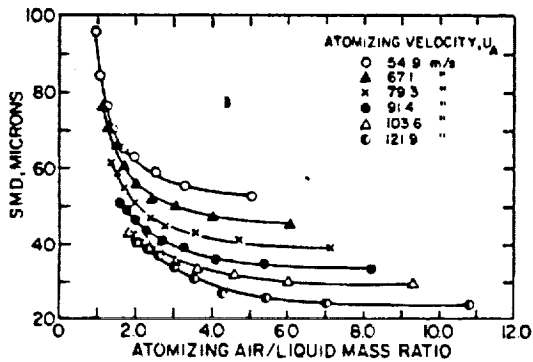
Figure B-7.   Effect on Mean Drop Size
             of Air/Liquid Mass Ratio
             (Ref. B-84)
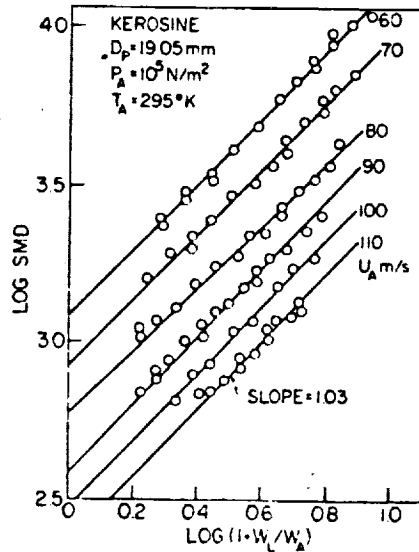
Figure B-8.   Graphs Illustrating
             Relationship Between Mean
             Drop Size and Air/Liquid
             Ratio (Ref. B-20)

air/liquid ratio is below about 4 and deteriorates rapidly below a ratio of
approximately 2. Increasing the air/liquid ratio beyond about 5 gives only mar-
ginal drop-size decreases.

The effects of air temperature and pressure on mean drop sizes are shown in Fig.
9 and 10 (Ref. B-84).
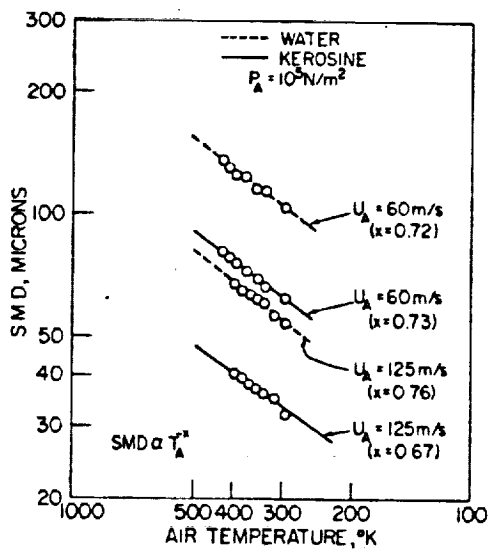
Figure B-9.   Influence of Air Tempera-
             ture on Mean Drop Size
             (Ref. B-84)
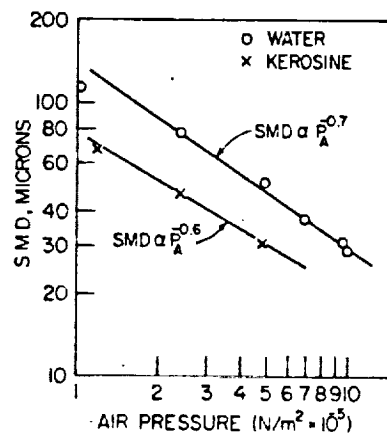
Figure B-10. Influence of Air Pressure
             on Mean Drop Size
             (Ref. B-84)

Summary of Property Effects. The effects of the major flow parameters on mean drop size, for low-viscosity liquids, are summarized in Ref. B-83, together with the ranges of test conditions that were covered in the experimental investigations, the liquids used, methods of measurement, and drop-size data.

Interestingly, the various expressions proposed for predicting the mean droplet sizes produced by prefilming airblast atomizers show some consistency. Thus, for low-viscosity liquids, the effects of the major variables on mean drop size may be expressed as power dependencies, with exponents in fairly narrow ranges:

Air velocity	-1.0 to -1.2
Air density	-0.6 to -0.7
Liquid density	0 to -0.25
Surface tension	0.5 to 0.6
$(1 + W_L/W_A)$	0.85 to 1.0
Linear scale	0.4 to 0.5

The dimensionally correct expression for mean drop sizes produced by prefilming airblast atomizers that best satisfies experimental data is (Ref. B-20):

$$SMD = \left[1 + \frac{W_L}{W_A}\right] \left[0.073 \left(\frac{\sigma}{\rho_A U_A^2}\right)^{0.6} \left(\frac{\rho_L}{\rho_A}\right)^{0.1} D_p^{0.4} + \right. \tag{B-47}$$

$$\left. 0.015 \left(\frac{\mu_L^2 D_p}{\sigma \rho_L}\right)^{0.5} \right]$$

where D_p is the prefilmer diameter.

This comparatively recent correlation was developed for the atomization of water and kerosene; drop sizes were measured by a Fraunhofer diffraction light-scattering technique. The variables used in this study were atomizer size (prefilmer lip diameter), and liquid density, viscosity, and surface tension. Agreement between measured SMD values and those predicted by Eq. B-47 was good (Fig. B-11).
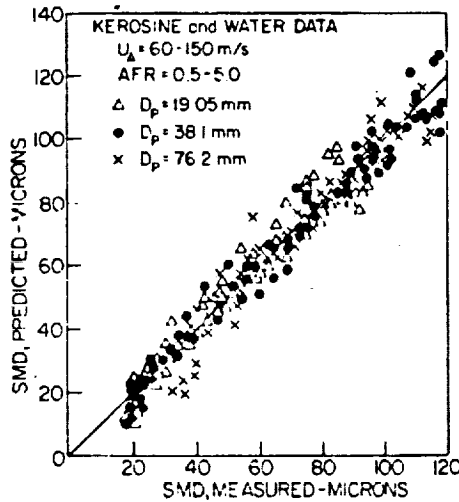
Figure B-11.   Comparison of SMD Values, Measured
vs Predicted From Eq. B-47 (Ref. B-58)

The most recent and reliable correlation for plain-jet atomization was reported by Jasuja (Ref. B-52), who varied liquid properties and air pressure. A Fraunhofer diffraction laser light-scattering technique was used for drop size measurements. The experimental data were fairly well correlated ($\pm30\%$) by the following expression:

$$SMD = 0.022 \left(\frac{\sigma}{\rho_G \, U_G^2}\right)^{0.45} \left(1 + \frac{W_L}{W_G}\right)^{0.5} + 1.43 \times 10^{-3} \left(\frac{\mu_L^2}{\sigma \, \rho_L}\right)^{0.4} \left(1 + \frac{W_L}{W_G}\right)^{0.8} \qquad (B-48)$$

This correlation does not include geometric (i.e., liquid orifice diameter) effects, since atomizer size was not varied in the investigation. A comparison of the performance of plain-jet and prefilming airblast atomizers is presented in Ref. B-42, which indicates that despite the simpler design of the former, its experimentally measured SMDs are only slightly larger, particularly for low-viscosity liquids.

Significant differences occur in the power dependencies in the drop size equations for prefilming and plain-jet atomizers. For example, liquid density appears to have opposite effects on the SMDs of the two types. This may be

caused by different mechanisms of bulk liquid conversion into a droplet spray, so that the SMD is proportional to $(\rho_L/\rho_A)^{0.1}$ in prefilming types and to $(\rho_L/\rho_A)^{-0.3}$ in plain-jet units.

The experimental data obtained from both prefilming and plain-jet airblast atomizers with low-viscosity liquids (water or kerosene) indicate that the main factors governing product drop size are the liquid surface tension, and the air velocity and density; with high-viscosity liquids, the effects of air properties are less significant, and the SMD is more dependent on the liquid properties, especially viscosity. The observation that the effects of liquid and gas properties are separate (Ref. B-20, -51, -53, -60, -73, and -83) suggests an expression for SMD consisting of the sum of two terms:

$$SMD = (SMD)_1 + (SMD)_2 \qquad\qquad (B-49)$$

where $(SMD)_1$ is dominated by air velocity and density and $(SMD)_2$ by liquid viscosity. The two different but complementary mechanisms of airblast atomization--one governed by the ratio of aerodynamic to surface tension forces, as embodied in the Weber number $(\rho_G U_G^2 D/\sigma)$, and the other by viscous forces, as expressed in the Z number $(\mu_L^2/\sigma\rho_L D)$--support the idea that any expression for SMD should consist of two terms to represent these effects.

This provides a theoretical basis for the SMD equations for airblast atomizers. In actual application of the equations to different atomizer designs, however, it is necessary to divide the calculated value of SMD by a factor, ϕ, which represents the overall efficiency of the atomizer, compared to the one for which the equation was developed, as well as to account for different methods of drop sampling and drop-size measurement. For prefilming atomizers, values of ϕ were found to be as low as 0.6 and were sensitive to minor changes in atomizer geometry. With the right values of ϕ, data from various experimentors agree fairly well with Eq. B-47, supporting its general validity to prefilming airblast atomizers. Unfortunately, the available data were obtained under conditions in which $(SMD)_1$ as very large compared to $(SMD)_2$. Tests in which the $(SMD)_2/(SMD)_1$ ratio is maximized are required for accurately checking the general applicability of the correlation.

The most acceptable expression for the SMD obtained from plain-jet airblast atomizers (Eq. B-48) has the same form as that for the prefilming type (i.e., it consists of the sum of a term dominated by air velocity and density and a term dominated by liquid viscosity). In fact, the similarity of the two correlations is strong evididence that both types of atomizer function by the same fundamental processes.

It has been suggested (Ref. B-58) that at least two different mechanisms are involved in airblast atomization; their relative importance depends on the level of liquid viscosity. For low-viscosity liquids injected into a comparatively low-velocity gas stream, capillary waves are produced on the liquid surface. These waves grow, become unstable, and break off as ligaments that disintegrate into droplets. Increased gas velocity causes earlier formation of the ligaments, which are thinner and shorter, and disintegrate into smaller drops. With liquids of high viscosity, the capillary wave mechanism may not be valid. Instead, the liquid is drawn out in the form of long ligaments that break up relatively slowly, in regions of lower gas velocity, into larger-size droplets.

An investigation of an external mixing* atomizer using kerosene/air (Ref. B-18) resulted in a drop-size correlation that was not of the two-term type, nor do the property exponents follow those of other empirical correlation

$$SMD = (1 \times 10^{-3})D_0 \ (Re)^{0.39}(We)^{0.18} \left(\frac{W_G}{W_L}\right)^{-0.29} \qquad \text{(B-50)}$$

where

$$Re = \rho_L \ D_0 \ \overline{\Delta V}/\mu_L$$

$$We = \rho_L \ D_0 \ \overline{\Delta V}^2/\sigma$$

---

*The prefilm and plain-jet airblast atomizers previously discussed are "internal mixing" types, in which the gas/liquid interaction occurs within the atomizer body. In external mixing, the interaction occurs outside the atomizer.

The characteristics of a Y-shaped airblast atomizer, in which the liquid jet is atomized by the air in an internal chamber, were studied by Prasad (Ref. B-77). His drop-size data conformed in general to the empirical correlation of Wigg (Ref. B-95):

$$MMD = 200 \left(\frac{\rho_L^{0.5}}{\rho_G^{0.3}} \right) \left(\frac{W_L^{0.1}}{\Delta V} \right) \left(1 + \frac{W_L}{W_G} \right)^{0.5} h^{0.1} \sigma^{0.2} \qquad (B-51)$$

where h is a characteristic atomizer dimension. The data of Mullinger and Chigier (Ref. B-70) were also in fair agreement with this expression.

Jet Atomization

Several investigators have studied the atomization of single jets of liquid in low- or moderate-velocity gas flow fields. Although these may be considered as types of plain-jet airblast atomizers, they are not generally so classified and will therefore be discussed separately.

Ingebo has worked extensively in this field. In Ref. B-43, he reported drop size data obtained for the conditions $V_G = 0$, $V_G > V_L$, and V_G increasing with constant acceleration. Maximum measured drop sizes were correlated in terms of several dimensionless numbers by the following expression:

$$\frac{D_o}{D_{max}} = 0.64 \left(\frac{D_o Bo}{D_t} \right)^{0.33} + \frac{(Re_G)^{0.5}}{(Re_L)^{0.1}(Bo)^{0.07}} \left[0.044 + \right.$$

$$\left. \frac{We_L}{(We_G)^{0.2}(Bo)^{0.09}} \left((1.25 \times 10^{-6}) + (3.5 \times 10^{-7}) \frac{(Ac)^{0.5}}{(Bo)^{0.66}} \right) \right] \qquad (B-52)$$

where

D_o = liquid orifice diameter

D_t = gas tip diameter

D_{max} = maximum droplet size

Bo = bond number = $\rho_L D_o^2/\sigma$

Re_G = gas Reynolds number = $\rho_G D_o V_G/\mu_G$

Re_L = liquid Reynolds number = $\rho_L D_o V_L/\mu_L$

We_G = gas Weber number = $\rho_G D_o \overline{\Delta V}^2/\sigma$

We_L = liquid Weber number = $\rho_L D_o \overline{\Delta V}^2/\sigma$

Ac = aerodynamic acceleration = $\rho_G D_o^2 a/\sigma$

a = gas stream acceleration (constant)

The maximum measured droplet diameter may be considered to be associated with the critical Weber number at the specified flow conditions and to constitute an experimental determination of this factor.

In an investigation of the effect of gas velocity on mean droplet sizes (Ref. B-44), Ingebo found that D_{32} was proportional to $V_G^{-0.75}$ with a subsonic air flow atomizer and to the product $(V_G)^{-0.75}(FN)^{0.4}$ in a pressure atomizer, where FN is the flow number:

$$FN = \frac{Q}{\sqrt{\Delta P}} \quad \frac{(\text{liters/hour})}{(N/m^2)^{0.5}} \tag{B-53}$$

Results of a study of the atomization of water jets (V_L = 5 and 23 m/sec) by a moderate-velocity air flow (V_G = 40 - 150 m/sec), swirled and unswirled, at wind tunnel pressures between one and two atmospheres, were reported in Ref. B-45. Swirl of the liquid jet reduced droplet sizes, compared to unswirled jets, and little difference was found between upstream, downstream, or cross-stream injection.

An experimental investigation of the acceleration wave breakup mode of liquid jets was reported by Ingebo (Ref. B-46). Water jets injected into stagnant air ($V_G = 0$) start to disintegrate at a distance of approximately 4.5 times the jet diameter (from Rayleigh analysis). Jets injected into high-velocity air streams break up by the capillary wave or acceleration wave mode, depending on the air velocity, with mean droplet sizes given by:

$$D_0/D_{10} = 0.21 \ (We_G Re_L)^{0.25} \tag{B-54}$$

for $(We_G Re_L) < 10^6$ (capillary wave breakup mode)

and

$$D_0/D_{10} = 0.27 \ (We_G Re_L)^{0.4} \tag{B-55}$$

for $(We_G Re_L) > 10^6$ (acceleration wave breakup mode)

The data showed that in acceleration wave breakup (very high gas velocity and/or density) the effect of relative gas/liquid velocity is magnified and the effect of orifice diameter is minimized, compared to the capillary wave breakup mode.

Further experimental work on acceleration wave breakup for various types of water injection into air streams (Ref. B-47) gave the following minor modifications of Eq. B-55:

(1) For downstream injection, nonswirling air flow,

$$D_0/D_{10} = 0.23 \ (We_G Re_L)^{0.4} \tag{B-56}$$

(2) For downstream injection, swirling airflow, Eq. B-55 is valid.

(3) For upstream injection, nonswirling air flow,

$$D_0/D_{10} = 0.0045 \ (We_G Re_L)^{0.5} \tag{B-57}$$

Ingebo (Ref. B-48) recently reported results of an experimental study of the atomization of liquid sheets in quiescent and high-velocity air. Empirical correlations were made in terms of the liquid Reynolds number ($Re_L = D_0 V_L \rho_L / \mu_L$), the air stream Reynolds number; ($Re_G = D_0 V_G \rho_G / \mu_G$); and the relative velocity Reynolds number ($Re_R = D_0 \overline{\Delta V} \rho_G / \mu_G$).

For like-doublet impinging jets*,

$$D_0/D_m = 0.023 \ (Re_L)^{0.5} + 0.002 \ (Re_R) \tag{B-58}$$

where D_0 is the orifice diameter and D_m is a "mean" droplet diameter, similar to D_{32}. (A nearly identical expression was derived by Ingebo for the heptane impinging jet data reported in Ref. B-8.)

For splash plate injectors,

$$D_0/D_m = 2.9 \times 10^{-4} \ (Re_L) + 2.4 \times 10^{-3} \ (Re_G) \tag{B-59}$$

For atomizers producing swirling, hollow-cone sheets,

$$D_0/D_m = (D_0/D_{m,h}) + 2.2 \times 10^{-3} \ (Re_G - Re_c) \tag{B-60}$$

where $D_{m,h}$ and Re_c are constants, defined as the hydrodynamic mean drop diameter and the critical Reynolds number for aerodynamic breakup, respectively. The same type of simplex swirl atomizer was recently used to spray jet and diesel fuels into ambient and heated air at pressures of 20 to 80 psia (Ref. B-17). Measured droplet sizes showed a strong effect of air density:

$$SMD \propto \rho_A^{-0.53} \tag{B-61}$$

---

*Impinging jets form a liquid sheet before breakup.

It is of interest that Eq. B-58, B-59, and B-60 are two-term expressions, one related to hydrodynamic forces (Re_L) and the other related to aerodynamic forces (Re_R) or (Re_G). This may be compared to the two-term correlations for airblast atomizers previously discussed.

In another study of the breakup of liquid jets by cross-flowing air streams, Hussein et al (Ref. B-40) constructed a model of stream breakup. Drop-size measurements made to verify the model showed that the SMD varied significantly over an axial distance of 5 cm from the injection point. Beyond 5 cm, the sizes were relatively constant and showed the following dependencies: with air velocity, SMD $\propto V_A^{-1.34}$; with orifice diameter, SMD $\propto D_o^{0.55}$; and with liquid jet velocity, no appreciable effect.

Matta (Ref. B-63) conducted an experimental investigation of the breakup behavior of viscoelastic liquids in high-velocity airstreams. He modeled the process as simply the breaking off of ligaments from the jet which then neck into a series of drops, with no significant interaction with the gas flow. For the fluids tested (e.g., glycerine, diethylmalonate, and various polymers), the "average" drop size was a function of the Ohnesorge number:

$$D_{mean} = 1.88 \, D_o \, (1 + 3Z)^{1/6} \tag{B-62}$$

where

$$Z = \mu_L / (D_o \rho_L \sigma)^{1/2}$$

Simmons and Harding (Ref. B-88) measured the drop sizes in sprays produced by simplex pressure-atomizing nozzles. They found that water and kerosene SMD values showed differing dependencies on surface tension. However, by defining a Weber number based on the liquid sheet thickness, t, ($We = \rho_G V_L^2 t / \sigma$), they could correlate their data by

$$SMD \propto \sigma^{0.51} \qquad (We < 1),$$
$$SMD \propto \sigma^{0.16} \qquad (We > 1),$$
$$SMD \propto \Delta P^{-0.275} \, We^{-0.4}$$

REFERENCES

B-1. Adelberg, M., "Breakup Rate and Penetration of a Liquid Jet in a Gas Stream," _AIAA J._, Vol. 5, No. 8, pp. 1405-1415 (1967)

B-2. Adelberg, M., "Mean Drop Size Resulting from the Injection of a Liquid Jet into a High-Speed Gas Stream," _AIAA J._, Vol. 6, No. 6, pp. 1143-1147 (1968)

B-3. Borisov, A., B. Gel'fand, M. Natanzon, and O. Kossor, "Droplet Breakup Regimes and Criteria for Their Existence," _J. Eng. Physics_, Vol. 40, No. 1 (1981)

B-4. Bryan, R., P.S. Godbole, and E.R. Norster, "Characteristics of Airblast Atomizers," _Combustion and Heat Transfer in Gas Turbine Systems_, Cranfield International Symposium Series, Pergamon Press, Vol. II, pp. 343-359 (1971)

B-5. Buzukov, A.A., "The Breakup of Drops and a Fluid Stream by an Air Shock Wave," _J. Appl. Mech. and Tech. Phys. (USSR)_, FTD-TT-63-839, AD-435996, AF Foreign Technology Division (1964)

B-6. Chiv, H., "Dynamics of Deformation of Liquid Drops," AF Aerospace Research Laboratory, Report ARL-0065 (1969)

B-7. Clark, B.J., "Breakup of a Liquid in a Transverse Flow of Gas," NASA TN-D-2424 (1964)

B-8. Clift, R., and W.H. Gauvin, "Motion of Entrained Particles in Gas Streams," _Canadian J. of Chem. Eng._, Vol. 49, p. 439 (1971)

B-9. Collins, R., and A.F. Charwat, "The Deformation and Mass Loss of Liquid Drops in a High-Speed Flow of Gas," _Israel J. of Technology_, Vol. 9, No. 5, p. 453 (1971)

B-10. Craig, J.E., "Conventional and Liquid Metal Droplet Breakup in Aerodynamic Nozzle Contractions," AIAA-84-0201, AIAA 22nd Aerospace Sciences Meeting, Reno, Nevada, January 1984

B-11. Crowe, C.T., J.A. Nicholls, and R.D. Morrison, "Drag Coefficients of Inert and Burning Particles Accelerating in Gas Streams," Ninth International Symposium on Combustion, Academic Press, pp. 394-406 (1963)

B-12. Crowe, C.T., and W. Comfort, "Atomization Mechanisms in Single-Component, Two-Phase, Nozzle Flows," Preprint UCRL-79656-Rev-1, Lawrence Livermore Laboratories, April 1978

B-13. Dabora, E.K., K.W. Ragland, A.A. Ranger, and J.A. Nicholls, "Detonation in Two-Phase Media and Drop Shattering Studies," NASA CR-72421 (1968)

B-14. Dickerson, R.A., and T.A. Coultas, "Breakup of Droplets in an Accelerating Gas Flow," AIAA No. 66-611, Second Propulsion Joint Specialist Conference, June 1966

B-15. Dickerson, R.A., and M.D. Schuman, "Atomization Rates of Droplets and Jets," Preprint No. 63-498, AIAA Heterogeneous Combustion Conference, Palm Beach, Florida, December 1963

B-16. Dickerson, R.A., and M.D. Schuman, "Rate of Atomization of Droplets," J. Spacecraft and Rockets, Vol. 2, No. 1, pp. 99-100 (1965)

B-17. Dodge, L.G., and J.A. Biaglow, "Effect of Elevated Temperature and Pressure on Sprays from Simplex Swirl Atomizers," 30th ASME International Gas Turbine Conference and Exhibit, Houston, Texas, March 1985

B-18. Elkotb, M.M., E. Mahdy, and M.E. Montaser, "Investigation of External Mixing Air Blast Atomizers," Proceedings of Second International Conference on Liquid Atomization and Spray Systems, Madison, Wisconsin, pp. 107-115 (1982)

B-19. Elliott, D., and E. Weinberg, "Acceleration of Liquids in Two-Phase Nozzles," NASA TR-32-987 (1968)

B-20. El-Shanawang, M.S., and A.H. Lefebvre, "Airblast Atomization: Effect of Linear Scale on Mean Drop Size," J. Energy, Vol. 4, No. 4, pp. 184-189 (1980)

B-21. Engel, O.G., "Fragmentation of Water Drops in the Zone Behind an Air Shock," J. Res. Nat. Bur. Stand., Vol. 60, No. 3, pp. 245-280 (1958)

B-22. Ferrenberg, A., and V. Jaqua, "Atomization and Mixing Study, Interim Report," Contract NAS8-34504, Report No. RI/RD83-170, Rocketdyne Division, Rockwell International Corporation, July 1983

B-23. Fishburn, B.D., "Boundary Layer Stripping of Liquid Drops Fragmented by Taylor Instability," Acta Astronautical, Vol. 1 (1974)

B-24. Forsnes, V.G., "A Literature Review and Discussion of Liquid Particle Breakup in Gas Streams," NWC-TP-4589, Naval Weapons Center, China Lake, California (1968)

B-25. Fox, G., and E.K. Dabora, "Breakup of Liquid Drops Due to Convective Flow in Shocked Sprays," Fourteenth International Combustion Symposium (1972)

B-26. Fraser, R.P., N. Dombrowski, and J.H. Routley, "The Atomization of a Liquid Sheet by an Impinging Air Stream," Chem. Eng. Sci., Vol. 18, pp. 339-353 (1963)

B-27. Fraser, R.P., P. Eisenklam, N. Dombrowski, and D. Hasson, "Drop Formation from Rapidly Moving Liquid Sheets," <u>Am. Inst. Chem. Eng. J.</u>, Vol. 8, No. 5, pp. 672-680 (1962)

B-28. Gel'fand, B., and A. Borisov, "The Effect of Droplet Disintegration on the Combustion of Sprayed Fuel," FTD-ID(RS)T-1407-82 (1982)

B-29. Gilbert, M., L. Davis, and D. Altman, "Velocity Lag of Particles in Linearly Accelerated Combustion Gases," Jet Propulsion, Vol. 25, pp. 26-30 (1955)

B-30. Gordon, G.D., "Mechanism and Speed of Breakup of Drops," <u>J. of App. Phys.</u>, Vol. 30, No. 11, pp. 1759-1761 (1959)

B-31. Gretzinger, J., and W.R. Marshall, "Characteristics of Pneumatic Atomization," <u>Am. Inst. Chem. Eng. J.</u>, Vol. 7, No. 2, pp. 312-318 (1961)

B-32. Groenweg, J.F., "The Statistical Description of a Spray in Terms of Drop Velocity, Size, and Position," Ph.D. dissertation, University of Wisconsin (1967)

B-33. Hanson, A.R., E.G. Domich, and H.S. Adams, "Shock Tube Investigation of the Breakup of Drops by Air Blast," <u>Phys. of Fluids</u>, Vol. 6, pp. 1070-1080 (1963)

B-34. Harper, E.Y., I.D. Chang, and G.W. Grube, "A Second-Order JWKB Approximation with One Turning Point and Two Singular Points: Stability of an Accelerating Liquid Sphere," <u>J. Math. Phys.</u>, Vol. 12, No. 9, pp. 1955-1960 (1971)

B-35. Harper, E.Y., and G.W. Grube, "The Deformation and Instability of a Suddenly Accelerated Liquid Drop," AIAA Paper 71-393 (1971)

B-36. Hinze, J.O., "Critical Speeds and Sizes of Liquid Globules," <u>App. Sci. Res.</u>, Series A, Vol. 1, No. 9, pp. 273-288 (1948)

B-37. Hinze, J.O., "Forced Deformations of Viscous Liquid Globules," <u>App. Sci. Res.</u>, Series A, Vol. 1, No. 9, pp. 263-272 (1948)

B-38. Hinze, J.O., "Fundamentals of the Hydrodynamic Mechanism of Splitting in Dispersion Processes," <u>Am. Inst. Chem. Eng. J.</u>, Vol. 1, No. 3, pp. 289-295 (1955)

B-39. Hughes, R.R., and E.R. Gilliland, "The Mechanics of Drops," <u>Chem. Eng. Progress</u>, Vol. 48, p. 497 (1952)

B-40. Hussein, G., A.K. Jasuja, and R. Fletcher, "Penetration and Breakup Studies of Discrete Liquid Jets in Cross-Flowing Airstreams," AMSE Paper 82-GT-25 (1982)

B-41. Ingebo, R.D., "Drag Coefficients for Droplets and Solid Spheres in Clouds Accelerating in Airstreams," NACA TN-3762 (1956)

B-42. Ingebo, R.D., and H.H. Foster, "Drop-Size Distribution for Crosscurrent Breakup of Liquid Jets in Airstreams," NACA TN-4087 (1957)

B-43. Ingebo, R.D., "Maximum Drop Diameters for the Atomization of Liquid Jets Injected Concurrently into Accelerating or Decelerating Gas Streams," NASA TN-D-4640 (1968)

B-44. Ingebo, R.D., "Effect of Airstream Velocity on Mean Drop Diameters of Water Sprays Produced by Pressure and Air Atomizing Nozzles," NASA TM-73740 (1977)

B-45. Ingebo, R.D., "Atomization of Water Jets and Sheets in Axial and Swirling Airflow," NASA TM-79043 (1979)

B-46. Ingebo, R.D., "Capillary and Acceleration Wave Breakup of Liquid Jets in Axial-Flow Airstreams," NASA TP-1791 (1981)

B-47. Ingebo, R.D., "Acceleration Wave Breakup of Liquid Jets," NASA TM-81717 (1981)

B-48. Ingebo, R.D., "Hydrodynamic and Aerodynamic Breakup of Liquid Sheets," Proceedings of Second International Conference on Liquid Atomization and Spray Systems, Madison, Wisconsin, pp. 9-17 (1982)

B-49. Ishikawa, M., and T. Murakami, "Characteristics of Intermittent Sprays Generated by an Orifice Atomizer," Proceedings of Second International Conference on Liquid Atomization and Spray Systems, Madison, Wisconsin, pp. 85-92 (1982)

B-50. Jaarsma, F., and W. Derksen, "Shock Tube Techniques for Fuel Droplet Combustion Studies," Report No. MP-251, National Aerospace Laboratory, The Netherlands (1967)

B-51. Jasuja, A.K., "Airblast Atomization of Alternative Liquid Petroleum Fuels under High Pressure Conditions," ASME Trans., J. of Eng. for Power, Vol. 103, pp. 514-518 (1981)

B-52. Jasuja, A.K., "Plain-Jet Airblast Atomization of Alternative Liquid Petroleum Fuels under High Ambient Air Pressure Conditions," ASME 82-Gt-32, 27th Annual International Gas Turbine Conference (April 1982)

B-53. Kim, K.Y., and W.R. Marshall, "Drop-Size Distributions from Pneumatic Atomizers," _Am. Inst. Chem. Eng. J.,_ Vol. 17, No. 3, pp. 575-584 (1971)

B-54. Korsunov, Y.A., and A.P. Tishin, "Experimental Study of the Atomization of Liquid Droplets at Low Reynolds Numbers," _J. Heat Transfer,_ Soviet Research, Vol. 3, No. 6, pp. 136-140 (1971)

B-55. Krzeczkowski, S.A., "Measurement of Liquid Droplet Disintegration Mechanisms," _Inter. J. of Multiphase Flow,_ Vol. 6, No. 3, pp. 227-239 (1980)

B-56. Lane, W.R., "Shatter of Drops in Streams of Air," _J. Ind. Eng. Chem.,_ Vol. 43, pp. 1312-1317 (1951)

B-57. Lapple, C.E., J.P. Henry, and D.E. Blake, "Atomization - A Survey and Critique of the Literature," Army Contract DA-18-035-AMC-122(A), SRI Technical Report No. 6, Stanford Research Institute, Menlo Park, California, ASTIA AD-821-314 (1967)

B-58. Lefebvre, A.H., "Airblast Atomization," _Prog. Energy and Combust. Sci.,_ Vol. 6, pp. 233-261 (1980)

B-59. Lefebvre, A.H., and D. Miller, "The Development of an Airblast Atomizer for Gas Turbine Applications," Cranfield College of Aeronautics, Report No. 193 (1960)

B-60. Lorenzetto, G.E., and A.H. Lefebvre, "Measurements of Drop Size on a Plain-Jet Airblast Atomizer," _AIAA J.,_ Vol. 15, No. 7, pp. 1006-1010 (1977)

B-61. Luna, N., and W. Klikoff, "On Aerodynamic Breakup of Liquid Drops," Report SC-RR-66-2716, Sandia National Laboratory, Albuquerque, New Mexico, (1967)

B-62. Magarvey, R.H., and B.W. Taylor, "Free Fall Breakup of Large Drops," _J. Appl. Phys.,_ Vol. 27, No. 10, pp. 1129-1135 (1956)

B-63. Matta, J.E., "Nonlinear Viscoelastic Breakup in a High-Velocity Airstream," Report ARCSL-TR-80067, Chemical Systems Laboratory, Aberdeen Proving Ground, Maryland (1981)

B-64. Mayer, E., "Theory of Liquid Atomization in High-Velocity Gas Streams," _ARS J.,_ Vol. 31, No. 12, pp. 1783-1785 (1961)

B-65. Mayer, E., "Capillary Mechanisms of Liquid Atomization in High-Velocity Gas Streams," _Proceedings of Twelfth International Astronautical Congress,_ Vol. 2, Academic Press, New York, pp. 731-740 (1963)

B-66. Merrington, A.C., and E.G. Richardson, "The Breakup of Liquid Jets," Proc. _Phys. Soc.,_ Vol. 59, p. 1 (1947)

B-67. Morrell, G., "Critical Conditions for Drop and Jet Shattering," NASA TN-D-677 (1961)

B-68. Morrell, G., "Rate of Liquid Jet Breakup by a Transverse Shock Wave," NASA TN-D-1728 (1963)

B-69. Morrell, G., and F.P. Povinelli, "Breakup of Various Liquid Jets by Shock Waves and Application to Resonant Combustion," NASA TN-D-2423 (1964)

B-70. Mullinger, P.H., and N.A. Chigier, "The Design and Performance of Internal Mixing, Multijet, Twin-Fluid Atomizers," J. Inst. Fuel, Vol. 47, pp. 251-261 (1974)

B-71. Nicholls, J.A., and A.A. Ranger, "Droplet Shattering," Fifth ICRPG Combustion Conference, CPIA Publ. No. 183, pp. 85-90 (1968)

B-72. Nicholson, J.E., and A.F. Hill, "Rain Erosion on Spike-Protected Supersonic Radomes," Report No. MC-61-6-R3, Mithas, Inc., Cambridge, Massachusetts (1963)

B-73. Nurick, W.H., and L.J. Zajac, "Physical Property Effect on Spray Atomization," Report No. ITR-72-058-C, Rocketdyne, Canoga Park, California (1972)

B-74. Nukiyama, S., and Y. Tanasawa, "Experiments on the Atomization of Liquids in an Airstream," Trans. Society of Mechanical Engineers, Japan, Vol. 5, pp. 68-75 (1939)

B-75. O'Rourke, P.J., "Collective Drop Effects on Vaporizing Liquid Sprays," LA-9069-T, Los Alamos National Laboratory, Los Alamos, New Mexico (1981)

B-76. Petela, R., "Analyses of Atomization Processes," Fuel, Vol. 61 (1982)

B-77. Prasad, K.S.L., "Spray Characterization of Airblast Atomizers," Proceedings of Second International Conference on Liquid Atomization and Spray Systems, Madison, Wisconsin, pp. 123-130 (1982)

B-78. Rabin, E., and R.B. Lawhead, "The Motion and Shattering of Burning and Nonburning Propellant Droplets," AFOSR-TN-59-129 Rocketdyne No. R-1503 (1959)

B-79. Rabin, E., A.R. Schallenmuller, and R.B. Lawhead, "Displacement and Shattering of Propellant Droplets," AFOSR-TR-60-75 (1960)

B-80. Ranger, A.A. and J.A. Nicholls, "Aerodynamic Shattering of Liquid Drops," AIAA J., Vol. 7, No. 2, pp. 285-290 (1969)

B-81. Rao, K.V.L., and A.H. Lefebvre, "Fuel Atomization in a Flowing Airstream," AIAA J., Vol. 13, No. 10, pp. 1413-1415 (1975)

B-82. Rizk, N.K., and A.H. Lefebvre, "Influence of Liquid Film Thickness on Air-blast Atomization," ASME, Gas Turbine and Fuels Technology Meeting, Atlanta, Georgia, pp. 37-42 (1977)

B-83. Rizkalla, A.A., and A.H. Lefebvre, "Influence of Liquid Properties on Air-blast Atomizer Spray Characteristics," Trans. ASME, J.Eng. Power, pp. 173-179 (1975)

B-84. Rizkalla, A.A., and A.H. Lefebvre, "The Influence of Air and Liquid Prop-erties on Airblast Atomization," Trans. ASME, J. Fluids Eng., Vol. 97, pp. 316-320 (1975)

B-85. Rojec, E.A., "Photographic Presentation of Shear-Type Droplet Breakup," Rocketdyne Research Report No. 63-39 (1963)

B-86. Shapiro, A.H., and A.J. Erickson, "On the Changing Size Spectrum of Parti-cle Clouds Undergoing Evaporation, Combustion, or Acceleration," Trans. ASME, Vol. 79, pp. 775-788 (1957)

B-87. Simmons, H.C., "The Correlation of Drop-Size Distributions in Fuel Nozzle Sprays," Trans. ASME, J. Eng. Power, Vol. 99, pp. 309-319 (1977)

B-88. Simmons, H.C., and C.F. Harding, "Some Effects of Using Water as a Test Fluid in Fuel Nozzle Spray Analysis," Trans. ASME, J. Eng. Power, Vol. 103, pp. 118-123 (1981)

B-89. Tate, R.W., "Some Problems Associated with the Accurate Representation of Droplet Size Distributions," Proceedings of Second International Confer-ence on Liquid Atomization and Spray Systems, Madison, Wisconsin, pp. 341-351 (1982)

B-90. Taylor, G.I., "The Shape and Acceleration of a Drop in a High Speed Air Stream," Scientific Papers of G.I.Taylor, G.K. Batchelor, Editor, Univer-sity Press, Cambridge, pp. 457-464 (1963) (paper written in 1949)

B-91. Volynskiy, M.S., and A.S. Lipatov, "Deformation and Breakup of Droplets in a Gas Flow," J. Heat Transfer, Soviet Research, Vol. 2, No. 6, pp. 30-36 (1970)

B-92. Weiss, M.A., and C.H. Warsham, "Atomization in High Velocity Airstreams," ARS J., Vol. 29, No. 4, pp. 252-259 (1959)

B-93. Wetzel, R.H., and W.R. Marshall, "Venturi Atomization," Am. Inst. Chem. Eng., Washington, DC (1954)

B-94. Wigg, L.D., "The Effects of Scale on Fine Sprays Produced by Large Air-blast Atomizers," NGTE Report No. 236 (1959)

B-95. Wigg, L.D., "Dropsize Predictions for Twin-Fluid Atomizers," <u>J. Inst. Fuel</u>, Vol. 27, pp. 500-505 (1974)

B-96. Williams, F.A., "Atomization Processes and Ignition Criteria for Supersonic Combustion with Liquid Fuel Ignition," <u>Astronautics Acta</u>, Vol. 15, p. 547 (1970)

B-97. Wolfe, H.E., and W.H. Anderson, "Kinetics, Mechanism and Resultant Droplet Sizes of the Aerodynamic Breakup of Liquid Drops," Aerojet-General Report No. 0395-04(18) SP, AD-437340 (1964)

B-98. Yuen, M.C., and L.W. Chen, "On Drag of Evaporating Droplets," Combustion Science Technology, Vol. 14, pp. 147-154 (1976)

APPENDIX C

DISTRIBUTION LIST FOR FINAL REPORT
ATOMIZATION AND MIXING STUDY
NAS8-34504

NAME	NUMBER OF COPIES
National Aeronautics & Space Administration Washington, DC 20546	
Attn: RP/F.W. Stephenson	1
George C. Marshall Space Flight Center National Aeronautics & Space Administration Marshall Space Flight Center, AL 35812	
Attn: AS24D	5
AT01	1
EM12-34	1
EP23/C.R. Bailey	1
EP22/F.W. Braam	2
EL24/K.W. Gross	1
Lewis Research Center National Aeronautics & Space Administration 21000 Brookpark Road Cleveland, OH 44135	
Attn: MS 60-3/Library	1
MS 500-219/S. Gorland	2
MS 500-200/L. Diehl	1
AMES Research Center National Aeronautics & Space Administration Moffett Field, CA 94035	
Attn: Library	1
Goddard Space Flight Center National Aeronautics & Space Administration Greenbelt, MD 20771	
Attn: Library	1
John F. Kennedy Space Center National Aeronautics & Space Administration Kennedy Space Center, FL 92899	
Attn: Library	1

Lyndon B. Johnson Space Center
National Aeronautics & Space Administration
Houston, TX 77058

Attn: Library   1
       EP2/C.R. Gibson   1

Langley Research Center
National Aeronautics & Space Administration
Langley Station
Hampton, VA 23665

Attn: Library   1

Jet Propulsion Laboratory
National Aeronautics & Space Administration
4800 Oak Grove Drive
Pasadena, CA 91109

Attn: Library   1

NASA-Scientific & Technical Information Facility
P.O. Box 8757
Baltimore-Washington International Airport
Baltimore, MD 21240

Attn: Accessing Department   5

Defense Documentation Center
Cameron Station, Building #5
5010 Duke Street
Alexandria, VA 22314

Attn: TISIA   5

Air Force Rocket Propulsion Laboratory
Edwards, CA 93523

Attn: Library   1

Arnold Engineering Development Center
Air Force Systems Command
Tullahoma, TN 37388

Attn: Library   1

U.S. Naval Research Laboratory
Washington, DC 20390

Attn: Library   1

U.S. Army Missile Command
Redstone Scientific Information Center
Redstone Arsenal, AL 35808

Attn: Documents Section   2

U.S. Naval Missile Center
Point Mugu, CA 93041

Attn: Technical Library   1

Battelle Memorial Institute
505 King Avenue
Columbus, OH 43201

Attn: Library   1

Bell Aerosystems, Inc.
Box 1
Buffalo, NY 14240

Attn: Library   1

Boeing Company
Space Division
P.O. Box 868
Seattle, WA 98124

Attn: Library   1

General Dynamics/Convair
P.O. Box 1128
San Diego, CA 92112

Attn: Library   1

Grumman Aerospace Corporation
Bethpage, Long Island, NY 11714

Attn: Library   1

Lockheed Missiles & Space Co.
P.O. Box 504
Sunnyvale, CA 94088

Attn: Library   1

Marquardt Corporation
16555 Saticoy Street
Box 2013 South Annex
Van Nuys, CA 91409

Attn: Library   1

Martin-Marietta Corporation
P.O. Box 179
Denver, CO 80201

Attn: Library   1

McDonnell Douglas Astronautics
5301 Bolsa Avenue
Huntington Beach, CA 92547

Attn: Library   1

Rocket Research Corporation
Willow Road at 116th Street
Redmond, WA 98052

Attn: Library   1

TRW Systems, Inc.
1 Space Park
Redondo Beach, CA 90278

Attn: Library   1

United Technologies Research Center
East Hartford, CT 06108

Attn: Library   1

United Technologies Pratt & Whitney
Government Products Division
P.O. Box 2691
West Palm Beach, FL 33402

Attn: Library   1

Aerojet Tech Systems Company
P.O. Box 13222
Sacramento, CA 95813

Attn: Library   1